INVESTIGATING THE ROLE OF GIBBERELLIC ACID (GA) AND ABSCISIC ACID (ABA) CROSS-TALK IN ENHANCING TUBEROUS ROOT DEVELOPMENT IN SWEET POTATOES

ARTICLES FOR FACULTY MEMBERS

Dynamic network biomarker analysis discovers IbNAC083 in the initiation and regulation of sweet potato root tuberization / He, S., Wang, H., Hao, X., Wu, Y., Bian, X., Yin, M., Zhang, Y., Fan, W., Dai, H., Yuan, L., Zhang, P., & Chen, L.

The Plant Journal
Volume 108 Issue 3 (2021) 1365313 Pages 793–813
https://doi.org/10.1111/tpj.15478
(Database: Wiley Online Library)

Genome-wide identification and expression analysis of sweet family genes in sweet potato and its two diploid relatives / Dai, Z., Yan, P., He, S., Jia, L., Wang, Y., Liu, Q., Zhai, H., Zhao, N., Gao, S., & Zhang, H.

International Journal of Molecular Sciences
Volume 23 Issue 24 (2022) 15848 Pages 1-23
https://doi.org/10.3390/ijms232415848
(Database: MDPI)

IbMYB73 targets abscisic acid-responsive IbGER5 to regulate root growth and stress tolerance in sweet potato / Wang, Z., Li, X., Gao, X. R., Dai, Z. R., Peng, K., Jia, L. C., Wu, Y. K., Liu, Q. C., Zhai, H., Gao, S. P., Zhao, N., He, S. Z., & Zhang, H.

Plant Physiology
Volume 194 Issue 2 (2024) Pages 787–804
https://doi.org/10.1093/plphys/kiad532
(Database: Oxford Academic)

INVESTIGATING THE ROLE OF GIBBERELLIC ACID (GA) AND ABSCISIC ACID (ABA) CROSS-TALK IN ENHANCING TUBEROUS ROOT DEVELOPMENT IN SWEET POTATOES

ARTICLES FOR FACULTY MEMBERS

Molecular characterization and target prediction of candidate miRNAs related to abiotic stress responses and/or storage root development in sweet potato / Sun, L., Yang, Y., Pan, H., Zhu, J., Zhu, M., Xu, T., Li, Z., & Dong, T.

Genes
Volume 13 Issue 1 (2022) 110 Pages 1-16
https://doi.org/10.3390/genes13010110
(Database: MDPI)

Overexpression of 9-cis-epoxycarotenoid dioxygenase gene, IbNCED1, negatively regulates plant height in transgenic sweet potato / Zhou, Y., Zhao, C., Du, T., Li, A., Qin, Z., Zhang, L., Dong, S., Wang, Q., & Hou, F.

International Journal of Molecular Sciences
Volume 24 Issue 13 (2023) 10421 Pages 1-14
https://doi.org/10.3390/ijms241310421
(Database: MDPI)

Salicylic acid protects sweet potato seedlings from drought stress by mediating abscisic acid-related gene expression and enhancing the antioxidant defense system / Huang, C., Liao, J., Huang, W., & Qin, N.

International Journal of Molecular Sciences
Volume 23 Issue 23 (2022) 14819 Pages 1-18
https://doi.org/10.3390/ijms232314819
(Database: MDPI)

INVESTIGATING THE ROLE OF GIBBERELLIC ACID (GA) AND ABSCISIC ACID (ABA) CROSS-TALK IN ENHANCING TUBEROUS ROOT DEVELOPMENT IN SWEET POTATOES

ARTICLES FOR FACULTY MEMBERS

The IbPYL8–IbbHLH66–IbbHLH118 complex mediates the abscisic acid-dependent drought response in sweet potato / Xue, L., Wei, Z., Zhai, H., Xing, S., Wang, Y., He, S., Gao, S., Zhao, N., Zhang, H., & Liu, Q.

New Phytologist
Volume 236 Issue 6 (2022) Pages 2151–2171
https://doi.org/10.1111/nph.18502
(Database: Wiley Online Library)

Transcriptome analysis reveals the impact of short-term biochar application on starch and sucrose metabolism in sweet potato tuberous roots / Zhang, J., Xu, X., Li, T., Lv, Z., Zhu, Y., Li, J., & Lu, G.

Industrial Crops and Products
Volume 223 (2025) 120050 Pages 1-11
https://doi.org/10.1016/j.indcrop.2024.120050
(Database: ScienceDirect)

Transcriptomic analysis of tuberous root in two sweet potato varieties reveals the important genes and regulatory pathways in tuberous root development. BMC / Cai, Z., Cai, Z., Huang, J., Wang, A., Ntambiyukuri, A., Chen, B., Zheng, G., Li, H., Huang, Y., Zhan, J., Xiao, D., & He, L.

BMC Genomics
Volume 23 (2022) 473 Pages 1-19
https://doi.org/10.1186/s12864-022-08670-x
(Database: Springer Nature)

ARTICLES FOR FACULTY MEMBERS

INVESTIGATING THE ROLE OF GIBBERELLIC ACID (GA) AND ABSCISIC ACID (ABA) CROSS-TALK IN ENHANCING TUBEROUS ROOT DEVELOPMENT IN SWEET POTATOES

Dynamic network biomarker analysis discovers IbNAC083 in the initiation and regulation of sweet potato root tuberization / He, S., Wang, H., Hao, X., Wu, Y., Bian, X., Yin, M., Zhang, Y., Fan, W., Dai, H., Yuan, L., Zhang, P., & Chen, L.

The Plant Journal
Volume 108 Issue 3 (2021) 1365313 Pages 793–813
https://doi.org/10.1111/tpj.15478
(Database: Wiley Online Library)

the plant journal

SEB SOCIETY FOR EXPERIMENTAL BIOLOGY

The Plant Journal (2021) **108,** 793–813 doi: 10.1111/tpj.15478

Dynamic network biomarker analysis discovers IbNAC083 in the initiation and regulation of sweet potato root tuberization

Shutao He[1,†], Hongxia Wang[2,†], Xiaomeng Hao[2,3,†], Yinliang Wu[2,3], Xiaofeng Bian[2], Minhao Yin[2,4], Yandi Zhang[2,3], Weijuan Fan[2], Hao Dai[1], Ling Yuan[5], Peng Zhang[2,3,*] and Luonan Chen[1,6,7,*]

[1]*State Key Laboratory of Cell Biology, CAS Center for Excellence in Molecular Cell Science, Shanghai Institute of Biochemistry and Cell Biology, Chinese Academy of Sciences, Shanghai 200031, China,*

[2]*National Key Laboratory of Plant Molecular Genetics, CAS Center for Excellence in Molecular Plant Sciences, Institute of Plant Physiology and Ecology, Chinese Academy of Sciences, Shanghai 200032, China,*

[3]*CAS Center for Excellence in Molecular Plant Sciences, University of Chinese Academy of Sciences, Beijing 100049, China,*

[4]*College of Tree Peony, Henan University of Science and Technology, Luoyang 471000, China,*

[5]*Department of Plant and Soil Sciences, University of Kentucky, Lexington, Kentucky 40506, USA,*

[6]*Key Laboratory of Systems Health Science of Zhejiang Province, Hangzhou Institute for Advanced Study, University of Chinese Academy of Sciences, Chinese Academy of Sciences, Hangzhou 310024, China, and*

[7]*School of Life Science and Technology, ShanghaiTech University, Shanghai 201210, China*

Received 2 December 2020; revised 19 August 2021; accepted 23 August 2021; published online 30 August 2021.
*For correspondence (e-mail lnchen@sibcb.ac.cn or zhangpeng@cemps.ac.cn).
† These authors contributed equally to this work.

SUMMARY

The initiation and development of storage roots (SRs) are intricately regulated by a transcriptional regulatory network. One key challenge is to accurately pinpoint the tipping point during the transition from pre-swelling to SRs and to identify the core regulators governing such a critical transition. To solve this problem, we performed a dynamic network biomarker (DNB) analysis of transcriptomic dynamics during root development in *Ipomoea batatas* (sweet potato). First, our analysis identified stage-specific expression patterns for a significant proportion (>9%) of the sweet potato genes and unraveled the chronology of events that happen at the early and later stages of root development. Then, the results showed that different root developmental stages can be depicted by co-expressed modules of sweet potato genes. Moreover, we identified the key components and transcriptional regulatory network that determine root development. Furthermore, through DNB analysis an early stage, with a root diameter of 3.5 mm, was identified as the critical period of SR swelling initiation, which is consistent with morphological and metabolic changes. In particular, we identified a NAM/ATAF/CUC (NAC) domain transcription factor, IbNAC083, as a core regulator of this initiation in the DNB-associated network. Further analyses and experiments showed that IbNAC083, along with its associated differentially expressed genes, induced dysfunction of metabolism processes, including the biosynthesis of lignin, flavonol and starch, thus leading to the transition to swelling roots.

Keywords: *Ipomoea batatas*, storage root development, transcriptome dynamics, co-expression network, dynamic network biomarker, tipping point, IbNAC083.

INTRODUCTION

Ipomoea batatas L. (sweet potato) is the sixth largest food crop in the world. The widely grown crop is high in nutrient content and is suitable for multiple food and industrial uses (Dong et al., 2019). The storage root (SR), the carbohydrate storage organ that is also used for vegetative propagation, is the most economically important part of the sweet potato and provides an excellent model for studying organogenesis and evolution. Therefore, much of the research on sweet potato focuses on the mechanisms underlying SR formation and development.

The initiation and development of SRs are complicated biological processes influenced by both internal and external factors. The SRs of sweet potato are specialized roots that develop from adventitious roots at the anatomical

level (Wilson and Lowe, 1973). In sweet potato, roots are classified into young, non-tuberous, pencil-like and tuberous roots according to the degree of stele lignification and primary cambium activity (Togari, 1950). First, the developmental process begins by the genesis of vascular cambiums from procambial cells between the primary phloem and the primary xylem of young fibrous roots, resulting in the formation of circular primary cambium (Ravi et al., 2009). Afterwards, secondary meristems, including the meristems around vessels and anomalous secondary cambiums, differentiate into the xylem. Furthermore, cell divisions and expansions proceed in the primary cambium and secondary meristems, accompanied by divisions of parenchyma cells in the xylem, resulting in root expansion. During this expansion phase, the parenchyma cells accumulate a mass of photosynthates, specifically starch (Firon et al., 2013). Pencil roots do not transform into SRs by the process of lignification (Villordon et al., 2009), indicating that stele lignification in the early root developmental stage influences the SR development process (Togari, 1950). To facilitate the study of root development in sweet potato, 20 stages (S1–S20) have been classified according to root diameter (Wang et al., 2016). Further, transcriptomics validated the downregulation of lignin biosynthesis and the upregulation of starch biosynthesis genes at an early stage of SR formation (Firon et al., 2013). The formation and development of SRs strongly correlate with the levels of endogenous phytohormones. SR swelling is the consequence of the synergistic interaction of several phytohormones, including abscisic acid (ABA), auxin (IAA), cytokinins (CTKs), gibberellins (GAs) and jasmonic acid (JA) (Nakatani, 1994; Nakatani and Komeichi, 1991; Noh et al., 2010; Ravi et al., 2009; Singh et al., 2019; Spence and Humphries, 1972; Tanaka et al., 2008).

Recently, considerable progress has been made regarding the isolation and characterization of genes related to SR formation, which can be grouped into four categories: (i) cell division-related genes, such as *Cyclin A-like* and *Cyclin D-like*, which are the key cell division regulator genes (Firon et al., 2013); (ii) expansion-related genes, including *IbEXP1*, which affect the weight and number of SRs (Noh et al., 2013); (iii) lignin biosynthesis-related genes, as lignification of the stele restrains the transition of adventitious roots to SRs (Belehu et al., 2004); (iv) transcription factor (TF) genes, such as *IbMADS*, which affects the enlargement of the SRs (Ku et al., 2008), *SRD1*, which is essential for the initiation and development of tuberous roots by influencing auxin synthesis (Noh et al., 2010), as well as KNOXI homeobox and NAM/ATAF/CUC (NAC) homeobox genes, which affect SR development and lignin content (Firon et al., 2013; Tanaka et al., 2008). Specification into distinctive xylem cells affecting lignin content can be affected by various NAM/ATAF/CUC (NAC) domain TFs, such as XND1, VND and AtNAC083 in Arabidopsis (Yamaguchi et al., 2011). AtNAC083 interacts with VND proteins and other NAC domain proteins, which regulates xylem cell differentiation, implying the significance of a transcriptional network regulating xylem specification (Yamaguchi et al., 2010).

Currently, the transcriptional mechanisms mediating the initiation and progression of root swelling, a non-linear transitional process, remain unclear. In other words, how the swelling process is initiated and what is the critical state (tipping point) with its core regulators during root swelling development are largely unknown. Transcriptomic analysis is an effective approach to study transcriptional mechanisms, which gives an overview of spatiotemporal gene expression profiles and associates biological functions with co-expressed genes (Silva et al., 2016; Vesty et al., 2016). The dynamic study of transcriptome data thus gives us a powerful tool to explore the mechanisms underlying the phase transition of developing roots on a genome-wide scale (Chen et al., 2016). However, the majority of the traditional studies concentrate on static molecular biomarkers, which mainly distinguish different development states of SR by their static features, e.g. using the 'differential expressions of molecules' (Dong et al., 2019; Firon et al., 2013; Wang et al., 2015). In other words, it is difficult to determine the critical state or catch the dynamic signals that occur at the tipping point, which is key to revealing the critical transition and core regulators of the transition from fibrous roots to SRs. Recently, the dynamic network biomarker (DNB) method, which is a model-free method, has been developed to recognize early signals of a critical transition as well as its core regulators in many biological problems, including hepatocellular carcinoma and type-2 diabetes, based on omics data and nonlinear dynamical theory (Chen et al., 2012; Jiang et al., 2020; Li et al., 2014, 2017; Liu et al., 2013; Yang et al., 2018; Zhang et al., 2019). Whereas DNB has been used successfully in medical research, its application in plant research remains rare (Zhang et al., 2019). Nevertheless, DNB is an ideal method to identify the tipping point or pre-swelling state (just before the dramatic transition to the swelling state) during SR developmental process, based on 'differential associations among molecules' (or differential networks) in a dynamical manner, and to further determine the corresponding core regulators or regulatory network, in contrast to the traditional strategy using 'differential expressions of molecules' (or differential molecules/genes).

Here, based on our gene expression profiles of sweet potato roots at different developmental stages, we studied the molecular mechanisms of SR development from the perspectives of dynamics and network, and identified the tipping point of the SR swelling process using the DNB method. In particular, we discovered that IbNAC083, a member of the DNB-associated network, not only regulates

the initiation of SRs in sweet potato but also quantifies the tipping point of this process, which was validated by biological experimental analysis. Collectively, our study not only identified the core regulator and its associated DNB network, which tightly regulates the critical developmental transition during the root-swelling process, but also provides an information-rich resource for investigating the functions of key components in SR development.

RESULTS

Characterizing root phenotypes at different developmental stages of sweet potato roots for RNA-seq analysis

Several important physiological parameters were analyzed in roots at seven developmental stages (S4–S20) representing major events occurring within the root, including the early fibrous and pencil root development and the later SR formation and swelling (Figure 1a). The initial swelling roots showed circular primary cambia (S10 and S12), and the SRs at later stages displayed secondary cambia and anomalous meristems (S16), which had more parenchyma cells (Figure 1b). Toluidine blue staining for lignin revealed a continuously decreased number of lignified cells surrounding xylem bundles and increased starch granules from fibrous roots (S4) to SRs (S16). To verify this result, the lignin and starch levels of roots at different developmental stages were measured. The lignin content decreased gradually from S8 (average of 73.6%) to S20 (average of 16.6%), whereas the starch content increased progressively from S8 (average of 1.9%) to S20 (average of 68.9%) (Figure 1c,d). In addition, the sucrose content increased from S4 and reached a plateau at S12–S16 before decreasing again. The levels of glucose and fructose remained low prior to S14, followed by a sharp increase at S16 before a decrease. The maltose level was barely detectable until S16, followed by a sharp increase (Figure 1e).

To decipher the molecular mechanism underlying the initiation and development of sweet potato SRs, we conducted RNA-seq analysis using total RNA extracted from roots at seven developmental stages. After the removal of adaptors and reads containing low-quality nucleotides, more than 47 million clean reads (on average approx. 56 million reads) were obtained for each sample (Table S1) and aligned with the sweet potato genome of 466 Mb in size using TOPHAT. More than 77% of the clean reads were aligned with the genome, and more than 72% of the clean reads were unique mapped reads (Table S1). The mapped files were processed with STRINGTIE 1.3.3b, which generated a transcriptome assembly with a total of 99 697 gene loci, including 75 502 annotated and 24 195 novel gene loci (Table S2). The uniquely mapped reads for each sample were processed via RSEM 1.3.1 to obtain the normalized expression level as transcripts per million reads (TPMs) for all sweet potato genes. Overall, a total of approximately 77% genes (TPM > 0.1) were identified as being expressed in at least one of the seven stages (Table S3), and the number of expressed genes in samples from different stages varied from 56.4% (S4) to 65.2% (S14).

Global transcriptome analysis of sweet potato roots at different developmental stages

To study the global differences of the transcriptome dynamics during root development of sweet potato, we performed principal component analysis (PCA), gene ontology (GO) analysis and unsupervised hierarchical clustering based on the TPM values for all the expressed genes in at least one of the seven developmental stages. PCA revealed that sweet potato root transcriptomes were clustered into four groups: (i) fibrous roots (S4 and S8); (ii) early stages of SR development (S10 and S12); (iii) middle stages of SR development (S14 and S16); and (iv) mature stage of SR development (S20) (Figure 2a), which reflects the progression from fibrous roots to mature SRs (Figure 1a). To explore the biological functions that distinguish these samples in different developmental stages, we selected the 500 genes with the largest load and the 500 genes with the smallest load in principal component 1 (PC1) and principal component 2 (PC2) and performed GO enrichment analysis. As shown in Figure 2(b), the biological functions with the most significant changes during the development of sweet potato roots included carbohydrate metabolic processes, cell wall metabolism, transcription regulator activity, protein metabolic processes, secondary metabolic processes and response to stress, in agreement with previous studies (Firon et al., 2013). Furthermore, the hierarchical clustering analysis (Figure 2c) showed that all samples were clustered into four independent groups, consistent with the clustering by PCA (Figure 2a). Clearly, only samples in stage S10 were dispersed in both the fibrous roots state and the early developmental state, indicating that they might be at a critical stage before the swelling transition to SRs.

Preferentially expressed genes at each root developmental stage of sweet potato

We analyzed the genes expressed at a particular stage of root development by using the stage specificity (SS) algorithm (Zhan et al., 2015), with an SS score of >0.5. According to this criterion, we characterized a total of 6791 genes particularly expressed at a special root developmental stage (Table S4). Collectively, 196 TFs belonging to 28 gene families displayed a developmental stage-specific expression profile. The members of several TF families, including basic helix-loop-helix (bHLH), homeobox (HB), heat shock factor (HSF) and myeloblastosis (MYB) TF families, showed high representation. Figure S1(a) depicts stage-specific gene expression patterns during root development in sweet potato. The variable number and

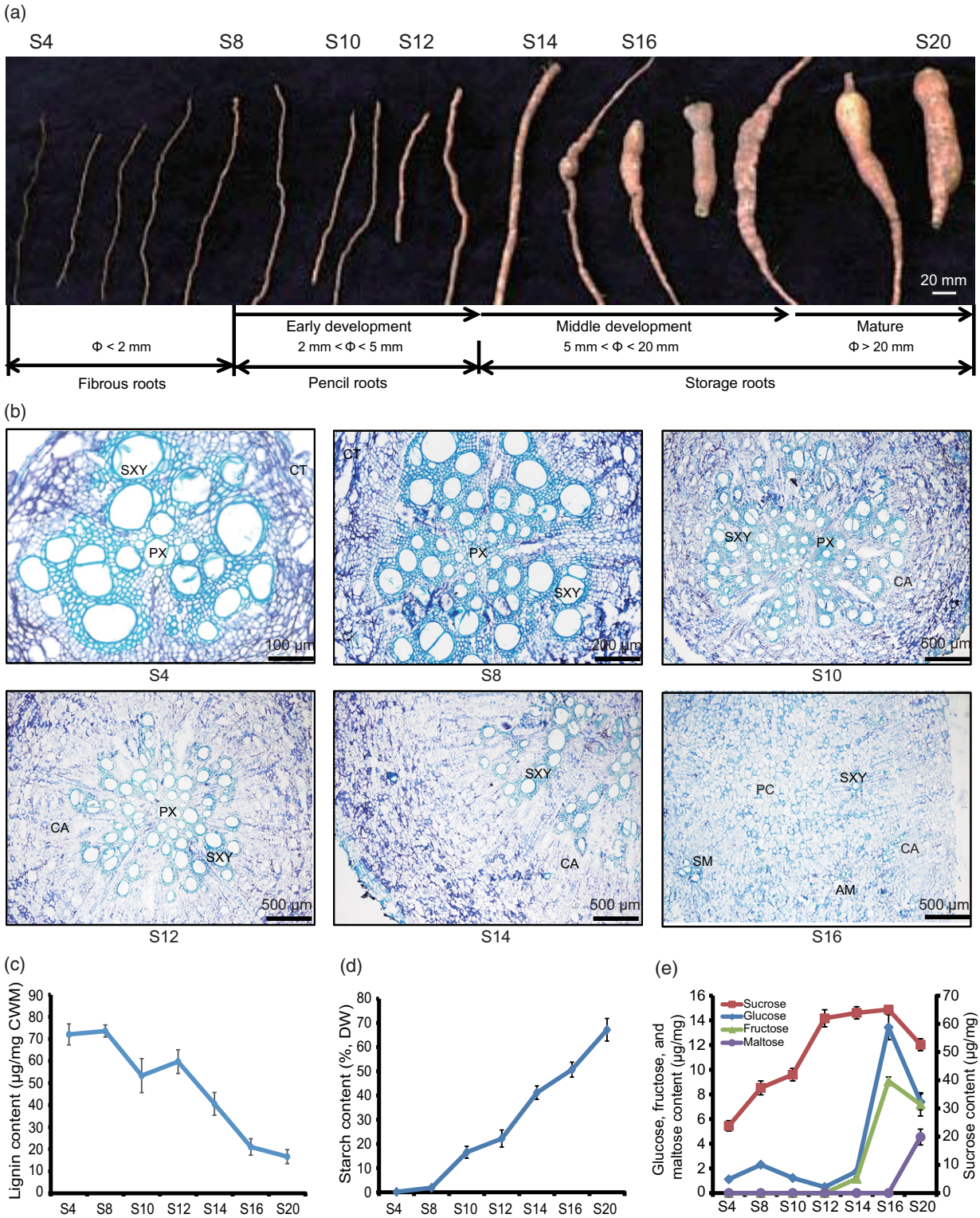

Figure 1. Physiological changes in different developmental stages of *Ipomoea batatas* (sweet potato).
(a) Morphology of sweet potato roots at different developmental stages.
(b) Transverse sections of sweet potato roots at different developmental stages after staining with toluidine blue. Abbreviations: AM, anomalous meristem; CA, cambium; CT, cortex; PC, parenchyma cell; PX, primary xylem; SM, secondary meristem; SXY, secondary xylem.
(c–e) Variation in lignin (c), starch (d) and sugar (e) contents of sweet potato roots at different developmental stages. CWM, cell wall material; DW, dry weight. Error bars indicates standard errors (n = 12).

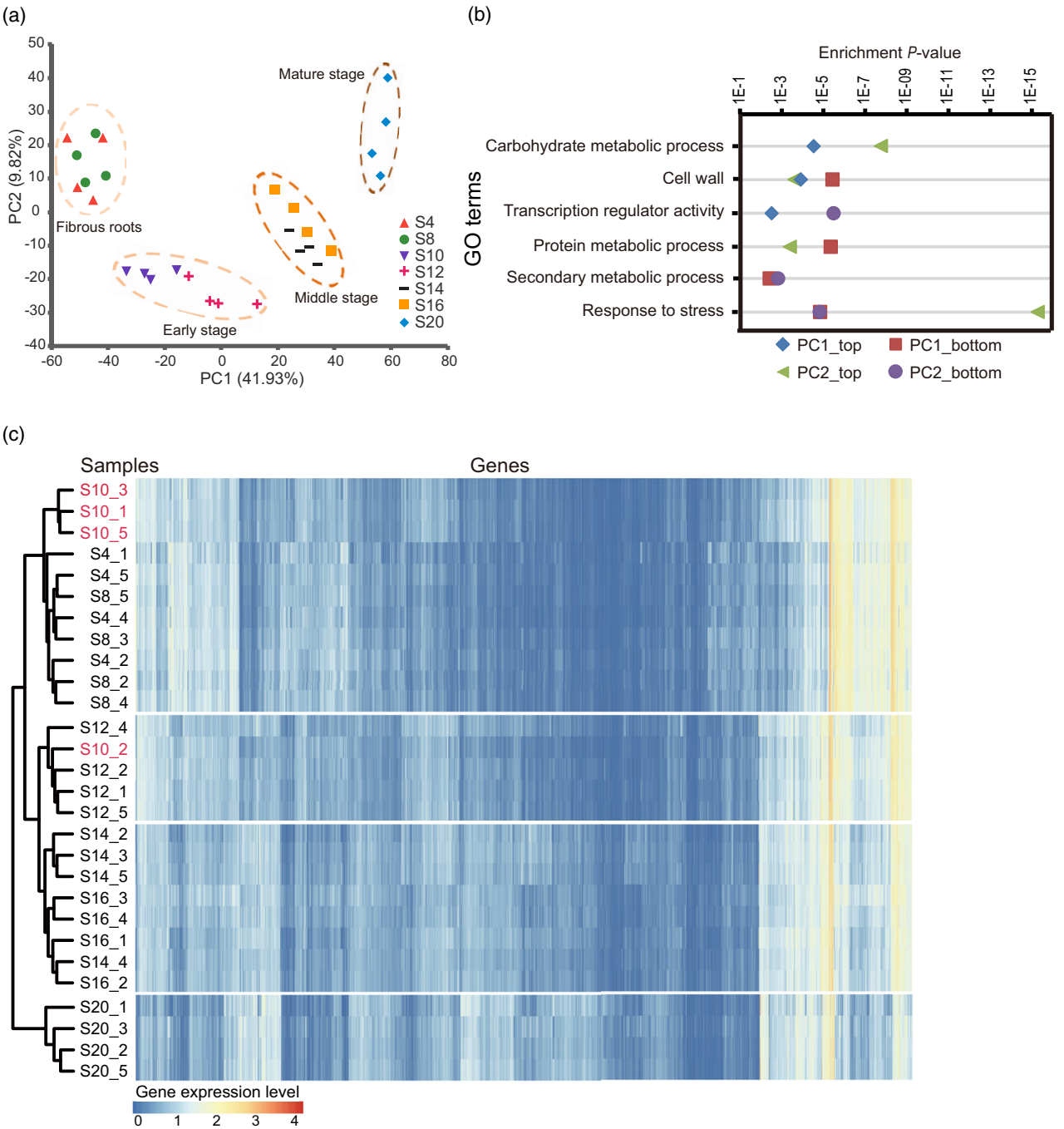

Figure 2. Global differences in transcriptome dynamics during the root development of *Ipomoea batatas* (sweet potato).
(a) Principal component analysis (PCA) plot showing the clustering of transcriptomes of sweet potato roots at different developmental stages.
(b) Biological functions that can best distinguish these samples at different developmental stages, analyzed by gene ontology (GO) enrichment of genes with the largest load (positive value) and genes with the smallest load (negative value) in PCA.
(c) Unsupervised hierarchical clustering of transcriptomes of sweet potato roots at different developmental stages.

proportion of preferentially/specifically expressed genes suggests that each stage has its own independent developmental program.

The GO enrichment analysis of all the stage-specific genes showed a representation of genes associated with reproductive processes, cell wall organization, carbohydrate metabolic processes and response to stress/hormones. These processes are related to various aspects of root development. In general, the fibrous root stages (S4 and S8) were marked by functions related to inorganic

anion transport, primary metabolic processes and response to stimulus (Figure S1b). The early stages (S10 and S12) were marked by functions associated with brassinosteroid biosynthetic processes and hormone biosynthetic processes. Interestingly, there were no significantly enriched GO terms at stage S10, indicating that, with no significant highly expressed biological function, S10 might represent the critical period of the SR swelling transition or represent a pre-swelling state, in line with the conclusion of the hierarchical clustering result (Figure 2c). During the middle stages (S14 and S16), biological processes related to cell wall reorganization, carbohydrate metabolic process, hormone metabolic regulation and regulation of transcription were over-represented. At the mature stage (S20), GO terms related to starch biosynthesis processes, ABA metabolism and cell wall functions were over-represented. In conclusion, a set of genes, containing those encoding TFs, implement stage-specific functions during root developmental process in sweet potato, potentially providing hints to the transition stage of tuberous root swelling.

We performed reverse-transcriptase quantitative polymerase chain reaction (RT-qPCR) analysis for 17 genes displaying stage-specific expression. The results revealed that the expression patterns and stage-specific expression of the genes tested resembled those obtained by RNA-seq (Figure S2), confirming the accuracy of the RNA-seq data. For most of the genes tested the correlation coefficient was $\geq$0.70 between the RNA-seq and RT-qPCR analysis (Figure S2).

Characterizing transcriptional reprogramming during sweet potato root development

DESEQ 2 identified 13 063 differentially expressed genes (DEGs), and the DEGs obtained at each stage of root development were compared with the previous adjacent stage (Table S5): seven DEGs were unique to stage S8, compared with stage S4; 3175 DEGs were unique to stage S10, compared with stage S8; 609 DEGs were unique to stage S12, compared with stage S10; 2412 DEGs were unique to stage S14, compared with stage S12; 336 DEGs were unique to stage S16, compared with stage S14; and 3044 DEGs were unique to stage S20, compared with stage S16. There were 3480 genes differentially expressed at more than one stage. Many of these DEGs have not been described previously as being related to root development. Previous study has analyzed the genome-wide transcriptional profiling of sweet potato root at seven different developmental stages using a customized microarray including 39 724 genes (Wang et al., 2015). Based on the root diameter, we matched our samples with the samples at the same developmental stage in the previous study. All DEGs identified in the microarray analysis in an earlier study (Wang et al., 2015) were also differentially expressed in our study, but only accounted for approximately 17.8% of the DEGs in our data set (Figure 3a, and larger image in Figure S3), indicating that our data set captures a larger proportion of root developmental transcriptional changes and can be used to model biologically relevant gene expression changes during root development.

Next, the genes were separated into sets of upregulated and downregulated DEGs and were sorted based on the time at which they were first differentially expressed. Several biological processes particularly enriched at various stages of root development were identified by the GO enrichment analysis of these gene sets (Figure 3b). The analysis showed that a massive onset of downregulation-enriched biological processes preceded that of upregulation, and various waves of coordinated biological functions of gene expression changes can be identified during root development. Various GO terms related to metabolic processes, such as cellular amino acid and derivative metabolic processes, lipid metabolic processes and secondary

Figure 3. Chronology of root developmental transcriptional reprogramming in *Ipomoea batatas* (sweet potato).
(a) Circos plots of developmental series expression profiles in comparison with previously published sweet potato root transcriptome data (Wang et al., 2015), as indicated underneath the plot. The stacked histograms indicate differential expression. The second to seventh circles indicate differentially expressed genes (DEGs) of stages S8–S4, S10–S8, S12–S10, S14–S12, S16–S14 and S20–S16, respectively. Genes differentially expressed in both data sets are marked by connecting bands (colors indicate first developmental stage of differential expression in our study). Each section within the circus plot represents a set of 500 DEGs.
(b) Enriched gene ontology (GO) terms of first downregulated and upregulated genes at different stages of root development. The color scale at the bottom represents significance (corrected *P*-value).
(c) Analysis of the major transcriptional states in the root developmental gene regulatory network of sweet potato. DEGs were divided into four sets according to their function as regulator or non-regulator (regulated), and their expression pattern being upregulated (red) or downregulated (blue) over time. Transcriptional states are indicated by boxes, aligned on the timeline. DEGs are assigned to the states according to the time point where they were differentially expressed; the over-represented functional categories are indicated (F). Colored squares indicate known transcription factor (TF) DNA-binding motifs that are over-represented in gene promoters (hypergeometric distribution; $P \leq 0.001$). Pie charts indicate the proportion of TF gene families. Abbreviations Develop., development; Diff., differentiation; Metab., Metabolism; Phos., protein phosphorylation; Reg., regulation; Str., response to stress.
(d) Predicted directional interactions in transcriptional states of the root developmental gene regulatory network. The promoter sequences of genes associated with a transcriptional state were tested for the over-representation of DNA motifs shown to be bound to TFs that are differentially transcribed during root development. Each TF with a known motif is represented by a colored circle and is plotted at the time point that its corresponding gene is first differentially expressed. Each regulated transcriptional state is represented by a square and plotted in time according to its onset (red and blue squares indicate up- and downregulated transcriptional states, respectively). An edge between a TF and a transcriptional state only indicates significant enrichment of the corresponding binding motif in that state, not the direction of regulation (positive regulation or negative regulation). The size of each TF node is proportional to the number of states in which its binding site is over-represented. To aid the interpretation of the network, nodes are grouped and colored according to the transcriptional state where they first become differentially expressed.

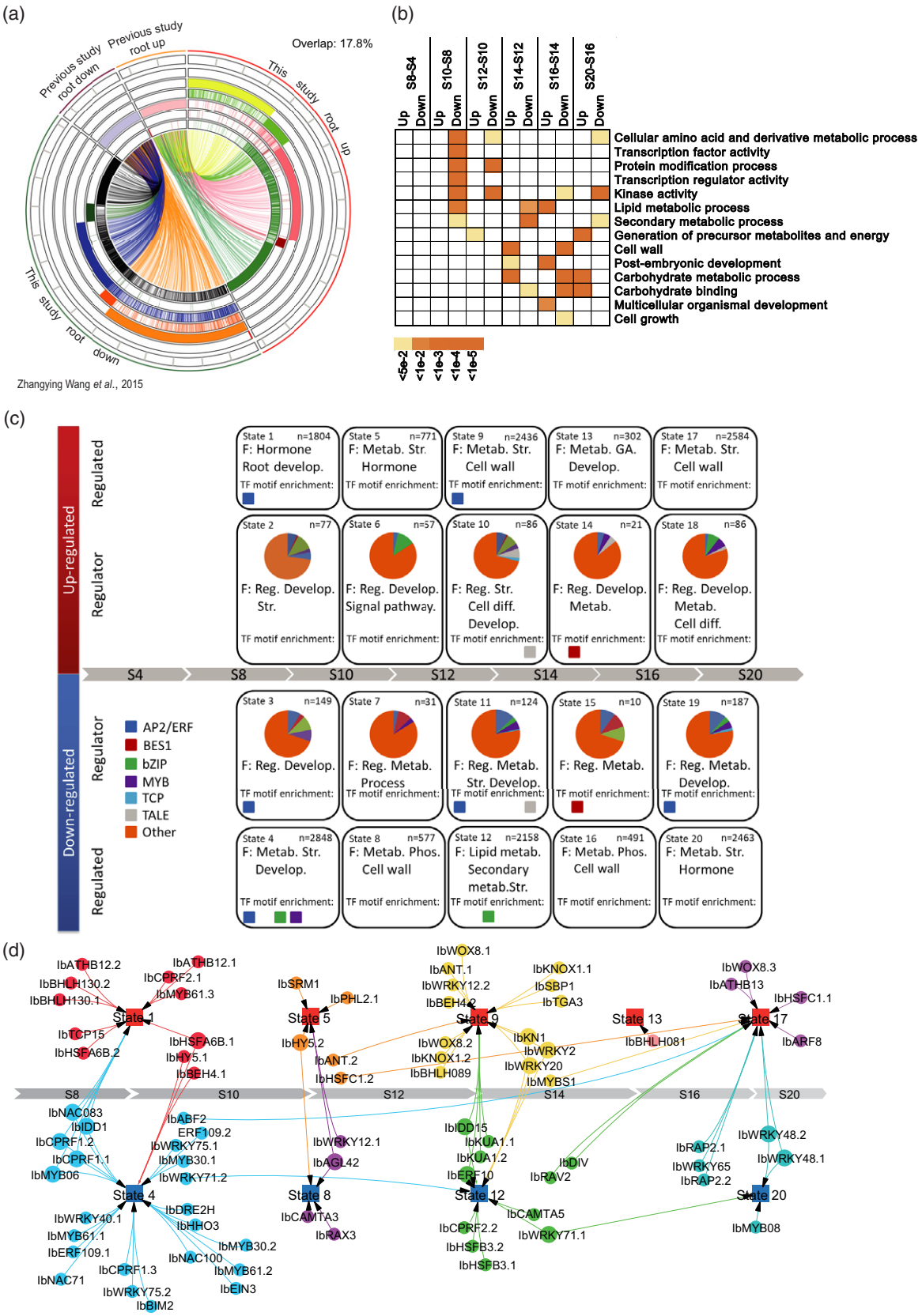

metabolic processes, were significantly repressed, particularly at stage S10 compared with stage S8. Likewise, compared with stage S8, regulation-related GO terms, including TF activity, transcription regulator activity, protein modification processes and kinase activity, were highly enriched at stage S10 in the downregulated genes. Additionally, development-related genes, involved in post-embryonic development and multicellular organismal development, exhibited transcriptional activation during the middle developmental stages (S14 and S16). Interestingly, we observed the significant activation of genes related to the GO terms for cell wall and carbohydrate metabolic processes at stage S14, followed by repression at stage S16, suggesting elevated activities of cell wall metabolism and starch accumulation during the middle stages of the root-swelling process. Thereafter, genes associated with carbohydrate metabolism were observed to be more active at stage S20.

Characterizing gene regulatory network rewiring during sweet potato root development

The chronology of transcriptional states during root development was discerned by mining our RNA-seq data. First, DEGs at each developmental stage were divided into two gene sets, i.e. upregulated and downregulated DEGs. Then, according to their predicted function as transcriptional regulators (termed regulator genes) or as having a different function (termed regulated genes), we divided these genes into two additional sets. In order to investigate the biological significance and regulatory directionality of each gene set (termed transcriptional state), the gene sets of the 20 transcriptional states were analyzed for the enrichment of functional categories and promoter motifs (Figure 3c). The first wave of transcriptional change is characterized by genes related to transcriptional regulation, including AP2/ERFs, bZIPs and MYBs, and other genes associated with metabolism and development, and begins at the transition from stages S8 to S10. These regulatory genes might be crucial to the regulation of other regulator genes, and regulated genes appear in the contemporaneous or subsequent developmental stage transitions, which are linked to root developmental processes such as cell differentiation, signal transduction, organ development, and cell wall and carbohydrate metabolism. For instance, in the DEGs of state 9, DNA motifs that can be bound by AP2/ERFs, which were transcribed in previous states 2, 3, 6, 7 and contemporaneous states 10 and 11, are enriched. In state 9, genes involved in stress responses, and in cell wall and metabolism processes, are enriched, which is consistent with previous studies showing that AP2/ERF genes play various roles in the regulation of several developmental processes, such as floral organ development and leaf epidermal cell development, and response to multiple forms of biotic and abiotic stress (Riechmann and Meyerowitz, 1998).

Further, to predict directional interactions between the regulator genes and the regulated genes related to the various transcriptional states, a gene regulatory network (GRN) was established using the TF DNA-binding motif information. As shown in Figure 3(d), when a specific DNA-binding motif is enriched in one transcriptional state, that state (indicated by a square node) is linked to corresponding differentially expressed TF genes (indicated by a circular node and sorted based on the time at which they were first differentially expressed). In the network, TFs were likely to regulate the transcriptional levels of genes in either single or several transcriptional states. Notably, TFs that become active in the states showing the first wave of transcriptional activity (states 1 and 4) might be crucial to the regulation of subsequent transcriptional activity, and the regulatory relationships between TFs assigned to these states were predicted using the network. States 1 and 4 contain the TFs IbWRKY75, IbMYB61, IbMYB30, IbHY5, IbHSFA6B, IbEIN3, IbERF109 and IbABF2, which are the most active TFs as there is an over-representation of their DNA binding motifs in the promoters of genes assigned to the majority of the differentially expressed transcriptional states. This prediction is consistent with previous reports indicating that these TFs are modulators of root development (Cai et al., 2014; Devaiah et al., 2007; Garcia et al., 2014; Van Gelderen et al., 2018; Huang et al., 2016; Li et al., 2020a; Romano et al., 2012; Sakaoka et al., 2018). Furthermore, other stages contain the TFs IbWOX8, IbTGA3, IbRAP2, IbPHL2, IbATHB3, IbMYB08, IbKN1, IbARF8, IbANT and IbAGL42, the corresponding mutants of which show altered root development (Bomal et al., 2008; Bonke et al., 2003; Eysholdt-Derzso and Sauter, 2017; Farinati et al., 2010; Gutierrez et al., 2009; Hacham et al., 2011; Petricka et al., 2012; Randall et al., 2015; Silva et al., 2016; Woerlen et al., 2017). Moreover, *IbKNOX1* genes have been shown to regulate cytokinin levels, thus affecting sweet potato SR development (Ravi et al., 2009; Tanaka et al., 2008).

Analysis of transcriptional modules associated with root development of sweet potato

Weighted gene co-expression network analysis (WGCNA) was used to identify co-expressed genes. Through this GRN analysis, several major subnetworks were revealed, characterized by the interaction relationships among genes showing similar expression patterns, termed co-expression modules. Fifteen modules (containing 33–3743 genes) were identified (Figure 4a; Table S6). We associated each co-expression module with root developmental stages and physiological phenotypes using Pearson correlation coefficient analysis. Twelve co-expression modules showed significant correlation ($r \geq 0.50$ and $P \leq 0.01$) with root developmental stages. Most of the modules were associated with one particular root development stage only; however, a few of them were correlated with more than

one root development stage, such as the black and blue modules in Figure 4(b).

Stage S10 seems to be a critical period for the swelling of sweet potato roots (Figures 2c and 3b–d; Figure S1b). Considering that modules associated with stage S10 might be responsible for the swelling during root development, we examined the GRNs that connect the TFs with corresponding co-expressed target genes harboring remarkably over-represented TF binding motifs at S10 and its adjacent developmental periods (S8 and S12) (Figure 4b,c). Co-expressed genes involved in the modules related to S8, S10 and S12 were used to perform this analysis, and we found co-expressed modules linking the over-represented TF binding motifs with the known TFs and specific GO categories that are remarkably enriched in their target genes. The transcriptional modules in S8 (black, salmon and blue modules) included TFs with significantly enriched motifs, like IbNAC083, IbERF109, IbWRKY53, IbMYB30 and IbBEH4, and target genes related to GO categories for the regulation of cell wall reorganization and response to hormone stimulus (Figure 4b). At S10 (tan and red modules), motifs associated with TFs like IbWOX8, IbPHL2, IbERF10, IbWRKY48 and IbKN1 were enriched (Figure 4c), and their associated target genes are involved in cellulose biosynthetic processes, cellular cell wall organization or biogenesis, chromatin silencing by small RNA and primary metabolism. Similarly, motifs associated with TFs, such as IbMYB08, IbNAC092, IbWRKY65, IbTCP15 and IbBH130, and target genes involved in secondary metabolic processes, hormone transport, gibberellin and salicylic acid metabolism, oxidation reduction and carbohydrate transport were enriched in the transcriptional modules at stage S12 (Figure 4d). Several of these regulatory motifs and TFs are related to root development and play vital roles coordinately in gene transcriptional activation. For instance, some TFs reported to be associated with root development and those are over-represented in the differential expression regulatory network (Figure 3d), such as IbERF109, IbMYB30, IbMYB61, IbHSFA6B, IbPHL2, IbWOX8, IbANT, IbKN1 and IbMYB08, were also enriched in the modules associated with stages S8, S10 and S12. Moreover, IbWRKY53 also plays a crucial role in root elongation (Li et al., 2020b). Overall, some key transcriptional modules were characterized as important modulators and their roles in regulating root development and determination of root phenotype were revealed.

IbNAC083 was identified as a core regulator of DNB members and played a key role in SR initiation

To precisely identify the tipping point for the initiation of root swelling, a phase transition model based on DNB was used. According to non-linear dynamic theory, the tipping point is the critical state just before the transition, and its DNB accords with a unique gene expression profile characterized by collective fluctuation and strong correlation. Previous studies (Chen et al., 2012; Liu et al., 2014, 2015) have shown that at the critical state: (i) the transcriptional level of a group of DNB genes begins to fluctuate strongly, indicated by changes in the coefficient of variance CV_{in}; (ii) the transcriptional level of the DNB genes exhibits high correlation, represented by the absolute Pearson correlation coefficient values, PCC_{in}; and (iii) associations between DNB genes and other genes significantly decrease, represented by the absolute PCC values (PCC_{out}). Considering all the above criteria, we used an index (criticality index, CI) as the comprehensive signal of the DNB method. When CI comes up to the peak or rises dramatically during the measured stages, the corresponding stage is the critical state of the biological system. As shown in Figure 5(a), stage S10 is the tipping point because of the highest CI score. This result was in line with the morphological changes of sweet potato roots (Figure 1a,b) and the dynamics of gene expression (Figures 2c and 3b,c; Figure S1b). We identified 86 genes crucial to the CI score as DNB members. Some of these DNB genes play important roles in root development. For instance, a reduction in root growth was observed in MGD mutants under phosphate (Pi) starvation (Kobayashi et al., 2009). In Arabidopsis, NAP1-RELATED PROTEIN 1/2 (NRP1/2), a H2A/H2B histone chaperone, is essential to maintain the root stem cell niche (Ma et al., 2018). In *Oryza sativa* (rice), the *VILLIN2* (*VLN2*) mutant seedling shows malformed organs, such as twisted roots and shoots (Wu et al., 2015). Additionally, DNB members including EDS1, RPS13, ELP2, RPL3 and CUL1 also play key roles in root growth and development (Ito et al., 2000; Jia et al., 2015; Kim et al., 2012; Popescu and Tumer, 2004; Woodward et al., 2007).

To explore the key regulators for the initiation of root swelling, we predicted interactions between TF genes and DNB genes based on the TF binding motif information and the expression correlation (absolute $|PCC| > 0.8$). We then ranked the DNB-regulating TFs according to the criteria of importance in the regulatory network of DNB members, differential patterns, dynamic regulatory patterns of DEGs, transcriptional regulatory patterns of co-expressed modules (see the ranking scheme for the regulators of DNB members in the Experimental procedures). Through this analysis, there were five TFs (IbNAC083, IbHFA6B.1, IbMYB61.1, IbERF109.1 and IbBEH4.1) that meet these screening criteria, i.e. belong to DEGs of S8–S12, with enriched motifs associated with TFs regulating DEGs during S8–S10 and with enriched motifs associated with TFs in the S8 module. Based on the ratio of DEGs in a DNB set regulated by each TF (IbNAC083, 67%; IbHFA6B.1, 50%; IbMYB61.1, 50%; IbERF109.1, 40%; IbBEH4.1, 33%), IbNAC083 was selected as the top candidate for further functional study because of its highest ratio.

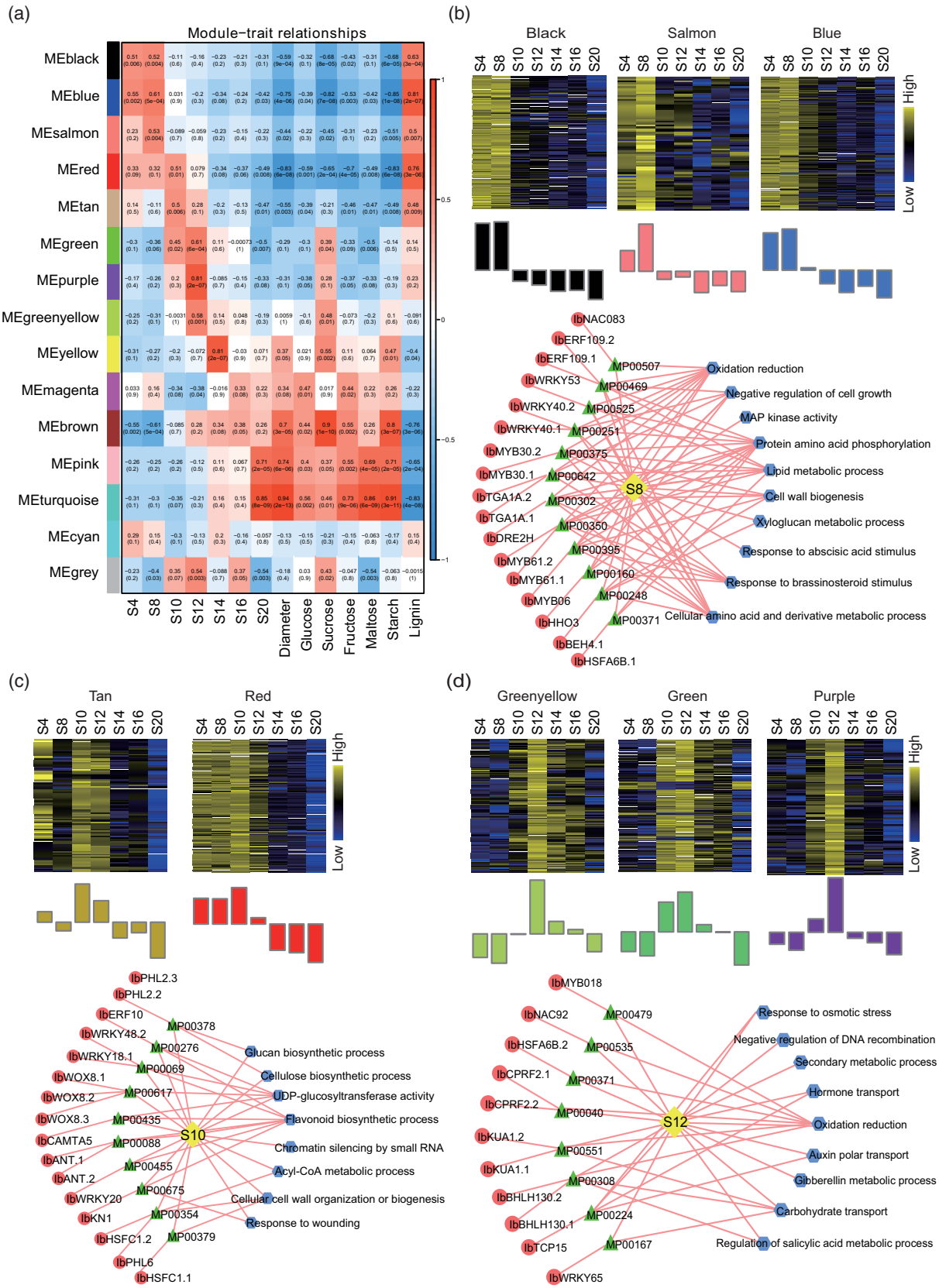

Figure 4. Analysis of transcription regulatory modules related to root development of *Ipomoea batatas* (sweet potato).
(a) Correlation heat map of module eigenvalues with root development stages and physiological phenotypes. The Pearson correlation coefficient and *P*-value of each module with different stages and phenotypes are given and colored according to the score.
(b–d) Expression profile and transcriptional regulatory network associated with the co-expressed modules at stages S8 (b), S10 (c) and S12 (d). Heat maps show the expression profile of all the co-expressed genes in the modules (labeled on top). The color scale represents the *Z*-score. Bar graphs (below the heat maps) show the consensus expression pattern of the co-expressed genes in each module. The predicted transcriptional regulatory network [significantly enriched transcription factor (TF)-binding sites along with the associated TFs and enriched gene ontology (GO) terms] associated with the co-expressed gene sets at stages S8, S10 and S12 of root development are given. The significantly enriched *cis*-regulatory motifs (green triangle) and GO terms (blue hexagons) within the given set of genes were linked by pink lines. The TFs are represented by magenta circles. Edges represent known interactions between the *cis*-regulatory motifs and TFs.

To determine the molecular function of IbNAC083 in SR development, the expression profile and the cellular localization of IbNAC083 were examined. *IbNAC083* was expressed in various root cell types, especially in the stele, and localized in the nucleus (Figure S4a–c). To further explore the function of IbNAC083 in SR initiation, transgenic sweet potato plants showing down-regulated *IbNAC083* expression by RNAi were generated. Compared with the wild type (WT), the expression levels of *IbNAC083* in four independent transgenic lines were decreased significantly (Figure 5b). Five-month-old transgenic and WT plants were collected from the field: the *IbNAC083*-RNAi transgenic plants showed decreased SR size and more pencil roots compared with the WT (Figure 5c). The root biomass per plant varied from 0.35 to 2.11 kg for the transgenic lines (Figure 5d), which was considerably less than the average fresh weight in the WT (2.86 kg). The average pencil root number per plant was 6.33 in the WT but ranged from 8.73 to 13.2 for the transgenic lines (Figure 5e). The average SR number per plant ranged from 0.40 to 2.11 for the transgenic lines (Figure 5f), which was dramatically less than the number for the WT (3.67). These results suggest that IbNAC083 affects the initiation of root swelling and promotes SR formation.

Rewiring of the IbNAC083 subnetwork before and after the tipping point

Storage root development is an intricate and dynamic process, including various genes working synergistically (Dong et al., 2019; Firon et al., 2013; Wang et al., 2015). DNB genes positioned in the upstream of the pathways are important for the initiation and development of complex biological progression (Chen et al., 2012; Li et al., 2014, 2017). Thus, IbNAC083-related regulations (or network rewiring) were analyzed to investigate systematically the function of IbNAC083 in SR swelling at a network level. Based on the well-known molecular interactions of plant biology found in the STRING database, IbNAC083 and its 78 neighboring genes were integrated into the IbNAC083-centered network and the nodes of this network were weighted based on the *Z*-score-converted data of their real transcriptional expressions throughout the three developmental stages (S8, S10 and S12) (Figure 6a; Table S7). The expression levels of 63 neighboring genes (80% of all IbNAC083 neighboring genes) are switching, from high (low) to low (high) levels, before and after the critical stage of SR initiation (stage S10). This result suggested that IbNAC083 has a significant influence on the initiation of SR swelling, directly or proximally affecting these DEGs with switching expression patterns at a molecular network level.

IbNAC083 is located upstream of processes associated with root swelling initiation

Further, we examined the association between the initiation of SR swelling and biological functions over-represented by IbNAC083 and 63 inversely expressed DEGs before and after the tipping point of SR swelling (Figure 6b). The enriched functions were related primarily to the regulation of gene expression and metabolic processes (e.g. lignin and flavonol biosynthesis). These enriched biological processes affect SR development by association with signals in cell growth and division (Belehu et al., 2004; Firon et al., 2013) and auxin transport (Brown et al., 2001; Peer et al., 2013; Tan et al., 2019). The dynamic phenotypes of IbNAC083 and its inversely expressed DEGs implied the complication and time dependence of dysfunctions in swelling-associated processes during the initiation of SR swelling (Figure 6a,b). The majority of biological processes related to the regulation of metabolism (e.g. macromolecule metabolism and flavonol biosynthesis) and oxidation reduction were dysregulated before the critical state, whereas the typical SR formation mechanism (i.e. organ development) was dysregulated after the critical stage. Dysfunction in lignin biosynthetic processes, particularly those including IbNAC083, happened across the root swelling initiation stage.

To further investigate how IbNAC083 affects the initiation of root swelling, we performed RNA-seq analysis of the initial swelling roots of WT (S12–S14) and *IbNAC083*-RNAi transgenic plants (S12–S14) grown in the field (Tables S8 and S9). Compared with the WT, 5443 DEGs (adjusted $P < 0.05$) were identified in the roots of transgenic plants. GO enrichment (Figure 6c) showed that the biological processes associated with the DEGs closely resemble those observed in the network analysis (Figure 6b). *IbNAC083*-RNAi resulted in significant changes in GO terms related to metabolic processes, including lignin

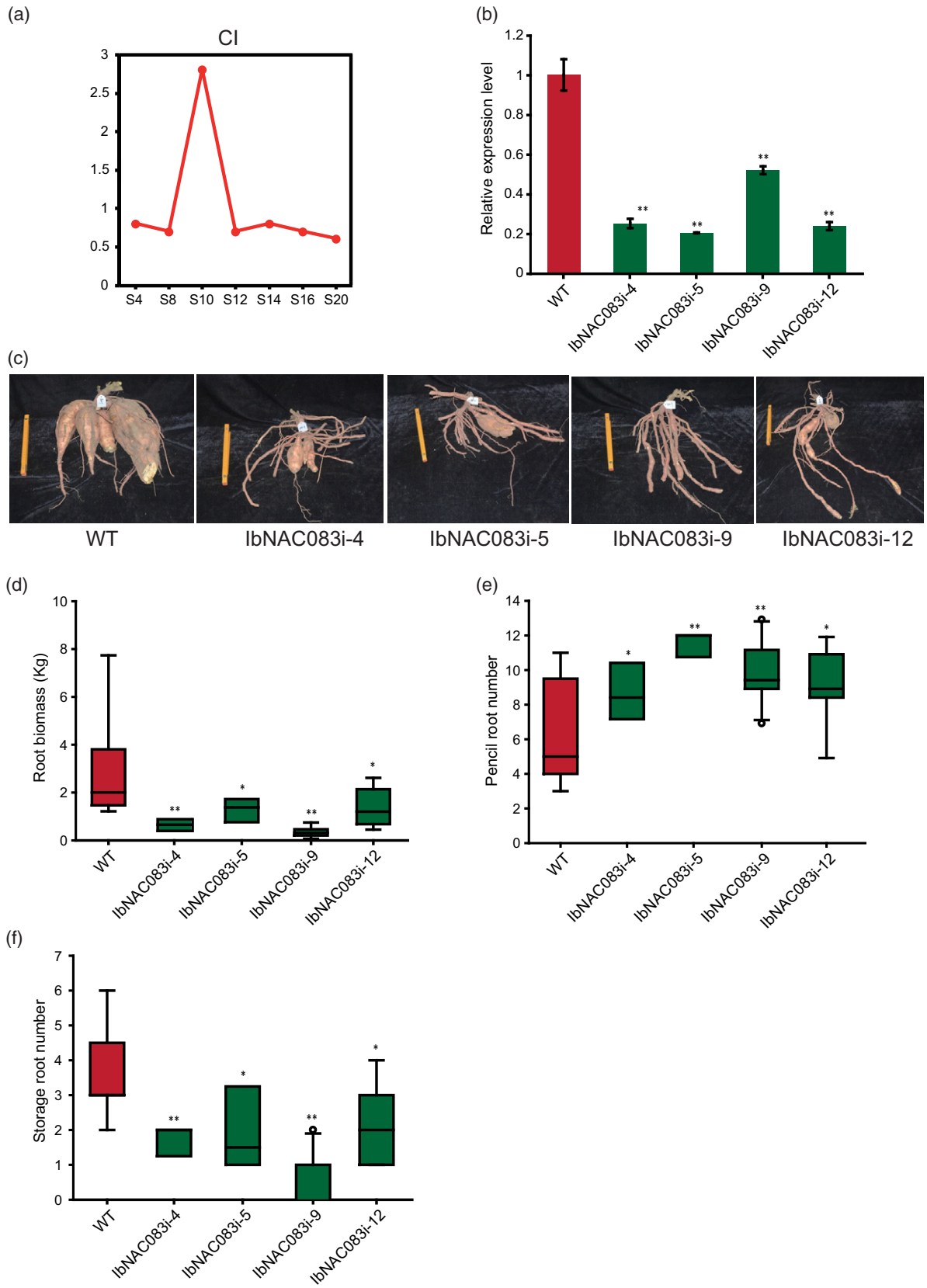

Figure 5. IbNAC083 ranked as one of the core regulators of dynamic network biomarker (DNB) members to promote storage root formation.
(a) The criticality index (CI) scores for each time point. The CI score of the S10 stage is higher than that of the other developmental stages, which indicates the critical state or tipping point just before the transition to the root-swelling process.
(b) The expression levels of *IbNAC083* in storage roots (S18–S20) of wild-type (WT) plants and *IbNAC083*-RNAi transgenic plants determined by reverse transcriptase-quantitative polymerase chain reaction (RT-qPCR). Error bars indicate standard errors ($n = 9$). Significant differences compared with the wild type (WT): $^{*}P < 0.05$ and $^{**}P < 0.01$, determined by Student's *t*-test.
(c) Phenotypes of field-grown WT and *IbNAC083*-RNAi (IbNAC083i) transgenic *Ipomoea batatas* (sweet potato) plants.
(d–f) Comparisons of root biomass (d), pencil root number (e) and storage root number (f). Root samples were collected from nine independent plants per line. Significant differences compared with the WT: $^{*}P < 0.05$ and $^{**}P < 0.01$, determined by Student's *t*-test.

and starch metabolism, which was supported by significant changes in lignin and starch content (Figure S5a,b). RT-qPCR analysis confirmed the significant changes of expression of many key genes related to lignin metabolism (*IbC4H*, *IbCAD*, *IbCCR*, *IbCOMT* and *IbCCoAOMT*) and starch metabolism (*IbAGPa*, *IbAGPb*, *IbGBSSI*, *IbSBEI*, *IbSBEII*, *IbSS*, *Ibα-amylase* and *Ibβ-amylase*) in the transgenic plants (Figure S5c,d).

According to the above analyses, the dynamic changes of biological processes resulted proximally from the function or dysregulation in IbNAC083 during the initiation of swelling in the SRs. Next, whether IbNAC083 could regulate well-known genes associated with root development in a cascade was investigated. We examined 66 root development related genes, e.g. those related to cell cycle, cell wall biogenesis and histone phosphorylation. The expression of 30 genes was affected by IbNAC083, as also found in our series of root developmental transcriptomic data (Figure 6d). Sixteen of these genes were identified as DEGs in the developmental transcriptomic analysis (Figure 6d). Seven genes co-expressed with *IbNAC083*, three of which positively correlated with *IbNAC083* expression and the rest were negatively correlated with *IbNAC083* (Figure 6d). These results suggest that IbNAC083 could affect the expression of genes related to root development in a cascade manner, which might be significant for the initiation of sweet potato SRs.

DISCUSSION

The molecular mechanisms underlying sweet potato root development are still poorly understood. The initiation of SR swelling is the critical stage that determines crop yield. It is difficult to elucidate the regulatory mechanism that determines the initiation or the tipping point of the conversion from fibrous root to SR and its core regulators. DNB is an analytical system that can explore the genome-wide dynamic gene network and dissect the critical transitions with their leading regulators during developmental process. In contrast, conventional transcriptomic analyses have provided insights into temporal gene expression associated with sweet potato root development (Dong et al., 2019; Firon et al., 2013; Wang et al., 2015); however, the approach is limited by a number of steady-state gene expression profiles. Compared with previous transcriptomic studies, the DNB analysis in our study has yielded considerably more comprehensive gene sets associated with the early developmental stages. Most importantly, we have identified the critical state of SR initiation and have confirmed that IbNAC083 is a core regulator of DNB members and is significant to SR initiation.

The expression data throughout the seven root development stages exhibited high reproducibility and differential expression during the formation and development of sweet potato SR. On the basis of PCA analysis, the root developmental stages were clustered into four prominent groups, signifying the differences in the gene expression profiles from one stage to another (Figure 2a). These clusters depicted similar kinds of gene expression during the progression from fibrous roots to mature SRs. Furthermore, the biological functions of these differently expressed genes in different developmental stages were drawn by GO analysis, which highlighted the significant changes in various metabolic processes, e.g. carbohydrate metabolic processes, cell wall metabolism, transcription regulator activity, protein metabolic processes, secondary metabolic processes and response to stress, and these findings are in line with previous findings (Firon et al., 2013). The data obtained during the root developmental process validated and established the chronology of gene expression events and revealed that the onset of downregulation-enriched biological functions preceded that of activation. The first state conversion began from stages S8 to S10 and was represented by the transcriptional regulators (Figure 3b,c), consistent with the apparent changes in lignin and starch contents during this period (Figure 1c,d). In our findings, hormonal metabolism and hormone-mediated signaling pathways were the first targets for activation, followed by primary and secondary metabolism, development processes, cell wall development and cell differentiation (Figure 3c). Previously, the hormonal activation and their functions during SR developmental processes were also highlighted (Dong et al., 2019). These observations correlated well with the activation of AP2/ERF TF genes, which play crucial roles in metabolism and development processes, and the over-representation of AP2/ERF regulatory motifs in the later stages. The TF-binding motifs of MYB and bZIP, which are linked to secondary metabolism, stress signaling and development, were only over-represented in down-regulated genes, in good agreement with the previous

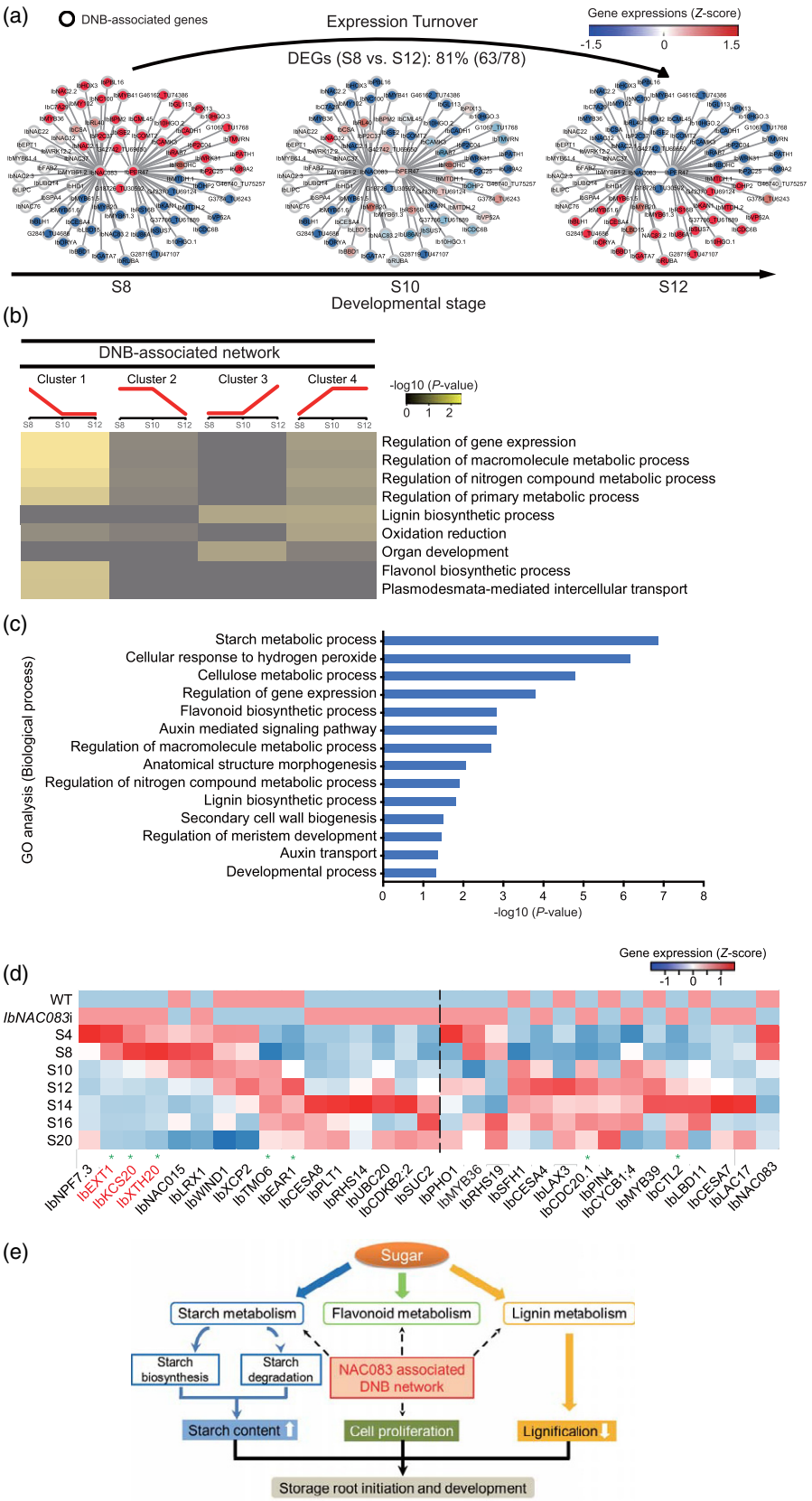

Figure 6. Dynamic network analysis of *Ipomoea batatas* (sweet potato) root developmental transcriptome.
(a) Dynamics of *IbNAC083*-associated genes in terms of expression before and after the critical period. Expression of *IbNAC083* and its 63 neighboring differentially expressed genes (DEGs) changes significantly (or inversed) from low (or high) at stage S8 to high (or low) at stage S12 (i.e. the expression levels of those genes are reversed before and after the critical period, at stage S10), implying key roles of dynamic network biomarker (DNB) members in coordinating the critical transition to root swelling at stage S10.
(b) Dynamic activity of the relative gene ontology (GO) terms that involved *IbNAC083* and its neighboring DEGs in different dynamic patterns.
(c) GO enrichment analysis of the DEGs in the initial swelling roots of *IbNAC083*-RNAi transgenic plants relative to the wild type (WT). The GO terms of biological processes with statistical significance ($P \leq 0.05$) are shown. Three biological replicates were performed for each genotype.
(d) A heat map illustrated the co-expression of *IbNAC083* and typical root development-related genes. The 16 genes listed on the left of the dashed line were also DEGs in the root developmental series transcriptomic data; seven genes labeled by a green star had co-expression relationships with *IbNAC083* by analysis of both the root developmental series transcriptomic expression profiling and the RNA-seq data of WT and *IbNAC083*-RNAi transgenic plants. Genes in red showed positive co-expression with *IbNAC083* (Pearson correlation coefficient, PCC > 0.8), whereas genes in black showed negative co-expression with *IbNAC083* (PCC < −0.8).
(e) A molecular model of IbNAC083-associated DNB network function in sweet potato initiation and development.

studies about the functions of these TFs (Jakoby et al., 2002; Martin and PazAres, 1997). By integrating the TF regulatory motif over-representation data with our chronological root developmental network, we established the potential causal regulatory relationships between TFs and target subnetworks (Figure 3d). Approximately 40% of these TFs were found to be key regulators in root growth and development, emphasizing the high reliability of our method in the detection of biological roles of novel genes in the root developmental network.

To further investigate the mechanisms underlying the process of SR formation and development, we performed gene co-expression network analysis and determined the gene modules involved in a mass of TFs related to developmental stages from fibrous root to mature SR (Figure 4). These TFs can play synergistic roles in regulating the expression of co-expressed genes within each module. The results of GO analysis emphasized the significant functions of several biological processes during root developmental progression. Furthermore, we established the transcriptional regulation networks connecting TFs with their putative regulatory motifs and target genes (TF-regulatory motifs and co-expressed genes) for the three (S8, S10 and S12) critical periods of root development that are supposed to play a decisive role in SR initiation in sweet potato. Several members of these regulatory networks were found to be involved in different aspects of root development in different plants (Bomal et al., 2008; Cai et al., 2014; Huang et al., 2016; Li et al., 2020b; Petricka et al., 2012; Randall et al., 2015; Romano et al., 2012; Sakaoka et al., 2018; Woerlen et al., 2017). Our results indicated that the analysis of transcriptional regulatory networks, except for the establishment of co-expression modules, can be extremely useful to investigate the molecular mechanisms of root development. However, to illustrate the details of these GRNs, it is necessary to conduct further functional investigations for each component in the network.

In order to determine potential biomarkers of the critical swelling stage and better investigate the molecular mechanisms governing SR initiation, we performed the DNB method and identified stage S10 as the tipping point of root swelling initiation (Figure 5a), which is also consistent with the progression of root development (Figure 1a,b) and the dynamics of gene expression (Figures 2c and 3b,c; Figure S1b). Furthermore, IbNAC083 was found to be one of the regulators in the DNB-associated network and might have an important influence on SR initiation. The downregulation of *IbNAC083* significantly inhibited SR initiation (Figure 5b–f). Previously, *Lc* transgenic sweet potato affected the SR development by enhancing lignification of vascular cells in the initiating SRs (Wang et al., 2016). Therefore, lignification could be the limited factor for initiating SRs. In Arabidopsis, IbNAC083 yields a TF belonging to the NAC gene family, which can negatively regulate xylem vessel formation by interacting with VND7 (Yamaguchi et al., 2010). IbNAC083 is also found to act with *COR/RD* genes to affect leaf senescence through integrating ABA signals (Yang et al., 2011b). Recently, IbNAC083 is identified as a root hair cell enriched TF gene by the analysis of accessible chromatin regions throughout various plant species and cell types (Maher et al., 2018). Furthermore, the function of IbNAC083 in the DNB-associated network was uncovered and the genes and biological functions that can be influenced by IbNAC083 during SR initiation were revealed (Figure 6a–c; Figure S5a–d; Table S7). By RNA-seq, we found that several known root development related genes can be regulated by IbNAC083 in a cascading manner (Figure 6d). These results confirmed that IbNAC083 played an important role in initiating the root swelling process by regulating multiple metabolic and signaling pathways (Figure 6e).

In summary, our work gives new insights into the dynamics and architecture of the root development regulatory network and provides a valuable data set for mining other genes associated with root growth and development in root crops like sweet potato. Our work is another successful example of identifying the tipping point of a critical developmental transition in plants using DNB. In particular, DNB identified IbNAC083 as an early indicator and a key regulator of the initiation of SRs in sweet potato.

EXPERIMENTAL PROCEDURES

Plant materials

Sweet potato (*I. batatas* L.) cv. Taizhong6 plants were cultivated in early May in the Wushe Plantation for Transgenic Crops,

Shanghai, China (31°13948.0099 N, 121°28912.0099 E). The WT and transgenic sweet potato plants were planted with a density of 50 cm × 50 cm (length by width), and each row had more than six plants. Sweet potato grew up under clay soils without fertilizer on rainfall conditions for 20 weeks. Fibrous roots at two stages (S4 and S8; root diameters of 1.5 and 2 mm, respectively), pencil roots at two stages (S10 and S12; root diameters of 3.5 and 5 mm, respectively) and SRs at three stages (S14, S16 and S20; root diameters of 10, 15 and 25 mm, respectively) were collected in early October to cover the entire SR initiation and development processes (Wang et al., 2016). Roots in each developmental stage have four independent biological replicates. These materials were separated into three parts: one part was rapidly frozen in liquid nitrogen and subsequently stored at −80°C for RNA isolation; another part was dried at 80°C for 48 h to acquire a stable dry weight, which was then used for the analysis of lignin, starch and sugar content; and the last part was used immediately for anatomical observations.

Plasmid and *Agrobacterium*-mediated sweet potato transformation and phenotypic characterization of *IbNAC083*-RNAi transgenic plants

Sweet potato cDNA was used to obtain the open reading frame (ORF) of *IbNAC083* (729 bp). The pRNAi-DFR vector was used to construct the pRNAi-*IbNAC083* binary vector to express hairpin RNA of the 250-bp *IbNAC083* fragment (451–700 bp) (Wang et al., 2013) by using the primers *IbNAC083-Kpn*I (5′-CGG**GGTACC**AACGAGAATTGGGTACTCTG-3′, *Kpn*I site in bold), *IbNAC083-Cla*I (5′-CC**ATCGAT**TACTGCAGCTGCACTCTCT-3′, *Cla*I site in bold), *IbNAC083*-BamHI (5′-CG**GGATCC**AACGAGAATTGGGTACTCTG-3′, *Bam*HI site in bold) and *IbNAC083*-XhoI (5′-CCG**CTCGAG**TACTGCAGCTGCTACTCTCT-3′, *Xho*I site in bold). Then, pRNAi-*IbNAC083* was transferred into *Agrobacterium tumefaciens* strain LBA4404 to transform sweet potato (Yang et al., 2011a). After obtaining transgenic plants, *IbNAC083* expression was detected by RT-qPCR and was normalized to the sweet potato *β-actin* internal control gene.

The phenotypes of the WT and *IbNAC083*-RNAi sweet potato were studied under field conditions in the Wushe Plantation. We recorded the field characteristics of roots at different developmental stages and the yield was examined as the average root weight of nine individual plants per line.

Anatomical observations

We used 4% neutral-buffered formalin to fix the cross sections from the middle of fibrous roots (S4 and S8), pencil roots (S10 and S12) and SRs (S14 and S16) of sweet potato for 24 h and then used paraffin wax to embed these cross sections. We cut 15-μm-thick sections and placed these samples on silane-coated slides to fix them. These sections were dewaxed and rehydrated after baking for 12 h at 37°C. Then, the samples were incubated with toluidine blue (0.05%) for 3 min at 25°C and were washed with water to remove the staining solution. Finally, an Olympus BX51 microscope (Olympus, https://www.olympus-global.com) was used to observe the tissues.

Analysis of lignin, starch and sugar contents

Lignin content was analyzed as previously described (Gui et al., 2019). Furthermore, we accurately weighed 30-mg dried samples and put them into 5-ml tubes, and then added 0.7 ml of ethanol (80%). After shaking and mixing thoroughly, these samples were held at 70°C for 2 h. Then, we added 0.7 ml of high-performance liquid chromatography (HPLC)-grade water and 0.7 ml of chloroform into the tube and vibrated these samples several times, followed by centrifugation at 12 000 ***g*** for 10 min. The sediments were used to examine starch content whereas the supernatants were collected to analyze the content of soluble sugars. We washed the sediments three times using 80% ethanol, and used the Total Starch Assay Kit (Megazyme, https://www.megazyme.com) to examine the total starch contents. We transferred 0.7 ml of supernatant to a 1.5-ml tube and added 0.7 ml of chloroform to each sample. After shaking and mixing thoroughly, these samples were centrifuged at 12 000 ***g*** for 10 min and then we transferred 0.5 ml of supernatant into a glass tube to analyze the content of each sugar component using HPLC. The sugar-separation method was performed according to the manufacturer's instructions, with some modification; the Agilent HPLC column (ZORBAX Carbohydrate column; 4.6 × 150 mm, 5 μm; Agilent, https://www.agilent.com) was used with a differential refraction detector. We used 75% acetonitrile as the mobile phase; the flow velocity was 0.8 ml min^{-1} and the column temperature was 35°C. The retention times of sugar standards were used to identify each sugar component and the sugar content was obtained based on the external standard curve. Data from at least three technical replicates are presented as the mean ± standard deviation.

Illumina sequencing, read mapping and differential expression analysis of genes

For RNA-seq analysis, total RNA was isolated from the middle sections of fibrous roots (S4 and S8), pencil roots (S10 and S12) and SRs (S14, S16 and S20) using the RNeasy Mini Kit (Qiagen, https://www.qiagen.com) with the protocol provided by the manufacturer. The RNA integrity number was used to analyze the quality of the RNA using an Agilent 2100 Bioanalyzer and Nanodrop 2000 (ThermoFisher Scientific, https://www.thermofisher.com). RNA-seq library preparation and sequencing were conducted by Majorbio (http://www.majorbio.com/). The Illumina TruSeq RNA Sample Prep Kit (Illumina, https://www.illumina.com) was used to prepare all 28 libraries (seven samples in four biological replicates), and these samples were sequenced by Illumina platform (Novaseq 6000) to generate 150-nucleotide-long paired-end sequence reads. We used various quality parameters to assess the raw sequence data and used NGS QC TOOLKIT 2.3 (Patel and Jain, 2012) to filter the high-quality reads. The mapping of filtered high-quality reads onto the sweet potato genome (Yang et al., 2017) was performed with TOPHAT 2.0.0. The mapped reads were processed by STRINGTIE 1.3.3b to generate a transcription assembly. The TPM values of each sweet potato gene were obtained by RSEM 1.3.1 using the mapped output. Two R packages, i.e. CORRPLT and PRCOMP, were used to perform hierarchical clustering and PCA analysis, respectively. The TPM values were used to determine DEGs with a false discovery rate (*q*-value) of ≤0.05 and a fold change of >2 with DESEQ2 1.30.0 (Love et al., 2014). The SS scoring algorithm was used to identify the developmental stage-specific/preferential genes through comparing the transcriptional level of one gene at a given stage with its maximum transcriptional level in other stages (Zhan et al., 2015). For a specific gene *i*, its expression values in seven stages are denoted as $EV_i = \left(E_1^i, E_2^i, E_3^i, \cdots, E_7^i\right)$, and the SS score of the gene in stage *j* is defined as: $SS(i,j) = 1 - (\max E_k^i / E_j^i)$, where $1 \le k \le 7$ and $k \ne j$. Therefore, a higher SS score of one gene at a specific stage indicates preferential expression in the corresponding stage. For a particular gene list, we calculated row-wise *Z*-scores and used HEATMAP2 in R to draw heat maps.

For RNA-sequencing analysis of WT and *IbNAC083*-RNAi transgenic plants, the RNeasy Mini Kit (Qiagen) was used to isolate total RNAs of initial swelling roots of WT (S12–S14) and transgenic plants (S12–S14) according to the protocol provided by the

manufacturer. The Illumina platform (Novaseq 6000) was used to sequence all six libraries (two samples with three biological replicates per sample) to generate sequence reads. Other processes and analyses were the same as described above.

GO enrichment analysis

Cytoscape (BiNGO plug-in) (Maere et al., 2005) was used to conduct the GO enrichment analysis of particular gene sets. The *P*-value of each represented GO category was adjusted by Benjamini–Hochberg error correction method. The GO terms with an adjusted *P*-value of ≤0.05 were considered to be remarkably over-represented. The background for the GO analysis was the total protein coding genes of sweet potato.

RT-qPCR analysis

To validate the results of RNA-seq, we conducted RT-qPCR assays using four biological replicates for each tissue sample and at least three technical replicates of each biological replicate. Furthermore, to quantify the gene expression levels of WT and *IbNAC083*-RNAi transgenic plants, total RNA was isolated from the middle sections of roots of WT (S12–S14) and transgenic plants (S12–S14) using at least three biological replicates per line and three technical replicates of each sample. After the RNA quality was confirmed, 2 μg of mRNA from each sample was reverse transcribed to cDNA. RT-qPCR analyses were conducted according to the previous study (Xu et al., 2013). PRIMER EXPRESS 3.0 was used to design the gene-specific primers (Table S10). Each gene was normalized to the *β*-actin internal control gene, and the fold change was calculated using the $2^{-\Delta\Delta Ct}$ method.

TF family and promoter motif analysis

To identify which TF families are over-represented among DEGs at each developmental stage, we analyzed for the enrichment of 58 TF families contained in the TF database PlantTFDB 4.0 (Jin et al., 2017). Cumulative hypergeometric distribution was used to analyze the enriched TF families within a gene list, and the total protein coding genes were treated as the background. *P*-values were adjusted using the Bonferroni method.

To predict directional interactions in transcriptional states of the root developmental GRN, TFs of sweet potato were first predicted by checking 'Best hit in *Arabidopsis thaliana*' in PlantTFDB, and the matching relationship between a given sweet potato TF and its putative binding motif was also obtained. Next, we analyzed 1-kb upstream sequences of all the genes in each gene set and identified significantly enriched DNA sequence motifs with HOMER 4.8.3, based on the high-quality TF binding motifs collected from the PlantTFDB database. Further, their association/binding with the TFs included in the same transcriptional state was identified by the matching relationships obtained above.

Co-expression network analysis for constructing modules

The WGCNA package (Langfelder and Horvath, 2008; Zhang and Horvath, 2005a) was used to establish the co-expression network. We obtained a matrix of pairwise Spearman correlation coefficients between all gene pairs according to $\log_2(1 + \text{TPM})$ values and converted it to an adjacency matrix using the formula: connection strength (adjacency value) = $|(1 + \text{correlation})/2|^{\beta}$. Here, based on the scale-free topology criterion, a soft threshold β-value of 15 was selected. Then, a toplogical overlap matrix (TOM) similarity algorithm was used to transform the above adjacency matrix to a TOM (Zhang and Horvath, 2005a), and a hierarchical clustering dendrogram was generated based on TO similarity and was cut by the dynamic tree-cutting algorithm to get the stable clustering groups. The module eigengene (ME) of each module was computed by PCA. To analyze the relationship of module with phenotypes, the correlation between each ME and the data of these characteristics was calculated. To determine the association of module with stage-specific expression, we determined the correlation between each ME with the binary indicator (stage = 1 and all other samples = 0) as described by Downs et al. (2013). A positive correlation indicates that genes in a module have higher/preferential expression in a particular stage relative to all other samples. Additionally, to predict directional interactions in the transcriptional regulatory network associated with the co-expressed modules, the same method as the 'TF family and promoter motif analysis' part was performed. To obtain GO terms, FIMO (Grant et al., 2011) was used to screen genes, the promoters of which have a given significantly enriched motif in one module/gene set. A motif with at least one match at $P \leq 10^{-4}$ in a particular promoter was considered to imply the existence of the motif in the corresponding promoter. Subsequently, these selected genes were used to perform GO enrichment analysis.

DNB analysis

Many investigations about complex biological processes (e.g. complex diseases, development processes and cell cycle processes) have indicated that the progression of a complex biological process is not always a smooth phenomenon, with linear changes, but occasionally includes drastic and non-linear transitions (Liu et al., 2014; Zhang et al., 2019). Such a transition has an important influence on biological processes because of its qualitative alterations of the biological system state. Notably, determining the tipping point just before this transition not only reveals the molecular mechanism of this dynamical process but can also infer its core regulators in the corresponding regulatory network. Therefore, to uncover the dynamical biomarkers and analyze the molecular mechanisms of swelling initiation in sweet potato SRs, we analyzed the RNA-seq data by using the DNB method. According to the non-linear dynamical theory, a biological system is near the tipping point when there is a dominant gene set, i.e. DNB, which meets the following three necessary conditions of gene expression (Chen et al., 2012; Li et al., 2014, 2017; Liu et al., 2013, 2019a,b; Yang et al., 2018):

i the transcript levels of DNB members widely fluctuate, represented by coefficient values of variation (CV_{in});
ii the correlation among DNB genes is dramatically increased, represented by the absolute Pearson correlation coefficient (PCC_{in});
iii the association between DNB genes and the other genes is drastically decreased, indicated by the absolute value of PCC (PCC_{out}).

To consider all the above conditions, a CI can be defined as:

$$CI = \frac{PCC_{in}}{PCC_{out}} CV_{in}$$

Here, CV_{in}, PCC_{in} and PCC_{out} are all average values. Based on the above conditions and the criticality index, genes with CV values lower than the 70% percentile throughout all the time points were filtered out, and the following steps were conducted to identify DNB members/genes at each time point:

i gene modules are obtained by clustering the selected genes, and the distance is defined as $1 - |\text{PCC}|$ with the cut-off set to 0.1;
ii the CI of each module is computed;
iii the maximum-CI module at each time point is selected, considering it as the potential DNB module;

iv the maximum-CI potential module of all the time points is selected through comparing all the candidate modules, and this potential module is the expected DNB module (with all genes in the module as DNB members) and the corresponding stage is the tipping point.

Clearly, the DNB method is mainly based on 'differential associations among genes' (differential network or the second-order statistics) rather than the 'differential expressions of genes' (differential genes or the first-order statistics) used in most of the traditional methods.

The STRING database (http://string-db.org) and CYTOSCAPE (http://www.cytoscape.org/) were used to build the molecular interactions (protein–protein interactions) network and visualization, respectively (Shannon et al., 2003; Szklarczyk et al., 2015). In the network, the nodes indicate genes and the edges indicate interactions. For a particular gene list, we calculated root developmental stage-wise *Z*-scores as the expression level of the corresponding genes.

Ranking scheme for core regulators of DNB members

We ranked the core regulators of DNB genes near the critical stage S10 based on the following criteria with four priorities.

i Priority one. We ranked the regulators of DNB members according to their significance to the network. Core TFs are regarded as playing dominant roles in the molecular network composed of DNB genes and their predicted TFs during the initiation of root swelling. Then, these genes were mapped into the network and the total number of DNB members directly connected with each TF member was calculated individually. This criterion is indicated as a ratio of target DNB genes belonging to DEGs from S8–S12 stages to the total target DNB genes regulated by each TF gene.

ii Priority two. We required that TFs need to be differentially expressed from stages S8 to S12 to regulate the expression of target genes, although this would ignore the regulatory effect of the non-differential expression of some TFs on target genes, such as protein modification. This criterion represents whether, or not, a TF belongs to DEGs from stages S8 to S12.

iii Priority three. To identify the TFs that play crucial regulatory roles in the initial expansion process of SR, we required that key TFs should be one of the enriched-motif-associated TFs regulating DEGs from stages S8 to S10 (Figure 3d). This criterion represents whether, or not, a TF belongs to the enriched-motif-associated TFs regulating DEGs from S8 to S10 stages (Figure 3d).

iv Priority four. To explore the key regulators in the initial swelling stage of SR, we selected TFs that might play crucial roles in the early stage of the tipping point, i.e. stage S8. This criterion represents whether, or not, a TF belongs to the enriched-motif-associated TFs in the S8 module (Figure 4b).

GUS staining and subcellular localization of IbNAC083

To study the tissue localization of IbNAC083, the promoter of *IbNAC083* (2573 bp) fused to an *uidA* gene was constructed into pCAMBIA1300 with *Pst*I and *Bam*HI and transformed to Arabidopsis through *Agrobacterium*-mediated DNA transformation. The positive transgenic lines were selected by kanamycin resistance for GUS staining. GUS staining of the root in Arabidopsis was conducted according to a previous study (Yu et al., 2013). For subcellular localization experiments, a vector yielding IbNAC083-GFP fusion proteins was constructed with the CaMV *35S* promoter and was transferred into *Nicotiana benthamiana* (tobacco) leaf by *Agrobacterium*-mediated transformation. Finally, the leaf was observed under an Olympus FV1000 microscope. The primers used in this study are listed in Table S10.

Statistical analysis

The independent samples Student's *t*-test was conducted in SPSS 17 (IBM, https://www.ibm.com). An alpha value of $P < 0.05$ was considered statistically significant.

Accession numbers

The RNA-seq data are available in the NCBI Sequence Read Archive under accession number PRJNA647694.

ACKNOWLEDGEMENTS

This work was supported by National Key R&D Program of China (grant nos 2017YFA0505500 and 2018YFD1000705), Priority Research Program of the Chinese Academy of Sciences (grant no. XDB38040400), the National Natural Science Foundation of China (grant nos 31930022, 12026608 and 31771476) and Japan Science and Technology Agency Moonshot R&D (grant no. JPMJMS2021).

AUTHOR CONTRIBUTIONS

LC, PZ and SH designed and conceived this project. SH performed the analysis of RNA-seq data. XH, YW, HW, YZ, XB, WF, MY and SH executed the experiment. SH and XH prepared the figures and drafted the article. LC, PZ, LY, SH and HW analyzed the data and revised the article with input from the other authors. All authors have read and approved the final version for publication.

CONFLICT OF INTEREST

The authors declare that they have no conflicts of interest associated with this work.

DATA AVAILABILITY STATEMENT

All relevant data can be found within the article and its supporting materials.

SUPPORTING INFORMATION

Additional Supporting Information may be found in the online version of this article.

Figure S1. Preferential/stage-specific expression of genes at different developmental stages of sweet potato roots.

Figure S2. Correlation between expression profiles of selected genes obtained from RNA-seq and RT-qPCR analysis.

Figure S3. Circos plots of developmental series expression profiles in comparison with previously published sweet potato root transcriptome data.

Figure S4. Expression profile and subcellular localization of IbNAC083.

Figure S5. Changes in lignin and starch contents and related metabolic gene expression profiles in the initial swelling roots of WT (S19–S20) and *IbNAC083*-RNAi transgenic plants (S13–S14).

Table S1. Summary of the transcriptome data in sweet potato roots.

Table S2. The novel gene sequences of sweet potato.

Table S3. TPM values for all genes detected in sweet potato roots.

Table S4. SS scores for all preferentially expressed genes in sweet potato roots.

Table S5. Differentially expressed genes (DEGs) between different root developmental stages of sweet potato.

Table S6. Gene modules identified by WGCNA.

Table S7. The relationships between members in the IbNAC083-centered DNB network.

Table S8. Summary of the transcriptome data of WT and IbNAC083-RNAi initial swelling roots

Table S9. TPM values of DEGs between WT and IbNAC083-RNAi initial swelling roots.

Table S10. Primer pairs used in this study.

REFERENCES

Belehu, T., Hammes, P.S. & Robbertse, P.J. (2004) The origin and structure of adventitious roots in sweet potato (*Ipomoea batatas*). *Australian Journal of Botany*, **52**, 551–558.

Bomal, C., Bedon, F., Caron, S., Mansfield, S.D., Levasseur, C., Cooke, J.E.K. *et al.* (2008) Involvement of *Pinus taeda* MYB1 and MYB8 in phenylpropanoid metabolism and secondary cell wall biogenesis: a comparative in planta analysis. *Journal of Experimental Botany*, **59**, 3925–3939.

Bonke, M., Thitamadee, S., Mahonen, A.P., Hauser, M.T. & Helariutta, Y. (2003) APL regulates vascular tissue identity in Arabidopsis. *Nature*, **426**, 181–186.

Brown, D.E., Rashotte, A.M., Murphy, A.S., Normanly, J., Tague, B.W., Peer, W.A. *et al.* (2001) Flavonoids act as negative regulators of auxin transport in vivo in Arabidopsis. *Plant Physiology*, **126**, 524–535.

Cai, X.T., Xu, P., Zhao, P.X., Liu, R., Yu, L.H. & Xiang, C.B. (2014) Arabidopsis ERF109 mediates cross-talk between jasmonic acid and auxin biosynthesis during lateral root formation. *Nature Communications*, **5**, 5833.

Chen, L.N., Liu, R., Liu, Z.P., Li, M.Y. & Aihara, K. (2012) Detecting early-warning signals for sudden deterioration of complex diseases by dynamical network biomarkers. *Scientific Reports*, **2**, 342.

Chen, P., Liu, R., Li, Y. & Chen, L. (2016) Detecting critical state before phase transition of complex biological systems by hidden Markov model. *Bioinformatics*, **32**, 2143–2150.

Devaiah, B.N., Karthikeyan, A.S. & Raghothama, K.G. (2007) WRKY75 transcription factor is a modulator of phosphate acquisition and root development in arabidopsis. *Plant Physiology*, **143**, 1789–1801.

Dong, T.T., Zhu, M.K., Yu, J.W., Han, R.P., Tang, C., Xu, T. *et al.* (2019) RNA-Seq and iTRAQ reveal multiple pathways involved in storage root formation and development in sweet potato (*Ipomoea batatas* L.). *BMC Plant Biology*, **19**, 136.

Downs, G.S., Bi, Y.M., Colasanti, J., Wu, W.Q., Chen, X., Zhu, T. *et al.* (2013) A developmental transcriptional network for maize defines coexpression modules. *Plant Physiology*, **161**, 1830–1843.

Eysholdt-Derzso, E. & Sauter, M. (2017) Root bending is antagonistically affected by hypoxia and ERF-mediated transcription via auxin signaling. *Plant Physiology*, **175**, 412–423.

Farinati, S., Dalcorso, G., Varotto, S. & Furini, A. (2010) The *Brassica juncea* BjCdR15, an ortholog of Arabidopsis TGA3, is a regulator of cadmium uptake, transport and accumulation in shoots and confers cadmium tolerance in transgenic plants. *New Phytologist*, **185**, 964–978.

Firon, N., LaBonte, D., Villordon, A., Kfir, Y., Solis, J., Lapis, E. *et al.* (2013) Transcriptional profiling of sweetpotato (*Ipomoea batatas*) roots indicates down-regulation of lignin biosynthesis and up-regulation of starch biosynthesis at an early stage of storage root formation. *BMC Genomics*, **14**, 460.

Garcia, M.N.M., Stritzler, M. & Capiati, D.A. (2014) Heterologous expression of Arabidopsis ABF4 gene in potato enhances tuberization through ABA-GA crosstalk regulation. *Planta*, **239**, 615–631.

Grant, C.E., Bailey, T.L. & Noble, W.S. (2011) FIMO: scanning for occurrences of a given motif. *Bioinformatics*, **27**, 1017–1018.

Gui, J.S., Luo, L.F., Zhong, Y., Sun, J.Y., Umezawa, T. & Li, L.G. (2019) Phosphorylation of LTF1, an MYB transcription factor in *Populus*, acts as a sensory switch regulating lignin biosynthesis in wood cells. *Molecular Plant*, **12**, 1325–1337.

Gutierrez, L., Bussell, J.D., Pacurar, D.I., Schwambach, J., Pacurar, M. & Bellini, C. (2009) Phenotypic plasticity of adventitious rooting in Arabidopsis is controlled by complex regulation of AUXIN RESPONSE FACTOR transcripts and microRNA abundance. *The Plant Cell*, **21**, 3119–3132.

Hacham, Y., Holland, N., Butterfield, C., Ubeda-Tomas, S., Bennett, M.J., Chory, J. *et al.* (2011) Brassinosteroid perception in the epidermis controls root meristem size. *Development*, **138**, 839–848.

Huang, Y.C., Niu, C.Y., Yang, C.R. & Jinn, T.L. (2016) The heat stress factor HSFA6b connects ABA signaling and ABA-mediated heat responses. *Plant Physiology*, **172**, 1182–1199.

Ito, T., Kim, G.T. & Shinozaki, K. (2000) Disruption of an Arabidopsis cytoplasmic ribosomal protein S13-homologous gene by transposon-mediated mutagenesis causes aberrant growth and development. *Plant Journal*, **22**, 257–264.

Jakoby, M., Weisshaar, B., Droge-Laser, W., Vicente-Carbajosa, J., Tiedemann, J., Kroj, T. *et al.* (2002) bZIP transcription factors in Arabidopsis. *Trends in Plant Science*, **7**, 106–111.

Jia, Y.B., Tian, H.Y., Li, H.J., Yu, Q.Q., Wang, L., Friml, J. *et al.* (2015) The *Arabidopsis thaliana* elongator complex subunit 2 epigenetically affects root development. *Journal of Experimental Botany*, **66**, 4631–4642.

Jiang, Z.L., Lu, L.N., Liu, Y.W., Zhang, S., Li, S.X., Wang, G.Y. *et al.* (2020) SMAD7 and SERPINE1 as novel dynamic network biomarkers detect and regulate the tipping point of TGF-beta induced EMT. *Science Bulletin*, **65**, 842–853.

Jin, J.P., Tian, F., Yang, D.C., Meng, Y.Q., Kong, L., Luo, J.C. *et al.* (2017) PlantTFDB 4.0: toward a central hub for transcription factors and regulatory interactions in plants. *Nucleic Acids Research*, **45**, D1040–D1045.

Kim, T.H., Kunz, H.H., Bhattacharjee, S., Hauser, F., Park, J., Engineer, C. *et al.* (2012) Natural variation in small molecule-induced TIR-NB-LRR signaling induces root growth arrest via EDS1-and PAD4-complexed R protein VICTR in Arabidopsis. *The Plant Cell*, **24**, 5177–5192.

Kobayashi, K., Awai, K., Nakamura, M., Nagatani, A., Masuda, T. & Ohta, H. (2009) Type-B monogalactosyldiacylglycerol synthases are involved in phosphate starvation-induced lipid remodeling, and are crucial for low-phosphate adaptation. *Plant Journal*, **57**, 322–331.

Ku, A.T., Huang, Y.S., Wang, Y.S., Ma, D.F. & Yeh, K.W. (2008) IbMADS1 (*Ipomoea batatas* MADS-box 1 gene) is involved in tuberous root initiation in sweet potato (*Ipomoea batatas*). *Annals of Botany*, **102**, 57–67.

Langfelder, P. & Horvath, S. (2008) WGCNA: an R package for weighted correlation network analysis. *BMC Bioinformatics*, **9**, 559.

Li, H., Yao, L., Sun, L. & Zhu, Z. (2020a) ETHYLENE INSENSITIVE 3 suppresses plant de novo root regeneration from leaf explants and mediates age-regulated regeneration decline. *Development*, **147**, dev179457.

Li, M.Y., Li, C., Liu, W.X., Liu, C.H., Cui, J.R., Li, Q.R. *et al.* (2017) Dysfunction of PLA2G6 and CYP2C44-associated network signals imminent carcinogenesis from chronic inflammation to hepatocellular carcinoma. *Journal of Molecular Cell Biology*, **9**, 489–503.

Li, M., Zeng, T., Liu, R. & Chen, L. (2014) Detecting tissue-specific early-warning signals for complex diseases based on dynamical network biomarkers: study of type-2 diabetes by cross-tissue analysis. *Briefings in Bioinformatics*, **15**, 229–243.

Li, S.X., Nayar, S., Jia, H., Kapoor, S., Wu, J. & Yukawa, Y. (2020b) The Arabidopsis hypoxia inducible AtR8 long non-coding RNA also contributes to plant defense and root elongation coordinating with WRKY genes under low levels of salicylic acid. *Non-Coding RNA*, **6**, 8.

Liu, R., Aihara, K. & Chen, L. (2013) Dynamical network biomarkers for identifying critical transitions and their driving networks of biologic processes. *Quantitative Biology*, **1**, 105–114.

Liu, R., Chen, P., Aihara, K. & Chen, L.N. (2015) Identifying early-warning signals of critical transitions with strong noise by dynamical network markers. *Scientific Reports*, **5**, 17501.

Liu, R., Wang, J.Z., Ukai, M., Sewon, K., Chen, P., Suzuki, Y. *et al.* (2019a) Hunt for the tipping point during endocrine resistance process in breast cancer by dynamic network biomarkers. *Journal of Molecular Cell Biology*, **11**, 649–664.

Liu, R., Wang, X.F., Aihara, K. & Chen, L. (2014) Early diagnosis of complex diseases by molecular biomarkers, network biomarkers, and dynamical network biomarkers. *Medicinal Research Reviews*, **34**, 455–478.

Liu, X.P., Chang, X., Leng, S.Y., Tang, H., Aihara, K. & Chen, L.N. (2019b) Detection for disease tipping points by landscape dynamic network biomarkers. *National Science Review*, **6**, 775–785.

Love, M.I., Huber, W. & Anders, S. (2014) Moderated estimation of fold change and dispersion for RNA-seq data with DESeq2. *Genome Biology*, **15**, 550.

Ma, J., Liu, Y.H., Zhou, W.B., Zhu, Y., Dong, A.W. & Shen, W.H. (2018) Histone chaperones play crucial roles in maintenance of stem cell niche during plant root development. *Plant Journal*, **95**, 86–100.

Maere, S., Heymans, K. & Kuiper, M. (2005) BiNGO: a Cytoscape plugin to assess overrepresentation of gene ontology categories in biological networks. *Bioinformatics*, **21**, 3448–3449.

Maher, K.A., Bajic, M., Kajala, K., Reynoso, M., Pauluzzi, G., West, D.A. *et al.* (2018) Profiling of accessible chromatin regions across multiple plant species and cell types reveals common gene regulatory principles and new control modules. *The Plant Cell*, **30**, 15–36.

Martin, C. & Pazares, J. (1997) MYB transcription factors in plants. *Trends in Genetics*, **13**, 67–73.

Nakatani, M.(1994) In-vitro formation of tuberous roots in sweet-potato. *Japanese Journal of Crop Science*, **63**, 158–159.

Nakatani, M. & Komeichi, M. (1991) Changes in the endogenous level of zeatin riboside, abscisic-acid and indole acetic-acid during formation and thickening of tuberous roots in sweet-potato. *Japanese Journal of Crop Science*, **60**, 91–100.

Noh, S.A., Lee, H.S., Huh, E.J., Huh, G.H., Paek, K.H., Shin, J.S. *et al.* (2010) SRD1 is involved in the auxin-mediated initial thickening growth of storage root by enhancing proliferation of metaxylem and cambium cells in sweetpotato (*Ipomoea batatas*). *Journal of Experimental Botany*, **61**, 1337–1349.

Noh, S.A., Lee, H.S., Kim, Y.S., Paek, K.H., Shin, J.S. & Bae, J.M. (2013) Down-regulation of the IbEXP1 gene enhanced storage root development in sweetpotato. *Journal of Experimental Botany*, **64**, 129–142.

Patel, R.K. & Jain, M. (2012) NGS QC toolkit: a toolkit for quality control of next generation sequencing data. *PLoS One*, **7**, e30619.

Peer, W.A., Cheng, Y. & Murphy, A.S. (2013) Evidence of oxidative attenuation of auxin signalling. *Journal of Experimental Botany*, **64**, 2629–2639.

Petricka, J.J., Winter, C.M. & Benfey, P.N. (2012) Control of Arabidopsis root development. *Annual Review of Plant Biology*, **63**(63), 563–590.

Popescu, S.C. & Tumer, N.E. (2004) Silencing of ribosomal protein L3 genes in *N. tabacum* reveals coordinate expression and significant alterations in plant growth, development and ribosome biogenesis. *Plant Journal*, **39**, 29–44.

Randall, R.S., Miyashima, S., Blomster, T., Zhang, J., Elo, A., Karlberg, A. *et al.* (2015) AINTEGUMENTA and the D-type cyclin CYCD3;1 regulate root secondary growth and respond to cytokinins. *Biology Open*, **4**, 1229–1236.

Ravi, V., Naskar, S., Makeshkumar, T., Babu, B. & Prakash Krishnan, B.S.(2009) Molecular physiology of storage root formation and development in sweet potato (*Ipomoea batatas* (L.) lam.). *J Root Crops*, **35**, 1–27.

Riechmann, J.L. & Meyerowitz, E.M. (1998) The AP2/EREBP family of plant transcription factors. *Biological Chemistry*, **379**, 633–646.

Romano, J.M., Dubos, C., Prouse, M.B., Wilkins, O., Hong, H., Poole, M. *et al.* (2012) AtMYB61, an R2R3-MYB transcription factor, functions as a pleiotropic regulator via a small gene network. *New Phytologist*, **195**, 774–786.

Sakaoka, S., Mabuchi, K., Morikami, A. & Tsukagoshi, H. (2018) MYB30 regulates root cell elongation under abscisic acid signaling. *Communicative & Integrative Biology*, **11**, e1526604.

Shannon, P., Markiel, A., Ozier, O., Baliga, N.S., Wang, J.T., Ramage, D. *et al.* (2003) Cytoscape: a software environment for integrated models of biomolecular interaction networks. *Genome Research*, **13**, 2498–2504.

Silva, A.T., Ribone, P.A., Chan, R.L., Ligterink, W. & Hilhorst, H.W.M. (2016) A predictive coexpression network identifies novel genes controlling the seed-to-seedling phase transition in *Arabidopsis thaliana*. *Plant Physiology*, **170**, 2218–2231.

Singh, V., Sergeeva, L., Ligterink, W., Aloni, R., Zemach, H., Doron-Faigenboim, A. *et al.* (2019) Gibberellin promotes sweetpotato root vascular lignification and reduces storage-root formation. *Frontiers in Plant Science*, **10**, 1320.

Spence, J.A. & Humphries, E.C. (1972) Effect of moisture supply, root temperature, and growth-regulators on photosynthesis of isolated rooted leaves of sweet potato (*Ipomoea batas*). *Annals of Botany*, **36**, 115–121.

Szklarczyk, D., Franceschini, A., Wyder, S., Forslund, K., Heller, D., Huerta-Cepas, J. *et al.* (2015) STRING v10: protein-protein interaction networks, integrated over the tree of life. *Nucleic Acids Research*, **43**, D447–D452.

Tan, H.J., Man, C., Xie, Y., Yan, J.J., Chu, J.F. & Huang, J.R. (2019) A crucial role of GA-regulated flavonol biosynthesis in root growth of Arabidopsis. *Molecular Plant*, **12**, 521–537.

Tanaka, M., Kato, N., Nakayama, H., Nakatani, M. & Takahata, Y. (2008) Expression of class I knotted1-like homeobox genes in the storage roots of sweetpotato (*Ipomoea batatas*). *Journal of Plant Physiology*, **165**, 1726–1735.

Togari, Y.(1950) A study of tuberous root formation in sweet potato. *Bulletin of the National Agricultural Experiment Station Tokyo*, **68**, 1–96.

Van Gelderen, K., Kang, C.K., Paalman, R., Keuskamp, D., Hayes, S. & Pierik, R. (2018) Far-red light detection in the shoot regulates lateral root development through the HY5 transcription factor. *The Plant Cell*, **30**, 101–116.

Vesty, E.F., Saidi, Y., Moody, L.A., Holloway, D., Whitbread, A., Needs, S. *et al.* (2016) The decision to germinate is regulated by divergent molecular networks in spores and seeds. *New Phytologist*, **211**, 952–966.

Villordon, A.Q., la Bonte, D.R., Firon, N., Kfir, Y., Pressman, E. & Schwartz, A. (2009) Characterization of adventitious root development in sweetpotato. *HortScience*, **44**, 651–655.

Wang, H.X., Fan, W.J., Li, H., Yang, J., Huang, J.R. & Zhang, P. (2013) Functional characterization of dihydroflavonol-4-reductase in anthocyanin biosynthesis of purple sweet potato underlies the direct evidence of anthocyanins function against abiotic stresses. *PLoS One*, **8**, e78484.

Wang, H.X., Yang, J., Zhang, M., Fan, W.J., Firon, N., Pattanaik, S. *et al.* (2016) Altered phenylpropanoid metabolism in the maize Lc-expressed sweet potato (*Ipomoea batatas*) affects storage root development. *Scientific Reports*, **6**, 18645.

Wang, Z.Y., Fang, B.P., Chen, X.L., Liao, M.H., Chen, J.Y., Zhang, X.J. *et al.* (2015) Temporal patterns of gene expression associated with tuberous root formation and development in sweetpotato (*Ipomoea batatas*). *BMC Plant Biology*, **15**, 180.

Wilson, L.A. & Lowe, S.B. (1973) The anatomy of the root system in west Indian sweet potato (*Ipomoea batatas* (L.) lam.) cultivars. *Annals of Botany*, **37**, 633–643.

Woerlen, N., Allam, G., Popescu, A., Corrigan, L., Pautot, V. & Hepworth, S.R. (2017) Repression of BLADE-ON-PETIOLE genes by KNOX homeodomain protein BREVIPEDICELLUS is essential for differentiation of secondary xylem in Arabidopsis root. *Planta*, **245**, 1079–1090.

Woodward, A.W., Ratzel, S.E., Woodward, E.E., Shamoo, Y. & Bartel, B. (2007) Mutation of E1-CONJUGATING ENZYME-RELATED1 decreases RELATED TO UBIQUITIN conjugation and alters auxin response and development. *Plant Physiology*, **144**, 976–987.

Wu, S.Y., Xie, Y.R., Zhang, J.J., Ren, Y.L., Zhang, X., Wang, J.L. *et al.* (2015) VLN2 regulates plant architecture by affecting microfilament dynamics and polar auxin transport in rice. *The Plant Cell*, **27**, 2829–2845.

Xu, J., Duan, X.G., Yang, J., Beeching, J.R. & Zhang, P. (2013) Enhanced reactive oxygen species scavenging by overproduction of superoxide dismutase and catalase delays postharvest physiological deterioration of Cassava storage roots. *Plant Physiology*, **161**, 1517–1528.

Yamaguchi, M., Mitsuda, N., Ohtani, M., Ohme-Takagi, M., Kato, K. & Demura, T. (2011) VASCULAR-RELATED NAC-DOMAIN 7 directly regulates the expression of a broad range of genes for xylem vessel formation. *Plant Journal*, **66**, 579–590.

Yamaguchi, M., Ohtani, M., Mitsuda, N., Kubo, M., Ohme-Takagi, M., Fukuda, H. *et al.* (2010) VND-INTERACTING2, a NAC domain transcription factor, negatively regulates xylem vessel formation in Arabidopsis. *The Plant Cell*, **22**, 1249–1263.

Yang, B.W., Li, M.Y., Tang, W.Q., Liu, W.X., Zhang, S., Chen, L.N. *et al.* (2018) Dynamic network biomarker indicates pulmonary metastasis at the tipping point of hepatocellular carcinoma. *Nature Communications*, **9**, 678.

Yang, J., Bi, H.P., Fan, W.J., Zhang, M., Wang, H.X. & Zhang, P. (2011a) Efficient embryogenic suspension culturing and rapid transformation of a range of elite genotypes of sweet potato (*Ipomoea batatas* [L.] Lam.). *Plant Science*, **181**, 701–711.

Yang, J., Moeinzadeh, M.H., Kuhl, H., Helmuth, J., Xiao, P., Haas, S. *et al.* (2017) Haplotype-resolved sweet potato genome traces back its hexaploidization history. *Nature Plants*, **3**, 696–703.

Yang, S.D., Seo, P.J., Yoon, H.K. & Park, C.M. (2011b) The Arabidopsis NAC transcription factor VNI2 integrates abscisic acid signals into leaf senescence via the COR/RD genes. *The Plant Cell*, **23**, 2155–2168.

Yu, L.L., Sun, J.Y. & Li, L.G. (2013) PtrCel9A6, an endo-1,4–glucanase, is required for cell wall formation during xylem differentiation in *Populus*. *Molecular Plant*, **6**, 1904–1917.

Zhan, J.P., Thakare, D., Ma, C., Lloyd, A., Nixon, N.M., Arakaki, A.M. *et al.* (2015) RNA sequencing of laser-capture microdissected compartments of the maize kernel identifies regulatory modules associated with endosperm cell differentiation. *The Plant Cell*, **27**, 513–531.

Zhang, B. & Horvath, S. (2005) A general framework for weighted gene co-expression network analysis. *Statistical Applications in Genetics and Molecular Biology*, **4**, 17.

Zhang, F.P., Liu, X.P., Zhang, A.D., Jiang, Z.L., Chen, L.N. & Zhang, X.J. (2019) Genome-wide dynamic network analysis reveals a critical transition state of flower development in Arabidopsis. *BMC Plant Biology*, **19**, 11.

ARTICLES FOR FACULTY MEMBERS

INVESTIGATING THE ROLE OF GIBBERELLIC ACID (GA) AND ABSCISIC ACID (ABA) CROSS-TALK IN ENHANCING TUBEROUS ROOT DEVELOPMENT IN SWEET POTATOES

Genome-wide identification and expression analysis of sweet family genes in sweet potato and its two diploid relatives / Dai, Z., Yan, P., He, S., Jia, L., Wang, Y., Liu, Q., Zhai, H., Zhao, N., Gao, S., & Zhang, H.

International Journal of Molecular Sciences
Volume 23 Issue 24 (2022) 15848 Pages 1-23
https://doi.org/10.3390/ijms232415848
(Database: MDPI)

International Journal of
Molecular Sciences

MDPI

Article

Genome-Wide Identification and Expression Analysis of SWEET Family Genes in Sweet Potato and Its Two Diploid Relatives

Zhuoru Dai [1,†], Pengyu Yan [1,†], Shaozhen He [1,2], Licong Jia [3], Yannan Wang [4], Qingchang Liu [1], Hong Zhai [1], Ning Zhao [1], Shaopei Gao [1] and Huan Zhang [1,2,*]

[1] Key Laboratory of Sweet Potato Biology and Biotechnology, Ministry of Agriculture and Rural Affairs/Beijing Key Laboratory of Crop Genetic Improvement/Laboratory of Crop Heterosis & Utilization and Joint Laboratory for International Cooperation in Crop Molecular Breeding, Ministry of Education, College of Agronomy & Biotechnology, China Agricultural University, Beijing 100193, China
[2] Sanya Institute, China Agricultural University, Sanya 572025, China
[3] Institute of Grain and Oil Crops, Yantai Academy of Agricultural Sciences, Yantai 265500, China
[4] Cereal Crops Research Institute, Henan Academy of Agricultural Sciences, Zhengzhou 450002, China
* Correspondence: zhanghuan1111@cau.edu.cn; Tel./Fax: +86-010-6273-2559
† These authors contributed equally to this work.

Abstract: Sugar Will Eventually be Exported Transporter (SWEET) proteins are key transporters in sugar transportation. They are involved in the regulation of plant growth and development, hormone crosstalk, and biotic and abiotic stress responses. However, SWEET family genes have not been explored in the sweet potato. In this study, we identified 27, 27, and 25 SWEETs in cultivated hexaploid sweet potato (*Ipomoea batatas*, 2n = 6x = 90) and its two diploid relatives, *Ipomoea trifida* (2n = 2x = 30) and *Ipomoea triloba* (2n = 2x = 30), respectively. These SWEETs were divided into four subgroups according to their phylogenetic relationships with *Arabidopsis*. The protein physiological properties, chromosome localization, phylogenetic relationships, gene structures, promoter *cis*-elements, protein interaction networks, and expression patterns of these 79 *SWEETs* were systematically investigated. The results suggested that homologous SWEETs are differentiated in sweet potato and its two diploid relatives and play various vital roles in plant growth, tuberous root development, carotenoid accumulation, hormone crosstalk, and abiotic stress response. This work provides a comprehensive comparison and furthers our understanding of the SWEET genes in the sweet potato and its two diploid relatives, thereby supplying a theoretical foundation for their functional study and further facilitating the molecular breeding of sweet potato.

Keywords: sweet potato; *SWEET*; tissue-specific expression; tuberous root development; hormone treatment; abiotic stress

Citation: Dai, Z.; Yan, P.; He, S.; Jia, L.; Wang, Y.; Liu, Q.; Zhai, H.; Zhao, N.; Gao, S.; Zhang, H. Genome-Wide Identification and Expression Analysis of SWEET Family Genes in Sweet Potato and Its Two Diploid Relatives. *Int. J. Mol. Sci.* **2022**, *23*, 15848. https://doi.org/10.3390/ijms232415848

Academic Editor: Endang Septiningsih

Received: 6 September 2022
Accepted: 10 December 2022
Published: 13 December 2022

1. Introduction

Sugar Will Eventually be Exported Transporters (SWEETs) play key roles in sugar transport across plasma and intracellular membranes in both prokaryotes and eukaryotes [1]. Almost all SWEETs are present in the membrane structure, such as the plasma membrane and Golgi membrane [2]. As membrane proteins, SWEETs have three transmembrane domains (3TMs) in bacteria but have seven transmembrane domains (7TMs) in eukaryotes [3]. The 3TMs are encoded by a PQ-loop called the Mtn3 domain, which carries conserved proline and glutamine motifs [4,5]. The 7TM helices are folded into two parallel three-helix bundles connected by one central TM [1,6,7]. Since the 7TMs in SWEETs may not be sufficient for creating a functional pore as other types of sugar transporters carrying 12TMs, two SWEETs usually form a functional pore that permits sugar substrate transportation by oligomerization [1,3,7,8]. Accumulating evidence has revealed that SWEETs could homo- or hetero-oligomerize. The co-expression of a mutated and non-functional

AtSWEET1 with a functional AtSWEET1 was found to inhibit sugar transport activity [9]. The oligomerization of the mutated form of OsSWEET11 with functional OsSWEET11 was found to disrupt sugar transport activity [10]. AtSWEET11 and AtSWEET12 undergo hetero-oligomerization to form a functional pore for sucrose transportation [11]. The hetero-oligomerization of SUT1 and SUT2 was found to be involved in the negative regulation of sucrose transportation [12].

In plants, the number of SWEETs varies among different species. The *Arabidopsis*, rice, potato, and soybean genomes encode 17, 21, 35, and 52 SWEETs, respectively [9,13–15]. These are critical in organ formation due to their controlling sugar transport [9,16]. In *Arabidopsis*, AtSWEET11, AtSWEET12, and AtWEET15 are important transporters for seed filling [17,18]. *AtSWEET11* and *AtSWEET12* are highly expressed in leaf phloem parenchyma cells, and the mutations of *AtSWEET11* and *AtSWEET12* result in defects in phloem loading [19]. Under dark or fructose accumulation, AtSWEET17, as a facilitator, was found to regulate the flow of fructose in vacuoles [16]. Mutations to *StSWEET11* were found to cause sucrose accumulation in leaves, leading to yield reductions in potato [20]. The overexpression of *PbSWEET4* caused reductions in sugar and early senescence in leaves in pears [21]. Moreover, SWEETs are also involved in the regulation of plant growth and development and hormone response. *AtSWEET8* is necessary for pollen growth [22]. *GmSWEET10a* and *GmSWEET10b* directly affect seed qualities in soybean [23]. The *AtSWEET13* and *AtSWEET14* double-mutant line failed to transport exogenous GA [24]. The rice *OsSWEET3a* was found to be involved in transporting glucose and gibberellin (GA) to leaves during early plant development [25]. The overexpression of *OsSWEET5* inhibited auxin concentration and signaling [26]. The triple mutants of *ZmSWEET13a*, *ZmSWEET13b*, and *ZmSWEET13c* resulted in a stunted phenotype in maize [27]. Furthermore, SWEETs are also involved in the regulation of biotic and abiotic stress responses. AtSWEET2 transports sugar from the cytosol to the vacuole, causing sugar leakage and thereby limiting pathogen growth [18]. The overexpression of *IbSWEET10* enhanced *Fusarium oxysporum* resistance by reducing the sugar content in the transgenic plants of the sweet potato [28]. *AtSWEET16* was found to enhance the freezing tolerance of transgenic plants [29]. Cucumber *CsSWEET2* was found to improve cold tolerance in *Arabidopsis* [30]. However, the biological functions and regulatory mechanisms of SWEETs remain unclear in sweet potato.

The sweet potato (*Ipomoea batatas* (L.) Lam., 2n = $B_1B_1B_2B_2B_2B_2$ = 6x = 90), belonging to the family Convolvulaceae, is an economically important root and tuber crop that is widely used as an industrial and bioenergy resource worldwide [31]. It provides a rich source of carbohydrates, dietary fiber, carotenoid, vitamins, and micronutrients. Due to its resilience and adaptability, it plays an important role in food security for subsistence farmers in Africa and Southeast Asia [31]. The formation and thickening of tuberous roots is one of the most important processes determining the yield of sweet potato. However, its diploids cannot form tuberous roots, and they exhibit slender stems and rattan characteristics [32–34]. In recent years, genome assemblies of a hexaploid sweet potato, Taizhong 6 [35], and two diploid species closely related to the hexaploid sweet potato, *Ipomoea trifida* NCNSP0306 (2n = 2x = 30) and *Ipomoea triloba* NCNSP0323 (2n = 2x = 30) [36], were released, making it possible to identify and analyze important gene families involved in tuberous root development at the whole-genome level in sweet potato.

In this study, SWEET family genes were identified from *I. batatas*, *Ipomoea trifida*, and *Ipomoea triloba*. We systematically investigated the protein physicochemical properties, chromosome localization, phylogenetic relationships, gene structure, *cis*-elements of promoters, and the protein interaction network of SWEETs in sweet potato. In addition, the tissue specificity and expression pattern analyses for tuberous root development in different varieties, and hormone responses (in leaves) of SWEETs were carried out using qRT-PCR and RNA-seq. The results play an important guiding role in the further study of their functions and the molecular breeding of the sweet potato.

2. Results

2.1. Identification and Characterization of SWEETs in the Sweet Potato and Two Diploid Relatives

The plant morphology of the cultivated hexaploid sweet potato is different from that of its diploid relatives, especially since the diploid relatives cannot form tuberous roots (Figure 1). To comprehensively identify all SWEETs in the sweet potato and its two diploid relatives, we employed three typical strategies (i.e., blastp search, hmmersearch, and the CD-search database). A total of 79 SWEETs were identified in *I. batatas* (27), *I. trifida* (27), and *I. triloba* (25), which were named "*Ib*", "*Itf*", and "*Itb*", respectively. The physicochemical properties were analyzed using the sequence of IbSWEETs (Table 1). The genomic length of the 27 *IbSWEETs* ranged from 1052 bp (*IbSWEET8.1*) to 5747 bp (IbSWEET15.7), and the CDS length varied from 823 bp (*IbSWEET9.1*) to 1557 bp (*IbSWEET2.3*). The amino acid lengths of IbSWEETs ranged from 153 aa (IbSWEET15.7) to 321 aa *(IbSWEET15.1*), with the molecular weight (MW) varying from 17.64 kDa (IbSWEET15.7) to 35.41 kDa (IbSWEET15.1). The isoelectric point (pI) of IbSWEET15.6 (5.81) was the lowest among all the IbSWEETs, indicating that it is an acidic protein. The pI of the other SWEETs was distributed from 7.61 (IbSWEET15.1) to 9.98 (IbSWEET8.3), suggesting that they are basic proteins. All the IbSWEETs contained Ser, Thr, and Tyr phosphorylation sites. All the IbSWEETs were stable with an aliphatic index of more than 100, except for IbSWEET3.1, which obtained an aliphatic index of 98.25. The grand average of the hydropathicity (GRAVY) value of all the IbSWEET proteins varied from 0.281 (IbSWEET3.1) to 1.070 (IbSWEET2.3), indicating that they are hydrophobic. The subcellular localization prediction assay showed that most of IbSWEETs were located in the cell membrane, except three IbSWEETs: IbSWEET15.6 and IbSWEET15.7, which were located in the cell membrane and chloroplasts, and IbSWEET1.1, which was located in the cell membrane and Golgi apparatus. Most of the IbSWEETs have seven transmembrane helical segments (TMHs); several (i.e., IbSWEET6.3, -8.1, -8.3, -9.2, -9.3, -15.2, -15.3, -15.4, and -15.7) have six TMHs; a few (i.e., IbSWEET2.3, -3.1, -6.2, and -10.5) have five TMHs, and IbSWEET15.6 has four TMHs. The three-dimensional structural models showed that there are three conserved α-helices in both N-terminal and C-terminal of all IbSWEETs (Figure S1).

Table 1. Characterization of *IbSWEETs* in sweet potato.

Gene ID	Gene Name	PI	MW/kDa	Genomic Length/bp	CDS Length/bp	Phosphorylation Site			Protein Size/aa	Aliphatic Index	GRAVY	TMHs	Subcellular Locations	*Arabidopsis* Homologous
						Ser	Thr	Tyr						
g42355	*IbSWEET1.1*	9.55	27.63	1949	1158	17	12	6	254	120.47	0.819	7	Cell membrane Golgi apparatus	*SWEET1*
g45970	*IbSWEET2.1*	9.18	30.50	2865	1303	30	11	12	273	114.58	0.788	7	Cell membrane	*SWEET2*
g37512	*IbSWEET2.2*	8.97	26.17	2620	1086	23	12	14	235	125.19	1.003	7	Cell membrane	*SWEET2*
g37574	*IbSWEET2.3*	9.44	19.99	4204	1557	17	11	9	179	125.70	1.070	5	Cell membrane	*SWEET2*
g20639	*IbSWEET3.1*	8.83	24.44	1825	829	20	12	10	217	98.25	0.281	5	Cell membrane	*SWEET3*
g39263	*IbSWEET6.1*	8.46	30.93	2934	1046	19	17	12	278	126.19	0.871	7	Cell membrane	*SWEET6*
g39260	*IbSWEET6.2*	9.15	25.53	2101	868	19	16	11	233	105.41	0.481	5	Cell membrane	*SWEET6*
g39262	*IbSWEET6.3*	9.30	25.79	2900	983	22	15	11	237	112.32	0.523	6	Cell membrane	*SWEET6*
g5800	*IbSWEET8.1*	9.83	22.47	1052	966	15	10	7	206	117.86	0.639	6	Cell membrane	*SWEET8*
g346	*IbSWEET8.2*	9.47	25.72	1977	1065	17	11	10	235	120.68	0.681	7	Cell membrane	*SWEET8*
g51687	*IbSWEET8.3*	9.98	26.48	2536	1055	16	14	7	239	108.20	0.592	6	Cell membrane	*SWEET8*
g41769	*IbSWEET9.1*	9.16	27.26	1912	823	12	7	14	241	119.71	0.747	7	Cell membrane	*SWEET9*
g49942	*IbSWEET9.2*	9.48	30.39	5035	1049	15	14	17	267	114.68	0.696	6	Cell membrane	*SWEET9*
g33162	*IbSWEET9.3*	8.72	30.49	2028	1395	16	22	13	275	122.15	0.691	6	Cell membrane	*SWEET9*
g6315	*IbSWEET10.1*	8.83	31.13	2310	1122	16	16	14	278	117.73	0.700	7	Cell membrane	*SWEET10*
g33248	*IbSWEET10.2*	9.34	34.07	3208	1235	17	18	11	305	114.72	0.549	7	Cell membrane	*SWEET10*
g55355	*IbSWEET10.3*	9.20	34.65	1851	1231	18	11	13	314	122.26	0.689	7	Cell membrane	*SWEET10*
g38390	*IbSWEET10.4*	9.19	34.25	2664	1264	21	17	11	304	117.57	0.607	7	Cell membrane	*SWEET10*
g14486	*IbSWEET10.5*	9.48	30.78	3130	1123	18	15	9	272	106.76	0.521	5	Cell membrane	*SWEET10*
g14649	*IbSWEET10.6*	9.39	32.65	3831	1188	17	17	11	288	116.39	0.678	7	Cell membrane	*SWEET10*
g4174	*IbSWEET15.1*	7.61	35.41	2008	1238	19	19	11	321	114.70	0.568	7	Cell membrane	*SWEET15*
g39828	*IbSWEET15.2*	8.19	33.64	2933	1057	19	16	12	302	115.79	0.541	6	Cell membrane	*SWEET15*
g13599	*IbSWEET15.3*	9.46	24.64	1780	896	16	10	8	221	127.87	0.802	6	Cell membrane	*SWEET15*
g13600	*IbSWEET15.4*	9.30	24.86	1917	920	19	12	8	222	124.19	0.821	6	Cell membrane	*SWEET15*
g13601	*IbSWEET15.5*	7.74	32.80	1767	1103	24	9	11	292	120.17	0.664	7	Cell membrane	*SWEET15*
g61464	*IbSWEET15.6*	5.81	31.87	1594	1026	29	13	9	278	119.10	0.729	4	Cell membrane Chloroplast	*SWEET15*
g61461	*IbSWEET15.7*	9.47	17.64	5747	988	14	9	7	153	127.97	0.907	6	Cell membrane Chloroplast	*SWEET15*

CDS, coding sequence; MW, molecular weight; pI, isoelectric point; Ser, serine; Thr, threonine; Tyr, tyrosine; TMHs, transmembra-ne helices.

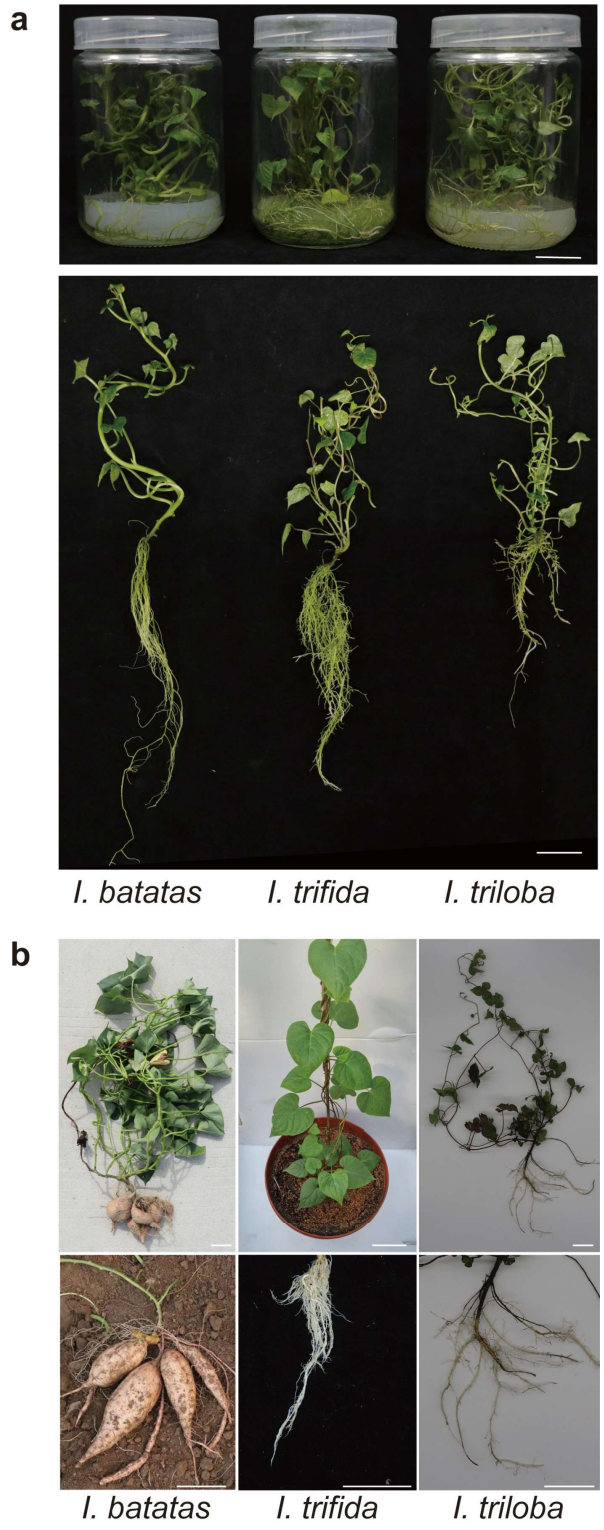

Figure 1. Plant morphology of in vitro grown (**a**) and field-grown plants. Scale bars, 2 cm. (**b**) of *I. batatas*, *I. trifida*, and *I.triloba*. Scale bars, 5 cm.

The *SWEETs* were distributed across 11, 10, and 11 chromosomes of *I. batatas*, *I. trifida*, and *I. triloba*, respectively (Figure 2). In *I. batatas*, five *IbSWEETs* were detected on LG4 and LG10; three on LG11; two on LG1, LG2, LG8, LG9, LG13, and LG15; and one on LG5 and LG12, whereas no genes were detected on LG3, LG6, LG7, or LG14 (Figure 2a). In *I. trifida* and *I. triloba*, the distribution of *SWEETs* on Chr01 (3), Chr04 (2), Chr11 (2), Chr12 (2), Chr13 (2), and Chr06 (1) was similar, but their distribution on other chromosomes

was different (Figure 2b,c). The results indicated a variation and loss of *SWEETs* during evolution, causing the difference between the distribution and disproportion of *SWEETs* on the chromosomes in sweet potato and its two diploid relatives.

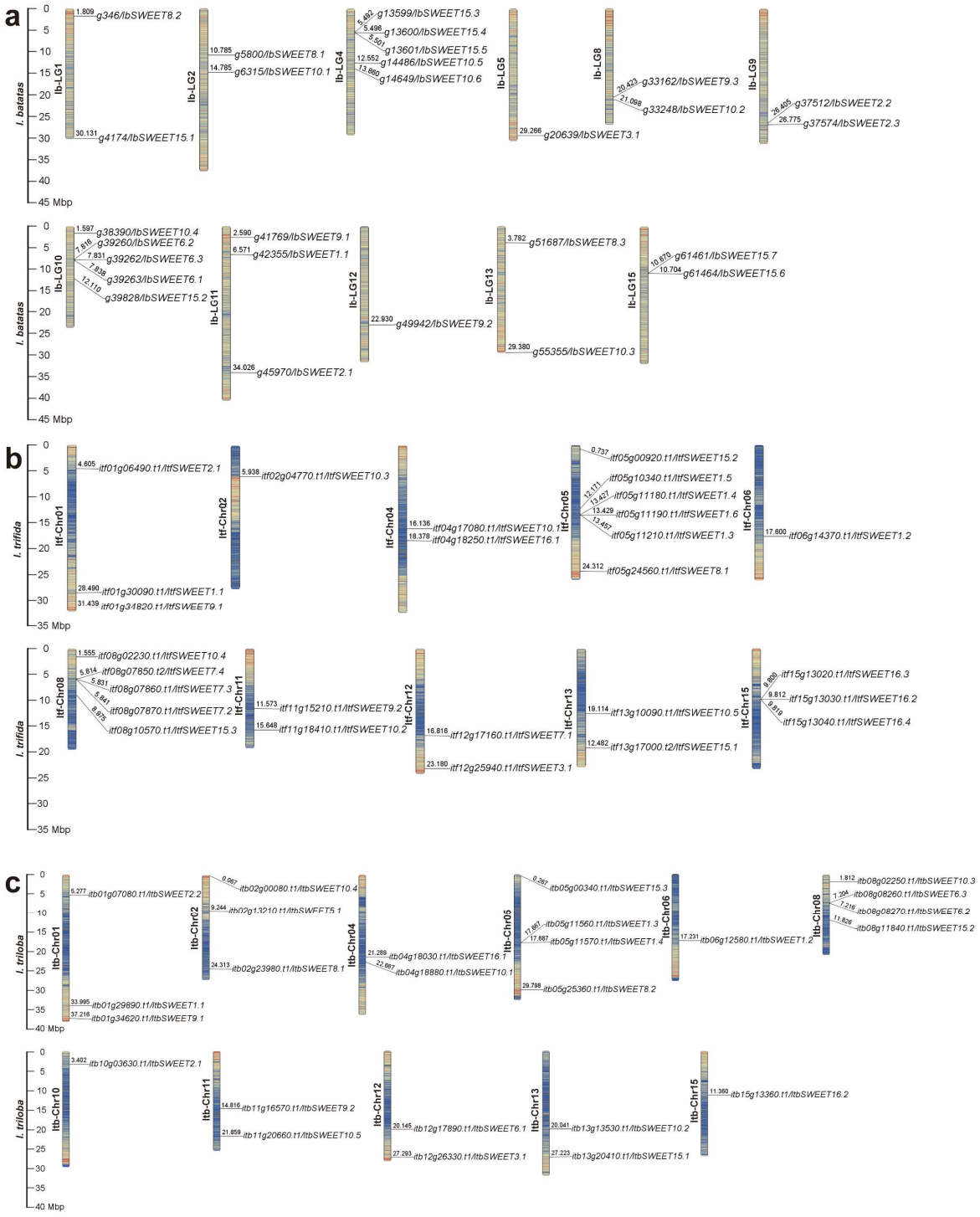

Figure 2. Chromosomal localization and distribution of *SWEETs* in *I. batatas* (**a**), *I. trifida* (**b**), and *I. triloba* (**c**). The bars represent chromosomes. The chromosome numbers are displayed on the left side, and the gene names are displayed on the right side. Each gene location is shown on the line. Detailed chromosomal location information is listed in Table S1.

2.2. Phylogenetic Relationship of SWEETs in the Sweet Potato and Its Two Diploid Relatives

To study the evolutionary relationship of SWEETs in *I. batatas*, *I. trifida*, *I. triloba*, and *Arabidopsis*, we constructed a phylogenetic tree for 96 SWEETs of these four species (i.e., 27 in *I. batatas*, 27 in *I. trifida*, 25 in *I. triloba*, and 17 in *Arabidopsis*) (Figure 3). All the SWEETs were unevenly distributed on each branch of the phylogenetic tree. Interestingly, the SWEETs in *I. trifida*, *I. triloba*, and *Arabidopsis* were divided into four subgroups (Groups I to IV), but in *I. batatas*, they were divided into three subgroups (Groups I to III) according to the evolutionary distance (Figure 3). The specific distribution of the SWEETs was as follows (total: *I.batatas*, *I. trifida*, *I. triloba*, and *Arabidopsis*): Group I (22:6, 5, 6, 5), Group II (23:5, 8, 7, 3), Group III (43:16, 10, 10, 7), and Group IV (8:0, 4, 2, 2) (Figure 3; Table S1). We named IbSWEETs, ItfSWEETs, and ItbSWEETs based on their homology with homologs in *Arabidopsis*, and only AtSWEET1/2/3/5/6/7/8/9/10/15/16 from *Arabidopsis* had homologous proteins in *I. batatas*, *I. trifida*, and *I. triloba*. These results indicate that the number and type of SWEETs distributed in each subgroup in the sweet potato differed from those of its two diploid relatives and Arabidopsis.

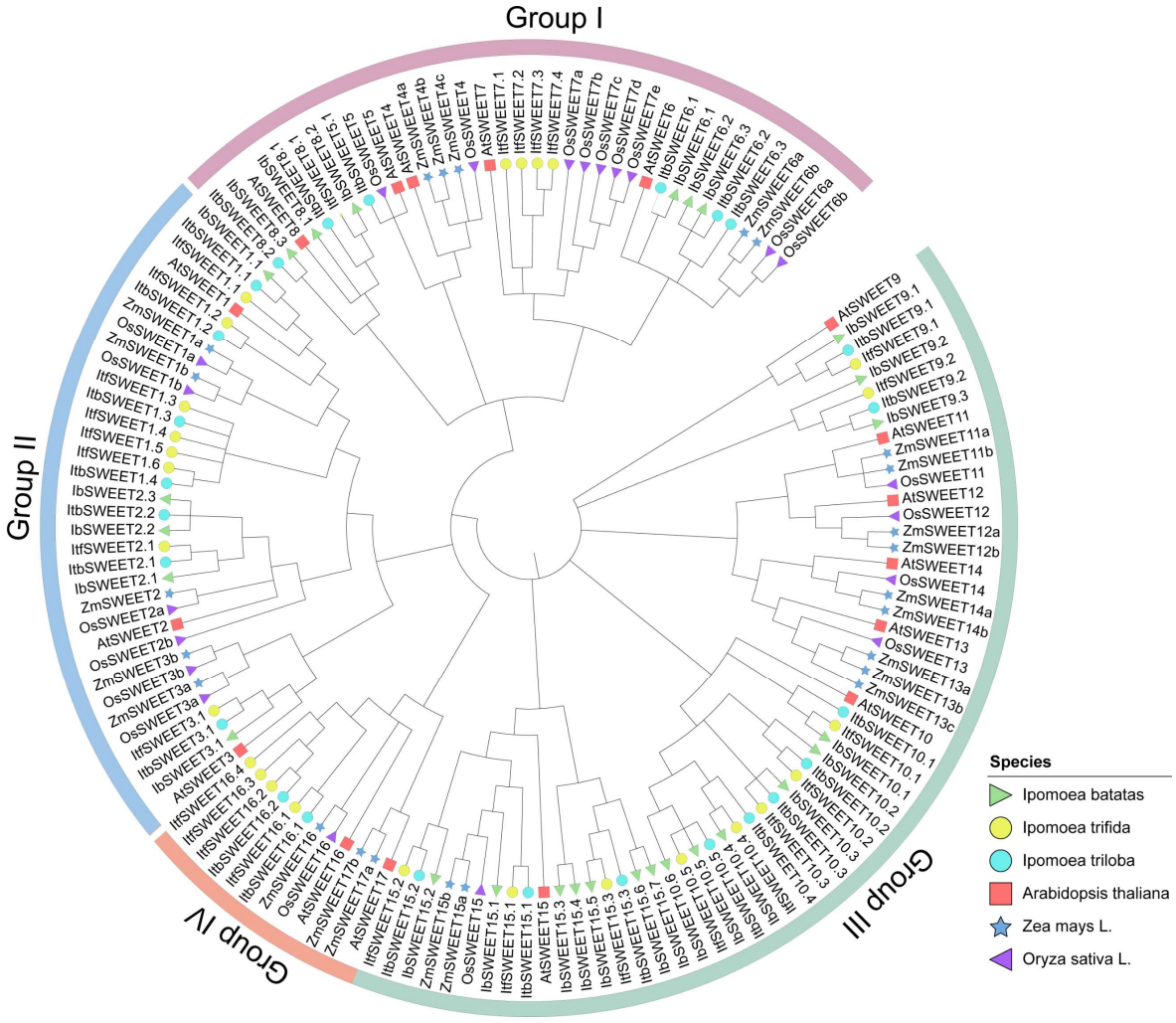

Figure 3. Phylogenetic analysis of the SWEET proteins from seven plant species (i.e., *I. batatas*, *I. trifida*, *I. triloba*, *Arabidopsis thaliana*, *Oryza sativa* L., and *Zea mays*). A total of 142 SWEETs were divided into four subgroups (GroupI to Group IV) according to the evolutionary distance. The green triangle, yellow circles, blue circles, red squares, purple triangle, and blue star represent the 27 IbSWEETs in *I. batatas*, 27 ItfSWEETs in *I. trifida*, 25 ItbSWEETs in I. *triloba*, 17 AtSWEETs in *Arabidopsis thaliana*, 21 OsSWEETs in *Oryza sativa* L., and 24 ZmSWEETs in *Zea mays*, respectively.

Furthermore, a total of 142 SWEET proteins from six plant species (i.e., 27 in *I.batatas*, 27 in *I. trifida*, 25 in *I.triloba*, 17 in *Arabidopsis*, 21 in rice, and 24 in maize) were used for the phylogenetic analysis. They were divided into four subgroups (Groups I to IV) (Figure 3), which indicated that the evolutionary relationship of the SWEETs was relatively conserved in the plant.

2.3. Conserved Motif and Exon–Intron Structure Analysis of SWEETs in the Sweet Potato and Two Diploid Relatives

Furthermore, sequence motifs in the 27 *IbSWEETs*, 27 *ItfSWEETs*, and 25 *ItbSWEETs* were analyzed using the MEME website, and the five most conserved motifs were identified (Figure 4a and Figure S2). Most of the SWEETs contained these five conserved motifs, except for a few SWEETs that were differentiated in the number and species of motifs in *I.batatas*, *I.trifida*, and *I.triloba*, such as IbSWEET15.2 (containing motifs 2–5), ItfSWEET15.2 (containing motifs 1–5), and ItbSWEET15.2 (containing motifs 1–5) (Figure 4a). The PQ-loop acts as a key structure for the helix of the SWEETs [9]—the first PQ-loop contains motifs 1 and 4 and the second PQ-loop contains motifs 2, 3, and 5; additionally, all the SWEETs contain two PQ-loops (Figure 4b). Moreover, only ItfSWEET9.1 and ItbSWEET9.1 contain an SANT domain, which is involved in the regulation of flower development [37] (Figure 4b).

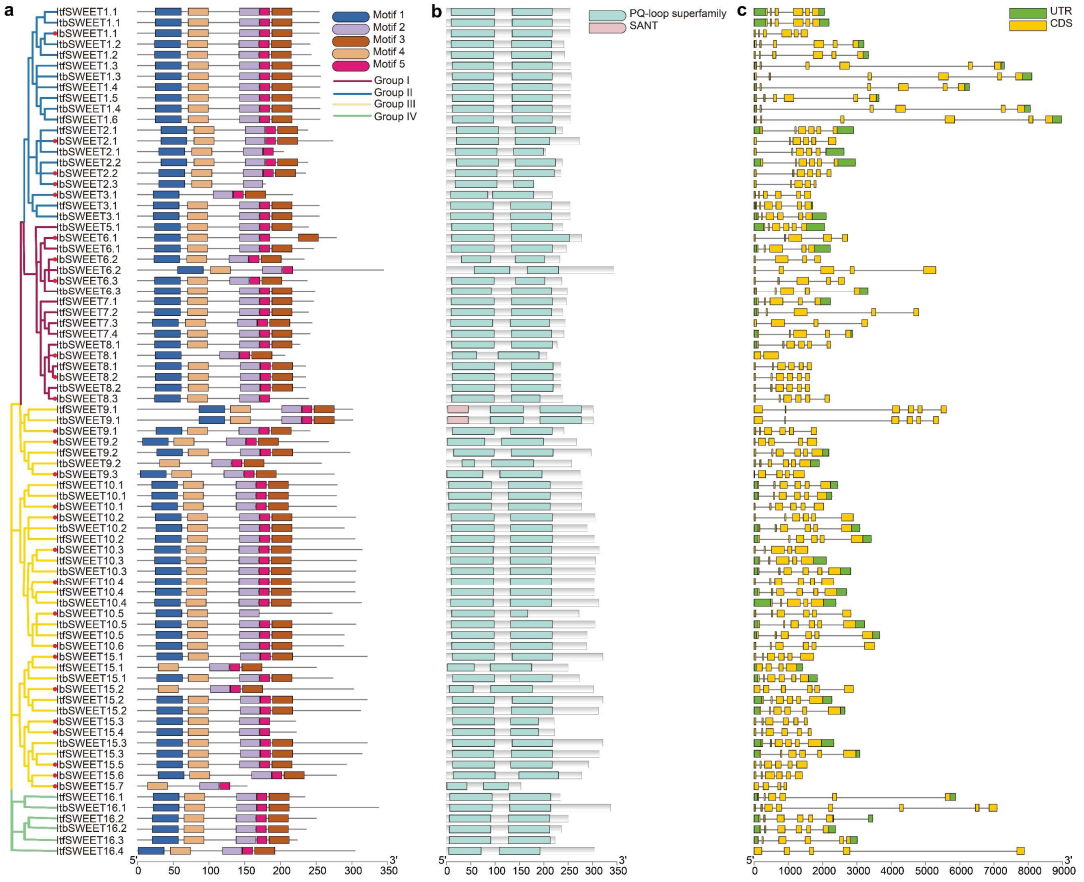

Figure 4. Conserved motifs and exon–intron structure analysis of the SWEET family in *I. batatas*, *I. trifida*, and, *I. triloba.* (**a**) The phylogenetic tree shows that SWEETs are distributed in four subgroups on the left, and the five conserved motifs are shown in different colors. The red circle represents the IbSWEETs. (**b**). Conserved domain structures of SWEETs. The blue box represents the PQ-loop domain. The red box represents the SANT domain. (**c**) Exon–intron structures of SWEETs. The green boxes, yellow boxes, and black lines represent the UTRs, exons, and introns, respectively.

To better understand the structural diversity among SWEETs, the exon–intron structures were analyzed (Figure 4c). The number of exons in the SWEETs ranged from two to eight. In more detail, the SWEETs of Group I contained two to six exons; the SWEETs of Group II contained five or six exons; the SWEETs of Group III contained four to six exons; and the SWEETs of Group IV contained five to eight exons (Figure 4c). The exon–intron structures of some homologous SWEETs were different in *I. batatas* compared to those in *I. trifida* and *I. triloba*, such as *IbSWEET8.1* (containing two exons), *ItfSWEET8.1* (containing six exons), and *ItbSWEET8.1* (containing six exons) in Group I, *IbSWEET9.2* (containing five exons) and *ItbSWEET9.2* (containing six exons) in Group III, and *ItfSWEET16.1* (containing six exons), and *ItbSWEET16.1* (containing eight exons) in Group IV (Figure 4c). These results indicated that the SWEET family may have undergone a lineage-specific differentiation event in the sweet potato genome.

2.4. Cis-Element Analysis in the Promoter of IbSWEETs in Sweet Potato

Promoter c*is*-elements in plants initiate the gene functions related to plant development, hormone regulation, and stress response. Therefore, we performed a *cis*-element analysis using the 1500 bp promoter region of *IbSWEETs*. According to the predicted functions, we divided the elements into five categories: core elements, development regulation elements, hormone-responsive elements, abiotic/biotic stress-responsive elements, and light-responsive elements (Figure 5). A large number of core elements were identified in the 27 *IbSWEETs* (CAAT-box and TATA-box) (Figure 5). Most of the *IbSWEETs* contained several development elements, such as the O2-site, which was a zein metabolism regulatory element (found in *IbSWEET3.1, -6.2, -8.1, -9.3, -10.1, -10.4*, and *-15.1*); the CAT-box, which was associated with meristem formation (found in *IbSWEET2.2, -2.3, -6.2, -8.2, -8.3, -9.2, -10.2*, and *-15.3*); and the GCN4 motif, which was involved in controlling seed-specific expression (found in *IbSWEET3.1* and *IbSWEET6.1*) (Figure 5). However, no development-related elements were found in the 1500 bp promoter region of *IbSWEET15.2, IbSWEET15.6*, and *IbSWEET15.7*. Moreover, light-responsive elements such as the G-box, BOX4, and AE-box were abundant in the promoters of *IbSWEETs* (Figure 5).

Additionally, some abiotic elements, such as the drought-responsive elements DRE-core, MYB, and MYC; the salt-responsive elements LTR, MBS, and W-box; the light-responsive elements ERE and LTR; and biotic elements, such as WRE3, W-box, and the WUN motif, were identified in most *IbSWEETs* (Figure 5). All the *IbSWEETs* possessed several hormone elements, including ABRE for ABA-responsive elements, TGA-element for IAA-responsive elements, TATC-box for GA-responsive elements, the CGTCA and TGACG motifs for MeJA-responsive elements, and the TCA motif for SA-responsive elements (Figure 5). These results suggest that *IbSWEETs* are involved in the regulation of plant growth and development, hormone crosstalk, and abiotic stress adaption in the sweet potato.

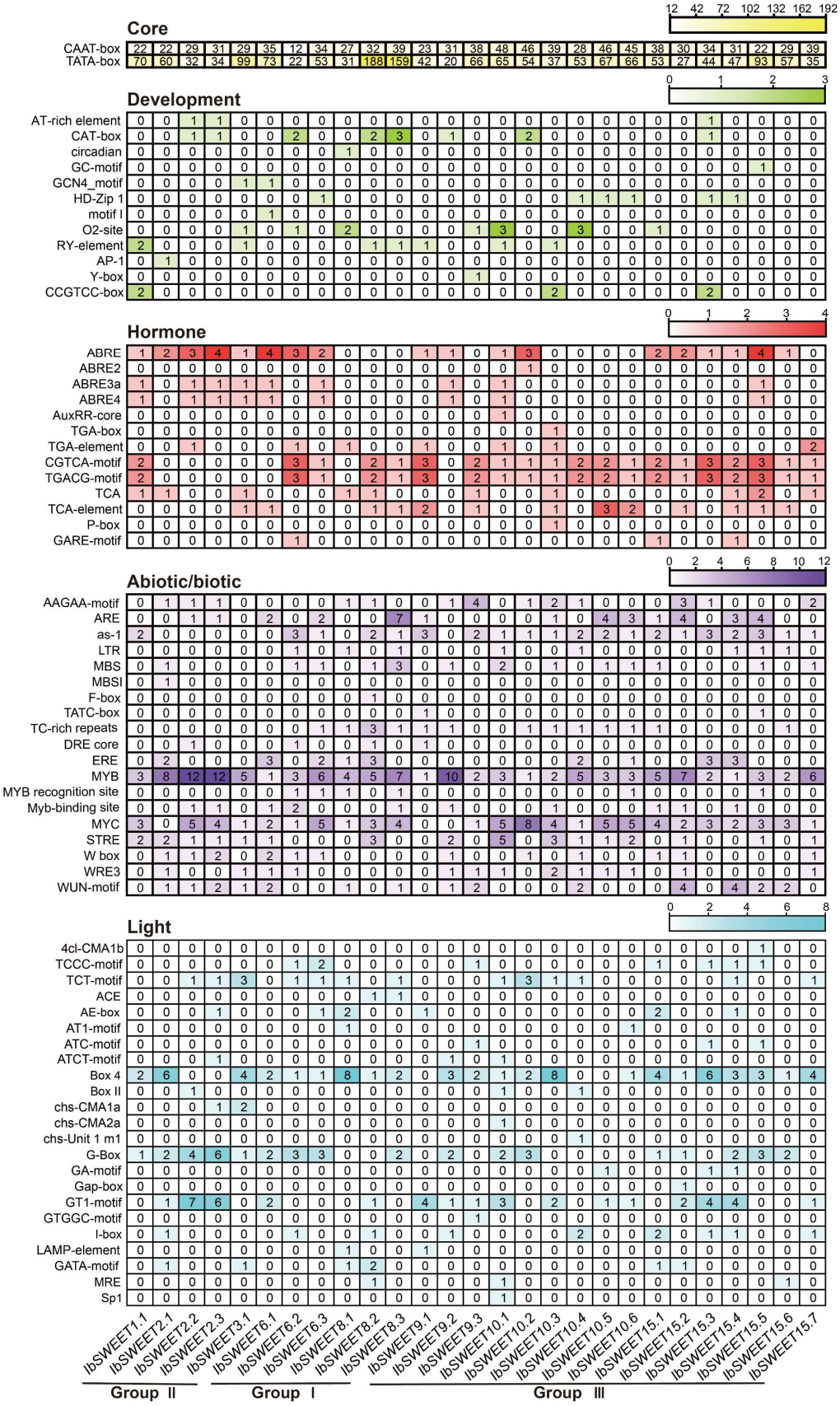

Figure 5. *Cis*-element analysis of *IbSWEET*s in *I. batatas*. The *cis*-elements were divided into five categories. The intensity of the different colors represents the number of *cis*-elements in the *IbSWEET* promoters.

2.5. Protein Interaction Network of IbSWEETs in the Sweet Potato

To explore the potential regulatory network of IbSWEETs, we constructed an IbSWEET interaction network based on *Arabidopsis* orthologous proteins (Figure 6). Protein interaction predictions indicated that some IbSWEETs (IbSWEET1, 6, 8, 9, and 10) could interact with other IbSWEETs to form heterodimers. In addition, SWEETs can interact with pollen development-related protein DEX1 [38], circadian rhythm-related protein FKF1 [39,40], and pathogen responsive-related protein RIN4 and RPM1 [41,42]. IbSWEET2, IbSWEET3, and IbSWEET9 can interact with translation regulation-related protein PUM23 [43]. IbSWEET15 can interact with plant senescence regulatory-related protein SAG12 [44]. These results indicate that IbSWEETs are involved in the regulation of plant growth and development and biotic stress adaption in the sweet potato.

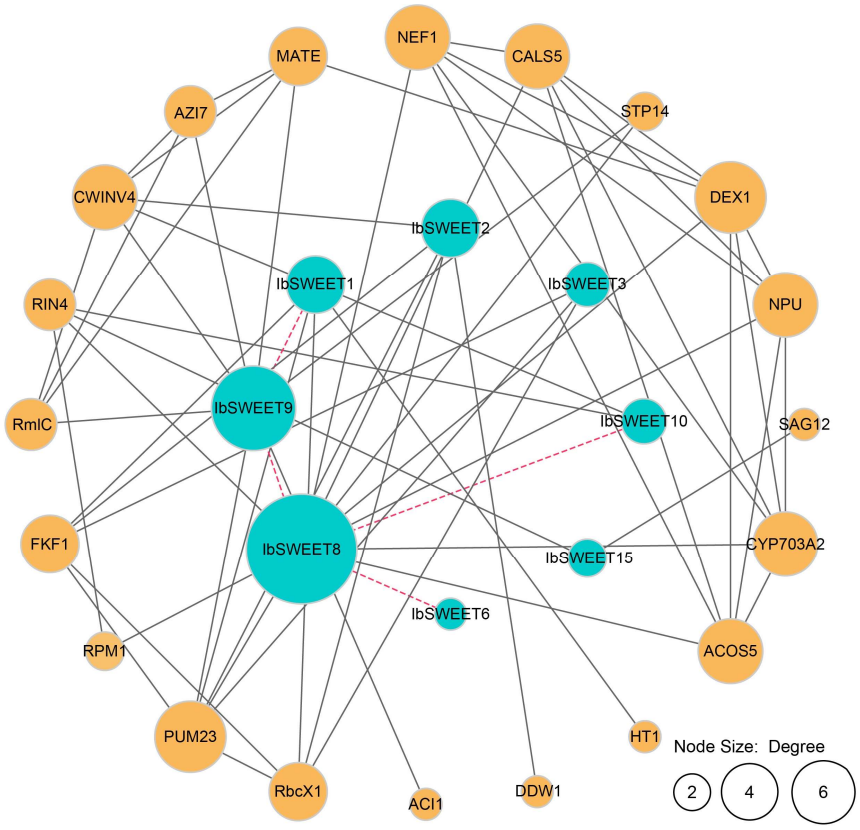

Figure 6. Functional interaction networks of IbSWEETs in *I. batatas* according to orthologues in *Arabidopsis.* Network nodes represent proteins, and lines represent protein–protein associations. The node size represents the number of proteins that interact with each other. The dotted line represents the interaction between the different SWEETs. The solid line represents the interaction between SWEETs and other proteins.

2.6. Expression Analysis of SWEETs in the Sweet Potato and Two Diploid Relatives

2.6.1. Expression Analysis in Various Tissues

To investigate the potential biological function of *IbSWEETs* in plant growth and development, the expression levels in six representative tissues (i.e., bud, petiole, leaf, stem, pencil root, and tuberous root) of *I. batatas* were analyzed using real-time quantitative PCR (qRT-PCR) (Figure 7). Nonetheless, different subgroups showed diversified expression patterns in six tissues. *IbSWEETs* in Group II showed higher expression levels in all the tissues as compared to the other subgroups. Among all the *IbSWEETs*, six *IbSWEETs* (i.e., *IbSWEET1.1*, *−2.1*, *−2.2*, *−2.3*, *−9.2*, and *−10.2*) were highly expressed in all the tissues, especially *IbSWEET10.2*, which was highly expressed by more than 1000-fold in all the tissues. Interestingly, all the *IbSWEETs* showed high expression levels in the petiole.

Moreover, some *IbSWEETs* showed tissue-specific expression—e.g., *IbSWEET1.1*, *-2.1*, *-2.2*, *-2.3*, and *−15.1* were highly expressed in buds; *IbSWEET2.1*, *-2.2*, *-2.3*, *-10.2*, and *-15.1* were highly expressed in leaves; *IbSWEET10.3* was highly expressed in stems and pencil roots; and *IbSWEET8.3* and *IbSWEET15.6* were highly expressed in tuberous roots (Figure 7a). These results indicate that *IbSWEETs* might play different roles in sugar transport and development in the various tissues of the sweet potato.

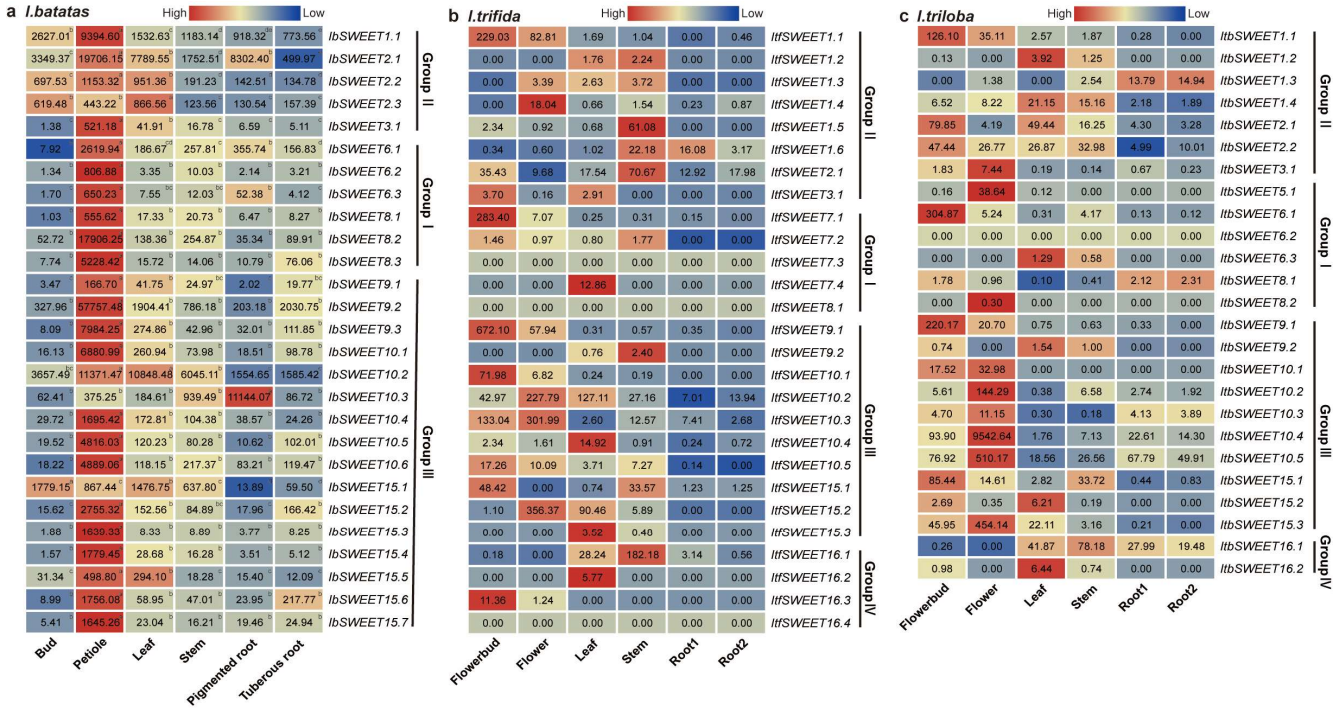

Figure 7. Gene expression patterns of SWEETs in different tissues of *I. batatas*, *I. trifida*, and *I. triloba*. (**a**) Expression analysis in the bud, petiole, leaf, stem, pencil root, and tuberous root of *I. batatas*. qRT-PCR determined the values from three biological replicates consisting of pools of three plants, and the results were analyzed using the comparative C_T method. The expression of *IbSWEET8.1* in the buds was considered as "1". The fold change is shown in the boxes. Different lowercase letters indicate a significant difference in each *IbSWEET* at $p < 0.05$ based on the Student's *t*-test. (**b**) Gene expression patterns of *ItfSWEETs* in the flower bud, flower, leaf, stem, root 1, and root 2 of *I. trifida* as determined by RNA-seq. The $\log_2$(FPKM) value is shown in the boxes. (**c**) Gene expression patterns of *ItbSWEETs* in the flower bud, flower, leaf, stem, root 1, and root 2 of *I. triloba* as determined by RNA-seq. The $\log_2$(FPKM) value is shown in the boxes.

In addition, we used RNA-seq data of six tissues (i.e., flower bud, flower, leaf, stem, root1, and root2) to study the expression patterns of SWEETs in *I. trifida* and *I. triloba* [43] (Figure 7b,c). In *I. trifida*, *ItfSWEET1.1*, *-2.1*, *-7.1*, *- 9.1*, *-10.1*, *-10.3*, *-10.5*, *-15.1*, and *-16.3* were highly expressed in flowerbuds; *ItfSWEET1.1*, *-1.4*, *-9.1*, *-10.2*, *-10.3*, and *-15.2* were highly expressed in flowers; *ItfSWEET7.4*, *-10.2*, *-10.4*, *-15.2*, and *-16.2* were highly expressed in leaves; and *ItfSWEET1.5*, *-1.6*, *-2.1*, *-9.2*, *-15.1*, and *-16.1* were highly expressed in stems (Figure 7b). Almost all the *ItfSWEETs* had a low expression on levels in root1 and root2, except *ItfSWEET1.6* (16.08-fold in root1). In *I. triloba*, *ItbSWEET1.1*, *-2.1*, *-2.2*, *-6.1*, *-9.1*, and *-15.1* were highly expressed in flowerbuds; *ItbSWEET3.1*, *-5.1*, *-10.1*, *-10.2*, *-10.3*, *-10.4*, *-10.5*, and *-15.3* were highly expressed in flowers; *ItbSWEET1.2*, *-1.4*, *-2.1*, *-6.3*, *-9.2*, *-15.2*, and *-16.2* were highly expressed in leaves; *ItbSWEET2.2* and *ItbSWEET16.1* were highly expressed in stems; and *ItbSWEET1.3*, *-8.1*, and *-16.1* were highly expressed in roots (Figure 7c). These results showed that SWEETs exhibit different expression patterns and play important roles in the growth and development of the sweet potato and the two diploids.

2.6.2. Expression Analysis in Different Developmental Stages

We further performed qRT-PCR to evaluate the expression levels of *IbSWEETs* in different developmental stages of sweet potato roots (i.e., at 3 d, 10 d, 20 d, 30 d, 40 d, 50 d, 60 d, 70 d, 80 d, and 90 d) (Figure 8). Notably, most *IbSWEETs* peaked at 20 d and 50 d, which were the initial development and the rapid expansion stage of tuberous roots, respectively. These results indicate that *IbSWEET*s are of vital importance to the growth and development of tuberous roots in the sweet potato.

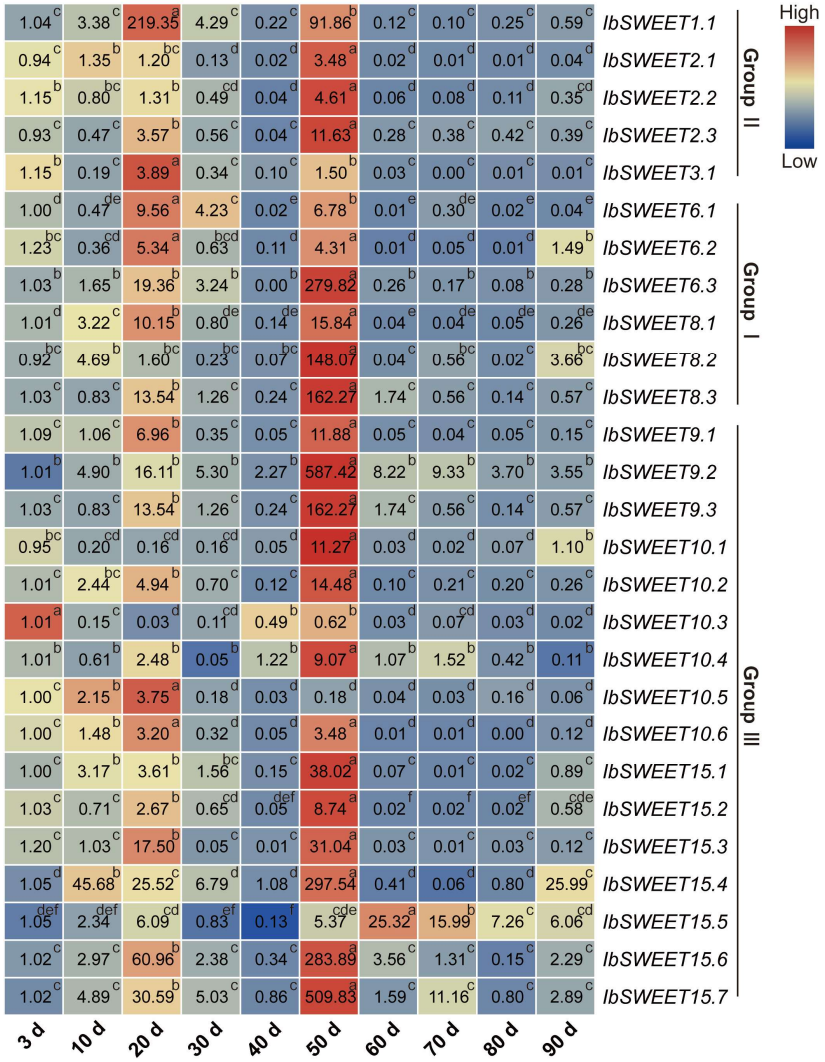

Figure 8. Gene expression patterns of *IbSWEETs* in different root developmental stages (i.e., at 3 d, 10 d, 20 d, 30 d, 40 d, 50 d, 60 d, 70 d, 80 d, and 90 d) as determined by qRT-PCR. The values were determined by qRT-PCR from three biological replicates consisting of pools of three plants, and the results (i.e., at 3 d, 10 d, 20 d, 30 d, 40 d, 50 d, 60 d, 70 d, 80 d, and 90 d) were analyzed using the comparative C_T method. The expression of 3 d was considered as "1". The fold changes are shown in the boxes. Different lowercase letters indicate a significant difference of each *IbSWEET* at $p < 0.05$ based on Student's *t*-test.

2.6.3. Expression Analysis in Different Varieties

We analyzed the expression levels of *IbSWEETs* in sweet potato varieties with different flesh colors (white flesh: Jiyuan3 and Shangshu19; yellow flesh: Longshu9 and Yanshu32; purple flesh: Luozi5 and Qin12-20-11) (Figure 9). Interestingly, the expression levels of most *IbSWEETs* in the yellow-fleshed varieties were higher than those in the white- and

purple-fleshed varieties. This data indicates that *IbSWEET*s may be involved in carotenoid accumulation in sweet potato tuberous roots.

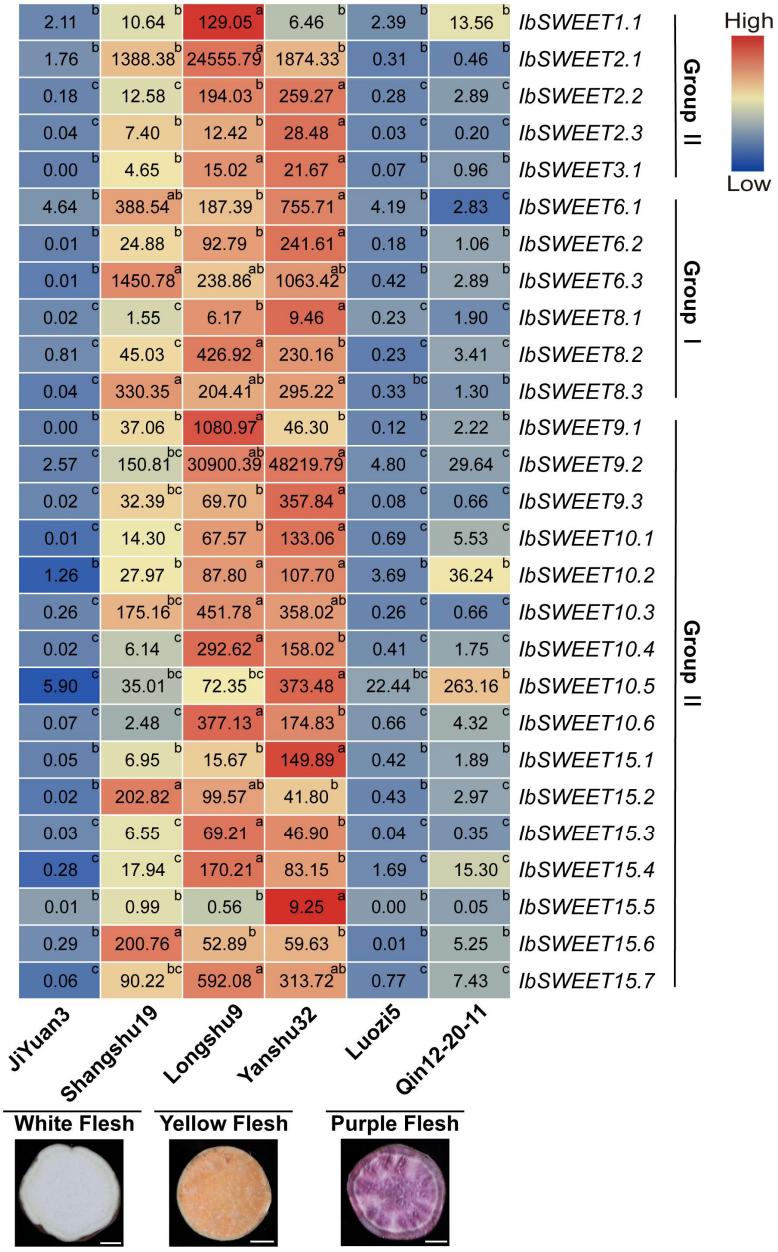

Figure 9. Gene expression patterns of *IbSWEETs* in different sweet potato varieties with different flesh colors. The values were determined by qRT-PCR from three biological replicates consisting of pools of three plants, and the results were analyzed using the comparative C_T method. The expression of *IbSWEET6.2* in Qin-12-20-11 was considered as "1". The fold changes are shown in the boxes. Different lowercase letters indicate a significant difference of each *IbSWEET* at $p < 0.05$ based on Student's *t*-test. Scale bars, 1 cm.

2.6.4. Expression Analysis of Hormone Response

To investigate the potential biological functions of *IbSWEETs* in the hormone signal transduction and crosstalk of plants, we investigated the expressions of SWEETs under various hormonal treatments in order to explore the relationships between SWEETs and hormones. We performed qRT-PCR to evaluate the expression levels of *IbSWEETs* in response to hormones, including ABA, GA, IAA, MeJA, and SA (Figure 10). Under ABA

treatment, *IbSWEET6.3* (10.30-fold), *IbSWEET10.4* (3.76-fold), and *IbSWEET15.7* (4.59-fold) were highly induced (Figure 10a). Under GA treatment, all of the *IbSWEETs* were strongly induced at 0.5 or 1 h (Figure 10b). Under IAA treatment, most of the *IbSWEETs* were repressed, except *IbSWEET9.2*, *-10.5*, and *-15.2* (Figure 10c). Under MeJA, most of the *IbSWEETs* were induced after 24 h. *IbSWEET2.1*, *-2.2*, and *-2.3* were induced by MeJA at all of the time points (Figure 10d). Under SA treatment, most of the *IbSWEETs* were sharply repressed at 0.5 h but induced at other time points (Figure 10e). These results indicate that *IbSWEETs* are differentially expressed in response to various types of hormone induction and that they participate in the crosstalk between various hormones.

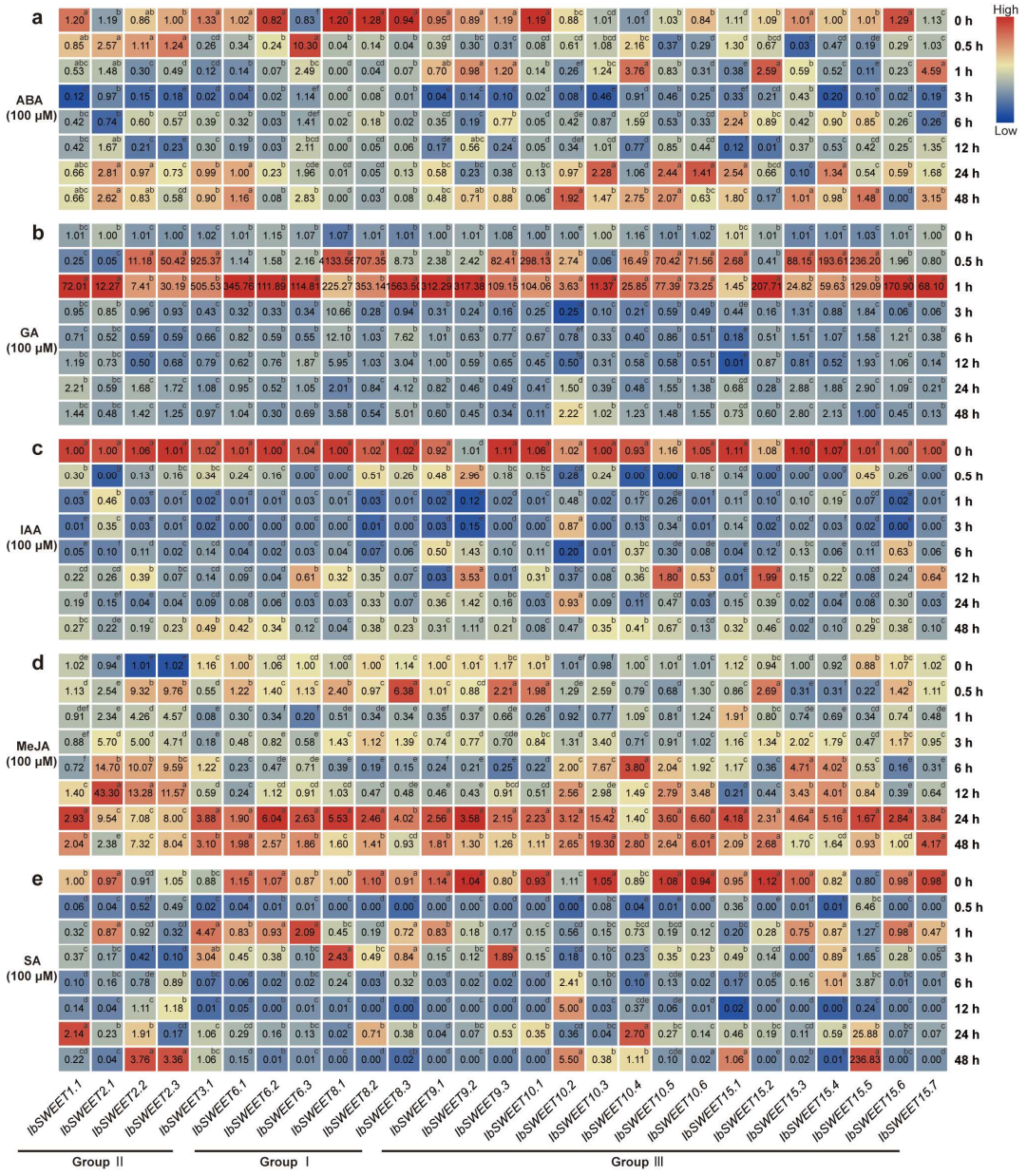

Figure 10. Gene expression patterns of *IbSWEETs* in response to different phytohormones ((**a**) ABA, (**b**) GA, (**c**) IAA, (**d**) MeJA, and (**e**) SA) of *I. batatas*. The values were determined by qRT-PCR from three biological replicates consisting of pools of three plants, and the results were analyzed using the comparative C_T method. The expression of 0 h in each treatment was considered as "1". The fold changes are shown in the boxes. Different lowercase letters indicate a significant difference of each *IbSWEET* at $p < 0.05$ based on Student's *t*-test.

In addition, we analyzed the expression patterns of *ItfSWEETs* and *ItbSWEETs* using the RNA-seq data of *I.trifida* and *I.triloba* under ABA, GA, and IAA treatments. In *I. trifida*, *ItfSWEET1.4*, *-1.6*, *-2.1*, *-7.1*, *-7.2*, *-7.4*, *-10.3*, *-10.5*, *15.1*, *-15.2*, and *-16.1* were induced by ABA. *ItfSWEET1.1*, *-1.3*, *-7.2*, *-7.3*, *-9.1*, *-10.4*, *-10.5*, and *-16.1* were induced by GA3. *ItfSWEET1.3*, *-3.1*, and *-15.1* were induced by IAA. *ItfSWEET16.1* was induced by all the hormones, but *ItfSWEET9.2* and *ItfSWEET10.2* were repressed by all the hormones (Figure 11). In *I.triloba*, the *ItbSWEETs* showed expression patterns that differed from the homologous gene in *I. trifida*. *ItbSWEET2.2*, *-5.1*, *-6.1*, and *-15.3* were induced by ABA. *ItbSWEET1.1*, *-1.2*, *-3.1*, *-6.1*, *-8.1*, *-10.3*, *-15.1*, and *-15.3* were induced by GA3. *ItbSWEET1.1*, *-2.1*, *-8.1*, *-10.5*, *-15.1*, and *-15.3* were induced by IAA. *ItbSWEET15.3* was induced by all the treatments, but *ItbSWEET1.2*, *-9.2*, *-10.2*, and *-16.1* were repressed under all the hormone treatments (Figure 11). These results indicate that *SWEETs* are involved in different hormonal pathways in the sweet potato and its two diploid relatives.

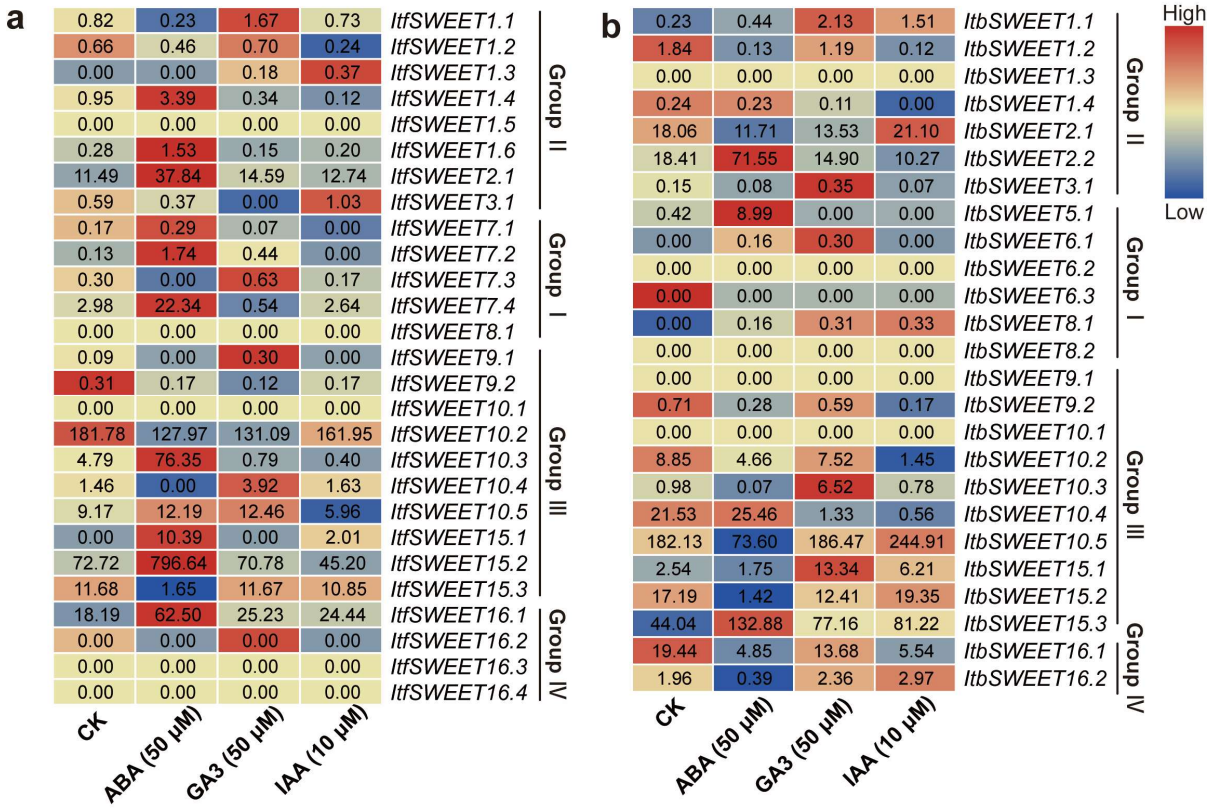

Figure 11. Gene expression patterns of SWEETs in response to different phytohormones (ABA, IAA, and GA) in *I. trifida* (**a**) and *I. triloba* (**b**) as determined by RNA-seq. The $\log_2$(FPKM+1) value is shown in the boxes.

2.6.5. Expression Analysis under Abiotic Stresses

To explore the possible roles of *IbSWEETs* in an abiotic stress response, we analyzed the expression patterns of *IbSWEETs* using the RNA-seq data of a drought-tolerant variety (Xu55-2) under drought stress, and the RNA-seq data of a salt-sensitive variety (Lizixiang) and a salt-tolerant line (ND98) under salt stress [45,46]. *IbSWEET2.1*, *-10.4*, *-15.1*, and *-15.7* were induced by both PEG and NaCl treatments in Xu55-2 and ND98 (Figure 12).

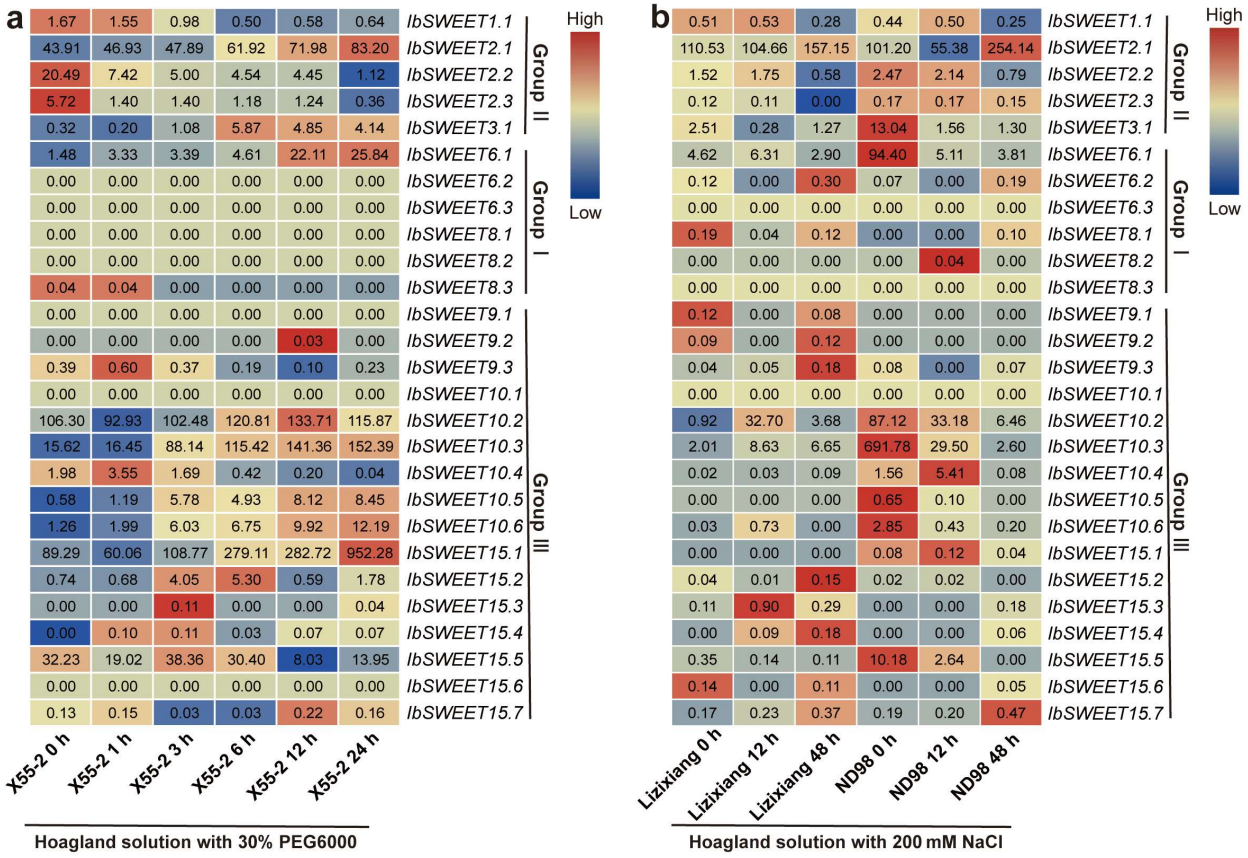

Figure 12. Gene expression patterns of *IbSWEETs* under drought and salt stresses as determined by RNA-seq. (**a**) Expression analysis of *IbSWEETs* under PEG treatment in a drought-tolerant variety, i.e., Xu55-2. (**b**) Expression analysis of *IbSWEETs* under NaCl treatment in a salt-sensitive variety, i.e., Lizixiang, and a salt-tolerant line, i.e., ND98. The $\log_2$(FPKM) value is shown in the boxes.

In addition, we also analyzed the expression patterns of SWEETs using the RNA-seq data of *I. trifida* and *I. triloba* under drought and salt treatments [36]. *ItfSWEET2.1, -7.4, -10.3, -10.5, -15.1, -15.2*, and *-16.2* and *ItbSWEET2.2, -5.1, -10.2, -10.4, -15.1*, and *-15.3* were induced by both drought and salt treatments (Figure S3). Taken together, these results indicate that SWEETs are differentially expressed in response to various abiotic stresses in the sweet potato and its two diploid relatives.

3. Discussion

Sugar transporters are major players in the distribution of photo-assimilates to various heterotrophic sink organs. SWEETs act as key sugar transporters and play a role in crop yield and quality formation, especially in tuberous-root crops [1–8]. However, the functions and transcriptional regulatory mechanisms of SWEETs remain largely unknown in sweet potato. Tuberous roots are the main tissues harvested from sweet potato, but sweet potato's probable progenitor diploids *I.trifida* and *I. triloba* cannot form tuberous roots. Due to the complex genetic background of cultivated sweet potato, recent studies on its gene families have mainly focused on *I.trifida* and *I. triloba* [36,47–49]. In this study, we systematically identified SWEETs and compared their characteristics between cultivated hexaploidy sweet potato and its two diploid relatives based on their genome sequences. A genome-wide study of SWEETs is necessary to gain a better understanding of their functions and the molecular breeding of sweet potato.

3.1. Evolution of the SWEET Gene Family in the Sweet Potato and Its Two Diploid Relatives

In this study, a total of 79 SWEETs were identified in sweet potato and its two diploid relatives. The number of SWEETs identified in *I. batatas* (27) was the same as that in *I. trifida* (27), but there were two fewer in *I. triloba* (25) (Figure 2; Table S1). Genomic alignment revealed the differentiation and evolution of chromosomes [50]. The chromosome localization and distribution of the SWEETs in each chromosome differed between *I. batatas, I. trifida*, and *I. triloba*; 11 chromosomes contained SWEET genes in *I.batatas* and *I. triloba*, but 10 chromosomes contained SWEET genes in *I.trifida* (Figure 2). Based on the phylogenetic relationship, the SWEETs were divided into four subgroups (Group I to IV). There were no IbSWEETs in Group III (Figure 3). Moreover, the number and type of SWEETs distributed in each subgroup of the sweet potato and its two diploid relatives were different from those in *Arabidopsis* and other plants (Figure 3). These results reveal that the SWEET gene family might have undergone a lineage-specific differentiation event in the terrestrial plant genome.

Five conserved motifs were identified in all 79 SWEETs, and all the SWEETs were found to contain a PQ-loop, indicating that these motifs are evolutionarily conserved among the sweet potato and its two diploid relatives. In *Arabidopsis*, four SANT-domain proteins (SANT1-4) were found to form a complex with HDA6 to regulate flowering [37]. Only ItfSWEET9.1 and ItbSWEET9.1, which were highly expressed in the flower and flower bud, were found to contain a SANT domain (Figure 4b). Introns usually act as buffer zones or mutation-resistant fragments that reduce adverse mutations and insertions. Moreover, introns also play essential roles in mRNA export, transcriptional coupling, alternative splicing, gene expression regulation, and other biological processes [50,51]. Here, the exon–intron distributions of some homologous SWEETs were different in *I. batatas* compared with those in *I. trifida* and *I. triloba* (Figure 4c). For example, in Group I, *IbSWEET8.1* contained one intron, but its homologous genes, *ItfSWEET8.1* and *ItbSWEET8.1,* contained five introns. In Group III, *IbSWEET15.1, ItfSWEET15.1*, and *ItbSWEET15.1* contained six, four, and six exons, respectively. In the sweet potato and the two diploids, these differences in the exon–intron structure may result in the different functions carried out by SWEETs in plant development [52–54].

3.2. Different Functions of SWEETs in Tuberous Root Development in Sweet Potato

In plants, SWEETs have been reported to be involved in root development and assimilate accumulation. The *atsweet11* and *atsweet12* double mutants exhibited delayed root development and severe modifications to the chemical composition of the xylem cell wall [19]. The knockout of *OsSWEET11* significantly decreased the sucrose concentration in mutant embryo sacs and led to defective grain filling [27,55]. For the sweet potato, the formation and development of tuberous roots is critical to the roots' yield and quality. Storage-root formation has been considered to be a process of assimilate accumulation [56]. As major transporters governing long-distance transport and sugar accumulation in sink cells, SWEETs may play vital roles in tuberous root development in the sweet potato [12,57]. In this study, most *IbSWEETs* peaked during the initial development stage (20 d) and the rapid expansion stage (50 d) of the tuberous roots, respectively (Figure 8). These results indicate that *IbSWEETs* may participate in tuberous root formation by regulating assimilate accumulation in sweet potato.

The flesh color of the tuberous root is one of the most important quality characteristics of the sweet potato. Most of the *IbSWEETs* were highly expressed in the yellow-fleshed varieties, which are rich in carotenoids (Figure 9). Carotenoids are derived from two isoprene isomers, isopentenyl diphosphate (IPP) and its allylic isomer, dimethylallyl diphosphate (DMAPP). IPP and DMAPP come from the Calvin–Benson cycle by fixed carbon [58,59]. Additionally, SWEETs' transport of sucrose is a key step for fixed-carbon transport in the phloem; thus, they may provide a sufficient precursor substance for carotenoid production in the sweet potato [11,60,61]. These data indicate that *IbSWEETs* may be involved in carotenoid accumulation in sweet potato tuberous roots by transporting photo-assimilates.

However, further study is required to underlie the regulatory mechanisms of SWEETs on tuberous root development and carotenoids accumulation.

3.3. Different Functions of SWEETs in Hormone Crosstalk in the Sweet Potato and Its Two Diploid Relatives

SWEETs have been reported to participate in the regulation of multiple hormones. The interaction between SWEETs and CWINV (cell wall invertase), which encodes an enzyme that catalyzes the hydrolysis of sucrose into glucose and fructose, may lead to the loss of apical dominance and the appearance of multiple shoots under cytokinins [62]. The *atsweet13* and *atsweet14* double mutant line showed function loss in transporting exogenous GA [24–26]. OsSWEET13a was found to be involved in the transport of GA to young leaves during the early developmental stage [24]. The overexpression of *OsSWEET5* inhibited auxin concentration, signaling, and translocation in rice [25]. In this study, each *IbSWEET* gene could be induced by at least two hormones. *IbSWEET2.1*, which contained an ABA-responsive element (i.e., ABRE, and an SA-responsive element, or the TCA motif), was induced by ABA, GA, and MeJA but repressed by IAA and SA. However, *ItbSWEET2.1* was induced by IAA, and there was no significant change in ItfSWEET2.1 under IAA treatment. *IbSWEET8.1*, which contained a TCA motif, was induced by GA, MeJA, and SA but repressed by ABA and IAA treatments (Figure 10). However, *ItbSWEET8.1* was induced by IAA. *IbSWEET15.5*, which contained a GA-responsive element (i.e., the TATC-box, and JA-responsive elements, or a TGACG motif, an ABRE, and a TCA motif), was significantly induced by GA and SA. *IbSWEET15.3*, which contained a TGACG motif and an ABRE was repressed under ABA treatment, but *ItbSWEET15.3* was induced by ABA, GA, and IAA. *ItbSWEET16.1* was repressed under ABA treatment, but *ItfSWEET16.1* was induced by ABA (Figure 11). These results indicate that SWEETs are involved in the crosstalk of multiple hormones and that homologous SWEET genes participate in different hormone pathways in sweet potato and its two diploid relatives (Tables S2 and S3). However, the roles of SWEETs in the regulation of hormone crosstalk still need further investigation.

3.4. Different Functions of SWEETs in Abiotic Stress Response in the Sweet Potato and Its Two Diploid Relatives

SWEETs have been reported to participate in the abiotic stress response in plants. In grapes, *VvSWEET11* and *VvSWEET15* were found to be significantly induced by heat treatment [63]. In Arabidopsis, *AtSWEET15* was highly expressed under cold and salinity treatments [64]. Here, SWEETs were differentially expressed in response to various abiotic stresses in the sweet potato and its two diploid relatives. In the sweet potato, *IbSWEET2.1, -10.4, -15.1,* and *-15.7* were induced by both PEG and NaCl treatments in Xu55-2 and ND98 (Figure 12). Moreover, the diploids *I. trifida* and *I. triloba* could be used to discover functional genes, particularly genes conferring resistance or tolerance to biotic and abiotic stress, which were possibly lost in the cultivated sweet potato during its domestication [57]. In the two diploid relatives, *ItfSWEET2.1, -7.4, -10.3, -10.5, -15.1, -15.2,* and *-16.2* and *ItbSWEET2.2, -5.1, -10.2, -10.4, -15.1,* and *-15.3* were induced by both drought and salt treatments (Figure S3). These SWEETs may serve as candidate genes for use in improving abiotic stress tolerance in sweet potato.

4. Materials and Methods

4.1. Identification of SWEETs

The whole-genome sequences of *I. batatas*, *I. trifida*, and *I. triloba* were downloaded from the *Ipomoea* Genome Hub (https://ipomoea-genome.org/, accessed on 26 July 2022) and the Sweetpotato Genomics Resource (http://sweetpotato.plantbiology.msu.edu/, accessed on 26 July 2022). To accurately identify all the SWEET family members, three different screening methods were combined. First, the BLAST algorithm was used to identify the predicted SWEETs using all the *AtSWEETs* from the *Arabidopsis* genome database (https://www.arabidopsis.org/, accessed on 27 July 2022) as queries (BLASTP, E value $\leq 1 \times 10^{-5}$). Next, the HMMER 3.0 software was used to identify potential

SWEETs through the Hidden Markov Model profiles (hmmsearch, E value $\leq 1 \times 10^{-5}$) of the PQ-loop domain (pfam04193), which were extracted from the Pfam databases (http://pfam.xfam.org/, accessed on 27 July 2022). Finally, all the putative SWEETs were ensured using SMART (http://smart.embl-heidelberg.de/, accessed on 27 July 2022) and CD-search (https://www.ncbi.nlm.nih.gov/Structure/cdd/wrpsb.cgi, accessed on 27 July 2022).

4.2. Chromosomal Distribution of SWEETs

The *IbSWEETs*, *ItfSWEETs*, and *ItbSWEETs* were separately mapped to the *I. batatas*, *I. trifida*, and *I. triloba* chromosomes, respectively, based on the chromosomal locations provided in the *Ipomoea* Genome Hub (https://ipomoea-genome.org/, accessed on 2 August 2022) and Sweetpotato Genomics Resource (http://sweetpotato.plantbiology.msu.edu/, accessed on 2 August 2022). The visualization was generated using the TBtools software (v.1.098696) (South China Agricultural University, Guangzhou, China) [65].

4.3. Protein Properties Prediction of SWEETs

The MW, theoretical pI, unstable index, and hydrophilic of the SWEETs were calculated using ExPASy (https://www.expasy.org/, accessed on 4 August 2022). The phosphorylation sites of the SWEETs were predicted using GPS 5.0 [66]. The subcellular localization of the SWEETs was predicted using Plant-mPLoc (http://www.csbio.sjtu.edu.cn/bioinf/plant-multi/, accessed on 4 August 2022). The TMHs of the SWEETs were predicted using TMHMM-2.0 (https://services.healthtech.dtu.dk/service.php?TMHMM-2.0, accessed on 4 August 2022). The 3D structural model of the SWEETs was built using SWISS-MODEL (https://swissmodel.expasy.org/, accessed on 4 August 2022) [67]

4.4. Phylogenetic Analysis of SWEETs

Multiple sequence alignment of the deduced amino acid sequences of the SWEETs from *I. batatas*, *I. trifida*, *I. triloba*, *Arabidopsis*, *Zea mays*, and *Oryza sativa* were aligned with Clustal X, and the alignment was imported into MEGA11 to create a phylogenetic tree using the neighbor-joining method with 1000 bootstrap replicates (www.megasoftware.net, accessed on 3 December 2022) [68]. Then, the phylogenetic tree was constructed using iTOL (http://itol.embl.de/, accessed on 3 December 2022).

4.5. Domain Identification and Conserved Motif Analysis of SWEETs

The conserved motifs of the SWEETs were analyzed using MEME software (https://meme-suite.org/meme/, accessed on 5 August 2022). The MEME parameters were set to search for a maximum of 15 motifs with a motif width comprised between 5 and 50 residues [69].

4.6. Exon–Intron Structures and Promoter Analysis of SWEETs

The exon–intron structures of the SWEETs were obtained from GSDS 2.0 (http://gsds.gao-lab.org/, accessed on 6 August 2022) and were visualized using the TBtools software. The *cis*-elements in the approximately 1500 bp promoter region of the SWEETs were predicted using PlantCARE (http://bioinformatics.psb.ugent.be/webtools/plantcare/html/, accessed on 6 August 2022) [70].

4.7. Protein Interaction Network of SWEETs

The protein interaction networks of the SWEETs were predicted using STRING (https://cn.string-db.org/, accessed on 7 August 2022) based on *Arabidopsis* homologous proteins. The network map was built using Cytoscape software [71].

4.8. qRT-PCR Analysis of SWEETs

The salt-tolerant sweet potato (*I. batatas*) line ND98 was used for qRT-PCR analysis in this study [45]. In vitro grown ND98 plants were cultured on Murashige and Skoog (MS)

medium at 27 ± 1 °C under a photoperiod consisting of 13 h of cool-white fluorescent light at 54 μmol m^{-2} s^{-1} and 11 h of darkness. The sweet potato plants were cultivated in a field in the campus of China Agricultural University, Beijing, China.

For expression analysis in various tissues, the total RNA was extracted from the buds, leaves, petioles, stems, pencil roots, and tuberous root tissues of 3-month-old field-grown ND98 plants; the different development stage of the tuberous root tissues of Y25 (3 d, 10 d, 20 d, 30 d, 40 d, 50 d, 60 d, 70 d, 80 d, and 90 d) and the tuberous root tissues of different field-grown plants at 90 d (Jiyuan3, Shangshu19, Longshu9, Yanshu32, Luozi5, and Qin12-20-11) were analyzed using the TRIzol method (Invitrogen). For the expression analysis of the hormone treatment, the leaves were sampled at 0, 0.5, 1, 3, 6, 12, 24, and 48 h after being treated with 100 μM ABA, 100 μM GA, 100 μM IAA, 100 μM MeJA, and 100 μM SA, respectively. Three independent biological replicates were taken, each with three plants. qRT-PCR was conducted using the SYBR detection protocol (TaKaRa, Kyoto, Japan) on a 7500 Real-Time PCR system (Applied Biosystems, Foster City, CA, USA). The reaction mixture was composed of first-strand cDNA, a primer mix, and an SYBR Green M Mix (TaKaRa; code RR420A) with a final volume of 20 μL. A sweet potato actin gene (GenBank AY905538) was used as an internal control. The relative gene expression levels were quantified using the comparative C_T method [72]. The specific primers used for the qRT-PCR analysis are listed in Table S4. The heat maps of the gene expression profiles were constructed using the TBtools software (v.1.098696) [65].

4.9. Transcriptome Analysis

The RNA-seq data of *ItfSWEETs* and *ItbSWEETs* in *I. trifida* and *I. triloba* were downloaded from the Sweetpotato Genomics Resource (http://sweetpotato.plantbiology.msu.edu/, accessed on 10 August 2022). The RNA-seq data of *IbSWEETs* in *I. batatas* were obtained from the NCBI SRA repository under the accession number SRP092215 [45,46]. The expression levels of the SWEETs were calculated as fragments per kilobase of exon per million fragments mapped (FPKM). The heat maps were constructed using the Tbtools software (v.1.098696) [65].

5. Conclusions

In this study, we identified and characterized 27, 27, and 25 SWEETs in cultivated hexaploidy sweet potato (*I. batatas*, 2n = 6x = 90) and its two diploid relatives, *I. trifida* (2n = 2x = 30) and *I. triloba* (2n = 2x = 30), respectively, based on genome and transcriptome data. The protein physicochemical properties, chromosome localization, phylogenetic relationships, gene structures, promoter *cis*-elements, and protein interaction networks of these 79 SWEETs were systematically investigated. Moreover, the tissue specificity and expression patterns of the SWEETs in tuberous root development, hormone responses, and abiotic stress responses were analyzed using qRT-PCR and RNA-seq. The results indicated that there was a differentiation in the functions of homologous SWEETs in the sweet potato and its two diploid relatives, and each SWEET gene played different vital roles in the plants' growth and development, carotenoid accumulation, hormone crosstalk, and abiotic stress response. This study provides valuable insights into the structure and function of SWEET genes in the sweet potato and its two diploid relatives.

Supplementary Materials: The supporting information can be downloaded at: https://www.mdpi.com/article/10.3390/ijms232415848/s1.

Author Contributions: H.Z. (Huan Zhang) and S.H. conceived and designed the research; Z.D., P.Y., L.J., Y.W. and N.Z. performed the experiments; Z.D., H.Z. (Huan Zhang) and S.G. analyzed the data; H.Z. (Huan Zhang) and Z.D. wrote the paper; Y.W., Q.L. and H.Z. (Hong Zhai) revised the paper. All authors have read and agreed to the published version of the manuscript.

Funding: This work was supported by grants from the Project of Sanya Yazhou Bay Science and Technology City (grant no. SCKJ-JYRC-2022-61/SYND-2022-09), the Beijing Natural Science Foundation (grant no. 6212017), the National Natural Science Foundation of China (grant no. 31901584),

the Beijing Food Crops Innovation Consortium Program (BAIC02-2022), the earmarked fund for CARS-10-Sweetpotato, and the Chinese Universities Scientific Fund (2022TC003).

Data Availability Statement: The data presented in this study are available on request from the corresponding author.

Conflicts of Interest: The authors declare no conflict of interest.

References

1. Wang, J.; Yan, C.; Li, Y.; Hirata, K.; Yamamoto, M.; Yan, N.; Hu, Q. Crystal structure of a bacterial homologue of SWEET transporters. *Cell Res.* **2014**, *24*, 1486–1489. [CrossRef] [PubMed]
2. Feng, L.; Frommer, W.B. Structure and function of SemiSWEET and SWEET sugar transporters. *Trends Biochem. Sci.* **2015**, *40*, 480–486. [CrossRef] [PubMed]
3. Xuan, Y.H.; Hu, Y.B.; Chen, L.Q.; Sosso, D.; Ducat, D.C.; Hou, B.H.; Frommer, W.B. Functional role of oligomerization for bacterial and plant SWEET sugar transporter family. *Proc. Natl. Acad. Sci. USA* **2013**, *110*, E3685–E3694. [CrossRef] [PubMed]
4. Anjali, A.; Fatima, U.; Manu, M.S.; Ramasamy, S.; Senthil-Kumar, M. Structure and regulation of SWEET transporters in plants: An update. *Plant Physiol. Biochem.* **2020**, *156*, 1–6. [CrossRef] [PubMed]
5. Gamas, P.; de Carvalho-Niebel, F.; Lescure, N.; Cullimore, J.V. Use of a subtractive hybridization approach to identify new Medicago truncatula genes induced during root nodule development. *Mol. Plant Microbe Interact.* **1996**, *9*, 233–242. [CrossRef]
6. Tao, Y.Y.; Cheung, L.S.; Li, S.; Eom, J.S.; Chen, L.Q.; Xu, Y.; Perry, K.; Frommer, W.B.; Feng, L. Structure of a eukaryotic SWEET transporter in a homotrimeric complex. *Nature* **2015**, *527*, 259–263. [CrossRef]
7. Lee, Y.; Nishizawa, T.; Yamashita, K.; Ishitani, R.; Nureki, O. Structural basis for the facilitative diffusion mechanism by SemiSWEET transporter. *Nat. Commun.* **2015**, *6*, 6112. [CrossRef]
8. Xu, Y.; Tao, Y.; Cheung, L.S.; Fan, C.; Chen, L.-Q.; Xu, S.; Perry, K.; Frommer, W.B.; Feng, L. Structures of bacterial homologues of SWEET transporters in two distinct conformations. *Nature* **2014**, *515*, 448–452. [CrossRef]
9. Chen, L.Q.; Hou, B.H.; Lalonde, S.; Takanaga, H.; Hartung, M.L.; Qu, X.Q.; Guo, W.J.; Kim, J.G.; Underwood, W.; Chaudhuri, B.; et al. Sugar transporters for intercellular exchange and nutrition of pathogens. *Nature* **2010**, *468*, 527–532. [CrossRef]
10. Gao, Y.; Zhang, C.; Han, X.; Wang, Z.Y.; Ma, L.; Yuan, D.P.; Wu, J.N.; Zhu, X.F.; Liu, J.M.; Li, D.P.; et al. Inhibition of OsSWEET11 function in mesophyll cells improves resistance of rice to sheath blight disease. *Mol. Plant Pathol.* **2018**, *19*, 2149–2161. [CrossRef]
11. Chen, L.Q.; Qu, X.Q.; Hou, B.H.; Sosso, D.; Osorio, S.; Fernie, A.R.; Frommer, W.B. Sucrose efflux mediated by SWEET proteins as a key step for phloem transport. *Science* **2012**, *335*, 207–211. [CrossRef] [PubMed]
12. Reinders, A.; Schulze, W.; Kuhn, C.; Barker, L.; Schulz, A.; Ward, J.M.; Frommer, W.B. Protein-protein interactions between sucrose transporters of different affinities colocalized in the same enucleate sieve element. *Plant Cell* **2002**, *14*, 1567–1577. [CrossRef] [PubMed]
13. Yuan, M.; Wang, S. Rice MtN3/Saliva/SWEET family genes and their homologs in cellular organisms. *Mol. Plant* **2013**, *6*, 665–674. [CrossRef] [PubMed]
14. Manck-Goetzenberger, J.; Requena, N. Arbuscular mycorrhiza symbiosis induces a major transcriptional reprogramming of the potato SWEET sugar transporter family. *Front. Plant Sci.* **2016**, *7*, 487. [CrossRef] [PubMed]
15. Patil, G.; Valliyodan, B.; Deshmukh, R.; Prince, S.; Nicander, B.; Zhao, M.Z.; Sonah, H.; Song, L.; Lin, L.; Chaudhary, J.; et al. Soybean (*Glycine max*) SWEET gene family: Insights through comparative genomics, transcriptome profiling and whole genome re-sequence analysis. *BMC Genom.* **2015**, *16*, 520. [CrossRef] [PubMed]
16. Guo, W.-J.; Nagy, R.; Chen, H.-Y.; Pfrunder, S.; Yu, Y.-C.; Santelia, D.; Frommer, W.B.; Martinoia, E. SWEET17, a facilitative transporter, mediates fructose transport across the tonoplast of Arabidopsis roots and leaves. *Plant Physiol.* **2014**, *164*, 777–789. [CrossRef]
17. Engel, M.L.; Holmes-Davis, R.; McCormick, S. Green sperm. Identification of male gamete promoters in arabidopsis. *Plant Physiol.* **2005**, *138*, 2124–2133. [CrossRef]
18. Chen, H.Y.; Huh, J.H.; Yu, Y.C.; Ho, L.H.; Chen, L.Q.; Tholl, D.; Frommer, W.B.; Guo, W.J. The Arabidopsis vacuolar sugar transporter SWEET2 limits carbon sequestration from roots and restricts *Pythium* infection. *Plant J.* **2015**, *83*, 1046–1058. [CrossRef]
19. Le Hir, R.; Spinner, L.; Klemens, P.A.W.; Chakraborti, D.; de Marco, F.; Vilaine, F.; Wolff, N.; Lemoine, R.; Porcheron, B.; Gery, C.; et al. Disruption of the sugar transporters AtSWEET11 and AtSWEET12 affects vascular development and freezing tolerance in Arabidopsis. *Mol. Plant.* **2015**, *8*, 1687–1690. [CrossRef]
20. Abelenda, J.A.; Bergonzi, S.; Oortwijn, M.; Sonnewald, S.; Du, M.; Visser, R.G.F.; Sonnewald, U.; Bachem, C.W.B. Source-Sink regulation is mediated by interaction of an ft homolog with a SWEET protein in potato. *Curr. Biol.* **2019**, *29*, 1178–1186. [CrossRef]
21. Ni, J.; Li, J.; Zhu, R.; Zhang, M.; Qi, K.; Zhang, S.; Wu, J. Overexpression of sugar transporter gene *PbSWEET4* of pear causes sugar reduce and early senescence in leaves. *Gene* **2020**, *743*, 144582. [CrossRef] [PubMed]
22. Guan, Y.F.; Huang, X.Y.; Zhu, J.; Gao, J.F.; Zhang, H.X.; Yang, Z.N. RUPTURED POLLEN GRAIN1, a member of the MtN3/saliva gene family, is crucial for exine pattern formation and cell integrity of microspores in arabidopsis. *Plant Physiol.* **2008**, *147*, 852–863. [CrossRef] [PubMed]

23. Wang, S.; Liu, S.; Wang, J.; Yokosho, K.; Zhou, B.; Yu, Y.-C.; Liu, Z.; Frommer, W.B.; Ma, J.F.; Chen, L.-Q.; et al. Simultaneous changes in seed size, oil content and protein content driven by selection of SWEET homologues during soybean domestication. *Nat. Sci. Rev.* **2020**, *7*, 1776–1786. [CrossRef] [PubMed]
24. Kanno, Y.; Oikawa, T.; Chiba, Y.; Ishimaru, Y.; Shimizu, T.; Sano, N.; Koshiba, T.; Kamiya, Y.; Ueda, M.; Seo, M. AtSWEET13 and AtSWEET14 regulate gibberellin-mediated physiological processes. *Nat. Commun.* **2016**, *7*, 13245. [CrossRef] [PubMed]
25. Morii, M.; Sugihara, A.; Takehara, S.; Kanno, Y.; Kawai, K.; Hobo, T.; Hattori, M.; Yoshimura, H.; Seo, M.; Ueguchi-Tanaka, M. The dual function of OsSWEET3a as a gibberellin and glucose transporter is important for young shoot development in rice. *Plant Cell Physiol.* **2020**, *61*, 1935–1945. [CrossRef]
26. Zhou, Y.; Liu, L.; Huang, W.; Yuan, M.; Zhou, F.; Li, X.; Lin, Y. Overexpression of *OsSWEET5* in rice causes growth retardation and precocious senescence. *PLoS ONE* **2014**, *9*, e94210. [CrossRef]
27. Bezrutczyk, M.; Hartwig, T.; Horschman, M.; Char, S.N.; Yang, J.; Yang, B.; Frommer, W.B.; Sosso, D. Impaired phloem loading in *zmsweet13a,b,c* sucrose transporter triple knock-out mutants in *Zea mays*. *New Phytol.* **2018**, *218*, 594–603. [CrossRef]
28. Li, Y.; Wang, Y.; Zhang, H.; Zhang, Q.; Zhai, H.; Liu, Q.; He, S. The Plasma membrane-localized sucrose transporter IbSWEET10 Contributes to the resistance of sweet potato to *Fusarium oxysporum*. *Front. Plant Sci.* **2017**, *8*, 197. [CrossRef]
29. Hu, B.; Wu, H.; Huang, W.; Song, J.; Zhou, Y.; Lin, Y. *SWEET* gene family in *Medicago truncatula*: Genome-wide identification, expression and substrate specificity analysis. *Plants* **2019**, *8*, 338. [CrossRef]
30. Hu, L.; Zhang, F.; Song, S.; Yu, X.; Ren, Y.; Zhao, X.; Liu, H.; Liu, G.; Wang, Y.; He, H. *CsSWEET2*, a hexose transporter from cucumber (*Cucumis sativus* L.), affects sugar metabolism and improves cold tolerance in Arabidopsis. *Int. J. Mol. Sci.* **2022**, *31*, 23. [CrossRef]
31. Liu, Q.C. Improvement for agronomically important traits by gene engineering in sweetpotato. *Breed. Sci.* **2017**, *67*, 15–26. [CrossRef]
32. Nhanala, S.E.C.; Yencho, G.C. Assessment of the potential of wild *Ipomoea spp.* for the improvement of drought tolerance in cultivated sweetpotato *Ipomoea batatas* (L.) Lam. *Crop. Sci.* **2021**, *61*, 234–249. [CrossRef]
33. Nakatani, M.; Komeichi, M. Changes in the endogenous level of zeatin riboside, abscisic-acid and indole acetic-acid during formation and thickening of tuberous roots in sweet-potato. *Jpn. J. Crop. Sci.* **1991**, *60*, 91–100. [CrossRef]
34. Komaki, K.; Katayama, K. Root thickness of diploid *Ipomoea trifida* (H. B. K.) G. Don and performance of progeny derived from the cross with sweetpotato. *Breed. Sci.* **1999**, *49*, 123–129. [CrossRef]
35. Yang, J.; Moeinzadeh, M.H.; Kuhl, H.; Helmuth, J.; Xiao, P.; Haas, S.; Liu, G.L.; Zheng, J.L.; Sun, Z.; Fan, W.J.; et al. Haplotype-resolved sweet potato genome traces back its hexaploidization history. *Nat. Plants* **2017**, *3*, 696–703. [CrossRef]
36. Wu, S.; Lau, K.H.; Cao, Q.H.; Hamilton, J.P.; Sun, H.H.; Zhou, C.X.; Eserman, L.; Gemenet, D.C.; Olukolu, B.A.; Wang, H.Y.; et al. Genome sequences of two diploid wild relatives of cultivated sweetpotato reveal targets for genetic improvement. *Nat. Commun.* **2018**, *9*, 4580. [CrossRef]
37. Zhou, X.; He, J.; Velanis, C.N.; Zhu, Y.; He, Y.; Tang, K.; Zhu, M.; Graser, L.; de Leau, E.; Wang, X.; et al. A domesticated Harbinger transposase forms a complex with HDA6 and promotes histone H3 deacetylation at genes but not TEs in Arabidopsis. *J. Integr. Plant Biol.* **2021**, *63*, 1462–1474. [CrossRef]
38. Paxson-Sowders, D.M.; Dodrill, C.H.; Owen, H.A.; Makaroff, C.A. DEX1, a novel plant protein, is required for exine pattern formation during pollen development in Arabidopsis. *Plant Physiol.* **2001**, *127*, 1739–1749. [CrossRef]
39. Toda, Y.; Kudo, T.; Kinoshita, T.; Nakamichi, N. Evolutionary insight into the clock-associated PRR5 transcriptional network of flowering plants. *Sci. Rep.* **2019**, *9*, 2983. [CrossRef]
40. Yan, J.; Li, X.; Zeng, B.; Zhong, M.; Yang, J.; Yang, P.; Li, X.; He, C.; Lin, J.; Liu, X.; et al. FKF1 F-box protein promotes flowering in part by negatively regulating DELLA protein stability under long-day photoperiod inArabidopsis. *J. Integr. Plant Biol.* **2020**, *62*, 1717–1740. [CrossRef]
41. Choi, S.; Prokchorchik, M.; Lee, H.; Gupta, R.; Lee, Y.; Chung, E.-H.; Cho, B.; Kim, M.-S.; Kim, S.T.; Sohn, K.H. Direct acetylation of a conserved threonine of RIN4 by the bacterial effector HopZ5 or AvrBsT activates RPM1-dependent immunity in Arabidopsis. *Mol. Plant* **2021**, *14*, 1951–1960. [CrossRef] [PubMed]
42. Redditt, T.J.; Chung, E.-H.; Zand Karimi, H.; Rodibaugh, N.; Zhang, Y.; Trinidad, J.C.; Kim, J.H.; Zhou, Q.; Shen, M.; Dangl, J.L.; et al. AvrRpm1 Functions as an ADP-Ribosyl Transferase to Modify NOI-domain Containing Proteins, Including Arabidopsis and Soybean RPM1-interacting Protein 4. *Plant Cell* **2019**, 2664–2681. [CrossRef] [PubMed]
43. Huang, K.-C.; Lin, W.-C.; Cheng, W.-H. Salt hypersensitive mutant 9, a nucleolar APUM23 protein, is essential for salt sensitivity in association with the ABA signaling pathway in Arabidopsis. *BMC Plant Biol.* **2018**, *18*, 40. [CrossRef] [PubMed]
44. Vatov, E.; Ludewig, U.; Zentgraf, U. Disparate dynamics of gene body and cis-regulatory element evolution illustrated for the senescence-associated cysteine protease gene *SAG12* of plants. *Plants* **2021**, *10*, 1380. [CrossRef] [PubMed]
45. Zhu, H.; Zhou, Y.; Zhai, H.; He, S.; Zhao, N.; Liu, Q. Transcriptome profiling reveals insights into the molecular mechanism of drought tolerance in sweetpotato. *J. Integr. Agri.* **2019**, *18*, 9–23. [CrossRef]
46. Zhang, H.; Zhang, Q.; Zhai, H.; Li, Y.; Wang, X.; Liu, Q.; He, S. Transcript profile analysis reveals important roles of jasmonic acid signalling pathway in the response of sweet potato to salt stress. *Sci. Rep.* **2017**, *7*, 40819. [CrossRef]
47. Li, Y.; Zhang, L.; Zhu, P.; Cao, Q.; Sun, J.; Li, Z.; Xu, T. Genome-wide identification, characterisation and functional evaluation of *WRKY* genes in the sweet potato wild ancestor *Ipomoea trifida* (HBK) G. Don. under abiotic stresses. *BMC Genet.* **2019**, *20*, 90. [CrossRef] [PubMed]

48. Lu, Y.; Sun, J.; Yang, Z.; Zhao, C.; Zhu, M.; Ma, D.; Dong, T.; Zhou, Z.; Liu, M.; Yang, D.; et al. Genome-wide identification and expression analysis of glycine-rich RNA-binding protein family in sweet potato wild relative *Ipomoea trifida*. *Gene* **2019**, *686*, 177–186. [CrossRef]
49. Wan, R.; Liu, J.; Yang, Z.; Zhu, P.; Cao, Q.; Xu, T. Genome-wide identification, characterisation and expression profile analysis of DEAD-box family genes in sweet potato wild ancestor *Ipomoea trifida* under abiotic stresses. *Genes Genom.* **2020**, *42*, 325–335. [CrossRef]
50. Mukherjee, D.; Saha, D.; Acharya, D.; Mukherjee, A.; Chakraborty, S.; Ghosh, T.C. The role of introns in the conservation of the metabolic genes of *Arabidopsis thaliana*. *Genomics* **2018**, *110*, 310–317. [CrossRef]
51. Morello, L.; Giani, S.; Troina, F.; Breviario, D. Testing the IMEter on rice introns and other aspects of intron-mediated enhancement of gene expression. *J. Exp. Bot.* **2011**, *62*, 533–544. [CrossRef]
52. Ma, J.; Deng, S.; Jia, Z.; Sang, Z.; Zhu, Z.; Zhou, C.; Ma, L.; Chen, F. Conservation and divergence of ancestral *AGAMOUS/SEEDSTICK* subfamily genes from the basal angiosperm *Magnolia wufengensis*. *Tree Physiol.* **2020**, *40*, 90–107. [CrossRef]
53. Ma, R.; Song, W.; Wang, F.; Cao, A.; Xie, S.; Chen, X.; Jin, X.; Li, H. A Cotton (*Gossypium hirsutum*) *Myo*-Inositol-1-Phosphate Synthase (*GhMIPS1D*) gene promotes root cell elongation in *Arabidopsis*. *Int. J. Mol. Sci.* **2019**, *20*, 1224. [CrossRef]
54. Pang, X.; Wei, Y.; Cheng, Y.; Pan, L.; Ye, Q.; Wang, R.; Ruan, M.; Zhou, G.; Yao, Z.; Li, Z.; et al. The Tryptophan decarboxylase in *Solanum lycopersicum*. *Molecules* **2018**, *23*, 5. [CrossRef]
55. Ma, L.; Zhang, D.; Miao, Q.; Yang, J.; Xuan, Y.; Hu, Y. Essential role of sugar transporter OsSWEET11 during the early stage of rice grain filling. *Plant Cell Physiol.* **2017**, *58*, 863–873. [CrossRef]
56. Rukundo, P.; Shimelis, H.; Laing, M.; Gahakwa, D. Storage root formation, dry matter synthesis, accumulation and genetics in sweet potato. *Aust. J. Crop. Sci.* **2013**, *7*, 2054–2061.
57. Bihmidine, S.; Julius, B.T.; Dweikat, I.; Braun, D.M. Tonoplast Sugar Transporters (SbTSTs) putatively control sucrose accumulation in sweet sorghum stems. *Plant Signal. Behav.* **2016**, *11*, e1117721. [CrossRef]
58. Michelet, L.; Zaffagnini, M.; Morisse, S.; Sparla, F.; Perez-Perez, M.E.; Francia, F.; Danon, A.; Marchand, C.H.; Fermani, S.; Trost, P.; et al. Redox regulation of the Calvin-Benson cycle: Something old, something new. *Front. Plant Sci.* **2013**, *4*, 470. [CrossRef]
59. Nisar, N.; Li, L.; Lu, S.; Khin, N.C.; Pogson, B.J. Carotenoid metabolism in plants. *Mol. Plant* **2015**, *8*, 68–82. [CrossRef]
60. Hu, Z.; Tang, Z.; Zhang, Y.; Niu, L.; Yang, F.; Zhang, D.; Hu, Y. Rice SUT and SWEET transporters. *Int. J. Mol. Sci.* **2021**, *22*, 20. [CrossRef]
61. Mizuno, H.; Kasuga, S.; Kawahigashi, H. The sorghum *SWEET* gene family: Stem sucrose accumulation as revealed through transcriptome profiling. *Biotechnol. Biofuels* **2016**, *9*, 127. [CrossRef]
62. Jameson, P.E.; Dhandapani, P.; Novak, O.; Song, J. Cytokinins and expression of *SWEET, SUT, CWINV* and *AAP* genes increase as *pea seeds* germinate. *Int. J. Mol. Sci.* **2016**, *17*, 12. [CrossRef]
63. Conde, A.; Soares, F.; Breia, R.; Geros, H. Postharvest dehydration induces variable changes in the primary metabolism of grape berries. *Food Res. Int.* **2018**, *105*, 261–270. [CrossRef]
64. Durand, M.; Porcheron, B.; Hennion, N.; Maurousset, L.; Lemoine, R.; Pourtau, N. Water deficit enhances C export to the roots in *Arabidopsis thaliana* plants with contribution of sucrose transporters in both shoot and roots. *Plant Physiol.* **2016**, *170*, 1460–1479. [CrossRef]
65. Chen, C.; Chen, H.; Zhang, Y.; Thomas, H.R.; Frank, M.H.; He, Y.; Xia, R. TBtools: An integrative toolkit developed for interactive analyses of big biological data. *Mol Plant* **2020**, *13*, 1194–1202. [CrossRef]
66. Wang, C.; Xu, H.; Lin, S.; Deng, W.; Zhou, J.; Zhang, Y.; Shi, Y.; Peng, D.; Xue, Y. GPS 5.0: An update on the prediction of kinase-specific phosphorylation sites in proteins. *Genom. Proteom. Bioinform.* **2020**, *18*, 72–80. [CrossRef]
67. Kopp, J.; Schwede, T. The SWISS-MODEL Repository of annotated three-dimensional protein structure homology models. *Nucleic Acids Res.* **2004**, *32*, D230–D234. [CrossRef]
68. Thompson, J.D.; Gibson, T.J.; Plewniak, F.; Jeanmougin, F.; Higgins, D.G. The Clustal_X windows interface: Flexible strategies for multiple sequence alignment aided by quality analysis Tools. *Nucleic Acids Res.* **1997**, *25*, 4876–4882. [CrossRef]
69. Bailey, T.L.; Johnson, J.; Grant, C.E.; Noble, W.S. The MEME Suite. *Nucleic Acids Res.* **2015**, *43*, W39–W49. [CrossRef]
70. Lescot, M.; Dehais, P.; Thijs, G.; Marchal, K.; Moreau, Y.; Van de Peer, Y.; Rouze, P.; Rombauts, S. PlantCARE, a database of plant cis-acting regulatory elements and a portal to tools for in silico analysis of promoter sequences. *Nucleic Acids Res.* **2002**, *30*, 325–327. [CrossRef]
71. Kohl, M.; Wiese, S.; Warscheid, B. Cytoscape: Software for visualization and analysis of biological networks. *Methods Mol. Biol.* **2011**, *696*, 291–303. [PubMed]
72. Schmittgen, T.D.; Livak, K.J. Analyzing real-time PCR data by the comparative C-T method. *Nat. Protoc.* **2008**, *3*, 1101–1108. [CrossRef] [PubMed]

ARTICLES FOR FACULTY MEMBERS

INVESTIGATING THE ROLE OF GIBBERELLIC ACID (GA) AND ABSCISIC ACID (ABA) CROSS-TALK IN ENHANCING TUBEROUS ROOT DEVELOPMENT IN SWEET POTATOES

IbMYB73 targets abscisic acid-responsive IbGER5 to regulate root growth and stress tolerance in sweet potato / Wang, Z., Li, X., Gao, X. R., Dai, Z. R., Peng, K., Jia, L. C., Wu, Y. K., Liu, Q. C., Zhai, H., Gao, S. P., Zhao, N., He, S. Z., & Zhang, H.

Plant Physiology
Volume 194 Issue 2 (2024) Pages 787–804
https://doi.org/10.1093/plphys/kiad532
(Database: Oxford Academic)

https://doi.org/10.1093/plphys/kiad532 PLANT PHYSIOLOGY 2024: 194: 787–804

Plant Physiology®

Research Article

IbMYB73 targets abscisic acid-responsive *IbGER5* to regulate root growth and stress tolerance in sweet potato

Zhen Wang [1,2,†] Xu Li [1,2,†] Xiao-ru Gao [2] Zhuo-ru Dai [2] Kui Peng [2] Li-cong Jia [3] Yin-kui Wu [2] Qing-chang Liu [2] Hong Zhai [2] Shao-pei Gao [2] Ning Zhao [2] Shao-zhen He [1,2,*] and Huan Zhang [1,2,*]

1 Sanya Institute of China Agricultural University, Sanya 572025, China
2 Key Laboratory of Sweet Potato Biology and Biotechnology, Ministry of Agriculture and Rural Affairs/Beijing Key Laboratory of Crop Genetic Improvement/Laboratory of Crop Heterosis & Utilization and Joint Laboratory for International Cooperation in Crop Molecular Breeding, Ministry of Education, College of Agronomy & Biotechnology, China Agricultural University, Beijing 100193, China
3 Institute of Grain and Oil Crops, Yantai Academy of Agricultural Sciences, Yantai 265500, China

*Author for correspondence: zhanghuan1111@cau.edu.cn (H.Z.), sunnynba@cau.edu.cn (S.-z.H.)
†These authors contributed equally to this work.
The author responsible for distribution of materials integral to the findings presented in this article in accordance with the policy described in the Instructions for Authors (https://academic.oup.com/plphys/pages/General-Instructions) is: Huan Zhang (zhanghuan1111@cau.edu.cn).

Abstract

Root development influences plant responses to environmental conditions, and well-developed rooting enhances plant survival under abiotic stress. However, the molecular and genetic mechanisms underlying root development and abiotic stress tolerance in plants remain unclear. In this study, we identified the MYB transcription factor-encoding gene *IbMYB73* by cDNA-amplified fragment length polymorphism and RNA-seq analyses. *IbMYB73* expression was greatly suppressed under abiotic stress in the roots of the salt-tolerant sweet potato (*Ipomoea batatas*) line ND98, and its promoter activity in roots was significantly reduced by abscisic acid (ABA), NaCl, and mannitol treatments. Overexpression of *IbMYB73* significantly inhibited adventitious root growth and abiotic stress tolerance, whereas *IbMYB73*-RNAi plants displayed the opposite pattern. IbMYB73 influenced the transcription of genes involved in the ABA pathway. Furthermore, IbMYB73 formed homodimers and activated the transcription of ABA-responsive protein *IbGER5* by binding to an MYB binding sites I motif in its promoter. *IbGER5* overexpression significantly inhibited adventitious root growth and abiotic stress tolerance concomitantly with a reduction in ABA content, while *IbGER5*-RNAi plants showed the opposite effect. Collectively, our results demonstrated that the IbMYB73-IbGER5 module regulates ABA-dependent adventitious root growth and abiotic stress tolerance in sweet potato, which provides candidate genes for the development of elite crop varieties with well-developed root-mediated abiotic stress tolerance.

Introduction

Soil salinization and drought represent abiotic stresses that critically affect crop distribution, growth, and productivity (Zhang et al. 2022a). The root system plays a key role in crop development by promoting growth and abiotic stress tolerance (Seo et al. 2020). Sweet potato (*Ipomoea batatas* [L.] Lam. [$2n = B_1B_1B_2B_2B_2B_2 = 6x = 90$]) is an economically important root and tuber crop. However, because it is mainly planted on marginal land, it is necessary to improve salt-sensitive and drought-sensitive germplasms of this plant through the enhancement of root-mediated abiotic stress tolerance (Mukhopadhyay et al. 2011). Although genetic engineering approaches have contributed to elucidating the mechanisms of abiotic stress tolerance in sweet potato (Zhai et al. 2016; Kang et al. 2018; Zhang et al. 2019;

Received August 29, 2023. Accepted September 15, 2023. Advance access publication October 10, 2023

Zhang et al. 2022b; Meng et al. 2023), the molecular and genetic mechanisms underlying root-mediated abiotic stress tolerance in this plant remain largely unknown.

The phytohormone abscisic acid (ABA), known as the "stress hormone," is a key regulator of plant responses to a variety of abiotic stresses, including high salinity and drought. Several genes, such as 9-*cis*-epoxycarotenoid dioxygenase *NCED3*, protein phosphatase *PP18*, NAC transcription factor *RD26*, and WRKY transcription factor *WRKY77*, have been reported to mediate abiotic stress through ABA signaling in plants (Iuchi et al. 2001; Fujita et al. 2004; You et al. 2014; Jiang et al. 2021). In addition, ABA plays a critical role in the resistance to abiotic stress in plants by promoting root development and growth. For instance, in *Populus*, the nuclear factor Y (NF-Y) transcription factor PdNF-YB21 interacts with the B3 domain transcription factor PdFUS3 and markedly upregulates the expression of *PdNCED3*, a key gene in ABA synthesis, resulting in increased drought tolerance and root growth (Zhou et al. 2020). Additionally, transgenic *Arabidopsis* expressing the ABA receptor *GhPYL9-11A* of cotton (*Gossypium hirsutum*) shows increased root growth and upregulation of drought stress-related genes under drought treatment (Liang et al. 2017). In soybean (*Glycine max*), meanwhile, the clustered regularly interspaced short palindromicrepeats (CRISPR) and CRISPR-associated protein 9 (Cas9)-mediated editing of the ABA-responsive gene *GmHdz4* shows to promote root growth and drought tolerance (Zhong et al. 2022). The glucosyltransferases, Rab-like GTPase activators and myotubularins (GRAM) domain, are highly conserved, and 9 proteins containing only a GRAM domain are annotated as being ABA-responsive in *Arabidopsis* (Mauri et al. 2016). In addition to ABA-responsiveness, several GRAM domain-containing members (GERs) have also been implicated in seed development (Baron et al. 2014; Mauri et al. 2016) and pathogen resistance (Choi and Hwang 2011).

V-myb avian myeloblastosis viral oncogene homolog (MYB) transcription factors, and particularly R2R3-MYB proteins, are involved in plant root growth and abiotic stress responses (Chen et al. 2022). In *Arabidopsis*, *MYB60* promotes root growth in the initial stage of drought stress, resulting in increased water uptake (Oh et al. 2011). In *Arabidopsis*, the *AtMYB30* mutant shows increased root cell elongation under hydrogen peroxide (H_2O_2) treatment (Mabuchi et al. 2018), while the overexpression of *AtMYB20* promotes root growth and enhances salt tolerance (Cui et al. 2013). In soybean, *GmMYB84* exhibits enhanced drought tolerance and greater primary root length (Wang et al. 2017). The ectopic expression of wheat (*Triticum aestivum*) *TaMpc1-D4* in *Arabidopsis* reduces root growth and drought tolerance (Li et al. 2020). The ectopic expression of *ThMYB8* in transgenic *Arabidopsis* significantly increases root growth and enhances salt tolerance (Liu et al. 2021). Although these studies have highlighted the importance of R2R3-MYB proteins in plant root growth and stress responses, the underlying molecular mechanisms remain largely unexplored.

In this study, we found that the MYB transcription factor IbMYB73 forms homodimers and binds to the promoter of the ABA-responsive gene *IbGER5* to activates its transcription. We further found that the overexpression of *IbMYB73* and *IbGER5* markedly inhibits adventitious root growth and abiotic stress tolerance by suppressing ABA signaling. Collectively, our data provide insight into the roles of MYB transcription factors in regulating ABA-dependent root growth and abiotic stress tolerance in plants.

Results

IbMYB73 is involved in ABA-dependent abiotic stress responses

To identify potential abiotic stress response factors in sweet potato roots, we selected genes that were highly expressed in sweet potato roots and responded to a variety of abiotic stresses. One transcription factor gene, *IbMYB73*, was found to be highly expressed in the roots compared with that in various other tissues (Tao et al. 2012; Wu et al. 2018). Our previously generated cDNA-amplified fragment length polymorphism (cDNA-AFLP) and RNA-seq data showed that *IbMYB73* was differentially expressed in the salt-tolerant sweet potato line ND98 and the salt-sensitive variety Lizixiang under salt stress (Zhang et al. 2017a; Zhang et al. 2017b). Accordingly, we focused on *IbMYB73* given its potential role in abiotic stress responses in sweet potato roots.

We performed reverse transcription quantitative PCR (RT-qPCR) to detect the relative transcript levels of *IbMYB73* in the adventitious roots of ND98 and Lizixiang plants under different stress conditions (Supplemental Table S1). Following NaCl, polyethylene glycol (PEG), and ABA treatment, the expression of *IbMYB73* was suppressed 5.53-fold (at 12 h), 2.37-fold (at 12 h), and 2.11-fold (at 12 h) in ND98 plants but was induced 1.32-fold (at 2 h), 4.84-fold (at 2 h), and 5.21-fold (at 6 h) in Lizixiang plants, respectively (Fig. 1, A to C). In addition, *IbMYB73* was highly expressed in the fibrous roots of 2-mo-old field-grown ND98 plants (Fig. 1D).

The 867-bp ORF of *IbMYB73* encodes a protein of 288 amino acids with a predicted molecular weight of 31.4 kDa. IbMYB73 contains conserved R2 and R3 MYB domain repeats characteristic of subgroup 22 of the R2R3-MYB transcription factor family (Fig. 1E). IbMYB73 shows higher sequence similarity to that of *Arabidopsis*, AtMYB73 (Fig. 1F). The genomic sequence of *IbMYB73* contains only one exon and is similar to that of *AtMYB73* (Fig. 1G).

The *IbMYB73* promoter regions of ND98 and Lizixiang both contain 2 ABA-responsive elements (ABREs; Narusaka et al. 2003; Fig. 1H; Supplemental Fig. S1A). Remarkably, a 142-bp deletion was detected in the *IbMYB73* promoter region (about 668 bp upstream of the initiation site) of Lizixiang, while this deletion was not present in ND98 (Supplemental Fig. S1A). To further investigate whether the 142-bp variation affects the activation of *IbMYB73*, we separately expressed the 2 types of *IbMYB73* promoters in sweet potato tissues. The results of histochemical staining and *GUS* expression showed that the GUS activity and *GUS* expression driven by the *IbMYB73* promoter of Lizixiang were significantly higher than those driven by in the *IbMYB73* promoter of ND98 (Supplemental Fig. S1, B and C).

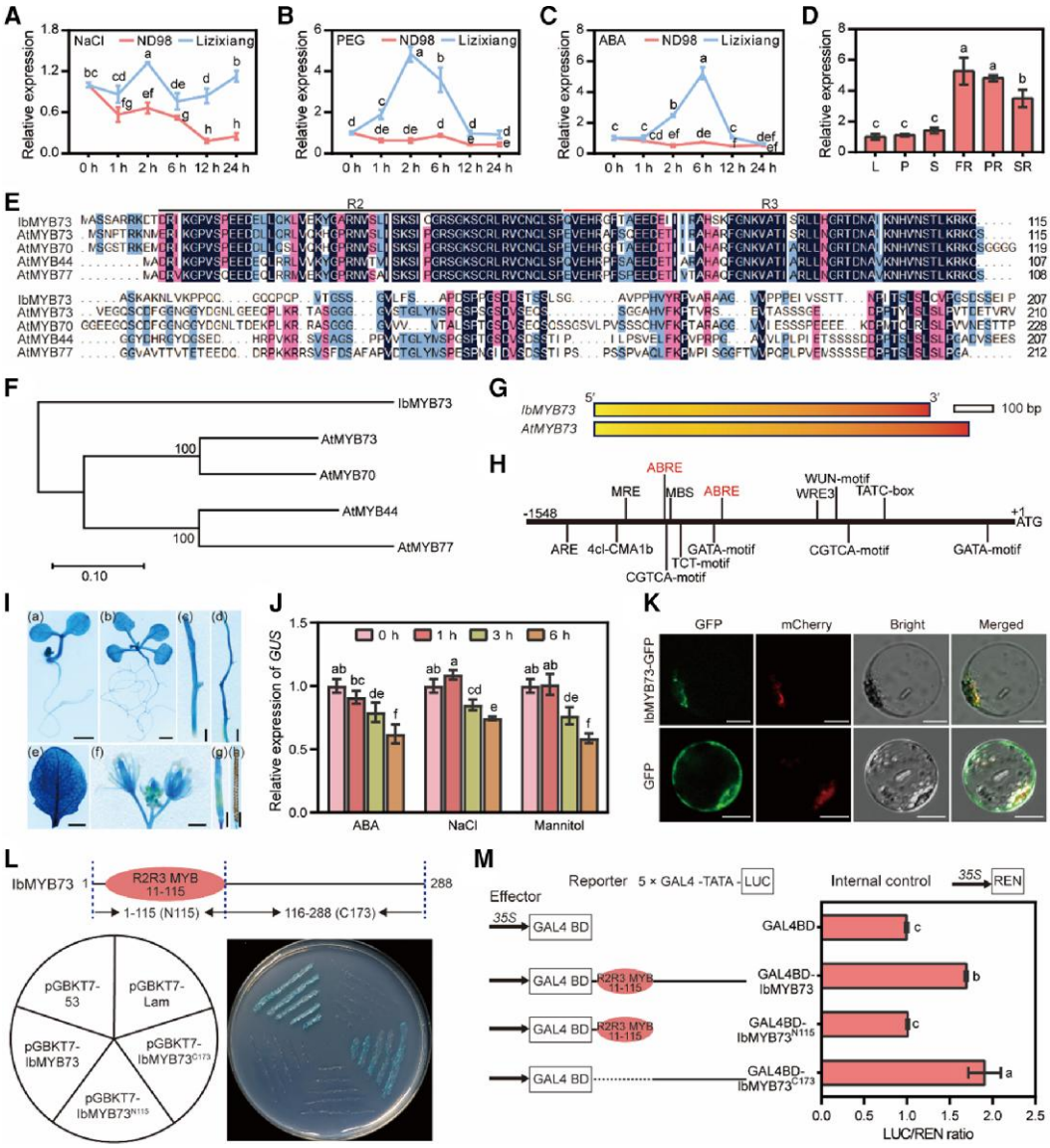

Figure 1. Expression analysis, sequence analysis, subcellular localization, and transactivation assay of IbMYB73. **A** to **C)** Expression analysis of *IbMYB73* in sweet potato lines ND98 and Lizixiang under 200 mM NaCl **A)**, 20% PEG **B)**, or 100 μM ABA **C)** treatments during a 24 h period. Data were presented as mean ± SD ($n = 3$). Different lowercase letters indicated statistically significant differences (2-way ANOVA, $P < 0.05$). **D)** Expression analysis of *IbMYB73* in different tissues of sweet potato line ND98. Data were presented as mean ± SD ($n = 3$). Different lowercase letters indicated statistically significant differences (One-way ANOVA, $P < 0.05$). **E)** Multiple protein sequence alignment of IbMYB73 and *Arabidopsis* MYBs, with conserved amino acids shaded on different colors. The entire lines represented the conserved R2 and R3 MYB domain repeats. **F)** Phylogenetic analysis of IbMYB73 and *Arabidopsis* MYBs using the neighbor-joining method in MEGA X with 1,000 bootstrap iterations. The numbers at the nodes of the tree indicated bootstrap value from 1,000 replicates. **G)** Comparison of genomic structure of *IbMYB73* and *AtMYB73*. Boxes indicated exons. **H)** Alignment of various *cis*-acting elements of *IbMYB73* promoter in sweet potato line ND98. **I)** GUS staining of 5 d seedlings (a), 12 d seedlings (b), stems (c), roots (d), mature leaves (e), flowers (f), immature siliques (g), and mature siliques (h) of transgenic *Arabidopsis* plants harboring *IbMYB73*pro: GUS conduct of sweet potato line ND98. Bars, 1 cm. **J)** The promoter activity of *IbMYB73* in roots of *Arabidopsis* plants subjected to treatment with ABA (50 μM), NaCl (100 mM), or mannitol (200 mM) for different times. The *Arabidopsis ACTIN* gene was used as internal control. Relative transcript expression of 0 h in each treatment was set to 1.0. Data were presented as mean ± SD ($n = 3$). Different lowercase letters indicated statistically significant differences (2-way ANOVA, $P < 0.05$). **K)** Subcellular localization of IbMYB73 in sweet potato protoplasts transformed with the fusion conduct (IbMYB73-GFP or GFP) and the nuclear marker NLS-mCherry. Bars, 10 μm. **L)** Transactivation assay of IbMYB73 in yeast. Fusion proteins of the GAL4 DNA-binding domain and different portions of IbMYB73 were expressed in yeast. Yeast cells were planted onto SD/−Trp/−Ade/−His with 20 mg/L X-α-gal medium. The pGBKT7-53 was used as a positive control, while pGBKT7-Lam was used as a negative control. **M)** Transactivation assay of IbMYB73 in rice protoplasts. The GAL4BD empty vector was used as a negative control. Data were presented as mean ± SD ($n = 3$). Different lowercase letters indicated statistically significant differences (1-way ANOVA, $P < 0.05$). MBS, MYB binding sites. WUN, wound-responsive element. ABRE, ABA-responsive elements; LUC, firefly luciferase. Ren, renilla luciferase; L, leaf; P, petiole; S, stem; FR, fibrous root; PR, pencil root; SR, storage root.

We further generated transgenic *Arabidopsis* plants expressing GUS driven by the *IbMYB73* promoter and found that all tissues exhibited GUS activity, as assessed by histochemical staining; however, RT-qPCR analysis showed that *GUS* expression was significantly inhibited in roots following ABA, NaCl, or mannitol treatment (Fig. 1, I and J). Collectively, these results indicated that *IbMYB73* is involved in abiotic stress responses in sweet potato.

IbMYB73 is a nucleus-localized transactivator

To identify the subcellular localization of IbMYB73, we transiently expressed an IbMYB73-GFP fusion protein in sweet potato protoplasts. Confocal microscopy indicated that IbMYB73-GFP was localized to the nucleus, whereas GFP alone (control) was localized throughout the cytosol (Fig. 1K).

We next tested the transactivation activity of IbMYB73 in a yeast 1-hybrid assay using full-length IbMYB73 or 2 fragments of the protein (the 174 C-terminal amino acid residues [IbMYB73^{C173}] and the 115 N-terminal amino acid residues [IbMYB73^{N115}]). We found that IbMYB73^{C173} was required for transcriptional activation (Fig. 1L). The full-length and the 2 fragments of IbMYB73 were then separately further fused to the DNA-binding domain of GAL4 and transiently transfected in protoplasts. Full-length IbMYB73 and IbMYB73^{C173} showed markedly stronger transactivation activity than IbMYB73^{N115} (Fig. 1M). These observations confirmed that IbMYB73 is a nucleus-localized transactivator and that its C-terminus is required for its transactivation activity.

IbMYB73 inhibits adventitious root growth and abiotic stress tolerance in sweet potato

To investigate the potential biological function of *IbMYB73* in sweet potato, we generated 3 *IbMYB73* overexpression lines (OE-M7, OE-M9, and OE-M11) and 4 *IbMYB73*-RNAi lines (Ri-M1 to Ri-M4) lines of the salt-sensitive sweet potato variety Lizixiang via *Agrobacterium tumefaciens*-mediated transformation. After 4 mo of growth in the field, there were no significant differences in the number of storage root, while the storage root weight of *IbMYB73*-OE lines was decreased (Supplemental Fig. S2). We then compared root morphology among in vitro-grown salt-tolerant ND98, WT, and *IbMYB73* transgenic plants (Fig. 2A; Supplemental Fig. S3). Under normal conditions, the *IbMYB73*-OE lines formed fewer adventitious roots than WT, whereas the opposite was seen for the ND98 and 2 *IbMYB73*-RNAi lines (Fig. 2B). Under ABA treatment, the *IbMYB73*-OE lines formed significantly more adventitious roots compared with WT, whereas those of the ND98 and *IbMYB73*-RNAi lines formed significantly fewer (Fig. 2B), indicating that *IbMYB73* influences ABA sensitivity in sweet potato. Under NaCl and PEG treatments, the number, length, and weight of the adventitious roots were significantly decreased in the *IbMYB73*-OE lines relative to that seen in WT, whereas the opposite was observed in the ND98 and *IbMYB73*-RNAi lines (Fig. 2, B to D). These findings indicated that *IbMYB73* is involved in root-mediated abiotic stress sensitivity.

We further observed the root growth of 2-mo-old field-grown plants (Fig. 2E). Consistent with that observed growth of the in vitro grown root system, under ABA treatment, the number of adventitious roots of the *IbMYB73*-OE lines was increased compared with that in WT, whereas that of the *IbMYB73*-RNAi lines was significantly decreased (Fig. 2F). Under normal conditions as well as under NaCl or PEG treatment, the *IbMYB73*-OE lines formed markedly fewer adventitious roots relative to the WT controls, whereas the *IbMYB73*-RNAi lines formed considerably more (Fig. 2F). Meanwhile, under NaCl and PEG treatment, the length and weight of the adventitious roots in the *IbMYB73*-OE lines were decreased compared with the WT; in contrast, those of the *IbMYB73*-RNAi lines were increased (Fig. 2, G and H). These results indicated that *IbMYB73* inhibits ABA-dependent adventitious root growth and abiotic stress tolerance in sweet potato.

To further evaluate the role of *IbMYB73* in abiotic stress, we grew both transgenic and WT plants in transplantation boxes and subjected all the plants to salt (200 mM NaCl) and drought stress. We found that compared with WT, growth and rooting were reduced in the *IbMYB73*-OE lines under normal condition (Fig. 3A). Under salt and drought stress, the *IbMYB73*-OE lines turned brown and showed significantly poorer rooting relative to WT plants; in contrast, *IbMYB73*-RNAi lines exhibited better growth and rooting and greater fresh weight and dry weight (Fig. 3, A and B; Supplemental Tables S2 and S3). In addition, we planted *IbMYB73* transgenic and WT plants in a greenhouse and subjected them to drought stress (no watering for 2 mo). We observed that most of the *IbMYB73*-OE plants exhibited difficulty in rooting, turned brown, and died earlier than WT plants; in contrast, the *IbMYB73*-RNAi lines showed more adventitious roots and increased fresh and dry weight (Fig. 3, C and D; Supplemental Fig. S4).

Salt and drought stresses are known to induce oxidative damage in plants (Cruz de Carvalho 2008; Bose et al. 2014). Here, we found that, under salt and drought stress, H_2O_2 and MDA contents were higher, whereas proline contents were lower, in the adventitious roots of *IbMYB73*-OE lines than in those of WT plants. By contrast, the *IbMYB73*-RNAi lines exhibited the opposite pattern for the respective physiological indices (Fig. 3, E to G). Under normal conditions as well as under NaCl and PEG treatment, the ABA content was significantly decreased in the adventitious roots of the *IbMYB73*-OE lines compared with that in WT plants, whereas the opposite was seen in the *IbMYB73*-RNAi lines (Fig. 3H). Collectively, our data demonstrated that the overexpression of *IbMYB73* inhibited ABA-dependent adventitious root growth and reduced abiotic stress tolerance in sweet potato.

IbMYB73 regulates the transcription of genes involved in the ABA pathway

As we found that *IbMYB73* was involved in ABA-mediated adventitious root growth and abiotic stress responses, we

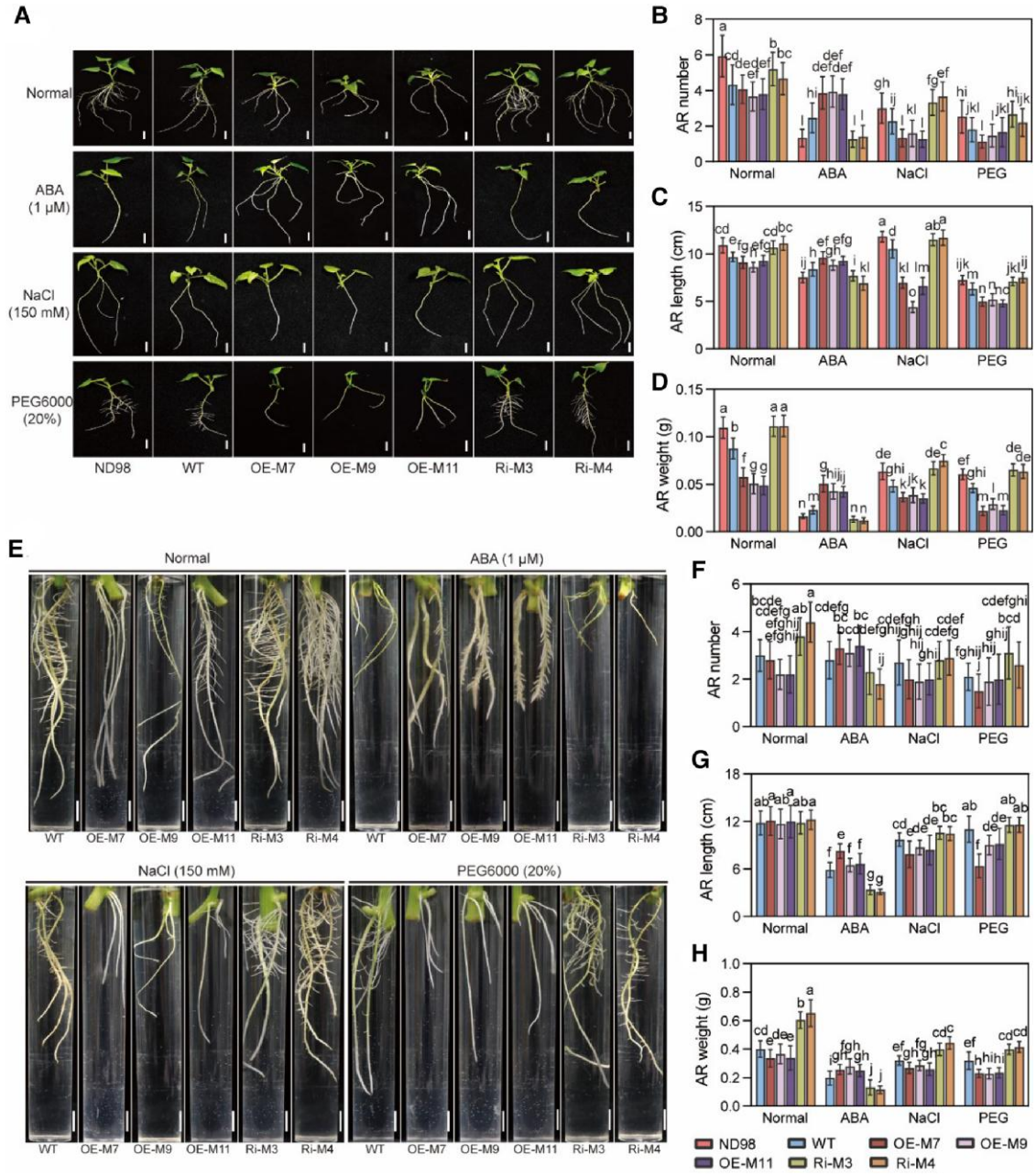

Figure 2. Overexpression of *IbMYB73* inhibits adventitious root growth and reduces ABA sensitivity and abiotic stress tolerance. **A** to **D**) Responses and adventitious root growth condition of salt-tolerant line ND98, Lizixiang (WT) and *IbMYB73* transgenic sweet potato plants grown on MS medium under normal condition or subjected to ABA (1 μM), NaCl (150 mM), or PEG6000 (20%) for 10 d. **E** to **H**) Responses and adventitious root growth condition of 2-mo-old field-grown *IbMYB73* transgenic and WT sweet potato plants grown hydroponically in Hoagland solution alone (normal) or with the addition of ABA (1 μM), NaCl (150 mM), or PEG6000 (20%) for 10 d. Bars, 1 cm. All data were presented as means ± SD. In **B** to **D**) adventitious root growth index was determined for 15 plants; in **F** to **H**) adventitious root growth index was determined for 10 plants. Different lowercase letters indicated statistically significant differences (2-way ANOVA, $P < 0.05$). AR, adventitious root; WT, the sweet potato variety Lizixiang; OE-M, the *IbMYB73*-overexpression lines; Ri-M, the *IbMYB73*-RNAi lines.

next determined the expression levels of key genes involved in ABA biosynthesis and signaling in the adventitious roots of transgenic plants. Under ABA treatment, compared with the WT, the ABA biosynthesis-related genes *IbNCED3* (encoding a 9-*cis*-epoxycarotenoid dioxygenase; Kalladan et al. 2019), *IbABA2* (encoding a short-chain dehydrogenase/reductase; Gonzalez-Guzman et al. 2002), and *IbAAO3* (encoding an aldehyde oxidase; Seo et al. 2000); the ABA signaling-related genes *IbABI2* (encoding an ABA-insensitive protein; Leung et al. 1997), and *IbSnRK2.3* (encoding a Snf1-related protein kinase 2; Feng et al. 2014); and the abiotic stress tolerance-related genes *IbDREB1D*, *IbRD22*, and *IbRD26*

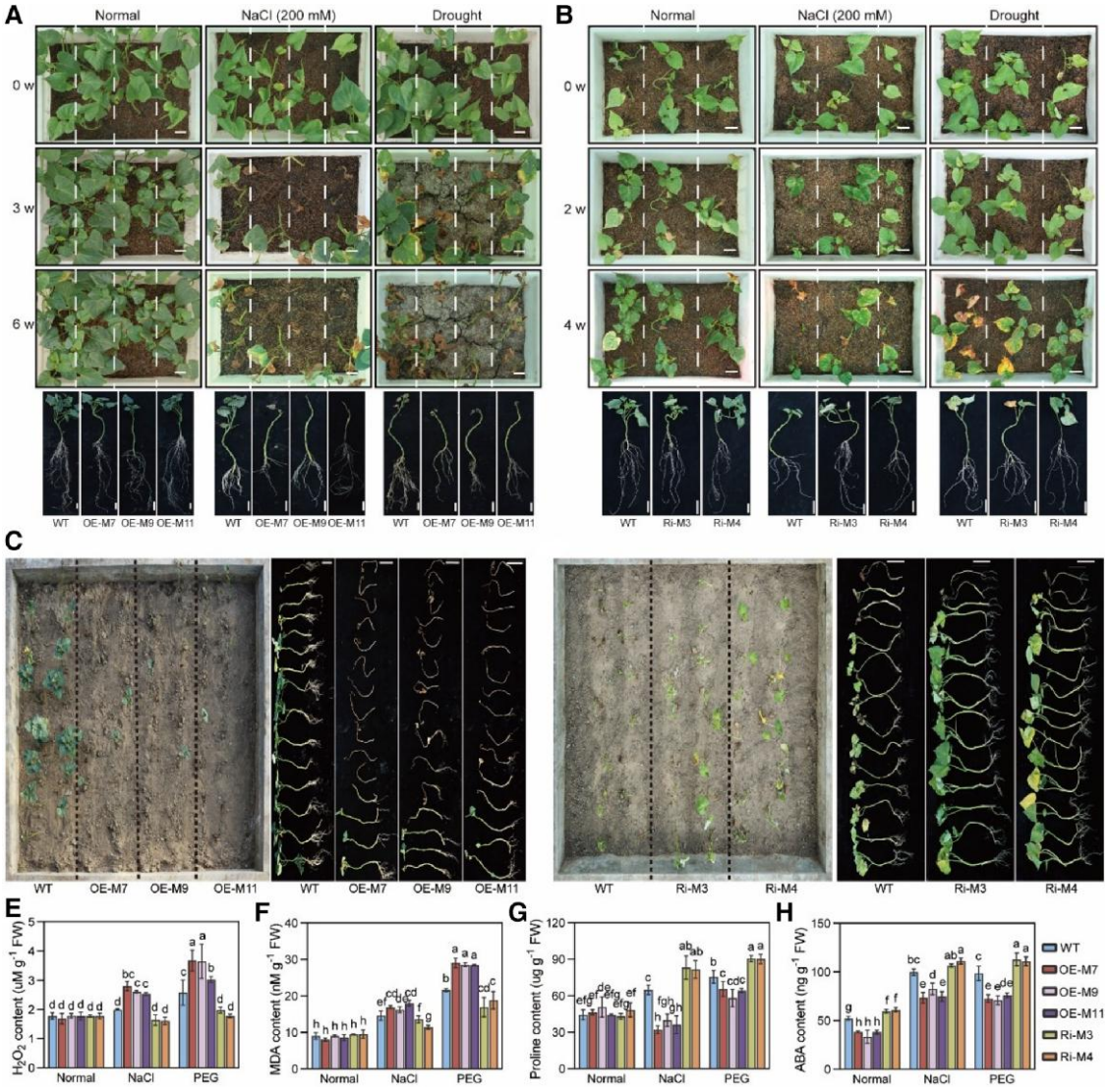

Figure 3. Overexpression of *IbMYB73* negatively regulates abiotic stress tolerance under soil conditions. **A** and **B)** Responses of 2-mo-old field-grown *IbMYB73*-OE, *IbMYB73*-RNAi, and WT sweet potato plants (separated by dotted lines) grown in transplantation boxes under normal condition or subjected to 200 mM NaCl or drought stress during 4- or 6-wk period. The representative photographs were taken after stress treatment. Bars, 4 cm. **C** and **D)** Responses of 2-mo-old field-grown *IbMYB73* overexpression and WT sweet potato plants (separated by dotted lines) grown in greenhouse for 8 wk without watering. Bars, 10 cm. **E** to **H**) H_2O_2 content **E)**, MDA content **F)**, proline content **G)**, and ABA content **H)** in the adventitious roots of *IbMYB73* transgenic and WT plants grown on MS medium under normal condition as well as under 150 mM NaCl and 20% PEG6000 treatment for 10 d. Data were presented as means ± SD ($n = 3$). Different lowercase letters indicated statistically significant differences (2-way ANOVA, $P < 0.05$). WT, the sweet potato variety Lizixiang; OE-M, the *IbMYB73*-overexpression lines; Ri-M, the *IbMYB73*-RNAi lines; MDA, malondialdehyde; FW, fresh weight.

(encoding dehydration-responsive proteins; Fujita et al. 2004; Wang et al. 2012; Alves et al. 2017) were significantly downregulated in *IbMYB73*-OE plants but were significantly upregulated in *IbMYB73*-RNAi plants (Fig. 4, A to H). However, the expression of an ABA-responsive gene, *IbGER5*, was significantly upregulated in *IbMYB73*-OE plants but significantly downregulated in *IbMYB73*-RNAi plants, relative to that in WT plants (Fig. 4I). These data indicated that *IbMYB73* regulates abiotic stress tolerance in sweet potato by influencing the transcription of genes involved in the ABA pathway.

IbMYB73 forms homodimers and activates the transcription of the ABA-responsive gene *IbGER5*

To better understand the regulatory mechanisms underlying *IbMYB73*-mediated adventitious root growth and abiotic stress responses, we used the $IbMYB73^{N115}$ fragment as bait to screen a sweet potato Y2H library. Notably, we found that IbMYB73 interacts strongly with itself, forming homodimers (Fig. 5A). We further verified this using bimolecular fluorescence complementation (BiFC) and co-immunoprecipitation (Co-IP) assays, with the results showing that IbMYB73

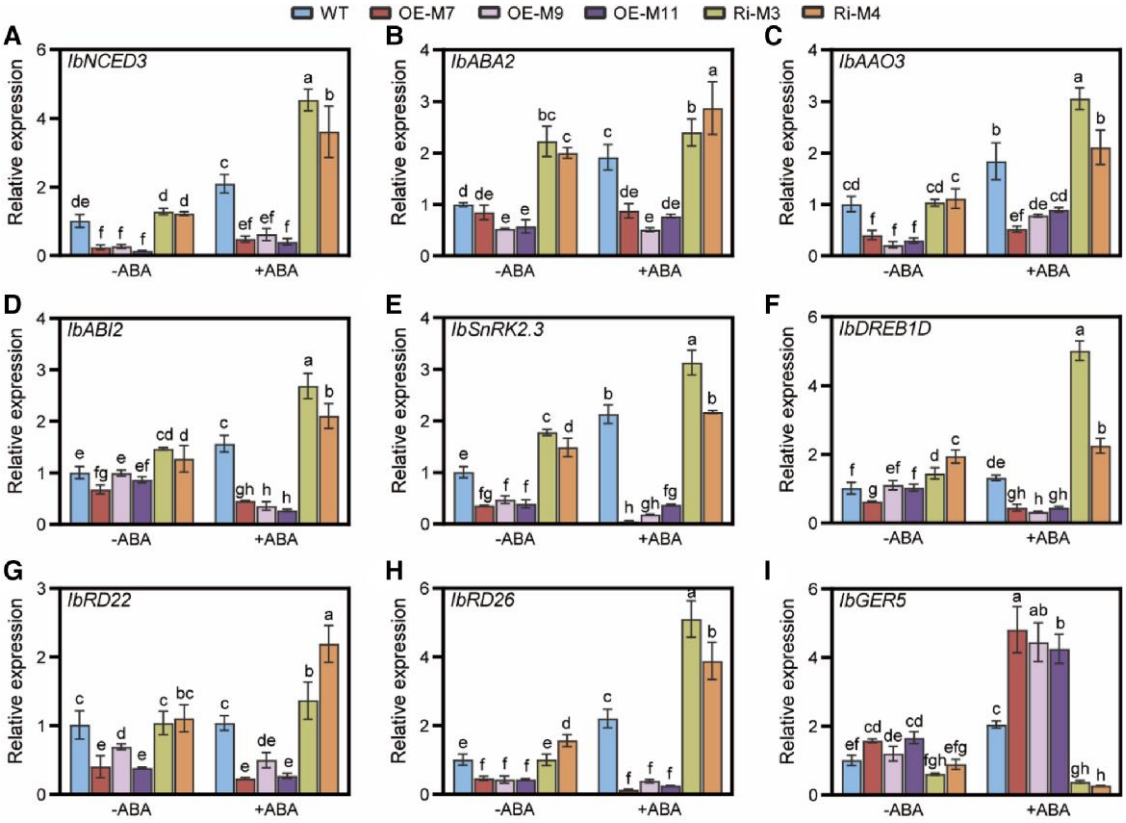

Figure 4. *IbMYB73* regulates the transcription of genes involved in ABA pathway with or without ABA treatment. **A** to **I**) Relative expression level of *IbNCED3* **A)**, *IbABA2* **B)**, *IbAAO3* **C)**, *IbABI2* **D)**, *IbSnRK2.3* **E)**, *IbDERB1D* **F)**, *IbRD22* **G)**, *IbRD26* **H)**, and *IbGER5* **I)** in the adventitious roots of *IbMYB73*-OE and *IbMYB73*-RNAi and WT plants grown on MS medium under normal condition and following 1 μM ABA treatment for 10 d. The sweet potato *β-actin* gene was used as internal control. Relative transcript level of WT plants under normal condition was set to 1.0. Data were presented as means ± SD ($n = 3$). Different lowercase letters indicated statistically significant differences (2-way ANOVA, $P < 0.05$). WT, the sweet potato variety Lizixiang; OE-M, the *IbMYB73*-overexpression lines; Ri-M, the *IbMYB73*-RNAi lines.

indeed formed homodimers in the nucleus of plant cells (Fig. 5, B and C).

In plants, MYB proteins bind to MYB binding sites (MBS) I and MBSII motifs in the promoters of their target genes (Romero et al. 1998; Yang et al. 2001). Additionally, binding sites adjacent to transcription start sites are more likely to be bound and regulated by transcription factors in sweet potato (Gao et al. 2023). Because we found that the ABA-responsive gene *IbGER5* was significantly upregulated in *IbMYB73*-OE plants and downregulated in *IbMYB73*-RNAi plants under different stress conditions, we investigated whether MBSI and MBSII motifs were present in the promoter region of *IbGER5* and identified a MBSI motif at −214 bp (Fig. 5D; Supplemental Fig. S5). We further performed chromatin immunoprecipitation-quantitative PCR (ChIP)-qPCR on the adventitious roots of the OE-M11 line and observed that IbMYB73 directly targets *IbGER5* in vivo (Fig. 5D). Then, we performed EMSA based on accumulated IbMYB73 protein abundance and a competitive probe. The addition of double the amount of IbMYB73 substantially increased its ability to bind to *IbGER5* (Fig. 5E). Meanwhile, the accumulation of the competitive probe gradually abolished the binding of IbMYB73 to the *IbGER5* promoter probe (Fig. 5E). Further transient dual-luciferase reporter assays showed that IbMYB73 directly activated the *IbGER5* promoter under normal condition and following ABA treatment, and doubling the amount of IbMYB73 protein significantly enhanced the activation of the *IbGER5* promoter (Fig. 5F). These results indicated that IbMYB73 forms homodimers and activates the transcription of the ABA-responsive gene *IbGER5* in sweet potato.

GERs have rarely been characterized in plants. We identified 12, 9, and 9 GERs in sweet potato (*I. batatas*, $2n = 6x = 90$) and in its 2 diploid relatives *I. triloba* ($2n = 2x = 30$) and *I. trifida* ($2n = 2x = 30$), respectively (Fig. 5G). Additionally, 9, 9, 14, and 27 GERs were identified in *Arabidopsis*, rice (*Oryza sativa*), maize (*Zea mays*), and wheat, respectively (Fig. 5G; Supplemental Table S4). These GERs could be divided into 6 subgroups according to their phylogenetic relationships (Fig. 5G). The 852-bp ORF of *IbGER5* encodes a protein of 283 amino acids with a predicted molecular weight of 31.32 kDa. The IbGER5 protein contains only one conserved GRAM domain and shows higher sequence similarity with AtGER5 (Supplemental Fig. S6A).

Like *AtGER5*, the genomic sequence of *IbGER5* contains 3 exons and 2 introns (Supplemental Fig. S6B). The promoter of

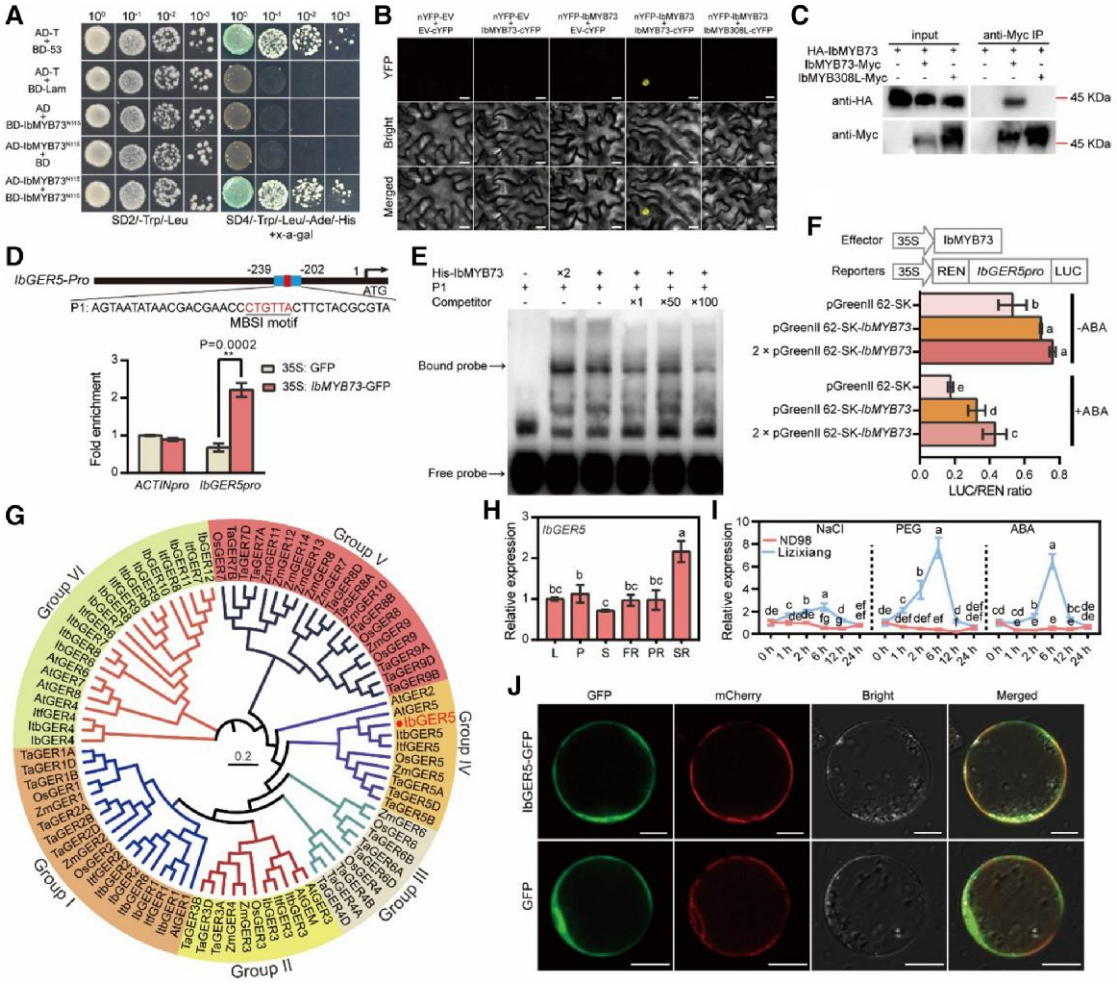

Figure 5. IbMYB73 forms homodimers and activates the transcription of the ABA-responsive gene *IbGER5*. **A)** Y2H analysis showed that IbMYB73 interacts with itself. Yeast cells were planted onto SD/−Trp/−Leu and SD/−Trp/−Leu/−Ade/−His with 20 mg/L X-α-gal medium to screen for possible interactions. BD-53 was used as a positive control, while BD-Lam was used as a negative control. **B)** BiFC analysis showed that IbMYB73 interacts with itself in *N. benthamiana* leaf epidermal cells. IbMYB308L from the MYB transcription factor family was used as a related noninteracting protein for a negative control. Bars = 20 μm. **C)** Co-IP analysis showed that IbMYB73 interacts with itself in vivo. IbMYB308L was used as a related noninteracting protein for a negative control. **D)** ChIP-qPCR analysis using 35S:*IbMYB73*-GFP and 35S:GFP plants with anti-GFP antibody, which showed that IbMYB73 could directly bind to the *IbGER5* promoters. The *ACTIN* promoter was used as an internal reference for ChIP-qPCR. Data were presented as means ± SD ($n = 3$). Different asterisks indicated statistically significant differences (Student's *t*-test; **, $P < 0.01$). **E)** EMSA showed that IbMYB73 could directly target *IbGER5* by binding to the MBSI motif. **F)** Dual-LUC assays showed that IbMYB73 activated the *IbGER5* promoters under normal condition and following ABA treatment. Data were presented as means ± SD ($n = 3$). Different lowercase letters indicated statistically significant differences (2-way ANOVA, $P < 0.05$). **G)** Phylogenetic analysis of GERs from *I. batatas* (IbGER5) and other plants (*I. triloba*, *I. trifida*, *A. thaliana*, *O. sativa*, *Z. mays*, and *T. aestivum*) using the neighbor-joining method in MEGA X with 1,000 bootstrap iterations. **H)** Expression analysis of *IbGER5* in different tissues of sweet potato line ND98. Data were presented as means ± SD ($n = 3$). Different lowercase letters indicated statistically significant differences (1-way ANOVA, $P < 0.05$). **I)** Expression analysis of *IbGER5* in sweet potato line ND98 under ABA (100 μM), NaCl (200 mM), or PEG (20%) treatments during a 24 h period. Data were presented as means ± SD ($n = 3$). Different lowercase letters indicated statistically significant differences (2-way ANOVA, $P < 0.05$). **J)** Subcellular localization of IbGER5 in sweet potato protoplasts transformed with the fusion conduct (IbGER5-GFP or GFP) and the plasma membrane marker PIP2-mCherry. Bars, 10 μm. REN, renilla luciferase; LUC, firefly luciferase; L, leaf; P, petiole; S, stem; FR, fibrous root; PR, pencil root; SR, storage root.

IbGER5 contains one ABA-responsive element (Supplemental Fig. S6C). RT-qPCR analysis revealed that *IbGER5* was highly expressed in the storage roots of 2-mo-old field-grown ND98 plants (Fig. 5H). Under NaCl, PEG, and ABA treatments, the expression of *IbGER5* was suppressed almost 2.11-fold (at 12 h), 4.86-fold (at 12 h), and 2.99-fold (at 2 h) in the ND98 line but was induced 2.40-fold (at 6 h), 7.65-fold (at 6 h), and 6.44-fold (at 6 h) in the Lizixiang plants, respectively (Fig. 5I). Subcellular localization analysis showed that IbGER5 was localized to the plasma membrane in protoplasts (Fig. 5J). Together, these results indicated that *IbMYB73* might regulate adventitious root growth and abiotic stress sensitivity in sweet potato through an *IbGER5*-mediated, ABA-dependent response.

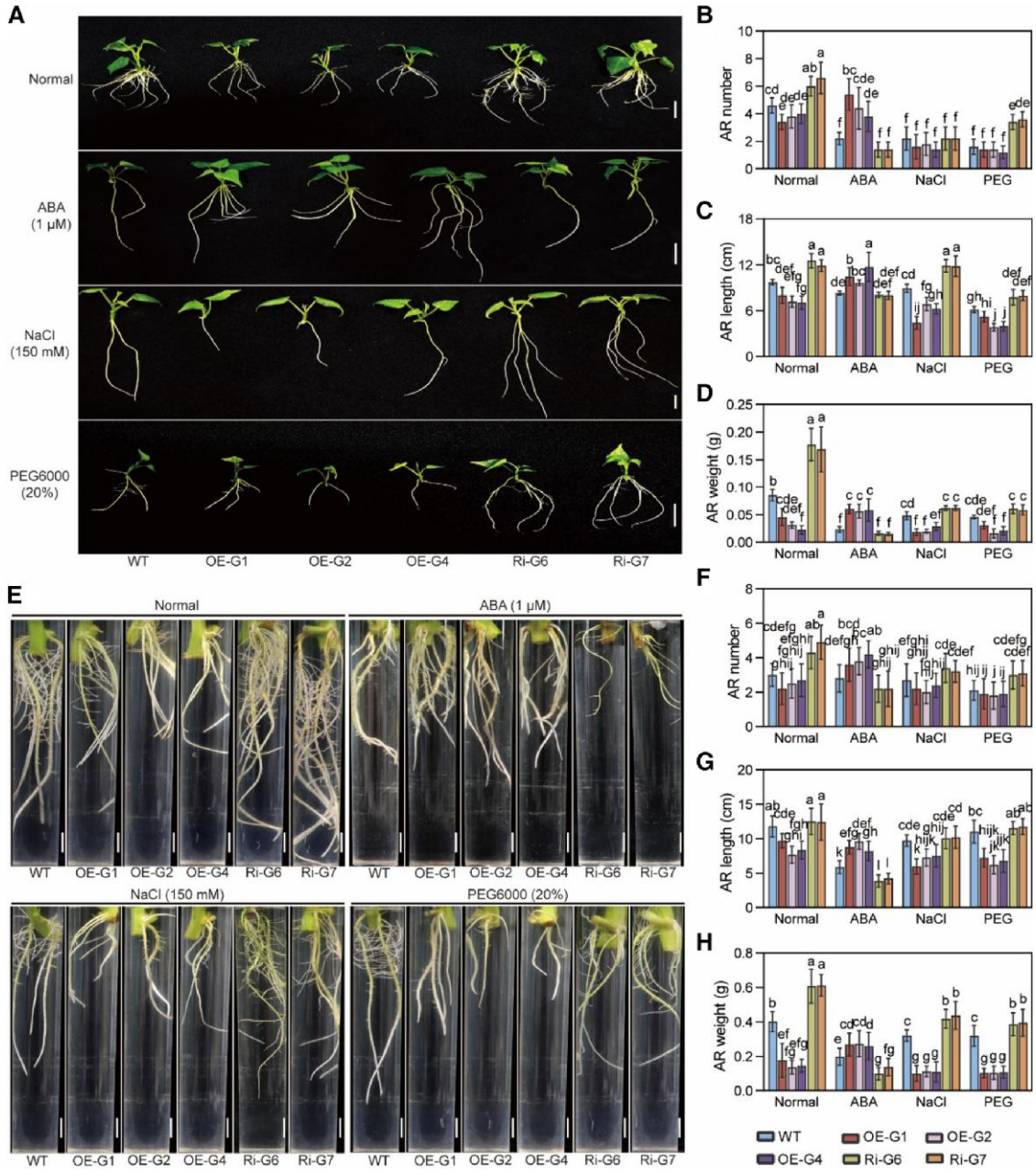

Figure 6. Overexpression of *IbGER5* inhibits adventitious root growth and reduces ABA sensitivity and abiotic stress tolerance. **A** to **D)** Responses and adventitious root growth condition of *IbGER5* transgenic and Lizixiang (WT) sweet potato plants grown on MS medium under normal condition or subjected to ABA (1 μM), NaCl (150 mM), or PEG6000 (20%) for 10 d. **E** to **H**) Responses and adventitious root growth condition of 2-mo-old field-grown *IbGER5* transgenic and WT sweet potato plants grown hydroponically in Hoagland solution alone (normal) or with the addition of ABA (1 μM), NaCl (150 mM), or PEG6000 (20%) for 10 d. Bars, 1 cm. All data were presented as means ± SD. In **B** to **D**) adventitious root growth index was determined for 5 plants, in **F** to **H**) adventitious root growth index was determined for 10 plants. Different lowercase letters indicated statistically significant differences (2-way ANOVA, $P < 0.05$). AR, adventitious root; WT, the sweet potato variety Lizixiang; OE-G, the *IbGER5*-overexpression lines; Ri-G, the *IbGER5*-RNAi lines.

IbGER5 inhibits ABA-dependent adventitious root growth and abiotic stress tolerance

To investigate the potential biological function of *IbGER5* in sweet potato, we generated 3 *IbGER5* overexpression lines (OE-G1, OE-G2, and OE-G4) and 2 *IbGER5*-RNAi lines (Ri-G6 and Ri-G7) from cell aggregates of the salt-sensitive sweet potato variety Lizixiang via *Agrobacterium*-mediated transformation (Supplemental Fig. S7). After 4 mo of growth in the field, the *IbGER5*-OE plants showed reduced storage root weight, whereas the *IbGER5*-RNAi plants showed more and heavier storage root compared with WT plants (Supplemental Fig. S7, K and L). Then, we investigated the morphological changes in in vitro-grown *IbGER5* transgenic plants (Fig. 6A; Supplemental Fig. S8). The *IbGER5*-OE lines

formed fewer, whereas those of the *IbGER5*-RNAi lines formed more adventitious roots compared with WT plants under normal condition as well as under NaCl or PEG treatment. Under ABA treatment, the *IbGER5*-OE plants formed significantly more, whereas the *IbGER5*-RNAi lines formed significantly fewer adventitious roots compared with that seen in WT plants (Fig. 6, B to D). Next, we cultured cuttings of field-grown plants in Hoagland solution with or without the addition of 1 μM ABA, 150 mM NaCl, or 20% (w/v) PEG6000 (Fig. 6E). Under ABA treatment, the *IbGER5*-OE lines displayed a significantly greater number of adventitious roots compared with WT plants, opposite to that recorded for *IbGER5*-RNAi plants (Fig. 6F). Under normal conditions as well as under NaCl or PEG treatment, the *IbGER5*-OE lines exhibited reduced rooting and weight relative to that seen in WT plants, whereas the *IbGER5*-RNAi lines formed observably more adventitious roots (Fig. 6, F to H).

To further evaluate the role of *IbGER5* under abiotic stress in soil, we grew the *IbGER5* transgenic and WT plants in transplantation boxes or a greenhouse. Under normal conditions as well as under salt or drought stress, the *IbGER5*-OE lines grown in transplantation boxes showed poorer rooting than WT plants, while the *IbGER5*-RNAi lines exhibited better growth and rooting (Fig. 7, A and B; Supplemental Tables S5 and S6). In the greenhouse, most of the *IbGER5*-OE plants had difficulty forming roots, turned brown, and died; however, the *IbGER5*-RNAi lines showed better growth and rooting than WT plants (Fig. 7, C and D; Supplemental Fig. S9). We further found that H_2O_2 and MDA contents were higher, whereas proline and ABA contents were lower, in the *IbGER5*-OE lines than in WT plants; however, the opposite effect was observed in *IbGER5*-RNAi plants (Fig. 7, E to H). Besides, the ABA signaling-related genes *IbABI2* and *IbSnRK2.3* were significantly downregulated in *IbGER5*-OE plants but were significantly upregulated in *IbGER5*-RNAi plants under different stress conditions (Supplemental Fig. S10). Taken together, these results indicated that *IbGER5* inhibits ABA-dependent adventitious root growth and plays a negative regulatory role in abiotic stress tolerance in sweet potato.

To further investigate the regulatory mechanism of IbMYB73-IbGER5 module in sweet potato, we overexpressed *IbMYB73* in the *IbGER5*-RNAi line (Ri-G6) and detected the adventitious roots growth conditions under normal, ABA, NaCl, and PEG treatment. The results showed that the number, length, and weight of adventitious roots in *IbMYB73*/Ri-G6 plants were similar to those in WT, suggesting that *IbMYB73* regulated the adventitious root growth and abiotic stress tolerance through *IbGER5* (Fig. 7, I to L). Collectively, our data demonstrate that under abiotic stress, IbMYB73-IbGER5 module regulates ABA-dependent adventitious roots growth and reduces abiotic stress tolerance in sweet potato.

Discussion

To improve the salt and drought tolerance of sweet potato such that it can grow on barren land may allow the expansion of farmland resources and the construction of an ecological environment (Gelfand et al. 2013). Genetic engineering, such as gene editing, is an effective approach for improving abiotic stress tolerance, and several genes that positively regulate abiotic stress in sweet potato have been identified (Zhai et al. 2016; Kang et al. 2018; Zhang et al. 2019; Zhang et al. 2022b; Meng et al. 2023). However, genes that enhance germplasm abiotic stress sensitivity in this plant are rarely reported. In this study, we showed that IbMYB73 inhibits ABA-dependent adventitious root growth by targeting *IbGER5*, leading to increased salt and drought stress sensitivity in sweet potato (Fig. 8).

Root architecture governs crop performance under abiotic stress. Soil moisture and salinity influence both the growth and development of plant roots and the programming and distribution of the root mass between main and lateral roots (Julkowska et al. 2017). A plant's capacity to alter its root system, such as growing thicker and deeper into the soil, is a crucial strategy for mitigating drought stress and adapting to salinity. This adaptive response helps the plant to access water and nutrients in the soil more efficiently, which ultimately enhances its overall growth and survival under stressful conditions. Hence, well-developed and deep rooting is a key aim of crop improvement programs (Kim et al. 2020). In *Arabidopsis*, *AtHKT1* and *AtCYP79B2/B3* play important roles in the modulation of lateral root development under conditions of salt stress (Julkowska et al. 2017). *AtAGL16* negatively regulates primary root elongation in response to abiotic stress (Zhao et al. 2021). Subclass 1 SnRK2s function in root development under salt stress by affecting the transcript levels of aquaporins (Kawa et al. 2020). In rice, transgenic *ASD16* plants (shallow-rooted) overexpressing *OsARD4* exhibit drought-adaptive traits of the rice genotype Nootripathu (deep-rooted), including a high root bulk (Ramanathan et al. 2018). In soybean, *GmSIN1* regulates root elongation and salt tolerance by boosting cellular ABA and ROS contents (Li et al. 2019a). However, key genes that regulate root development-mediated abiotic stress have rarely been characterized in sweet potato. In this study, *IbMYB73* and *IbGER5* were found to be predominantly expressed in fibrous roots and storage roots, respectively (Figs. 1D and 5H). Under normal conditions as well as under NaCl or PEG treatment, compared with WT plants, the *IbMYB73*-OE and *IbGER5*-OE lines formed fewer adventitious roots, and the length and weight of the adventitious roots were significantly decreased; meanwhile, *IbMYB73*-RNAi and *IbGER5*-RNAi plants showed the opposite pattern (Figs. 2 and 6). Moreover, overexpressing *IbMYB73* and *IbGER5* led to reduced storage root yields, whereas knockdown of *IbMYB73* and *IbGER5* resulted in increased yields after 4 mo of growth in the field (Supplemental Figs. S2 and S7). In the greenhouse, compared with WT plants, *IbMYB73*-RNAi and *IbGER5*-RNAi plants displayed better growth and rooting, whereas *IbMYB73*-OE and *IbGER5*-OE exhibited poorer rooting under normal condition as well as under salt and drought stress (Figs. 3 and 7). Moreover, compared with

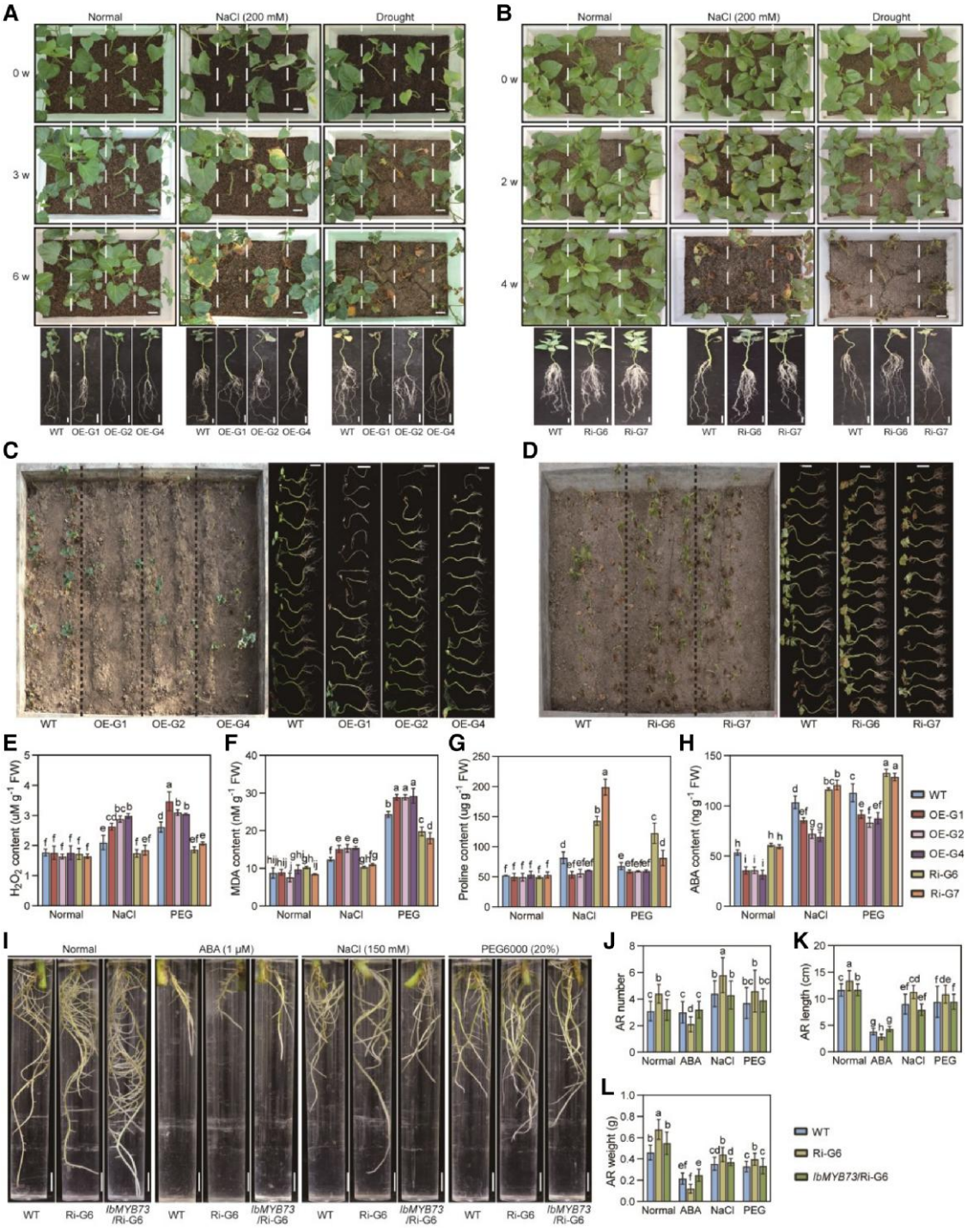

Figure 7. Overexpression of *IbGER5* negatively regulates abiotic stress tolerance under soil conditions. **A** and **B)** Responses of 2-mo-old field-grown *IbGER5* transgenic and WT sweet potato plants (separated by dotted lines) grown in transplantation boxes with addition of 200 mM NaCl or drought stress during 4 or 6 wk period. The representative photographs were taken after stress treatment. Bars, 4 cm. **C** and **D)** Responses of 2-mo-old field-grown *IbGER5* transgenic and WT sweet potato plants (separated by dotted lines) grown for 8 wk in greenhouse without watering. Bars, 10 cm. **E** to **H)** H_2O_2 content **E)**, MDA content **F)**, proline content **G)**, and ABA content **H)** in the adventitious root of *IbGER5* transgenic and WT plants grown on MS medium under normal condition as well as under 150 mM NaCl and 20% PEG6000 treatment for 10 d. Data were presented as means ± SD ($n = 3$). Different lowercase letters indicated statistically significant differences (2-way ANOVA, $P < 0.05$). **I** to **L**), Responses and adventitious root growth condition of 8 d incubation transgenic and WT sweet potato plants grown hydroponically in Hoagland solution alone (normal) or with the addition of ABA (1 μM), NaCl (150 mM), or PEG6000 (20%) for 10 d. Bars, 1 cm. Data were presented as means ± SD ($n = 10$). Different lowercase letters indicated statistically significant differences (2-way ANOVA, $P < 0.05$). AR, adventitious root; WT, the sweet potato variety Lizixiang; OE-G, the *IbGER5*-overexpression lines; Ri-G, the *IbGER5*-RNAi lines; MDA, malondialdehyde; FW, fresh weight.

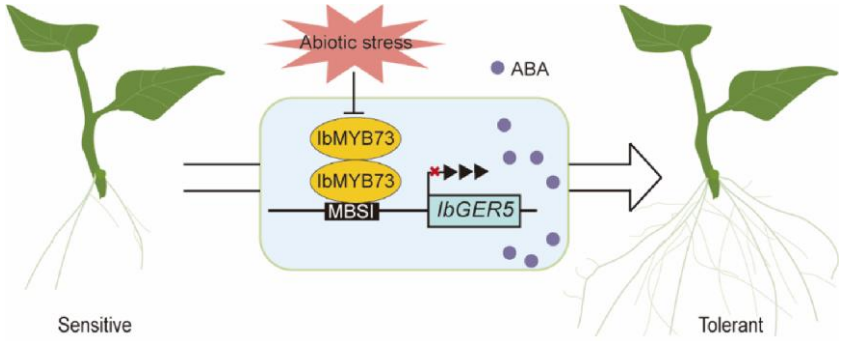

Figure 8. Proposed working model of IbMYB73-IbGER5 regulating ABA-dependent adventitious root growth and abiotic stress tolerance. The expressions of *IbMYB73* and *IbGER5* are suppressed under abiotic stresses. IbMYB73 forms homodimers and activates the transcription of the ABA-responsive gene *IbGER5* by binding to a MBSI motif in its promoter. In addition, the decreased expression of *IbMYB73* and *IbGER5* concomitants with active ABA biosynthesis and signaling and promotes adventitious root growth and abiotic stress tolerance. The circle represents ABA. The arrow represents promotion, and the bar and the cross represent inhibition.

WT plants, the contents of H_2O_2 and MDA were higher, whereas those of proline and ABA were lower, in the adventitious roots of *IbMYB73*-OE and *IbGER5*-OE plants, while the *IbMYB73*-RNAi and *IbGER5*-RNAi lines followed the opposite pattern for the respective physiological indices (Figs. 3 and 7). These data indicated that the overexpression of *IbMYB73* and *IbGER5* inhibited adventitious root growth and reduced storage root yields and abiotic stress tolerance.

ABA has a pervasive role in regulating plant root growth and development as well as responses to abiotic stress. Several genes that positively regulate ABA-dependent root growth and abiotic stress tolerance have been identified. In *Arabidopsis*, *AtWRKY46* promotes lateral root development under abiotic stress via the regulation of ABA signaling and auxin homeostasis (Ding et al. 2015). Meanwhile, the ectopic expression of *SiMYB305* of the high oil-bearing crop sesame in *Arabidopsis* was reported to promote root growth and abiotic stress responses through an ABA-mediated pathway (Dossa et al. 2020). Moreover, the heterologous expression of poplar *PtrSSR1* in transgenic *Arabidopsis* plants mitigates salt stress by integrating the regulation of lateral root emergence and ABA signaling (Fang et al. 2017). In maize, meanwhile, *ZmPTF1* overexpression contributes to an improved root system and an increase in ABA content, thereby enhancing drought tolerance (Li et al. 2019b). *ZmbZIP4* contributes to abiotic stress tolerance by regulating ABA synthesis and root development (Ma et al. 2018). In rice, the overexpression of *OsMADS25* enhances primary root length and lateral root density and confers tolerance to salinity and oxidative stress in an ABA-dependent and ROS scavenging-dependent manner (Xu et al. 2018). However, the genes that regulate ABA-dependent root growth and abiotic stress tolerance in sweet potato have rarely been reported. Here, we found that the expression of *IbMYB73* and *IbGER5* was suppressed by ABA treatment (Figs. 1C and 5I). The overexpression of *IbMYB73* and *IbGER5* inhibited adventitious root growth and abiotic stress tolerance concomitant with a reduction in ABA content (Figs. 2, 3, 6, and 7). Under ABA treatment, genes involved in ABA synthesis (*IbNCED3*, *IbABA2*, and *IbAAO3*), ABA signaling (*IbABI2* and *IbSnRK2.3*), and abiotic stress responses (*IbDREB1D*, *IbRD22*, and *IbRD26*) were downregulated in the *IbMYB73*-OE lines but were upregulated in *IbMYB73*-RNAi plants (Fig. 4). Notably, regulatory network involved in root growth and abiotic stress tolerance have been identified. In *Populus*, PdNF-YB21 interacts with PdFUS3, which activates *PdNCED3* to improve root growth under drought conditions (Zhou et al. 2020). In rice, OsDOF15 binds to the promoter of *OsACS1* to mediate the salt-induced inhibition of root growth (Qin et al. 2019). In this study, we found that IbMYB73 forms homodimers and acts as a nucleus-localized transactivator (Figs. 1 and 5). Furthermore, IbMYB73 significantly increased its ability to bind to the promoter of the ABA-responsive gene *IbGER5* and activate its transcription under both normal and ABA treatment conditions (Fig. 5, E and F). The *IbMYB73*/Ri-G6 plants showed the similar phenotype of adventitious roots with that in WT under abiotic stress, which may be due to the regulation of IbMYB73 targeting *IbGER5* (Fig. 7). Collectively, these results indicated that *IbMYB73* plays critical roles in the regulation of adventitious root growth and abiotic stress tolerance through an *IbGER5*-mediated, ABA-dependent response.

Several GERs involved in ABA signaling have been identified. In *Arabidopsis*, *GEM* acts in the ABA signaling pathway and is a positive effector of germination, being necessary for the breaking of seed dormancy (Mauri et al. 2016). *GER5* has been implicated in the regulation of ABA-dependent seed development and inflorescence architecture (Baron et al. 2014). The silencing of *CaABR1* substantially compromises the hypersensitive response in pepper, and the heterologous expression of *CaABR1* in transgenic *Arabidopsis* confers enhanced resistance to pathogen infection via ABA-salicylic acid antagonism (Choi and Hwang 2011). However, the functions of GERs and the associated molecular regulatory mechanisms remain largely unclear. In this study, we found that there are 3 more GERs in sweet potato than in its 2 diploid relatives *I. triloba* and *I. trifida* (12 vs, respectively, 9 and 9), suggesting that GERs have expanded during evolutionary process (Yang et al. 2019;

Fig. 5G). In addition, the number of GERs in *Arabidopsis* (9), rice (9), maize (14), and wheat (27) differ from that in sweet potato (Fig. 5G; Supplemental Table S4). Meanwhile, the intron of *AtGER5* is substantially shorter than that of *IbGER5*, although the exon–intron patterns are similar (Supplemental Fig. S6B). The functions of GERs and the associated molecular mechanisms merit further investigation.

The results of the present study shed light on the regulatory mechanisms underlying the role of the IbMYB73-IbGER5 module in regulating ABA-dependent adventitious root growth and abiotic stress tolerance in sweet potato. Namely, we found that IbMYB73 forms homodimers and binds to the promoter of *IbGER5* to activate its transcription. For future germplasm improvement, repressing the expression of *IbMYB73* and *IbGER5* in abiotic stress-sensitive germplasms may enable the activation of the ABA response, thereby promoting root development and enhancing the yield and abiotic stress tolerance of sweet potato plants.

Materials and methods

Plant materials and growth conditions

The salt-tolerant sweet potato (*I. batatas*) line "ND98," the salt-sensitive sweet potato variety "Lizixiang" (Zhang et al. 2017a; Zhang et al. 2017b), the Arabidopsis (*Arabidopsis thaliana*) Col-0 ecotype, and *Nicotiana benthamiana* were used in this study. The ND98 line was employed for the cloning of *IbMYB73* and *IbGER5*. Lizixiang, Col-0, and *N. benthamiana* were used to characterize the functions of the 2 genes. In vitro grown transgenic sweet potato ND98 and Lizixiang plants were cultured on MS medium at 27 ± 1 °C under a photoperiod comprising 13 h of cool-white fluorescent light (1500 lx) and 11 h of darkness. The sweet potato plants were cultivated in the field, a greenhouse, or a growth chamber at China Agricultural University, Beijing, China. The *Arabidopsis* seeds were sown on MS medium plates, and seedlings were grown at 22 °C under a 16 h light/8 h dark photoperiod. The seedlings were transplanted into soil and grown under the same conditions.

DNA sequencing and analysis

Genomic DNA (*EasyPure* Plant Genomic DNA Kit, TransGen Biotech Co., Ltd, Beijing, China) and total RNA (TRIzol Reagent, Mei5 Biotechnology Co., Ltd, Beijing, China) were extracted from fresh adventitious root of ND98 plants. Genomic DNA, cDNA, and promoter sequences were amplified using the primers listed in Supplemental Table S1. Conserved domains were searched using InterPro (http://www.ebi.ac.uk/interpro/). Multiple sequence alignment was performed using DNAMAN software. Phylogenetic analysis was conducted using the neighbor-joining method in MEGA X with 1,000 bootstrap iterations (Kumar et al. 2018). The exon–intron structures of genes were analyzed using GSDS 2.0 (http://gsds.gao-lab.org/) (Hu et al. 2015). The *cis*-elements in the promoter regions were analyzed using PlantCARE (http://bioinformatics.psb.ugent.be/webtools/plantcare/html/) (Lescot et al. 2002). The GERs in 7 plant genomes (sweet potato [*I. batatas*, *I. triloba*, *I. trifida*], Arabidopsis, rice [*O. sativa*], maize [*Z. mays*], and wheat [*T. aestivum*]) were identified using HMMER software through the HMM profiles of the GRAM domain (PF02893).

Expression analysis

The adventitious roots of 4-wk-old in vitro grown ND98 and Lizixiang plants were sampled at 0, 1, 2, 6, 12, and 24 h after treatment with 100 μM ABA, 200 mM NaCl, or 20% (w/v) PEG 6000 in Hoagland solution. Total RNA was extracted from leaf, stem, petiole, fibrous root, pencil root, and storage root tissues of 2-mo-old field-grown ND98 plants using the TRIzol method. The experiments were conducted with 3 biological replicates, each with 3 plants. The transcript levels were determined by RT-qPCR. The relative expression levels of the target genes were measured using the comparative C_T method (Schmittgen and Livak 2008). The sweet potato *β-actin* gene served as an internal control (Supplemental Table S1).

Promoter expression analysis

The promoter sequence of *IbMYB73* of ND98 and Lizixiang was inserted into the pMDC162 vector. The resulting plasmids were transformed into *A. tumefaciens* strain GV3101 and then introduced into sweet potato variety Lizixiang or *Arabidopsis* Col-0 plants (Zhang et al. 2006; Gao et al. 2023). The sweet potato transgenic plants were generated by *Agrobacterium*-mediated vacuum infiltration (Gao et al. 2023). The *Arabidopsis* transgenic plants were generated by the flora-dip method, and T1 seedlings were grown on MS medium supplemented with 30 mg/L hygromycin. T3-generation plants were used for subsequent analysis. GUS activity was measured in various tissues as described by Jefferson et al (1987). Twelve-day-old seedlings were cultured separately in Hoagland solution with NaCl (100 mM), mannitol (200 mM), or ABA (50 μM) for 1, 3, and 6 h. *GUS* transcript levels were measured by RT-qPCR using the comparative C_T method (Schmittgen and Livak 2008). The *Arabidopsis ACTIN* and sweet potato *β-actin* gene served as an internal control, respectively (Supplemental Table S1). Three independent biological replicates were performed, each with 5 plants.

Subcellular localization

The entire *IbMYB73* and *IbGER5* coding regions minus the stop codons were cloned into pCAMBIA1300-GFP. These constructs and those expressing the nuclear marker NLS-mCherry or the membrane marker PIP2-mCheery were transformed into sweet potato protoplasts by PEG-calcium transfection (Hayashimoto et al. 1990). Protoplasts from sweet potato petioles were isolated as described previously (Zhang et al. 2020). Fluorescent signals were detected using a confocal laser scanning microscope (LSM900, Zeiss Co., Ltd, Oberkochen, Germany) with excitation at the 488 and

561-nm wavelengths. The experiment was independently repeated 3 times, with similar results.

Transactivation assay in yeast

The full-length coding sequence of *IbMYB73* and fragments encoding amino acids 1 to 115 and 116 to 288 were inserted into the pGBKT7 vector. These constructs, pGBKT7-53 (positive control) or pGBKT7-Lam (negative control), were transferred into yeast strain AH109 according to the Yeast Protocol Handbook (Clontech Co., Ltd, New York, USA). The transformed yeast colonies were cultured on SD/−Trp/−Ade/−His/+X-α-gal medium at 30 °C for 3 d. The primers used for the transcriptional activation assay are listed in Supplemental Table S1. Three independent biological replicates were performed.

Transactivation assay in protoplasts

The *IbMYB73*, *IbMYB73*^{N115}, and *IbMYB73*^{C173} sequences were cloned in-frame with the GAL4 DNA-binding domain of the Pro35S:GAL4 BD vector to use as effectors. The firefly *LUC* gene driven by 5 copies of the GAL4 UAS was used as a reporter. The *REN* (encoding *Renilla* LUC) gene driven by the 35S promoter served as an internal control. The effector, reporter, and internal control plasmids were cotransfected into rice protoplasts by PEG-mediated transformation (Hayashimoto et al. 1990). LUC and REN activity levels were measured using the dual-luciferase reporter assay system (Promega Co., Ltd, Madison, WI, USA). The primers used in this assay are listed in Supplemental Table S1. Three independent biological replicates were performed.

Transgenic plant generation

The 35S:*IbMYB73*-GFP, 35S:*IbGER5*-GFP, and 35S:GFP (pCAMBIA1300-GFP) vectors were transfected into *A. tumefaciens* strain EHA105. In addition, a pair of forward and reverse nonconserved fragments of *IbGER5* was inserted into the plant RNA interference (RNAi) vector pFGC5941 and subsequently transfected into *A. tumefaciens* strain EHA105. Transformation and plant regeneration were performed using embryogenic suspension cultures of the variety Lizixiang via *Agrobacterium*-mediated transformation, as previously described (Liu et al. 2001; Zhang et al. 2022b). A pair of forward and reverse nonconserved fragments of *IbMYB73* was inserted into pFGC5941 and subsequently transfected into *Agrobacterium rhizogenes* strain K599. These clones were dispersed into 200 mL of LB broth and cultured overnight to an OD_{600} of one. Subsequently, the bacteria were centrifuged and resuspended in a buffer solution (10 mM MES and 10 mM $MgCl_2$). The cut–dip–budding delivery system was used for the generation of transformed roots in the Lizixiang variety (Cao et al. 2023). The stems of field-grown sweet potato seedlings were cut 20 cm from the tip, and the cut seedlings were then dipped in *A. rhizogenes* for 1 h. The inoculated plants were incubated in a greenhouse for 3 d and then transplanted into the field. Storage roots were harvested, and transformed roots were identified. Eight plants of storage root number and weight were determined after 4 mo of cultivation.

The transgenic plants of overexpression *IbMYB73* in *IbGER5*-RNAi line were generated by cut–dip–budding delivery system, and the inoculated plants were incubated in a greenhouse for 8 d with short adventitious roots formation.

Abiotic stress tolerance assays

The conditions and times for the ABA, salt, and drought treatments were established based on the stress adaptability of the transgenic plants during a pilot experiment.

Stem tip cuttings (3 cm) from in vitro-grown *IbMYB73* and *IbGER5* transgenic plants, Lizixiang (WT), and ND98 sweet potato plants were grown on MS medium containing 1 μM ABA, 150 mM NaCl, or 20% (w/v) PEG6000 for 10 d. Adventitious root number, length, and weight were determined. Fifteen plants from each line were taken.

Stem segment cuttings (10 cm) from field-grown transgenic and WT plants were cultured in Hoagland solution containing 1 μM ABA, 150 mM NaCl, or 20% (w/v) PEG6000 for 10 d. The number, length, and weight of adventitious roots were determined. Ten cuttings from each line were taken.

Stem tip cuttings (20 cm) from field-grown transgenic and WT plants were planted in a transplantation box in a greenhouse and irrigated with Hoagland solution for 1 wk. For salt and drought tolerance assays, each plant was irrigated with 400 mL of a 200 mM NaCl solution once every 3 d for 4 or 6 wk or submitted to drought stress for 4 or 6 wk. At harvest, the adventitious root number, length, fresh weight, and dry weight were determined. Three independent biological replicates were performed, each with 3 plants.

Stem tip cuttings (20 cm) from field-grown transgenic and WT plants were planted in a greenhouse without watering for 8 wk. At harvest, adventitious root number, length, fresh weight, and dry weight were determined. Fifteen cuttings from each line were taken.

Measurement of abiotic stress tolerance indices

H_2O_2, malondialdehyde (MDA), proline, and ABA contents in the adventitious roots of transgenic and WT plants were measured using the respective assay kits (Comin Biotechnology Co. Ltd., Suzhou, China). Three independent biological replicates were performed, each with 5 plants. The transcript levels of ABA-related genes in the adventitious roots of transgenic and WT plants were measured by RT-qPCR using the comparative C_T method (Schmittgen and Livak 2008). The sweet potato *β-actin* gene was used as an internal control (Supplemental Table S1). Three independent biological replicates were performed, each with 5 plants.

Yeast 2-hybrid assay

The *IbMYB73*^{N115} sequence was cloned into pGADT7 and pGBKT7, and the resulting constructs were transferred into yeast strain AH109. Positive clones were selected on SD/−Trp/−Leu and SD/−Trp/−Leu/−Ade/−His/+X-α-gal medium at 30 °C according to the Yeast Protocol Handbook

(Clontech). The primer sequences used for the Y2H assay are listed in Supplemental Table S1. The experiment was independently repeated 3 times, with similar results.

BiFC assay

The full-length *IbMYB73* sequence was cloned into the pSPYNE-35S vector and fused to the N-terminus of yellow fluorescent protein (nYFP), and the sequences of *IbMYB73* and *IbMYB308L* were also cloned into the pSPYCE-35S vector and fused to the C-terminus of YFP (cYFP) (Walter et al. 2004). The resulting constructs were introduced into *N. benthamiana* leaves by *Agrobacterium*-mediated infiltration. The YFP signal was observed using a confocal laser scanning microscope (LSM 880, Zeiss). The primer sequences are listed in Supplemental Table S1. The experiment was independently repeated 3 times, with similar results.

Co-IP assay

The HA-IbMYB73, IbMYB73-Myc, and IbMYB308L-Myc vectors were transiently expressed in *N. benthamiana* leaves. Total protein was extracted from the leaves using extraction buffer (Zhang et al. 2020), mixed with Myc agarose beads (B26301, Bimake Co., Ltd, Houston, TX, USA), incubated at 4 °C for 2 h, washed at least 5 times with extraction buffer, and boiled in 5× SDS loading buffer for 15 min to separate the proteins from the agarose beads. The proteins were detected using polyclonal anti-HA (1:10,000, H3663, Sigma Co., Ltd, St. Louis, MO, USA) and anti-Myc antibodies (1:10,000, M4439, Sigma). Horseradish peroxidase-conjugated rabbit antimouse IgG (H + L) (1:20,000, 31450, Thermo Fisher Co., Ltd, Waltham, MA, USA) was used as the secondary antibody. The primer sequences are listed in Supplemental Table S1. The experiment was independently repeated 3 times, with similar results.

ChIP assay

The adventitious roots of plants expressing 35S:*IbMYB73*:GFP (OE-M11) or 35S:GFP were used for the ChIP assays, as previously described (Zhang et al. 2020). Anti-GFP (1:5,000, BE2002, EASYBIO Co., Ltd, Beijing, China) antibody was used to immunoprecipitate the protein–DNA complexes, and the precipitated DNA was recovered. An equal amount of chromatin sample without antibody precipitation was used as input control. ChIP DNA was analyzed by qPCR, and the ChIP values were normalized against the values of the respective controls. The primers used for ChIP-qPCR are listed in Supplemental Table S1. Three independent biological replicates were performed.

Electrophoretic mobility shift assay

EMSAs were performed according to the method described in Zhang et al (2020), with minor modifications. pET-28a-*IbMYB73* was transferred into competent *Escherichia coli* strain DE3 cells to produce His-IbMYB73 proteins. Probes labeled or not labeled with biotin at their 5′ ends were used as binding and competitive probes, respectively. The experiment was independently repeated 3 times, with similar results.

Dual-luciferase assay

The full-length IbMYB73 sequence was inserted into pGreenII 62-SK downstream of the CaMV 35S promoter. The *IbGER5* promoter sequences were cloned into pGreenII 0800-LUC. Rice protoplasts were isolated and used for the dual-luciferase assays, as previously described (Zhang et al. 2020). After transient transfection, the protoplasts were incubated in W1 solution for 16 h with or without 1 μM ABA in the dark. LUC and REN activity levels were measured using the dual-luciferase reporter assay system (Promega). The primers are listed in Supplemental Table S1. Three independent biological replicates were performed.

Statistical analysis

All data were analyzed using 1-way ANOVA, 2-way ANOVA, or Student's *t*-tests followed by post hoc Tukey's multiple comparisons in GraphPad Prism 7 (Supplemental Data Set 1). Data were presented as mean ± SD.

Accession numbers

Sequence data from this article can be found in the Sweetpotato Genomics Resource (http://sweetpotato.uga.edu) under accession numbers *IbMYB73* (itb01g33150.t1), *IbNCED3*(itb11g03190.t1), *IbABA2*(itb10g18200.t1), *IbAAO3* (itb12g22200.t1), *IbABI2*(itb03g18390.t2), *IbSnRK2.3*(itb05g18150.t1), *IbDREB1D*(itb03g13510.t1), *IbRD22*(itb15g22680.t1), *IbRD26*(itb15g03720.t1), *IbMYB308L*(itb08g08240.t1), and *ItfGER5*(itf08g10140.t1).

Author contributions

S.-z.H., Hu.Z., and Z.W. conceived and designed the research. Z.W., X.L., X.-r.G., and Y.-k.W. performed the experiments. Z.W., Z.-r.D., K.P., L.-c.J., and S.-p.G. analyzed the data. Z.W. and Hu.Z. wrote the paper. Q.-c.L., H.Z., N.Z., and S.-z.H. revised the paper. All authors read and approved the final version of the paper.

Supplemental data

The following materials are available in the online version of this article.

Supplemental Figure S1. Promoter analysis of *IbMYB73*.

Supplemental Figure S2. Production of *IbMYB73* transgenic sweet potato plants.

Supplemental Figure S3. Responses of salt-tolerant line ND98, WT, and *IbMYB73* transgenic sweet potato plants grown on MS medium.

Supplemental Figure S4. Adventitious root growth indexes of *IbMYB73* transgenic and WT sweet potato plants after 8 wk of grown in greenhouse without watering.

Supplemental Figure S5. Relative expression level of *IbGER5* in the adventitious roots of *IbMYB73* transgenic and WT plants grown on MS medium.

Supplemental Figure S6. Sequence analysis of *IbGER5*.

Supplemental Figure S7. Production of *IbGER5* transgenic sweet potato plants.

Supplemental Figure S8. Responses of *IbGER5* transgenic and WT sweet potato plants grown on MS medium.

Supplemental Figure S9. Adventitious root growth indexes of *IbGER5* transgenic and WT sweet potato plants after 8 wk of grown in greenhouse without watering.

Supplemental Figure S10. Relative expression level of *IbABI2 and IbSnRK2.3* in the adventitious roots of *IbGER5* transgenic and WT plants grown on MS medium.

Supplemental Table S1. Sequence of the primers used in this study.

Supplemental Table S2. Adventitious root growth indexes of *IbMYB73*-OE and WT sweet potato plants after 6 wk of grown in transplantation boxes under normal condition or subjected to 200 mM NaCl or drought stress.

Supplemental Table S3. Adventitious root growth indexes of *IbMYB73*-RNAi and WT sweet potato plants after 4 wk of grown in transplantation boxes under normal condition or subjected to 200 mM NaCl or drought stress.

Supplemental Table S4. Information of *GERs* in different species.

Supplemental Table S5. Adventitious root growth indexes of *IbGER5*-OE and WT sweet potato plants after 6 wk of grown in transplantation boxes under normal condition or subjected to 200 mM NaCl or drought stress.

Supplemental Table S6. Adventitious root growth indexes of *IbGER5*-RNAi and WT sweet potato plants after 4 wk of grown in transplantation boxes under normal condition or subjected to 200 mM NaCl or drought stress.

Supplemental Data Set 1. ANOVA tables.

Funding

This work was supported by grants from the Project of Sanya Yazhou Bay Science and Technology City (grant no. SCKJ-JYRC-2022-61/SYND-2022-09), the Beijing Natural Science Foundation (grant no. 6212017), the Beijing Food Crops Innovation Consortium Program (BAIC02-2023), the Chinese Universities Scientific Fund (2023TC057/2022TC003), and the earmarked fund for CARS-10-Sweetpotato.

Conflict of interest statement. None declared.

Data availability

The data underlying this article are available in the article and in its online supplementary material.

References

Alves G, Torres LF, Dechamp E, Breitler JC, Joet T, Gatineau F, Andrade AC, Bertrand B, Marraccini P, Etienne H. Differential fine-tuning of gene expression regulation in coffee leaves by *CcDREB1D* promoter haplotypes under water deficit. J Exp Bot. 2017:**68**(11): 3017–3031. https://doi.org/10.1093/jxb/erx166

Baron KN, Schroeder DF, Stasolla C. GEm-related 5 (GER5), an ABA and stress-responsive GRAM domain protein regulating seed development and inflorescence architecture. Plant Sci. 2014:**223**: 153–166. https://doi.org/10.1016/j.plantsci.2014.03.017

Bose J, Rodrigo-Moreno A, Shabala S. ROS homeostasis in halophytes in the context of salinity stress tolerance. J Exp Bot. 2014:**65**(5): 1241–1257. https://doi.org/10.1093/jxb/ert430

Cao X, Xie H, Song M, Lu J, Ma P, Huang B, Wang M, Tian Y, Chen F, Peng J, et al. Cut-dip-budding delivery system enables genetic modifications in plants without tissue culture. Innovation (Camb). 2023:**4**(1):100345. https://doi.org/10.1016/j.xinn.2022.100345

Chen Z, Wu ZX, Dong WY, Liu SY, Tian LL, Li JN, Du H. MYB transcription factors becoming mainstream in plant roots. Int J Mol Sci. 2022:**23**(16):9262. https://doi.org/10.3390/ijms23169262

Choi DS, Hwang BK. Proteomics and functional analyses of pepper abscisic acid-responsive 1 (ABR1), which is involved in cell death and defense signaling. Plant Cell. 2011:**23**(2):823–842. https://doi.org/10.1105/tpc.110.082081

Cruz de Carvalho MH. Drought stress and reactive oxygen species: production, scavenging and signaling. Plant Signal Behav. 2008:**3**(3): 156–165. https://doi.org/10.4161/psb.3.3.5536

Cui MH, Yoo KS, Hyoung S, Nguyen HT, Kim YY, Kim HJ, Ok SH, Yoo SD, Shin JS. An *Arabidopsis* R2R3-MYB transcription factor, *AtMYB20*, negatively regulates type 2C serine/threonine protein phosphatases to enhance salt tolerance. FEBS Lett. 2013:**587**(12): 1773–1778. https://doi.org/10.1016/j.febslet.2013.04.028

Ding ZJ, Yan JY, Li CX, Li GX, Wu YR, Zheng SJ. Transcription factor *WRKY46* modulates the development of *Arabidopsis* lateral roots in osmotic/salt stress conditions *via* regulation of ABA signaling and auxin homeostasis. Plant J. 2015:**84**(1):56–69. https://doi.org/10.1111/tpj.12958

Dossa K, Mmadi MA, Zhou R, Liu A, Yang Y, Diouf D, You J, Zhang X. Ectopic expression of the sesame MYB transcription factor *SiMYB305* promotes root growth and modulates ABA-mediated tolerance to drought and salt stresses in *Arabidopsis*. AoB Plants. 2020:**12**(1): plz81. https://doi.org/10.1093/aobpla/plz081

Fang Q, Jiang T, Xu L, Liu H, Mao H, Wang X, Jiao B, Duan Y, Wang Q, Dong Q, et al. A salt-stress-regulator from the *Poplar* R2R3 MYB family integrates the regulation of lateral root emergence and ABA signaling to mediate salt stress tolerance in *Arabidopsis*. Plant Physiol Biochem. 2017:**114**:100–110. https://doi.org/10.1016/j.plaphy.2017.02.018

Feng CZ, Chen Y, Wang C, Kong YH, Wu WH, Chen YF. *Arabidopsis* RAV1 transcription factor, phosphorylated by SnRK2 kinases, regulates the expression of *ABI3, ABI4*, and *ABI5* during seed germination and early seedling development. Plant J. 2014:**80**(4):654–668. https://doi.org/10.1111/tpj.12670

Fujita M, Fujita Y, Maruyama K, Seki M, Hiratsu K, Ohme-Takagi M, Tran LS, Yamaguchi-Shinozaki K, Shinozaki K. A dehydration-induced NAC protein, RD26, is involved in a novel ABA-dependent stress-signaling pathway. Plant J. 2004:**39**(6): 863–876. https://doi.org/10.1111/j.1365-313X.2004.02171.x

Gao XR, Zhang H, Li X, Bai YW, Peng K, Wang Z, Dai ZR, Bian XF, Zhang Q, Jia LC, et al. The B-box transcription factor *IbBBX29* regulates leaf development and flavonoid biosynthesis in sweet potato. Plant Physiol. 2023:**191**(1):496–514. https://doi.org/10.1093/plphys/kiac516

Gelfand I, Sahajpal R, Zhang X, Izaurralde RC, Gross KL, Robertson GP. Sustainable bioenergy production from marginal lands in the US Midwest. Nature. 2013:**493**(7433):514–517. https://doi.org/10.1038/nature11811

Gonzalez-Guzman M, Apostolova N, Belles JM, Barrero JM, Piqueras P, Ponce MR, Micol JL, Serrano R, Rodriguez PL. The short-chain alcohol dehydrogenase ABA2 catalyzes the conversion of xanthoxin to abscisic aldehyde. Plant Cell. 2002:**14**(8):1833–1846. https://doi.org/10.1105/tpc.002477

Hayashimoto A, Li Z, Murai N. A polyethylene glycol-mediated protoplast transformation system for production of fertile transgenic rice plants. Plant Physiol. 1990:**93**(3):857–863. https://doi.org/10.1104/pp.93.3.857

Hu B, Jin JP, Guo AY, Zhang H, Luo JC, Gao G. GSDS 2.0: an upgraded gene feature visualization server. Bioinformatics. 2015:**31**(8): 1296–1297. https://doi.org/10.1093/bioinformatics/btu817

Iuchi S, Kobayashi M, Taji T, Naramoto M, Seki M, Kato T, Tabata S, Kakubari Y, Yamaguchi-Shinozaki K, Shinozaki K. Regulation of drought tolerance by gene manipulation of 9-*cis*-epoxycarotenoid dioxygenase, a key enzyme in abscisic acid biosynthesis in *Arabidopsis*. Plant J. 2001:**27**(4):325–333. https://doi.org/10.1046/j.1365-313x.2001.01096.x

Jefferson RA, Kavanagh TA, Bevan MW. GUS Fusions—beta-glucuronidase as a sensitive and versatile gene fusion marker in higher-plants. EMBO J. 1987:**6**(13):3901–3907. https://doi.org/10.1002/j.1460-2075.1987.tb02730.x

Jiang Y, Tong S, Chen N, Liu B, Bai Q, Chen Y, Bi H, Zhang Z, Lou S, Tang H, et al. The *PalWRKY77* transcription factor negatively regulates salt tolerance and abscisic acid signaling in *Populus*. Plant J. 2021:**105**(5):1258–1273. https://doi.org/10.1111/tpj.15109

Julkowska MM, Koevoets IT, Mol S, Hoefsloot H, Feron R, Tester MA, Keurentjes J, Korte A, Haring MA, de Boer GJ, et al. Genetic components of root architecture remodeling in response to salt stress. Plant Cell. 2017:**29**(12):3198–3213. https://doi.org/10.1105/tpc.16.00680

Kalladan R, Lasky JR, Sharma S, Kumar MN, Juenger TE, Des Marais DL, Verslues PE. Natural variation in 9-*cis*-epoxycartenoid sioxygenase 3 and ABA accumulation. Plant Physiol. 2019:**179**(4):1620–1631. https://doi.org/10.1104/pp.18.01185

Kang C, He SZ, Zhai H, Li RJ, Zhao N, Liu QC. A sweetpotato auxin response factor gene (*IbARF5*) is involved in carotenoid biosynthesis and salt and drought tolerance in transgenic *Arabidopsis*. Front Plant Sci. 2018:**9**:1307. https://doi.org/10.3389/fpls.2018.01307

Kawa D, Meyer AJ, Dekker HL, Abd-El-Haliem AM, Gevaert K, Van De Slijke E, Maszkowska J, Bucholc M, Dobrowolska G, De Jaeger G, et al. SnRK2 protein kinases and mRNA decapping machinery control root development and response to salt. Plant Physiol. 2020:**182**(1):361–377. https://doi.org/10.1104/pp.19.00818

Kim Y, Chung YS, Lee E, Tripathi P, Heo S, Kim KH. Root response to drought stress in rice (*Oryza sativa* L.). Int J Mol Sci. 2020:**21**(4):1513. https://doi.org/10.3390/ijms21041513

Kumar S, Stecher G, Li M, Knyaz C, Tamura K. MEGA X: molecular evolutionary genetics analysis across computing platforms. Mol Biol Evol. 2018:**35**(6):1547–1549. https://doi.org/10.1093/molbev/msy096

Lescot M, Dehais P, Thijs G, Marchal K, Moreau Y, Van de Peer Y, Rouze P, Rombauts S. PlantCARE, a database of plant *cis*-acting regulatory elements and a portal to tools for in silico analysis of promoter sequences. Nucleic Acids Res. 2002:**30**(1):325–327. https://doi.org/10.1093/nar/30.1.325

Leung J, Merlot S, Giraudat J. The *Arabidopsis* ABSCISIC ACID-INSENSITIVE2 (ABI2) and ABI1 genes encode homologous protein phosphatases 2C involved in abscisic acid signal transduction. Plant Cell. 1997:**9**(5):759–771. https://doi.org/10.1105/tpc.9.5.759

Li S, Wang N, Ji D, Zhang W, Wang Y, Yu Y, Zhao S, Lyu M, You J, Zhang Y, et al. A GmSIN1/GmNCED3s/GmRbohBs feed-forward loop acts as a signal amplifier that regulates root growth in soybean exposed to salt stress. Plant Cell. 2019a:**31**(9):2107–2130. https://doi.org/10.1105/tpc.18.00662

Li X, Tang Y, Li H, Luo W, Zhou C, Zhang L, Lv J. A wheat R2R3 MYB gene *TaMpc1-D4* negatively regulates drought tolerance in transgenic *Arabidopsis* and wheat. Plant Sci. 2020:**299**:110613. https://doi.org/10.1016/j.plantsci.2020.110613

Li Z, Liu C, Zhang Y, Wang B, Ran Q, Zhang J. The bHLH family member *ZmPTF1* regulates drought tolerance in maize by promoting root development and abscisic acid synthesis. J Exp Bot. 2019b:**70**(19): 5471–5486. https://doi.org/10.1093/jxb/erz307

Liang C, Liu Y, Li Y, Meng Z, Yan R, Zhu T, Wang Y, Kang S, Ali AM, Malik W, et al. Activation of ABA receptors gene *GhPYL9-11A* is positively correlated with cotton drought tolerance in transgenic *Arabidopsis*. Front Plant Sci. 2017:**8**:1453. https://doi.org/10.3389/fpls.2017.01453

Liu QC, Zhai H, Wang Y, Zhang DP. Efficient plant regeneration from embryogenic suspension cultures of sweetpotato. In Vitro Cell Dev Biol Plant. 2001:**37**(5):564–567. https://doi.org/10.1007/s11627-001-0098-7

Liu ZY, Li XP, Zhang TQ, Wang YY, Wang C, Gao CQ. Overexpression of *ThMYB8* mediates salt stress tolerance by directly activating stress-responsive gene expression. Plant Sci. 2021:**302**:110668. https://doi.org/10.1016/j.plantsci.2020.110668

Ma H, Liu C, Li Z, Ran Q, Xie G, Wang B, Fang S, Chu J, Zhang J. *ZmbZIP4* contributes to stress resistance in maize by regulating ABA synthesis and root development. Plant Physiol. 2018:**178**(2): 753–770. https://doi.org/10.1104/pp.18.00436

Mabuchi K, Maki H, Itaya T, Suzuki T, Nomoto M, Sakaoka S, Morikami A, Higashiyama T, Tada Y, Busch W, et al. MYB30 Links ROS signaling, root cell elongation, and plant immune responses. Proc Natl Acad Sci U S A. 2018:**115**(20):E4710–E4719. https://doi.org/10.1073/pnas.1804233115

Mauri N, Fernández-Marcos M, Costas C, Desvoyes B, Pichel A, Caro E, Gutierrez C. GEM, a member of the GRAM domain family of proteins, is part of the ABA signaling pathway. Sci Rep. 2016:**6**(1):22660. https://doi.org/10.1038/srep22660

Meng X, Liu S, Zhang C, He J, Ma D, Wang X, Dong T, Guo F, Cai J, Long T, et al. The unique sweet potato NAC transcription factor *IbNAC3* modulates combined salt and drought stresses. Plant Physiol. 2023:**191**(1):747–771. https://doi.org/10.1093/plphys/kiac508

Mukhopadhyay SK, Chattopadhyay A, Chakraborty I, Bhattacharya I. Crops that feed the world 5. Sweetpotato. Sweetpotatoes for income and food security. Food Secur. 2011:**3**(3):283–305. https://doi.org/10.1007/s12571-011-0134-3

Narusaka Y, Nakashima K, Shinwari ZK, Sakuma Y, Furihata T, Abe H, Narusaka M, Shinozaki K, Yamaguchi-Shinozaki K. Interaction between two *cis*-acting elements, ABRE and DRE, in ABA-dependent expression of Arabidopsis *rd29A* gene in response to dehydration and high-salinity stresses. Plant J. 2003:**34**(2): 137–148. https://doi.org/10.1046/j.1365-313X.2003.01708.x

Oh JE, Kwon Y, Kim JH, Noh H, Hong SW, Lee H. A dual role for *MYB60* in stomatal regulation and root growth of *Arabidopsis thaliana* under drought stress. Plant Mol Biol. 2011:**77**(1–2):91–103. https://doi.org/10.1007/s11103-011-9796-7

Qin H, Wang J, Chen X, Wang F, Peng P, Zhou Y, Miao Y, Zhang Y, Gao Y, Qi Y, et al. Rice *OsDOF15* contributes to ethylene-inhibited primary root elongation under salt stress. New Phytol. 2019:**223**(2): 798–813. https://doi.org/10.1111/nph.15824

Ramanathan V, Rahman H, Subramanian S, Nallathambi J, Kaliyaperumal A, Manickam S, Ranganathan C, Muthurajan R. OsARD4 encoding an acireductone dioxygenase improves root architecture in rice by promoting development of secondary roots. Sci Rep. 2018:**8**(1):15713. https://doi.org/10.1038/s41598-018-34053-y

Romero I, Fuertes A, Benito MJ, Malpica JM, Leyva A, Paz-Ares J. More than 80R2R3-MYB regulatory genes in the genome of *Arabidopsis thaliana*. Plant J. 1998:**14**(3):273–284. https://doi.org/10.1046/j.1365-313X.1998.00113.x

Schmittgen TD, Livak KJ. Analyzing real-time PCR data by the comparative C-T method. Nat Protoc. 2008:**3**(6):1101–1108. https://doi.org/10.1038/nprot.2008.73

Seo DH, Seomun S, Choi YD, Jang G. Root development and stress tolerance in rice: the key to improving stress tolerance without yield penalties. Int J Mol Sci. 2020:**21**(5):1807. https://doi.org/10.3390/ijms21051807

Seo M, Peeters A, Koiwai H, Oritani T, Marion-Poll A, Zeevaart J, Koornneef M, Kamiya Y, Koshiba T. The *Arabidopsis* aldehyde oxidase 3 (*AA03*) gene product catalyzes the final step in abscisic acid biosynthesis in leaves. Proc Natl Acad Sci U S A. 2000:**97**(23): 12908–12913. https://doi.org/10.1073/pnas.220426197

Tao X, Gu YH, Wang HY, Zheng W, Li X, Zhao CW, Zhang YZ. Digital gene expression analysis based on integrated de novo transcriptome

assembly of sweet potato [*Ipomoea batatas* (L.) Lam]. PLoS One. 2012:**7**(4):e36234. https://doi.org/10.1371/journal.pone.0036234

Walter M, Chaban C, Schutze K, Batistic O, Weckermann K, Nake C, Blazevic D, Grefen C, Schumacher K, Oecking C, et al. Visualization of protein interactions in living plant cells using bimolecular fluorescence complementation. Plant J. 2004:**40**(3):428–438. https://doi.org/10.1111/j.1365-313X.2004.02219.x

Wang H, Zhou L, Fu Y, Cheung MY, Wong FL, Phang TH, Sun Z, Lam HM. Expression of an apoplast-localized BURP-domain protein from soybean (GmRD22) enhances tolerance towards abiotic stress. Plant Cell Environ. 2012:**35**(11):1932–1947. https://doi.org/10.1111/j.1365-3040.2012.02526.x

Wang N, Zhang W, Qin M, Li S, Qiao M, Liu Z, Xiang F. Drought tolerance conferred in soybean (*Glycine max. L)* by *GmMYB84*, a novel R2R3-MYB transcription factor. Plant Cell Physiol. 2017:**58**(10): 1764–1776. https://doi.org/10.1093/pcp/pcx111

Wu S, Lau KH, Cao Q, Hamilton JP, Sun H, Zhou C, Eserman L, Gemenet DC, Olukolu BA, Wang H, et al. Genome sequences of two diploid wild relatives of cultivated sweetpotato reveal targets for genetic improvement. Nat Commun. 2018:**9**(1):4580. https://doi.org/10.1038/s41467-018-06983-8

Xu N, Chu Y, Chen H, Li X, Wu Q, Jin L, Wang G, Huang J. Rice transcription factor *OsMADS25* modulates root growth and confers salinity tolerance via the ABA-mediated regulatory pathway and ROS scavenging. PLoS Genet. 2018:**14**(10):e1007662. https://doi.org/10.1371/journal.pgen.1007662

Yang S, Sweetman JP, Amirsadeghi S, Barghchi M, Huttly AK, Chung WI, Twell D. Novel anther-specific myb genes from tobacco as putative regulators of phenylalanine ammonia-lyase expression. Plant Physiol. 2001:**126**(4):1738–1753. https://doi.org/10.1104/pp.126.4.1738

Yang Z, Sun J, Chen Y, Zhu P, Zhang L, Wu S, Ma D, Cao Q, Li Z, Xu T. Genome-wide identification, structural and gene expression analysis of the bZIP transcription factor family in sweet potato wild relative *Ipomoea trifida*. BMC Genet. 2019:**20**(1):41. https://doi.org/10.1186/s12863-019-0743-y

You J, Zong W, Hu H, Li X, Xiao J, Xiong L. A STRESS-RESPONSIVE NAC1-regulated protein phosphatase gene rice protein phosphatase 18 modulates drought and oxidative stress tolerance through abscisic acid-independent reactive oxygen species scavenging in rice. Plant Physiol. 2014:**166**(4):2100–2114. https://doi.org/10.1104/pp.114.251116

Zhai H, Wang F, Si Z, Huo J, Xing L, An Y, He S, Liu Q. A myo-inositol-1-phosphate synthase gene, *IbMIPS1*, enhances salt and drought tolerance and stem nematode resistance in transgenic sweet potato. Plant Biotechnol J. 2016:**14**(2):592–602. https://doi.org/10.1111/pbi.12402

Zhang H, Gao X, Zhi Y, Li X, Zhang Q, Niu J, Wang J, Zhai H, Zhao N, Li J, et al. A non-tandem CCCH-type zinc-finger protein, *IbC3H18*, functions as a nuclear transcriptional activator and enhances abiotic stress tolerance in sweet potato. New Phytol. 2019:**223**(4): 1918–1936. https://doi.org/10.1111/nph.15925

Zhang H, Wang Z, Li X, Gao X, Dai Z, Cui Y, Zhi Y, Liu Q, Zhai H, Gao S, et al. The IbBBX24-IbTOE3-IbPRX17 module enhances abiotic stress tolerance by scavenging reactive oxygen species in sweet potato. New Phytol. 2022b:**233**(3):1133–1152. https://doi.org/10.1111/nph.17860

Zhang H, Zhang Q, Wang YN, Li Y, Zhai H, Liu QC, He SZ. Characterization of salt tolerance and *Fusarium wilt* resistance of a sweetpotato mutant. J Integr Agric. 2017a:**16**(9):1946–1955. https://doi.org/10.1016/S2095-3119(16)61519-8

Zhang H, Zhang Q, Zhai H, Gao S, Yang L, Wang Z, Xu Y, Huo J, Ren Z, Zhao N, et al. *IbBBX24* promotes the jasmonic acid pathway and enhances *Fusarium wilt* resistance in sweet potato. Plant Cell. 2020:**32**(4):1102–1123. https://doi.org/10.1105/tpc.19.00641

Zhang H, Zhang Q, Zhai H, Li Y, Wang X, Liu Q, He S. Transcript profile analysis reveals important roles of jasmonic acid signalling pathway in the response of sweet potato to salt stress. Sci Rep. 2017b:**7**(1): 40819. https://doi.org/10.1038/srep40819

Zhang H, Zhu J, Gong Z, Zhu JK. Abiotic stress responses in plants. Nat Rev Genet. 2022a:**23**(2):104–119. https://doi.org/10.1038/s41576-021-00413-0

Zhang X, Henriques R, Lin SS, Niu QW, Chua NH. *Agrobacterium*-mediated transformation of *Arabidopsis thaliana* using the floral dip method. Nat Protoc. 2006:**1**(2):641–646. https://doi.org/10.1038/nprot.2006.97

Zhao PX, Zhang J, Chen SY, Wu J, Xia JQ, Sun LQ, Ma SS, Xiang CB. *Arabidopsis* MADS-box factor *AGL16* is a negative regulator of plant response to salt stress by downregulating salt-responsive genes. New Phytol. 2021:**232**(6):2418–2439. https://doi.org/10.1111/nph.17760

Zhong X, Hong W, Shu Y, Li J, Liu L, Chen X, Islam F, Zhou W, Tang G. CRISPR/Cas9 mediated gene-editing of *GmHdz4* transcription factor enhances drought tolerance in soybean (*Glycine max* [L.] Merr.). Front Plant Sci. 2022:**13**:988505. https://doi.org/10.3389/fpls.2022.988505

Zhou Y, Zhang Y, Wang X, Han X, An Y, Lin S, Shen C, Wen J, Liu C, Yin W, et al. Root-specific NF-Y family transcription factor, *PdNF-YB21*, positively regulates root growth and drought resistance by abscisic acid-mediated indoylacetic acid transport in *Populus*. New Phytol. 2020:**227**(2):407–426. https://doi.org/10.1111/nph.16524

ARTICLES FOR FACULTY MEMBERS

INVESTIGATING THE ROLE OF GIBBERELLIC ACID (GA) AND ABSCISIC ACID (ABA) CROSS-TALK IN ENHANCING TUBEROUS ROOT DEVELOPMENT IN SWEET POTATOES

Molecular characterization and target prediction of candidate miRNAs related to abiotic stress responses and/or storage root development in sweet potato / Sun, L., Yang, Y., Pan, H., Zhu, J., Zhu, M., Xu, T., Li, Z., & Dong, T.

Genes
Volume 13 Issue 1 (2022) 110 Pages 1-16
https://doi.org/10.3390/genes13010110
(Database: MDPI)

genes

MDPI

Article

Molecular Characterization and Target Prediction of Candidate miRNAs Related to Abiotic Stress Responses and/or Storage Root Development in Sweet Potato

Li Sun [1,†], Yiyu Yang [1,†], Hong Pan [2,†], Jiahao Zhu [1], Mingku Zhu [1,2], Tao Xu [2], Zongyun Li [2,*] and Tingting Dong [1,*]

[1] Institute of Integrative Plant Biology, School of Life Science, Jiangsu Normal University, Xuzhou 221008, China; 15165542391@163.com (L.S.); hongzhuang00140020@163.com (Y.Y.); f2694635698@gmail.com (J.Z.); mingkuzhu007@126.com (M.Z.)

[2] Jiangsu Key Laboratory of Phylogenomics & Comparative Genomics, School of Life Sciences, Jiangsu Normal University, Xuzhou 221008, China; A2627147086@126.com (H.P.); xutao_yr@126.com (T.X.)

* Correspondence: zongyunli@jsnu.edu.cn (Z.L.); dtt@jsnu.edu.cn (T.D.); Tel.: +86-516-8340-3172 (Z.L.); +86-516-8350-0083 (T.D.)

† These authors contributed equally to this work.

Abstract: Sweet potato is a tuberous root crop with strong environmental stress resistance. It is beneficial to study its storage root formation and stress responses to identify sweet potato stress- and storage-root-thickening-related regulators. Here, six conserved miRNAs (miR156g, miR157d, miR158a-3p, miR161.1, miR167d and miR397a) and six novel miRNAs (novel 104, novel 120, novel 140, novel 214, novel 359 and novel 522) were isolated and characterized in sweet potato. Tissue-specific expression patterns suggested that miR156g, miR157d, miR158a-3p, miR167d, novel 359 and novel 522 exhibited high expression in fibrous roots or storage roots and were all upregulated in response to storage-root-related hormones (indole acetic acid, IAA; zeaxanthin, ZT; abscisic acid, ABA; and gibberellin, GAs). The expression of miR156g, miR158a-3p, miR167d, novel 120 and novel 214 was induced or reduced dramatically by salt, dehydration and cold or heat stresses. Moreover, these miRNAs were all upregulated by ABA, a crucial hormone modulator in regulating abiotic stresses. Additionally, the potential targets of the twelve miRNAs were predicted and analyzed. Above all, these results indicated that these miRNAs might play roles in storage root development and/or stress responses in sweet potato as well as provided valuable information for the further investigation of the roles of miRNA in storage root development and stress responses.

Keywords: miRNA; abiotic stress; hormone; storage root; sweet potato

Citation: Sun, L.; Yang, Y.; Pan, H.; Zhu, J.; Zhu, M.; Xu, T.; Li, Z.; Dong, T. Molecular Characterization and Target Prediction of Candidate miRNAs Related to Abiotic Stress Responses and/or Storage Root Development in Sweet Potato. *Genes* **2022**, *13*, 110. https://doi.org/10.3390/genes13010110

Academic Editors: Dan Milbourne and Bin Yu

Received: 30 November 2021
Accepted: 4 January 2022
Published: 6 January 2022

1. Introduction

MicroRNAs (miRNAs) are a series of single-stranded sRNAs that usually consist of 20–24 nucleotides [1,2]. They are produced by complex biological processes. First, pri-miRNAs are transcribed by miRNA-coding genes. Then, pri-miRNAs are cut by the drosha–DGCR8 complex to produce pre-miRNAs that have hairpin secondary structures. Subsequently, pre-miRNAs are identified and cut by RNase Dicer, and mature miRNA as well as miRNA* are produced. Finally, most miRNA*s are degraded, and the miRNAs form RISC [3,4].

The main function of miRNAs is to play crucial roles in post-transcriptional regulation [5]. In plants, miRNAs are related to plant development and resistance. For instance, miR319 regulates the formation of leaf serrations by inhibiting *TCP* (*TEOSINTE-BRANCHED1*, *CYCLOIDEA* and *PROLIFERATING CELL NUCLEAR ANTIGEN BINDING FACTOR*) genes [6]. miR172 functions in the determination of flower development and flowering by targeting *AP2* (*APETALA2*) and/or *AP2-like* genes [7]. miR390 regulates lateral root formation and growth by negatively regulating auxin response factors (ARFs) [8].

Additionally, a set of miRNAs have been confirmed to play essential roles in plant stress resistance. miR164 is characterized as an important player in salt and drought stress resistance by regulating the expression of NAC genes [9,10]. miR398 could mediate the accumulation of ROS and the response to high-temperature stress by impacting its target genes: *CSDs*, *CCS1* and/or *COX5b-1* [11,12]. Moreover, plants that overexpressed miR319 exhibited improved tolerance to salt stress [13].

Sweet potato (*Ipomoea batatas* (L.) Lam.) is a tuberous root crop with strong environmental stress resistance and poor soil tolerance. It is beneficial for finding regulators related both to storage root development and stress resistance to investigate the characteristics of sweet potato; research has confirmed that miRNAs play crucial roles in both aspects [14,15]. Thus, we predict that there may be some miRNAs related to both sweet potato storage root development and stress resistance. In recent years, several miRNAs have been identified by high-throughput sequencing in sweet potato. Saminathan and Reddy reported that 32 known miRNAs and 25 novel miRNAs were differentially expressed during drought and that CO_2 stresses were identified in sweet potato by small RNA sequencing [16]. A total of 190 conserved miRNAs and 191 novel miRNAs were identified from sweet potato storage roots under cold stress treatment [17]. Fifty-one miRNAs were markedly induced and 76 miRNAs were significantly reduced in sweet potato leaves; 13 miRNAs were strikingly upregulated and nine miRNAs were obviously downregulated in sweet potato roots by salt stress treatment [18]. The sRNA sequencing results of He et al. reported 121 differentially expressed miRNAs between white flesh sweet potato (Xushu 18) and purple flesh sweet potato (Xuzishu 3) [19]. Above all, there have been many high-throughput sequencing data on sweet potato miRNA. Unfortunately, only a few of them have been analyzed deeply. The relationship between miRNAs and sweet potato resistance and/or storage root thickening is largely unknown.

In this study, six conserved miRNAs and six novel miRNAs were isolated and characterized in sweet potato. The structures of the novel miRNAs and the expression profiles of all twelve miRNAs were investigated. In addition, the expression patterns of these twelve miRNAs under abiotic stresses (salt, dehydration and cold as well as heat stress) and development/stress-related hormone treatments (IAA, indole acetic acid; ZT; zeaxanthin; GAs, gibberellin; and ABA, abscisic acid) were analyzed. Moreover, the candidate targets of these miRNAs were predicted. These results provide valuable information for the further investigation of miRNA roles in storage root development and stress responses of sweet potato.

2. Materials and Methods

2.1. Plant Materials

Sweet potatoes (Xushu 22) were grown in a greenhouse at 18–28 °C under a long-day photoperiod (16/8 h, light/dark). For organ-specific expression profiling of miRNAs and target genes, the tissues of stems, leaves, fibrous roots and storage roots in different stages were collected and promptly frozen in liquid nitrogen and stored at −80 °C until required.

2.2. Identification of Sweet Potato miRNAs

Six known miRNAs (miR156g, miR157d, miR158a-3p, miR161.1, miR167d and miR397a) and six novel miRNAs (novel 104, novel 120, novel 140, novel 214, novel 359 and novel 522) were identified by using our high-throughput sequencing analysis of sweet potato [20]. Sweet potato fibrous roots and four different developmental stages of storage roots were collected for small RNA sequencing. Twelve miRNAs that differentially expressed in fibrous roots compared with storage roots were chosen.

2.3. Predicted Hairpin Secondary Structures of Novel miRNAs

The hairpin secondary structures of novel miRNAs were predicted by RNAfold (http://rna.tbi.univie.ac.at//cgi-bin/RNAWebSuite/RNAfold.cgi, accessed on 17 December

2021). For fold algorithms and basic options, "minimum free energy (MFE) and partition function" and "avoid isolated base pairs" were used.

2.4. Abiotic Stress and Hormone Treatments

Abiotic stress (salt, dehydration and cold as well as heat treatments) and plant hormone treatments (IAA, ZT, ABA and GAs) were performed as described by Dong et al. [21]. Sweet potato plants with 5–6 leaves and 8–10 cm adventitious roots were chosen and cultured in water. For the salt, dehydration and hormone treatments, 150 mM NaCl, 100 mM PEG (polyethylene glycol), 100 μM IAA, 100 μM ZT, 100 μM ABA and 100 μM GAs were used and the plants were cultured in a greenhouse. For the cold and heat treatments, the pants were cultured in water at 4 °C and 40 °C. Then, adventitious roots were collected after 0, 1, 12, 24 and 48 h for analysis.

2.5. QRT-PCR Analysis of miRNAs

Total RNA was isolated from sweet potato leaves (leaves obtained from three-month-old plants), stems (stems obtained from three-month-old plants) and roots at five stages (FR, fibrous roots; D1, 1 cm storage roots; D3, 3 cm storage roots; D5, 5 cm storage roots; and D10, 10 cm storage roots) by a RNAprep Pure Plant Plus Kit (Polysaccharides & Polyphenolics-rich; TIANGEN, Beijing, China). Reverse transcription and qRT-PCR were performed as described by Tang et al. [20]. An adaptor (5′ GTC GTA TCC AGT GCA GGG TCC GAG GTA TTC GCA CTG GAT ACG AC 3′) was added to the 3′ end of the miRNAs through a reverse transcription program; the reverse transcription of the miRNAs was performed by a PrimeScript™ RT reagent kit with gDNA Eraser (TaKaRa, Dalian, China). qRT-PCR was performed by using TB Green™ Premix Ex Taq™ II (TaKaRa, Dalian, China) and CFX96™ Real-Time System (Bio-Rad, Hercules, CA, USA) with the following procedures: 95 °C for 30 s, then 95 °C for 5 s and 60 °C for 40 s for 40 cycles. The primers used for miRNA qRT-PCR analysis are listed in Table S2. Sweet potato *ARF* (ADP-ribosylation factor) was used as the reference gene for the normalization of gene expression [22].

2.6. Target Prediction and Analysis

The target genes of the miRNAs were predicted by combined analysis of RNA-seq and sRNA-seq, and a set of potentail targets of each miRNA have been identified [20]. Then, one predicted target of each miRNA was chosen and its expression in sweet potato leaves, stems and roots was analyzed by qRT-PCR. The methods used for the qRT-PCR of the target genes were performed by using TB Green™ Premix Ex Taq™ II (TaKaRa, Dalian, China) and a CFX96™ Real-Time System (Bio-Rad, Hercules, CA, USA) with the procedures below: 95 °C 30 s, then 95 °C 5 s, 60 °C 40 s for 40 cycles. Sweet potato *ARF* was used as the reference gene and the primers used for target qRT-PCR analysis are listed in Supplementary Materials Table S2.

2.7. Statistical Analysis

The data were statistically analyzed by SPSS software (IBM Corp., Armonk, NY, USA) with an ANOVA (one-way analysis of variance), and differences in means were determined to be significant by a Dunnett's test at $p < 0.05$ and $p < 0.01$. Additionally, to make the statistical inference more convenient and reasonable, a log10 transformation of the expression data was performed.

3. Results

3.1. Isolation and Structure Analysis of Sweet Potato miRNAs

Six known miRNAs (miR156g, miR157d, miR158a-3p, miR161.1, miR167d and miR397a) and six novel miRNAs (novel 104, novel 120, novel 140, novel 214, novel 359 and novel 522) were identified and selected by high-throughput sequencing analysis of sweet potato. The mature sequences and pre-miRNA sequences of these miRNAs are listed in Table S1. Then,

the secondary structures of the novel pre-miRNAs were predicted. The results showed that all six novel miRNAs could form hairpin structures (Figure 1).

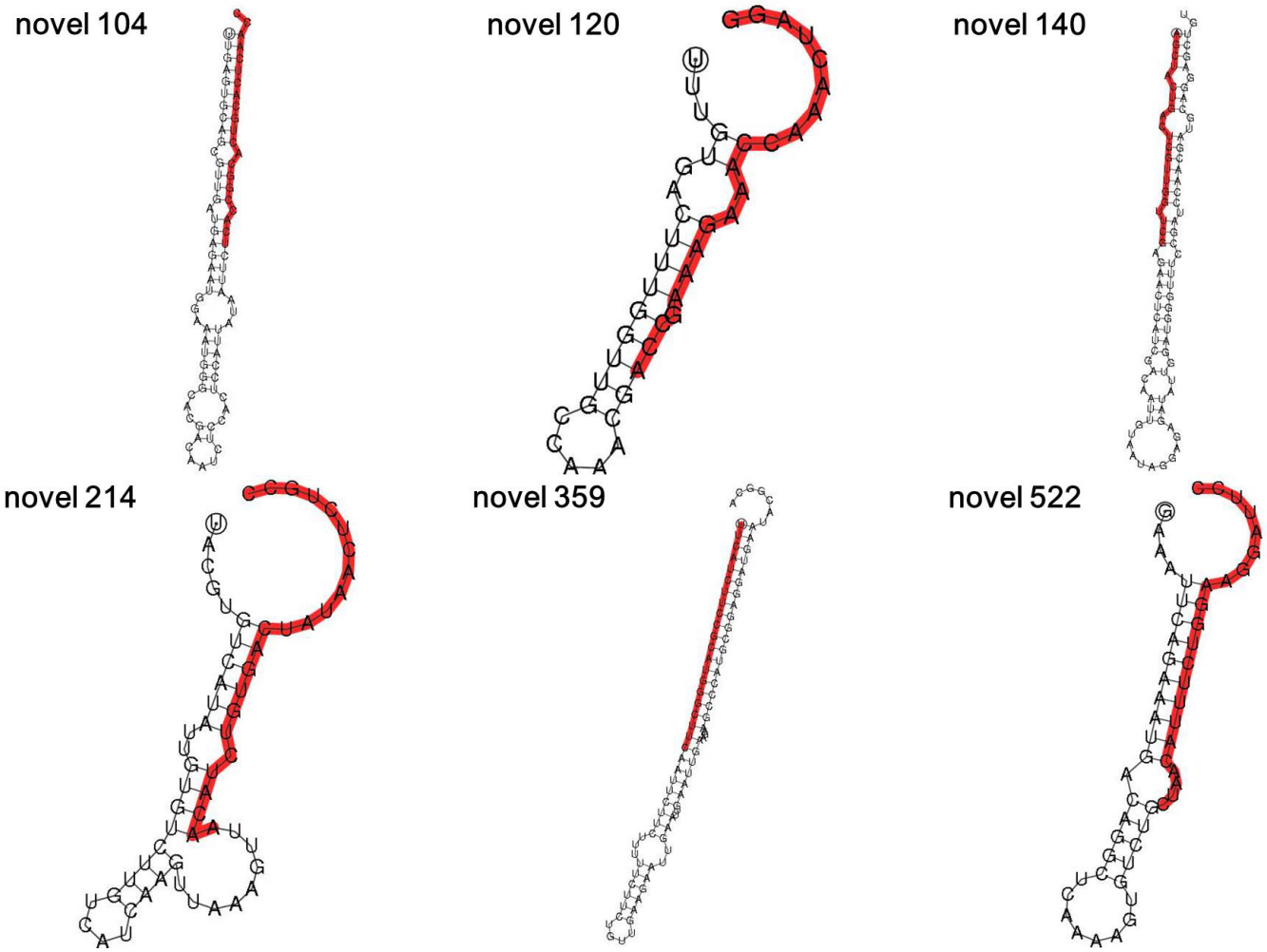

Figure 1. Hairpin secondary structures of novel miRNAs. The hairpin secondary structures of novel 104, novel 120, novel 140, novel 214, novel 359 and novel 522. The mature sequences of the six novel miRNAs are marked red.

3.2. Organ-Specific Expression of miRNAs in Sweet Potato

Organ-specific expression profiles of the miRNAs were analyzed by qRT-PCR. The results showed that the twelve miRNAs exhibited different levels of expression in different sweet potato tissues (Figure 2). miR156g, miR158a-3p and novel 522 exhibited high expression in fibrous roots of sweet potato, while lower levels of expression were observed in other tissues (Figure 2). Similar to these three miRNAs, miR167d and miR397a not only exhibited high expression in fibrous roots but were also expressed highly in stems and mature storage roots, respectively (Figure 2). In contrast, miR157d, novel 120 and novel 359 were expressed highly in the D5 stage of storage roots than in other tissues, and novel 104 showed high expression in D10 stage of storage roots (Figure 2). In addition, the predominant expression of miR161.1, novel 140 and novel 214 was detected in stems, while a small number of these miRNAs were accumulated in other tissues (Figure 2). These sundry tissue-specific expression profiles suggested that the twelve miRNAs might play multiple functions during the growth and development of sweet potato.

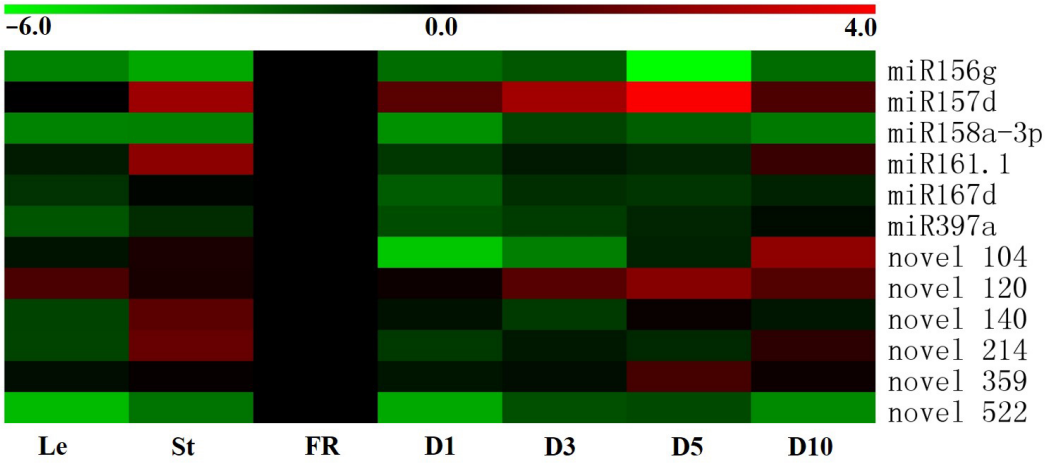

Figure 2. Expression profiles of six conserved and six novel miRNAs in different tissues of sweet potato. The tissues were obtained from Xushu 22 and the expression profiles of the miRNAs were detected by qRT-PCR. Log2-transformed fold-change data were used to create a heatmap via MeV4.9. The relative expression of FR was normalized to 0. Le, leaves obtained from three-month-old plants; St, stems obtained from three-month-old plants; FR, fibrous roots; D1, 1 cm storage roots; D3, 3 cm storage roots; D5, 5 cm storage roots; and D10, 10 cm storage roots.

3.3. The miRNAs Participate in Resistance to Various Abiotic Stresses in Sweet Potato

To screen sweet potato miRNAs participating in stress resistance and explore the potential functions of these twelve miRNAs under stress conditions, qRT-PCR was performed. Under the salt treatment, varying degrees of changes were observed in the expression of these twelve miRNAs (Figure 3). Weak induction was detected in miR156g, miR158a-3p and miR161.1 (Figure 3). The expression of miR157d, miR167d, miR397a and novel 120 was induced gradually and reached a maximum level at 12 h after the salt treatment; the expression level of miR167d increased by more than 20-fold (Figure 3). Novel 104 and novel 522 reached their maximum levels at 24 h after the salt treatment, and the expression level of novel 522 was increased by approximately 25-fold (Figure 3). In contrast, the expression of novel 140 and novel 359 was seriously inhibited by the salt treatment (Figure 3).

After the dehydration treatment, the great majority of miRNAs were upregulated significantly (Figure 3). The expression of miR156g, miR167d, novel 104, novel 120 and novel 214 was induced gradually from 1 h to 48 h of the PEG treatment (Figure 3). Among them, the levels of two miRNAs, miR167d and novel 120, were increased by more than 100-fold after 48 h the PEG treatment (Figure 3). miR157d and novel 359 were accumulated markedly after 1 h PEG treatment (Figure 3). Four miRNAs, miR158a-3p, miR161.1, miR397a and novel 140, exhibited their maximum induction after 24 h of the PEG treatment, and the expression of miR158a-3p was increased by more than 800-fold (Figure 3). The level of novel 522 was reduced by approximately 80% (Figure 3).

The significant inhibition of the expression of five miRNAs, miR156g, miR158a-3p, miR167d, novel 104 and novel 359, was detected after the cold treatment (Figure 4). The expression of the other seven miRNAs was all increased, and the maximum induction was detected after 48 h of the cold treatment with miR397a (Figure 4). For the heat treatment the expression of most of the miRNAs was increased (Figure 4). miR156g was increased gradually from 1 h to 48 h, and reached a maximum value at 48 h with an approximately 60-fold increase under high temperature (Figure 4). miR158a-3p, miR397a, novel 104 and novel 359 were accumulated heavily after 1 h of heat treatment (Figure 4). The levels of miR157d and miR167d were increased dramatically after 24 h of heat treatment (Figure 4). The significant inhibition of miR161.1, novel 140, novel 214 and novel 522 was observed under heat treatment (Figure 4). Overall, the results indicated that these miRNAs are stress-responsive.

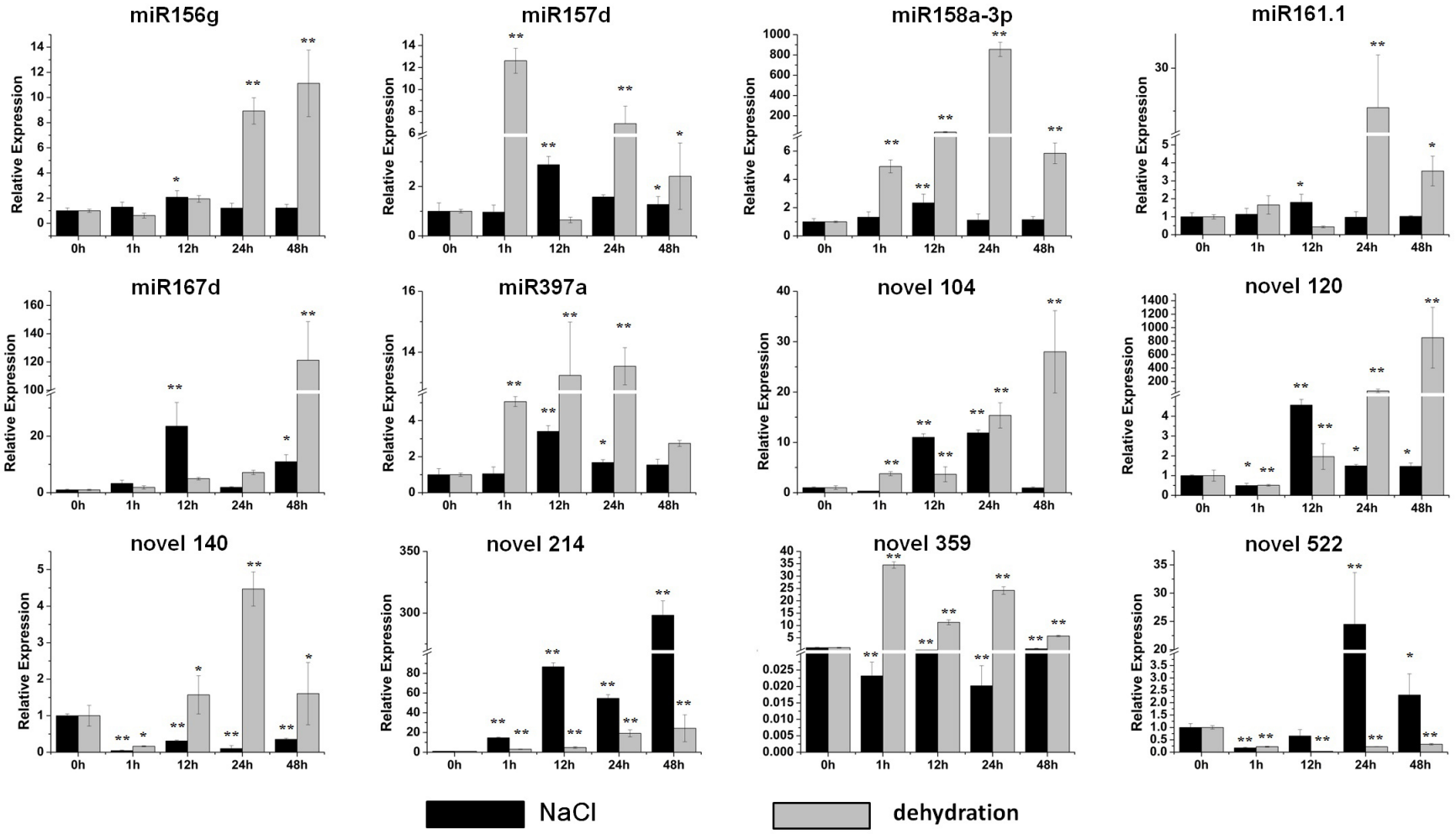

Figure 3. Expression profiles of six conserved and six novel miRNAs under salt and dehydration stresses. The relative expression levels of unstressed plants (0 h) were normalized to 1. One asterisk (*) indicates statistically significant differences between control (0 h) and stress-treated plants ($p < 0.05$); two asterisks (**) indicate statistically extremely significant differences between control (0 h) and stress-treated plants ($p < 0.01$). The black columns represent the salt treatment and the grey columns represent the dehydration treatment.

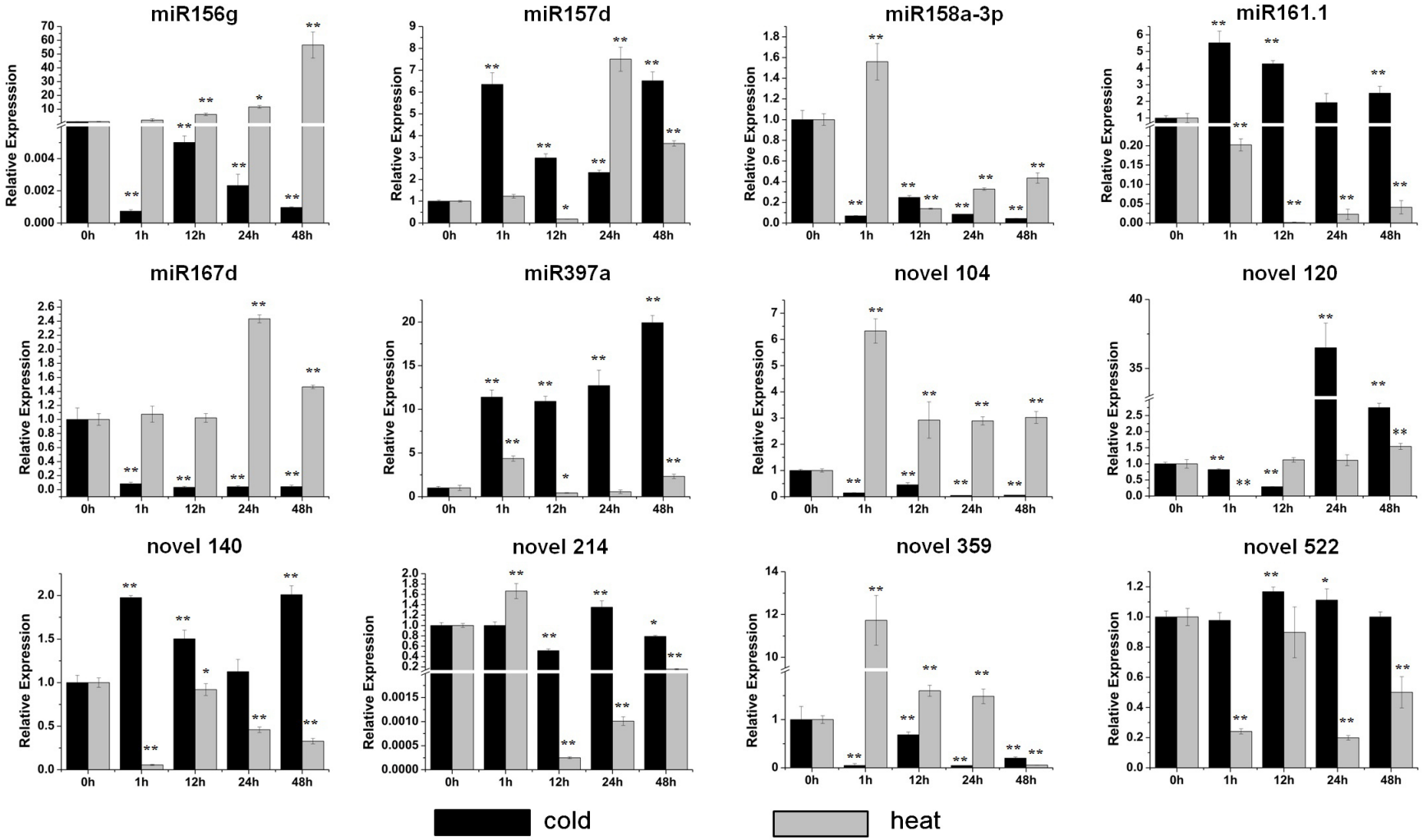

Figure 4. Expression profiles of six conserved and six novel miRNAs under cold and heat stresses. The relative expression levels of unstressed plants (0 h) were normalized to 1. One asterisk (*) indicates statistically significant differences between control (0 h) and stress-treated plants ($p < 0.05$), and two asterisks (**) indicate statistically extremely significant differences between control (0 h) and stress-treated plants ($p < 0.01$). The black columns represent the cold treatment and the grey columns represent the heat treatment.

3.4. The Expression of Sweet Potato miRNAs Was Impacted by Multiple Hormones

The expression of these miRNAs under stress-related and storage-root-development-related hormone treatments was investigated by qRT-PCR to further explore miRNA functions in stress responses and sweet potato development. For the IAA treatment, there were no obvious changes in miR158a-3p or miR167d (Figure 5), while miR156g, miR161.1, novel 214 and novel 359 showed their highest expression at 24 h of the IAA treatment (Figure 5). The most upregulated miRNA by IAA was miR161.1, which was upregulated by more than 45-fold (Figure 5). miR157d, novel 120 and novel 522 accumulated the highest at 1 h, 12 h and 48 h of the IAA treatment, respectively (Figure 5). In contrast, the levels of miR397a, novel 104 and novel 140 decreased dramatically (Figure 5). Five miRNAs, miR158a-3p, miR161.1, novel 120, novel 214 and novel 522, barely changed in response to the ZT treatment (Figure 5). The levels of miR156g and novel 359 increased the most at 24 h of the IAA treatment (Figure 5). Novel 104 and novel 140 were upregulated gradually and reached a maximum at 48 h of the IAA treatment (Figure 5). miR157d and miR397a showed their highest expression at 1 h and 12 h of the IAA treatment, respectively (Figure 5). The expression of miR167d was inhibited dramatically after the IAA treatment (Figure 5).

Most of the miRNAs were upregulated by ABA and GAs. In particular, miR167d was the most induced miRNA under the ABA treatment and was up-regulated by more than 1000-fold compared with the control (Figure 6). Novel 359 was the most upregulated miRNA by GAs, with an increase of approximately 17-fold (Figure 6). Above all, these data indicated that the level of these miRNAs is impacted by multiple hormones.

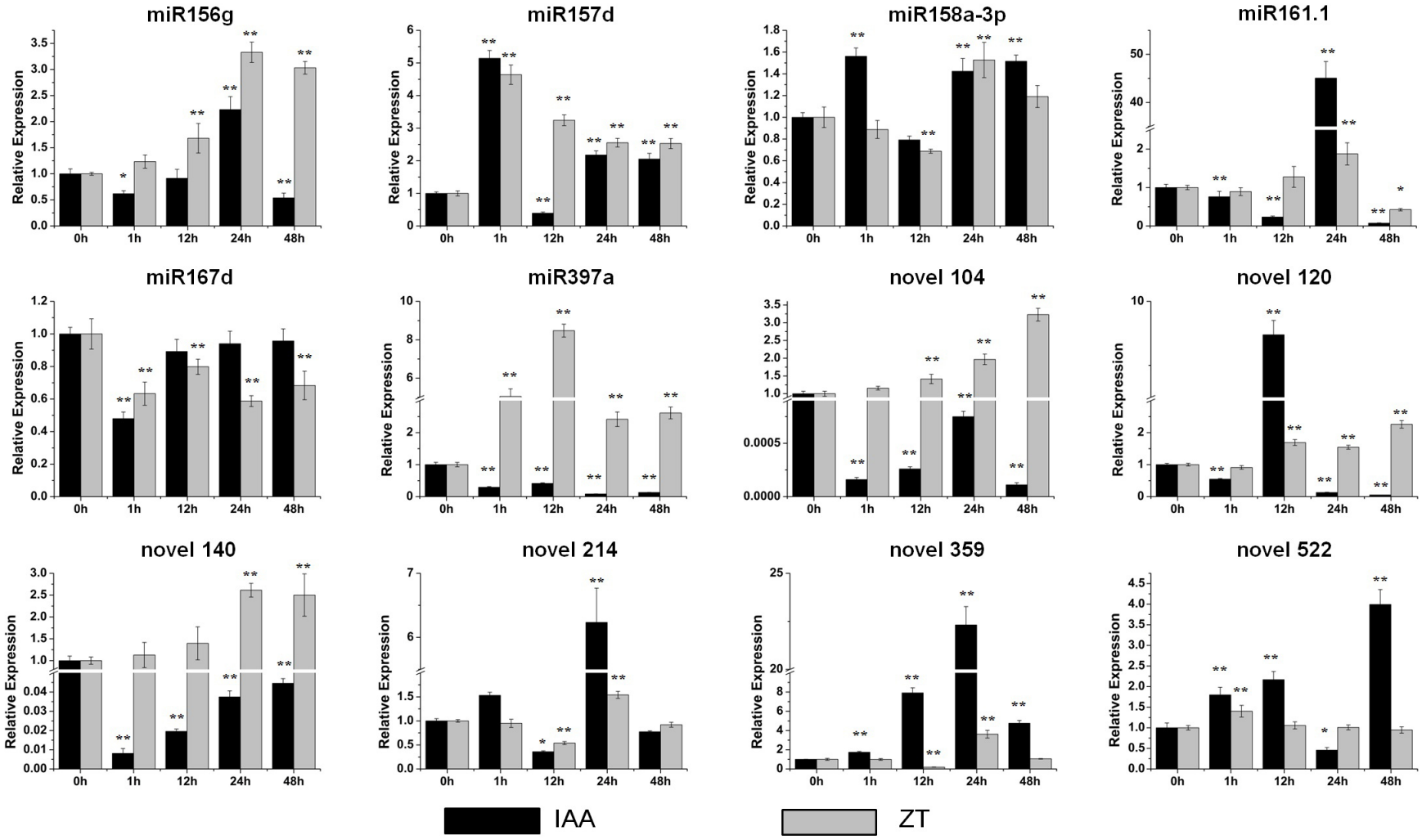

Figure 5. Expression profiles of six conserved and six novel miRNAs under the IAA (indole acetic acid) and ZT (zeaxanthin) treatments. The relative expression levels of unstressed plants (0 h) were normalized to 1. One asterisk (*) indicates statistically significant differences between control (0 h) and hormone-treated plants ($p < 0.05$), and two asterisks (**) indicate statistically extremely significant differences between control (0 h) and hormone-treated plants ($p < 0.01$). The black columns represent the IAA treatment and the grey columns represent the ZT treatment.

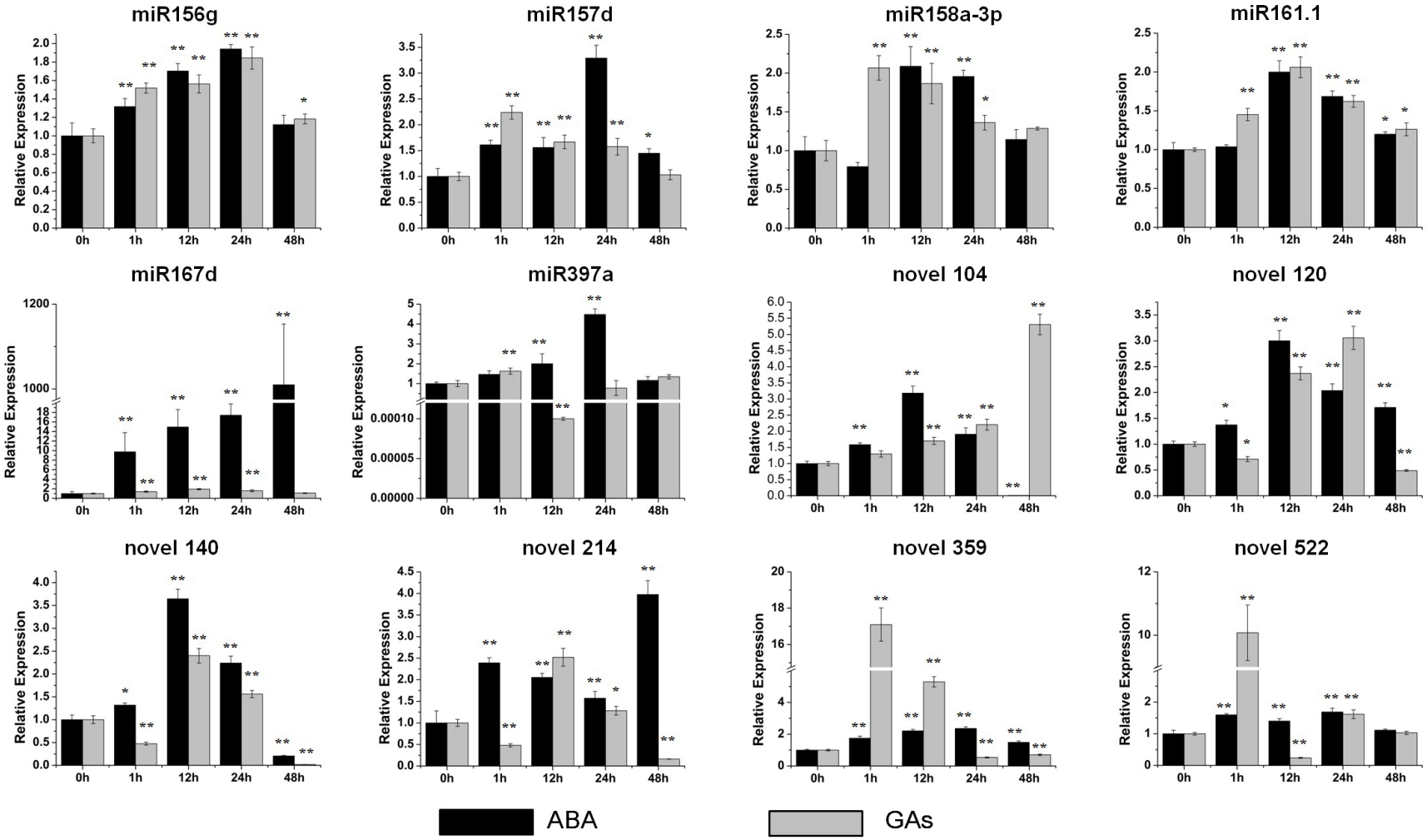

Figure 6. Expression profiles of six conserved and six novel miRNAs under the ABA (abscisic acid) and GAs (gibberellin) treatments. The relative expression levels of unstressed plants (0 h) were normalized to 1. One asterisk (*) indicates statistically significant differences between control (0 h) and hormone-treated plants ($p < 0.05$), and two asterisks (**) indicate statistically extremely significant differences between control (0 h) and hormone-treated plants ($p < 0.01$). The black columns represent the ABA treatment and the grey columns represent the GAs treatment.

3.5. The Target Prediction of the Twelve miRNAs

To predict the targets of these miRNAs, the RNA-seq and sRNA-seq data were combined and analyzed, and a set of potential targets of each miRNA were identified [20]. Then, qRT-PCR was performed to validate the predicted target expression. As with previous reports in other species, the potential targets of miR156g and miR157d were two SPL (squamosa promoter-binding-like) genes (*IbSPL3-like* and *IbSPL1-like*) (Figure 7). A BEL1-like gene (*IbBEL7-like*) was predicted to be a potential target of miR158a-3p (Figure 7). The expression of *IbARF8-like*, an ARF gene, showed a reverse trend compared with the miR167d expression profile (Figure 7). One PPR (pentatricopeptide repeat) gene (*IbPPR-like*) was predicted to be a potential target of miR161.1 (Figure 7). The candidate target of 397a was a laccase gene (*IbLaccase 3-like*) (Figure 7). Moreover, a homeobox-leucine zipper gene (*IbHB6-like*), a soluble acid invertase (*IbFRUCT2-like*), an ethylene biosynthesis gene 1-aminocyclopropane-1-carboxylate oxidase gene (*IbACCox1-like*), a pyruvate kinase gene (*IbPyruvate kinase-like*), a WRKY transcription factor gene (*IbWRKY51-like*) and a lycopene β cyclase gene (*Iblycopene-β-cyclase-like*) were predicted to be the candidate targets of novel 104, novel 120, novel 140, novel 214, novel 359 and novel 522, respectively (Figure 7).

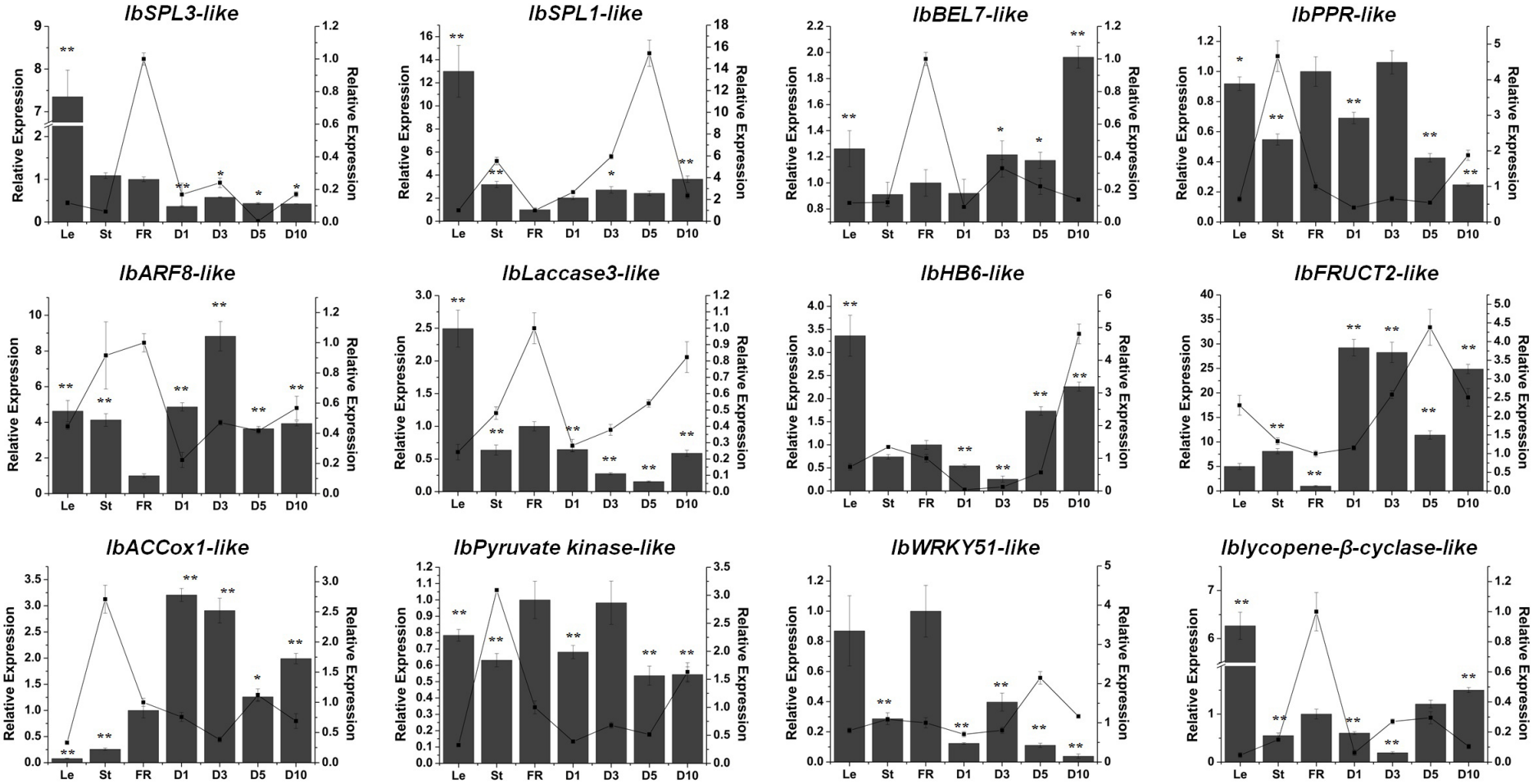

Figure 7. The potential targets of six conserved and six novel miRNAs. The relative expression levels of FR were normalized to 1. One asterisk (*) indicates statistically significant differences between FR and other tissues ($p < 0.05$), and two asterisks (**) indicate statistically extremely significant differences between FR and other tissues ($p < 0.01$). The tissues were obtained from Xushu 22. Le, leaves obtained from three-month-old plants; St, stems obtained from three-month-old plants; FR, fibrous roots; D1, 1 cm storage roots; D3, 3 cm storage roots; D5, 5 cm storage roots; and D10, 10 cm storage roots. The columns represent the potential target expression, and the lines represent the corresponding miRNA expression.

4. Discussion

4.1. Twelve miRNAs May Play a Role in Storage Root Development of Sweet Potato

Much evidence of miRNAs being involved in development has been found. For instance, miR156, miR319 and miR775 have been confirmed to play a role in leaf development [6,23,24]. miR172 and miR156 play a role in flower initiation and the flowering of plants [7,25]. Several miRNAs, including miR160, miR390, miR393 and miR847, affect root formation and development [8,26–28]. A set of miRNAs, such as miR164 and miR165, have been proven to impact stem development [29,30]. However, there are few reports about the roles of miRNAs in storage root thickening. Here, we identified and characterized six conserved miRNAs and six new miRNAs from sweet potato (Table S1). Our expression analysis results showed that miR156g, miR158a-3p, miR167d and novel 522 were highly expressed in fibrous roots but exhibited low expression in storage roots (Figure 2). In contrast, the level of miR157d and novel 359 was much higher in storage roots than in fibrous roots (Figure 2). These results indicated that these miRNAs might participate in sweet potato storage root development.

The hormone treatments suggested that miR156g, miR157d and novel 359 were all upregulated by the primary thickening growth of storage-root-related hormones (IAA/ZT) [31,32] (Figure 5). In particular, the level of novel 359 was induced by more than 20-fold after the IAA treatment (Figure 5). In addition, the expression of miR158a-3p, miR167d and novel 522 was upregulated by the hormones that mainly play roles in the later stage of storage root development (ABA/GAs) [31,32] (Figure 6). Among them, miR167d was upregulated by approximately 1000-fold by ABA, and novel 522 was increased by approximately 10-fold by ZT (Figure 5).

Moreover, the potential targets of these miRNAs have been predicted by high-throughput sequencing; one predicted target of each miRNA has been chosen and its expression validated by qRT-PCR (Figure 7). Although the relationship between target genes and miRNAs requires further confirmation, these results provide some information for exploring the functions of these miRNAs. The results showed that two *SPLs*, the important lateral root formation regulators, were potential targets of miR156g and miR157d [33]. The target of miR158a-3p and novel 104 are two homeobox genes (Figure 7), which have been reported to be an important regulator in plant development, including root growth and development [34,35]. The potential targets of miR167d and novel 140 are related to hormone biosynthesis or response (Figure 7). The potential target of miR167d is an auxin response factor which has been shown to regulate root formation in other species [36]. *ACCox1*, a potential target of novel 140, is an ethylene biosynthesis gene, indicating that novel 140 is related to ethylene biosynthesis. Additionally, ethylene has been reported to be related to the formation and development of potato as well as sugar accumulation. Additionally, in order to further explore the function of these miRNAs, the sequences of these twelve mature miRNAs and pre-miRNAs have been screened in the genome of wild sweet potato species *I. trifida* and *I. triloba*, whose roots cannot thicken. The results showed that, apart from novel 522, the other eleven miRNAs can be identified, indicating that novel 522 may be a miRNA unique to sweet potato. Combining the tissue expression and hormone response results, we speculate that novel 522 may be an essential regulator in the formation and development of sweet potato storage roots. Altogether, these results suggest that these miRNAs might play crucial roles in storage root thickening and development.

4.2. miRNAs May Play a Role in Sweet Potato Abiotic Stress Responses

Plant miRNAs have a close relationship with various stress resistances. For example, miR164, miR394 and miR408 have been reported to be related to salt tolerance [9,10,37]. miR168, miR169 and miR319 are important regulators of the drought stress response [38–40]. Several miRNAs, including miR166 and miR319, play critical roles in cold/heat tolerance [41]. In addition, some miRNAs have been confirmed to help plants cope with oxidative and flood stresses [11,12].

Here, most miRNAs were shown to respond to abiotic stresses in sweet potato (Figures 3 and 4). Among them, miR156g was distinctly induced by drought and high-temperature stresses (Figures 3 and 4). miR167d was markedly induced by salt and drought stresses but significantly inhibited by cold stress (Figures 3 and 4). miR158a-3p was dramatically upregulated by drought stress (Figure 3). Additionally, our results showed that novel 120 was significantly induced by drought and low-temperature stresses, and that the level of novel 214 increased sharply under salt stress treatment (Figures 3 and 4). The three conserved miRNAs (miR156g, miR158a-3p and miR167d) have all been defined as stress responders in other species [33,42,43]. Furthermore, the candidate targets of these miRNAs have also been reported to be related to plant stress responses. *SPL3*, the target of miR156g, belongs to SBP box family, which is an important regulator in recurring environmental stress [33]. The candidate target of miR167d is an auxin response factor that is reported to be related to salinity tolerance and low-temperature resistance [36]. The expression of soluble acid invertase gene, the candidate targe of novel 120, has been reported to be impacted by salt, drought and heat stresses [44–46]. In addition, the overexpression of the lycopene β cyclase gene, a candidate target of novel 522, increased salt and drought tolerance [47]. Moreover, these five miRNAs were all induced by ABA, a crucial hormone modulator in regulating abiotic stresses (Figure 6). Above all, the data indicate that these miRNAs have functions in stress responses.

4.3. Some miRNAs May Play Roles in Abiotic Stress Responses and Storage Root Development of Sweet Potato Simultaneously

Sweet potato is a tuberous root crop with strong environmental stress resistance and tolerance of poor soil. Thus, it is beneficial to study the storage root formation and stress responses of sweet potato to identify the mechanisms involved. Plant miRNAs are essential regulators of both stress responses and plant development, and some miRNAs have been stated to play roles in both aspects. For instance, miR319 is critical for leaf and flower development, and simultaneously regulates salt and drought tolerances [6,13,48]. miR160 is an important regulator in root development, salt tolerance and heat tolerance [28,49]. Moreover, miR166 plays essential roles in shoot apical meristem development, leaf development and cold tolerance [30,41]. Our results showed that miR156g, miR158a-3p, miR157d, miR167d, novel 359 and novel 522 were differentially expressed in fibrous roots and storage roots, and simultaneously responded to one or more stresses (Figures 2–4). In addition, these miRNAs were all impacted by storage-root-related or stress-response-related hormones (Figures 5 and 6). Together, these results suggested that these miRNAs might simultaneously play roles in both the abiotic stress responses and storage root development of sweet potato.

Collectively, our results identified and thoroughly analyzed the stress- and storage-root-thickening-related miRNAs, which would provide useful information for the further study of miRNA functions and sweet potato breeding.

Supplementary Materials: The following are available online at https://www.mdpi.com/article/10.3390/genes13010110/s1, Table S1: The sequences of the mature miRNAs and pre-miRNAs, Table S2: Primers used in qRT-PCR and reverse transcription of miRNAs.

Author Contributions: L.S., Y.Y. and H.P. performed the main experiments; J.Z. and M.Z. analyzed the data; T.X. analyzed the data and revised the manuscript; Z.L. revised the manuscript; T.D. designed the experiments; T.D., L.S., Y.Y. and H.P. wrote the paper. All authors have read and agreed to the published version of the manuscript.

Funding: This work was jointly supported by the Natural Science Foundation of China (32072117 and 32172062), the Key R&D Program of Xuzhou-Modern Agriculture (KC20039), China Agriculture Research System of MOF and MARA (CARS-10-B02), the Priority Academic Program Development of Jiangsu Higher Education Institutions (PAPD), the Research and Practice Innovation Project for Postgraduates of Jiangsu Province (KYCX20_2289), the Research and Practice Innovation Project for

Postgraduates of Jiangsu Normal University (2021XKT0749) and the National Training Programs of Innovation and Entrepreneurship for Undergraduates (202010320008Z).

Informed Consent Statement: Informed consent was obtained from all subjects involved in the study.

Conflicts of Interest: The authors declare that they have no known competing financial interests or personal relationships that could have appeared to influence the work reported in this paper.

References

1. Lee, R.C.; Feinbaum, R.L.; Ambros, V. The *C. elegans* heterochronic gene lin-4 encodes small RNAs with antisense complementarity to lin-14. *Cell* **1993**, *75*, 843–854. [CrossRef]
2. Lee, R.C.; Ambros, V. An Extensive Class of Small RNAs in Caenorhabditis elegans. *Science* **2001**, *294*, 862–864. [CrossRef] [PubMed]
3. Hutvagner, G.; Zamore, P.D. A microRNA in a Multiple-Turnover RNAi Enzyme Complex. *Science* **2002**, *297*, 2056–2060. [CrossRef]
4. Lee, Y.; Jeon, K.; Lee, J.; Kim, S.; Kim, V.N. MicroRNA maturation: Stepwise processing and subcellular localization. *Embo J.* **2002**, *21*, 4663–4670. [CrossRef] [PubMed]
5. Bartel, D.P. MicroRNAs: Genomics, Biogenesis, Mechanism, and Function. *Cell* **2004**, *116*, 281–297. [CrossRef]
6. Koyama, T.; Sato, F.; Ohme-Takagi, M. Roles of miR319 and TCP Transcription Factors in Leaf Development. *Plant Physiol.* **2017**, *175*, 874–875. [CrossRef]
7. Zhu, Q.-H.; Helliwell, C.A. Regulation of flowering time and floral patterning by miR172. *J. Exp. Bot.* **2010**, *62*, 487–495. [CrossRef]
8. Kyung, Y.E.; Yang, J.H.; Jun, L.; Hwan, K.S.; Seong-Ki, K.; Sung, L.W. Auxin regulation of the microRNA390-dependent transacting small interfering RNA pathway in Arabidopsis lateral root development. *Nucleic Acids Res.* **2010**, *38*, 1382–1391.
9. Fang, Y.; Xie, K.; Xiong, L. Conserved miR164-targeted NAC genes negatively regulate drought resistance in rice. *J. Exp. Bot.* **2014**, *65*, 2119–2135. [CrossRef] [PubMed]
10. Shan, T.; Fu, R.; Xie, Y.; Chen, Q.; Wang, B. Regulatory Mechanism of Maize (*Zea mays* L.) miR164 in Salt Stress Response. *Russ. J. Genet.* **2020**, *56*, 835–842. [CrossRef]
11. Ramanjulu Sunkar, J.K.Z. Posttranscriptional induction of two Cu/Zn superoxide dismutase genes in Arabidopsis is mediated by downregulation of miR398 and important for oxidative stress tolerance. *Plant Cell* **2006**, *18*, 2051–2065. [CrossRef] [PubMed]
12. Li, Y.; Li, X.; Yang, J.; He, Y. Natural antisense transcripts of MIR398 genes suppress microR398 processing and attenuate plant thermotolerance. *Nat. Commun.* **2020**, *11*, 5331. [CrossRef]
13. Liu, Y.; Li, D.; Yan, J.; Wang, K.; Zhang, W. MiR319 ediated ethylene biosynthesis, signaling and salt stress response in switchgrass. *Plant Biotechnol. J.* **2019**, *17*, 2370–2383. [CrossRef]
14. Li, C.; Zhang, B. MicroRNAs in control of plant development. *J. Cell. Physiol.* **2015**, *231*, 303–313. [CrossRef] [PubMed]
15. Xu, T.; Zhang, L.; Yang, Z.; Wei, Y.; Dong, T. Identification and functional characterization of plant miRNA under salt stress shed light on the salinity resistance improvement through miRNA manipulation in crops. *Front. Plant Sci.* **2021**, *12*, 665439. [CrossRef]
16. Saminathan, T.; Reddy, U. Elevated carbon dioxide and drought modulate physiologyand storage-root development in sweet potato by regulating microRNAs. *Funct. Integr. Genom.* **2019**, *19*, 171–190. [CrossRef]
17. Xie, Z.; Wang, A.; Li, H.; Yu, J.; Jiang, J.; Tang, Z.; Ma, D.; Zhang, B.; Han, Y.; Li, Z. High throughput deep sequencing reveals the important roles of microRNAs during sweetpotato storage at chilling temperature. *Sci. Rep.* **2017**, *7*, 16578. [CrossRef]
18. Yang, Z.; Zhu, P.; Kang, H.; Liu, L.; Xu, T. High-throughput deep sequencing reveals the important role that microRNAs play in the salt response in sweet potato (*Ipomoea batatas* L.). *BMC Genom.* **2020**, *21*, 164. [CrossRef]
19. He, L.; Tang, R.; Shi, X.; Wang, W.; Jia, X. Uncovering anthocyanin biosynthesis related microRNAs and their target genes by small RNA and degradome sequencing in tuberous roots of sweetpotato. *BMC Plant Biol.* **2019**, *19*, 232. [CrossRef] [PubMed]
20. Tang, C.; Han, R.; Zhou, Z.; Yang, Y.; Dong, T. Identification of candidate miRNAs related in storage root development of sweet potato by high throughput sequencing. *J. Plant Physiol.* **2020**, *251*, 153224. [CrossRef]
21. Dong, T.; Song, W.; Tang, C.; Zhou, Z.; Yu, J.; Han, R.; Zhu, M.; Li, Z. Molecular characterization of nine sweet potato (*Ipomoea batatas* Lam.) MADS-box transcription factors during storage root development and following abiotic stress. *Plant Breed.* **2018**, *137*, 790–804. [CrossRef]
22. Park, S.-C.; Yun-Hee, K.; Ji, C.Y.; Seyeon, P.; Cheol, J.J.; Haeng-Soon, L.; Sang-Soo, K.; Alexander, V.B. Stable Internal Reference Genes for the Normalization of Real-Time PCR in Different Sweetpotato Cultivars Subjected to Abiotic Stress Conditions. *PLoS ONE* **2012**, *7*, e51502. [CrossRef]
23. Xie, K.; Shen, J.; Hou, X.; Yao, J.; Li, X.; Xiao, J.; Xiong, L. Gradual Increase of miR156 Regulates Temporal Expression Changes of Numerous Genes during Leaf Development in Rice. *Plant Physiol.* **2012**, *158*, 1382–1394. [CrossRef]
24. Zhang, H.; Guo, Z.; Zhuang, Y.; Suo, Y.; Li, L. MicroRNA775 promotes intrinsic leaf size and reduces cell wall pectin level via a target galactosyltransferase in Arabidopsis. *BioRxiv* **2020**. [CrossRef]
25. Zhou, Q.; Shi, J.; Li, Z.; Zhang, S.; Liu, G. miR156/157 targets SPLs to regulate flowering transition, plant architecture and flower organ size in petunia. *Plant Cell Physiol.* **2021**, *62*, 24. [CrossRef] [PubMed]

26. Lin, D.; Yang, Y.; Khalil, R.; Xian, Z.; Li, Z. SlmiR393 controls the auxin receptor homologous genes expression, and regulates sensitivity to auxin in tomato root growth. *Sci. Hortic.* **2013**, *162*, 90–99. [CrossRef]
27. Wang, J.J.; Guo, H.S. Cleavage of INDOLE-3-ACETIC ACID INDUCIBLE28 mRNA by MicroRNA847 Upregulates Auxin Signaling to Modulate Cell Proliferation and Lateral Organ Growth in Arabidopsis. *Plant Cell* **2015**, *27*, 574–590. [CrossRef] [PubMed]
28. Meng, Y.; Mao, J.; Tahir, M.M.; Wang, H.; Wei, Y.; Zhao, C.; Li, K.; Ma, D.; Zhang, D. Mdm-miR160 Participates in Auxin-Induced Adventitious Root formation of apple rootstock. *Sci. Hortic.* **2020**, *270*, 109442. [CrossRef]
29. Peaucelle, A.; Morin, H.; Traas, J.; Laufs, P. Plant expressing a miR164-resistant CUC2 gene reveal the importance of post-meristematic maintenance of phyllotaxy in Arabidopsis. *Development* **2007**, *134*, 1045–1050. [CrossRef]
30. Du, F.; Gong, W.; Boscá, S.; Tucker, M.; Laux, T. Dose-Dependent AGO1-Mediated Inhibition of the miRNA165/166 Pathway Modulates Stem Cell Maintenance in Arabidopsis Shoot Apical Meristem. *Plant Commun.* **2019**, *1*, 100002. [CrossRef]
31. Hou, F.; Zhang, L.; Xie, B.; Dong, S.; Zhang, H.; Li, A.; Wang, Q. Effect of plastic mulching on the photosynthetic capacity, endogenous hormones and root yield of summer-sown sweet potato (*Ipomoea batatas* (L). Lam.) in Northern China. *Acta Physiol. Plant.* **2015**, *37*, 164. [CrossRef]
32. Dong, T.; Zhu, M.; Yu, J.; Han, R.; Tang, C.; Xu, T.; Liu, J.; Li, Z. RNA-Seq and iTRAQ reveal multiple pathways involved in storage root formation and development in sweet potato (*Ipomoea batatas* L.). *BMC Plant Biol.* **2019**, *19*, 136. [CrossRef]
33. Cui, L.; Shan, J.; Shi, M.; Gao, J.; Lin, H. The miR156-SPL9-DFR pathway coordinates the relationship between development and abiotic stress tolerance in plants. *Plant J.* **2014**, *180*, 1108. [CrossRef]
34. Hake, S.; Char, B.R.; Chuck, G.; Foster, T.; Long, J.; Jackson, D. Homeobox genes in the functioning of plant meristems. Philosophical Transactions of the Royal Society of London. *Ser. B Biol. Sci.* **1995**, *350*, 45–51.
35. Meng, L.; Fan, Z.; Zhang, Q.; Wang, C.; Gao, Y.; Deng, Y.; Zhu, B.; Zhu, H.; Chen, J.; Shan, W.; et al. BEL 1-LIKE HOMEODOMAIN 11 regulates chloroplast development and chlorophyll synthesis in tomato fruit. *Plant J.* **2018**, *94*, 1126–1140. [CrossRef]
36. Xu, L.; Wang, D.; Liu, S.; Fang, Z.; Tang, Y. Comprehensive Atlas of Wheat (*Triticum aestivum* L.) AUXIN RESPONSE FACTOR Expression During Male Reproductive Development and Abiotic Stress. *Front. Plant Sci.* **2020**, *11*, 586144. [CrossRef]
37. Guo, X.; Niu, J.; Cao, X. Heterologous Expression of Salvia miltiorrhiza MicroRNA408 Enhances Tolerance to Salt Stress in Nicotiana benthamiana. *Int. J. Mol. Sci.* **2018**, *19*, 3985. [CrossRef] [PubMed]
38. Man, Z.; Li, D.; Li, Z.; Qian, H.; Hong, L. Overexpression of a Rice MicroRNA319 Gene Enhances Drought and Salt Tolerance in Transgenic Creeping Bentgrass (*Agrostis stolonifera* L.). *Vitr. Cell. Dev. Biol. Anim.* **2011**, *47*, S37.
39. Li, W.; Cui, X.; Meng, Z.; Huang, X.; Xie, Q.; Wu, H.; Jin, H.; Zhang, D.; Liang, W. Transcriptional Regulation of Arabidopsis MIR168a and ARGONAUTE1 Homeostasis in Abscisic Acid and Abiotic Stress Responses. *Plant Physiol.* **2012**, *158*, 1279–1292. [CrossRef] [PubMed]
40. Yy, A.; Zn, A.; Yi, W.A.; Hw, A.; Zheng, H.B.; Qj, B.; Xs, B.; Hui, Z.B. Overexpression of soybean miR169c confers increased drought stress sensitivity in transgenic Arabidopsis thaliana. *Plant Sci.* **2019**, *285*, 68–78.
41. Valiollahi, E.; Farsi, M.; Kakhki, A.M. Sly-miR166 and Sly-miR319 are components of the cold stress response in Solanum lycopersicum. *Plant Biotechnol. Rep.* **2014**, *8*, 349–356. [CrossRef]
42. Lv, D.; Ying, G.; Bei, J.; Xi, B.; Bao, P.; Hua, C.; Wei, J.; Zhu, Y. miR167c is induced by high alkaline stress and inhibits two auxin response factors in Glycine soja. *J. Plant Biol.* **2012**, *55*, 373–380. [CrossRef]
43. Zhang, X.D.; Sun, J.Y.; You, Y.Y.; Song, J.B.; Yang, Z.M. Identification of Cd-responsive RNA helicase genes and expression of a putative BnRH 24 mediated by miR158 in canola (*Brassica napus*). *Ecotoxicol. Environ. Saf.* **2018**, *157*, 159–168. [CrossRef] [PubMed]
44. Andersen, M.N.; Asch, F.; Wu, Y.; Jensen, C.R.; Næsted, H.; Mogensen, V.O.; Koch, K.E. Soluble invertase expression is an early target of drought stress during the critical, abortion-sensitive phase of young ovary development in maize. *Plant Physiol.* **2002**, *130*, 591–604. [CrossRef] [PubMed]
45. Aloni, B.; Karni, L.; Daie, J. Effect of heat stress on the growth, root sugars, acid invertase and protein profile of pepper seedlings following transplanting. *J. Hortic. Sci.* **1992**, *67*, 717–725. [CrossRef]
46. Mišić, D.; Dragićević, M.; Šiler, B.; Živković, J.N.; Maksimović, V.; Momčilović, I.; Nikolic, M. Sugars and acid invertase mediate the physiological response of Schenkia spicata root cultures to salt stress. *J. Plant Physiol.* **2012**, *169*, 1281–1289. [CrossRef]
47. Shi, Y.; Guo, J.; Zhang, W.; Jin, L.; Liu, P.; Chen, X.; Li, F.; Wei, P.; Li, Z.; Li, W.; et al. Cloning of the Lycopene β-cyclase Gene in Nicotiana tabacum and Its Overexpression Confers Salt and Drought Tolerance. *Int. J. Mol. Sci.* **2015**, *16*, 30438–30457. [CrossRef]
48. Man, Z.; Li, D.; Li, Z.; Hu, Q.; Hong, L. Constitutive expression of a miR319 gene alters plant development and enhances salt and drought tolerance in transgenic creeping bentgrass. *Plant Physiol.* **2014**, *161*, 1375–1391.
49. Anl, B.A.; Gke, Z. Investigating effect of miR160 through overexpression in potato cultivars under single or combination of heat and drought stresses. *Plant Biotechnol. Rep.* **2021**, *15*, 335–348.

ARTICLES FOR FACULTY MEMBERS

INVESTIGATING THE ROLE OF GIBBERELLIC ACID (GA) AND ABSCISIC ACID (ABA) CROSS-TALK IN ENHANCING TUBEROUS ROOT DEVELOPMENT IN SWEET POTATOES

Overexpression of 9-cis-epoxycarotenoid dioxygenase gene, IbNCED1, negatively regulates plant height in transgenic sweet potato / Zhou, Y., Zhao, C., Du, T., Li, A., Qin, Z., Zhang, L., Dong, S., Wang, Q., & Hou, F.

International Journal of Molecular Sciences
Volume 24 Issue 13 (2023) 10421 Pages 1-14
https://doi.org/10.3390/ijms241310421
(Database: MDPI)

International Journal of
Molecular Sciences

MDPI

Article

Overexpression of 9-*cis*-Epoxycarotenoid Dioxygenase Gene, *IbNCED1*, Negatively Regulates Plant Height in Transgenic Sweet Potato

Yuanyuan Zhou, Chunling Zhao, Taifeng Du, Aixian Li, Zhen Qin, Liming Zhang, Shunxu Dong, Qingmei Wang * and Fuyun Hou *

Crop Research Institute, Shandong Academy of Agricultural Sciences, Jinan 250100, China; zhou_yy_2020@163.com (Y.Z.)
* Correspondence: wangqingmei@shandong.cn (Q.W.); houfuyun@shandong.cn (F.H.)

Abstract: Plant height is one of the key agronomic traits for improving the yield of sweet potato. Phytohormones, especially gibberellins (GAs), are crucial to regulate plant height. The enzyme 9-*cis*-epoxycarotenoid dioxygenase (NCED) is the key enzyme for abscisic acid (ABA) biosynthesis signalling in higher plants. However, its role in regulating plant height has not been reported to date. Here, we cloned a new NCED gene, *IbNCED1*, from the sweet potato cultivar Jishu26. This gene encoded the 587-amino acid polypeptide containing an NCED superfamily domain. The expression level of *IbNCED1* was highest in the stem and the old tissues in the in vitro-grown and field-grown Jishu26, respectively. The expression of *IbNCED1* was induced by ABA and GA3. Overexpression of *IbNCED1* promoted the accumulation of ABA and inhibited the content of active GA3 and plant height and affected the expression levels of genes involved in the GA metabolic pathway. Exogenous application of GA3 could rescue the dwarf phenotype. In conclusion, we suggest that *IbNCED1* regulates plant height and development by controlling the ABA and GA signalling pathways in transgenic sweet potato.

Keywords: sweet potato; *IbNCED1*; plant height; ABA; GA

Citation: Zhou, Y.; Zhao, C.; Du, T.; Li, A.; Qin, Z.; Zhang, L.; Dong, S.; Wang, Q.; Hou, F. Overexpression of 9-*cis*-Epoxycarotenoid Dioxygenase Gene, *IbNCED1*, Negatively Regulates Plant Height in Transgenic Sweet Potato. *Int. J. Mol. Sci.* **2023**, *24*, 10421. https://doi.org/10.3390/ijms241310421

Academic Editor: Tomotsugu Koyama

Received: 3 April 2023
Revised: 8 June 2023
Accepted: 16 June 2023
Published: 21 June 2023

1. Introduction

Sweet potato, *Ipomoea batatas* (L.) Lam., is an important root crop worldwide [1,2]. In actual production, due to the genotype, excessive nitrogen application, uneven rainfall distribution, and improper irrigation, sweet potato is easily overgrown; this seriously impacts the yield, mechanization degree and the sustainable development of the sweet potato industry [3]. The ideal plant height of sweet potato helps to break through the bottleneck. However, research to date has yet to establish a clear genetic basis and the constituent elements in sweet potato.

Plant height is an agronomic trait with a complex genetic basis [4,5]. It is confined by stem elongation and plays important role in crop yield and quality [6]. With the rise of the green revolution, a large number of dwarf mutants, quantitative trait loci (QTLs), and genes have been identified to control plant height [7–10]. In wheat, the Reduced height (Rht) alleles, such as *Rht-1*, *Rht-B1b*, and *Rht-D1b* were introduced to reduce plant height, providing improved lodging resistance through interfering with the action or production of the gibberellins (GAs), plant hormones [11–13].

GAs are a class of tetracyclic diterpenoid phytohormones that mediate different processes of plant development including stem elongation, seed germination, trichome development, leaf expansion, induction of flowering, and pollen maturation [14,15]. More than 130 GAs have been identified, and GA1, GA3, GA4, and GA7 show capital biological activity that controls plant development [16–18]. Higher GA levels and more active GA biosynthesis were found to be correlated with plant height [19–21]. GA metabolism or

signalling conferred grain productivity during the Green Revolution by reshaping plant stature [22,23]. Many genes have been identified relating to plant height through the GA signalling pathway. In rice, *OsDREB2B*, *OsAP2-39*, and *OsWRKY21* reduce plant height development through the GA biosynthesis pathway [24]. TaLecRK-IV.1 and TaRht24 are regulators of plant height through the gibberellic acid and auxin-signalling pathways in wheat [25,26]. Overexpression of *CmDRP* resulted in a semi-dwarf phenotype with a significantly decreased active GA3 content, while reduced expression generated the opposite phenotype inchrysanthemum [27].

It has always been clear that GAs interact with other plant hormones [28]. GA and ABA usually play antagonistic roles in the regulation of germination, growth, and flowering in plants [29,30]. ABA affect the GA pathway through a different mechanism, such as an ABA-induced Ser/Thr protein kinase (PKABA1) and transcriptional regulators of ABA-induced WRKY, DELLA, and MYB [31–35]. *Arabidopsis* ABF2 and ABF4 transcription factors positively regulate potato tuber induction by regulating the expression of ABA- and GA-metabolism genes [36].

The enzyme 9-*cis*-epoxycarotenoid dioxygenase (NCED) is the key enzyme for ABA biosynthesis signalling [37,38]. NCED genes are associated with development and tolerance by the ABA signalling pathway in plants. Overexpression of *VaNCED1* delayed the development of transgenic *Vitis vinifera* [39]. *OsNCED3* and *OsNCED5* mediated seed dormancy, plant growth, abiotic stress tolerance, and leaf senescence by regulating ABA biosynthesis in rice [40,41]. *LeNCED1* overexpression in tomato increased ABA concentration and prevented the induction of genes involved in ABA metabolism and the deactivations of GA and auxin that occurred in WT [42]. The expression of NCED genes in dwarf cotton accession was higher than that in taller ones, and *GhNCED1*-silenced cotton plants increased in height [43]. Up to now, NCED genes have not been identified in sweet potato. In this study, we cloned a new *IbNCED1* gene for the 587aa from sweet potato. Functional analysis showed that *IbNCED1* enhanced the accumulation of ABA and inhibited plant height, affected the expression levels of genes involved in the GA metabolic pathway, and affected the content of active GA.

2. Results

2.1. Cloning and Sequence Analysis of IbNCED1

The novel *IbNCED1* gene was isolated from the sweet potato cultivar Jishu26. The 1764-bp ORF sequence of *IbNCED1* encoded a protein of 587 aa with a molecular weight of 65.33 kDa and a predicted *p*I of 6.12, which belongs to the RPE65 superfamily (Figure 1A). Phylogenetic analysis of NCED proteins with a neighbor-joining method revealed that *IbNCED1* has high homology with NCED proteins from *Ipomoea triloba* (*ItNCED1*, XP_031110150.1), *Ipomoea nil* (*InNCED1*, XP_019153780.1), and *Solanum lycopersicum* (*SlNCED1*, NP_001234455.1) (Figure 1B).

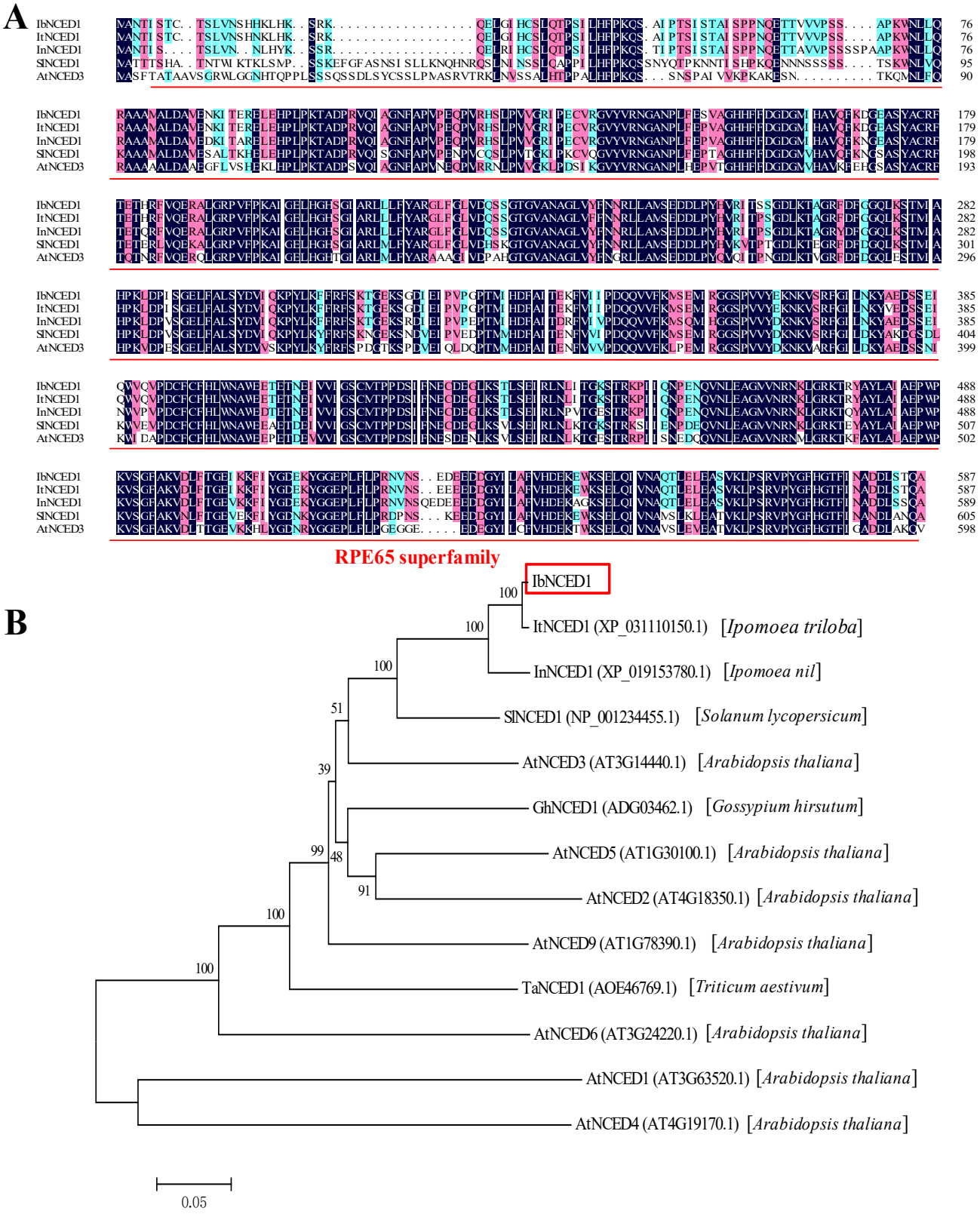

Figure 1. Sequence alignment (**A**) and phylogenetic tree (**B**) of *IbNCED1* with its homologs from other plants.

2.2. Expression Analysis of *IbNCED1*

To study the potential function of *IbNCED1* in sweet potato, its expression in different tissues and treatments of Jishu26 was analyzed with qRT-PCR. The expression level of *IbNCED1* was the highest in the stem of the in vitro-grown Jishu26 plants (Figure 2A). For the field-grown Jishu26 plants, the expression level of *IbNCED1* was higher in the old stem, pencil root, and storage root tissues than in other young tissues (Figure 2B).

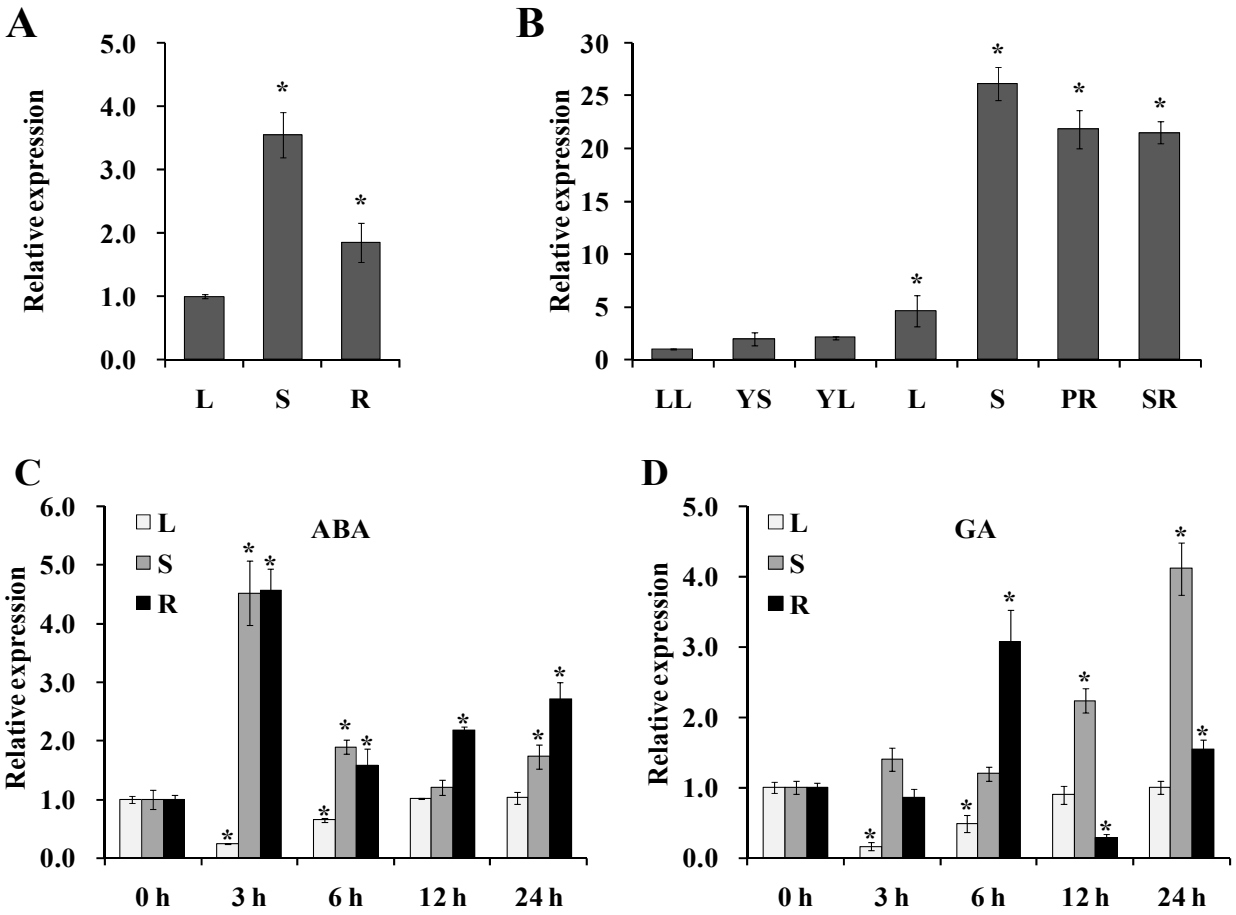

Figure 2. Expression analysis of *IbNCED1* in different tissues of Jishu26 plants. The expression analysis of *IbNCED1* in different tissues of in vitro-grown (**A**) and field-grown (**B**) plants of Jishu26. LL: Leaflet; L: Leaf; PR: Pencil root; R: Root; S: Stem; SR: Storage root; YS: Young stem. The transcript levels of *IbNCED1* in the leaf tissue or leaflet were set to 1. The expression analysis of *IbNCED1* in different tissues of Jishu26 plants after different time points (h) in response to 100 mM ABA (**C**) and 100 mM GA (**D**), respectively. The expression level of *IbNCED1* in the plant sampled at 0 h was set to 1. The data are presented as the means ± SEs (n = 3). * indicates significant differences from that of WT at $p < 0.05$, according to Student's t-test.

The expression of *IbNCED1* was downregulated in the leaf and upregulated in the stem and root after ABA and GA treatments. The expression level peaked at 3 h (4.520-fold in the stem and 4.56-fold in the root) after ABA treatment (Figure 2C), while it peaked at 12 h in the stem and at 6 h in the root (4.11- and 3.08-fold, respectively) after GA treatment (Figure 2D). These results suggest that *IbNCED1* might be involved in ABA and GA response pathways.

2.3. Regeneration of the Transgenic Sweet Potato Plants

The overexpression vector pCAMBIA1301s-*IbNCED1* was introduced into the *Agrobacterium tumefaciens* strain EHA105 (Figure 3A). Cell aggregates of Xushu22 (Figure 3B) co-cultivated with EHA105 carrying pCAMBIA1301-*IbNCED1* were cultured on the selective

MS medium with 2.0 mg L^{-1} 2,4-dichlorophenoxyacetic acid (2,4-D), 100 mg L^{-1} carbenicillin (Carb), and 10 mg L^{-1} hygromycin (Hyg) (Figure 3C). Seventeen Hyg-resistant embryogenic calluses of 132 cell aggregates were obtained after 6 weeks. These Hyg-resistant embryogenic calluses were transferred to MS medium with 1.0 mg L^{-1} ABA and 100 mg L^{-1} Carb, and after 4 weeks of transfer, they formed plantlets (Figure 3D). Nine regenerated plants were transferred to MS medium and seven of them showed dwarf phenotype (Figure 3E). The seven regenerated plants were proved to be transgenic by PCR and GUS analyses, named L1, L2, . . . , L7, respectively (Figure 3F,G). qRT-PCR analysis revealed that the expression level of *IbNCED1* was significantly increased in most of the transgenic plants compared with that of WT (Figure 3H).

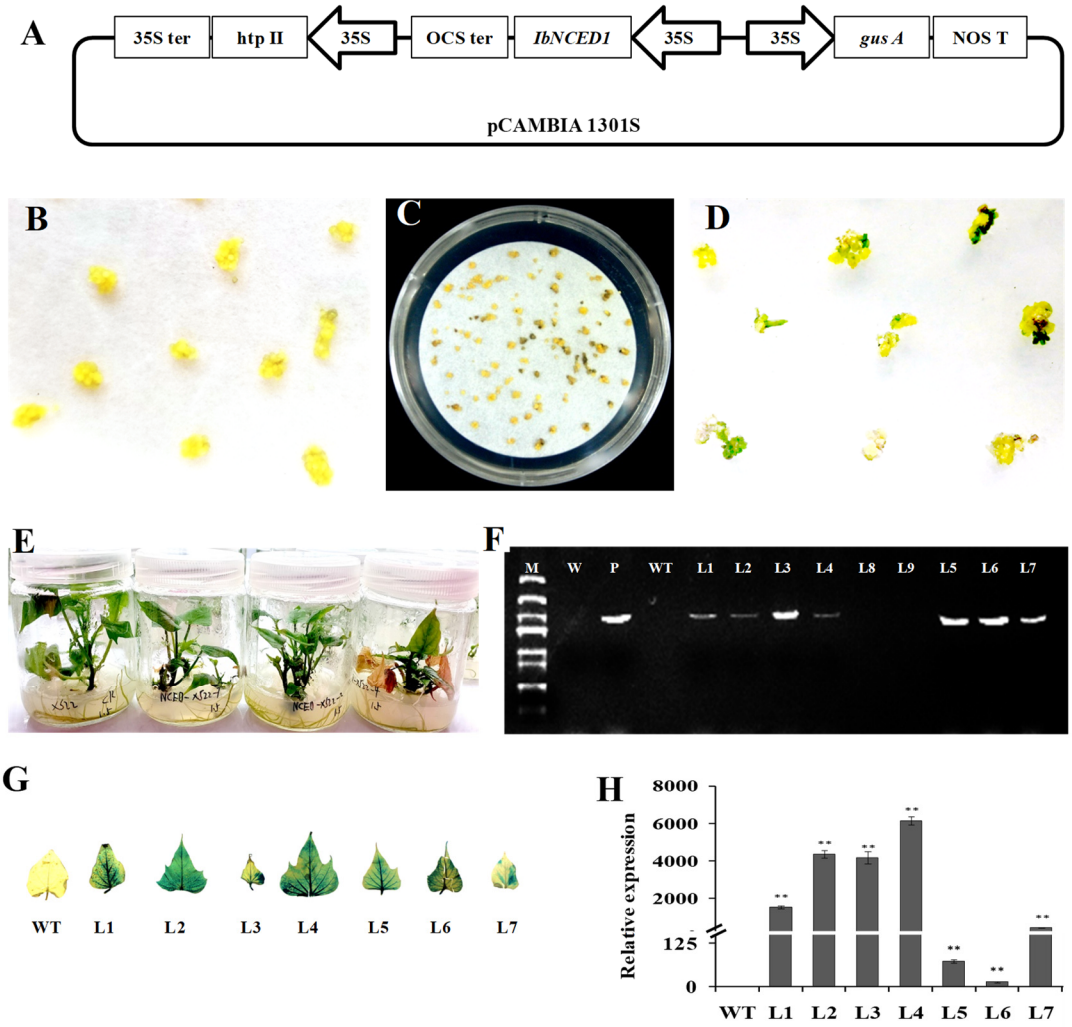

Figure 3. Production of the *IbNCED1*-overexpressing sweet potato plants. (**A**) Diagram of constitutive expression of the 35S promoter::*IbNCED1* construct. (**B**) Embryogenic cultures proliferating in MS medium with 2.0 mg L^{-1} 2,4-D. (**C**) Hyg-resistant calluses formedafter 4 weeks of selection on MS medium with 2.0 mg L^{-1} 2,4-D, 100 mg L^{-1} Carb and 10 mg L^{-1} Hyg. (**D**) Germination of somatic embryos from Hyg-resistant calluses on MS medium with 1.0 mg L^{-1} ABA and 100 mg L^{-1} Carb. (**E**) Whole regenerated plantlets. (**F**) PCR analysis of the transgenic plants. Lane M: BL2000 plus DNA marker; Lane W: Water; Lane P: plasmid pCAMBI1301::*IbNCED1* as a positive control; Lane WT: Xushu22 plant as a negative control. (**G**) GUS analysis of the transgenic plants. (**H**) qRT-PCR analysis of *IbNCED1* in the transgenic plants. ** indicates a significant difference from that of WT at $p < 0.01$ according to Student's *t*-test.

2.4. Plant Height Assay

In vitro propagation of sweet potato is a basic step for routine gene bank and biotechnology research activities. The seven regenerated sweet potato lines were raised in plant numbers by vegetative propagation using an MS medium. The three transgenic sweet potato plants L1, L2, and L4, with high relative expression of *IbNCED1* and stable dwarf phenotype, were selected to test plant height. The result show that overexpression of *IbNCED1* conferred a reduction in height of in vitro-grown and greenhouse-grown transgenic plants (Figure 4A,B). The histological analysis of the longitudinal section showed that the pith cell length of the transgenic plants decreased in comparison to the WT (Figure 4C). All the results demonstrated that *IbNCED1* demoted stem elongation primarily by reducing cell length.

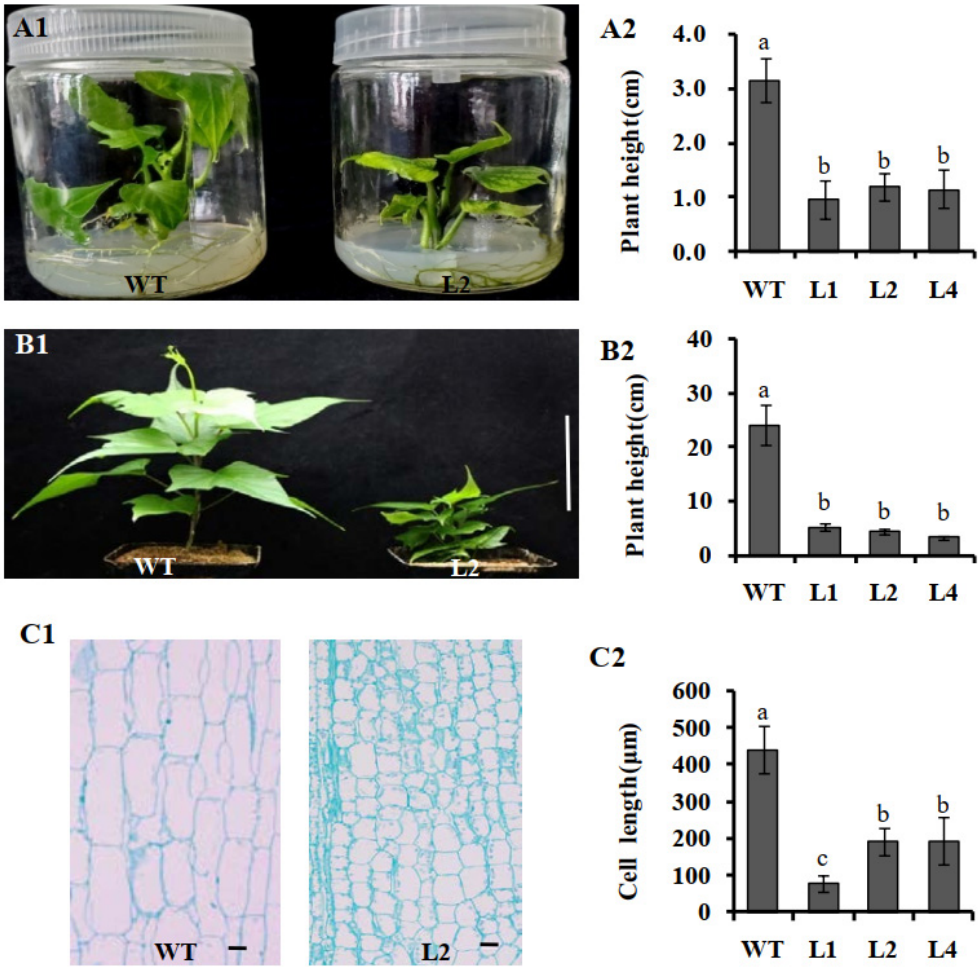

Figure 4. Plant height of transgenic sweet potato plants and WT. (**A1**,**A2**) Phenotypes and plant height of in vitro-grown transgenic sweet potato plants and WT cultured on MS medium for 4 weeks. The data are presented as the means ± SEs (n = 5). (**B1**,**B2**) Phenotypes and plant height of transgenic sweet potato plants and WT grown in transplanting boxes for 6 weeks. Bar = 10 cm. The data are presented as the means ± SEs (n = 5). (**C1**,**C2**)The histological analysis and cell length of in vitro-grown transgenic sweet potato plants and WT cultured on MS medium for 4 weeks. Bar = 100 μm. The data are presented as the means ± SEs (n = 20). The data are presented as the means ± SEs (n = 5). The different small letters indicate a significant difference at $p < 0.05$ according to Student's t-test.

2.5. Underlying Mechanism of IbNCED1 in Plant Height

To explore the dwarfing mechanism and the dwarf genes of sweet potato, differentially expressed genes and metabolic pathways in transgenic sweet potato were analyzed by RNA sequencing (RNA-Seq) using 4-week-old in vitro-grown WT and transgenic line L2

(OE). After removing the adapter and low-quality reads, a total of 614,283,286 clean reads were obtained from two lines (three biological replicates per line), and the quality control and quality assessment of RNA-Seq data showed that the sample quality was reliable and can be analyzed later (Table S1 and Figure S1). Using WT as the control group and $|\log2(\text{Fold Change})| > 1$ & $q < 0.05$ as the standard of gene differential expression, we obtained a total of 2938 differential expressed genes (DEGs), of which 1827 genes were downregulated, and 1111 genes were upregulated. KEGG enrichment analysis showed that the DEGs were primarily enriched metabolism, biosynthesis of secondary metabolites, plant MAPK signalling, and plant hormone signal transduction pathway (Figure 5A). The DEGs of GA biosynthesis and signal transduction pathway were downregulated (Figure 5B).

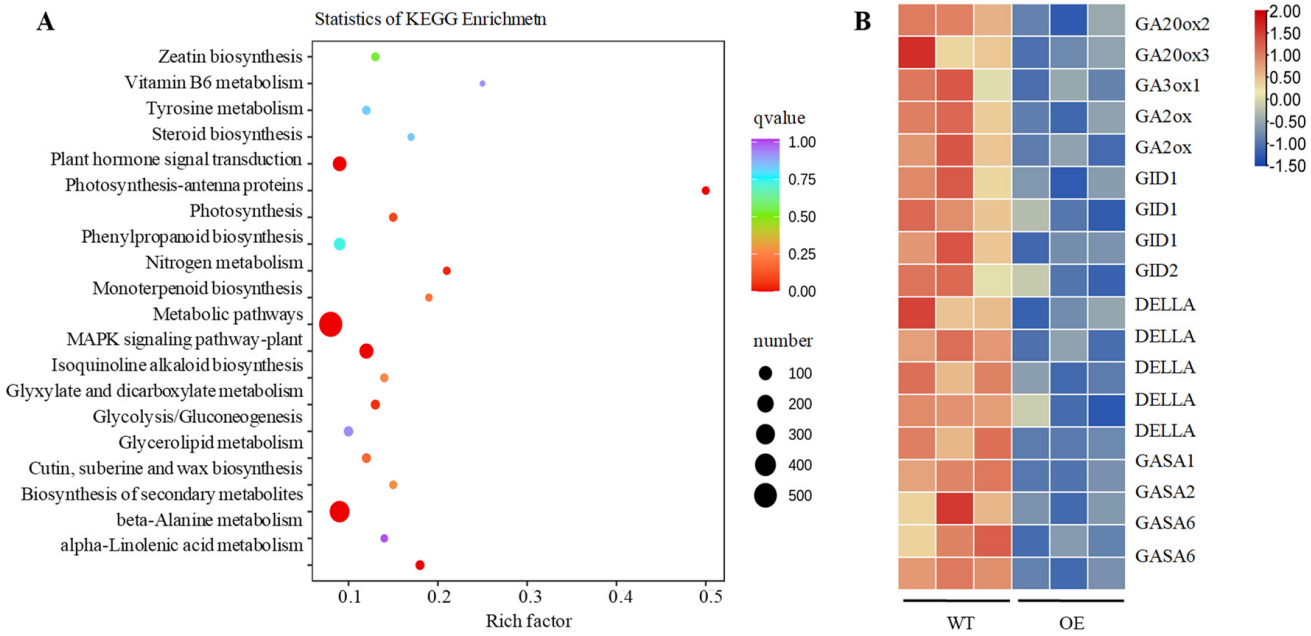

Figure 5. The analysis of KEGG pathway in transgenic sweet potato (**A**) and the expression analysis of DEGs in GA signalling pathway (**B**).

To investigate the underlying mechanism of *IbNCED1* in plant height, the phytohormone components of 4−week−old in vitro-grown sweet potato plants were measured. The results showed that the ABA and ABA−GE contents of the transgenic plants were significantly increased, while the GA3 content was significantly decreased compared with those of WT (Table 1). Exogenous GA3 treatment was performed on WT and transgenic sweet potato to determine the factors of height reduction. The WT plant and transgenic sweet potato could not grow on MS with 10 ng L^{-1} GA3 and 30 ng L^{-1} GA3, respectively (Figure S2). These results indicated that overexpression of *IbNCED1* could reduce the GA sensitivity of transgenic sweet potato. To further prove the function of GA in plant height, we analyzed the plant height of transgenic sweet potato plants and WT after GA3 treatment, and the results showed that exogenous GA3 can restore the plant height of transgenic sweet potato (Figure 6). In conclusion, we suggest that *IbNCED1* negatively regulates plant height by controlling the GA biosynthesis and signal transduction pathway.

Table 1. The contents of ABA and GAs (mg g^{-1}).

Class	Index	WT	L2
ABA	ABA	7.60 ± 0.68	83.42 ± 1.77
	ABA-GE	133.91 ± 4.82	355.59 ± 8.22
GA	GA1	N/A	N/A
	GA3	5.02 ± 0.16	N/A
	GA4	N/A	N/A
	GA7	N/A	N/A
	GA9	N/A	N/A
	GA15	N/A	N/A
	GA19	21.15 ± 0.53	23.85 ± 0.84
	GA20	N/A	N/A
	GA24	N/A	N/A
	GA53	6.36 ±0.68	11.34 ± 0.30

N/A—Not applicable.

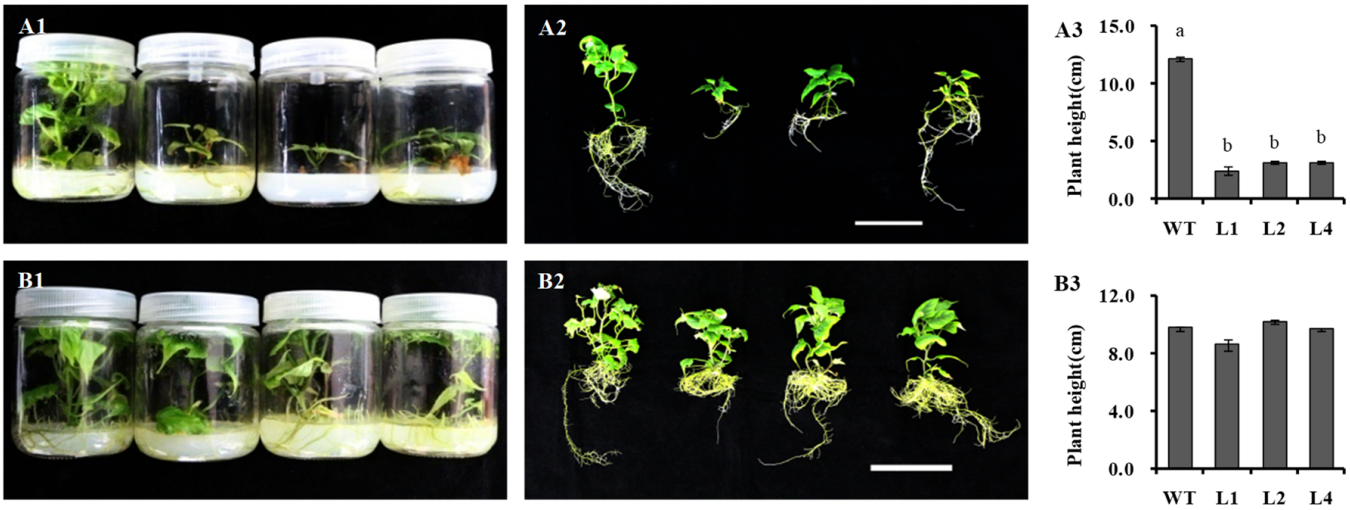

Figure 6. Plant height of transgenic sweet potato plants and WT after GA3 treatment. (**A1**–**A3**) Phenotypes and plant height of in vitro-grown transgenic sweet potato plants and WT cultured on MS medium for 6 weeks. (**B1**–**B3**) Phenotypes and plant height of in vitro-grown transgenic sweet potato plants and WT cultured on MS medium with 10 ng L^{-1} GA3 for 6 weeks. Bar = 10 cm. The data are presented as the means ± SEs (n = 3). The different small letters indicate a significant difference at $p < 0.05$ according to Student's t-test.

3. Discussion

The Green Revolution has promoted a significant yield increase through the development of semi-dwarf plant architecture in rice, wheat, maize, and soybean [21,44–46]. The ideal architecture for sweet potato also could promote the mechanization degree and yield of storage roots. However, the dwarfing mechanism and the dwarf genes of sweet potato are still unclear. In this study, we cloned an *IbNCED1* from the sweet potato cv. Jishu26 (Figure 1). The expression of *IbNCED1* was downregulated in the leaf and upregulated in the stem and root after ABA and GA treatments (Figure 2). Its overexpression significantly conferred a reduction in the height of the transgenic sweet potato plants and promoted the accumulation of ABA and ABA−GE in transgenic sweet potato (Table 1). It is thought that *IbNCED1* is key enzyme gene for ABA biosynthesis signalling in sweet potato.

The other functions of NCED genes have been identified in different plants. *GhNCED1* reduced plant height in cotton [47]. *AtNCED3* and *AtNCED5* contributed to ABA production affecting vegetative growth and drought tolerance in *Arabidopsis* [48,49]. *OsNCED3* mediates seed dormancy, plant growth, abiotic stress tolerance, and leaf senescence by regulating ABA biosynthesis in rice [40]. In our study, overexpression of *IbNCED1* reduced

plant height and cell length of the stem in transgenic sweet potato (Figure 4). The results indicated that *IbNCED1* plays an important role in reducing the growth of transgenic sweet potato by regulating ABA biosynthesis.

To date, many Rht genes have been identified in regulating plant height via participating in GA biosynthesis regulation in different plants [11–13]. The antagonistic regulations of GA and ABA have been reported in seed germination, cell development of the hypocotyls and plant height [50–54]. The miR528 and its target gene *DWARF3* (D3) negatively regulate rice plant height by triggering a reduction of GA content and a significant increase in ABA accumulation in transgenic plants [55]. Overexpression of *LeNCED1* limited biomass accumulation increased ABA concentration and prevented the induction of genes in ABA metabolism and GA deactivation [42]. GA20−oxidases (GA20oxs) that produce GA precursors, GA3−oxidases (GA3oxs) that produce bioactive GAs, and GA2−oxidases (GA2oxs) that deactivate precursors and bioactive GAs, were kay enzymes of the GA biosynthesis pathway [56,57]. GA20oxs are known to affect cell division and cell expansion, resulting in larger plants [58,59]. GA3ox1 and GA3ox2, which encode a GA3 beta-hydroxylase in GA biosynthesis, are significantly associated with cell lengths and plant height [60,61]. GA2oxs regulate plant growth by regulating endogenous bioactive Gas [62,63]. In the GA signal transduction pathway, the gibberellin receptor GIBBERELLIN INSENSITIVE DWAR (GID) was a putative candidate gene controlling plant height [64–67]. Interactions between GID1 and DELLAs mediated the GA signalling in land plants [68,69]. The plant-specific gibberellic acid-stimulated *Arabidopsis* (GASA) gene family plays roles in hormone response, promoted seedling germination and root extension, and plant development [70]. In this study, the expression of genes in GA biosynthesis and signal transduction pathways was downregulated in transgenic sweet potato (Figure 5B). Overexpression of *IbNCED1* reduced the accumulation of GA3 and exogenous application of GA3 could rescue the dwarf phenotype (Table 1, Figures 6 and S2). These results suggest that *IbNCED1* regulates plant height and development by controlling the GA signalling pathway in transgenic sweet potato. All the analyses revealed that the occurrence of dwarfing in transgenic sweet potatoes with high ABA content was likely to be caused by the GA signalling pathway.

In wheat and rice, the Rht alleles were introduced to reduce plant height allowing the application of higher fertilizer rates to substantially increase grain yield [11]. The fertilizer rates of the dwarf transgenic sweet potato would impact the yield of storage roots. The main objective of future dwarf sweet potato research should be to optimize fertilizer rates.

4. Materials and Methods

4.1. Plant Material

Sweet potato cv. Jishu26 was used for isolation and expression analysis of the *IbNCED1* gene. Sweet potato cv. Xushu22 was employed to characterize the function of *IbNCED1*.

4.2. Cloning and Sequence Analysis of IbNCED1

Total RNA from sweet potato cv. Jishu26 plants was extracted using the Trozol Up Kit (ET111, Transgen, Beijing, China). The first-strand cDNA was transcribed from the total RNA with the PrimeScript^{TM} RT reagent Kit with gDNA Eraser (PR047A, Takara, Beijing, China). Amino acid sequence alignment was analyzed using DNAMAN V6 software. The phylogenetic tree was constructed with MEGA 7.0 software with 1000 bootstrap replicates. The molecular weight and theoretical isoelectric point (*p*I) of *IbNCED1* were calculated with ProtParam tool (https://web.expasy.org/protparam/) accessed on 9 May 2023.

4.3. Expression Analysis of IbNCED1

The transcript levels of *IbNCED1* in leaf, stem and root tissues of the 4-week-old in vitro-grown plants and leaflet, leaf, stem, pencil root, and storage root tissues of the 80-day-old field-grown plants of Jishu26 were analyzed with qRT-PCR using SYBR Green Pro Taq HS kit (AG11701, ACCURATE BIOLOGY). Furthermore, the 4-week-old Jishu26 plants were stressed in Hoagland solution with 100 mM ABA and 100 mM GA, respectively,

and sampled at 0, 3, 6, 12, and 24 h after stresses for analyzing the expression of *IbNCED1*. *Ibactin* (AY905538) was used to normalize the expression levels in sweet potato [71]. All the specific primers are shown in Supplementary Table S2.

4.4. Regeneration of the Transgenic Sweet Potato Plants

Embryogenic suspension cultures of sweetpotato cv. Xushu22 were prepared using MS medium with 2.0 mg L^{-1} 2,4-D [72]. The overexpression vector pCAMBIA1301-*IbNCED1* was introduced into the *A. tumefaciens* strain EHA105. The transformation and plant regeneration were performed as previously described [70]. The identification of the transgenic plants was conducted by PCR with specific primers (Supplementary Table S2). The expression levels of *IbNCED1* in the in vitro-grown transgenic and WT plants were analyzed using specific primers designed in the non-conserved domain (Supplementary Table S2).

4.5. Plant Height Analysis

The phenotypic of the 4-week-old in vitro-grown transgenic sweet potato plants and WT cultured on MS medium and the 6-week-old plants grown in transplanting boxes in the greenhouse were analyzed. At least 5 plants were measured for plant height. For paraffin section, the stem tissues were collected from WT and transgenic lines. The methods of paraffin section are dissected as described by Fang et al. (2021) [73]. At least 20 cells were measured in length.

4.6. RNA-Sequencing and Hormone Analysis

Due to the dwarf phenotype, total RNA was extracted from 4-week-old in vitro-grown sweet potato plant Xushu22 (WT) and transgenic lines L2 (OE) using a plant RNA kit (DP441, TIANGEN). The sequencing library was constructed using Ultra RNA sample preparation kit (Illumina) and then sequenced using an Illumina HiSeq 2500 according to the standard method (Illumina). Total reads were mapped to the *I. Trifida* genome (Sweet potato). Differentially expressed genes were identified using Cuffdiff with default criteria (fold change >1.5) and adjusted false discovery rate (p value < 0.05). Three independent biological replicates were used for the RNA-sequencing analysis. Analysis using the Kyoto Encyclopedia of Genes and Genomes (KEGG) pathway was conducted according to database instructions (KEGG PATHWAY Database). The gene expression patterns were graphically represented in a heat map by cluster analysis using TBtools software (version number 1.108). The hormone contents of 4-week-old in vitro-grown WT and transgenic lines L2 plants were determined using high-performance liquid chromatography (HPLC).

4.7. Exogenous GA3 Treatment Analysis

In order to investigate the effect of GA3 on plants, the in vitro-grown transgenic and WT plants were cultured on MS medium with 0 (control), 5, 10, 20, 30, and 50 ng L^{-1} GA3 for 4 weeks. Furthermore, we measured the plant height of the in vitro-grown transgenic and WT plants culturing on MS medium with 0 (control) and 10 ng L^{-1} GA3 for 6 weeks.

4.8. Statistical Analysis

For cell length, at least 20 biological replicates were analysed. Data were presented as the mean ± SE and analyzed using Student's *t*-test (two-tailed analysis). For biochemical and molecular biology analysis, all experiments were donefor at least three biological replicates. Significance levels at $p < 0.05$ and $p < 0.01$ are denoted by * (or different small letters) and **, respectively.

5. Conclusions

A novel 9-*cis*-epoxycarotenoid dioxygenase gene, *IbNCED1*, was isolated and characterized from sweet potato. Its overexpression in sweet potato led to a semi-dwarf phenotype, increased contents of ABA, decreased levels of GA3, and downregulated gene expression of the GA3 signal transduction pathway. *IbNCED1* overexpression reduced sensitivity to

GA3, and exogenous GA3 treatment rescued the dwarfism phenotype. It is suggested that *IbNCED1* regulates plant height by the ABA and GA signalling pathways in transgenic sweet potato.

Supplementary Materials: The following supporting information can be downloaded at: https://www.mdpi.com/article/10.3390/ijms241310421/s1.

Author Contributions: Y.Z., Q.W. and F.H. conceived and designed the experiments. Y.Z., C.Z. and T.D. performed the experiments. Y.Z., A.L. and Z.Q. analysed the data. Y.Z., C.Z., T.D., A.L., Z.Q., L.Z., S.D., Q.W. and F.H. contributed reagents, materials and analysis tools. Y.Z., Q.W. and F.H. wrote the paper. All authors have read and agreed to the published version of the manuscript.

Funding: This study was supported by the China Agriculture Research System of Sweet potato (CARS-10-B06 and CARS-10-GW08), Taishan industry leading talents project (LJNY202002, LJNY202113), the Agricultural Seed Project of Shandong Province (2020LZGC004), and the Agricultural scientific and technological innovation project of Shandong Academy of Agricultural Sciences (CXGC2022E01).

Institutional Review Board Statement: Not applicable.

Informed Consent Statement: Not applicable.

Data Availability Statement: The raw data supporting the conclusions of this article will be made available by the authors, without undue reservation, to any qualified researcher.

Conflicts of Interest: The authors declare no conflict of interest.

References

1. El Sheikha, A.F.; Ray, R.C. Potential impacts of bioprocessing of sweet potato: Review. *Crit. Rev. Food Sci. Nutr.* **2017**, *57*, 455–471. [CrossRef]
2. Escobar-Puentes, A.A.; Palomo, I.; Rodriguez, L.; Fuentes, E.; Villegas-Ochoa, M.A.; Gonzalez-Aguilar, G.A.; Olivas-Aguirre, F.J.; Wall-Medrano, A. Sweet potato (*Ipomoea batatas* L.) phenotypes: From agroindustry to health effects. *Foods* **2022**, *11*, 1058. [CrossRef]
3. Gobena, T.L.; Asemie, M.M.; Firisa, T.B. Evaluation of released sweet potato [*Ipomoea batatas* (L.) Lam] varieties for yield and yield-related attributes in Semen-Bench district of Bench-Sheko-Zone, South-Western Ethiopia. *Heliyon* **2022**, *8*, e10950. [CrossRef]
4. Alqudah, A.M.; Koppolu, R.; Wolde, G.M.; Graner, A.; Schnurbusch, T. The genetic architecture of barley plant stature. *Front. Genet.* **2016**, *7*, 117. [CrossRef] [PubMed]
5. Wurschum, T.; Langer, S.M.; Longin, C.F. Genetic control of plant height in European winter wheat cultivars. *Theor. Appl. Genet.* **2015**, *128*, 865–874. [CrossRef] [PubMed]
6. Mo, Y.; Vanzetti, L.S.; Hale, I.; Spagnolo, E.J.; Guidobaldi, F.; Al-Oboudi, J.; Odle, N.; Pearce, S.; Helguera, M.; Dubcovsky, J. Identification and characterization of Rht25, a locus on chromosome arm 6AS affecting wheat plant height, heading time, and spike development. *Theor. Appl. Genet.* **2018**, *131*, 2021–2035. [CrossRef]
7. Greene, A.D.; Reay-Jones, F.; Kirk, K.R.; Peoples, B.K.; Greene, J.K. Spatial associations of key lepidopteran pests with defoliation, NDVI, and plant height in soybean. *Environ. Entomol.* **2021**, *50*, 1378–1392. [CrossRef] [PubMed]
8. Hassan, M.A.; Yang, M.; Fu, L.; Rasheed, A.; Zheng, B.; Xia, X.; Xiao, Y.; He, Z. Accuracy assessment of plant height using an unmanned aerial vehicle for quantitative genomic analysis in bread wheat. *Plant Methods* **2019**, *15*, 37. [CrossRef] [PubMed]
9. Sera, B. Simple traits among diaspore weight/number, plant height and ability of vegetative propagation. *J. Integr. Plant Biol.* **2008**, *50*, 1563–1569. [CrossRef]
10. Trini, J.; Maurer, H.P.; Neuweiler, J.E.; Wurschum, T. Identification and fine-mapping of quantitative trait loci controlling plant height in central european winter *Triticale* (×*Triticosecale Wittmack*). *Plants* **2021**, *10*, 1592. [CrossRef]
11. Hedden, P. The genes of the Green Revolution. *Trends Genet.* **2003**, *19*, 5–9. [CrossRef]
12. Borojevic, K.; Borojevic, K. The transfer and history of "reduced height genes" (Rht) in wheat from Japan to Europe. *J. Hered.* **2005**, *96*, 455–459. [CrossRef]
13. Van De Velde, K.; Thomas, S.G.; Heyse, F.; Kaspar, R.; Van Der Straeten, D.; Rohde, A. N-terminal truncated RHT-1 proteins generated by translational reinitiation cause semi-dwarfing of wheat Green Revolution alleles. *Mol. Plant* **2021**, *14*, 679–687. [CrossRef] [PubMed]
14. Olszewski, N.; Sun, T.P.; Gubler, F. Gibberellin signaling: Biosynthesis, catabolism, and response pathways. *Plant Cell* **2002**, *14* (Suppl. S1), S61–S80. [CrossRef]
15. Nagel, R. Gibberellin signaling in plants: Entry of a new MicroRNA player. *Plant Physiol.* **2020**, *183*, 5–6. [CrossRef] [PubMed]
16. Hedden, P. A novel gibberellin promotes seedling establishment. *Nat. Plants* **2019**, *5*, 459–460. [CrossRef] [PubMed]
17. Hedden, P.; Sponsel, V. A century of gibberellin research. *J. Plant Growth Regul.* **2015**, *34*, 740–760. [CrossRef]

18. Binenbaum, J.; Weinstain, R.; Shani, E. Gibberellin localization and transport in plants. *Trends Plant Sci.* **2018**, *23*, 410–421. [CrossRef]
19. Zhang, Y.; Ni, Z.; Yao, Y.; Nie, X.; Sun, Q. Gibberellins and heterosis of plant height in wheat (*Triticum aestivum* L.). *BMC Genet.* **2007**, *8*, 40. [CrossRef] [PubMed]
20. Zhong, J.; Peng, Z.; Peng, Q.; Cai, Q.; Peng, W.; Chen, M.; Yao, J. Regulation of plant height in rice by the polycomb group genes *OsEMF2b*, *OsFIE2* and *OsCLF*. *Plant Sci.* **2018**, *267*, 157–167. [CrossRef] [PubMed]
21. Lee, J.; Moon, S.; Jang, S.; Lee, S.; An, G.; Jung, K.H.; Park, S.K. *OsbHLH073* negatively regulates internode elongation and plant height by modulating GA homeostasis in rice. *Plants* **2020**, *9*, 547. [CrossRef] [PubMed]
22. Wang, S.; Wang, Y. Harnessing hormone gibberellin knowledge for plant height regulation. *Plant Cell Rep.* **2022**, *41*, 1945–1953. [CrossRef]
23. Siekmann, D.; Jansen, G.; Zaar, A.; Kilian, A.; Fromme, F.J.; Hackauf, B. A genome-wide association study pinpoints quantitative trait genes for plant height, heading date, grain quality, and yield in rye (*Secale cereale* L.). *Front. Plant Sci.* **2021**, *12*, 718081. [CrossRef] [PubMed]
24. Ma, Z.M.; Jin, Y.M.; Wu, T.; Hu, L.J.; Zhang, Y.; Jiang, W.Z.; Du, X.L. OsDREB2B, an AP2/ERF transcription factor, negatively regulates plant height by conferring GA metabolism in rice. *Front. Plant Sci.* **2022**, *13*, 1007811. [CrossRef]
25. Saidou, M.; Zhang, Z.Y. The L-Type Lectin-like receptor kinase gene *TaLecRK-IV.1* regulates the plant height in wheat. *Int. J. Mol. Sci.* **2022**, *23*, 8208. [CrossRef]
26. Tian, X.L.; Xia, X.C.; Xu, D.G.; Liu, Y.Q.; Xie, L.; Hassan, M.A.; Song, J.; Li, F.J.; Wang, D.S.; Zhang, Y.; et al. Rht24b, an ancient variation of TaGA2ox-A9, reduces plant height without yield penalty in wheat. *New Phytol.* **2022**, *233*, 738–750. [CrossRef] [PubMed]
27. Zhang, X.; Ding, L.; Song, A.P.; Li, S.; Liu, J.Y.; Zhao, W.Q.; Jia, D.W.; Guan, Y.X.; Zhao, K.K.; Chen, S.M.; et al. DWARF and Robust Plant regulates plant height via modulating gibberellin biosynthesis in chrysanthemum. *Plant Physiol.* **2022**, *190*, 2484–2500. [CrossRef]
28. Weiss, D.; Ori, N. Mechanisms of cross talk between gibberellin and other hormones. *Plant Physiol.* **2007**, *144*, 1240–1246. [CrossRef]
29. Abley, K.; Formosa-Jordan, P.; Tavares, H.; Chan, E.Y.; Afsharinafar, M.; Leyser, O.; Locke, J.C. An ABA-GA bistable switch can account for natural variation in the variability of *Arabidopsis* seed germination time. *Elife* **2021**, *10*, e59485. [CrossRef]
30. Lando, A.P.; Viana, W.G.; Vale, E.M.; Santos, M.; Silveira, V.; Steiner, N. Cellular alteration and differential protein profile explain effects of GA3 and ABA and their inhibitor on *Trichocline catharinensis* (Asteraceae) seed germination. *Physiol. Plant.* **2020**, *169*, 258–275. [CrossRef]
31. Griffiths, J.; Murase, K.; Rieu, I.; Zentella, R.; Zhang, Z.L.; Powers, S.J.; Gong, F.; Phillips, A.L.; Hedden, P.; Sun, T.P.; et al. Genetic characterization and functional analysis of the GID1 gibberellin receptors in *Arabidopsis*. *Plant Cell* **2006**, *18*, 3399–3414. [CrossRef] [PubMed]
32. Gomez-Cadenas, A.; Zentella, R.; Walker-Simmons, M.K.; Ho, T.H. Gibberellin/abscisic acid antagonism in barley aleurone cells: Site of action of the protein kinase PKABA1 in relation to gibberellin signaling molecules. *Plant Cell* **2001**, *13*, 667–679. [CrossRef] [PubMed]
33. Achard, P.; Herr, A.; Baulcombe, D.C.; Harberd, N.P. Modulation of floral development by a gibberellin-regulated microRNA. *Development* **2004**, *131*, 3357–3365. [CrossRef] [PubMed]
34. Xie, Z.; Zhang, Z.L.; Zou, X.L.; Yang, G.X.; Komatsu, S.; Shen, Q.X.J. Interactions of two abscisic-acid induced *WRKY* genes in repressing gibberellin signaling in aleurone cells. *Plant J.* **2006**, *46*, 231–242. [CrossRef] [PubMed]
35. Lang, J.; Fu, Y.X.; Zhou, Y.; Cheng, M.P.; Deng, M.; Li, M.L.; Zhu, T.T.; Yang, J.; Guo, X.J.; Gui, L.X.; et al. Myb10-D confers PHS-3D resistance to pre-harvest sprouting by regulating NCED in ABA biosynthesis pathway of wheat. *New Phytol.* **2021**, *230*, 1940–1952. [CrossRef]
36. García, M.N.M.; Stritzler, M.; Capiati, D.A. Heterologous expression of Arabidopsis *ABF4* gene in potato enhances tuberization through ABA-GA crosstalk regulation. *Planta* **2014**, *239*, 615–631. [CrossRef]
37. Chen, K.; Li, G.J.; Bressan, R.A.; Song, C.P.; Zhu, J.K.; Zhao, Y. Abscisic acid dynamics, signaling, and functions in plants. *J. Integr. Plant Biol.* **2020**, *62*, 25–54. [CrossRef]
38. Iuchi, S.; Kobayashi, M.; Taji, T.; Naramoto, M.; Seki, M.; Kato, T.; Tabata, S.; Kakubari, Y.; Yamaguchi-Shinozaki, K.; Shinozaki, K. Regulation of drought tolerance by gene manipulation of 9-*cis*-epoxycarotenoid dioxygenase, a key enzyme in abscisic acid biosynthesis in *Arabidopsis*. *Plant J.* **2001**, *27*, 325–333. [CrossRef]
39. He, R.R.; Zhuang, Y.; Cai, Y.M.; Aguero, C.B.; Liu, S.L.; Wu, J.; Deng, S.H.; Walker, M.A.; Lu, J.; Zhang, Y.L. Overexpression of 9-*cis*-epoxycarotenoid dioxygenase cisgene in grapevine increases drought tolerance and results in pleiotropic effects. *Front. Plant Sci.* **2018**, *9*, 970. [CrossRef]
40. Huang, Y.; Guo, Y.M.; Liu, Y.T.; Zhang, F.; Wang, Z.K.; Wang, H.Y.; Wang, F.; Li, D.P.; Mao, D.D.; Luan, S.; et al. 9-*cis*-epoxycarotenoid dioxygenase 3 regulates plant growth and enhances multi-abiotic stress tolerance in rice. *Front. Plant Sci.* **2018**, *9*, 162. [CrossRef]
41. Huang, Y.; Jiao, Y.; Xie, N.K.; Guo, Y.M.; Zhang, F.; Xiang, Z.P.; Wang, R.; Wang, F.; Gao, Q.M.; Tian, L.F.; et al. *OsNCED5*, a 9-*cis*-epoxycarotenoid dioxygenase gene, regulates salt and water stress tolerance and leaf senescence in rice. *Plant Sci.* **2019**, *287*, 110188. [CrossRef] [PubMed]

42. Martinez-Andujar, C.; Martinez-Perez, A.; Ferrandez-Ayela, A.; Albacete, A.; Martinez-Melgarejo, P.A.; Dodd, I.C.; Thompson, A.J.; Perez-Perez, J.M.; Perez-Alfocea, F. Impact of overexpression of 9-*cis*-epoxycarotenoid dioxygenase on growth and gene expression under salinity stress. *Plant Sci.* **2020**, *295*, 110268. [CrossRef]
43. Iuchi, S.; Kobayashi, M.; Yamaguchi-Shinozaki, K.; Shinozaki, K. A stress-inducible gene for 9-*cis*-epoxycarotenoid dioxygenase involved in abscisic acid biosynthesis under water stress in drought-tolerant cowpea. *Plant Physiol.* **2000**, *123*, 553–562. [CrossRef]
44. Agarwal, P.; Balyan, H.S.; Gupta, P.K. Identification of modifiers of the plant height in wheat using an induced dwarf mutant controlled by RhtB4c allele. *Physiol. Mol. Biol. Plants* **2020**, *26*, 2283–2289. [CrossRef] [PubMed]
45. Teng, F.; Zhai, L.H.; Liu, R.X.; Bai, W.; Wang, L.Q.; Huo, D.G.; Tao, Y.S.; Zheng, Y.L.; Zhang, Z.X. *ZmGA3ox2*, a candidate gene for a major QTL, qPH3.1, for plant height in maize. *Plant J.* **2013**, *73*, 405–416. [CrossRef] [PubMed]
46. Bhat, J.A.; Karikari, B.; Adeboye, K.A.; Ganie, S.A.; Barmukh, R.; Hu, D.; Varshney, R.K.; Yu, D. Identification of superior haplotypes in a diverse natural population for breeding desirable plant height in soybean. *Theor. Appl. Genet.* **2022**, *135*, 2407–2422. [CrossRef]
47. Pei, X.X.; Wang, X.Y.; Fu, G.Y.; Chen, B.J.; Nazir, M.F.; Pan, Z.; He, S.P.; Du, X.M. Identification and functional analysis of 9-*cis*-epoxy carotenoid dioxygenase (NCED) homologs in *G. hirsutum*. *Int. J. Biol. Macromol.* **2021**, *182*, 298–310. [CrossRef]
48. Frey, A.; Effroy, D.; Lefebvre, V.; Seo, M.; Perreau, F.; Berger, A.; Sechet, J.; To, A.; North, H.M.; Marion-Poll, A. Epoxycarotenoid cleavage by NCED5 fine-tunes ABA accumulation and affects seed dormancy and drought tolerance with other NCED family members. *Plant J.* **2012**, *70*, 501–512. [CrossRef]
49. Behnam, B.; Iuchi, S.; Fujita, M.; Fujita, Y.; Takasaki, H.; Osakabe, Y.; Yamaguchi-Shinozaki, K.; Kobayashi, M.; Shinozaki, K. Characterization of the promoter region of an *Arabidopsis* gene for 9-*cis*-epoxycarotenoid dioxygenase involved in dehydration-inducible transcription. *DNA Res.* **2013**, *20*, 315–324. [CrossRef]
50. Lee, S.A.; Jang, S.; Yoon, E.K.; Heo, J.O.; Chang, K.S.; Choi, J.W.; Dhar, S.; Kim, G.; Choe, J.E.; Heo, J.B.; et al. Interplay between ABA and GA modulates the timing of asymmetric cell divisions in the *Arabidopsis* root ground tissue. *Mol. Plant* **2016**, *9*, 870–884. [CrossRef]
51. Murcia, G.; Fontana, A.; Pontin, M.; Baraldi, R.; Bertazza, G.; Piccoli, P.N. ABA and GA3 regulate the synthesis of primary and secondary metabolites related to alleviation from biotic and abiotic stresses in grapevine. *Phytochemistry* **2017**, *135*, 34–52. [CrossRef]
52. Kozaki, A.; Aoyanagi, T. Molecular aspects of seed development controlled by gibberellins and abscisic acids. *Int. J. Mol. Sci.* **2022**, *23*, 1876. [CrossRef]
53. Tuan, P.A.; Kumar, R.; Rehal, P.K.; Toora, P.K.; Ayele, B.T. Molecular mechanisms underlying abscisic acid/gibberellin balance in the control of seed dormancy and germination in cereals. *Front. Plant Sci.* **2018**, *9*, 668. [CrossRef]
54. Golldack, D.; Li, C.; Mohan, H.; Probst, N. Gibberellins and abscisic acid signal crosstalk: Living and developing under unfavorable conditions. *Plant Cell Rep.* **2013**, *32*, 1007–1016. [CrossRef]
55. Zhao, J.; Liu, X.; Wang, M.; Xie, L.J.; Wu, Z.X.; Yu, J.M.; Wang, Y.C.; Zhang, Z.Q.; Jia, Y.F.; Liu, Q.P. The miR528-D3 module regulates plant height in rice by modulating the gibberellin and abscisic acid metabolisms. *Rice* **2022**, *15*, 27. [CrossRef]
56. Katyayini, N.U.; Rinne, P.; Tarkowska, D.; Strnad, M.; van der Schoot, C. Dual role of gibberellin in perennial shoot branching: Inhibition and activation. *Front. Plant Sci.* **2020**, *11*, 736. [CrossRef]
57. Pearce, S.; Huttly, A.K.; Prosser, I.M.; Li, Y.D.; Vaughan, S.P.; Gallova, B.; Patil, A.; Coghill, J.A.; Dubcovsky, J.; Hedden, P.; et al. Heterologous expression and transcript analysis of gibberellin biosynthetic genes of grasses reveals novel functionality in the GA3ox family. *BMC Plant Biol.* **2015**, *15*, 130. [CrossRef]
58. Voorend, W.; Nelissen, H.; Vanholme, R.; De Vliegher, A.; Van Breusegem, F.; Boerjan, W.; Roldan-Ruiz, I.; Muylle, H.; Inze, D. Overexpression of *GA20-OXIDASE1* impacts plant height, biomass allocation and saccharification efficiency in maize. *Plant Biotechnol. J.* **2016**, *14*, 997–1007. [CrossRef]
59. Filo, J.; Wu, A.; Eliason, E.; Richardson, T.; Thines, B.C.; Harmon, F.G. Gibberellin driven growth in elf3 mutants requires PIF4 and PIF5. *Plant Signal. Behav.* **2015**, *10*, e992707. [CrossRef]
60. Itoh, H.; Ueguchi-Tanaka, M.; Sentoku, N.; Kitano, H.; Matsuoka, M.; Kobayashi, M. Cloning and functional analysis of two gibberellin 3 beta-hydroxylase genes that are differently expressed during the growth of rice. *Proc. Natl. Acad. Sci. USA* **2001**, *98*, 8909–8914. [CrossRef]
61. Mares, D.; Derkx, A.; Cheong, J.; Zaharia, I.; Asenstorfer, R.; Mrva, K. Gibberellins in developing wheat grains and their relationship to late maturity alpha-amylase (LMA). *Planta* **2022**, *255*, 119. [CrossRef] [PubMed]
62. Lo, S.F.; Yang, S.Y.; Chen, K.T.; Hsing, Y.I.; Zeevaart, J.A.; Chen, L.J.; Yu, S.M. A novel class of gibberellin 2-oxidases control semidwarfism, tillering, and root development in rice. *Plant Cell* **2008**, *20*, 2603–2618. [CrossRef] [PubMed]
63. Zhao, C.; Ma, J.J.; Zhang, Y.H.; Yang, S.X.; Feng, X.Z.; Yan, J. The miR166 mediated regulatory module controls plant height by regulating gibberellic acid biosynthesis and catabolism in soybean. *J. Integr. Plant Biol.* **2022**, *64*, 995–1006. [CrossRef] [PubMed]
64. Liu, X.L.; Yang, W.C.; Wang, J.; Yang, M.X.; Wei, K.; Liu, X.Y.; Qiu, Z.K.; van Giang, T.; Wang, X.X.; Guo, Y.M.; et al. *SlGID1a* is a putative candidate gene for qtph1.1, a major-effect quantitative trait locus controlling tomato plant height. *Front. Genet.* **2020**, *11*, 881. [CrossRef]
65. Gazara, R.K.; Moharana, K.C.; Bellieny-Rabelo, D.; Venancio, T.M. Expansion and diversification of the gibberellin receptor gibberellin insensitive dwarf1 (GID1) family in land plants. *Plant Mol. Biol.* **2018**, *97*, 435–449. [CrossRef]

66. Yoshida, H.; Tanimoto, E.; Hirai, T.; Miyanoiri, Y.; Mitani, R.; Kawamura, M.; Takeda, M.; Takehara, S.; Hirano, K.; Kainosho, M.; et al. Evolution and diversification of the plant gibberellin receptor GID1. *Proc. Natl. Acad. Sci. USA* **2018**, *115*, E7844–E7853. [CrossRef]
67. Ueguchi-Tanaka, M.; Nakajima, M.; Motoyuki, A.; Matsuoka, M. Gibberellin receptor and its role in gibberellin signaling in plants. *Annu. Rev. Plant Biol.* **2007**, *58*, 183–198. [CrossRef]
68. Ito, T.; Okada, K.; Fukazawa, J.; Takahashi, Y. DELLA-dependent and -independent gibberellin signaling. *Plant Signal. Behav.* **2018**, *13*, e1445933. [CrossRef]
69. Daviere, J.M.; Wild, M.; Regnault, T.; Baumberger, N.; Eisler, H.; Genschik, P.; Achard, P. Class I TCP-DELLA interactions in inflorescence shoot apex determine plant height. *Curr. Biol.* **2014**, *24*, 1923–1928. [CrossRef]
70. Roxrud, I.; Lid, S.E.; Fletcher, J.C.; Schmidt, E.D.; Opsahl-Sorteberg, H.G. GASA4, one of the 14-member Arabidopsis GASA family of small polypeptides, regulates flowering and seed development. *Plant Cell Physiol.* **2007**, *48*, 471–483. [CrossRef]
71. Liu, D.G.; Wang, L.J.; Zhai, H.; Song, X.J.; He, S.Z.; Liu, Q.C. A novel alpha/beta-hydrolase gene *IbMas* enhances salt tolerance in transgenic sweet potato. *PLoS ONE* **2014**, *9*, e115128. [CrossRef]
72. Liu, Q.C.; Zhai, H.; Wang, Y.; Zhang, D.P. Efficient plant regeneration from embryogenic suspension cultures of sweet potato. *Vitr. Cell. Dev. Biol.-Plant* **2001**, *37*, 564–567. [CrossRef]
73. Fang, X.; Bo, C.; Wang, M.J.; Yuan, H.T.; Li, W.; Chen, H.W.; Ma, Q.; Cai, R.H. Overexpression of the maize *WRKY114* gene in transgenic rice reduce plant height by regulating the biosynthesis of GA. *Plant Signal. Behav.* **2021**, *16*, 1967635. [CrossRef]

ARTICLES FOR FACULTY MEMBERS

INVESTIGATING THE ROLE OF GIBBERELLIC ACID (GA) AND ABSCISIC ACID (ABA) CROSS-TALK IN ENHANCING TUBEROUS ROOT DEVELOPMENT IN SWEET POTATOES

Salicylic acid protects sweet potato seedlings from drought stress by mediating abscisic acid-related gene expression and enhancing the antioxidant defense system / Huang, C., Liao, J., Huang, W., & Qin, N.

International Journal of Molecular Sciences
Volume 23 Issue 23 (2022) 14819 Pages 1-18
https://doi.org/10.3390/ijms232314819
(Database: MDPI)

International Journal of
Molecular Sciences

MDPI

Article

Salicylic Acid Protects Sweet Potato Seedlings from Drought Stress by Mediating Abscisic Acid-Related Gene Expression and Enhancing the Antioxidant Defense System

Chongping Huang [1,2,3,*], Junlin Liao [1,2], Wenjie Huang [1,2] and Nannan Qin [1]

[1] Department of Agronomy, College of Agriculture and Biotechnology, Zhejiang University, 866 Yu-Hang-Tang Road, Hangzhou 310058, China
[2] Hainan Institute of Zhejiang University, Sanya 572025, China
[3] Agricultural Experiment Station of Zhejiang University, 866 Yu-Hang-Tang Road, Hangzhou 310058, China
* Correspondence: hcping@zju.edu.cn; Tel.: +86-571-8820-8490

Abstract: China has the largest sweet potato planting area worldwide, as well as the highest yield per unit area and total yield. Drought is the most frequently encountered environmental stress during the sweet potato growing season. In this study, we investigated salicylic acid (SA)-mediated defense mechanisms under drought conditions in two sweet potato varieties, Zheshu 77 and Zheshu 13. Drought stress decreased growth traits, photosynthetic pigments and relative water contents, as well as the photosynthetic capability parameters net photosynthetic rate, stomatal conductance and transpiration rate, whereas it increased reactive oxygen species production, as well as malondialdehyde and abscisic acid contents. The application of SA to drought-stressed plants reduced oxidative damage by triggering the modulation of antioxidant enzyme activities and the maintenance of optimized osmotic environments in vivo in the two sweet potato varieties. After SA solution applications, *NCED-like3* expression was downregulated and the abscisic acid contents of drought-stressed plants decreased, promoting photosynthesis and plant growth. Thus, foliar spraying an appropriate dose of SA, 2.00–4.00 mg·L^{-1}, on drought-stressed sweet potato varieties may induce resistance in field conditions, thereby increasing growth and crop yield in the face of increasingly frequent drought conditions.

Keywords: sweet potato; drought stress; salicylic acid; photosynthetic capability; antioxidant enzymes; *NCED-like3* expression

Citation: Huang, C.; Liao, J.; Huang, W.; Qin, N. Salicylic Acid Protects Sweet Potato Seedlings from Drought Stress by Mediating Abscisic Acid-Related Gene Expression and Enhancing the Antioxidant Defense System. *Int. J. Mol. Sci.* **2022**, *23*, 14819. https://doi.org/10.3390/ijms232314819

Academic Editors: Masayuki Fujita, Mirza Hasanuzzaman and Kamrun Nahar

Received: 26 October 2022
Accepted: 24 November 2022
Published: 26 November 2022

1. Introduction

Drought is the most frequent environmental problem in crop production worldwide. Owing to climate change, seasonal and regional droughts are showing trends of increasing [1]. Plants have evolved complex morphological, physiological and biochemical mechanisms to cope with drought stress [2]. When the soil moisture is insufficient, the stomata often close partially or completely to decrease the transpiration rate, which reduces water loss and CO_2 entry, resulting in a photosynthetic rate decrease. Deficiencies in CO_2 and H_2O lead to excessive energy production by electron transmission during photosynthesis, which further induces the overgeneration of various reactive oxygen species (ROS) [3]. Plants have developed an antioxidant system, including the antioxidant enzymes superoxide dismutase (SOD), catalase (CAT), peroxidase (POD) and ascorbate peroxidase, as well as the low-molecular antioxidant compounds ascorbate, glutathione, α-tocopherol, β-carotene and flavonoids, to scavenge high levels of ROS [4,5]. To maintain water balance in vivo, plants produce soluble sugars and proteins that increase the osmotic potential. Furthermore, drought induces changes in the expression levels of related genes, resulting in the inhibition of normal and stress-specific protein synthesis [6]. However, there are

limited reports regarding the physiological responses of sweet potato, *Ipomoea batatas*, to the foliar spraying of SA under drought conditions.

As an important plant hormone, SA plays a key regulatory role in plants growing under environmentally stressed conditions. Applying an appropriate SA dose results in plant tolerance to drought, salt, cold and heat, as well as to heavy metal toxicity stress, and it enhances systemic acquired resistance when plants are infected by pathogens [7]. The exogenous application of SA can alleviate the impacts of chilling stress on *Dendrobium. officinale* seedlings by protecting the chloroplast membrane, including PS II D1 protein, and it enhances the antioxidant capacity of plants [8]. In a high temperature environment, SA treatments of ornamental pepper crops increase the germination rate and germination potential, and they reduce oxidative damage to seeds [9]. Additionally, SA remarkably increases the total polyphenolic content and potentiates the radical scavenging activity of *Ammi visnaga* L. when grown in drought-stress conditions [10]. In tomato plants, SA treatments obviously alleviate cadmium-induced growth inhibition by decreasing the cadmium accumulation and malondialdehyde (MDA) level as well as increasing CAT activity and chlorophyll content [11]. Treatments also regulate root cell-wall composition through nitric oxide signaling in rice (*Oryza sativa* L.) [12]. In maize, SA increases crop yield through the enhancement of photosynthesis and antioxidant capacity under salt-stress conditions [13]. Exogenous SA at low concentrations alleviates the accumulation of pesticides and mitigates pesticide-induced oxidative stress in cucumber plants (*Cucumis sativus* L.) by increasing biomass, chlorophyll and proline contents, as well as ascorbate peroxidase and glutathione S-transferase activities, and by decreasing the MDA and H_2O_2 contents [14].

Sweet potato, *I. batatas* (L.) Lam, is an important food crop in China, which has the largest planting area in the world. In 2018, the sweet potato planting area in China reached 2.374 million hectares, accounting for 29.1% of the world planting area. The total output of fresh potato was 62.347 million tons, accounting for 57.11% of the worldwide output. The average yield per hectare was 22.44 tons, the highest in the world [15]. As a significant crop, it provides calories, proteins, vitamins, edible fiber and minerals for humans. In the past, its consumption has saved millions of people from starvation, and it is presently popular with city dwellers in southeastern coastal China for obesity prevention and weight reduction. With economic development, many snack foods based on fresh and processed potatoes have been developed, and this has effectively increased farmer income and alleviated poverty. Therefore, sweet potato production has increased in China in recent years, especially in the southeast coastal areas [2]. As an upland crop, sweet potato is highly tolerant to water deficits. In the south of China, sweet potato is usually planted in hilly areas, where the farmlands are mostly rainfed, but in the north of China water deficits are very common [16]. A water deficiency usually results in a reduced crop yield. Thus, there is a need to develop new measures to alleviate the negative impacts of drought stress on sweet potato production.

Although SA can protect plants from biotic and abiotic stresses through varied metabolic mechanisms, the complete regulatory process is not clear. Moreover, there are limited reports regarding the effects of SA applications on sweet potato plant protection. In this study, we investigated the extent to which SA improves sweet potato tolerance in multiple manners, including seedling growth, chloroplast membrane protection, osmotic adjustment, oxidative stress, antioxidant balance and ABA-related gene expression levels under drought conditions.

2. Results and Analysis

2.1. SA Protects Photosynthetic Pigments and Increases the Photosynthetic Rate

Drought stress resulted in a significant decrease in the total chlorophyll content of sweet potato leaves and spraying appropriate concentrations of SA solutions on the leaves effectively reversed this adverse impact (Table 1). Chlorophyll a (Chl a) represents a portion of the total amount of chlorophyll and is a major component of the photosystem (PS) I. As

shown in Figure 1a,b, with the extension of drought-stress time, the Chl a contents in the leaves of 'Zheshu 77' ('ZS77') and 'Zheshu 13' ('ZS13') showed downward trends.

Table 1. Effects of exogenous SA on total chlorophyll content of sweet potato under drought stress.

Cultivars	Treatment Duration (h)	Total Chlorophyll Content (mg·g^{-1}FW)				
		C0 0.0	C1 1.00	C2 2.00	C3 4.00	C4 8.00
ZS77	24	3.41 ± 0.08 b	3.68 ± 0.14 a	3.54 ± 0.16 a	3.43 ± 0.09 ab	3.26 ± 0.11 b
	48	2.78 ± 0.11 d	3.43 ± 0.11 ab	3.31 ± 0.09 b	3.11 ± 0.14 c	2.79 ± 0.07 d
	72	2.38 ± 0.07 e	2.74 ± 0.14 d	2.92 ± 0.13 c	2.91 ± 0.09 c	2.60 ± 0.07 d
ZS13	24	3.50 ± 0.08 b	3.62 ± 0.13 a	3.76 ± 0.09 a	3.52 ± 0.11 b	3.47 ± 0.15 b
	48	3.02 ± 0.10 c	3.42 ± 0.09 b	3.38 ± 0.13 b	3.27 ± 0.17 c	2.75 ± 0.12 d
	72	2.62 ± 0.14 d	2.62 ± 0.09 d	2.89 ± 0.08 c	3.07 ± 0.11 c	2.31 ± 0.13 e

The different lowercase letters show significant differences ($p < 0.05$).

For 'ZS77', there was no significant difference in the Chl a content among the treatments after 24 h. At 48 h, C1 and C2 were significantly increased by 21.68% and 17.25%, respectively, compared with C0. At 72 h, C2 and C3 were significantly increased by 20.10% and 21.16%, respectively, compared with C0. For 'Zheshu13', the C1, C2 and C3 treatments all alleviated the decline in the Chl a content, but the C4 treatment showed a greater decline than C0. The two sweet potato varieties showed limited differences in SA concentrations, but the concentrations used in the C2 and C3 treatments, 2.0 mg·L^{-1} and 4.0 mg·L^{-1}, respectively, significantly alleviated the decline in the Chl a content in both varieties.

The drought treatment caused pronounced reductions in the chlorophyll b (Chl b) contents in both varieties. For 'ZS77', Chl b contents at 48 h and 72 h decreased by 17.46% and 22.22%, respectively, compared with 24 h after the C0 treatment (Figure 1c). The application of exogenous SA increased the Chl b content. The contents of Chl b after the C2 and C3 treatments significantly increased by 9.52% and 15.87%, respectively, 26.92% and 25.00%, respectively, and 28.57% and 26.53%, respectively, compared with after C0 at 24, 48 and 72 h, respectively. For 'ZS13', only the C3 treatment significantly increased the Chl b contents at 24, 48 and 72 h (Figure 1d).

For 'ZS77', at 24, 48 and 72 h after drought treatments, the net photosynthetic rate (Pn) decreased by 14.18%, 49.55% and 60.67%, respectively. The drought stress also resulted in considerable decreases in the transpiration rate (Tr) and leaf stomatal conductance (Gs) and an increase in the intracellular CO_2 concentration (Ci) for both varieties after 24, 48 and 72 h of drought stress (Table 2).

Seedling leaves receiving different concentrations of exogenous SA demonstrated obvious increases in the Pn, especially after 24 h and 48 h. The Pn values at 48 h after C1, C2 and C3 treatments increased 45.88%, 62.52%, and 36.97%, respectively, for 'ZS77', and by 13.90%, 52.70% and 6.42%, respectively, for 'ZS13', when compared with C0 (Figure 2a,b). Applications of SA solutions also modulated the decrease in Tr. Under drought conditions, after 24, 48 and 72 h of treatments, all the plant Tr values increased by different amounts. After 48 h of drought stress, the Tr values of the C1, C2, C3 and C4 treatments for 'ZS77' were significantly increased by 39.27%, 49.57%, 34.31% and 16.74%, respectively, compared with C0. For 'ZS13', the Tr values of the four treatments significantly increased by 52.91%, 61.70%, 79.19% and 35.33%, respectively (Figure 2c,d).

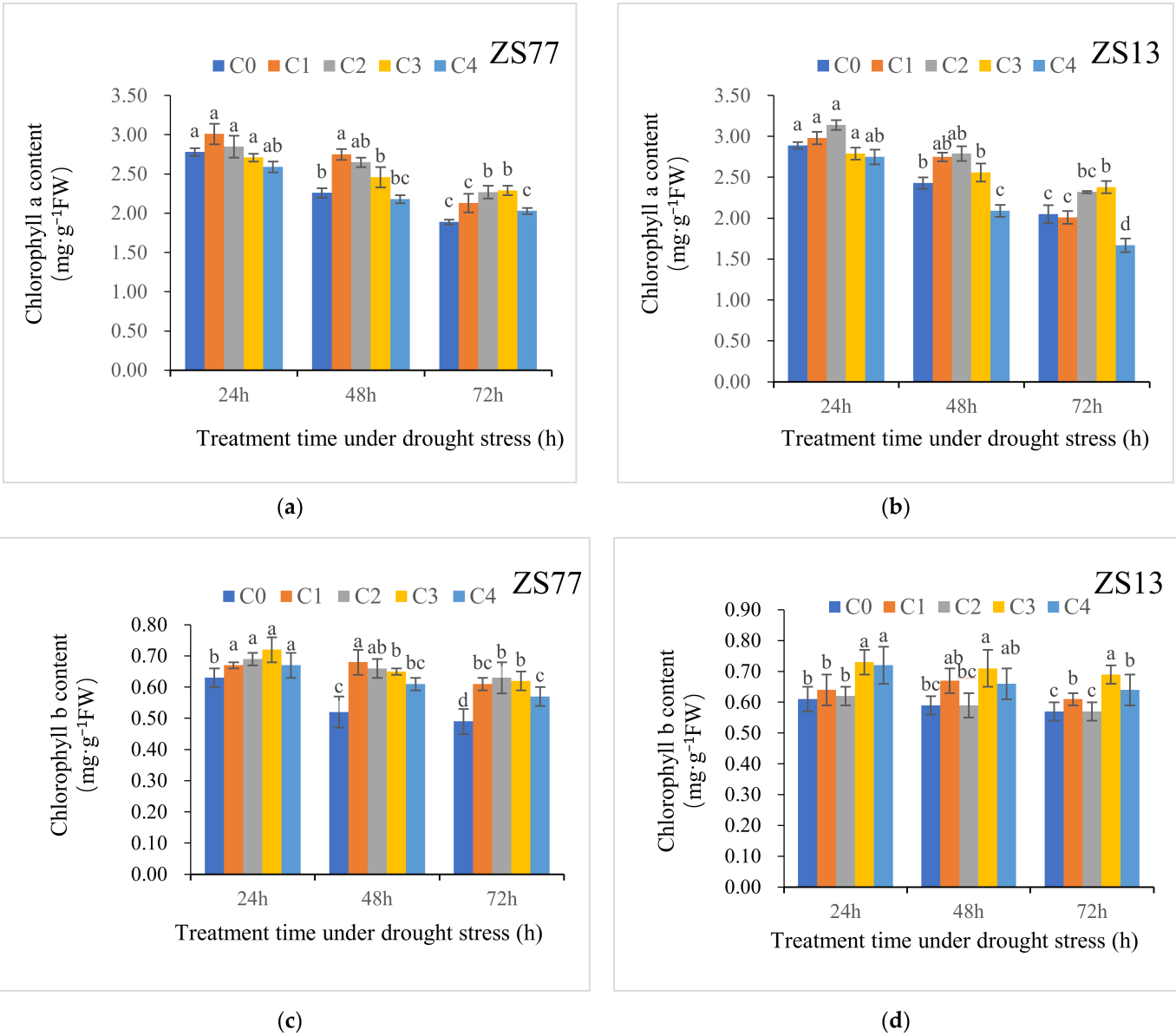

Figure 1. Effect of different concentrations of exogenous SA solution 0 (C0), 1.00 (C1), 2.00 (C2), 4.00 (C3), and 8.00 mg·L^{-1} (C4) on chlorophyll a (**a**,**b**) and b (**c**,**d**) content in sweet potato leaves under drought stress. ZS77 and ZS 13 refer to sweet potato varieties Zheshu 77 and Zheshu 13 respectively, the same as in following figures Bars with different letters indicate significant differences ($p < 0.05$).

Table 2. Effects of drought stress on photosynthetic characteristics of sweet potato leaves.

Item	Treatments	Duration of Drought Stress (h)					
		ZS77			ZS13		
		24 h	48 h	72 h	24 h	48 h	72 h
Pn (CO_2 μmol·m^{-2} s^{-1})	CK	18.34 ± 0.57	19.05 ± 0.82	18.74 ± 0.77	16.58 ± 0.92	16.37 ± 1.11	17.05 ± 0.98
	C0	15.74 ± 0.77	9.61 ± 0.82	7.37 ± 0.54	14.04 ± 0.62	10.24 ± 0.73	5.78 ± 0.59
Tr (H_2O mmol·m^{-2} s^{-1})	CK	5.38 ± 0.10	5.62 ± 0.09	5.55 ± 0.07	3.77 ± 0.08	3.69 ± 0.11	3.73 ± 0.09
	C0	2.71 ± 0.05	2.04 ± 0.11	1.58 ± 0.09	2.02 ± 0.06	1.14 ± 0.04	0.84 ± 0.07
Gs (H_2O mol·m^{-2} s^{-1})	CK	0.214 ± 0.007	0.228 ± 0.005	0.237 ± 0.08	0.188 ± 0.04	0.170 ± 0.07	0.183 ± 0.10
	C0	0.035 ± 0.002	0.026 ± 0.001	0.018 ± 0.004	0.025 ± 0.001	0.016 ± 0.001	0.009 ± 0.002
Ci (CO_2 μmol·mol^{-1})	CK	250.4 ± 4.8	256.8 ± 8.5	255.6 ± 10.1	223.9 ± 7.3	240.3 ± 5.2	239.2 ± 6.7
	C0	143.4 ± 4.6	190.6 ± 7.9	223.7 ± 8.1	155.6 ± 6.4	210.4 ± 8.0	244.3 ± 9.0

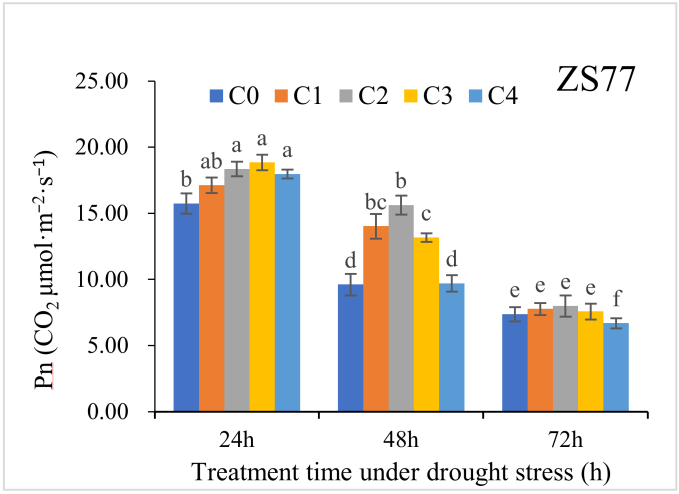

(**a**)

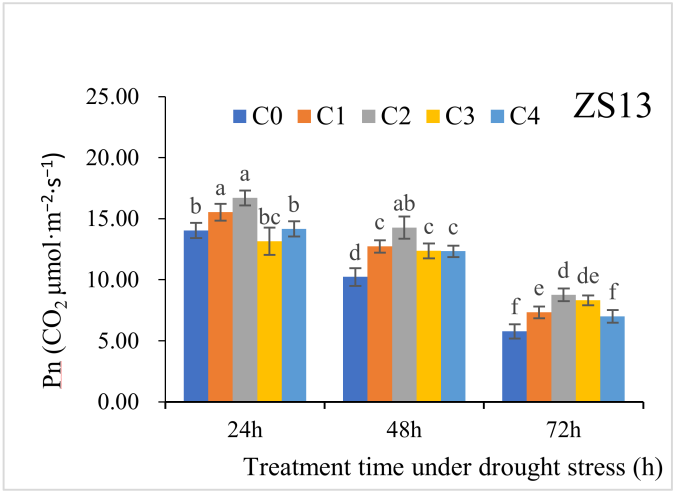

(**b**)

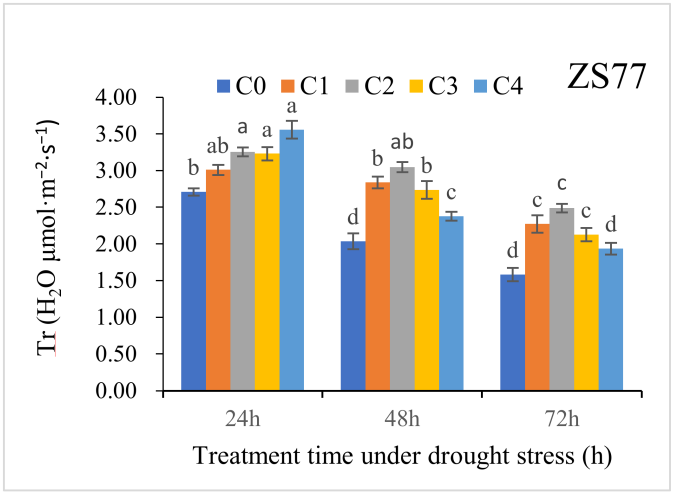

(**c**)

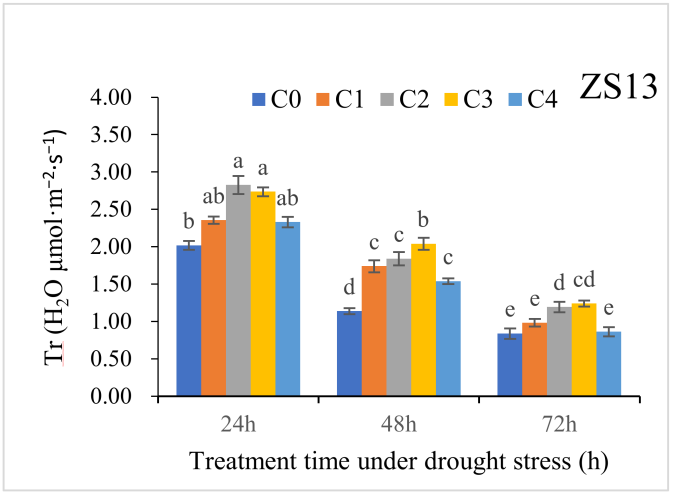

(**d**)

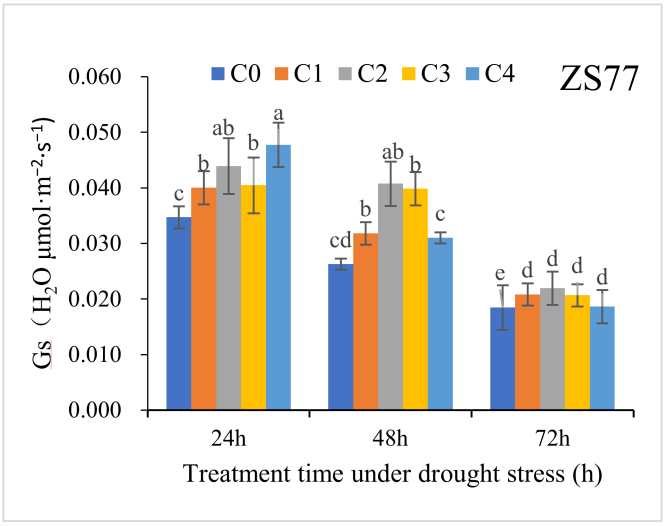

(**e**)

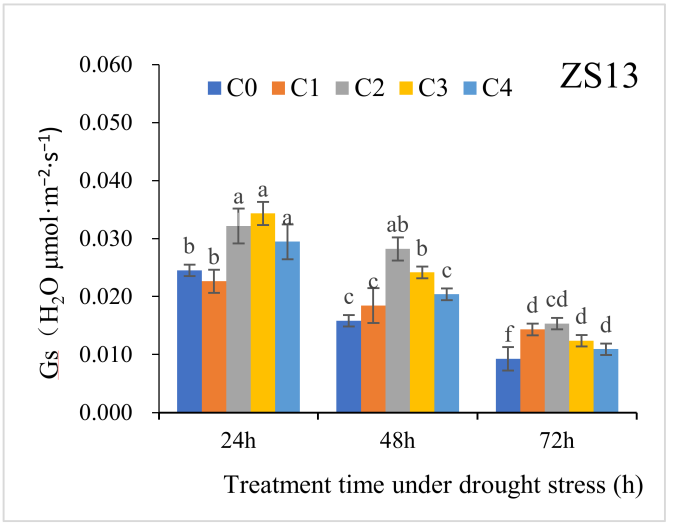

(**f**)

Figure 2. *Cont.*

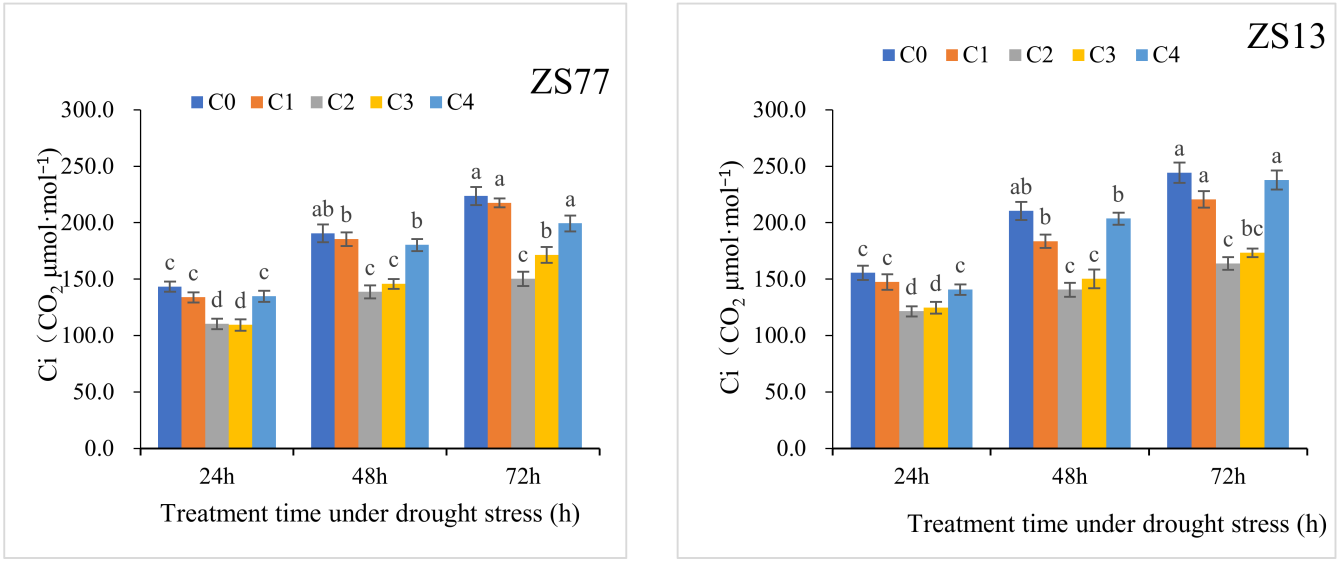

(**g**) (**h**)

Figure 2. Effect of different concentrations of exogenous SA solution 0 (C0), 1.00 (C1), 2.00 (C2), 4.00 (C3), and 8.00 mg·L^{-1} (C4) on Pn (**a**,**b**), Tr (**c**,**d**), Gs (**e**,**f**), and Ci (**g**,**h**) in sweet-potato leaves under drought stress. Bars with different letters indicate significant differences among treatments at 0.05 level (Duncan).

Spraying SA on leaves mitigated the decline in Gs caused by drought for both varieties. In general, C2 was more efficacious. At 24, 48 and 72 h after treatments, the Gs values in the two varieties increased by 26.56%, 55.16% and 18.95% and by 31.19% 78.40% and 65.48%, respectively (Figure 2e,f). The SA application also modulated an adverse increase in Ci values. The Ci values after the C2 and C3 treatments decreased by 27.23% and 23.45%, respectively, after 48 h and by 32.81% and 23.33%, respectively, after 72 h compared with those of C0. The mitigation effects were significantly different ($p < 0.05$) (Figure 2g,h).

2.2. SA Reduces Oxidative Stress and Enhances Antioxidant Enzyme Activities

Drought stress led to strict increases in the H_2O_2 and MDA contents. For 'ZS77', at 24, 48 and 72 h after drought treatment, the H_2O_2 content increased by 32.50%, 74.96% and 95.90%, respectively, and the MDA content increased by 15.96%, 43.41% and 72.95%, respectively. There were similar changes for 'ZS13' (Table 3). SA applications significantly decreased the H_2O_2 and MDA contents at 24, 48 and 72 h after treatments (Figures 3 and 4).

Table 3. Effects of drought stress on H_2O_2, MDA contents in sweet potato leaves.

Item	Treatments	Duration of Drought Stress					
		ZS77			ZS13		
		24 h	48 h	72 h	24 h	48 h	72 h
H_2O_2 content (μmol·g^{-1} FW)	CK	6.43 ± 0.38	6.71 ± 0.44	6.59 ± 0.51	7.55 ± 0.49	7.63 ± 0.33	7.59 ± 0.50
	C0	8.52 ± 0.49	11.74 ± 0.35	12.91 ± 0.66	8.58 ± 0.32	12.45 ± 0.43	13.07 ± 0.47
MDA content (μmol·g^{-1} FW)	CK	7.77 ± 0.31	7.81 ± 0.47	7.69 ± 0.62	8.40 ± 0.69	8.77 ± 0.63	8.64 ± 0.29
	C0	9.01 ± 0.41	11.20 ± 0.39	13.30 ± 0.70	11.38 ± 0.77	13.26 ± 0.48	15.16 ± 0.65

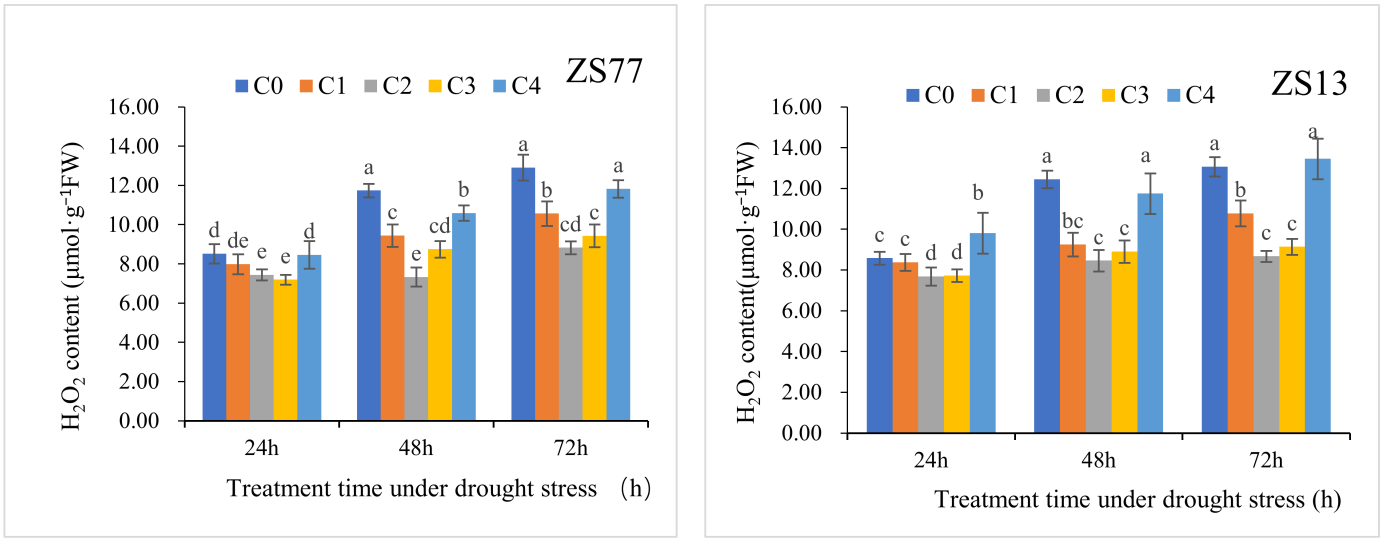

(**a**) (**b**)

Figure 3. Effect of different concentrations of exogenous SA solution 0 (C0), 1.00 (C1), 2.00 (C2), 4.00 (C3), and 8.00 mg·L^{-1} (C4) on H_2O_2 content of sweet-potato leaves under drought stress. Bars with different letters indicate significant differences among treatments at 0.05 level (Duncan).

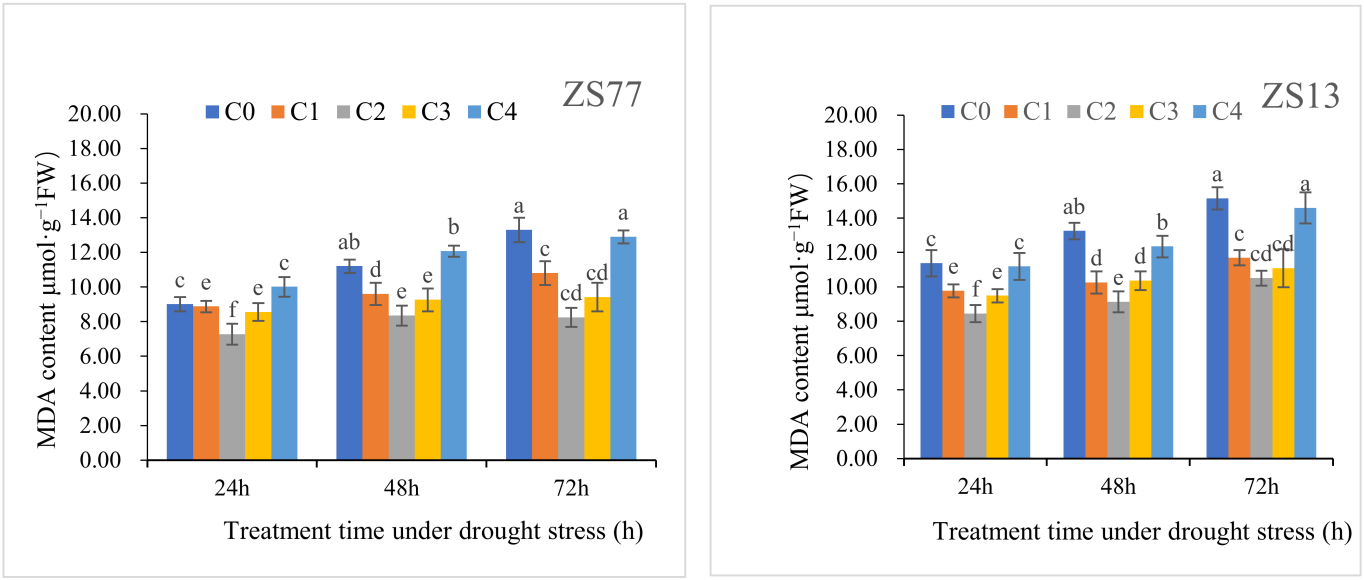

(**a**) (**b**)

Figure 4. Effect of different concentrations of exogenous SA solution 0 (C0), 1.00 (C1), 2.00 (C2), 4.00 (C3), and 8.00 mg·L^{-1} (C4) on MDA content of sweet-potato leaves under drought stress. Bars with different letters indicate significant differences among treatments at 0.05 level (Duncan).

At 72 h after foliar spraying SA, the H_2O_2 contents of 'ZS77' receiving C1, C2 and C3 treatments significantly decreased by 18.20%, 31.65% and 26.95%, respectively, compared with C0, whereas the H_2O_2 contents of 'ZS13' significantly decreased by 17.50%, 33.60% and 30.05%, respectively (Figure 3). At 48 h after treatment with SA, the MDA contents in 'ZS77' receiving C1, C2 and C3 treatments decreased by 14.28%, 25.47% and 17.29%, respectively, compared with the C0, and they decreased by 18.77%, 37.99% and 29.17%, respectively, after 72 h. 'ZS13' plants receiving the C1, C2 and C3 treatments showed similar trends (Figure 4). The MDA content after the C4 treatment maintained the same upward trend as that of the C0, with no significant difference.

Under drought conditions, the SOD activity levels in 'ZS77' and 'ZS13' leaves increased along with time (Figure 5a,b). For 'ZS77', after 48 h and 72 h of drought stress, the SOD activity increased by 8.44% and 28.72%, respectively, compared with C0 after 24 h. The SA treatment further increased the SOD activity. At 24, 48 and 72 h after the C2 treatment the SOD activities increased by 34.90%, 37.63% and 42.31%, respectively, and after the C3 treatment they increased by 42.03%, 51.41% and 43.64%, respectively, compared with those of the C0 treatment. The C1 and C4 treatments also significantly increased the SOD activities, but to lesser degrees than C2 and C3. The changes in the SOD activities of 'ZS13' showed similar trends for all the treatments.

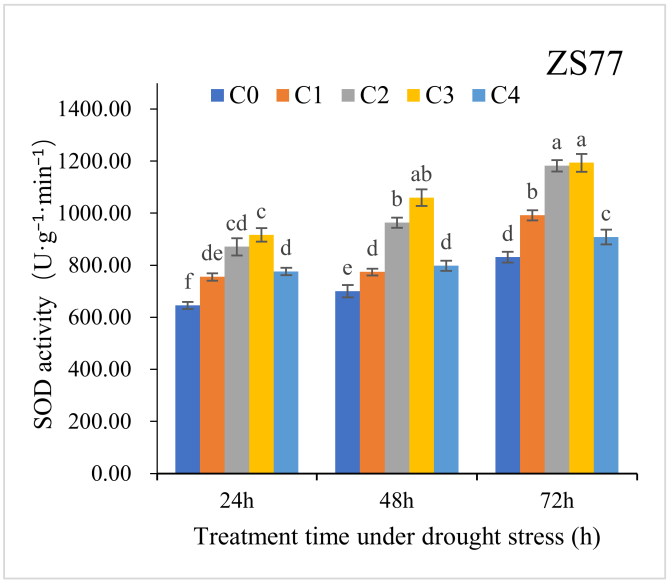

(**a**)

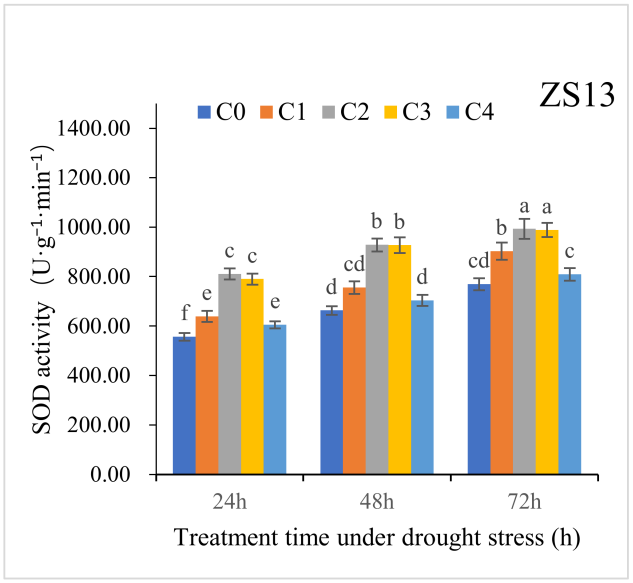

(**b**)

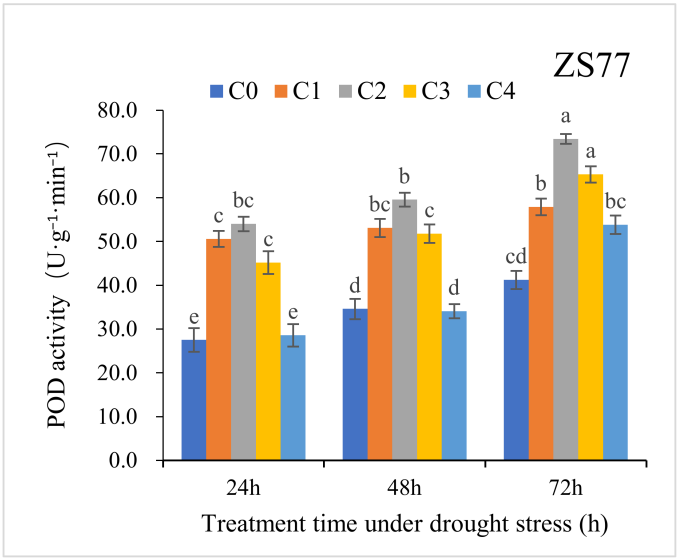

(**c**)

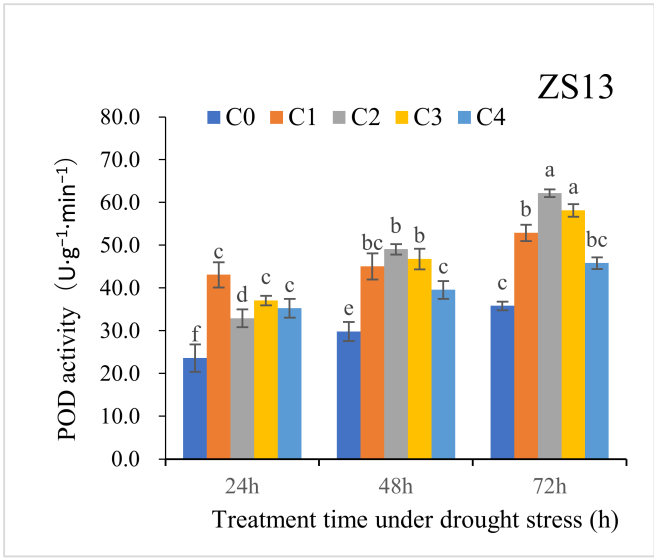

(**d**)

Figure 5. *Cont.*

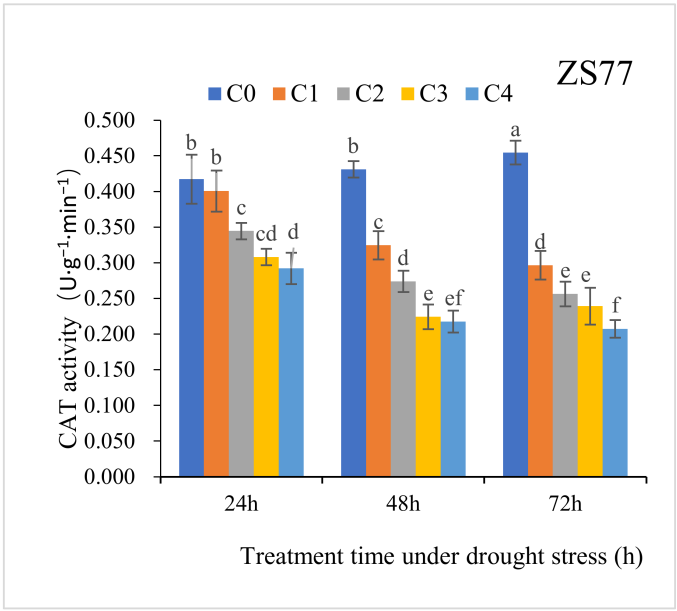

(**e**)

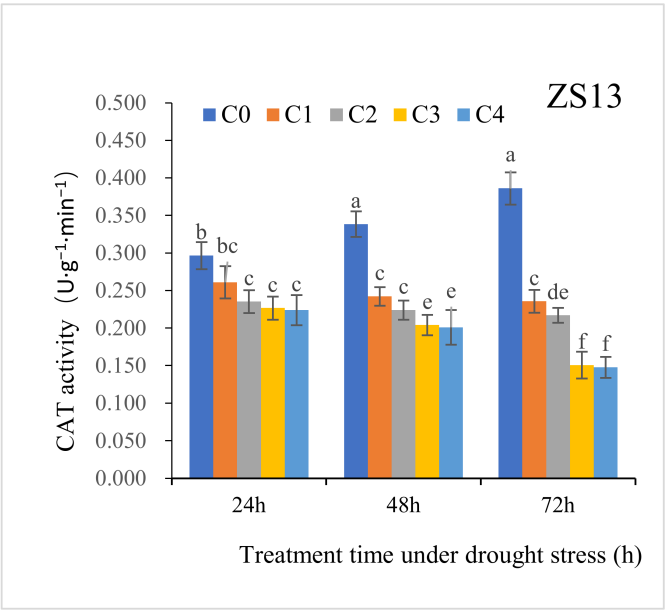

(**f**)

Figure 5. Effect of different concentrations of exogenous SA solution 0 (C0), 1.00 (C1), 2.00 (C2), 4.00 (C3), and 8.00 mg·L^{-1} (C4) on SOD (**a**,**b**), POD (**c**,**d**), CAT (**e**,**f**) activities in sweet-potato leaves under drought stress. Bars with different letters indicate significant differences among treatments at 0.05 level (Duncan).

POD works in cooperation with SOD and CAT to scavenge ROS. With the extension of drought-stress treatment times, the POD activity levels in the two sweet potato variety leaves increased significantly, and SA applications promoted a further increase in the POD activities. The variety 'ZS77' showed a higher POD activity level independent of the SA treatments (Figure 5c,d). For 'ZS77', at 24, 48 and 72 h after the C2 treatment, the POD activities increased by 96.39%, 72.08% and 78.09%, respectively, compared with C0, whereas for 'ZS13', the POD activities increased by 39.35%, 64.38% and 73.58%, respectively. The differences between varieties were significant ($p < 0.05$).

CAT catalyzes the decomposition of H_2O_2 into H_2O and O_2 in vivo to help plants cope with drought stress. With the extension of the C0 drought-treatment time, the CAT activity levels in leaves of the two sweet potato varieties increased gradually. After spraying different concentrations of SA solutions on the leaves, the CAT activities showed varying degrees of a downward trend, and the resulting activity range positively correlated with the SA concentration (Figure 5e,f). For 'ZS77', the CAT activity levels decreased by 3.99%, 17.41%, 26.20% and 29.95% after C1–4 treatments, respectively, at 24 h compared with the C0 treatment, and at 48 h, the values had decreased by 24.67%, 36.43%, 47.95% and 49.50%, respectively. After 72 h, the levels were 34.75%, 43.62%, 47.36% and 54.40%, respectively, compared with C0. The 'ZS13' variety showed a similar trend.

2.3. SA Mediates the Plant Osmotic Status

Compared with normally growing plants, after 24, 48 and 72 h of drought stress, the leaf relative water content (RWC) values decreased by 9.16%, 12.48% and 17.48%, respectively. SA treatments, especially C2 and C3, mediated the RWC decreases at 24, 48 and 72 h. At 48 h after the SA treatment of 'ZS77', the RWC values of C2- and C3-treated plant leaves significantly increased by 4.83% and 3.97%, respectively, compared with C0, whereas for 'ZS13', the RWC values significantly increased by 10.39% and 10.04%, respectively (Figure 6a,b).

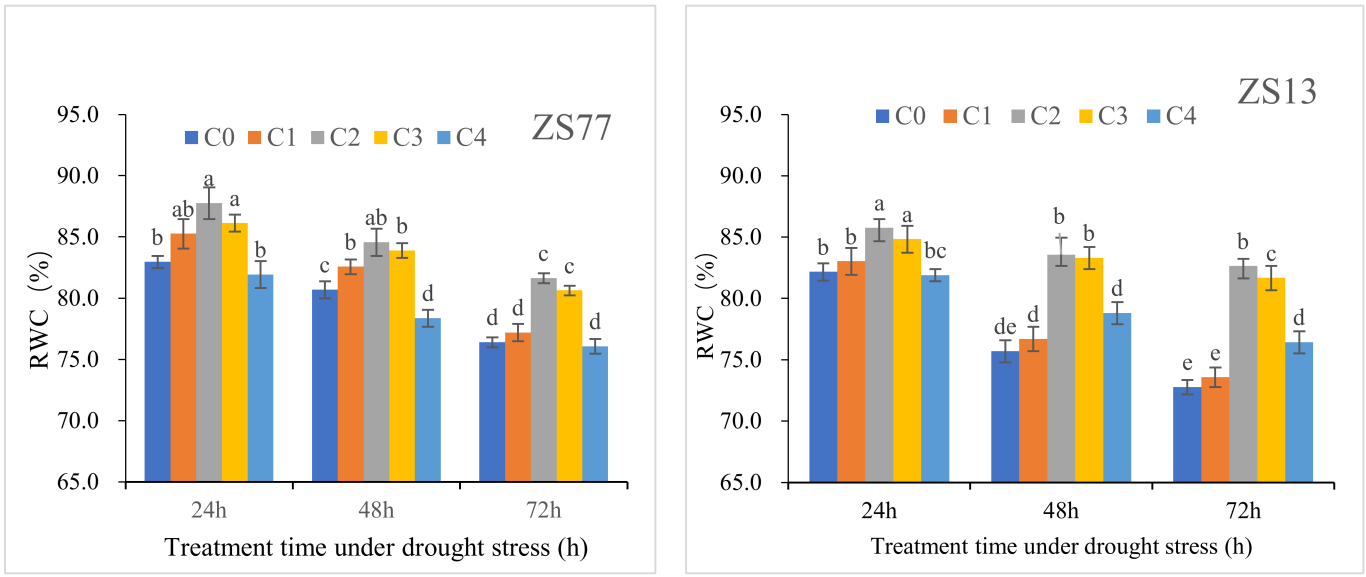

(**a**) (**b**)

Figure 6. Effect of different concentrations of exogenous SA solution 0 (C0), 1.00 (C1), 2.00 (C2), 4.00 (C3), and 8.00 mg·L^{-1} (C4) on RWC of sweet-potato leaves under drought stress. Bars with different letters indicate significant differences among treatments at 0.05 level (Duncan).

At 24, 48 and 72 h after drought treatments, compared with normally growing plants, the soluble sugar contents increased by 42.99%, 80.84% and 81.21%, respectively. Spraying exogenous SA further increased the soluble sugar contents independent of the concentration (Figure 7a,b). The C2 and C3 treatments were the most efficacious. For 'ZS77' at 24, 48 and 72 h after treatment, C2 increased by 28.78%, 30.19% and 51.96%, respectively, and C3 increased by 17.28%, 24.79% and 55.93%, respectively, compared with C0. There was a similar trend in 'ZS13'. After SA treatments, the soluble protein contents in leaves also increased (Figure 7c,d). For 'ZS77' after 24 h of drought, the soluble protein contents of the C1–4 treatments significantly increased by 8.22%, 27.03%, 32.22% and 21.51%, respectively, compared with C0. The content range increased further at 48 h and 72 h after treatment. Similar changes occurred in 'ZS13'.

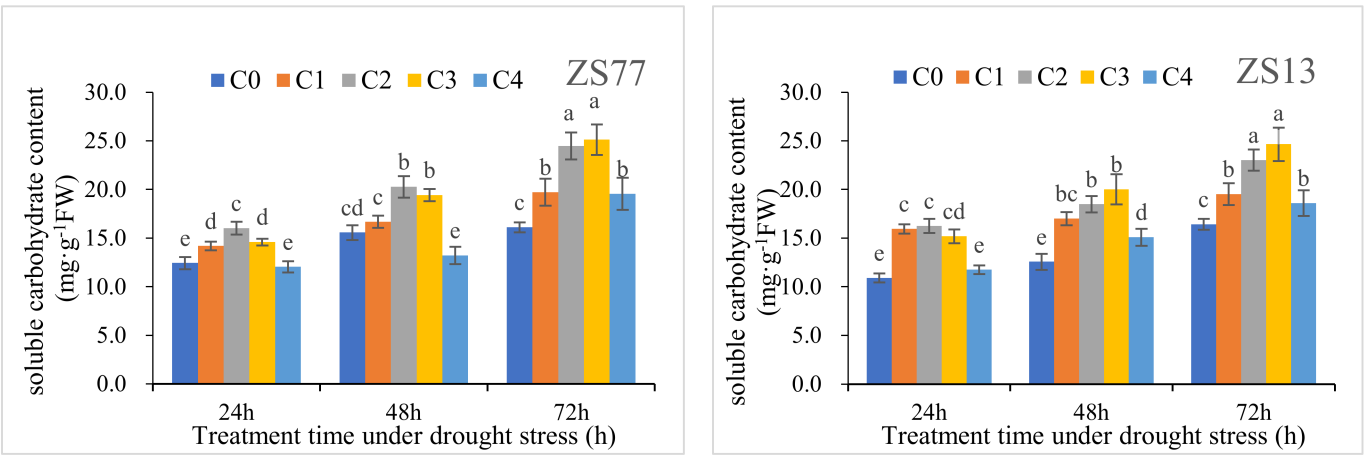

(**a**) (**b**)

Figure 7. *Cont.*

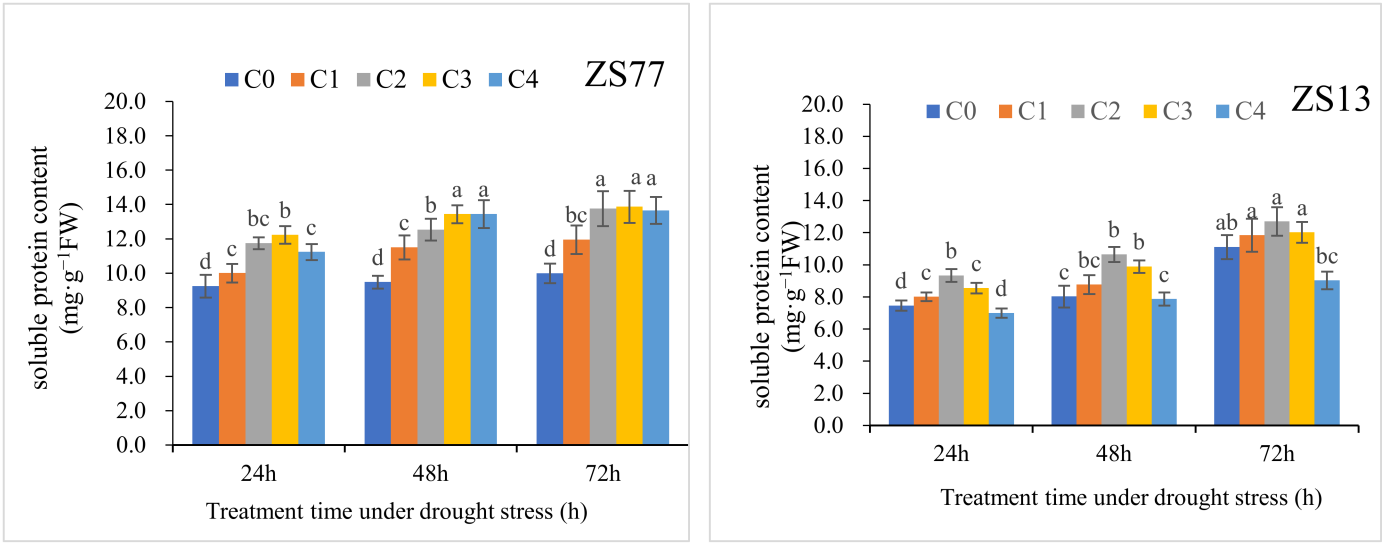

(**c**) (**d**)

Figure 7. Effect of different concentrations of exogenous SA solution 0 (C0), 1.00 (C1), 2.00 (C2), 4.00 (C3), and 8.00 mg·L^{-1} (C4) on soluble sugar (**a**,**b**) and protein (**c**,**d**) in sweet-potato leaves under drought stress. Bars with different letters indicate significant differences among treatments at 0.05 level (Duncan).

2.4. SA Effects on Abscisic Acid (ABA) Content and NCED3-like Gene Express

The ABA content of a plant is closely correlated with cell metabolism and growth. Under drought-stress conditions, at 24 h the ABA contents in C0-treated leaves of 'ZS77' plant increased by 146.45% compared with CK leaves (Figure 8a). For 'ZS77', the ABA contents in leaves treated with C1–4 decreased by 26.18%, 40.98%, 34.74% and 26.99%, respectively, compared with C0. The C2 and C3 treatment effects were good. Similar changes occurred in 'ZS13'.

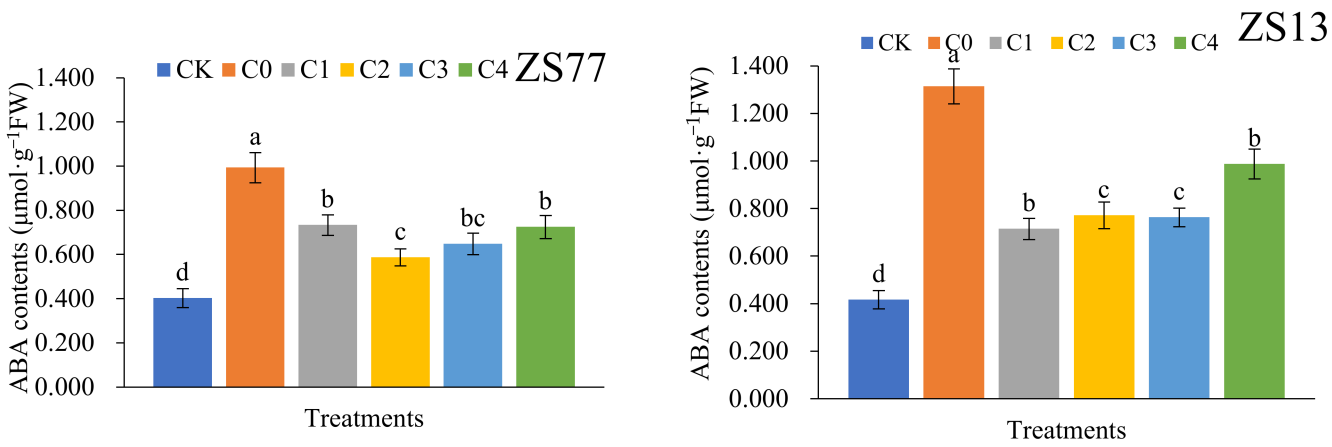

(**a**) (**b**)

Figure 8. Effect of different concentrations of exogenous SA solution 0 (C0), 1.00 (C1), 2.00 (C2), 4.00 (C3), and 8.00 mg·L^{-1} (C4) on ABA content of sweet-potato leaves under drought stress. CK is the treatment with normal irrigation. Bars with different letters indicate significant differences among treatments at 0.05 level (Duncan).

As shown in Figure 9, the expression status of the *NCED3-like* gene in sweet potato showed an induced trend under drought-stress conditions, with the expression level increasing accordingly. However, the expression levels of the *NCED3-like* gene in sweet

potato after exogenous SA treatments were lower than those of the C0, but still greater than those of the CK (normal water supply). The results of the two varieties were consistent.

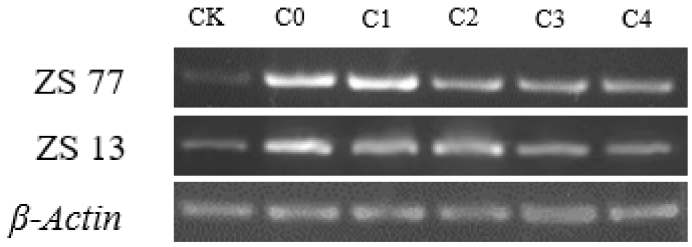

Figure 9. Semi-quantitative RT-PCR of *NCED3-like* gene. RNA was isolated from the leaves of normal irrigated (CK) and drought treated sweet potato plants foliar spraying 0 (C0), 1.00 (C1), 2.00 (C2), 4.00 (C3), and 8.00 mg·L^{-1} (C4) SA solution after 24 h treatment. Actin was used as an internal control. The experiment was repeated twice with the similar results.

2.5. SA Improves Growth Traits under Drought-Stress Conditions

Without drought stress, the two sweet potato varieties 'ZS77'and 'ZS13' grow rapidly, with 2–3 cm of vine elongation per day. The vine and leaf growth were greatly reduced, as well as the dry matter accumulation, under drought conditions (Table S1). The foliar spraying of SA mitigated the impacts of drought stress on sweet potato growth (Table 4). For 'ZS77', the vine length significantly increased 20.32%, 19.10% and 11.01% after C2, C3 and C4 treatments, respectively, compared with the C0 treatment. Similar results were obtained in 'ZS13'.

Table 4. Effects of exogenous SA on growth traits of sweet potato under drought stress.

	Vine Length (cm)		Dry Matter Weight (g)		Leaf Area (cm^2)	
	ZS77	**ZS13**	**ZS77**	**ZS13**	**ZS77**	**ZS13**
C0	14.81 ± 1.67 b	15.46 ± 1.42 b	15.35 ± 1.78 b	16.43 ± 1.03 b	19.58 ± 1.35 c	20.71 ± 1.22 c
C1	15.62 ± 0.64 b	16.74 ± 0.67 ab	16.94 ± 2.37 ab	17.85 ± 2.78 ab	20.66 ± 1.67 cb	21.95 ± 1.54 bc
C2	17.82 ± 0.55 a	18.08 ± 0.85 a	19.36 ± 1.08 a	19.94 ± 1.47 a	22.82 ± 0.89 ba	24.44 ± 1.04 ab
C3	17.64 ± 0.61 a	18.18 ± 0.65 a	18.93 ± 0.78 a	19.81 ± 0.95 a	23.91 ± 0.89 a	25.35 ± 1.08 a
C4	16.44 ± 0.59 ab	16.76 ± 0.58 ab	17.75 ± 1.57 ab	17.6 ± 1.63 ab	21.41 ± 2.41 abc	22.45 ± 2.47 abc

The dry matter weight and leaf area were given for per plant, and the different lowercase letters show significant differences ($p < 0.05$).

The dry matter weight (DW) is closely correlated with vine and root growth. For 'ZS13', the DWs of plants receiving C1–4 treatments increased 8.64%, 21.36%, 20.57% and 7.12% compared with C0. The C2 and C3 treatments reached the significance level. The variation in characteristics and difference in the significance of the 'ZS77' DW were consistent with those of 'ZS13'. The leaf area per plant (LA) showed noticeable increases in the two varieties. For 'ZS77' and 'ZS13' the LA values of the C2 treatment significantly increased 16.44% and 18.01%, whereas those of the C3 treatment increased 22.11% and 22.40% compared with C0. The LA values of treatments C1 and C4 increased but did not reach the significance level in either variety.

3. Discussion

The seedling stage of sweet potato is the key period for root and vine growth and is followed by the early part of the rooting and branching stage. Zhang [17] reported that drought during the rooting and branching stage has the greatest negative impact on the final sweet potato yield. Field experiments conducted by Li [18] also showed that drought in the early sweet potato growth periods have the greatest negative impacts on root development. Until now, most experiments investigating SA applications alleviating

drought, high or low temperature and other stresses have been conducted under non-field conditions. Fan [19] reported that under field experimental conditions, spraying 0.1 mmol·L^{-1} SA at the flowering stage mediates the high temperature stress of wheat and that it is more effective than spraying at other growth stages. In this study, the application of a proper SA concentration to drought plants improved all the studied growth traits (Table 4), with the most efficacious treatments, C2 and C3, having 2–4 mg·L^{-1} SA. The improvement was attributed to the SA-mediated ameliorating impact under drought-stress conditions that results from complex biochemical and physiological machinery. Similarly, SA-mediated improvements in growth traits under drought-stress conditions have been reported in wheat crops [20,21]. After reviewing the literature, this experiment sprayed SA for 3 days (twice daily) consecutively. However, this application rate would increase the cost of farming. Therefore, it is necessary to explore effective ways to reduce the spraying times to alleviate drought stress during production.

The application of the appropriate dose of an SA solution can promote the growth of sweet potato seedlings under drought conditions. To reduce water transpiration, sweet potato, as with other plants, will close or partially close the stomata under drought conditions, and this leads to reductions in the Ci and Pn. In this study, the Gs and Tr values of leaves from two sweet potato varieties decreased along with drought time, where the Ci increased, indicating that under drought conditions, the inhibition of photosynthesis in sweet potato was not primarily due to stomatal-related factors [2]. However, after the C2 and C3 treatments, the Gs, Tr and Pn values of 'ZS 77' and 'ZS13' leaves increased compared with the C0 (0.0 mg·L^{-1}). An increase in Gs is conducive to the photosynthetic system obtaining more CO_2 and increasing the Pn. Additionally, SA modulates the decline in Pn, which may be related to its protection of the D1 protein in chloroplast PS II. Huang [8] found that SA protects the D1 protein in chloroplasts of *Dendrobium officinale* under low temperature-stress conditions. Wang [22] reported that SA maintains a higher level of D1 protein phosphorylation, enhances the light energy capture efficiency of the PS II reaction center under heat and high irradiance stress, and inhibits the decline in the maximum photochemical efficiency (Fv/Fm) of PS II in wheat crops. Additionally, SA may effectively alleviate the stress of active oxygen in plants, stimulate the antioxidant defense system of plants and protect the photosynthetic apparatus from being damaged by excessive active oxygen to ensure photosynthesis progresses.

ROS are collections of several types of active molecules, including superoxide anion (O_2^-), hydroxyl radical (^-OH), hydroperoxyl radical (HO_2^-), an alkoxy radical (RO^-), and non-radicals such as hydrogen peroxide (H_2O_2) and singlet oxygen ($^1O_2$), which are inevitable products of normal plant growth and metabolism [23,24]. When plants are exposed to biotic or abiotic stresses, a growth disorder normally occurs, such as membrane damage, ROS generation and excessive accumulation, which can lead a serious injury. To alleviate or prevent ROS-induced oxidative injury, plants have evolved mechanisms to scavenge these toxic and reactive species through the antioxidation of enzymatic and nonenzymatic systems [25]. Drought leads to excess electrons being captured by plant chloroplasts and in the production of ROS. ROS damages the membrane lipid systems of cells and leads to increased MDA levels [11]. Here, SA applications decreased the MDA content, which suggested that the exogenous SA protected the membrane lipid system. The declines in Chl a and b may be related to ROS over-accumulation. High levels of ROS destroy the chloroplast membrane, resulting in the chlorophyll synthesis of sweet potato being faster than the decomposition under drought conditions [2]. SA is involved in the regulation of plant antioxidant enzyme systems as a signal molecule. Recently, Ma [26] showed that exogenous SA treatments induce the upregulation of *PIP1* expression in *Lycium ruthenicu* leaves under drought conditions, increase the contents of plant plasma membrane intrinsic proteins, enhance the H_2O_2 transport capacities of plasma membranes, and help trigger the activities of SOD, POD and other antioxidant enzymes. Peng [27] reported that exogenous SA applications induce the over-expression of the SA-binding protein 2 gene, which plays active roles in regulating the expression of antioxidant enzyme-related genes

and the activities of antioxidant enzymes in tobacco plants. In this study, foliar spraying of an appropriate SA dose increased the SOD and POD activities, which is consistent with these previous results. However, after SA applications, the CAT activity levels in all treatments decreased. This may be because exogenous SA specifically binds to CAT and inhibits its activity, thereby increasing the H_2O_2 contents of cells. H_2O_2, as the second messenger in cells, can activate the expression of corresponding resistance genes in plants and promote the responses of antioxidant defense systems in cells [28]. In agreement with our results, several other studies have suggested that the SA applications inhibit CAT activity in other plants [29–31], which suggests that the applications do not positively regulate CAT activity.

SA applications appeared to increase the RWC, which is very beneficial for maintaining normal physiological functions of leaves under drought conditions (Figure 6). A similar increase in leaf RWC was observed during drought stress in a wheat crop [32]. SA also increased osmolytes, including soluble sugar and protein, under drought conditions (Figure 7). The low-molecular antioxidants, such as ascorbic acid, glutathione, α-tocopherol, β-carotene, flavonoids and proline, are important soluble protein compounds and play vital roles in maintaining the reducing environment [4,20]. Here, the soluble carbohydrates cooperated with soluble proteins in maintaining cell turgor pressure and helped stabilize cell membranes, providing a stable internal environment for optimum metabolic and physiological activities under drought-stress conditions. Khalvandi et al. [33] found that SA applications on six ecotypes of wheat crops under drought-stress conditions cause marked increases in osmolytes (soluble carbohydrates and protein contents), which supports our results.

When plants are in a drought environment, the ABA contents of roots increase and are transported to the leaves to guide stomatal closure or partial closure. In this study, the ABA contents in leaves decreased after they were sprayed with SA. Furthermore, the expression of ABA synthesis-related *NECD-like3* decreased in leaves. The results suggest that SA regulates the ABA content, perhaps through the expression of *NECD-like3*. Thus, the metabolic pathway of exogenous SA acting on *NECD-like3* expression deserves further study. Zhang [34] reported that SA not only promotes seed dormancy and inhibits the transformation of seed from dormancy to germination, but it also produces a strong germination inhibition effect by increasing the sensitivity of seed to exogenous ABA. Whether SA enhances the sensitivity of sweet potato to endogenous ABA when applied for drought tolerance improvement deserves further study.

In conclusion, foliar spraying of an appropriate SA concentration enhanced the activity levels of SOD and POD and protected the photosynthetic apparatus of leaves. Then, the leaf Pn increased and plant growth indicators were upregulated in sweet potato under drought conditions. The SA downregulated the expression of ABA-related genes, such as *NECD-like3*, in sweet potato leaves and decreased the ABA content in leaves. These functions may be important for the enhancement of drought tolerance in sweet potato plants and; therefore, have practical application potentials.

4. Materials and Methods

4.1. Plant Materials and Growing Conditions

The sweet potato varieties 'Zheshu 77' (ZS77) with chicken claw leaves and 'Zheshu 13' (ZS13) with horseshoe leaves planted in Zhejiang Province were selected as experimental plants. The seedlings were transferred to plastic pots (top and bottom pot diameters of 16 cm and 12 cm, respectively; pot depth of 17 cm) containing 1.0 kg clay loam soil from the Zijingang Campus experimental field at the Agricultural Experiment Station of Zhejiang University (AES-ZJU). The soil pH was 6.7, and it contained 28.48 $g \cdot kg^{-1}$ total soil organic matter, 1.68 $g \cdot kg^{-1}$ total nitrogen, 62.1 $mg \cdot kg^{-1}$ available phosphorus and 52.4 $mg \cdot kg^{-1}$ available potassium. Every pot contained one seedling, which had three grown leaves and was 8 cm high at planting. The seedlings were grown in a greenhouse at the Zijingang Campus of AES-ZJU with a temperature regime of 25/20 °C day/night and natural sunlight

before the drought treatment. The plants were irrigated once every 2 or 3 d to avoid water stress. After a new leaf was fully spread, healthy and uniform seedlings (with 4–4.5 leaves and 12-cm heights) were selected for experiments. The experiments were carried out at the AES-ZJU from April to June 2020. Owing to the COVID-19 pandemic, some laboratory tests were completed in 2021.

4.2. SA Treatment and Drought Stress

The sweet potato seedlings were cultured in three climate chambers (AGCM-113DC01, Hangzhou, China) at 25/20 °C with a 14-h/10-h light/dark regime, with a photosynthetic photon flux density of 360 μmol.$m^{-2}.s^{-1}$ and 80% ± 5% relative humidity for 3 d as a pretreatment. During the pretreatment, the pots were irrigated regularly to maintain the soil water content (SWC) at the field capacity, which is 35.21% (*w*/*w*) and used as the CK status. After the SWC pretreatment, the drought and SA treatment pots were adjusted to 30% of field capacity, at 10.5 ± 0.5% SWC. The detail methods were described as previously reported [2]. After the SWC pretreatment, the plots were maintained at drought and CK states, the seedlings underwent independent foliar spraying with one of four SA concentrations (1.00, 2.00, 4.00 and 8.00 mg·L^{-1}, abbreviated as C1, C2, C3 and C4, respectively). There was also a distilled water control (C0) treatment. Plants in each pot were sprayed with 10 mL of a SA solution twice daily at 8 a.m. and 5 p.m. for 3 consecutive days (six times total). There were 30 trays of plants in every treatment set, with three replications of 10 trays per replication, and the trays were randomly arranged. The third and fourth leaves from the tops of the stems were sampled at 24, 48 and 72 h after treatments. Half of each replication plant set was transported back to the greenhouse and cultured for an additional 7 d at the original SWC of either the treatment or CK. Then, the agronomic traits were investigated. All the green leaves from the sample plants in each treatment were sampled, frozen in liquid nitrogen and stored at −70 °C.

4.3. Determination of the Agronomy Traits

The agronomy traits were analyzed on the end day and at 7 d after treatment. The leaf area was determined using LI-6400 portable photosynthesis equipment (LI-COR, Lincoln, NE, USA). The vine length represents the length from the apical of the shoot to the pot soil surface. Five plants from every replication were taken and dried at 80 °C to determine the dry weights (DWs), and the averages of each agronomic trait used data from five plants.

4.4. Determination of Chlorophyll Content and Photosynthetic Parameters

The chlorophyll content was determined using the method proposed by Lichtenthaler [35] and described previously [4]. The photosynthetic parameters of net photosynthetic rate (Pn), leaf stomatal conductance (Gs), intracellular CO_2 concentration (Ci) and transpiration rate (Tr) were determined in the treated plants using LI-6400 equipment. The air temperature, relative humidity, CO_2 concentration and photosynthetic photon flux density were maintained at 25 °C, 85%, 380 μmol·mol^{-1} and 1000 μmol·m^{-2}·s^{-1}, respectively.

4.5. Determination of H_2O_2 and Malondialdehyde (MDA) Content

The H_2O_2 levels were measured by monitoring the absorbance at 410 nm of the titanium–peroxide complex following the method described by Lin et al. [36] and briefly described in a previous report [8]. The MDA level was determined using the thiobarbituric acid reaction as described by Wu et al. [37].

4.6. Determination of Antioxidant Enzyme Activities

The total SOD activity was determined as described by Prochazkova et al. [38] and as used in our previous studies [4,8]. The methods to determine CAT and POD activity levels have been described previously [2,4].

4.7. Determination of Relative Water Content (RWC) and Soluble Carbohydrate and Protein Contents

Similar or the same leaves after chlorophyll determination were used in the RWC assay. The fresh weights (FWs), FWs at full turgor (TWs) and DWs of sample leaves were measured to determine the RWC [RWC (%) = (FW − DW/TW − DW) × 100%]. The soluble sugar content was measured using the anthrone colorimetry method [39]. The soluble protein content was estimated using the Coomassie brilliant blue staining method [40].

4.8. Determination of the ABA Content and Semi-Quantitative RT-PCR Analysis of NCED3-like Genes

The leaf ABA content was determined as described by Liu et al. [41] and analyzed using a Shanghai Jinkang ELISA kit (Shanghai Jinkang Bioengineering Co., Ltd., Shanghai, China) in accordance with the manufacturer's instructions. The absorbance was recorded at 450 nm.

Total RNA extraction from treated and control plant leaves and cDNA preparation were performed as described by Lin et al. [42]. The RNA extractions were carried out using a TRIzol reagent kit (Invitrogen, Carlsbad, CA, USA) in accordance with the protocol provided by the manufacturer. The ReverTra Ace qPCR RT Kit (Toyobo, Osaka, Japan) was used for cDNA synthesis following the manufacturer's protocol. Independent PCR reactions with equal amounts of cDNA were performed using *NCED3-like* and *β-actin* primers (Table S2). The PCR conditions used were an initial denaturation at 94 °C for 3 min, followed by 35 cycles of denaturation at 94 °C for 15 s, annealing at 54 °C for 15 s and extension at 72° C for 1 min, with a final extension at 72 °C for 10 min. PCR products were resolved on a 1.2% (*w*/*v*) agarose gel for size verification.

4.9. Statistical Analyses

The statistical analysis was performed using a one-way analysis of variance. Comparisons between the treatment means were performed using a least significant difference test at the $p \leq 0.05$ level.

Supplementary Materials: The following supporting information can be downloaded at: https://www.mdpi.com/article/10.3390/ijms232314819/s1.

Author Contributions: C.H. conceived and designed the experiments. J.L., W.H. and N.Q. performed the experiments, while J.L. and C.H. analyzed the data. C.H. and J.L. wrote the manuscript. All authors reviewed the manuscript. All authors have read and agreed to the published version of the manuscript.

Funding: This work was supported by the National Key Research and Development Program of Ministry of Science and Technology of the PRC (2016YFD0300203).

Institutional Review Board Statement: Not applicable.

Informed Consent Statement: Not applicable.

Data Availability Statement: The raw data supporting the conclusions of this article will be made available by the authors without undue reservation.

Conflicts of Interest: The authors declare no conflict of interest.

References

1. Munson, S.M.; Bradford, J.B.; Hultine, K.R. An integrative ecological drought framework to span plant stress to ecosystem transformation. *Ecosystems* **2021**, *24*, 739–754. [CrossRef]
2. Huang, C.P.; Yu, M.Y.; Sun, L.; Wei, L. Physiological responses of sweet potato seedlings under drought-stress conditions with selenium applications. *J. Agric. Crop Res.* **2020**, *8*, 98–112. [CrossRef]
3. Rao, D.E.; Chaitanya, K.V. Photosynthesis and antioxidative defense mechanisms in deciphering drought stress tolerance of crop plants. *Biol. Plant.* **2016**, *60*, 201–218. [CrossRef]
4. Huang, C.P.; Qin, N.N.; Sun, L.; Yu, M.Y.; Hu, W.Z.; Qi, Z.Y. Selenium improves physiological parameters and alleviates oxidative stress in strawberry seedlings under low-temperature stress. *Int. J. Mol. Sci.* **2018**, *19*, 1913. [CrossRef] [PubMed]

5. Huang, C.P.; Huang, W.J.; Liao, J.L. Selenium- and nano-selenium-mediated cold-stress tolerance in crop plants. In *Selenium and Nano-Selenium in Environmental Stress Management and Crop Quality Improvement*; Sustainable Plant Nutrition in a Changing World; Hossain, M.A., Ahammed, G.J., Kolbert, Z., El-Ramady, H., Islam, M.T., Schiavon, M., Eds.; Springer: Cham, Switzerland, 2022; pp. 173–190. [CrossRef]
6. Zhang, M.; Jin, Z.Q.; Zhao, J.; Zhang, G.P.; Wu, F.B. Physiological and biochemical responses to drought stress in cultivated and Tibetan wild barley. *Plant Growth Regul.* **2015**, *75*, 567–574. [CrossRef]
7. Ding, P.T.; Ding, Y.L. Stories of salicylic acid: A plant defense hormone. *Trends Plant Sci.* **2020**, *25*, 549–565. [CrossRef]
8. Huang, C.P.; Wang, D.; Sun, L.; Wei, L. Effects of exogenous salicylic acid on the physiological characteristics of *Dendrobium officinale* under chilling stress. *Plant Growth Regul.* **2016**, *79*, 199–208. [CrossRef]
9. Zhang, Z.Z.; Lan, M.F.; Han, X.Y.; Wu, J.H.; Wang-Pruski, G. Response of ornamental pepper to high-temperature stress and role of exogenous salicylic acid in mitigating high temperature. *J. Plant Growth Regul.* **2020**, *39*, 133–146. [CrossRef]
10. Osama, S.; Sherei, M.E.; Al-Mahdy, D.A.; Bishr, M.; Salama, O. Effect of salicylic acid foliar spraying on growth parameters, γ-pyrones, phenolic content and radical scavenging activity of drought stressed *Ammi visnaga* L. plant. *Ind. Crop Prod.* **2019**, *134*, 1–10. [CrossRef]
11. Guo, J.K.; Zhou, R.; Ren, X.H.; Jia, H.L.; Hua, L.; Xu, H.H.; Lv, X.; Zhao, J.; Wei, T. Effects of salicylic acid, Epi-brassinolide and calcium on stress alleviation and Cd accumulation in tomato plants. *Ecotoxicol. Environ. Saf.* **2018**, *157*, 491–496. [CrossRef]
12. Yotsova, E.K.; Dobrikova, A.G.; Stefanov, M.A.; Kouzmanova, M.; Apostolova, E.L. Improvement of the rice photosynthetic apparatus defence under cadmium stress modulated by salicylic acid supply to roots. *Theor. Exp. Plant Physiol.* **2018**, *30*, 57–70. [CrossRef]
13. Tahjib-Ul-Arif, M.; Siddiqui, M.N.; Sohag, A.A.M.; Sakil, M.A.; Rahman, M.M.; Polash, M.A.S.; Mostofa, M.G.; Tran, L.S.P. Salicylic acid-mediated enhancement of photosynthesis attributes and antioxidant capacity contributes to yield improvement of maize plants under salt stress. *J. Plant Growth Regul.* **2018**, *37*, 1318–1330. [CrossRef]
14. Liu, T.T.; Li, T.T.; Zhang, L.Y.; Li, H.L.; Liu, S.K.; Yang, S.; An, Q.S.; Pan, C.P.; Zou, N. Exogenous salicylic acid alleviates the accumulation of pesticides and mitigates pesticide-induced oxidative stress in cucumber plants (*Cucumis sativus* L.). *Ecotoxicol. Environ. Saf.* **2021**, *208*, 111654. [CrossRef]
15. Wang, X.; Li, Q.; Cao, Q.H.; Ma, D.F. Current status and future prospective of sweet potato production and seed industry in China. *Sci. Agric. Sin.* **2021**, *54*, 483–492. (In Chinese) [CrossRef]
16. Lu, J.Z.; Yi, Z.Y.; Xu, X.G.; Qing, J.J.; Wang, X. Evaluation of international competitiveness of China sweet potato industry. *J. Jiangsu Norm. Uni. Nat. Sci. Ed.* **2021**, *39*, 35–39. (In Chinese)
17. Zhang, H.Y.; Duan, W.X.; Xie, B.T.; Dong, S.X.; Wang, B.Q.; Shi, C.Y.; Zhang, L.M. Effects of drought stress at different growth stages on endogenous hormones and its relationship with storage root yield in sweet potato. *Acta Agron. Sin.* **2018**, *44*, 126–136. [CrossRef]
18. Li, C.Z.; Li, H.; Liu, Q.; Shi, Y.X. Comparison of root development and fluorescent physiological characteristics of sweet potato exposure to drought stress in different growth stages. *J. Plant Nutr. Fertil.* **2016**, *22*, 511–517. (In Chinese) [CrossRef]
19. Fan, Y.H.; Li, Y.X.; Ma, L.L.; Lyu, Z.Y.; Wu, Q.Q.; Zhang, W.J.; Ma, S.Y.; Huang, Z.L. Effects of exogenous salicylic acid on antioxidant physiological characteristics of wheat flag leaves under high temperature stress at grain filling stage. *Acta Agric. Nucl. Sin.* **2022**, *36*, 1878–1886. (In Chinese) [CrossRef]
20. Dawood, M.F.A.; Zaid, A.; Latef, A.A.H.A. Salicylic acid spraying-induced resilience strategies against the damaging impacts of drought and/or salinity stress in two varieties of *Vicia faba* L. seedlings. *J. Plant Growth Regul.* **2022**, *41*, 1919–1942. [CrossRef]
21. Kareem, F.; Rihan, H.; Fuller, M.P. The Effect of exogenous applications of salicylic acid on drought tolerance and up-regulation of the drought response regulon of Iraqi wheat. *J. Crop Sci. Biotech.* **2019**, *22*, 37–45. [CrossRef]
22. Wang, H.L. Protective Effect of SA on Photosynthetic Apparatus of Wheat Leaves under Heat and High Irradiance Stress. Master's Thesis, Henan Agricultural University, Zhengzhou, China, 2011. (In Chinese)
23. Rai, K.K. Revisiting the critical role of ROS and RNS in plant defense. *J. Plant Growth Regul.* **2022**. [CrossRef]
24. Chen, Q.H.; Yang, G.W. Signal function studies of ROS, especially RBOH-dependent ROS, in plant growth, development and environmental stress. *J. Plant Growth Regul.* **2020**, *39*, 157–171. [CrossRef]
25. Yaqoob, U.; Jan, N.; Raman, P.V.; Siddique, K.H.M.; John, R. Crosstalk between brassinosteroid signaling, ROS signaling and phenylpropanoid pathway during abiotic stress in plants: Does it exist? *Plant Stress* **2022**, *4*, 100075. [CrossRef]
26. Ma, Y.H.; Li, J.; Ke, J. Cloning and identification of *LrPIP1* gene of *Lycium ruthenicum* and effect of exogenous SA on its expression under drought stress. *Acta Agric. Boreali-Occident. Sin.* **2022**, *31*, 310–319. (In Chinese) [CrossRef]
27. Peng, D.L.; Zhang, Y.; Li, Q.; Song, Y.; Li, X. Exogenous application and endogenous elevation of salicylic acid levels by overexpressing a salicylic acid-binding protein 2 gene enhance nZnO tolerance of tobacco plants. *Plant Soil* **2020**, *450*, 443–461. [CrossRef]
28. Shu, P.; Zhang, S.J.; Li, Y.J.; Wang, X.Y.; Yao, L.; Sheng, J.P.; Shen, L. Over-expression of *SlWRKY46* in tomato plants increases susceptibility to *Botrytis cinerea* by modulating ROS homeostasis and SA and JA signaling pathways. *Plant Physiol. Biochem.* **2021**, *166*, 1–9. [CrossRef]
29. Torun, H. Time-course analysis of salicylic acid effects on ROS regulation and antioxidant defense in roots of hulled and hulless barley under combined stress of drought, heat and salinity. *Physiol. Plant* **2019**, *165*, 169–182. [CrossRef]

30. Haghighi, S.R.; Hosseininaveh, V.; Maali-Amiri, R.; Talebi, K.; Irani, S. Improving the drought tolerance in pistachio (*Pistacia vera*) seedlings by foliar application of salicylic acid. *Gesunde Pflanz.* **2021**, *73*, 495–507. [CrossRef]
31. Mehrasa, H.; Farnia, A.; Kenarsari, M.J.; Nakhjavan, S. Endophytic bacteria and SA application improve growth, biochemical properties, and nutrient uptake in white beans under drought stress. *J. Soil Sci. Plant Nutr.* **2022**, *22*, 3268–3279. [CrossRef]
32. Munsif, F.; Shah, T.; Arif, M.; Jehangir, M.; Afridi, M.Z.; Ahmad, I.; Jan, B.L.; Alansi, S. Combined effect of salicylic acid and potassium mitigates drought stress through the modulation of physio-biochemical attributes and key antioxidants in wheat. *Saudi J. Biol. Sci.* **2022**, *29*, 103294. [CrossRef]
33. Khalvandi, M.; Siosemardeh, A.; Roohi, E.; Keramati, S. Salicylic acid alleviated the effect of drought stress on photosynthetic characteristics and leaf protein pattern in winter wheat. *Heliyon* **2021**, *7*, e05908. [CrossRef]
34. Zhang, X.; Zhao, C.Q.; Huang, J.; Xu, D.A.; Zhang, C.H.; Chen, J. Effect of exogenous abscisic acid and salicylic acid on germination and physiological characteristics of wheat seed. *Chin. J. Appl. Environ. Biol.* **2014**, *20*, 139–143. (In Chinese) [CrossRef]
35. Lichtenthaler, H.K. Chlorophylls and carotenoids: Pigments of photosynthetic biomembranes. *Methods Enzymol.* **1987**, *148*, 350–382. [CrossRef]
36. Lin, Z.F.; Li, S.S.; Lin, G.Z.; Guo, J.Y. The accumulation of hydrogen peroxide in senescing leaves and chloroplasts in relation to lipid peroxidation. *Acta Photophysiol. Sin.* **1988**, *14*, 16–22. (In Chinese)
37. Wu, F.B.; Zhang, G.P.; Dominy, P. Four barley genotypes respond differently to cadmium: Lipid peroxidation and activities of antioxidant capacity. *Environ. Exp. Bot.* **2003**, *50*, 67–78. [CrossRef]
38. Prochazkova, D.; Sairam, R.K.; Srivastava, G.C.; Singh, D.V. Oxidative stress and antioxidant activity as the basis of senescence in maize leaves. *Plant Sci.* **2001**, *161*, 765–771. [CrossRef]
39. Yemm, E.W.; Willis, A.J. The estimation of carbohydrates in plant extracts by anthrone. *Biochem. J.* **1954**, *57*, 508–514. [CrossRef]
40. Bradford, M.M. A rapid and sensitive method for the quantitation of microgram quantities of protein utilizing the principle of protein-dye binding. *Anal. Biochem.* **1976**, *72*, 248–254. [CrossRef]
41. Liu, S.; Dong, Y.; Kong, X.J. Effects of foliar application of nitric oxide and salicylic acid on salt-induced changes in photosynthesis and antioxidative metabolism of cotton seedlings. *Plant Growth Regul.* **2014**, *73*, 67–78. [CrossRef]
42. Lin, A.; Wang, Y.; Tang, J.; Xue, P.; Li, C.; Liu, L.; Hu, B.; Loake, Y.G.; Chu, C.C. Nitric oxide and protein S-nitrosylation are integral to hydrogen peroxide-induced leaf cell death in rice. *Plant Physiol.* **2012**, *158*, 451–464. [CrossRef]

ARTICLES FOR FACULTY MEMBERS

INVESTIGATING THE ROLE OF GIBBERELLIC ACID (GA) AND ABSCISIC ACID (ABA) CROSS-TALK IN ENHANCING TUBEROUS ROOT DEVELOPMENT IN SWEET POTATOES

The IbPYL8–IbbHLH66–IbbHLH118 complex mediates the abscisic acid-dependent drought response in sweet potato / Xue, L., Wei, Z., Zhai, H., Xing, S., Wang, Y., He, S., Gao, S., Zhao, N., Zhang, H., & Liu, Q.

New Phytologist
Volume 236 Issue 6 (2022) Pages 2151–2171
https://doi.org/10.1111/nph.18502
(Database: Wiley Online Library)

New Phytologist

Research

The IbPYL8–IbbHLH66–IbbHLH118 complex mediates the abscisic acid-dependent drought response in sweet potato

Luyao Xue*, Zihao Wei*, Hong Zhai, Shihan Xing, Yuxin Wang, Shaozhen He, Shaopei Gao, Ning Zhao, Huan Zhang and Qingchang Liu

Key Laboratory of Sweet Potato Biology and Biotechnology, Ministry of Agriculture and Rural Affairs/Beijing Key Laboratory of Crop Genetic Improvement/Laboratory of Crop Heterosis & Utilization and Joint Laboratory for International Cooperation in Crop Molecular Breeding, Ministry of Education, College of Agronomy & Biotechnology, China Agricultural University, Beijing 100193, China

Authors for correspondence:
Qingchang Liu
Email: liuqc@cau.edu.cn

Huan Zhang
Email: zhanghuan1111@cau.edu.cn

Received: *1 May 2022*
Accepted: *6 September 2022*

New Phytologist (2022) **236:** 2151–2171
doi: 10.1111/nph.18502

Key words: ABA, drought, *IbABF2*, *IbABI5*, *IbbHLH118*, *IbbHLH66*, *IbPYL8*, sweet potato.

Summary

- Drought limits crop development and yields. bHLH (basic helix–loop–helix) transcription factors play critical roles in regulating the drought response in many plants, but their roles in this process in sweet potato are unknown.
- Here, we report that two bHLH proteins, IbbHLH118 and IbbHLH66, play opposite roles in the ABA-mediated drought response in sweet potato. ABA treatment repressed *IbbHLH118* expression but induced *IbbHLH66* expression in the drought-tolerant sweet potato line Xushu55-2. Overexpressing *IbbHLH118* reduced drought tolerance, whereas overexpressing *IbbHLH66* enhanced drought tolerance, in sweet potato.
- IbbHLH118 directly binds to the E-boxes in the promoters of *ABA-insensitive 5* (*IbABI5*), *ABA-responsive element binding factor 2* (*IbABF2*) and *tonoplast intrinsic protein 1* (*IbTIP1*) to suppress their transcription. IbbHLH118 forms homodimers with itself or heterodimers with IbbHLH66. Both of the IbbHLHs interact with the ABA receptor IbPYL8. ABA accumulates under drought stress, promoting the formation of the IbPYL8–IbbHLH66–IbbHLH118 complex. This complex interferes with IbbHLH118's repression of ABA-responsive genes, thereby activating ABA responses and enhancing drought tolerance.
- These findings shed light on the role of the IbPYL8–IbbHLH66–IbbHLH118 complex in the ABA-dependent drought response of sweet potato and identify candidate genes for developing elite crop varieties with enhanced drought tolerance.

Introduction

Sweet potato (*Ipomoea batatas*) is an economically important root and tuber crop that is widely used as an industrial and bioenergy resource worldwide. This crop is planted mainly on marginal lands (Jata *et al.*, 2011). Extreme or prolonged drought conditions lead to significant reductions in sweet potato yield, prompting the need to improve the drought tolerance of this crop (Motsa *et al.*, 2015). Genetic engineering is an effective approach for improving drought tolerance in sweet potato (Zhai *et al.*, 2016; Kang *et al.*, 2018; Mbinda *et al.*, 2018; Zhang *et al.*, 2019, 2021). However, the transcriptional regulatory mechanisms underlying sweet potato's response to drought stress remain largely unknown.

Abscisic acid is a crucial phytohormone involved in plant responses to drought stress (Fujita *et al.*, 2006). This phytohormone plays essential roles in integrating a wide range of stress signals and regulating multiple downstream stress responses (Assmann & Jegla, 2016). ABA biosynthesis and signaling have been well-studied in plants. Key enzymes involved in ABA biosynthesis include zeaxanthin epoxidase (ZEP), 9-*cis*-epoxycarotenoid dioxygenase (NCED) and aldehyde oxidase (AAO) (Xiong & Zhu, 2003). In the ABA signaling pathway, ABA binds to its receptor Pyrabactin resistance 1/PYR-like (PYR/PYL), forming the ABA–PYR/PYL complex. This complex interacts with ABA-insensitive (ABI)-clade protein phosphatase 2Cs (PP2Cs) and represses their phosphatase activity, consequently releasing activated Snf1-related Kinase 2s (SnRK2s) to phosphorylate downstream ABA-bound transcription factors (ABFs) to promote ABA responses (Tuteja, 2007; Sun *et al.*, 2011; Danquah *et al.*, 2014).

The basic helix–loop–helix (bHLH) superfamily, the second largest transcription factor (TF) family, is widely present in eukaryotes (Pires & Dolan, 2010). bHLH TFs are classified into six subgroups, A, B, C, D, E and F, based on their phylogenetic relationships and DNA binding functions; most plant bHLH proteins belong to subgroups A and B. Subgroup A members

*These authors contributed equally to this work.

specifically bind to the E-box core sequence in the promoters of their target genes, but subgroup B members preferentially bind to the G-box sequence (Atchley & Fitch, 1997; C. Li *et al.*, 2021; J. Li *et al.*, 2021; Q. Li *et al.*, 2021). bHLH proteins usually consist of *c.* 60 amino acids with two functionally distinct regions: the basic region, which contains 13–17 primarily basic amino acids for DNA binding; and the HLH region, which enables the formation of homodimers or heterodimers with one or several different partners (Tian *et al.*, 2019). Therefore, bHLH proteins usually function by DNA binding and dimerization (Martínez-García *et al.*, 2000; Hao *et al.*, 2021).

The bHLH TFs are important regulators of plant growth and development, including seed germination (Penfield *et al.*, 2005; Oh *et al.*, 2006; Groszmann *et al.*, 2010), flowering (Ito *et al.*, 2012; Kumar *et al.*, 2012; Sharma *et al.*, 2016; Wang *et al.*, 2017), cell fate determination (Menand *et al.*, 2007; Yi *et al.*, 2010; Chen *et al.*, 2011; Qi *et al.*, 2015), anthocyanin biosynthesis (Zhao *et al.*, 2019; Liu *et al.*, 2021), environmental responses (Yuan *et al.*, 2008; Balazadeh *et al.*, 2010; Guan *et al.*, 2013; Tanabe *et al.*, 2019), and signaling pathways of phytohormones such as auxin (IAA), JA and ABA (Varaud *et al.*, 2011; Schweizer *et al.*, 2013; C. Li *et al.*, 2019; L. Li *et al.*, 2019; Z. Li *et al.*, 2019). Although several bHLH proteins, such as AtbHLH68, AtbHLH112, AtbHLH122 and ZmPTF1, have been reported to mediate abiotic stress responses by regulating the ABA signaling pathway in plants such as Arabidopsis, maize and peanut (Liu *et al.*, 2014, 2015; Le *et al.*, 2017; C. Li *et al.*, 2019, 2021; L. Li *et al.*, 2019; Z. Li *et al.*, 2019; J. Li *et al.*, 2021; Q. Li *et al.*, 2021), the biological functions and regulatory mechanisms of bHLH proteins in the drought response of sweet potato remain unclear.

In this study, we demonstrate that two bHLH proteins, IbbHLH118 and IbbHLH66, play opposite roles in the ABA-mediated drought stress responses of sweet potato. ABA promotes the formation of the IbPYL8–IbbHLH66–IbbHLH118 complex, which activates the expression of ABA-responsive genes, thereby enhancing ABA signaling and drought adaptation. These findings provide novel insights into the regulatory mechanisms of bHLH TFs in plants.

Materials and Methods

Plant materials

All of the plant materials are stored in laboratory stock. The drought-tolerant sweet potato (*Ipomoea batatas* (L.) Lam.) line 'Xushu55-2' (Zhu *et al.*, 2019, reported by our laboratory), the drought-sensitive sweet potato variety 'Lizixiang' (Zhang *et al.*, 2017, reported by our laboratory) and the tobacco (*Nicotiana tabacum* L.) cultivar 'Wisconsin38 (W38)' were cultivated in the field, glasshouse, or growth chamber at China Agricultural University, Beijing, China. Xushu55-2 was employed for cloning *IbbHLH118*, *IbbHLH66*, *IbPYL8* and *IbTIP1*. Lizixiang and W38 was used to characterize their functions. *In vitro*-grown transgenic sweet potato Xushu55-2 and Lizixiang plants were cultured on Murashige & Skoog (MS) medium at 27 ± 1°C under a photoperiod consisting of 13 h : 11 h, light : dark (cool-white fluorescent light at 54 μmol m^{-2} s^{-1}).

DNA sequencing and analysis

Genomic DNA (OminiPlant RNA Kit) and total RNA (Fast Plasmid Miniprep Kit) were extracted from fresh leaves of Xushu55-2 plants. The genomic DNA and cDNA sequences were amplified using primers listed in Table S1. The conserved domains were searched using InterPro (http://www.ebi.ac.uk/interpro/). Multiple sequence alignment was performed using Dnaman software (Lynnon-BioSoft, San Ramon, CA, USA). Phylogenetic analysis was conducted using the neighbor-joining method in Mega11.0 with 1000 bootstrap iterations (Tamura *et al.*, 2021). The exon-intron structures of genes were analyzed using the Splign program (https://www.ncbi.nlm.nih.gov/sutils/splign). The *cis* elements in the promoter regions were analyzed using PlantCare (http://bioinformatics.psb.ugent.be/webtools/plantcare/html/).

Expression analysis

The leaves of 4-wk-old *in vitro*-grown Xushu55-2 and Lizixiang plants were sampled at 0, 0.5, 1, 3, 6 and 12 h after treatment with 20% polyethylene glycol (PEG) 6000, 100 μM ABA or 200 mM hydrogen peroxide (H_2O_2) in half-strength Hoagland solution. Total RNA was extracted from leaf, stem and root tissues of 4-wk-old *in vitro*-grown Xushu55-2 plants, and from leaf, stem, petiole, storage root and fibrous root tissues of 2-month-old field-grown Xushu55-2 plants using the TRIzol method (CWBIO). The transcript levels were measured using quantitative reverse-transcription (qRT)-PCR. The sweet potato *ACTIN* (AY905538) gene was used as an internal control (Table S1).

Promoter activity assay

The promoter sequence of *IbbHLH118* of Lizixiang or Xushu55-2 was inserted into the pMDC162 vector. The plasmids were separately transformed into the sweet potato protoplasts, *Nicotiana benthamiana*, and tobacco cv W38 by *Agrobacterium*-mediated transformation according to Horsch *et al.* (1985). Four-wk-old transgenic tobacco plants were cultured separately in half-strength Hoagland solution with PEG6000 (10%) or ABA (100 μM) for 24 and 48 h. β-Glucuronidase (GUS) activity in leaves was measured as described by Jefferson (1987). Three independent biological replicates were performed.

Subcellular localization

The entire *IbbHLH118*, *IbbHLH66* and *IbPYL8* coding regions without the stop codon were cloned into pCAMBIA1300. The constructs and the membrane marker PIP2A-mCherry were transformed into *N. benthamiana* leaf epidermal cells by *Agrobacterium*-mediated infiltration. The fluorescent signals were detected using a confocal laser-scanning microscope (LSM880; Zeiss).

Transcriptional activation assay

The full-length coding sequence of *IbbHLH118* or fragments encoding amino acids (aa) 1–175 and 176–298 and the full-length coding sequence of *IbbHLH66* or fragments encoding aa 1–100, 101–350 and 351–465 were inserted into the pGBKT7 vector (10148; Yeasen, Shanghai, China). These constructs, pGBKT7-53 (positive control) and pGBKT7-Lam (negative control) were transferred into yeast strain AH109 according to the Yeast Protocols Handbook (Clontech). The transformed yeast colonies were cultured on SD/−Trp medium for 2 d and streaked onto SD/−Trp/−His/−Ade medium.

Transgenic plant generation

The *35S:IbbHLH118-GFP*, *35S:IbbHLH66-GFP*, *35S:IbPYL8-GFP* and *35S:IbTIP1-GFP* (pCAMBIA1300) vectors were transfected into *Agrobacterium* strain EHA105 (GFP, green fluorescent protein). In addition, a pair of forward and reverse nonconserved fragments of *IbbHLH118* were inserted into the plant RNA interference (RNAi) vector pCAMBIA1300-35SI-X which was transfected into *Agrobacterium* strain EHA105. Transformation and plant regeneration were performed using embryogenic suspension cultures of the drought-sensitive variety Lizixiang, or transformed into W38 via *A. tumefaciens*-mediated transformation (Liu *et al.*, 2001; Zhang *et al.*, 2020).

pTRV2-*IbbHLH66*, pTRV2-*IbABI5*, pTRV2-*IbABF2*, pTRV2 and pTRV1 were transferred into *Agrobacterium* strain EHA105 for tobacco rattle virus (TRV)-based virus-induced gene silencing (VIGS) in the drought-sensitive sweet potato variety 'Lizixiang'. The VIGS and VIGS wild-type (VWT) plants were generated by *Agrobacterium*-mediated transformation (Yan *et al.*, 2012). The transgenic plants transiently overexpressing *IbbHLH66* or *IbPYL8* in *IbbHLH118*-OE lines were generated by *Agrobacterium*-mediated vacuum infiltration (Bi & Zhang, 2014).

Drought tolerance assays

The conditions for the drought treatments were established based on stress adaptability of transgenic plants. The *IbbHLH118* (4 wk), *IbbHLH66* (4 wk), *IbTIP1* (4 wk), *IbbHLH66*-VIGS (2 wk), *IbABI5*-VIGS (2 wk), *IbABF2*-VIGS (2 wk) and the wild-type (WT) plants were grown on MS medium containing 30% PEG. Three independent biological replicates were taken. *IbPYL8* transgenic tobacco plants were grown on ½MS medium containing 10% PEG for 4 wk. Three independent biological replicates were taken.

Cuttings (*c.* 20 cm) from field-grown transgenic and WT plants were cultured in Hoagland solution containing 15% (*IbbHLH118*-OE lines) or 30% (*IbbHLH66*-OE lines) PEG, transferred to Hoagland solution, and cultured for 2 wk. The *IbbHLH118*-OE, *IbbHLH66* (*IbbHLH118*-OE), *IbPYL8*/*IbbHLH66* (*IbbHLH118*-OE) and WT plants were cultured in Hoagland solution with or without 20% PEG for 6 h. Three independent biological replicates were taken. Furthermore, cuttings were planted in a transplanting box in a glasshouse and grown without watering for 4 wk (*IbbHLH118*-OE lines) or 6 wk (*IbbHLH118*-RNAi and *IbbHLH66*-OE lines). Three independent biological replicates were taken.

Cuttings of *IbbHLH118*-OE and WT plants were planted in a glasshouse and grown without watering for 3 months. For normal conditions, the soil moisture was maintained at *c.* 65–75% for 3 months. Twenty independent biological replicates were taken. At harvest, the aboveground weight (AW) and storage root (belowground) weight (BW) of five consecutive plants from each genotype/treatment were measured.

Stomatal aperture assay

The leaves of field-grown transgenic and WT plants were incubated in stomatal opening solution (50 mM KCl, 10 mM MES-KOH, and 10 mM $CaCl_2$, pH 6.1) for 3 h and transferred to stomatal opening solution containing 20 μM ABA, followed by incubation for 2 h. Eighty stomata were selected randomly and measured using a fluorescence microscope (Revolve; Echo, San Diego, CA, USA).

Measurement of drought tolerance indices

The 3,3′-Diaminobenzidine (DAB) staining and nitro blue tetrazolium (NBT) staining were performed according to Zhang *et al.* (2022). The superoxide dismutase (SOD) and peroxidase (POD) activities, and ABA (Ruixinbio, Quanzhou, China), H_2O_2, proline and malondialdehyde (MDA) contents in the leaves of transgenic and WT plants were measured using assay kits (Comin Biotechnology Co. Ltd, Suzhou, China). The photosynthesis rate, stomatal conductance and transpiration rate were measured according to Zhang *et al.* (2019). For the measurement of the relative electrical conductivity (REC), 10 leaf discs (1-cm diameter) from each line were placed in 10 ml of distilled water, vacuumed for 10 min, and then surged for 1 h to measure the initial electric conductivity (S_1). The materials were boiled for 10 min and then cooled to room temperature to measure the final electric conductivity (S_2). The distilled water was used as a blank control and its electric conductivity (S_0) was measured. REC was calculated as $REC = (S_1 - S_0)/(S_2 - S_0) \times 100$.

Yeast-two-hybrid (Y2H) assay

The full-length *IbbHLH118*, *IbbHLH66* and *IbPYL8* sequences were cloned into pGADT7. The sequences encoding aa 1–175 of *IbbHLH118* and aa 101–350 of *IbbHLH66* were cloned into pGBKT7 (Table S1). These constructs were transferred into yeast strain AH109. Positive clones were selected on SD/−Ade/−His/−Leu/−Trp/+3AT/+X-α-gal medium with or without 100 μM ABA at 30°C according to the Yeast Protocols Handbook (Clontech/TaKaRa, Tokyo, Japan).

Co-immunoprecipitation (CoIP) assay

The HA-IbbHLH118-FLAG, HA-IbPYL8-FLAG, IbbHLH118-GFP and IbbHLH66-GFP vectors were transiently expressed in *N. benthamiana* leaves. Total proteins were extracted from the

leaves using extraction buffer (Zhang *et al.*, 2020). The total proteins were mixed with HA agarose beads (B26201; Bimake, Houston, TX, USA) and incubated at 4°C for 4 h. The agarose was washed at least five times with extraction buffer and boiled in 5× SDS loading buffer for 15 min to separate the proteins from the agarose beads. The proteins were detected using polyclonal anti-HA (1 : 10 000, H3663; Sigma) and anti-GFP antibodies (1 : 10 000, BE2002; EasyBio, Seoul, Korea).

Bimolecular fluorescence complementation (BiFC) assay

The full-length *IbbHLH118*, *IbbHLH66* and *IbPYL8* sequences were cloned into the pSPYNE-35S vector and fused to the N-terminus of yellow fluorescent protein (nYFP), and the full-length *IbbHLH118*, *IbbHLH66* and *IbPYL8* sequences were cloned into pSPYCE-35S and fused to the C-terminus of YFP (cYFP; Walter *et al.*, 2004) (Table S1). These constructs were introduced into *N. benthamiana* leaves by *Agrobacterium*-mediated infiltration. The yellow fluorescence signal was observed using a confocal laser-scanning microscope (LSM880; Zeiss).

Firefly luciferase complementation imaging (LCI) assay

The full-length *IbbHLH118* and *IbbHLH66* sequences were cloned into the C-terminus–encoding regions, and the full-length *IbPYL8* sequences were cloned into N-terminus–encoding regions of the luciferase, respectively (Chen *et al.*, 2008) (Table S1). These constructs were coinfiltrated into *N. benthamiana*, and the infiltrated leaves were analyzed for LUC activity at 48 h after infiltration using chemiluminescence imaging (LB985; Berthold Technologies GmbH, Bad Wildbad, Germany) and enzyme-labeled instrument (Glomax Discover; Promega).

Immunoblot analysis

The HA-IbbHLH118-FLAG, IbbHLH66-Myc and IbPYL8-GFP vectors were transiently expressed in *N. benthamiana* leaves with or without 100 μM ABA treatment. Total proteins were extracted and detected using polyclonal anti-HA (1 : 10 000, H3663; Sigma), anti-Myc (1 : 10 000, M4439; Sigma), and anti-GFP antibodies (1 : 10 000, BE2002; EasyBio), respectively.

Yeast-one-hybrid (Y1H) assay

The coding sequences of *IbbHLH118*, *IbbHLH66* and *IbPYL8* were fused to the activation domain of the pB42AD vector. The *IbNCED3*, *IbNCED5*, *IbABI5*, *IbABF2* and *IbTIP1* promoters were separately inserted into the pLacZi2μ vector to drive LacZ reporter expression. These effector and reporter plasmids were co-transformed into yeast strain EGY48, which were cultured on SD/−Trp/−Ura/+X-gal medium to screen positive clones.

Dual-luciferase assay

The full-length *IbbHLH118*, *IbbHLH66* and *IbPYL8* coding sequences were inserted into pGreenII 62-SK driven by the CaMV 35S promoter. The *IbABI5*, *IbABF2* and *IbTIP1* promoter sequences were cloned into pGreenII 0800-LUC. Sweet potato protoplasts were isolated and used for the dual-luciferase assays as described previously (Zhang *et al.*, 2020). The Firefly LUC and Renilla luciferase (REN) activity levels were measured using the Dual-Luciferase Reporter Assay System (Glomax Discover; Promega). Three independent biological replicates were taken.

Electrophoretic mobility shift assay

Electrophoretic mobility shift assays (EMSAs) were performed according to the method of Zhang *et al.* (2020) with minor modifications. The pCold-SUMO-*IbbHLH118*, pCold-SUMO-*IbbHLH66* and pCold-SUMO-*IbPYL8* constructs were transferred into competent *E. coli* strain Transetta (DE3) cells to produce the 6His-IbbHLH118, 6His-IbbHLH66 and 6His-IbPYL8 proteins. These proteins were treated with SUMO protease to remove the SUMO proteins. Probes labeled with or without biotin at their 5′ ends were used as binding or competitive probes.

Chromatin immunoprecipitation (ChIP) assay

The leaves of OE-X9 and OE-a5 plants were used for the ChIP assays according to Zhang *et al.* (2020). Anti-GFP (1 : 5000, BE2002; EasyBio) antibodies were used to immunoprecipitate the protein–DNA complex, and the precipitated DNA was recovered. An equal amount of chromatin sample without antibody precipitation was used as an input control. ChIP DNA was analyzed by qPCR, and the ChIP values were normalized against the values of the respective input. The primers used for ChIP-qPCR are listed in Table S1. The experiment was independently repeated three times with similar results.

Results

Differential expression of *IbbHLH118* in drought-tolerant and -sensitive germplasms

In order to identify potential regulators of the drought response in sweet potato, we analyzed the expression of bHLH TF family genes using the transcriptomes of several sweet potato varieties under drought stress (Lau *et al.*, 2018; Zhu *et al.*, 2019; Arisha *et al.*, 2020). *IbbHLH118* was differentially expressed in drought-tolerant vs -sensitive germplasms. We performed qRT-PCR to detect the relative transcript levels of *IbbHLH118* in the drought-tolerant sweet potato line Xushu55-2 and drought-sensitive sweet potato variety Lizixiang under various stress conditions. Under PEG, ABA and H_2O_2 treatment, the expression of *IbbHLH118* was suppressed almost 0.54-fold (at 1 h), 0.18-fold (at 1 h) and 0.14-fold (at 6 h) in Xushu55-2, but induced almost 6.75-fold (at 6 h), 3.75-fold (at 1 h) and 2.16-fold (at 6 h) in Lizixiang, respectively (Fig. 1a–c). In addition, *IbbHLH118* was highly expressed in the leaves of 4-wk-old *in vitro*-grown (Fig. S1a) and 2-month-old field-grown Xushu55-2 plants (Fig. S1b).

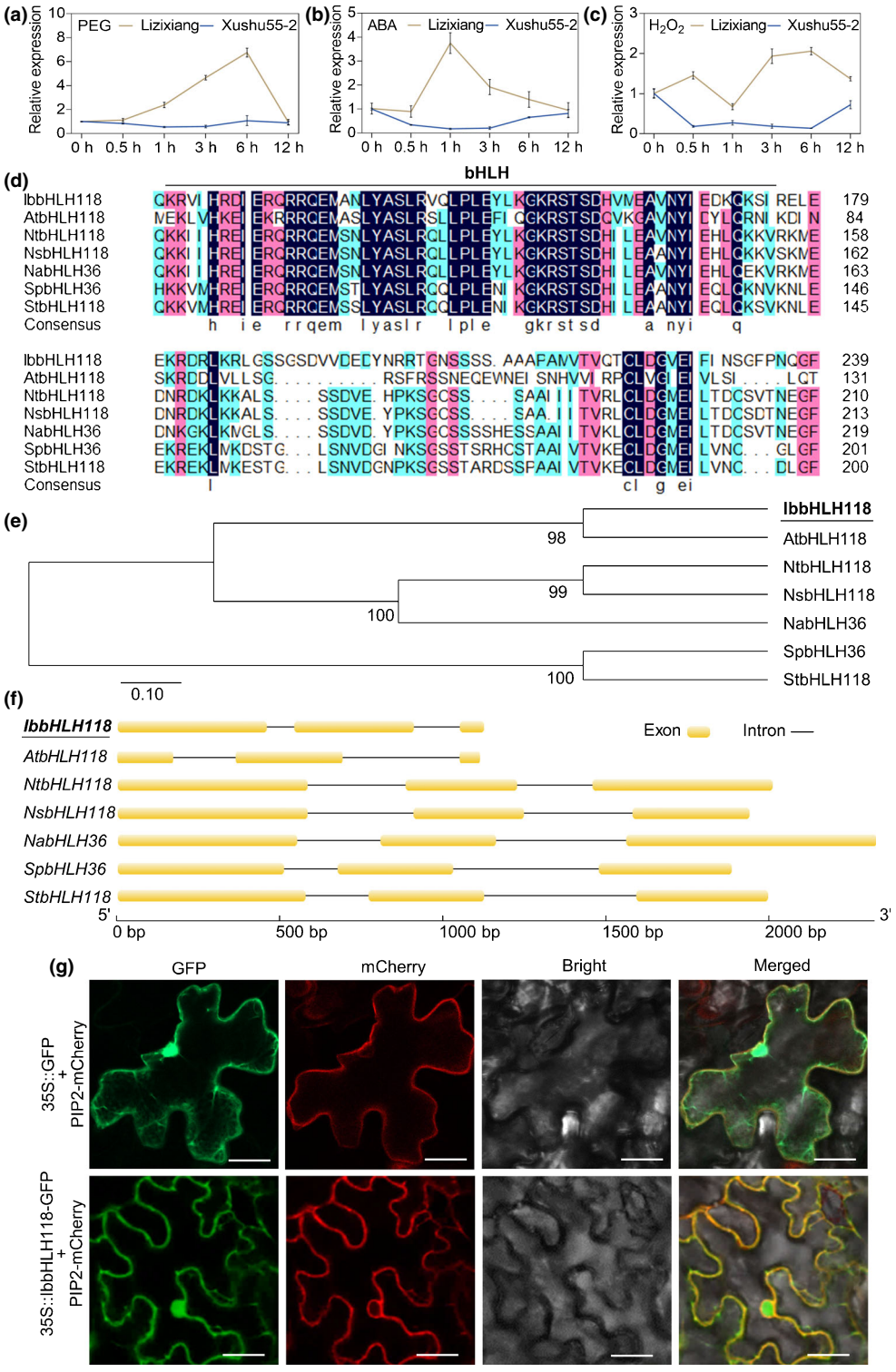

Fig. 1 Expression analysis, sequence analysis and subcellular localization of IbbHLH118. (a–c) Expression analysis of *IbbHLH118* in 4-wk-old *in vitro* grown sweet potato line Xushu55-2 and variety Lizixiang upon exposure to 20% PEG, 100 μM ABA or 200 mM H_2O_2 over a 24-h period. The sweet potato *ACTIN* gene was used as a reference. The expression at 0 h in each treatment was considered as "1". Data are shown as mean ± SD ($n = 3$). (d) Multiple protein sequence alignment of IbbHLH118 and other plant bHLHs, with conserved amino acids shaded in different colors. The entire black line represents the conserved bHLH domain. (e) Phylogenetic analysis of bHLH proteins from *Ipomoea batatas* (IbbHLH118) and other plants using the neighbor-joining method in MEGA 6.0 with 1000 bootstrap iterations. The numbers at the nodes of the tree indicate bootstrap values from 1000 replicates. (f) Comparison of the genomic structures of *IbbHLH118* and other plant *bHLHs*. Boxes indicate exons and lines indicate introns. (g) Subcellular localization of IbbHLH118. *Nicotiana benthamiana* leaf epidermal cells were transformed with the fusion construct (IbbHLH118-GFP) and the membrane marker PIP2-mCherry. Bar, 20 μm. bHLH, basic helix–loop–helix.

The 897-bp open reading frame (ORF) of *IbbHLH118* encodes a protein of 298 aa with a predicted molecular weight of 33.54 kDa. IbbHLH118, belonging to subgroup A of the bHLH TF family, contains one conserved bHLH domain and is most closely related to its homolog in Arabidopsis, AtbHLH118 (Fig. 1d,e). The genomic sequence of *IbbHLH118* contains three exons and two introns, and its length is similar to that of its Arabidopsis homolog but is shorter than the homologous genes in the other plants (Fig. 1f).

The *IbbHLH118* promoter regions in Xushu55-2 and Lizixiang both contain various abiotic stress-responsive elements, such as ACGT-containing ABA response elements (ABREs; Sonal *et al.*, 2014), MYB binding sites (MBSs; Karkute *et al.*, 2018), and long terminal repeats (LTRs; Wu *et al.*, 2019) (Fig. S1c). More abiotic stress-responsive elements, such as TCA- and ABRE-elements are present in the *IbbHLH118* promoter of Lizixiang (Fig. S1c). The *IbbHLH118* promoter of Xushu55-2 contains an $(ACGT)_{N15}(ACGT)$ *cis*-element, which may act as a negative regulator leading to reduced promoter activity (Armstrong *et al.*, 1992; Horn & Boutros, 2010; Mehrotra *et al.*, 2013). Consistent with that, the *GUS* expression and GUS activity driven by the *IbbHLH118* promoter of Xushu55-2 were significantly lower than those driven in Lizixiang (Fig. S1d,e). We further generated transgenic tobacco plants expressing GUS driven by the *IbbHLH118* promoter of Lizixiang. Histochemical staining showed that the leaves exhibited higher GUS activity than stems or roots, and the promoter activity was significantly induced by PEG and ABA treatment in leaves (Fig. S1f,g). Collectively, these results indicate that *IbbHLH118* is involved in drought and ABA responses in sweet potato.

IbbHLH118 is a nuclear and cell membrane-localized transcriptional activator

We examined the subcellular localization of IbbHLH118 by transiently expressing the IbbHLH118-GFP fusion protein in *N. benthamiana* epidermal cells. Analysis of the fluorescent signal indicated that IbbHLH118 was localized to the nucleus and cell membrane (Fig. 1g).

In order to explore whether IbbHLH118 harbors transcriptional activation activity, we separately inserted three fragments encoding the full-length IbbHLH118 protein, aa 1–175 and aa 176–298 of this protein into the GAL4 pGBKT7 vector and separately transformed the fusion constructs into yeast cells. Yeast colonies harboring either BD-IbbHLH118 or BD-176-298 grew well and turned blue on SD medium lacking Trp, His and Ade, and containing X-α-gal (Fig. S1h). These results indicate that IbbHLH118 is a nuclear- and cell membrane-localized transcriptional activator.

Knockdown of *IbbHLH118* enhances drought tolerance in sweet potato

In order to explore how *IbbHLH118* affects the drought response in sweet potato, we generated 15 overexpression (designated as OE-X1 to OE-X15) and five knockdown (designated as Ri-X1 to Ri-X5) lines from cell aggregates of the drought-sensitive sweet potato variety Lizixiang via *A. tumefaciens*-mediated transformation (Fig. S2). After examining the expression levels of *IbbHLH118* in these transgenic lines, we selected three overexpression (OE-X4, 6 and 9) and three knockdown (Ri-X2, 3 and 5) lines for further study.

We planted the transgenic and the WT plants on MS culture medium containing 30% PEG for *in vitro* assays. Under PEG treatment, the *IbbHLH118*-RNAi lines exhibited significantly stronger growth and rooting and higher FW and DW than WT plants, whereas the *IbbHLH118*-OE lines displayed opposite changes (Fig. 2a,b; Table S2).

The transgenic and WT plants then were transferred to soil in the glasshouse or the field. We cultured cuttings of the transgenic and WT plants in a transplanting box and subjected them to drought stress. Under normal conditions, the *IbbHLH118*-OE plants showed shorter stems and roots compared with WT plants, but no obvious morphological differences were observed in *IbbHLH118*-RNAi plants (Fig. 2c,d,f,g; Table S3). Under drought conditions, the *IbbHLH118*-RNAi lines exhibited better growth and rooting and greater FW and DW, whereas the *IbbHLH118*-OE lines became brown and dried earlier than WT plants (Figs 2c–h, S3). These results indicate that knockdown of *IbbHLH118* enhances the drought tolerance of sweet potato.

ABA stimulates stomatal closure to maintain osmotic pressure in plants in response to drought stress (Munemasa *et al.*, 2015). We therefore quantified endogenous ABA levels in the transgenic plants. Under drought stress, the ABA contents were significantly lower in *IbbHLH118*-OE but higher in *IbbHLH118*-RNAi vs WT plants (Fig. 3a). We then examined whether exogenous ABA treatment would affect the stomatal aperture of *IbbHLH118* transgenic plants. The *IbbHLH118*-OE lines exhibited reduced but *IbbHLH118*-RNAi lines exhibited increased ABA-induced stomatal closure compared to WT plants (Fig. 3b,c). These results indicated that knockdown of *IbbHLH118* led to increased ABA accumulation and a sharp response to ABA.

Drought stress causes excessive reactive oxygen species (ROS) generation, resulting in oxidative damage to plants (Sharma *et al.*, 2012; Foyer, 2018). Proline acts as an osmoticum and a ROS scavenger under drought stress (Ghosh *et al.*, 2022). DAB and NBT staining and H_2O_2 measurement revealed that the *IbbHLH118*-RNAi plants accumulated less H_2O_2 and superoxide anion radical (O^{2-}) than the WT (Fig. 3d–h). Moreover, significantly higher POD and SOD activities and proline contents were detected in *IbbHLH118*-RNAi vs WT plants (Fig. 3i–k; Table S4). By contrast, the *IbbHLH118*-OE lines showed the opposite pattern for the respective physiological indices. These results indicate that knockdown of *IbbHLH118* activated the ROS scavenging system of sweet potato.

IbbHLH118 forms homodimers or heterodimers

In order to better understand the regulatory mechanisms of *IbbHLH118*-mediated drought and ABA responses, we used aa 1–175 of IbbHLH118 as a bait to screen a yeast Y2H library constructed using RNA from sweet potato leaves. Two bHLH proteins, IbbHLH118 itself and IbbHLH66, were identified as interacting

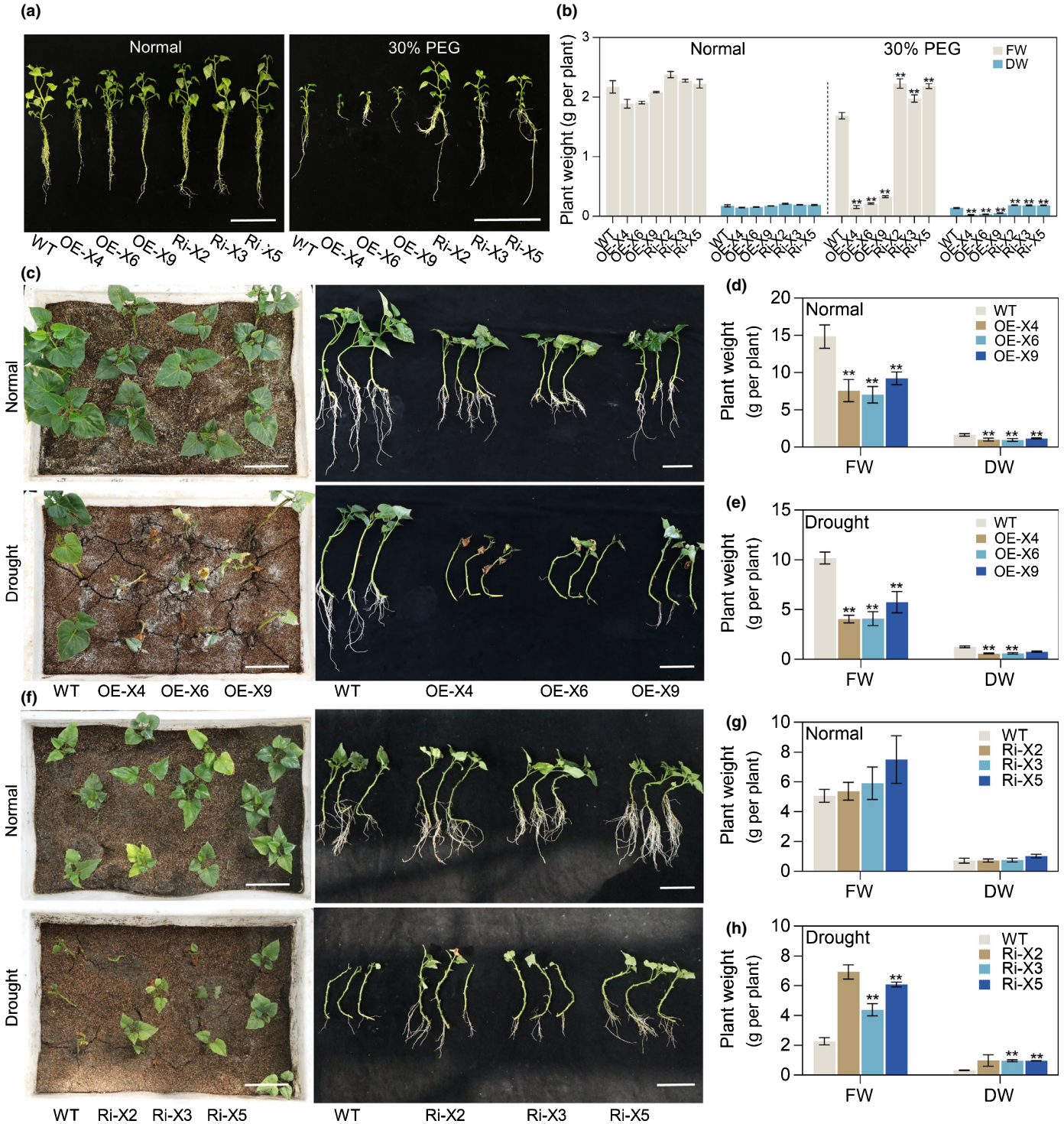

Fig. 2 Knockdown of *IbbHLH118* enhances drought tolerance in sweet potato (*Ipomoea batatas*). (a, b) Responses and plant weight of *IbbHLH118* transgenic and wild-type (WT) sweet potato plants grown for 4 wk on Murashige & Skoog medium under normal conditions or subjected to 30% polyethylene glycol (PEG). Bar, 10 cm. (c–e) Responses and plant weight of 2-month-old field-grown *IbbHLH118*-OE and WT sweet potato plants grown in transplanting boxes under normal conditions or subjected to drought stress for 4 wk. Bar, 10 cm. (f–h) Responses and plant weight of 1-month-old field-grown *IbbHLH118*-RNAi and WT plants grown in a transplanting box under normal or subjected to drought stress for 6 wk. RNAi, RNA interference. Bar, 10 cm. Time-course of the phenotypes of *IbbHLH118* transgenic and WT plants under normal and drought conditions is shown in Fig. S3. All data are presented as means ± SD ($n = 3$). **, $P < 0.01$; Student's *t*-test. bHLH, basic helix–loop–helix.

proteins of IbbHLH118 (Fig. 4a). A transcriptional activation assay showed that IbbHLH66 is a transcriptional activator (Fig. 4b), but it could not form a homodimer with itself (Fig. 4a).

Next, we performed BiFC and CoIP assays to verify the interaction of IbbHLH118 with itself and with IbbHLH66. IbbHLH118 indeed formed homodimers as well as heterodimers with IbbHLH66

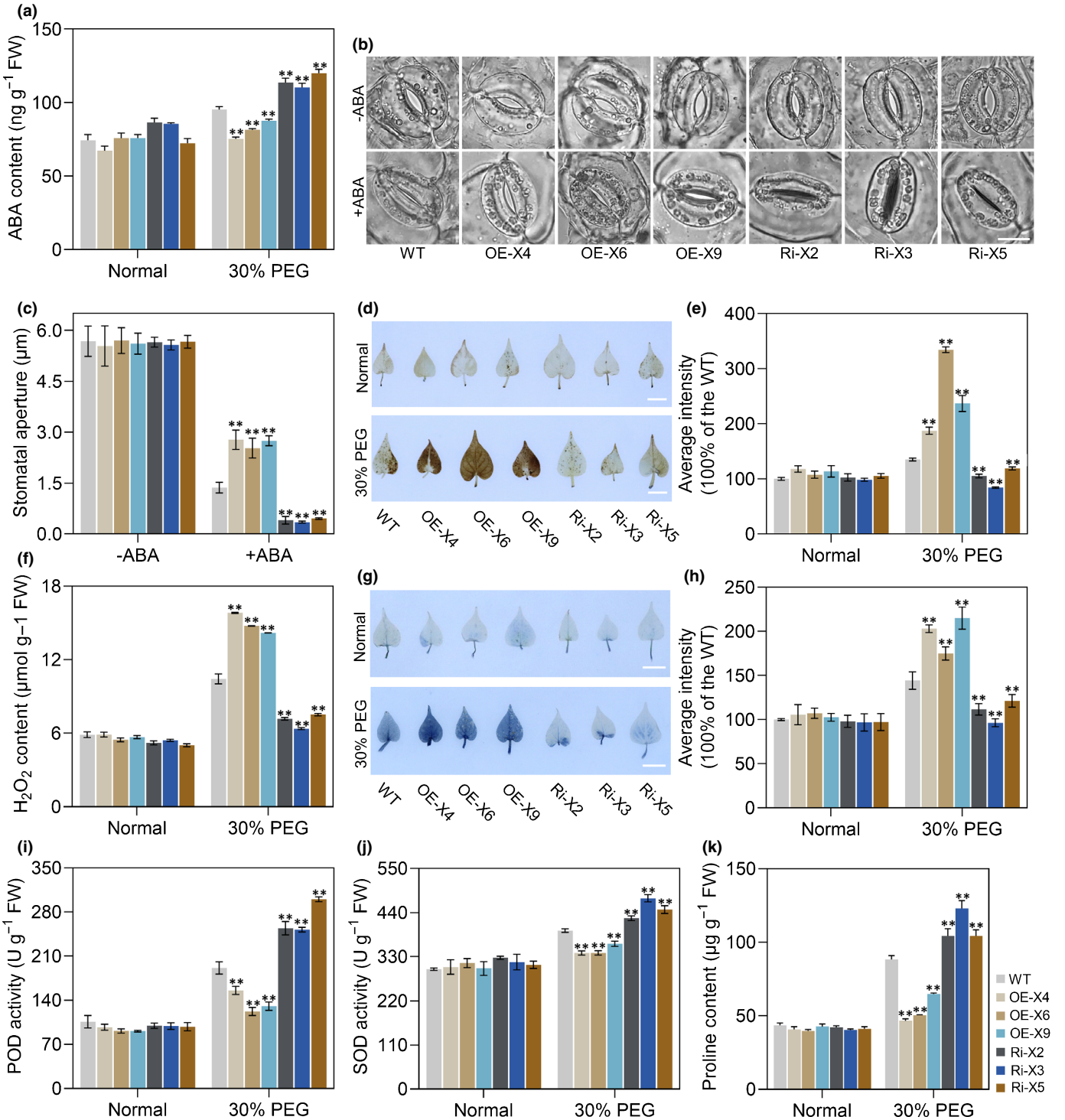

Fig. 3 Knockdown of *IbbHLH118* activates the ABA signaling pathway and reactive oxygen species (ROS) scavenging under drought stress in sweet potato (*Ipomoea batatas*). (a) ABA content in the leaves of 4 wk *IbbHLH118* transgenic and wild-type (WT) plants under normal conditions or subjected to 30% PEG. Data are presented as the means ± SD ($n = 3$). **, $P < 0.01$; Student's *t*-test. (b, c) Stomatal apertures of 2-month-old field-grown *IbbHLH118* transgenic and WT plants under normal conditions or treated with 20 μM ABA for 2 h. Bar, 10 μm. Data are presented as the means ± SD ($n = 80$). **, $P < 0.01$; Student's *t*-test. (d, e) DAB staining (Bar, 1 cm), (f) H_2O_2 content, (g, h) nitroblue tetrazolium (NBT) staining, (i) peroxidase (POD) activity, (j) superoxide dismutase (SOD) activity and (k) proline content in leaves of 4-wk-old *IbbHLH118* transgenic and WT plants under normal conditions or subjected to 30% PEG. Data are presented as the means ± SD ($n = 3$). **, $P < 0.01$; Student's *t*-test. bHLH, basic helix–loop–helix.

in plant cells, and both pairs interacted in the nucleus and cell membranes (Fig. 4c–e). We then investigated the subcellular localization of IbbHLH66 in *N. benthamiana* leaf epidermal cells. IbbHLH66 localized to the nucleus and cell membranes (Fig. 4f), which matches the subcellular localization of IbbHLH118 and the sites of the interaction between IbbHLH118 and IbbHLH66 (Figs 1g, 4c).

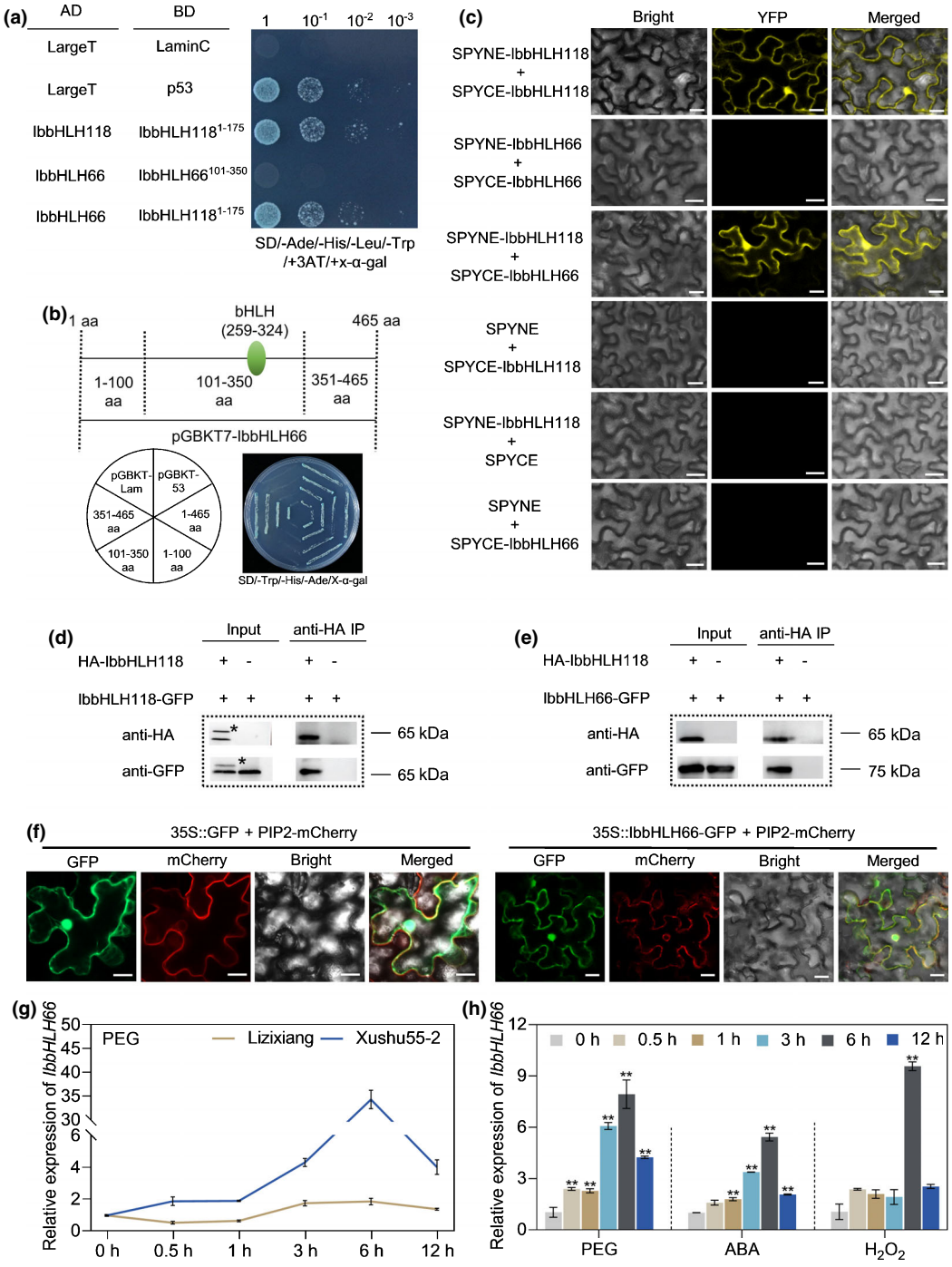

Fig. 4 IbbHLH118 forms homodimers with itself, or forms heterodimers with the drought- and ABA-responsive protein IbbHLH66. (a) Yeast-two-hybrid (Y2H) analysis showing that IbbHLH118 interacts with itself or IbbHLH66. aa, amino acid. IbbHLH118$^{1–175}$ contains IbbHLH118 aa residues 1 to 175, and IbbHLH66$^{101–350}$ contains IbbHLH66 aa residues 101–350, both without transcriptional activation activity. Yeast cells were plated onto SD/−Ade/−His/−Leu/−Trp + 3 mM 3AT medium to screen for possible interactions. (b) Transcriptional activation assay of IbbHLH66. Fusion proteins between the GAL4 DNA binding domain and different portions of IbbHLH66 were produced in yeast strain Y2H Gold. pGBKT7-Lam was used as a negative control, whereas pGBKT7-53 was used as a positive control. The positive transformants were streaked onto sabourauds dextrose (SD) medium –Trp –His –Ade + X-α-gal. (c) BiFC analysis showing that IbbHLH118 interacts with itself or IbbHLH66 in *Nicotiana benthamiana* leaf epidermal cells. Bar, 20 μm. (d, e) Co-immunoprecipitation (Co-IP) analysis showing that IbbHLH118 interacts with itself or IbbHLH66 *in vivo*. *, nonspecific protein band. (f) Subcellular localization of IbbHLH66. *N. benthamiana* leaf epidermal cells were transformed with the fusion construct (IbbHLH66-GFP) and the membrane marker PIP2-mCherry. GFP, green fluorescent protein. Bar, 20 μm. (g) Expression analysis of *IbbHLH66* in 4-wk-old *in vitro*-grown Xushu55-2 and Lizixiang upon exposure to 20% polyethylene glycol (PEG) over a 12-h period. The sweet potato (*Ipomoea batatas*) *ACTIN* gene was used as a reference. The expression at 0 h in each treatment was considered as '1'. Data are shown as mean ± SD ($n = 3$). (h) Expression analysis of *IbbHLH66* in 4-wk-old *in vitro*–grown Xushu55-2 upon exposure to 20% PEG, 100 μM ABA, or 200 mM H_2O_2 over a 12-h period. The expression at 0 h in each treatment was considered as '1'. Data are shown as mean ± SD ($n = 3$). **, $P < 0.01$; Student's *t*-test. bHLH, basic helix–loop–helix.

The 1395-bp ORF of *IbbHLH66* encodes a protein of 465 aa with a predicted molecular weight of 48.5 kDa. IbbHLH66, also belonging to subgroup A of the bHLH TF family, contains one conserved bHLH domain and is most closely related to its Arabidopsis homolog, AtbHLH66 (Fig. S4a,b). *IbbHLH66* contains seven exons and six introns, whereas *AtbHLH66* contains four exons and three introns (Fig. S4c). Under PEG treatment, the expression of *IbbHLH66* was induced to higher levels in Xushu55-2 than in Lizixiang (Fig. 4g). *IbbHLH66* was upregulated 7.93-fold (at 6 h), 5.42-fold (at 6 h) and 9.56-fold (at 6 h) in Xushu55-2 under PEG, ABA and H_2O_2 treatment, respectively (Fig. 4h). These results indicate that IbbHLH118 forms homodimers with itself or forms heterodimers with the drought- and ABA-responsive protein IbbHLH66 in sweet potato.

IbbHLH66 enhances drought tolerance in sweet potato

In order to study the role of *IbbHLH66* in drought tolerance, we overexpressed this gene in sweet potato (Fig. S5) and selected five lines with high *IbbHLH66* transcript levels, as determined by qRT-PCR (OE-a1 to a5; Fig. S5j), for drought tolerance assays. The five overexpression lines and the WT were planted on MS culture medium containing 30% PEG for the *in vitro* assays. Notably, *IbbHLH66*-OE plants exhibited significantly better growth and rooting than WT plants (Fig. 5a,b; Table S2).

Then, three randomly selected overexpression lines (OEa3, a4 and a5) and WT plants were transferred to soil and grown in the glasshouse or field (Fig. S5e,f). The cuttings of these lines and the WT were cultured in half-strength Hoagland solution containing 30% PEG for 3 wk, followed by standard Hoagland solution for 2 wk. Under PEG stress, the transgenic plants formed new leaves and longer roots, whereas the WT plants died (Figs 5c–e, S6; Table S3). Finally, we grew OEa3, a4, a5 and WT plants in a transplanting box and subjected them to drought stress. The *IbbHLH66*-OE plants exhibited better growth and rooting and greater FW and DW than the WT, with higher photosynthetic rates and transpiration rates, whereas the WT plants turned brown and died sooner (Fig. 6a,b).

Under drought stress, the ABA contents were significantly higher in *IbbHLH66*-OE plants than in WT plants (Fig. 6c). Upon exogenous ABA treatment, the *IbbHLH66*-OE plants were more sensitive to ABA-induced changes in stomatal aperture than WT plants (Fig. 6d,e). In addition, DAB and NBT staining and H_2O_2 measurement revealed that the *IbbHLH66*-OE plants accumulated less H_2O_2 and O^{2-} than the WT under drought stress (Fig. 6f–j). Upon exposure to drought stress, the SOD activities and proline contents were significantly higher in *IbbHLH66*-OE vs WT plants, whereas the MDA contents were significantly lower in these lines (Fig. 6k–m; Table S5).

We further examined knockdown phenotypes of *IbbHLH66* by VIGS. qRT-PCR analysis showed that *IbbHLH66* was significantly reduced in *IbbHLH66*-silenced sweet potato leaves (Fig. S7b,e), indicating that *IbbHLH66* was effectively silenced in sweet potato. After treatment with 30% PEG for 14 d, the VWT plants exhibited better growth with a lower browning rate than the *IbbHLH66*-VIGS plants (Fig. S7). These results indicate that overexpressing *IbbHLH66* led to increased, whereas knockdown of *IbbHLH66* resulted in decreased drought tolerance in sweet potato.

ABA promotes IbPYL8–IbbHLH66–IbbHLH118 complex formation

In order to explore the possible interacting partners of IbbHLH66 involved in ABA-mediated drought response in sweet potato, we screened the Y2H library. Because the 1–100 and 351–465 aa residues of IbbHLH66 were required for its transactivation activity in yeast (Fig. 4b), we used 101–350 aa residues of IbbHLH66, which included a bHLH domain, as the bait in Y2H screens. The ABA receptor IbPYL8 was identified as an interacting partner of IbbHLH66 (Figs 7a, S8a). The Y2H assays demonstrated that IbbHLH118 also interacts with IbPYL8 (Figs 7a, S8a). We then performed CoIP and BiFC assays to verify the interaction of IbPYL8 with IbbHLH66 or with IbbHLH118. IbbHLH66 and IbbHLH118 both interacted with IbPYL8 in plant cells, and both pairs interacted in the nucleus and cell membranes (Fig. 7b–d). These three proteins formed an IbPYL8–IbbHLH66–IbbHLH118 ternary complex.

The PYL8 was reported to mediate ABA perception, and in turn ABA specifically stabilizes PYL8 and induces its accumulation in plant (Belda-Palazon *et al.*, 2018; Garcia-Maquilon *et al.*, 2021). Therefore, we examined whether exogenous ABA treatment would affect the interactions of IbPYL8 by Y2H and LCI assays. Notably, ABA treatment enhanced the interactions of IbPYL8 with IbbHLH66 or IbbHLH118 in both yeast and *N. benthamiana* (Figs 7a,e,f, S8a,b). Furthermore, IbbHLH118, IbbHLH66 and IbPYL8 protein levels were determined after transiently expressing for different combinations in *N. benthamiana*. The protein levels of IbbHLH66 and IbPYL8 were induced, but IbbHLH118 was repressed after exogenous treatment with 100 μM of ABA. Being consistent with this trend, inside the IbPYL8–IbbHLH66–IbbHLH118 ternary complex, IbbHLH66 and IbPYL8 protein increased, but IbbHLH118 protein decreased after ABA treatment (Fig. 7g). Collectively, these results indicate that a ternary complex formed by IbbHLH66 and IbbHLH118 with the ABA receptor IbPYL8 functions in the ABA-dependent drought response in sweet potato.

IbPYL8 enhances drought tolerance in transgenic tobacco plants

Further qRT-PCR analysis showed that *IbPYL8* was significantly induced by PEG (3.18-fold at 1 h), ABA (2.46-fold at 6 h) and H_2O_2 (2.12-fold at 3 h) treatment in Xushu55-2 (Fig. S8c). Subcellular localization analysis indicated that IbPYL8-GFP was located in the nucleus and cell membranes (Fig. S8d). To investigate the role *IbPYL8* in drought tolerance, we generated transgenic tobacco (*N. tabacum*) plants overexpressing *IbPYL8* and challenged them with drought stress. *In vitro*-grown *IbPYL8*-OE plants showed better growth than the WT W38 when grown on ½MS medium containing 10% PEG (Fig. S9a).

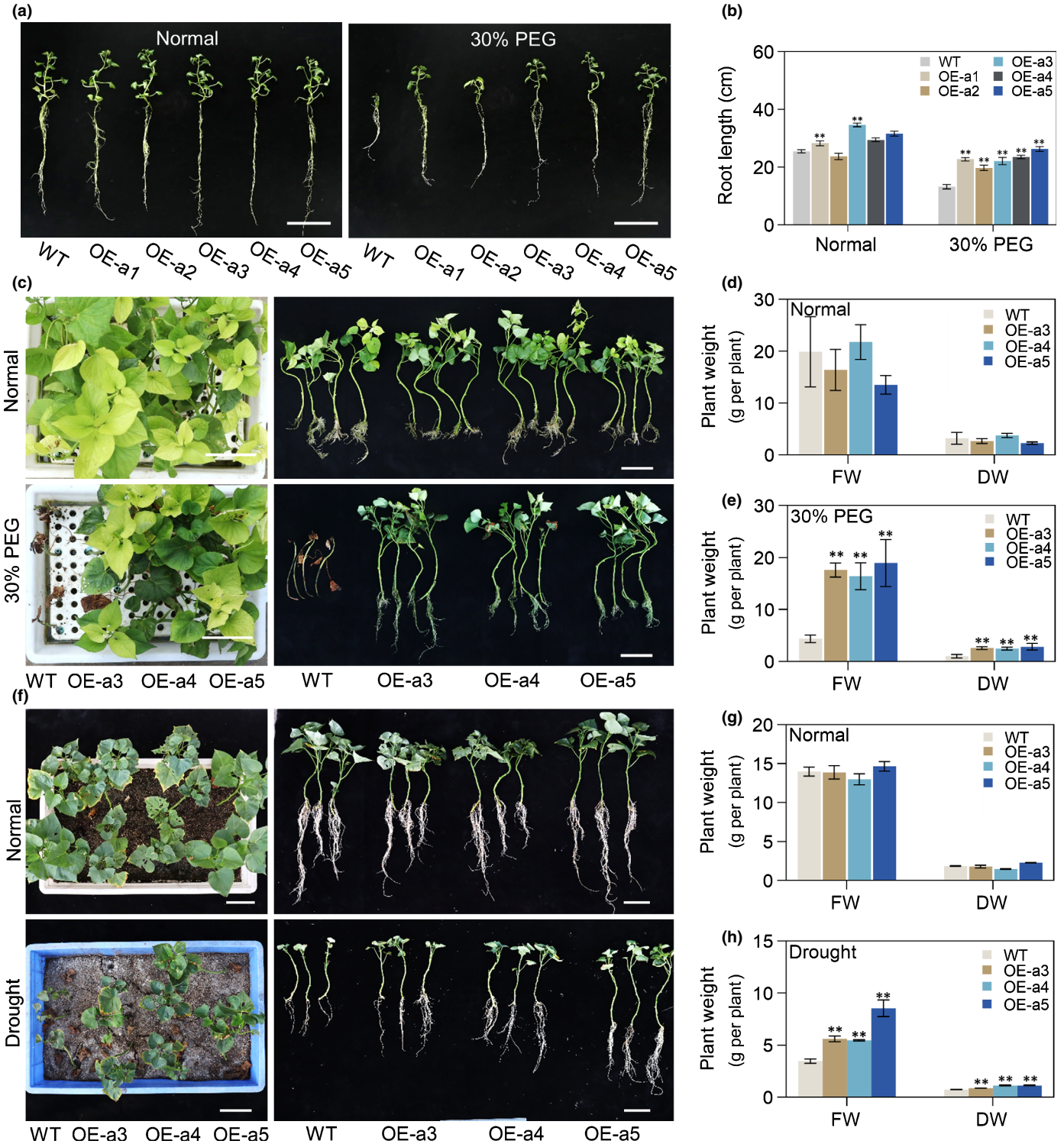

Fig. 5 Overexpression of *IbbHLH66* enhances drought tolerance in sweet potato (*Ipomoea batatas*). (a, b) Responses and plant weight of *IbbHLH66* transgenic and wild-type (WT) sweet potato plants grown for 4 wk on MS medium under normal conditions or subjected to 30% polyethylene glycol (PEG). Bar, 10 cm. (c–e) Responses and plant weight of 2-month-old field-grown *IbbHLH66*-OE and WT sweet potato plants grown hydroponically in half-strength Hoagland solution alone (Normal) or with the addition of 30% PEG6000 for 3 wk. Bar, 10 cm. (f–h) Responses and plant weight of 2-month-old field-grown *IbbHLH66*-OE and WT sweet potato plants grown in transplanting boxes under normal conditions or subjected to drought stress for 6 wk. Bar, 10 cm. All data are presented as the means ± SD ($n = 3$). **, $P < 0.01$; Student's *t*-test. bHLH, basic helix–loop–helix.

In addition, we measured higher ABA and proline contents, and POD and SOD activities, but lower MDA and H_2O_2 contents in the *IbPYL8*-OE lines compared to W38 (Fig. S9b–g). These results indicate that *IbPYL8* is a positive regulator against drought stress, probably by ABA signaling and ROS scavenging in plants.

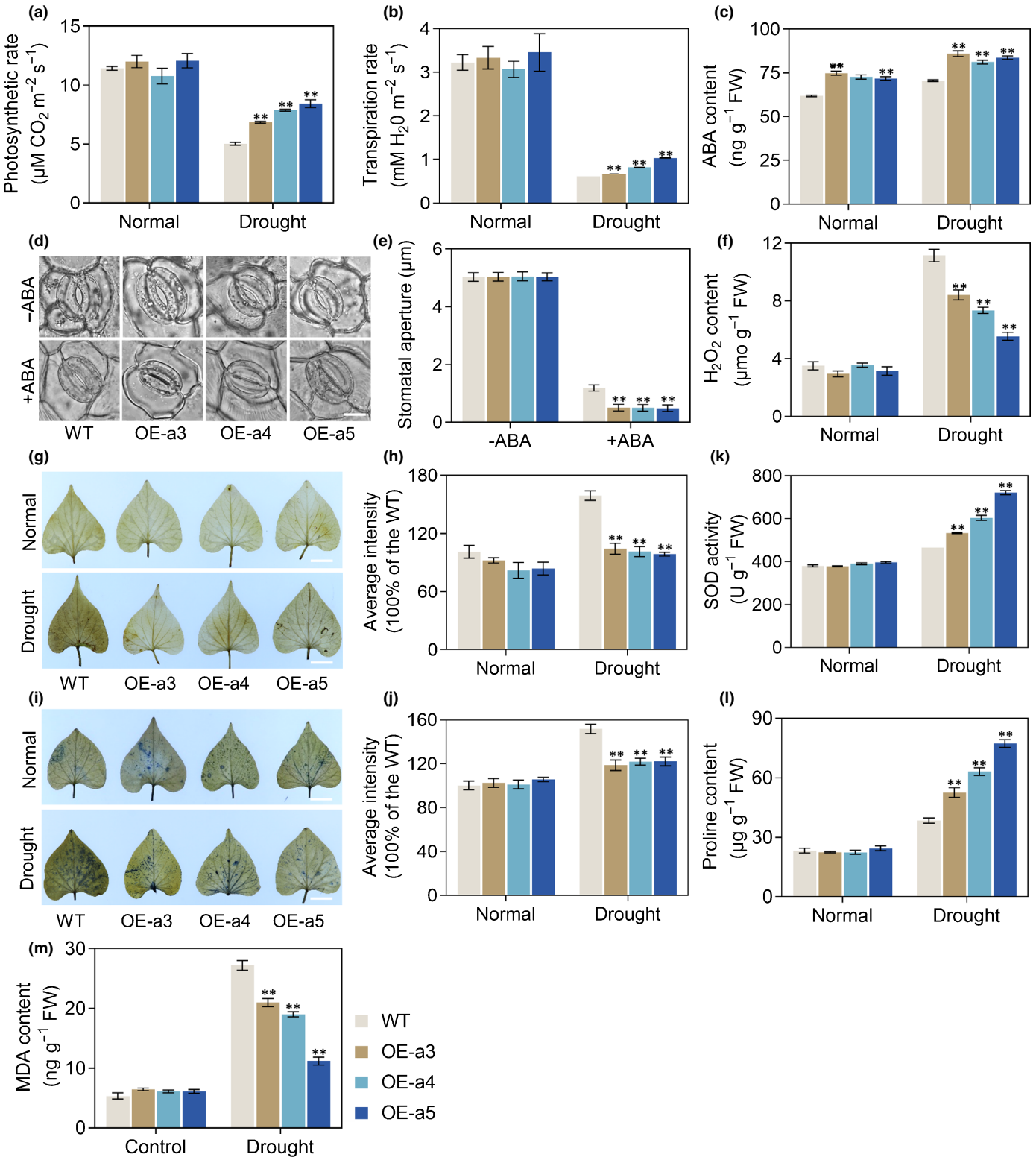

Fig. 6 Overexpression of *IbbHLH66* activates ABA signaling pathway and reactive oxygen species (ROS) scavenging under drought stress in sweet potato (*Ipomoea batatas*). (a) Photosynthetic rate, (b) transpiration rate, (c) ABA content in leaves of *IbbHLH66*-OE transgenic and wild-type (WT) plants under normal conditions or drought stress for 5 wk. Data are presented as the means ± SD ($n = 3$). **, $P < 0.01$; Student's *t*-test. (d, e) Stomatal apertures of 2-month-old field-grown *IbbHLH66* transgenic and WT plants under normal conditions or treated with 20 μM ABA for 2 h. Bar, 10 μm. Data are presented as the means ± SD ($n = 80$). **, $P < 0.01$; Student's *t*-test. (f) Hydrogen peroxide (H_2O_2) content, (g, h) DAB staining (Bar, 1 cm), (i, j) nitroblue tetrazolium (NBT) staining, (k) superoxide dismutase (SOD) activity, (l) proline content and (m) malondialdehyde (MDA) content in leaves of *IbbHLH66* transgenic and WT plants under normal conditions or drought stress for 5 wk. Data are presented as the means ± SD ($n = 3$). **, $P < 0.01$; Student's *t*-test. bHLH, basic helix–loop–helix.

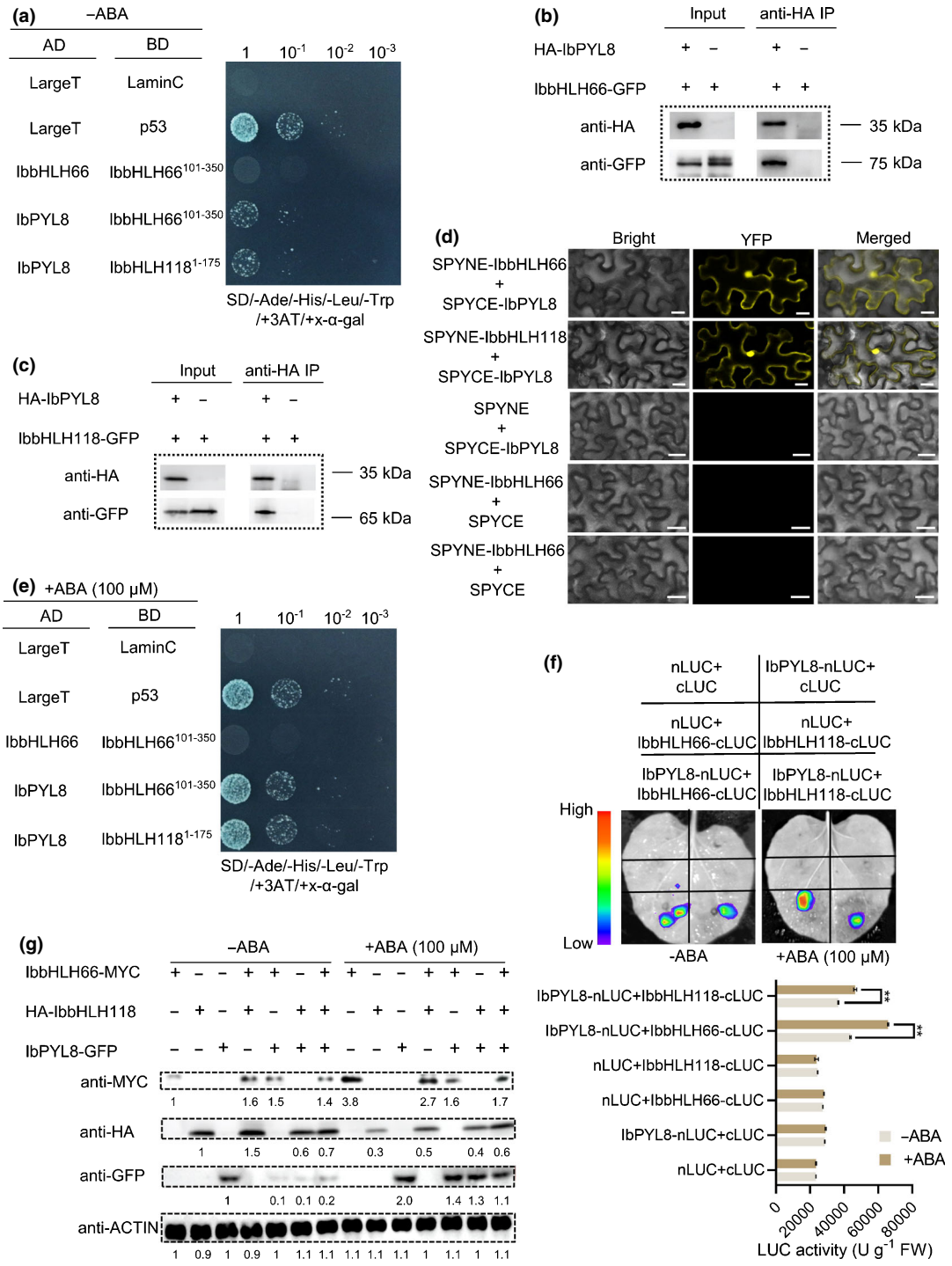

Fig. 7 Interaction of IbPYL8 with IbbHLH66 or IbbHLH118 *in vitro* and *in vivo*. (a) Yeast-two-hybrid (Y2H) analysis showing that IbPYL8 interacts with IbbHLH66 or IbbHLH118. IbbHLH66$^{101–350}$ contains IbbHLH66 amino acid (aa) residues 101–350, whereas IbbHLH118$^{1–175}$ contains IbbHLH118 aa residues 1–175, both without transcriptional activation activity. Yeast cells were plated onto SD/−Ade/−His/−Leu/−Trp + 3 mM 3AT medium to screen for possible interactions. (b, c) Co-immunoprecipitation (Co-IP) analysis showing that IbPYL8 interacts with IbbHLH66 or IbbHLH118 *in vivo*. (d) BiFC analysis showing that IbPYL8 interacts with IbbHLH66 or IbbHLH118 in *Nicotiana benthamiana* leaf epidermal cells. Bar, 20 μm. (e) ABA treatment enhanced the interactions of IbPYL8 with IbbHLH66 or IbbHLH118 in yeast. Yeast cells were plated onto SD/−Ade/−His/−Leu/−Trp + 3 mM 3AT + 100 μM ABA medium. (f) Luciferase complementation imaging (LCI) assay showing that ABA treatment enhanced the interactions of IbPYL8 with IbbHLH66 or IbbHLH118 in *Nicotiana benthamiana*. The N-terminus of LUC was fused to IbPYL8, and the C-terminus of LUC was fused to IbbHLH66 and IbbHLH118, respectively. The LUC activities were detected 2 d later. For ABA treatment, the tobacco leaves were sprayed with 100 μM ABA. Error bars indicate ± SD ($n = 3$). **, $P < 0.01$; Student's *t*-test. (g) Immunoblots showing that ABA induced the accumulation of IbbHLH66 and IbPYL8 protein, but repressed the accumulation of IbbHLH118 protein, under both conditions of alone expression or as components of IbPYL8–IbbHLH66–IbbHLH118 complex. Anti-ACTIN was used as a sample loading control. bHLH, basic helix–loop–helix.

New Phytologist

IbbHLH118 directly targets ABA signaling-related genes *IbABI5* and *IbABF2*

Because IbbHLH118 and IbbHLH66 are involved in the ABA-mediated drought response, we examined the expression levels of key genes involved in ABA biosynthesis and signaling in the transgenic plants. Under normal and drought conditions, key genes related to ABA biosynthesis (*IbNCED3* and *IbNCED5*) and ABA signaling (*IbABI5* and *IbABF2*) were significantly downregulated in *IbbHLH118*-OE plants, but significantly upregulated in *IbbHLH66*-OE plants compared to the WT (Figs 8a,b, S10).

In order to investigate whether IbbHLH118 and IbbHLH66 directly regulate these genes, we conducted Y1H assays. Neither IbbHLH118 nor IbbHLH66 bound to the promoter region of *IbNCED3* or *IbNCED5*. IbbHLH118 directly bound to the

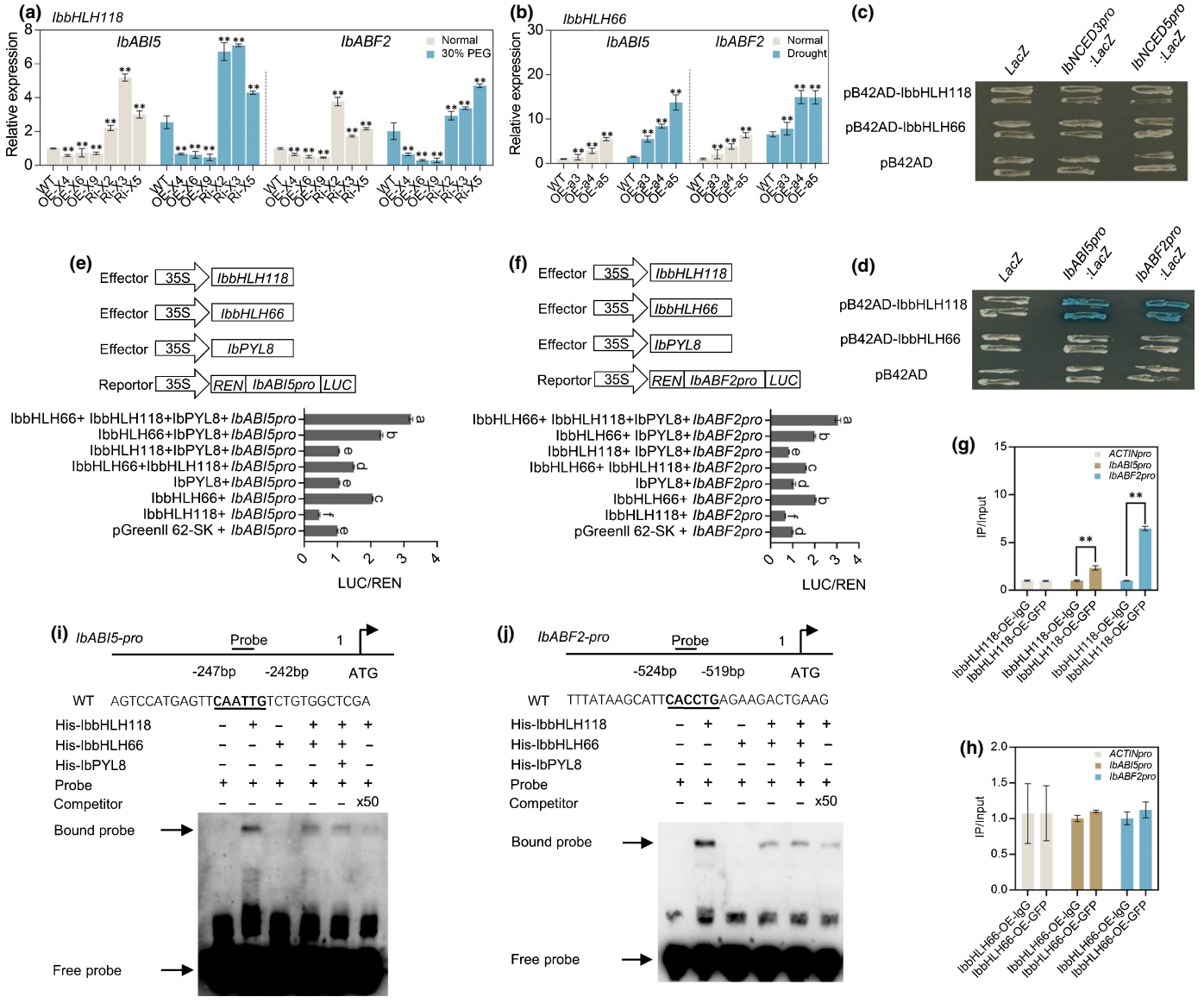

Fig. 8 The IbPYL8–IbbHLH66–IbbHLH118 complex interferes with IbbHLH118's repression of ABA-responsive genes *ABA-insensitive 5* (*IbABI5*) and *ABA-responsive element binding factor 2* (*IbABF2*) in sweet potato (*Ipomoea batatas*). (a, b) Expression analysis of *IbABI5* and *IbABF2* in 4-wk-old *IbbHLH118* and *IbbHLH66* transgenic and WT plants under normal conditions or subjected to 30% PEG. values were determined by quantitative reverse-transcription (qRT)-PCR from three biological replicates consisting of pools of three plants. Error bars indicate ±SD ($n = 3$). **, $P < 0.01$; Student's *t*-test. (c, d) Yeast-one-hybrid (Y1H) assays showing that IbbHLH118 binding to the *IbABI5* and *IbABF2* promoters. (e, f) Dual-LUC assays showing that IbbHLH118 suppressed the *IbABI5* and *IbABF2* promoters, but the IbPYL8–IbbHLH66–IbbHLH118 complex interferes with IbbHLH118's repression of *IbABI5* and *IbABF2*. Data are shown as mean ± SD ($n = 3$). Different letters indicate significant differences for each treatment at $P < 0.05$ based on Student's *t*-test. (g, h) Chromatin immunoprecipitation (ChIP)-qPCR analysis using 35S:IbbHLH118-GFP, 35S:IbbHLH66-GFP, and 35S:GFP plants with anti-GFP antibody, which showed that IbbHLH118 could directly bind to the *IbABI5* and *IbABF2* promoters, but IbbHLH66 could not. GFP, green fluorescent protein. The *ACTIN* promoter was used as an internal reference for ChIP-qPCR. Data are shown as mean ± SD ($n = 3$). (**) Significant difference from 35S:GFP at $P < 0.01$ based on Student's *t*-test. (i, j) EMSA showing that IbbHLH118, but not IbbHLH66, could directly target *IbABI5* and *IbABF2* by binding to E-boxes in their promoters. The addition of IbbHLH66 inhibited the DNA binding activity of IbbHLH118. bHLH, basic helix–loop–helix.

promoter regions of *IbABI5* and *IbABF2* to drive *LacZ* reporter gene expression in yeast cells, whereas IbbHLH66 did not (Fig. 8c,d). Therefore, IbbHLH118, but not IbbHLH66, directly targets and represses the key ABA signaling genes *IbABI5* and *IbABF2* that induce the ABA response in sweet potato.

We further explored the function of *IbABI5* and *IbABF2* in drought response using VIGS. qRT-PCR analysis showed that *IbABI5* and *IbABF2* were significantly reduced in gene-silenced sweet potato leaves during PEG stress (Fig. S11e,k). After treatment with 30% PEG for 14 d, the *IbABI5*-VIGS and *IbABF2*-VIGS plants exhibited worse growth with a higher browning rate than the VWT plants (Fig. S11). These results indicate that *IbABI5* and *IbABF2* function as positive regulators to drought tolerance in sweet potato.

IbbHLH66 inhibits the DNA binding activity of IbbHLH118

Because bHLHs usually function as dimers to bind to their target DNAs (Toledo-Ortiz *et al.*, 2003), we asked how IbbHLH66 and IbPYL8 affect the transcriptional activity of *IbbHLH118*. We performed transient dual-luciferase assays using sweet potato protoplasts and a reporter construct in which the expression of the *LUC* reporter gene was driven by the *IbABI5* or *IbABF2* promoter. LUC activity analysis indicated that IbbHLH118 directly suppressed the *IbABI5* and *IbABF2* promoters, whereas IbbHLH66 activated these promoters (Figs 8e,f, S12a,b). When IbbHLH66 or IbbHLH66 and IbPYL8 were co-expressed with IbbHLH118, *LUC* expression significantly gradually increased, whereas the addition of IbPYL8 alone had no effect on its expression, indicating that IbbHLH66 inhibits the function of IbbHLH118.

IbbHLH118, a subgroup A bHLH protein, specifically binds to E-box elements in its target gene promoters (Dennis *et al.*, 2019). Further ChIP-qPCR and EMSA assays indicated that IbbHLH118, but not IbbHLH66, could directly target *IbABI5* and *IbABF2* to suppress their expression by binding to particular E-boxes in their promoters (Fig. 8g–j). However, the addition of IbbHLH66 inhibited the DNA binding activity of IbbHLH118 to *IbABI5* and *IbABF2* (Fig. 8g–j). These results suggested that IbbHLH66 suppresses the inhibitory activity of IbbHLH118 towards *IbABI5* and *IbABF2*, thereby leading to their activation.

In order to further verify the regulation mode of IbPYL8–IbbHLH66–IbbHLH118 complex in sweet potato, we transiently overexpressed *IbbHLH66*, or *IbbHLH66* and *IbPYL8* into the *IbbHLH118*-OE lines (OE-X4 and OE-X6), and detected the transcript levels of *IbABI5* and *IbABF2* under normal or PEG treatment. The results showed that the expressions of *IbABI5* and *IbABF2* were gradually upregulated with the sequential overexpression of IbbHLH118, IbbHLH66–IbbHLH118 and IbPYL8–IbbHLH66–IbbHLH118 (Fig. S13). Collectively, our data demonstrate that under drought stress, IbPYL8–IbbHLH66–IbbHLH118 complex interferes with IbbHLH118's repression of *IbABI5* and *IbABF2*, thereby promoting ABA signaling and drought tolerance in sweet potato.

The IbPYL8–IbbHLH66–IbbHLH118 complex targets the ABA-responsive gene *IbTIP1*

Aquaporins respond to ABA, and are usually involved in helping maintain a balance of cellular water levels by modifying membrane permeability and stomatal opening (Kaldenhoff *et al.*, 2008; Maurel *et al.*, 2021). We identified *tonoplast intrinsic protein 1* (*IbTIP1*), encoding an aquaporin, whose expression level was significantly downregulated in *IbbHLH118*-OE plants but significantly upregulated in *IbbHLH66*-OE plants (Fig. 9a,b). The Y1H assay revealed that IbbHLH118 directly bound to the promoter region of *IbTIP1* to drive *LacZ* reporter gene expression in yeast cells, but IbbHLH66 did not (Fig. 9c). Transient dual-luciferase assays indicated that IbbHLH118 suppressed, but IbbHLH66 activated, the *IbTIP1* promoter. When IbbHLH66 or IbbHLH66 and IbPYL8 were co-expressed with IbbHLH118, *IbTIP1* promoter activity significantly gradually increased (Figs 9d, S12c). Further ChIP-qPCR and EMSA assays showed that IbbHLH118, but not IbbHLH66, directly targets *IbTIP1* by binding to the E-box element in its promoter, but the addition of IbbHLH66 or IbbHLH66 and IbPYL8 abolished this binding (Fig. 9e–g). These results indicate that IbbHLH66 suppresses the inhibitory activity of IbbHLH118 towards *IbTIP1*, thereby leading to its activation.

In drought-tolerant sweet potato line Xushu55-2, *IbTIP1* was significantly induced by almost 1.96-fold (at 3 h), 1.59-fold (at 1 h) and 2.06-fold (at 6 h) under PEG, ABA and H_2O_2 treatment, respectively (Fig. S14a), and this gene was highly expressed in leaves and stems (Fig. S14b). To investigate the role of *IbTIP1* in drought tolerance, we overexpressed it in sweet potato (Fig. S15) and selected five lines with high *IbTIP1* transcript levels, as determined by qRT-PCR (OE-t3, t4, t6, t9 and t12; Fig. S15f), for a drought tolerance assay. Under 30% PEG and drought treatment, the *IbTIP1*-OE plants exhibited significantly better growth and rooting and lower relative electrical conductivity compared to WT plants (Figs 9h–j, S16a–d). Upon exogenous ABA treatment, the *IbTIP1*-OE plants were more sensitive to ABA-induced changes in stomatal aperture than WT plants (Fig. S16e,f). Together, these results indicate that under drought stress, ABA promotes the formation of the IbPYL8–IbbHLH66–IbbHLH118 complex, which targets the ABA-responsive gene *IbTIP1* and activates its expression, thereby reducing membrane damage and enhancing drought tolerance in sweet potato (Fig. S13).

Discussion

Drought causes oxidative stress and metabolic and osmotic damage in plants, and inhibits cell growth and photosynthesis (Fàbregas & Fernie, 2019). Plants have evolved complex regulatory hormonal signaling networks to respond and adapt to drought conditions. ABA has emerged as a crucial regulator of the drought response (C. Li *et al.*, 2021; J. Li *et al.*, 2021; Q. Li *et al.*, 2021). bHLH TFs are involved in regulating ABA signaling to help plants cope with drought stress (Hao *et al.*, 2021).

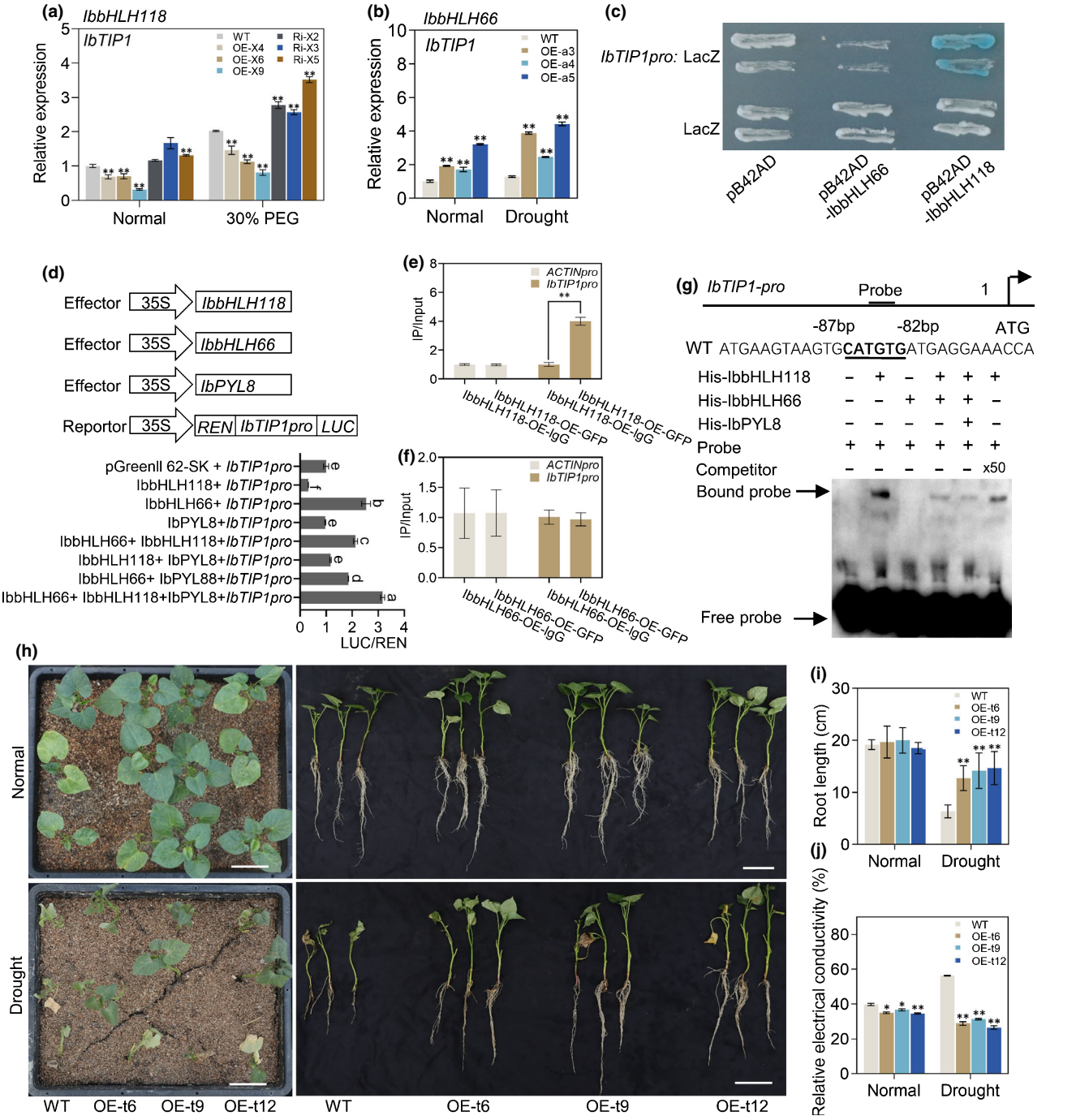

Fig. 9 The IbPYL8–IbbHLH66–IbbHLH118 complex targets the ABA-responsive gene *IbTIP1*. (a) Expression analysis of *tonoplast intrinsic protein 1* (*IbTIP1*) in 4-wk-old *IbbHLH118* transgenic and wild-type (WT) plants under normal conditions or subjected to 30% PEG. Data are presented as the means ± SD ($n = 3$). **, $P < 0.01$; Student's *t*-test. (b) Expression analysis of *IbTIP1* in 5-wk-old *IbbHLH66* transgenic and WT plants under normal conditions or drought stress for 6 wk. Data are presented as the means ± SD ($n = 3$). **, $P < 0.01$; Student's *t*-test. (c) Yeast-one-hybrid (Y1H) assay showing that IbbHLH118 bound to the *IbTIP1* promoter. (d) Dual-LUC assays showing that IbbHLH118 suppressed the *IbTIP1* promoter, but the IbPYL8–IbbHLH66–IbbHLH118 complex interferes with IbbHLH118's repression of *IbTIP1*. Data are shown as mean ± SD ($n = 3$). Different letters indicate significant differences for each treatment at $P < 0.05$ based on Student's *t*-test. (e, f) Chromatin immunoprecipitation (ChIP)-qPCR analysis using 35S:IbbHLH118-GFP, 35S:IbbHLH66-GFP and 35S:GFP plants with anti-GFP antibody, which showed that IbbHLH118 could directly bind to the *IbTIP1* promoter, but IbbHLH66 could not. GFP, green fluorescent protein. The *ACTIN* promoter was used as an internal reference for ChIP-qPCR. Data are shown as mean ± SD ($n = 3$). **, significant difference from 35S:GFP at $P < 0.01$ based on Student's *t*-test. (g) EMSA showing that IbbHLH118, but not IbbHLH66, could directly target *IbTIP1* by binding to the E-box in its promoter. The addition of IbbHLH66 inhibited the DNA binding activity of IbbHLH118. 50× indicates the usage of excess nonlabeled probe as a competitor. (h–j) Responses, root length and relative electrical conductivity of 2-month-old field-grown *IbbHLH66*-OE and WT sweet potato (*Ipomoea batatas*) plants grown in transplanting boxes under normal conditions or subjected to drought stress for 2 wk. Bar, 5 cm. All data are presented as the means ± SD ($n = 3$). *, $P < 0.05$; **, $P < 0.01$; Student's *t*-test. bHLH, basic helix–loop–helix.

Arabidopsis plants overexpressing *AtbHLH68* displayed significantly increased tolerance to drought stress, likely due to enhanced sensitivity to ABA and increased ABA contents (Le *et al.*, 2017). Overexpression of the bHLH TF gene *ZmPTF1* in maize activated ABA-mediated stress responses, thereby increasing drought tolerance (C. Li *et al.*, 2019; L. Li *et al.*, 2019; Z. Li *et al.*, 2019). Heterologous expression of *Myrothamnus flabellifolia bHLH38* in Arabidopsis improved drought tolerance and increased stomatal closure in response to mannitol and ABA (Qiu *et al.*, 2020). Overexpressing *AhHLH112* improved drought tolerance in peanut, along with increased ABA accumulation (C. Li *et al.*, 2021; J. Li *et al.*, 2021; Q. Li *et al.*, 2021). However, the biological functions and regulatory mechanisms of bHLH proteins in sweet potato remain unclear.

In this study, we showed that IbbHLH118 forms homodimers with itself and heterodimers with IbbHLH66. These two proteins play different roles in the ABA-mediated drought response. ABA treatment repressed *IbbHLH118* expression but significantly induced *IbbHLH66* expression in the drought-tolerant sweet potato line Xushu55-2 (Figs 1a–c, 4g,h). Overexpressing *IbbHLH118* reduced drought tolerance, whereas overexpressing *IbbHLH66* enhanced drought tolerance in sweet potato (Figs 2, 5). In Arabidopsis, *AtbHLH66* was involved in root development by regulating root epidermis growth (Lin *et al.*, 2015), and *AtbHLH118* was involved in cell division orientation during vascular development (Smet, 2018).

Drought triggers ABA accumulation in plant tissues. The accumulated ABA is sensed by PYL proteins to initiate the ABA signaling cascade, promoting the expression of key ABA-responsive factors such as ABIs and ABFs, which regulate the ABA response, leading to drought tolerance (Daszkowska-Golec, 2016). *AtPYL8*-overexpressing Arabidopsis plants were hypersensitive to ABA and exhibited high degrees of stomatal closure in response to ABA (Lim *et al.*, 2013). In date palm (*Phoenix dactylifera*), the PdPYL8-like receptor Pd27 accumulated after ABA treatment, and *Pd27*-overexpressing plants were more efficient than the WT in reducing transpiration under a negative soil water potential, leading to enhanced drought tolerance (Garcia-Maquilon *et al.*, 2021). *HvABI5* is involved in the ABA-dependent drought response in barley (Collin *et al.*, 2021). Overexpressing *AtABF2* altered ABA sensitivity, dehydration tolerance and the expression levels of ABA-regulated genes in Arabidopsis (Kim *et al.*, 2004).

In the current study, IbbHLH66, which positively regulates the drought response, did not directly target the ABA-responsive genes *IbABI5* and *IbABF2* (Fig. 8d–j). By contrast, IbbHLH118, which negatively regulates the drought response, directly bound to the E-box elements in the promoters of these two genes, repressing their transcription (Fig. 8d–j). We propose that in sweet potato, IbbHLH118 forms homodimers with itself or heterodimers with IbbHLH66 (Fig. 4a–e), and IbbHLH66 suppresses the inhibitory activity of IbbHLH118 (Fig. 8e,f,i,j). In addition, IbPYL8, a positive regulator to drought stress (Fig. S9), interacts with IbbHLH66 and IbbHLH118 to form the IbPYL8–IbbHLH66–IbbHLH118 complex (Fig. 7a–f). Under drought stress, accumulated ABA promotes and enhances the formation of the IbPYL8–IbbHLH66–IbbHLH118 complex, interfering with IbbHLH118's repression of *IbABI5* and *IbABF2*, thereby promoting ABA signaling and drought tolerance (Figs 7a,e–g, 8e,f, 10).

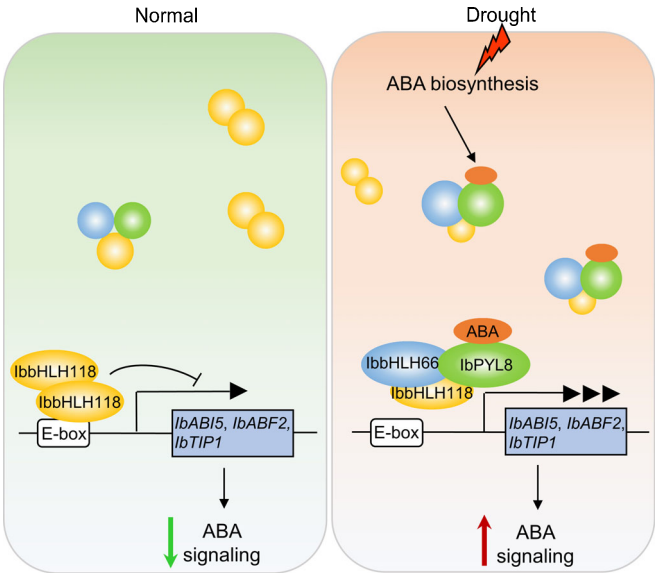

Fig. 10 Proposed working model of the IbPYL8-IbbHLH66-IbbHLH118 regulatory module in the ABA-dependent drought response of sweet potato (*Ipomoea batatas*). Under normal conditions, IbbHLH118 forms homodimers that bind to the promoters of *ABA-insensitive 5* (*IbABI5*), *ABA-responsive element binding factor 2* (*IbABF2*) and *tonoplast intrinsic protein 1* (*IbTIP1*), inhibiting their expression. Under drought conditions, IbbHLH66 and IbPYL8 proteins are induced, but IbbHLH118 is repressed. Accumulated ABA is sensed by IbPYL8 and promotes the formation of the IbPYL8–IbbHLH66–IbbHLH118 complex, which relieves IbbHLH118's repression of ABA-responsive genes, such as *IbABI5*, *IbABF2* and *IbTIP1*, thereby promoting ABA signaling and drought tolerance. Orange circle, ABA; yellow circle, IbbHLH118; blue circle, IbbHLH66; green circle, IbPYL8. Blunt-ended black arrow, promote gene expression; pointed green arrow, suppression; pointed red arrow, activation. bHLH, basic helix–loop–helix.

Accumulating evidence indicates that bHLH TFs usually function as binary or ternary complexes that bind to target DNA (Zhang *et al.*, 2021). The bHLH proteins MyoD, SREBP-2, and Max form homodimers and function in transcriptional regulation (Ma *et al.*, 1994; Parraga *et al.*, 1998; Grandori *et al.*, 2000). The bHLH TFs MYC2, MYC3 (bHLH5), and MYC4 (bHLH4) form homodimers and bind to the G-boxes in the promoters of genes in the JA signaling pathway (Fernández-Calvo *et al.*, 2011; Schweizer *et al.*, 2013). Several bHLHs were reported to form heterodimers with other proteins (Heim *et al.*, 2003). In Arabidopsis, MYC3 interacts with Jasmonate ZIM-domain proteins (JAZs) to mediate JA responses (Cheng *et al.*, 2011). In blueberry, the MYB-bHLH-WD40 regulatory complex controls anthocyanidin biosynthesis during fruit development (An *et al.*, 2012). In *Artemisia annua*, AabHLH1 interacts with AaMYB3 to regulate the accumulation of procyanidine (C. Li *et al.*, 2019; L. Li *et al.*, 2019; Z. Li *et al.*, 2019). In Arabidopsis, AtbHLH104 interacts with another bHLH protein, IAA-LEUCINE RESISTANT3 (ILR3), to modulate iron homeostasis (Zhang *et al.*, 2015). Here, we demonstrated that IbbHLH118 forms

homodimers, but IbbHLH66 does not (Fig. 4a,c). Both IbbHLH118 and IbbHLH66 form heterodimers with IbPYL8 and play important roles in regulating the ABA-mediated drought response (Figs 7, 10).

The IbPYL8–IbbHLH66–IbbHLH118 complex also is involved in the induction of other ABA-responsive genes in sweet potato under drought conditions. Our study showed that IbbHLH118 directly bound to the E-box element in the *IbTIP1* promoter to inhibit its expression (Fig. 9c–g). Under drought stress, ABA promotes the formation of the IbPYL8–IbbHLH66–IbbHLH118 complex, which targets the ABA-responsive gene *IbTIP1* and activates its expression (Fig. S14a). In plants, aquaporins play vital roles in cellular water and osmotic homeostasis under both normal and water deficit conditions (Ding *et al.*, 2016; Kayum *et al.*, 2017). Aquaporin genes usually are induced or suppressed by ABA in plants, and involved in regulating water efflux and stomatal closure (Zhu *et al.*, 2005; Guo *et al.*, 2006; Maurel *et al.*, 2021). In *Eucalyptus grandis*, *EgTIP2* promoter activity was induced by mannitol treatment (Rodrigues *et al.*, 2013). *HvTIP1;1* and *HvTIP1;2* play important roles in the adaptation of barley to drought stress conditions (Kurowska *et al.*, 2019). However, the functions and regulatory mechanisms of most *TIPs* in plants are still unclear. Here, we showed that *IbTIP1* was highly expressed in the leaves and stems of the drought-tolerant sweet potato line Xushu55-2 and was significantly induced by PEG, ABA and H_2O_2 treatment (Fig. S14a). Overexpressing *IbTIP1* reduced membrane damage and enhanced ABA-mediated drought tolerance in sweet potato (Figs 9h–j, S16a–d).

In order to adapt to harsh environments, plants have evolved elaborate mechanisms involving the stress-responsive phytohormones ABA and JA (Peleg & Blumwald, 2011), the ROS scavengers PODs and SODs (Li *et al.*, 2015), and the osmoprotectant proline (Kavi Kishor & Sreenivasulu, 2014). Under drought stress, the ABA contents, SOD activity, proline contents, photosynthetic rate, stomatal conductance and transpiration rate were higher, whereas H_2O_2 and MDA contents were lower in *IbbHLH66*-OE plants compared to the WT (Fig. 6). In addition, the leaves of *IbbHLH66*-OE plants were more sensitive than the WT to ABA-induced changes in stomatal aperture (Fig. 6d,e); *IbbHLH118*-OE plants showed the opposite patterns (Fig. 3). These data indicate that IbbHLH66 and IbbHLH118 have opposite regulatory effects on the physiological responses of sweet potato plants to drought stress, with IbbHLH66 functioning as a positive regulator and IbbHLH118 functioning as a negative regulator of these responses (Fig. 10).

In summary, we elucidated the regulatory mechanism underlying the role of the IbPYL8–IbbHLH66–IbbHLH118 complex in sweet potato's response to drought stress. Under drought, accumulated ABA is sensed by IbPYL8 and promotes the formation of the IbPYL8–IbbHLH66–IbbHLH118 complex, which relieves IbbHLH118's repression of ABA-responsive genes, such as *IbABI5*, *IbABF2* and *IbTIP1*, thereby promoting ABA signaling and drought tolerance. Our study provides insights into the roles of bHLH TFs in regulating ABA and drought responses in plants.

Acknowledgements

This work was supported by the National Key R&D Program of China (2019YFD1001301/2019YFD1001300), the Earmarked Fund for CARS-10-Sweetpotato, and the Beijing Food Crops Innovation Consortium Program (BAIC09-2021).

Author contributions

QL, LX, H Zhang and H Zhai conceived and designed the research; LX, ZW, SX and YW performed the experiments; ZW, LX, H Zhang, SH, SG and NZ analyzed the data; LX and ZW wrote the paper; LX, H Zhang, and QL revised the paper; and all authors read and approved the final version of the paper. LX and ZW contributed equally to this work.

ORCID

Shaopei Gao https://orcid.org/0000-0003-1084-0516
Shaozhen He https://orcid.org/0000-0003-0212-5803
Qingchang Liu https://orcid.org/0000-0002-9127-3885
Yuxin Wang https://orcid.org/0000-0002-6087-6544
Zihao Wei https://orcid.org/0000-0002-1868-4290
Shihan Xing https://orcid.org/0000-0002-3668-5246
Luyao Xue https://orcid.org/0000-0002-0016-9098
Hong Zhai https://orcid.org/0000-0001-9797-9961
Huan Zhang https://orcid.org/0000-0002-6190-296X
Ning Zhao https://orcid.org/0000-0002-2979-7602

Data availability

The data that support the findings of this study are available in the Supporting Information of this article.

References

An XH, Tian Y, Chen KQ, Wang XF, Hao YJ. 2012. The apple WD40 protein MdTTG1 interacts with bHLH but not MYB proteins to regulate anthocyanin accumulation. *Journal of Plant Physiology* **169**: 710–717.

Arisha MH, Ahmad MQ, Tang W, Liu Y, Yan H, Kou M, Wang X, Zhang Y, Li Q. 2020. RNA-sequencing analysis revealed genes associated drought stress responses of different durations in hexaploid sweet potato. *Scientific Reports* **10**: 1–17.

Armstrong GA, Weisshaar B, Hahlbrock K. 1992. Homodimeric and heterodimeric leucine zipper proteins and nuclear factors from parsley recognize diverse promoter elements with ACGT cores. *Plant Cell* **4**: 525–537.

Assmann SM, Jegla T. 2016. Guard cell sensory systems: recent insights on stomatal responses to light, abscisic acid, and CO_2. *Current Opinion in Plant Biology* **33**: 157–167.

Atchley WR, Fitch WM. 1997. A natural classification of the basic helix–loop–helix class of transcription factors. *Proceedings of the National Academy of Sciences, USA* **94**: 5172–5176.

Balazadeh S, Siddiqui H, Allu AD, Matallana-Ramirez LP, Caldana C, Mehrnia M, Zanor MI, Kohler B, Mueller-Roeber B. 2010. A gene regulatory network controlled by the NAC transcription factor ANAC092/AtNAC2/ORE1 during salt-promoted senescence. *The Plant Journal* **62**: 250–264.

Belda-Palazon B, Gonzalez-Garcia MP, Lozano-Juste J, Coego A, Antoni R, Julian J, Peirats-Llobet M, Rodriguez L, Berbel A, Dietrich D *et al.* 2018. PYL8 mediates ABA perception in the root through non-cell-autonomous and

ligand-stabilization–based mechanisms. *Proceedings of the National Academy of Sciences, USA* **115**: E11857–E11863.

Bi H, Zhang P. 2014. Agroinfection of sweet potato by vacuum infiltration of an infectious sweepovirus. *Virologica Sinica* **29**: 148–154.

Chen H, Zou Y, Shang Y, Lin H, Wang Y, Cai R, Tang X, Zhou J. 2008. Firefly luciferase complementation imaging assay for protein-protein interactions in plants. *Plant Physiology* **146**: 368–324.

Chen Q, Sun J, Zhai Q, Zhou W, Qi L, Xu L, Wang B, Chen R, Jiang H, Qi J *et al.* 2011. The basic helix-loop-helix transcription factor MYC2 directly represses *plethora* expression during jasmonate-mediated modulation of the root stem cell niche in *Arabidopsis*. *Plant Cell* **23**: 3335–3352.

Cheng Z, Sun L, Qi T, Zhang B, Peng W, Liu Y, Xie D. 2011. The bHLH transcription factor MYC3 interacts with the jasmonate ZIM-domain proteins to mediate jasmonate response in *Arabidopsis*. *Molecular Plant* **4**: 279–288.

Collin A, Daszkowska-Golec A, Szarejko I. 2021. Updates on the role of abscisic acid insensitive 5 (ABI5) and abscisic acid-responsive element binding factors (ABFs) in ABA signaling in different developmental stages in plants. *Cell* **10**: 1996.

Danquah A, de Zelicourt A, Colcombet J, Hirt H. 2014. The role of ABA and MAPK signaling pathways in plant abiotic stress responses. *Biotechnology Advances* **32**: 40–52.

Daszkowska-Golec A. 2016. The role of abscisic acid in drought stress: how ABA helps plants to cope with drought stress. *Drought Stress Tolerance in Plants* **2016**: 123–151.

Dennis DJ, Han S, Schuurmans C. 2019. bHLH transcription factors in neural development, disease, and reprogramming. *Brain Research* **1705**: 48–65.

Ding L, Li Y, Wang Y, Gao L, Wang M, Chaumont F, Shen Q, Guo S. 2016. Root ABA accumulation enhances rice seedling drought tolerance under ammonium supply: interaction with aquaporins. *Frontiers in Plant Science* **7**: 1206.

Fàbregas N, Fernie AR. 2019. The metabolic response to drought. *Journal of Experimental Botany* **70**: 1077–1085.

Fernández-Calvo P, Chini A, Fernández-Barbero G, Chico JM, Gimenez-Ibanez S, Geerinck J, Eeckhout D, Schweizer F, Godoy M, Franco-Zorrilla JM *et al.* 2011. The *Arabidopsis* bHLH transcription factors MYC3 and MYC4 are targets of JAZ repressors and act additively with MYC2 in the activation of jasmonate responses. *Plant Cell* **23**: 701–715.

Foyer CH. 2018. Reactive oxygen species, oxidative signaling and the regulation of photosynthesis. *Environmental and Experimental Botany* **154**: 134–142.

Fujita M, Fujita Y, Noutoshi Y, Takahashi F, Narusaka Y, Yamaguchi-Shinozaki K, Shinozaki K. 2006. Crosstalk between abiotic and biotic stress responses: a current view from the points of convergence in the stress signaling networks. *Current Opinion in Plant Biology* **9**: 436–442.

Garcia-Maquilon I, Coego A, Lozano-Juste J, Messerer M, de Ollas C, Julian J, Ruiz-Partida R, Pizzio G, Belda-Palazón B, Gomez-Cadenas A *et al.* 2021. PYL8 ABA receptors of *Phoenix dactylifera* play a crucial role in response to abiotic stress and are stabilized by ABA. *Journal of Experimental Botany* **72**: 757–774.

Ghosh UK, Islam MN, Siddiqui MN, Cao X, Khan MAR. 2022. Proline, a multifaceted signalling molecule in plant responses to abiotic stress: understanding the physiological mechanisms. *Plant Biology* **24**: 227–239.

Grandori C, Cowley SM, James LP, Eisenman RN. 2000. The Myc/Max/Mad network and the transcriptional control of cell behavior. *Annual Review of Cell and Developmental Biology* **16**: 653–699.

Groszmann M, Bylstra Y, Lampugnani ER, Smyth DR. 2010. Regulation of tissue-specific expression of *SPATULA*, a bHLH gene involved in carpel development, seedling germination, and lateral organ growth in *Arabidopsis*. *Journal of Experimental Botany* **61**: 1495–1508.

Guan Q, Wu J, Yue X, Zhang Y, Zhu J. 2013. A nuclear calcium-sensing pathway is critical for gene regulation and salt stress tolerance in *Arabidopsis*. *PLoS Genetics* **9**: e1003755.

Guo L, Wang ZY, Lin H, Cui WE, Chen J, Li M, Chen Zl QLJ, Gu H. 2006. Expression and functional analysis of the rice plasma-membrane intrinsic protein gene family. *Cell Research* **16**: 277–286.

Hao Y, Zong X, Ren P, Qian Y, Fu A. 2021. Basic helix–loop–helix (bHLH) transcription factors regulate a wide range of functions in *Arabidopsis*. *International Journal of Molecular Sciences* **22**: 7152.

Heim MA, Jakoby M, Werber M, Martin C, Weisshaar B, Bailey PC. 2003. The basic helix–loop–helix transcription factor family in plants: a genome-wide study of protein structure and functional diversity. *Molecular Biology and Evolution* **20**: 735–747.

Horn T, Boutros M. 2010. E-RNAi: a web application for the multi-species design of RNAi reagents—2010 update. *Nucleic Acids Research* **38**: W332–W339.

Horsch RB, Fry JE, Hoffmann NL, Eichholtz D, Rogers SG, Fraley RT. 1985. A simple and general method for transferring genes into plants. *Science* **227**: 1229–1231.

Ito S, Song YH, Josephson-Day AR, Miller RJ, Breton G, Olmstead RG, Imaizumi T. 2012. FLOWERING BHLH transcriptional activators control expression of the photoperiodic flowering regulator *constans* in *Arabidopsis*. *Proceedings of the National Academy of Sciences, USA* **109**: 3582–3587.

Jata SK, Nedunchezhian M, Misra SR. 2011. The triple 'f' (food, fodder and fuel) crop sweet potato [*Ipomoea batatas* (L.) Lam.]. *Orissa Review* **5**: 82–92.

Jefferson RA. 1987. Assaying chimeric genes in plants: the GUS gene fusion system. *Plant Molecular Biology Reporter* **5**: 387–405.

Kaldenhoff R, Ribas-Carbo M, Sans JF, Lovisolo C, Heckwolf M, Uehlein N. 2008. Aquaporins and plant water balance. *Plant, Cell & Environment* **31**: 658–666.

Kang C, He S, Zhai H, Li R, Zhao N, Liu Q. 2018. A sweetpotato auxin response factor gene (*IbARF5*) is involved in carotenoid biosynthesis and salt and drought tolerance in transgenic *Arabidopsis*. *Frontiers in Plant Science* **9**: 1307.

Karkute SG, Gujjar RS, Rai A, Akhtar M, Singh M, Singh B. 2018. Genome wide expression analysis of WRKY genes in tomato (*Solanum lycopersicum*) under drought stress. *Plant Gene* **13**: 8–17.

Kavi Kishor PB, Sreenivasulu N. 2014. Is proline accumulation per se correlated with stress tolerance or is proline homeostasis a more critical issue? *Plant, Cell & Environment* **37**: 300–311.

Kayum M, Park JI, Nath UK, Biswas MK, Kim HT, Nou IS. 2017. Genome-wide expression profiling of aquaporin genes confer responses to abiotic and biotic stresses in Brassica rapa. *BMC Plant Biology* **17**: 1–18.

Kim S, Kang JY, Cho DI, Park JH, Kim SY. 2004. ABF2, an ABRE-binding bZIP factor, is an essential component of glucose signaling and its overexpression affects multiple stress tolerance. *The Plant Journal* **40**: 75–87.

Kumar SV, Lucyshyn D, Jaeger KE, Alós E, Alvey E, Harberd NP, Wigge PA. 2012. Transcription factor PIF4 controls the thermosensory activation of flowering. *Nature* **48**: 242–245.

Kurowska MM, Wiecha K, Gajek K, Szarejko I. 2019. Drought stress and re-watering affect the abundance of TIP aquaporin transcripts in barley. *PLoS ONE* **14**: e0226423.

Lau KH, del Rosario HM, Crisovan E, Wu S, Fei Z, Khan MA, Robin Buell C, Gemenet DC. 2018. Transcriptomic analysis of sweet potato under dehydration stress identifies candidate genes for drought tolerance. *Plant Direct* **2**: e00092.

Le R, Castelain M, Chakraborti D, Moritz T, Dinant S, Bellini C. 2017. *AtbHLH68* transcription factor contributes to the regulation of ABA homeostasis and drought stress tolerance in *Arabidopsis thaliana*. *Physiologia Plantarum* **160**: 312–327.

Li C, Qiu J, Huang S, Yin J, Yang G. 2019. AaMYB3 interacts with AabHLH1 to regulate proanthocyanidin accumulation in *Anthurium andraeanum* (Hort.) —another strategy to modulate pigmentation. *Horticulture Research* **6**: 14.

Li C, Yan C, Sun Q, Wang J, Yuan C, Mou Y, Shan S, Zhao X. 2021. The bHLH transcription factor *AhbHLH112* improves the drought tolerance of peanut. *BMC Plant Biology* **21**: 1–12.

Li J, Li X, Han P, Liu H, Gong J, Zhou W, Shi B, Liu A, Xu L. 2021. Genome-wide investigation of *bHLH* genes and expression analysis under different biotic and abiotic stresses in *Helianthus annuus* L. *International Journal of Biological Macromolecules* **189**: 72–83.

Li JB, Luan YS, Liu Z. 2015. *SpWRKY1* mediates resistance to *Phytophthora infestans* and tolerance to salt and drought stress by modulating reactive oxygen species homeostasis and expression of defense-related genes in tomato. *Plant Cell, Tissue and Organ Culture* **123**: 67–81.

Li L, Hao X, Liu H, Wang W, Fu X, Ma Y, Shen Q, Chen M, Tang K. 2019. Jasmonic acid-responsive AabHLH1 positively regulates artemisinin

biosynthesis in *Artemisia annua*. *Biotechnology and Applied Biochemistry* **66**: 369–375.

Li Q, Xu F, Chen Z, Teng Z, Sun K, Li X, Yu J, Zhang G, Liang Y, Huang X *et al.* 2021. Synergistic interplay of ABA and BR signal in regulating plant growth and adaptation. *Nature Plants* **7**: 1108–1118.

Li Z, Liu C, Zhang Y, Wang B, Ran Q, Zhang J. 2019. The bHLH family member ZmPTF1 regulates drought tolerance in maize by promoting root development and abscisic acid synthesis. *Journal of Experimental Botany* **70**: 5471–5486.

Lim CW, Baek W, Han SW, Lee SC. 2013. *Arabidopsis* PYL8 plays an important role for ABA signaling and drought stress responses. *The Plant Pathology Journal* **29**: 471–476.

Lin Q, Ohashi Y, Kato M, Tsuge T, Gu H, Qu LJ, Aoyama T. 2015. GLABRA2 directly suppresses basic helix-loop-helix transcription factor genes with diverse functions in root hair development. *Plant Cell* **27**: 2894–2906.

Liu Q, Zhai H, Wang Y, Zhang D. 2001. Efficient plant regeneration from embryogenic suspension cultures of sweetpotato. *In Vitro Cellular & Developmental Biology – Plant* **37**: 564–567.

Liu W, Tai H, Li S, Gao W, Zhao M, Xie C, Li WX. 2014. *bHLH122* is important for drought and osmotic stress resistance in *Arabidopsis* and in the repression of ABA catabolism. *New Phytologist* **201**: 1192–1204.

Liu Y, Ji X, Nie X, Qu M, Zheng L, Tan Z, Zhang H, Huo L, Liu S, Zhang B *et al.* 2015. *Arabidopsis* AtbHLH112 regulates the expression of genes involved in abiotic stress tolerance by binding to their E-box and GCG-box motifs. *New Phytologist* **207**: 692–709.

Liu Y, Ma K, Qi Y, Lv G, Ren X, Liu Z, Ma F. 2021. Transcriptional regulation of anthocyanin synthesis by MYB-bHLH-WDR complexes in Kiwifruit (*Actinidia chinensis*). *Journal of Agricultural and Food Chemistry* **69**: 3677–3691.

Ma PC, Rould MA, Weintraub H, Pabo CO. 1994. Crystal structure of MyoD bHLH domain-DNA complex: perspectives on DNA recognition and implications for transcriptional activation. *Cell* **77**: 451–459.

Martínez-García JF, Huq E, Quail PH. 2000. Direct targeting of light signals to a promoter element-bound transcription factor. *Science* **288**: 859–863.

Maurel C, Tournaire-Roux C, Verdoucq L, Santoni V. 2021. Hormonal and environmental signaling pathways target membrane water transport. *Plant Physiology* **187**: 2056–2070.

Mbinda W, Ombori O, Dixelius C, Oduor R. 2018. *Xerophyta viscosa* aldose reductase, XvAld1, enhances drought tolerance in transgenic sweetpotato. *Molecular Biotechnology* **60**: 203–214.

Mehrotra R, Sethi S, Zutshi I, Bhalothia P, Mehrotra S. 2013. Patterns and evolution of ACGT repeat *cis*-element landscape across four plant genomes. *BMC Genomics* **14**: 203.

Menand B, Yi K, Jouannic S, Hoffmann L, Ryan E, Linstead P, G. Schaefer D, Dolan L. 2007. An ancient mechanism controls the development of cells with a rooting function in land plants. *Science* **316**: 1477–1480.

Motsa NM, Modi AT, Mabhaudhi T. 2015. Sweet potato (*Ipomoea batatas* L.) as a drought tolerant and food security crop. *South African Journal of Science* **111**: 1–8.

Munemasa S, Hauser F, Park J, Waadt R, Brandt B, Schroeder JI. 2015. Mechanisms of abscisic acid-mediated control of stomatal aperture. *Current Opinion in Plant Biology* **28**: 154–162.

Oh E, Yamaguchi S, Kamiya Y, Bae G, Chung WI, Choi G. 2006. Light activates the degradation of PIL5 protein to promote seed germination through gibberellin in *Arabidopsis*. *The Plant Journal* **47**: 124–139.

Parraga A, Bellsolell L, Ferre-D'Amare AR, Burley SK. 1998. Co-crystal structure of sterol regulatory element binding protein 1a at 2.3 Å resolution. *Structure* **6**: 661–672.

Peleg Z, Blumwald E. 2011. Hormone balance and abiotic stress tolerance in crop plants. *Current Opinion in Plant Biology* **14**: 290–295.

Penfield S, Josse EM, Kannangara R, Gilday AD, Halliday KJ, Graham IA. 2005. Cold and light control seed germination through the bHLH transcription factor SPATULA. *Current Biology* **15**: 1998–2006.

Pires N, Dolan L. 2010. Origin and diversification of basic–helix–loop–helix proteins in plants. *Molecular Biology and Evolution* **27**: 862–874.

Qi T, Huang H, Song S, Xie D. 2015. Regulation of jasmonate-mediated stamen development and seed production by a bHLH-MYB complex in *Arabidopsis*. *Plant Cell* **27**: 1620–1633.

Qiu JR, Huang Z, Xiang XY, Xu WX, Wang JT, Chen J, Song L, XiaoY LX, Ma J *et al.* 2020. MfbHLH38, a *Myrothamnus flabellifolia* bHLH transcription factor, confers tolerance to drought and salinity stresses in *Arabidopsis*. *BMC Plant Biology* **20**: 1–14.

Rodrigues MI, Bravo JP, Sassaki FT, Severino FE, Maia IG. 2013. The tonoplast intrinsic aquaporin (TIP) subfamily of *Eucalyptus grandis*: characterization of *EgTIP2*, a root-specific and osmotic stress-responsive gene. *Plant Science* **213**: 106–113.

Schweizer F, Fernández-Calvo P, Zander M, Diez-Diaz M, Fonseca S, Glauser GG, Lewsey MR, Ecker J, Solano R, Reymond P. 2013. *Arabidopsis* basic helix-loop-helix transcription factors MYC2, MYC3, and MYC4 regulate glucosinolate biosynthesis, insect performance, and feeding behavior. *Plant Cell* **25**: 3117–3132.

Sharma N, Xin R, Kim DH, Sung S, Lange T, Huq E. 2016. No flowering in short day (NFL) is a bHLH transcription factor that promotes flowering specifically under short-day conditions in *Arabidopsis*. *Development* **143**: 682–690.

Sharma P, Jha AB, Dubey RS, Pessarakli M. 2012. Reactive oxygen species, oxidative damage, and antioxidative defense mechanism in plants under stressful conditions. *Journal of Botany* **2012**: 2012.

Smet WMS. 2018. *Control of cell division orientation during vascular development in* Arabidopsis thaliana. PhD thesis, Wageningen University and Research, Wageningen, the Netherlands.

Sonal M, Aparna S, Swati U, Sanchita PS, Seema S, Ujjal J, Phukan AM, Feroz K, Tripathi V, Shukla RK *et al.* 2014. *Retracted*: identification, occurrence, and validation of DRE and ABRE *cis*-regulatory motifs in the promoter regions of genes of *Arabidopsis thaliana*. *Journal of Integrative Plant Biology* **4**: 388–398.

Sun L, Wang YP, Pei C, Ren J, Ji K, Qian L, Ping L, Dai S-J, Ping L. 2011. Transcriptional regulation of *SlPYL*, *SlPP2C*, and *SlSnRK2* gene families encoding ABA signal core components during tomato fruit development and drought stress. *Journal of Experimental Botany* **62**: 5659–5669.

Tamura K, Stecher G, Kumar S. 2021. MEGA11: molecular evolutionary genetics analysis v.11. *Molecular Biology and Evolution* **7**: 38–3027.

Tanabe N, Noshi M, Mori D, Nozawa K, Tamoi M, Shigeoka S. 2019. The basic helix–loop–helix transcription factor, bHLH11 functions in the iron-uptake system in *Arabidopsis thaliana*. *Journal of Plant Research* **132**: 93–105.

Tian S, Li L, Wei M, Yang F. 2019. Genome-wide analysis of basic helix–loop–helix superfamily members related to anthocyanin biosynthesis in eggplant (*Solanum melongena* L.). *PeerJ* **7**: e7768.

Toledo-Ortiz G, Huq E, Quail PH. 2003. The *Arabidopsis* basic/helix-loop-helix transcription factor family. *Plant Cell* **15**: 1749–1770.

Tuteja N. 2007. Abscisic acid and abiotic stress signaling. *Plant Signaling & Behavior* **2**: 135–138.

Varaud E, Brioudes F, Szécsi J, Leroux J, Brown S, Perrot-Rechenmann C, Bendahmane M. 2011. Auxin response factor 8 regulates *Arabidopsis* petal growth by interacting with the bHLH transcription factor BIGPETALp. *Plant Cell* **23**: 973–983.

Walter M, Chaban C, Schütze K, Batistic O, Weckermann K, Näke C, Blazevic D, Grefen C, Schumacher K, Oecking C *et al.* 2004. Visualization of protein interactions in living plant cells using bimolecular fluorescence complementation. *The Plant Journal* **40**: 428–438.

Wang H, Li Y, Pan J, Lou D, Hu Y, Yu D. 2017. The bHLH transcription factors MYC2, MYC3, and MYC4 are required for jasmonate-mediated inhibition of flowering in *Arabidopsis*. *Molecular Plant* **10**: 1461–1464.

Wu C, Zheng CY, Ji GS, Jiang P. 2019. Synergistic effects of HSE and LTR elements from *hsp70* gene promoter of *Ulva prolifera* (Ulvophyceae, Chlorophyta) upon temperature induction. *Journal of Phycology* **3**: 55.

Xiong L, Zhu JK. 2003. Regulation of abscisic acid biosynthesis. *Plant Physiology* **133**: 29–36.

Yan HX, Fu DQ, Zhu BZ, Liu HP, Shen XY, Luo YB. 2012. Sprout vacuum-infiltration: a simple and efficient agroinoculation method for virus-induced gene silencing in diverse solanaceous species. *Plant Cell Reports* **31**: 1713–1722.

Yi K, Menand B, Bell E, Dolan L. 2010. A basic helix-loop-helix transcription factor controls cell growth and size in root hairs. *Nature Genetics* **42**: 264–267.

Yuan Y, Wu H, Wang N, Li J, Zhao W, Du J, Wang D, Ling HQ. 2008. FIT interacts with AtbHLH38 and AtbHLH39 in regulating iron uptake gene expression for iron homeostasis in *Arabidopsis*. *Cell Research* **18**: 385–397.

Zhai H, Wang F, Si Z, Huo J, Xing L, An Y, He S, Liu Q. 2016. A *myo*-inositol-1-phosphate synthase gene, *IbMIPS1*, enhances salt and drought tolerance and stem nematode resistance in transgenic sweet potato. *Plant Biotechnology Journal* **14**: 592–602.

Zhang H, Gao X, Zhi Y, Li X, Zhang Q, Niu J, Wang J, Zhai H, Zhao N, Li J *et al.* 2019. A non-tandem CCCH-type zinc-finger protein, IbC3H18, functions as a nuclear transcriptional activator and enhances abiotic stress tolerance in sweet potato. *New Phytologist* **223**: 1918–1936.

Zhang H, Wang Z, Li X, Gao X, Dai Z, Cui Y, Zhi Y, Liu Q, Zhai H, Gao S *et al.* 2022. The IbBBX24–IbTOE3–IbPRX17 module enhances abiotic stress tolerance by scavenging reactive oxygen species in sweet potato. *New Phytologist* **233**: 1133–1152.

Zhang H, Zhang Q, Wang Y, Li Y, Zhai H, Liu Q, He S. 2017. Characterization of salt tolerance and fusarium wilt resistance of a sweetpotato mutant. *Journal of Integrative Agriculture* **16**: 1946–1955.

Zhang H, Zhang Q, Zhai H, Gao S, Yang L, Wang Z, Xu Y, Huo J, Ren Z, Zhao N *et al.* 2020. IbBBX24 promotes the jasmonic acid pathway and enhances fusarium wilt resistance in sweet potato. *Plant Cell* **32**: 1102–1123.

Zhang J, Liu B, Li M, Feng D, Jin H, Wang P, Liu J, Xiong F, Wang J, Wang HB. 2015. The bHLH transcription factor bHLH104 interacts with IAA-leucine resistant 3 and modulates iron homeostasis in *Arabidopsis*. *Plant Cell* **27**: 787–805.

Zhang Y, Mitsuda N, Yoshizumi T, Horii Y, Oshima Y, Ohme-Takagi M, Matsui M, Kakimoto T. 2021. Two types of bHLH transcription factor determine the competence of the pericycle for lateral root initiation. *Nature Plants* **7**: 633–643.

Zhao M, Li J, Zhu L, Chang P, Li L, Zhang L. 2019. Identification and characterization of MYB-bHLH-WD40 regulatory complex members controlling anthocyanidin biosynthesis in blueberry fruits development. *Genes* **10**: 496.

Zhu C, Schraut D, Hartung W, Schäffner AR. 2005. Differential responses of maize *MIP* genes to salt stress and ABA. *Journal of Experimental Botany* **56**: 2971–2981.

Zhu H, Zhou Y, Zhai H, He S, Zhao N, Liu Q. 2019. Transcriptome profiling reveals insights into the molecular mechanism of drought tolerance in sweetpotato. *Journal of Integrative Agriculture* **1**: 9–23.

Supporting Information

Additional Supporting Information may be found online in the Supporting Information section at the end of the article.

Fig. S1 Tissue-specific expression, the promoter characterization and transcriptional activation assays of IbbHLH118.

Fig. S2 Production of *IbbHLH118* transgenic sweet potato plants.

Fig. S3 Detailed time-course analysis of *IbbHLH118* transgenic and WT sweet potato plants grown in transplanting boxes without stress (Normal) or subjected to drought stress for the indicated times (weeks).

Fig. S4 Sequence, expression and genomic structure analysis of *IbbHLH66* in sweet potato and other plants.

Fig. S5 Production of *IbbHLH66*-OE transgenic sweet potato plants.

Fig. S6 Detailed time-course analysis of *IbbHLH66* transgenic and WT sweet potato plants grown in Hoagland solution with or without 30% PEG for the indicated times (weeks).

Fig. S7 Tobacco rattle virus-based virus-induced gene silencing of *IbbHLH66* in the drought-sensitive sweet potato variety 'Lizixiang' reduces drought tolerance of sweet potato.

Fig. S8 Y2H analysis, expression analysis and subcellular localization of IbPYL8.

Fig. S9 *IbPYL8* overexpression enhances drought tolerance in transgenic tobacco plants.

Fig. S10 Relative expression of *IbbHLH118, IbbHLH66, IbNCED3* and *IbNCED5* in *IbbHLH118* and *IbbHLH66* transgenic and WT sweet potato plants.

Fig. S11 TRV-based VIGS of *IbABI5* and *IbABF2* in the drought-sensitive sweet potato variety 'Lizixiang' reduce drought tolerance of sweet potato.

Fig. S12 Immunoblot detection of effector protein levels in dual-luciferase assays.

Fig. S13 Relative transcript levels of ABA-responsive genes under normal or 20% PEG treatment for 6 h in transgenic sweet potato plants.

Fig. S14 Expression analysis of *IbTIP1* in sweet potato.

Fig. S15 Production of *IbTIP1*-OE transgenic sweet potato plants.

Fig. S16 Overexpression of *IbTIP1* enhances drought tolerance in sweet potato.

Table S1 Sequences of the primers used in this study.

Table S2 Comparison of *IbbHLH118* and *IbbHLH66* transgenic plants with WT after 4 wk of culture on MS medium with or without 30% PEG.

Table S3 Comparison of *IbbHLH66* transgenic plants with WT grown in Hoagland solution with or without 30% PEG.

Table S4 Comparison of *IbbHLH118* transgenic plants with WT under 30% PEG treatment.

Table S5 Comparison of *IbbHLH66*-OE with WT plants under drought treatment.

Please note: Wiley Blackwell are not responsible for the content or functionality of any Supporting Information supplied by the authors. Any queries (other than missing material) should be directed to the *New Phytologist* Central Office.

ARTICLES FOR FACULTY MEMBERS

INVESTIGATING THE ROLE OF GIBBERELLIC ACID (GA) AND ABSCISIC ACID (ABA) CROSS-TALK IN ENHANCING TUBEROUS ROOT DEVELOPMENT IN SWEET POTATOES

Transcriptome analysis reveals the impact of short-term biochar application on starch and sucrose metabolism in sweet potato tuberous roots / Zhang, J., Xu, X., Li, T., Lv, Z., Zhu, Y., Li, J., & Lu, G.

Industrial Crops and Products
Volume 223 (2025) 120050 Pages 1-11
https://doi.org/10.1016/j.indcrop.2024.120050
(Database: ScienceDirect)

Industrial Crops & Products 223 (2025) 120050

Contents lists available at ScienceDirect

Industrial Crops & Products

journal homepage: www.elsevier.com/locate/indcrop

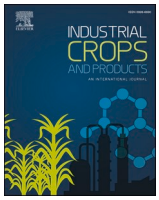

Transcriptome analysis reveals the impact of short-term biochar application on starch and sucrose metabolism in sweet potato tuberous roots

Jingzhen Zhang [a], Ximing Xu [a,b,*], Taojun Li [a], Zunfu Lv [a], Yueming Zhu [a], Jing Li [c], Guoquan Lu [a]

[a] The Key Laboratory for Quality Improvement of Agricultural Products of Zhejiang Province, Institute of Root and Tuber Crops, College of Advanced Agricultural Sciences, Zhejiang A&F University, Hangzhou 311300, China
[b] Key Laboratory of Biotechnology in Plant Protection of MARA and Zhejiang Province, Institute of Plant Virology, Ningbo University, Ningbo 315211, China
[c] Zhejiang Agricultural Technology Extension Center, Hangzhou 310020, China

ARTICLE INFO

Keywords:
Sweet potato
Short-term biochar application
Starch
Transcriptome sequencing

ABSTRACT

Biochar has been proven to be an effective method for enhancing sweet potato yield. However, limited research has been conducted on the molecular and physiological mechanisms underlying biochar's regulation of starch biosynthesis. This study aimed to investigate the transcriptome sequencing, which revealed the effects of short-term biochar application (STBA) on tuberous roots of sweet potato and the. We designed four STBA treatments: 0 t·hm^{-2} (CK), 5 t·hm^{-2} (X5t), 10 t·hm^{-2}(X10t), and 20 t·hm^{-2}(X20t), through a comprehensive analysis encompassing physiological data and RNA-seq analysis. The investigation included a comprehensive analysis integrating physiological measurements with RNA-seq data to elucidate the underlying mechanisms. The results showed that STBA enhanced the availability of nitrogen and potassium significantly, while also elevating the soil's pH levels. The 20 t·hm^{-2} STBA substantially enhanced sweet potato yields by 72.21 %, and the starch content of all STBA was not significantly different with CK. STBA decreased the sucrose, starch, glucose, and fructose content of tuberous root by 3–12 %, 1–5 %, 5–8 %, and 5–16 %. DEGs analysis identified distinct gene regulation patterns following biochar treatments, with the 5–10 t·hm^{-2} dosages predominantly down-regulating genes, including those in starch and sucrose metabolism pathways. WGCNA analysis uncovered 11 modules, highlighting biochar's influence on hormone signal transduction pathways, which was validated through qRT-PCR of five key genes. The study's findings light on the impact of STBA on the starch quality of sweet potatoes and inform biochar application strategies in agriculture.

1. Introduction

Agricultural organic waste (AOW) is a significant challenge for agriculture, with annual accumulations reaching nearly 3 billion tons (Alengebawy et al., 2023). Its smart recycling can stimulate soil fertility and decrease the need for chemical fertilizers, thus enhancing agricultural sustainability (Chen et al., 2020; Sayara et al., 2020). Addressing AOW effectively is now a key scientific pursuit. Biochar as a Bio-based material from crop materials has garnered significant attention as it provides a fantastic alternative for utilizing AOW (Tisserant and Cherubini, 2019). Biochar was produced from AOW under high-temperature, oxygen-limited conditions, and possesses a porous framework that alleviates soil compaction and optimizes nutrient and moisture retention, fostering robust crop development (Gabhane et al., 2020; Singh Yadav et al., 2023). Furthermore, its natural alkalinity (from straw sources) counters soil acidity, alleviates the adverse effects of aluminum and iron, and boosts phosphorus accessibility (Zhang et al., 2024).

Biochar studies are bifurcated into short-term (STBA) and long-term (LTBA) studies. STBA focuses on immediate soil and plant responses within a single season, examining biochar's rapid effects on soil fertility and plant development (Singh Yadav et al., 2023). Plants treated with 0.75 % STBA experienced less oxidative stress (Abideen et al., 2020). STBA significantly enhances the synthesis of stress-responsive proteins and proline in plants, thereby preserving their osmotic protection and potential under environmental stress (Haider et al., 2022). Starch is a key determinant of crops' quality. The effects of STBA on starch

* Corresponding author at: The Key Laboratory for Quality Improvement of Agricultural Products of Zhejiang Province, Institute of Root and Tuber Crops, College of Advanced Agricultural Sciences, Zhejiang A&F University, Hangzhou 311300, China.
E-mail address: xuximing@zafu.edu.cn (X. Xu).

https://doi.org/10.1016/j.indcrop.2024.120050
Received 19 September 2023; Received in revised form 6 November 2024; Accepted 10 November 2024
Available online 17 November 2024

properties and the activities of enzymes and expression levels of genes related to starch in two *Japonica* rice cultivars, and 5–10 t/hm^2 can regulate the activity of starch-related enzymes, and this affects the type, content, and fine structure of starch (Gong et al., 2020). STBA elevated the starch content and amylopectin ratio in broomcorn millet (Zhang et al., 2023), and increased the solubility, resistant starch, and swelling capacity in buckwheat, but decreased the amylopectin (Tao et al., 2023). Hence, starch properties across various crops display diverse responses to STBA.

Sweet potato *(Ipomoea batatas* L.) is an industrial crop with high starch content (50–80 % on a dry weight basis), starch extraction rate and its quality are pivotal in assessing the suitability of sweet potatoes for use in the starch industry and as a source for bioenergy production (Lyu et al., 2021). The positive influence of biochar on the levels of key nutrients such as nitrogen, phosphorus, potassium, calcium, magnesium, and sulfur, which are vital for the growth and quality of sweet potatoes (Agbede et al., 2024; Singh et al., 2022; Walter and Rao, 2015). However, the direct effect of biochar on the enzymes and pathways involved in starch synthesis has not been extensively studied. Understanding these effects could provide insights into how biochar application might be optimized to improve the yield and quality of sweet potato starch, which is a significant component of the crop's economic and nutritional value (Lai et al., 2016). The impact of biochar on starch synthesis in sweet potatoes is a topic that warrants further investigation. While it is known that biochar can improve soil health and potentially enhance crop yields and quality by affecting various soil properties, the specific influence on the starch synthesis process in sweet potatoes remains less explored. Further investigation is warranted to clarify the mechanisms of biochar's interaction with soil and plant systems concerning starch synthesis.

Consequently, in this study, we applied four STBA treatments: 0 t·hm^{-2} (CK), 5 t·hm^{-2} (X5t), 10 t·hm^{-2} (X10t), and 20 t·hm^{-2}(X20t), through a comprehensive analysis encompassing physiological data and RNA-seq analysis, which aimed to improve both the yield and quality of sweet potato by applying different biochar to soil and analyzing transcriptional modification in tuberous roots. We hope this research could provide a novel insight that deepens our comprehension of biochar's influence on crops and also furnishes a theoretical foundation and practical guidance for achieving high-yield sweet potato cultivation in reclaimed land and extending biochar applications to other crops.

2. Materials and methods

2.1. Plant materials and growth environment

The pot experiment was conducted from April to October across the years 2022 and 2023 at the farm of Zhejiang A & F University, Hangzhou, Zhejiang Province, China (30°15′N, 119°43′E). The sweet potato cultivar tested was Xinxiang, a high-quality conventional sweet potato cultivar. The soil bulk density is 1.35 g/cm^3, and soil quality was calculated for the top 20 cm layer. The biochar was produced and supplied by Liaoning Golden Future Agricultural Development Co., Ltd. China. The experimental treatments comprised four STBA treatments: 0 t·hm^{-2} (CK), 5 t·hm^{-2} (X5t), 10 t·hm^{-2}(X10t) and 20 t·hm^{-2}(X20t). The amount of biochar was calculated according to Gong et al. (2009). The biochar was mixed with soil into the pots 2 days before sweet potato transplanting. Plastic buckets with a diameter of 40 cm and height of 30 cm were filled with 8 kg of dry soil and then mixed with biochar, with 30 pots per treatment, and two holes for planting sweet potatoes in each pot. The experimental setup incorporated a precise drip irrigation system, featuring a specifically chosen drip tape with a radius of 10 millimeters, and drip emitters delivering a flow rate of 3.0 liters per hour at intervals of 0.3 m. Following the planting of sweet potato slips, an initial irrigation of 100 liters per pot was administered for three days to establish the crop. Subsequently, a reduced watering regimen of 50 liters per pot was maintained and applied every two days. Samples of the tuberous roots, leaves, and stems were meticulously collected in triplicate for each treatment and site 130 days after planting, employing a randomized selection process to ensure representativeness and minimize bias in the data.

2.2. Soil nutrients properties

The biochar specimens were procured in advance of the experimental procedures, whereas the soil samples from the various treatments were gathered after the sweet potato harvest, providing a post-experimental analysis of soil conditions. The soil's nutritional properties, encompassing carbon, available nitrogen, available phosphorus, and available potassium content, were precisely determined using an elemental analyzer (Vario EL cube, Elementar, Germany) across the spectrum of experimental treatments. (Ye et al., 2020). The pH values of the biochar, soil, and treatment samples were analyzed using a pH/ion meter (SDT-60, Zhejiang Top Cloud Agriculture Technology Co., Ltd).

2.3. Dry matter rate, root/shoot ratio(R/S), and texture properties

The dry matter content was determined following the method outlined by Yu et al. (2023). Tuberous roots, leaf, and stem samples were dried to constant mass at 80°C. The root/shoot ratio (R/S) was calculated for each of the nine samples, considering both aboveground and underground biomass, triplicate. Yield was calculated by tuberous root number per plant, fresh weight per tuberous root and planting density. Texture properties of the tuberous roots were ascertained through Textural Profile Analysis (TPA), a technique outlined by Understanding these effects could provide insights into how biochar application might be optimized to improve the yield and quality of sweet potato starch, which is a significant component of the crop's economic and nutritional value analyzed four pivotal textural attributes of tuberous roots: Hardness, Adhesiveness, Cohesiveness, and Springiness. Hardness, measured in Newtons (N), represents the maximum force encountered during the initial extrusion cycle, signifying the point at which the tuberous roots surpass its biological yield point under continuous external pressure, thereby reflecting the sample's resistance to deformation. Adhesiveness, also measured in Newtons (N), denotes the work done by the probe as it detaches from the sample surface, indicative of the root's gelling properties upon contact with the palate, teeth, and tongue during mastication. Cohesiveness is expressed as the ratio of the positive peak area during the second extrusion cycle to that of the first, mirroring the sample's resilience to fragmentation and its capacity to maintain structural integrity during chewing. Springiness is conveyed by the ratio of the heights of the second compression relative to the first, measured in millimeters (mm), which denotes the sample's ability to revert to its original form post-compression, reflecting its springiness.

2.4. Soluble sugar and starch content

Following a 130-day growth period, triplicate samples were randomly selected from each experimental pot to serve as materials for subsequent experiments. The Chinoy iodine colorimetric method quantified the starch content (Chinoy, 1939; Gur et al., 1969; McGrance et al., 1998). Meanwhile, sucrose content was evaluated through the conventional anthrone colorimetric assay. Following the manufacturer's protocols, glucose, and fructose contents were respectively determined using the glucose content detection kit (GOPOD oxidase method) and the fructose content detection kit (Resorcinol process), both provided by Ruixinbio, Quanzhou, China.

2.5. Enzymes activity of starch synthesis

The enzyme activity of starch debranching enzyme (DBE), granule-bound starch synthase (GBSS), starch branching enzyme (SBE), and soluble starch synthase (SSS) were assayed according to Nakamura et al.

(1989) and measured by the kits from Ruixinbio (Quanzhou, China). SBE activity was measured by monitoring the decrease in absorbance at 660 nm due to the reduction of the amylose-iodine complex. The reaction mixture included 65 μL of heat-inactivated enzyme solution or crude enzyme solution, 85 μL of reagent one, 10 μL of reagent two (dissolved in boiling water bath if precipitated), 130 μL of reagent three, and 10 μL of reagent four. After incubation at 37°C for 20 min and heat treatment at 95°C for 5 min, the mixture was cooled, and 200 μL was transferred to a micro-quartz cuvette or a 96-well plate for absorbance measurement at 660 nm. One unit (U) of SBE activity is defined as the amount of enzyme that causes a 1 % decrease in the absorbance of the amylose-iodine complex per milligram of protein at 37°C.SSS activity was determined using a coupled enzyme assay that measures the formation of NADPH. The reaction mixture contained 40 μL of sample, 140 μL of reagent one, 30 μL of reagent two (shaken well before use), 10 μL of reagent three, and 30 μL of reagent four. The mixture was incubated at 30°C for 20 min, followed by heat inactivation at 95–100°C for 2 min. After centrifugation at 12,000 rpm and 4°C for 10 min, the supernatant was used for the colorimetric reaction in a 96-well plate with reagents five, six, and seven. The absorbance was measured at 450 nm. One unit (U) of SSS activity is defined as the amount of enzyme catalyzing the formation of 1 nmol of NADPH per minute at 30°C.GBSS activity was assayed using a coupled enzyme assay that measures the formation of NADPH. The reaction mixture consisted of 40 μL of sample suspension, 140 μL of reagent one, 30 μL of reagent two (shaken well before use), 10 μL of reagent three, and 30 μL of reagent four. The mixture was incubated at 30°C for 20 min, followed by heat inactivation at 95–100°C for 2 min. The absorbance was measured at 450 nm. One unit (U) of GBSS activity is defined as the amount of enzyme catalyzing the formation of 1 nmol of NADPH per minute at 30°C.DBE activity was determined using a modified 3,5-dinitrosalicylic acid method. The reaction mixture contained 20 μL of sample, 200 μL of reagent two, and 280 μL of reagent three. After incubation at 37°C for 30 min, 100 μL of reagent four was added, followed by color development at 95°C for 10 min. The absorbance (ΔA) was measured at 540 nm. One unit (U) of DBE activity is defined as the amount of enzyme that releases 1.0 μmol of soluble sugars (as maltose) from branched starch per hour at 37°C.

2.6. RNA extraction and sequencing

The total RNA extraction was performed from twelve samples at four different biochar treatments by using Tiangen RNA prep Pure Plant Kit (Polysaccharides & Polyphenolics-rich) following the manufacturer's instructions (Yu et al., 2020). RNA purity and concentration were assessed on NanoDrop 2000 (Thermo Fisher Scientific, Wilmington, DE, USA), and the RNA integrity was checked using Agilent Bioanalyzer 2100 (Agilent Technologies, Palo Alto, CA, USA). The NEB Next Ultra small RNA Sample Library Prep Kit for Illumina (NEB, Ipswich, MA, USA) was used to create sequencing libraries by the manufacturer's instructions, and index codes were applied to assign sequences to specific samples. According to the manufacturer's instructions, the TruSeq PE Cluster Kit v4-cBotHS (Illumina, San Diego, CA, USA) was used to cluster the index-coded sample data on a cBot Cluster Generation System. The library preparations were sequenced and paired-end reads were generated on an Illumina HiSeqXten platform after cluster generation. The Biomarker Technologies Co., Ltd. (Beijing, China) has taken charge of mRNA isolation, fragment interruption, cDNA synthesis, adapter addition, PCR amplification, and RNA-seq. There were triplicates for each treatment.

2.7. Sequence data and differential expressed genes (DEGs) analysis

High-quality clean data (clean reads) were filtered from the raw data by removing reads containing adapters and poly-Ns as well as low-quality reads comprising more than 5 % of unknown nucleotides, which were further calculated the GC content, the Phred values, sequence duplication level. The remaining high-quality clean sequencing reads were mapped onto 'Taizhong6' database (https://www.sweetpotao.com/) using HISAT2 software (Kim et al., 2019), and then StringTie (Pertea et al., 2015) was used to assemble the above reads, and the transcriptome of which was reconstructed for subsequent analysis.

The fragments per kilobase of transcript per million fragments mapped (FPKM) as a measure of the transcript or gene expression level, were used to estimate and normalize the sweet potato gene expression levels (Li and Dewey, 2011). The DESeq2 software was used to identify differentially expressed genes (DEGs) across samples or groups (Anders and Huber, 2010). An absolute value of expression difference fold | log2FoldChange | > 1 and significance p-value< 0.05 and FDR (False Discovery Rate)<0.01 were used as thresholds to identify the DEGs (Zhou et al., 2016). The DEGs were applied to the enrichment analysis of GO functions and the KEGG pathway.

2.8. Sequence annotation and weighted gene co-expression network analysis (WGCNA)

Gene function was annotated based on the following databases by using BLAST(E value<1×10–5): Nr (the National Center for Biotechnology Information, non-redundant protein database, ftp://ftp.ncbi.nlm.nih.gov/blast/db/) COG (the Clusters of Orthologous Groups database, ftp://ftp.ncbi.nih.gov/pub/COG/COG2014/data/), Swiss-Prot database (http://web.expasy.org/docs/swiss-prot_guideline.htmL) , KOG(Clusters of orthologous groups for eukaryotic complete genomes, ftp://ftp.ncbi.nih.gov/pub/COG/KOG/kyva), Pfam (http://pfam.xfam.org/), GO (Gene Ontology, http://www.geneontology.org) and KEGG (Kyoto Encyclopedia of Genes and Genomes, http://www.genome.jp/kegg/) . To annotate the gene with Gene Ontology functional enrichment and the Kyoto Encyclopedia of Genes and Genomes (KEGG) pathway, the GOseq R package and KOBAS software were used. DEGs were significantly enriched in GO terms, and KEGG pathways were determined at p-values<0.05. Pathways analysis of upregulated and downregulated genes was performed using KEGG mapper (https://www.genome.jp/kegg/mapper.html) and Plant MetGenMAP.

2.9. qRT-PCR analysis

Total RNA from all the collected samples was extracted using SteadyPure Plant RNA Extraction Kit (AG21019, Accurate Biotechnology, Hunan, Co., Ltd.) following the manufacturer's instructions to validate the RNA-seq data. Reverse transcription was performed on 1 μg of RNA from each sample using the Evo M-MLV RT Mix Kit with gDNA Clean for qPCR (AG11728, Accurate Biotechnology, Hunan, Co., Ltd). Five representative genes from the key pathways of husk biochar were chosen for qRT-PCR analysis. qRT-PCR assay was conducted by a CFX Connect Real-Time System (Bio-Rad, USA) using SYBR Green Premix Pro Taq HS qPCR Kit (AG11701, Accurate Biotechnology, Hunan, Co., Ltd). The primer of genes for qRT-PCR detection is designed by Primer6 software listed in the supplementary Tab. S8. The sweet potato β-Actin gene (GenBank, AY905538) was applied as the internal control. The experiments were conducted for biological triplicates for each gene and the $2^{-\triangle\triangle CT}$ method was used to calculate the result (Mistry et al., 2021). Statistical significance was set to $P < 0.05$.

2.10. Statistic analysis

Statistical analysis employed one-factor analysis of variance with SPSS 23.0 (IBM, Armonk, NY, USA), and Duncan's method was utilized for mean comparisons within varieties at a significance level of $P < 0.05$. Tables were built using Excel 2021 (Microsoft Corporation, Redmond, WA, USA), and Figures were created using Excel 2021 and Adobe Illustrator 2020 software (Adobe Systems Incorporated, San Jose, CA, USA).

3. Results

3.1. Soil nutrients properties

The data on STBA's effect on soil nutrient properties is presented in Table1. The STBA increased the pH, total carbon content, nitrogen(N), and potassium(K) in the soil. It merits attention that with the escalation of biochar application concentration, there is a proportional increment in the concentrations of available nitrogen and potassium. These nutrients attain their apex levels at X20t treatment with respective values of 184.10 and 225.10. It indicated that sufficient STBA can effectively improve the nitrogen and potassium content in the soil ($P < 0.05$). Although the available phosphorus(P) of biochar(64.88±0.13) was higher than CK(37.10±0.03), the available phosphorus(P) of STBA treatments (7.85–11.66) was lower than CK.

3.2. Dry matter rate and R/S of sweet potato

As shown in Tables 2,3 the R/S and yield of all STBA treatments were higher than CK, especially X20t treatment (2132.73±30.45 g/plant) was higher than CK(1238.76±49.0 g/plant) significantly in this study ($P<0.05$). As biochar amount was increased, the yield of sweet potato was increased by 47.19–72.21 %. However, the dry matter of leaves, stems and roots of STBA treatments was not significantly different with CK.

3.3. Texture properties of tuberous root

As Table 3 shown, upon incrementing the biochar application rate, the hardness, cohesiveness, and springiness, exhibited negligible variation ($P > 0.05$). In stark contrast, adhesiveness underwent a biphasic response, initially plummeting from 10.17 N/mm in the control group (CK) to 3.50 N/mm under the 5 t·hm^{-2} biochar treatment (X5t), before a subsequent ascent. The adhesiveness of the tuberous roots after X5t and X10t application was lower than CK significantly ($P < 0.05$).

3.4. Soluble sugar and starch content

For applications such as starch extraction or serving as a resource for industrial starch, the quantity of starch in sweet potatoes is paramount (Kumar et al., 2023). As Fig. 1 shown, the starch content of sweet potato ranged from 53.45 % to 55.83 % under four different STBA treatments in this study, they are not significantly different ($P > 0.05$). The Amylose/amylopectin ratio (AM/AP) of X10t was 47.22 %, which was higher than X5t significantly in this study ($P < 0.05$). AM/AP of all STBA treatments was insignificant with CK ($P > 0.05$). Soluble sugars fulfill the crucial role of precursors in starch synthesis, offering the initial substrates necessary for this metabolic pathway (Zhai et al., 2021, Zhang et al., 2021). The sucrose, glucose, and fructose content of X5t were lower than CK and other STBA treatments significantly. However, the sucrose and glucose content of CK were the highest among all STBA treatments, with 37.41±0.83 mg/g and 72.45±1.28 mg/g, respectively. 5–10 t·hm^{-2} STBA decreased sucrose, fructose, and glucose content of tuberous root.

Table1
Soil nutrients status of the experimental soils.

Soil sample	pH	Carbon (%)	Available nitrogen (mg/kg)	Available phosphorus (mg/kg)	Available potassium (mg/kg)
Biochar	9.32 ±0.05^{a}	0.95 ±0.11^{b}	49.68 ±0.33^{b}	64.88±0.13^{a}	464.00 ±1.93^{a}
CK	6.71 ±0.03^{b}	0.71 ±0.10^{c}	2.62±0.10^{e}	37.10±0.03^{b}	50.92±0.03^{e}
X5t	6.77 ±0.01^{b}	0.76 ±0.10^{c}	28.07 ±0.21^{d}	7.85±0.15^{e}	74.74±0.05^{d}
X10t	6.81 ±0.02^{b}	1.03 ±0.26^{ab}	39.71 ±0.16^{c}	11.66±0.17^{c}	187.70 ±0.06^{c}
X20t	6.90 ±0.03^{b}	1.26 ±0.12^{a}	184.10 ±0.24^{a}	8.28±0.02^{d}	225.10 ±0.08^{b}

Note: Data are means ± SD of biological triplicates. Means denoted by the same letter do not significantly differ at $P < 0.05$, as determined by Duncan's multiple range test.

Table2
R/S, Dry matter rate, and yield of sweet potato.

Treatment	R/S	Yield (Fresh, g/plant)	Dry matter rate (%)			
			Leaf	Stem	Root (except tuberous root)	Tuberous root
CK	1.34 ±0.20^{b}	1238.76 ±49.06^{c}	19.03 ±1.02^{a}	10.05 ±1.01^{a}	28.95 ±2.55^{a}	31.18 ±2.02^{a}
X5t	1.55 ±0.23^{a}	1822.20 ±23.10^{b}	19.02 ±1.12^{a}	10.45 ±1.22^{a}	26.18 ±2.02^{a}	33.77 ±1.32^{a}
X10t	1.56 ±0.20^{a}	1881.80 ±25.18^{b}	18.43 ±1.55^{a}	9.91 ±1.04^{a}	31.47 ±3.02^{a}	31.62 ±2.55^{a}
X20t	1.57 ±0.20^{a}	2132.73 ±30.45^{a}	18.97 ±1.44^{a}	8.87 ±1.62^{a}	25.40 ±2.42^{a}	29.38 ±1.02^{a}

Note: Data are means ± SD of biological triplicates. Means denoted by the same letter do not significantly differ at $P < 0.05$, as determined by Duncan's multiple range test.

Table 3
Texture properties of tuberous root.

Treatment	Hardness N	Adhesiveness N/mm	Cohesiveness Ratio	Springiness mm
CK	106.33±8.90^{a}	10.17±3.44^{a}	0.22±0.03^{a}	5.32±0.43^{a}
X5t	110.99±9.56^{a}	3.50±2.12^{b}	0.21±0.04^{a}	4.95±0.62^{a}
X10t	109.14±9.98^{a}	4.24±2.66^{b}	0.21±0.02^{a}	4.82±0.72^{a}
X20t	107.53±8.42^{a}	6.70±3.78^{ab}	0.21±0.03^{a}	4.75±0.58^{a}

Note: Data are means ± SD of biological triplicates. Means denoted by the same letter do not significantly differ at $P < 0.05$, as determined by Duncan's multiple range test.

3.5. Enzymes activity of starch synthesis

The intricate process of starch synthesis metabolism is inextricably linked to the essential roles played by enzymes specifically associated with its production. These biological catalysts are responsible for the transformation of glucose molecules into complex carbohydrates such as starch and dextrin, highlighting their fundamental importance in carbohydrate metabolism (Zhang et al., 2021). As shown in Figs. 1, 2 and Tab. S3, the activity of the debranching enzyme (DBE) and the granule-bound starch synthase (GBSS) activity of sweet potato tuberous root under X5t STBA had the lowest activity (1.38U/g and 813.74 U/g, respectively) and significantly lower than other treatments ($P < 0.05$). For the DBE activity, the treatments were ranked as follows: X10t > X20t > CK >X5t with no significant difference between the treatment and CK ($P < 0.05$). The soluble starch synthase (SSS) activity of sweet potato tuberous root at X5t and X10t STBA was significantly lower than CK, while X20t showed similar activity to CK ($P < 0.05$). Regarding the enzymes, the treatments could be ranked, from highest SBE activity to lowest, as follows: X20t > CK > X5t> X10t, also with no significant difference between X5t and X20t ($P < 0.05$).

3.6. RNA-sequencing analysis

RNA sequencing analysis serves as a powerful tool for deciphering the complex regulatory mechanisms that crops employ to adapt their gene expression patterns in response to varying biochar environments. This approach allows researchers to peer into the genetic fine-tuning that underlies crop resilience and productivity in soils amended with

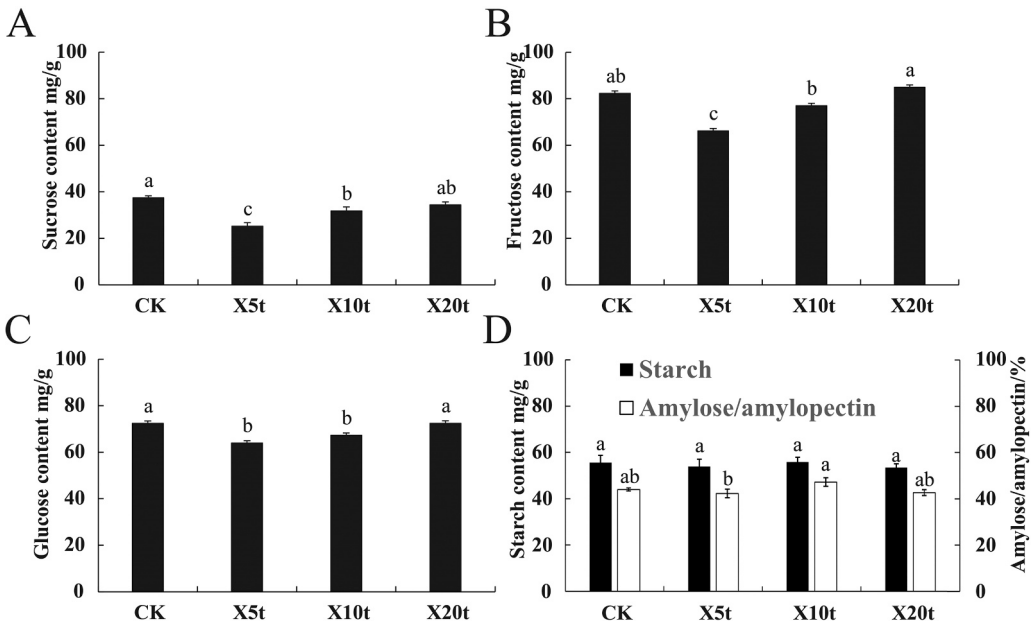

Fig. 1. Sucrose, fructose, glucose, and starch content of tuberous roots of sweet potato under STBA. (A) Sucrose content, (B) Fructose content, (C) Glucose content, (D) Starch content, and Amylose/Amylopectin ratio (AM/AP). Note: The bar plot means starch content and the red line chart means the rate of AM/AP of tuberous roots. Data are means ± SD of biological triplicates. Means denoted by the same letter do not significantly differ at $P < 0.05$, as determined by Duncan's multiple range test.

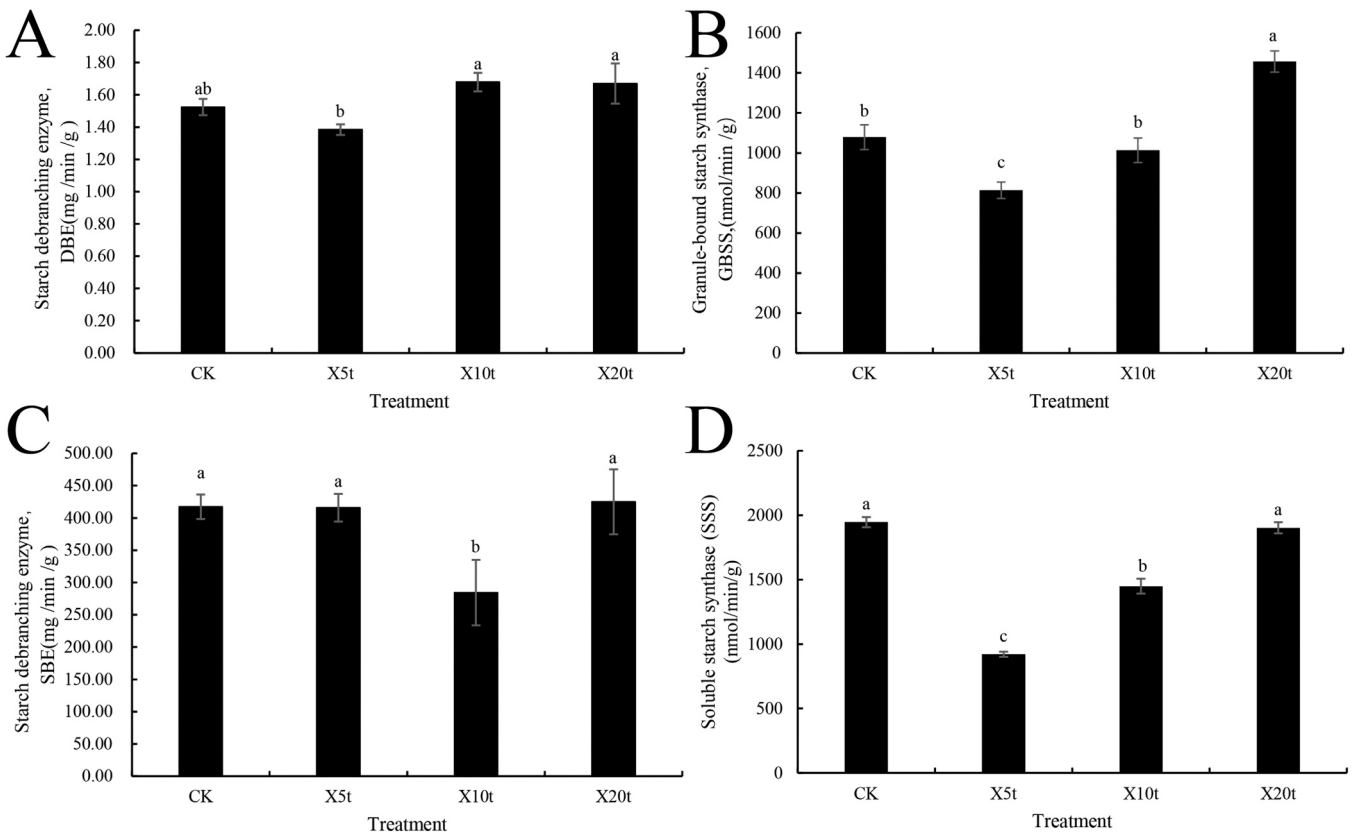

Fig. 2. Starch-related enzymes A: DBE, starch debranching enzyme; B: GBSS, granule-bound starch synthase; C: SBE, starch branching enzyme; D: SSS, soluble starch synthase.

biochar (Zhang et al., 2024). Approximately 517,237,214 clean reads and 77.40 Gb of data were generated after filtering from 12 samples of different STBA treatments. An average of 94.90 % of raw reads had a quality score of Q30 (an error probability for base calling of less than 0.1 %). A total of 432,896,245 multiple-mapped reads were obtained by comparing them to the reference genomes after removing ribosomal RNAs. The sequencing saturation curves for each sample showed that the sequencing depth met the requirements for subsequent analysis 64,

295. Overall, 64,610 genes were detected across samples, which accounted for 74.70 % of the total number of genes (74,088) in the reference group. PCA analysis and clustering of samples were performed based on gene expression level. The results of PCA analysis showed that the differences between STBA treatments and CK were more pronounced at 10 t·hm^{-2} biochar treatment (Fig. S1).

3.7. Differential gene expression (DEGs) analysis

A total of three pairwise comparative analyses (X5t_vs_CK, X10t_vs_CK, X20t_vs_CK) systematically investigated the potential molecular mechanisms of different STBA treatments (Fig. 3, Tab. S5). In total, 504 DEGs (158 up-regulated and 346 down-regulated) were detected in X5t_vs_CK, 1302 DEGs (353 up-regulated and 949 down-regulated) were detected in X10t_vs_CK, and 598 DEGs (407 up-regulated and 191 down-regulated) were detected in X20t_vs_CK (Fig. 3A). A Venn diagram illustrated the distribution of DEGs among the three comparisons (Figs. 2B, 2C). Specifically, 28 down-regulated genes and 7 up-regulated genes overlapped in X5t_vs_CK, X10t_vs_CK, X20t_vs_CK. The BLAST algorithm was utilized to annotate 6961 DEGs based on the Gene Ontology (GO), Kyoto Encyclopedia of Genes and Genomes (KEGG), Clusters of Orthologous Groups (COG), Nr, Swiss-Prot and Pfam databases to functionally characterize expression genes (Table 4). The X5t_vs_CK, X10t_vs_CK, and X20t_vs_CK comparisons exhibited 493 (97.8 %), 1287 (98.8 %), and 589 (98.50 %) DEGs, respectively.

3.8. Enrichment analysis of GO and KEGG of DEGs

GO analysis was used to classify DEGs based on their functions. The number of DEGs assigned GO terms was 401(79.56 %), 1062(81.56 %), 489(81.77 %) DEGs in the X5t_vs_CK, X10t_vs_CK and X20t_vs_CK comparisons, respectively. The GO terms included three aspects: biological process (BP), cellular component (CC), and molecular function (MF). Significant changes in BP were observed in areas such as development, reproduction, growth, and immune system functions. Large changes in MF occurred in the structural molecule, nutrition reservoir, and enzyme activity categories, while those in CC were concentrated in the cell, organelle, and macromolecular complex regions.

According to the GO enrichment analysis, it was worth noting that exposure to biochar greatly influenced the BP, CC, and MF(Fig. 4). The most common biological process GO term among the DEGs was the 'response to stimulus', which had the largest number of genes detected in the three comparisons. Notably, three cellular components GO terms were significantly enriched in the comparisons of X5t_vs_CK and X10t_vs_CK, such as 'intrinsic component of plasma membrane', 'apoplast', and 'plasma membrane part', while no cellular component was detected in the X20t_vs_CK comparison.

We conducted a KEGG pathway analysis to identify active biological processes in the selected STBA treatments. In this analysis, we identified 14, 36, and 14 enriched functional categories in the X5t_vs_CK, X10t_vs_CK, and X20t_vs_CK, comparisons, respectively. Additionally, 1, 16, and 8 significantly enriched functional categories($P<0.05$) were identified for the DEGs in the three comparisons, respectively. Under the 5 t·hm^{-2} STBA (Fig. 5A), 504 DEGs were analyzed for KEGG enrichment. map09101 (Carbohydrate metabolism), was significantly enriched ($P<0.05$). For the 10 t·hm^{-2} STBA treatment, 1302 DEGs were employed for KEGG enrichment analysis. Sixteen representative pathways were significantly enriched. including map00194 (Photosynthesis proteins), map00195(Photosynthesis), map00196 (Photosynthesis - antenna proteins), map09101 (Carbohydrate metabolism), map02000 (Transporters), map00860 (Porphyrin and chlorophyll metabolism), map00500 (Starch and sucrose metabolism) and map00400 (Phenylalanine, tyrosine and tryptophan biosynthesis).

We employed 598 DEGs from the X20t_vs_CK for KEGG enrichment analysis (Fig. 5C). Eight representative pathways were significantly enriched, including map04075 (Plant hormone signal transduction), map09132(Signal transduction), map00860 (Porphyrin and chlorophyll metabolism). Additionally, map00500 (Starch and sucrose metabolism), and map09101 (Carbohydrate metabolism) were enriched under all biochar applications, which indicated that with an increase in biochar application, certain representative pathways also become more prominent. Sweet potatoes exhibited significant biological changes in carbon metabolism, nitrogen metabolism, photosynthesis, sucrose metabolism, and amino acid metabolism among other pathways. It is noteworthy that protein and amino acid metabolism were significantly altered by biochar application.

3.9. Expression of genes involved in metabolic pathways of sucrose and starch metabolic pathways

In this study, there are 48 DEGs involved in starch and sucrose metabolism showed special expression patterns (Fig. 6, Tab. S6). Specifically, under 5t·t·hm^{-2} biochar treatment compared to CK, three DEGs were upregulated, 10 DEGs were downregulated. Similarly, under 10 t·t·hm^{-2} biochar treatment, four DEGs were upregulated, and 21 DEGs were downregulated compared to CK. 11 DEGs were upregulated, and 5 DEGs were downregulated compared to CK in X20t biochar

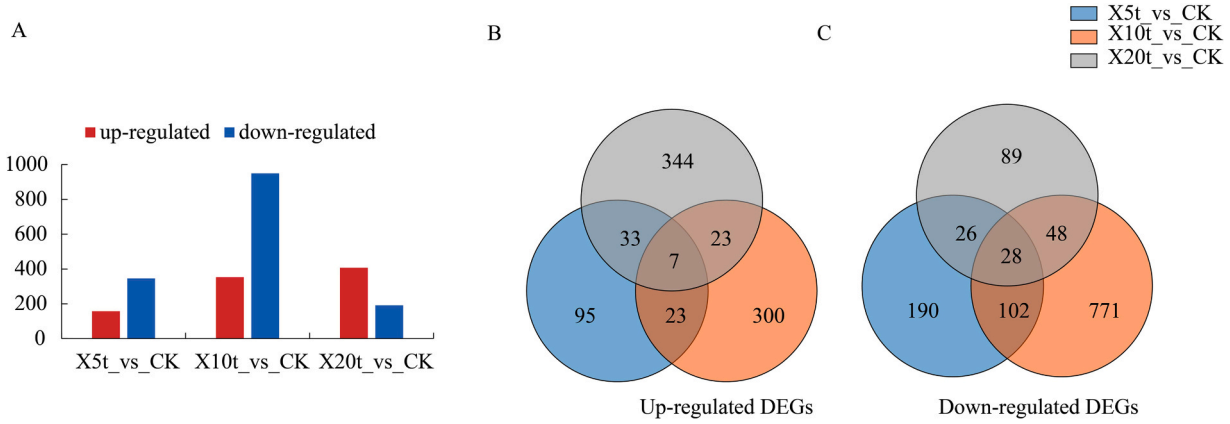

Fig. 3. DEGs between different STBA treatments. (A) Numbers of DEGs in X5t_vs_CK, X10t_vs_CK, X20t_vs_CK. the x-axis shows the paired samples; the y-axis shows the number of DEGs; the red bars represent significantly up-regulated genes($P< 0.05$); the blue bars represent significantly down-regulated genes($P< 0.05$). (B) Venn diagrams of up-regulated DEGs numbers and distributions among three comparisons. (C) Venn diagrams of down-regulated DEGs numbers and distributions among three comparisons. The blue circles represent the number of DEGs in X5t_vs_CK; The yellow circles represent the number of DEGs in X10t_vs_CK; the gray circles represent the number of DEGs in X20t_vs_CK.

Table4
Annotation summaries of DEGs.

DEG set	Annotated DEGs	GO	KEGG	COG	Nr	Swiss-Prot	Pfam
X5t_vs_CK	493	401	195	464	492	420	442
X10t_vs_CK	1287	1062	610	1234	1284	1141	1185
X20t_vs_CK	589	489	231	555	587	496	532

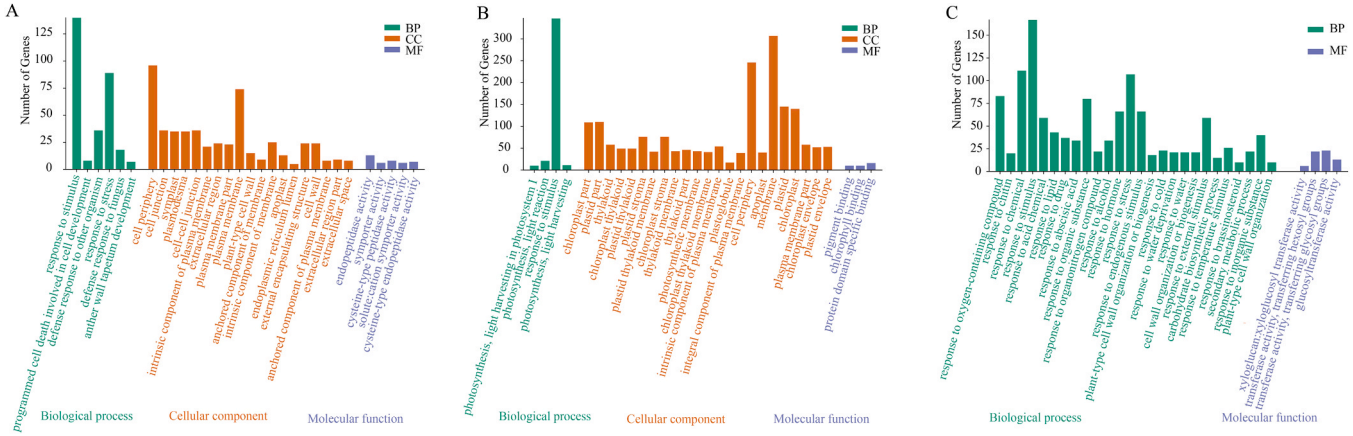

Fig. 4. The enrichment analysis of the DEGs using GO enrichment. (A–C) GO classifications of DEGs in X5t_vs_CK, X10t_vs_CK and X20t_vs_CK, respectively. The y-axis indicates the number of DEGs, and the X-axis indicates the top 30 enriched GO terms. The green-orange and purple colors represent biological processes, cellular components and molecular function, respectively.

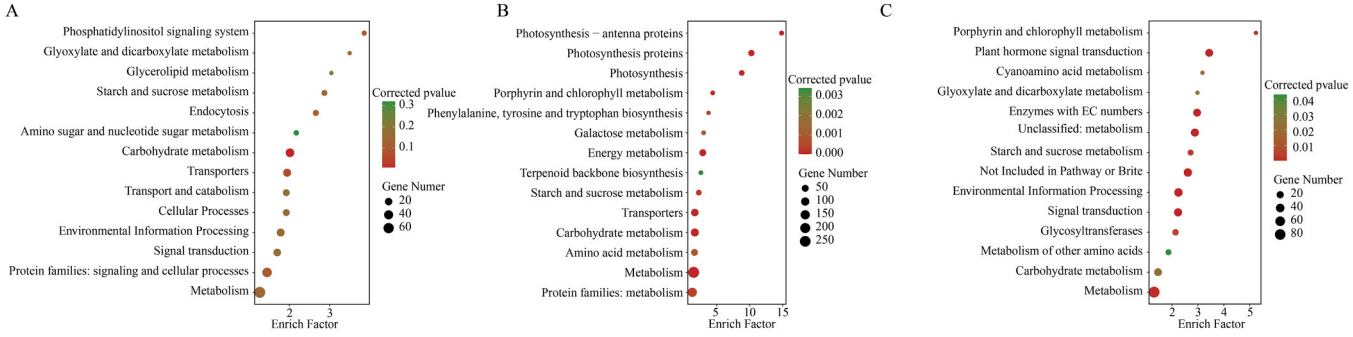

Fig. 5. KEGG pathway enrichment of DEGs under different STBA treatments. A) KEGG enrichment map of DEGs in X5t_vs_CK; B) KEGG enrichment map of DEGs in X10t_vs_CK; C) KEGG enrichment map of DEGs in X20t_vs_CK.

treatment. Sucrose synthesis and hydrolysis are catalyzed by Sucrose Phosphate Synthase (SPS) and Sucrose Synthase (SuSy). SuSy primarily catalyzed sucrose hydrolysis rather than its synthesis (Li et al., 2014). SuSy decomposes sucrose into UDP-glucose and fructose, providing substrates for starch synthesis, and can also convert UDP-glucose and fructose back into sucrose (Zhai et al., 2021). We detected a total of 13 *SuSy* genes with diverse expression patterns, showing low expression across all treatments. Among these, nine *SuSy* genes included two up-regulated genes (*g49561*, *g55056*) and seven down-regulated genes (*g20167, g30039, g505, g55342, g60893, g9231, g9241*) in X10t and four DEGs (3 up-regulated (*g57705, g9225, g9227*) and one down-regulated (*g20130*)) in X20t, while no DEGs were detected in X5t biochar treatment.

It was obvious that no DEGs were involved in the starch synthesis pathway. indicating a consistent pattern in starch conversion to sugars during tuberous root development in sweet potatoes. Starch degradation primarily occurs via the phosphorolytic pathway, catalyzed by the phosphorylase and amylolytic enzymes. Key enzymes such as β-glucosidase(bglX), α-amylase (AMY), and β-amylase (BMY) play crucial roles in starch and sucrose metabolism. In this study, two *IbAMY* genes (*g59290*, *g59297*), one *IbbglB* gene (*g46466*), and one *IbbglX* (*g51057*) were down-regulated in X5t_vs_CK, while the gene(*g13691*) encoding *IbBMY*, along with two genes (*g59316*, *g31641*) encoding *IbbglB* were down-regulated in X10t_vs_CK. In X20t_vs_CK, three genes (*g24112*, *g24863*, *g4495*) encoding *IbbglX*, *g59316* encoding *IbbglB* and *g38231* encoding *IbBMY* were up-regulated while *g13691* encoding *IbBMY* and *g51057*(*bglX*) were down-regulated.

Sucrose degradation into trehalose is facilitated by trehalose 6-phosphate phosphatase (*otsB*) and trehalose-phosphate synthase (*TPS*). However, compared to CK, *g16754* encoding *IbotsB* was down-regulated under X5t and X10t treatment but up-regulated under X20t biochar treatment. The starch was converted into dextrin under the regulation of *g38321*, *g13691*, *g59290,* and *g59297*. The synthesis and metabolism of cellobiose and D-glucose were mediated by β-glucosidase (*IbbglX*, *IbbglB*) and endoglucanase (*IbGN*). RNA-seq data revealed that *IbbglX* and *IbbglB* showed down-regulation in X5t and X10t but showed up-regulation (*g24112, g24863, g4495, g59316*) in X20t biochar treatment.

Note: INV, invertase; GN, glucan endo^{-1},3-β-glucosidase; SuSy, sucrose synthase; SPS, sucrose-phosphate synthase; bglX, β-glucosidase; bglB, β-glucosidase; malZ, α-glucosidase; EG, endoglucanase; AMY, α-amylase; BMY, β- amylase; TPS, trehalose 6-phosphate synthase; otsB, trehalose 6-phosphate phosphatase; TREH, α-trehalase

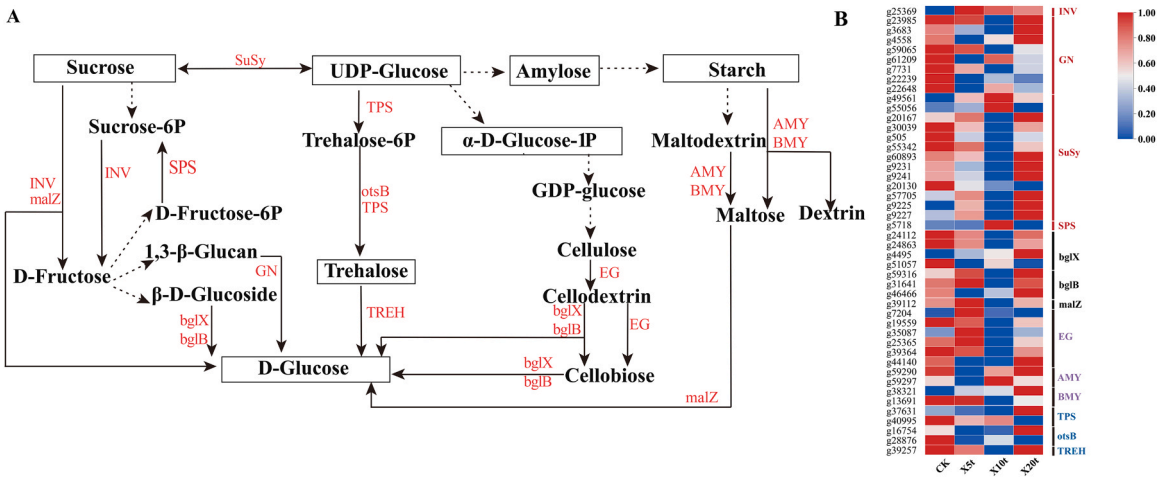

Fig. 6. Starch and sucrose metabolism pathway and expression pattern heatmap of related genes. A) Hypothetical representation of the expression patterns of DEGs involved in the starch and sucrose metabolism in tuberous roots. Upregulated Genes were shown in red, downregulated genes in blue, and non-DEGs in white. B) Expression pattern of related genes in starch and sucrose metabolism pathway.

3.10. Classified the DEGs by WGCNA

Due to the extensive number of samples analyzed by using transcriptome sequencing, we classified the DEGs by WGCNA (Fig. 7A). All genes were classified into eight modules with a particular focus on the magenta module based on its gene expression pattern. Overall, with the increase of biochar application, the expression of the magenta module exhibited higher levels in the X5t, X10t, and X20t compared to the control group. KEGG enrichment of the DEGs within this module revealed significant enrichment in the processes related to plant hormone signal transduction (Fig. 7B). By mapping the genes involved in plant hormone signal transduction, we found that the application of biochar altered the regulation of abscisic acid, auxin, and brassinosteroid (Fig. S3, Tab. S7).

3.11. qRT-PCR validation of the expression of selected genes

We selected five genes that showed substantial change in the RNA-data, including *g26948*(*IAA*) and *g13864* (*SAUR*) for plant hormone signal transduction and two genes namely *α-amylase* gene(*AMY*, *g59297*), *β-amylase* gene (*BMY*, *g13691*) and glucan endo^{-1},3-β-glucosidase (*GN*, *g61209*) in starch and sucrose metabolism verified by qRT-PCR. Specifically, *g26948* and *g13691* displayed down-regulation while *g13864* was up-regulated under 5 t·hm^{-2} and 10 t·hm^{-2} biochar application. Additionally, *g59297* showed down-regulated under 5 t·hm^{-2} biochar application. We observed that the changes in gene expression between different biochar treatments matched the RNA-seq results. However, the fold changes differed, possibly indicating differences in sensitivity between the two methods. The consistent results obtained from the qRT-PCR and RNA-seq analyses suggested that the RNA-seq data were reproducible and reliable (Fig. 8).

4. Discussion

Biochar can enrich soil nutrients and enhance soil particle structure, thereby fostering a more conducive environment for plant growth (Edussuriya et al., 2023). The nutritional profile of biochar is contingent upon the source materials used in its preparation. Biochar derived from fecal matter and sludge tends to be replete with phosphorus, whereas that derived from plant materials is often abundant in potassium (Hossain et al., 2020). Sweet potato has higher K requirements, and K plays key roles in the growth and the economic yield (Wang et al., 2017; Adekiya et al., 2022). In the present study, biochar treatment resulted in a significantly higher available K content in the soil (74.74(X5t)-225.10 mg/kg(X20t)) and higher yield, which indicated that available K exhibited significant positive correlation with yield and improve soil K

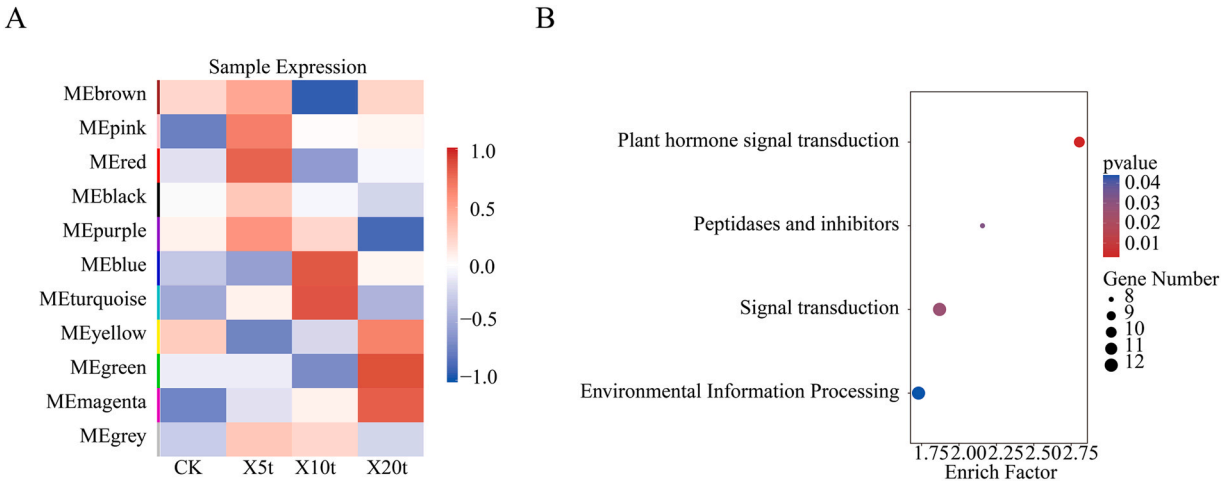

Fig. 7. Functional analysis of key expression patterns of WGCNA. A) Expression patterns of different modules of WGCNA; B) KO enrichment bubble diagram of genes in the magenta module;.

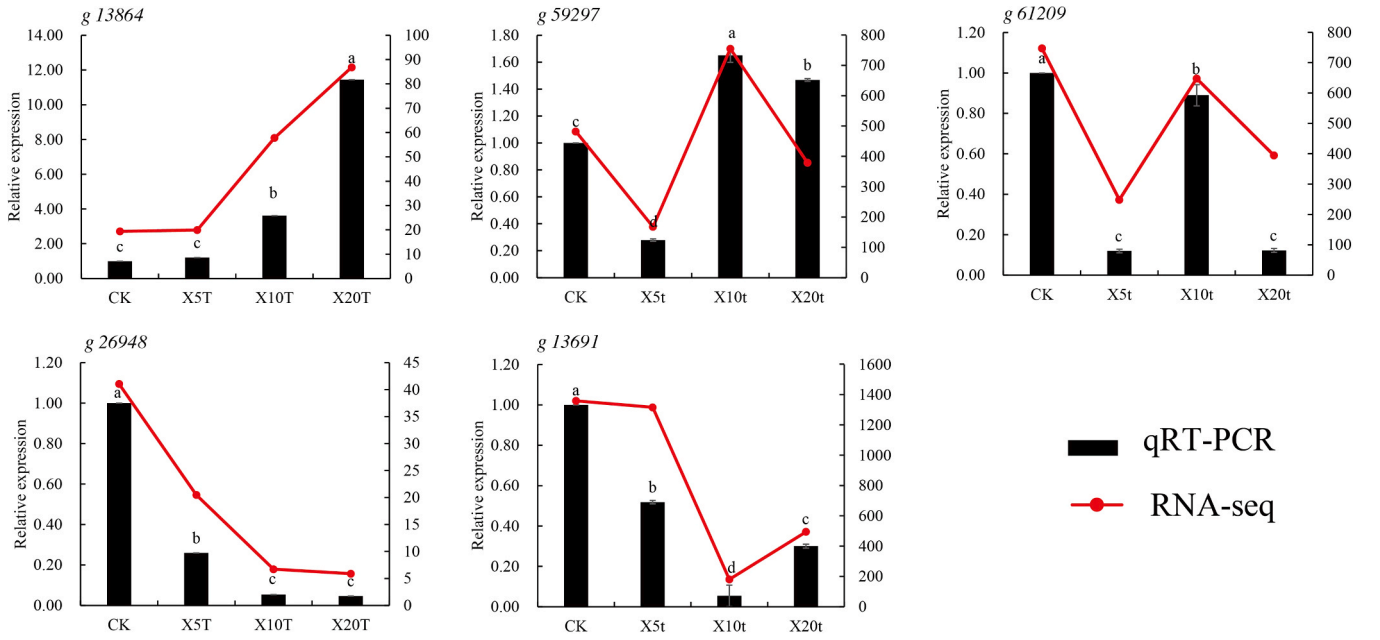

Fig. 8. qRT-PCR validation of representative genes in key pathways affected by biochar application.

availability. Additionally, the soil's pH value increased after biochar application might due to the alkaline nature of biochar. Although biochar is rich in available phosphorus and promotes the efficiency of phosphorus application (Luo et al., 2023), the available phosphorus content of the treatments' soil was lower than that of the control group (CK), indicating that the quantity of biochar ($\geq$5 t·hm^{-2}) applied could potentially sequester available phosphorus within the soil matrix, consequently diminishing its bioavailability to plants. In acid soils, elevated levels of reactive iron and aluminum can react with phosphates to form insoluble compounds, thereby diminishing the phosphorus uptake by plants (Bouray et al., 2021). Previous studies found that the application of biochar significantly reduces the available phosphorus in the rice rhizosphere at long-term (4–9 years) (Yuan et al., 2024; Chen et al., 2022; Jiang et al., 2021). In this study, first-year found this phenomenon. Therefore, to address the potential reduction in phosphorus availability due to increased soil pH from biochar application, it is suggested that future soil management practices include the incorporation of phosphorus fertilizers or the modification of biochar properties. These proactive measures are intended to optimize phosphorus accessibility, ensuring that plants can more effectively absorb this vital nutrient for their growth and development (Luo et al., 2023).

Starch is the main component of sweet potato tuberous roots. It determines the yield of sweet potatoes (Guo et al., 2019). Previous studies have reported that the nitrogen (N) level of soil can influence the growth and development of sweet potato as well as the correlation of starch content and physical properties. Recently, the properties of starches from sweet potato Jishu 25 with the application of N fertilizer (0, 75, and 150 kg/ha), concluded that the level of N treatment affects the amylose content and pasting properties of starch, but shows little effect on starch size and thermal properties (Duan et al., 2019).However, Noda et al. (1996) reported that the level of fertilizer cannot affect the physicochemical properties of starch in two purple- and two yellow-fleshed sweet potato varieties. In this study, compared with CK, biochar treatments resulted in a significantly higher available N content in the soil which increased by 10.70(X5t) to 70.26 times(X20t), but showed a significantly lower starch content(53.43 mg/g) and amylose content (34.71 mg/kg) in X20t. These results might due to the reason that the high N fertilization decreases the amylose content of starch. Li et al. (2013) reported that the high N fertilization treatment decreases the amylose of wheat. Zhu et al. (2017) observed that the application of high nitrogen levels enhances the swelling and gelatinization properties of rice starch, while concurrently reducing its granule size, amylose content, gelatinization temperature, and pasting viscosity.

In this study, we found the available nitrogen and potassium content of the soil increased in STBA treatments. However, the texture properties and starch quality of sweet potatoes were not significantly different from CK, although the enzyme of starch synthesis of sweet potato changed significantly after STBA. A potential explanation for this observation is that STBA upregulates the expression of SPS and SuSy, which in turn stimulates the synthesis of precursors required for starch production. It has a greater effect on starch accumulation than SSS, DBE, etc. This observation is consistent with prior findings in soybeans, where short-term biochar application (STBA) was found to elevate the activity of SPS and SuSy, thereby influencing carbohydrate metabolism. (Zhu et al., 2019). Furthermore, sweet potatoes may exhibit growth-stage-specific responses to biochar, which could dynamically adjust over time. The plants might counteract the synthetic effects of biochar on starch by fine-tuning the rate of starch degradation, thereby maintaining a relatively stable starch content. It is well-known that sucrose converts into glucose and fructose catalyzed by INV. UDP-glucose, synthesized from sucrose degradation catalyzed by sucrose synthase SuSy, served as a substrate for trehalose-6P synthesis mediated by trehalose-6-phosphate synthase (TPS, EC 2.4.1.15). Additionally, we also identified several transcripts encoding pivotal enzymes involved in sucrose and starch metabolic pathways, including sucrose degradation, synthesis pathways, starch degradation, and trehalose degradation pathways. (Chen et al., 2018) Trehalose-6P represents an initial product in trehalose biosynthesis, which is for plant signal metabolic pathways (Li et al., 2014; Paul et al., 2008). Furthermore, studies in *Arabidopsis thaliana*, showed that the sucrose induction would elevate the TPS substrates and UDP-glucose, suggesting that sucrose might activate TPS, ultimately promoting an increase in trehalose-6P levels (Li et al., 2014). KEGG pathway analysis revealed a potential new sucrose hydrolysis pathway in sweet potato tuberous roots under biochar treatment (Fig. 6), implying that sucrose might convert into trehalose-6P through *SuSy* and *TPS*, subsequently converting into trehalose by trehalose 6-phosphate phosphatase (otsB and TPS, EC: 3.1.3.12). We further validated gene expression related to sucrose and starch metabolism in different biochar treatments using qRT-PCR analyses, confirming the expression of DEGs. In summary, biochar application positively

influenced sucrose degradation through its impact on sucrose and starch metabolic pathways.

Plant hormones like gibberellic acid (GA), auxin (IAA), abscisic acid (ABA), cytokinin (CTK), and jasmonic acid, play major roles in root development and growth regulation (Wang and Irving, 2011). CTK and ABA are specifically involved in the formation of stored roots (Matsuo et al., 1983, 1988; Nakatani and Komeichi, 1991). WGCNA analysis showed that the plant hormone signal transduction pathway was enriched in tuberous roots under different biochar treatments. Auxin, essential for cambium cell multiplication and proliferation (Noh et al., 2010), also maintains cambium cells in a meristem state and enhances xylem component quality. The expression of auxin-related genes AUX/IAA and SAUR, were dramatically up-regulated during the tuberous root expansion stage of the *Raphanus sativus*, *Rehmannia glutinosa,* and *Callerya speciosa* (Li et al., 2015; Yu et al., 2016; Yao et al., 2021)., suggesting their role in cell expansion during secondary growth of cambium. ABA plays a role in tuberous root thickening by stimulating meristem cell division (Cai et al., 2022). Two distinct ABA signal transduction pathways have been identified: the PYLs-PP2C-SnRK2 pathway (Liu et al., 2022) and the CHLH-WRAKY pathway, which have been demonstrated to play a role in the regulation of fruit ripening (Sun et al., 2011; Chai et al., 2011; Jia et al., 2011). Additionally, ABA plays a role in tuberous root thickening by stimulating meristem cell division (Cai et al., 2022). Previous research has linked PP2C to plant abiotic stress tolerance (Saez et al., 2004; Lu et al., 2019; Zhang et al., 2017), while ABA has been associated with the sugar response pathway (Rook et al., 2006). Low sucrose levels induced *AtSUC9*, increasing ABA levels through ABA-inducible genes, and enhancing resilience to abiotic stress (Jia et al., 2015). In our study, *g26948* encoding PP2C showed down-regulated under X10t and X20t biochar applications. These findings suggest that biochar application may influence in plant tolerance to abiotic stress. In summary, the application of biochar exerts a complex influence on the tuberous roots of sweet potatoes, affecting both starch and sucrose metabolic processes, as well as plant hormone signaling pathways. These impacts collectively lead to enhancements in yield and the sweet potatoes' resilience against environmental stressors.

5. Conclusions

This study demonstrates that STBA substantially increased sweet potato yields and enhanced soil fertility, with optimal effects of 20 $t \cdot hm^{-2}$ STBA. While the adhesiveness and soluble sugar of tuberous root decreased at 5–10 $t \cdot hm^{-2}$ STBA, it had no significant impact on starch content or the AM/AP ratio. STBA enhances sweet potato yields without compromising starch quality, crucial for producing industrial-grade sweet potatoes. Biochar likely augments sweet potato yields and stress tolerance by modulating key enzymatic activities and plant hormone signaling, such as SPS, SuSy, IAA, and ABA. STBA effectively increases the yield of sweet potatoes without negatively affecting their quality, confirming its status as a potent strategy for yield enhancement in sweet potato cultivation. Consequently, STBA not only boosts the yields and stress tolerance of sweet potatoes but also maintains the integrity of their starch, establishing a solid scientific foundation for the application of biochar in agricultural practices.

CRediT authorship contribution statement

Ximing Xu: Writing – review & editing, Writing – original draft, Visualization, Resources, Project administration, Methodology, Investigation, Funding acquisition, Data curation, Conceptualization. **Jingzhen Zhang:** Writing – original draft, Visualization. **Zunfu Lv:** Resources, Project administration, Funding acquisition. **Taojun Li:** Formal analysis, Data curation. **Jing Li:** Funding acquisition. **Yueming Zhu:** Validation. **Guoquan Lu:** Software, Funding acquisition.

Declaration of Competing Interest

Authors declared that they have no conflicts of interest to this work. We declare that we do not have any commercial or associative interest that represents a conflict of interest in connection with the work submitted.

Acknowledgements

This research was funded by Research funding project of Zhejiang Provincial Department of Education (Y202147184), Scientific Research Foundation for the Introduction of Talent by Zhejiang A&F University (2021LFR017), China Agriculture Research System (CARS-10), the Natural Science Foundation of China (32071897, 32272222, and 32372075), the Key Research and Development Program of Zhejiang Province (2021C02057), and Huzhou Public Welfare Application Research Key Project (2023GZ47).

Appendix A. Supporting information

Supplementary data associated with this article can be found in the online version at doi:10.1016/j.indcrop.2024.120050.

Data availability

Data will be made available on request.

References

Abideen, Z., Koyro, H.W., Huchzermeyer, B., Ansari, R., Zulfiqar, F., Gul, B., 2020. Ameliorating effects of biochar on photosynthetic efficiency and antioxidant defence of Phragmites karka under drought stress. Plant Biol. 22, 259–266.

Adekiya, A.O., Adebiyi, O.V., Ibaba, A.L., Aremu, C., Ajibade, R.O., 2022. Effects of wood biochar and potassium fertilizer on soil properties, growth and yield of sweet potato (Ipomoea batatas). Heliyon 8, e11728.

Agbede, T.M., Oyewumi, A., Agbede, G.K., Adekiya, A.O., Adebiyi, O.T.V., Abisuwa, T. A., Ijigbade, J.O., Ogundipe, C.T., Wewe, A.O., Olawoye, O.D., Eifediyi, E.K., 2024. Impacts of poultry manure and biochar amendments on the nutrients in sweet potato leaves and the minerals in the storage roots. Sci. Rep. 14, 16598.

Alengebawy, A., Ran, Y., Ghimire, N., Osman, A.I., Ai, P., 2023. Rice straw for energy and value-added products in China: a review. Environ. Chem. Lett. 1–32.

Anders, S., Huber, W., 2010. Differential expression analysis for sequence count data. Genome Biol. 11, R106.

Bouray, M., Moir, J.L., Lehto, N.J., Condron, L.M., Touhami, D., Hummel, C., 2021. Soil pH effects on phosphorus mobilization in the rhizosphere of *Lupinus angustifolius*. Plant Soil 469, 387–407.

Cai, Z., Cai, Z., Huang, J., Wang, A., Ntambiyukuri, A., Chen, B., Zheng, G., Li, H., Huang, Y., Zhan, J., Xiao, D., He, L., 2022. Transcriptomic analysis of tuberous root in two sweet potato varieties reveals the important genes and regulatory pathways in tuberous root development. BMC Genom. 23, 473.

Chai, Y.M., Jia, H.F., Li, C.L., Dong, Q.H., Shen, Y.Y., 2011. *FaPYR1* is involved in strawberry fruit ripening. J. Exp. Bot. 62, 5079–5089.

Chen, H., Yuan, J., Chen, G., Zhao, X., Wang, S., Wang, D., Wang, L., Wang, Y., Wang, Y., 2022. Long-term biochar addition significantly decreases rice rhizosphere available phosphorus and its release risk to the environment. Biochar 4, 54.

Chen, L., Sun, P., Zhou, F., Li, Y., Chen, K., Jia, H., Yan, M., Gong, D., Ouyang, P., 2018. Synthesis of rebaudioside D, using glycosyltransferase UGTSL2 and in situ UDP-glucose regeneration. Food Chem. 259, 286–291.

Chen, S., Zhang, X., Shao, L., Sun, H., Niu, J., Liu, X., 2020. Effects of straw and manure management on soil and crop performance in North China Plain. CATENA 187, 104359.

Chinoy, J.J., 1939. A new colorimetric method for the determination of starch applied to soluble starch, natural starches, and flour. *Mikrochemie vereinigt.* Mit. Mikrochim. Acta 26, 132–142.

Duan, W.X., Zhang, H.Y., Xie, B.T., Wang, B.Q., Zhang, L.M., 2019. Impacts of nitrogen fertilization rate on the root yield, starch yield and starch physicochemical properties of the sweet potato cultivar Jishu 25. PLoS One 14, e0221351.

Edussuriya, R., Rajapaksha, A.U., Jayasinghe, C., Pathirana, C., Vithanage, M., 2023. Influence of biochar on growth performances, yield of root and tuber crops and controlling plant-parasitic nematodes. Biochar 5, 68.

Gabhane, J.W., Bhange, V.P., Patil, P.D., Bankar, S.T., Kumar, S., 2020. Recent trends in biochar production methods and its application as a soil health conditioner: a review. SN Appl. Sci. 2, 1307.

Gong, D.K., Xu, X.M., Wu, L.A., Dai, G.J., Zheng, W.J., Xu, Z.J., 2020. Effect of biochar on rice starch properties and starch-related gene expression and enzyme activities. Sci. Rep. 10, 16917.

Gong, W., Yan, X., Wang, J., Hu, T., Gong, Y., 2009. Long-term manure and fertilizer effects on soil organic matter fractions and microbes under a wheat–maize cropping system in northern China. Geoderma 149, 318–324.
Guo, K., Liu, T., Xu, A., Zhang, L., Bian, X., Wei, C., 2019. Structural and functional properties of starches from root tubers of white, yellow, and purple sweet potatoes. Food Hydrocoll. 89, 829–836.
Gur, A., Cohen, A., Bravdo, B.-A., 1969. Colorimetric method for starch determination. J. Agric. Food Chem. 17, 347–351.
Haider, F.U., Wang, X., Farooq, M., Hussain, S., Cheema, S.A., Ain, N.U., Virk, A.L., Ejaz, M., Janyshova, U., Liqun, C., 2022. Biochar application for the remediation of trace metals in contaminated soils: implications for stress tolerance and crop production. Ecotoxicol. Environ. Saf. 230, 113165.
Hossain, M.Z., Bahar, M.M., Sarkar, B., Donne, S.W., Ok, Y.S., Palansooriya, K.N., Kirkham, M.B., Chowdhury, S., Bolan, N., 2020. Biochar and its importance on nutrient dynamics in soil and plant. Biochar 2, 379–420.
Jia, H.F., Chai, Y.M., Li, C.L., Lu, D., Luo, J.J., Qin, L., Shen, Y.Y., 2011. Abscisic acid plays an important role in the regulation of strawberry fruit ripening. Plant Physiol. 157, 188–199.
Jia, W., Zhang, L., Wu, D., Liu, S., Gong, X., Cui, Z., Cui, N., Cao, H., Rao, L., Wang, C., 2015. Sucrose transporter AtSUC9 mediated by a low sucrose level is involved in Arabidopsis abiotic stress resistance by regulating sucrose distribution and aba accumulation. Plant Cell Physiol. 56, 1574–1587.
Jiang, B., Shen, J., Sun, M., Hu, Y., Jiang, W., Wang, J., Li, Y., Wu, J., 2021. Soil phosphorus availability and rice phosphorus uptake in paddy fields under various agronomic practices. Pedosphere 31, 103–115.
Kim, D., Paggi, J.M., Park, C., Bennett, C., Salzberg, S.L., 2019. Graph-based genome alignment and genotyping with HISAT2 and HISAT-genotype. Nat. Biotechnol. 37, 907–915.
Kumar, Y., Shikha, D., Guzmán-Ortiz, F.A., Sharanagat, V.S., Kumar, K., Saxena, D.C., 2023. Starch: current production and consumption trends. Starch: Advances in Modifications, Technologies and Applications. Springer International Publishing, Cham, pp. 1–10.
Lai, Y.C., Wang, S.Y., Gao, H.Y., Nguyen, K.M., Nguyen, C.H., Shih, M.C., Lin, K.H., 2016. Physicochemical properties of starches and expression and activity of starch biosynthesis-related genes in sweet potatoes. Food Chem. 199, 556–564.
Li, B., Dewey, C.N., 2011. RSEM: accurate transcript quantification from RNA-Seq data with or without a reference genome. BMC Bioinform. 12, 323.
Li, M., Yang, Y., Li, X., Gu, L., Wang, F., Feng, F., Tian, Y., Wang, F., Wang, X., Lin, W., Chen, X., Zhang, Z., 2015. Analysis of integrated multiple 'omics' datasets reveals the mechanisms of initiation and determination in the formation of tuberous roots in Rehmannia glutinosa. J. Exp. Bot. 66, 5837–5851.
Li, W.H., Shan, Y.L., Xiao, X.L., Zheng, J.M., Luo, Q.G., Ouyang, S.H., Zhang, G.Q., 2013. Effect of nitrogen and sulfur fertilization on accumulation characteristics and physicochemical properties of a- and b-wheat starch. J. Agric. Food Chem. 61, 2418–2425.
Li, X., Wang, C., Cheng, J., Zhang, J., Da Silva, J.A., Liu, X., Duan, X., Li, T., Sun, H., 2014. Transcriptome analysis of carbohydrate metabolism during bulblet formation and development in *Lilium davidii* var. unicolor. BMC Plant Biol. 14, 358.
Liu, S., Lu, C., Jiang, G., Zhou, R., Chang, Y., Wang, S., Wang, D., Niu, J., Wang, Z., 2022. Comprehensive functional analysis of the PYL-PP2C-SnRK2s family in *Bletilla striata* reveals that BsPP2C22 and BsPP2C38 interact with BsPYLs and BsSnRK2s in response to multiple abiotic stresses. Front. Plant Sci. 13, 963069.
Lu, T., Zhang, G., Wang, Y., He, S., Sun, L., Hao, F., 2019. Genome-wide characterization and expression analysis of PP2CA family members in response to ABA and osmotic stress in Gossypium. PeerJ 7, e7105.
Luo, D., Wang, L., Nan, H., Cao, Y., Wang, H., Kumar, T.V., Wang, C., 2023. Phosphorus adsorption by functionalized biochar: a review. Environ. Chem. Lett. 21, 497–524.
Lyu, R., Ahmed, S., Fan, W., Yang, J., Wu, X., Zhou, W., Zhang, P., Yuan, L., Wang, H., 2021. Engineering properties of sweet potato starch for industrial applications by biotechnological techniques including genome editing. Int. J. Mol. Sci. 22, 9533.
Matsuo, T., Mitsuzono, H., Okada, R., Itoo, S., 1988. Variations in the levels of major free cytokinins and free abscisic acid during tuber development of sweet potato. J. Plant Growth Regul. 7, 249–258.
Matsuo, T., Yoneda, T., Itoo, S., 1983. Identification of free cytokinins and the changes in endogenous levels during tuber development of sweet potato (*Ipomoea batatas* Lam.). Plant Cell Physiol. 24, 1305–1312.
McGrance, S.J., Cornell, H.J., Rix, C.J., 1998. A Simple and Rapid Colorimetric Method for the Determination of Amylose in Starch Products. Starch - Stärke 50, 158–163.
Mistry, J., Chuguransky, S., Williams, L., Qureshi, M., Salazar, G.A., Sonnhammer, E.L.L., Tosatto, S.C.E., Paladin, L., Raj, S., Richardson, L.J., Finn, R.D., Bateman, A., 2021. Pfam: the protein families database in 2021. Nucleic Acids Res. 49, D412–D419.
Nakamura, Y., Yuki, K., Park, S.-Y., Ohya, T., 1989. Carbohydrate metabolism in the developing endosperm of rice grains. Plant Cell Physiol. 30, 833–839.
Nakatani, M., Komeichi, M., 1991. Changes in the endogenous level of zeatin riboside, abscisic acid and indole acetic acid during formation and thickening of tuberous roots in sweet potato. Jpn J. Crop Sci. 60, 91–100.
Noda, T., Takahata, Y., Sato, T., Ikoma, H., Mochida, H., 1996. Physiochemical properties of starches from purple and orange fleshed sweet potato roots at two levels of fertilizer. Starch 48, 395–399.
Noh, S.A., Lee, H.S., Huh, E.J., Huh, G.H., Paek, K.H., Shin, J.S., Bae, J.M., 2010. SRD1 is involved in the auxin-mediated initial thickening growth of storage root by enhancing proliferation of metaxylem and cambium cells in sweetpotato (Ipomoea batatas). J. Exp. Bot. 61, 1337–1349.
Paul, M.J., Primavesi, L.F., Jhurreea, D., Zhang, Y., 2008. Trehalose metabolism and signaling. Annu Rev. Plant Biol. 59, 417–441.
Pertea, M., Pertea, G.M., Antonescu, C.M., Chang, T.C., Mendell, J.T., Salzberg, S.L., 2015. StringTie enables improved reconstruction of a transcriptome from RNA-seq reads. Nat. Biotechnol. 33, 290–295.
Rook, F., Hadingham, S., Li, Y., Bevan, M., 2006. Sugar and ABA response pathways and the control of gene expression. Plant, Cell Environ. 29, 426–434.
Saez, A., Apostolova, N., Gonzalez-Guzman, M., Gonzalez-Garcia, M.P., Nicolas, C., Lorenzo, O., Rodriguez, P.L., 2004. Gain-of-function and loss-of-function phenotypes of the protein phosphatase 2C HAB1 reveal its role as a negative regulator of abscisic acid signalling. Plant J. 37, 354–369.
Sayara, T., Basheer-Salimia, R., Hawamde, F., Sánchez, A., 2020. Recycling of organic wastes through composting: process performance and compost application in agriculture. Agronomy 10, 1838.
Singh, H., Northup, B.K., Rice, C.W., Prasad, P.V.V., 2022. Biochar applications influence soil physical and chemical properties, microbial diversity, and crop productivity: a meta-analysis. Biochar 4, 8.
Singh Yadav, S.P., Bhandari, S., Bhatta, D., Poudel, A., Bhattarai, S., Yadav, P., Ghimire, N., Paudel, P., Paudel, P., Shrestha, J., Oli, B., 2023. Biochar application: a sustainable approach to improve soil health. J. Agric. Food Res. 11, 100498.
Sun, L., Wang, Y.P., Chen, P., Ren, J., Ji, K., Li, Q., Li, P., Dai, S.J., Leng, P., 2011. Transcriptional regulation of SlPYL, SlPP2C, and SlSnRK2 gene families encoding ABA signal core components during tomato fruit development and drought stress. J. Exp. Bot. 62, 5659–5669.
Tao, J., Wan, C., Leng, J., Dai, S., Wu, Y., Lei, X., Wang, J., Yang, Q., Wang, P., Gao, J., 2023. Effects of biochar coupled with chemical and organic fertilizer application on physicochemical properties and in vitro digestibility of common buckwheat (Fagopyrum esculentum Moench) starch. Int. J. Biol. Macromol. 246, 125591.
Tisserant, A., Cherubini, F., 2019. Potentials, limitations, co-benefits, and trade-offs of biochar applications to soils for climate change mitigation. Land 8, 179.
Walter, R., Rao, B.K.R., 2015. Biochars influence sweet-potato yield and nutrient uptake in tropical Papua New Guinea. J. Plant Nutr. Soil Sci. 178, 393–400.
Wang, J.D., Hou, P., Zhu, G.P., Dong, Y., Hui, Z., Ma, H., Xu, X.J., Nin, Y., Ai, Y., Zhang, Y., 2017. Potassium partitioning and redistribution as a function of K-use efficiency under K deficiency in sweet potato (*Ipomoea batatas* L.). Field Crops Res. 211, 147–154.
Wang, Y.H., Irving, H.R., 2011. Developing a model of plant hormone interactions. Plant Signal. Behav. 6, 494–500.
Yao, S., Lan, Z., Huang, R., Tan, Y., Huang, D., Gu, J., Pan, C., 2021. Hormonal and transcriptional analyses provides new insights into the molecular mechanisms underlying root thickening and isoflavonoid biosynthesis in Callerya speciosa (Champ. ex Benth.) Schot. Sci. Rep. 11, 9.
Ye, X., Abe, S., Zhang, S., 2020. Estimation and mapping of nitrogen content in apple trees at leaf and canopy levels using hyperspectral imaging. Precis. Agric. 21, 198–225.
Yu, J.J., Su, D., Yang, D.J., Dong, T.T., Tang, Z.H., Li, H.M., Han, Y.H., Li, Z.Y., Zhang, B. H., 2020. Chilling and heat stress-induced physiological changes and microrna-related mechanism in sweetpotato (*Ipomoea batatas* L.). Front. Plant Sci. 11, 687.
Yu, R., Wang, J., Xu, L., Wang, Y., Wang, R., Zhu, X., Sun, X., Luo, X., Xie, Y., Everlyne, M., Liu, L., 2016. Transcriptome profiling of taproot reveals complex regulatory networks during taproot thickening in radish (*Raphanus sativus* L.). Front. Plant Sci. 7, 1210.
Yu, Y., Kleuter, M., Dinani, S.T., Trindade, L.M., Van Der Goot, A.J., 2023. The role of plant age and leaf position on protein extraction and phenolic compounds removal from tomato (*Solanum lycopersicum*) leaves using food-grade solvents. Food Chem. 406, 135072.
Yuan, J., Chen, H., Chen, G., Pokharel, P., Chang, S.X., Wang, Y., Wang, D., Yan, X., Wang, S., Wang, Y., 2024. Long-term biochar application influences phosphorus and associated iron and sulfur transformations in the rhizosphere. Carbon Res. 3, 25.
Zhai, Z.Y., Keereetaweep, J., Liu, H., Xu, C.C., Shanklin, J., 2021. The role of sugar signaling in regulating plant fatty acid synthesis. Front. Plant Sci. 12, 643843.
Zhang, K., Wu, Z., Tang, D., Luo, K., Lu, H., Liu, Y., Dong, J., Wang, X., Lv, C., Wang, J., Lu, K., 2017. Comparative transcriptome analysis reveals critical function of sucrose metabolism related-enzymes in starch accumulation in the storage root of sweet potato. Front. Plant Sci. 8, 914.
Zhang, M., Mukhamed, B., Yang, Q., Luo, Y., Tian, L., Yuan, Y., Huang, Y., Feng, B., 2023. Biochar and nitrogen fertilizer change the quality of waxy and non-waxy broomcorn millet (*Panicum miliaceum* L.) starch. Foods 12, 3009.
Zhang, X., Feng, X., Chai, N., Kuzyakov, Y., Zhang, F., Li, F.-M., 2024. Biochar effects on crop yield variability. Field Crops Res. 316, 109518.
Zhang, X., Guo, D., Blennow, A., Zörb, C., 2021. Mineral nutrients and crop starch quality. Trends Food Sci. Technol. 114, 148–157.
Zhou, Q., Guo, J.-J., He, C.-T., Shen, C., Huang, Y.-Y., Chen, J.-X., Guo, J.-H., Yuan, J.-G., Yang, Z.-Y., 2016. Comparative transcriptome analysis between low- and high-cadmium-accumulating genotypes of pakchoi (Brassica chinensis L.) in response to cadmium stress. Environ. Sci. Technol. 50, 6485–6494.
Zhu, D., Zhang, H., Guo, B., Xu, K., Dai, Q., Wei, C., Zhou, G., Huo, Z., 2017. Effects of nitrogen level on structure and physicochemical properties of rice starch. Food Hydrocoll. 63, 525–532.
Zhu, Q., Kong, L.J., Shan, Y.Z., Yao, X.D., Zhang, H.J., Xie, F.T., Ao, X., 2019. Effect of biochar on grain yield and leaf photosynthetic physiology of soybean cultivars with different phosphorus efficiencies. J. Integr. Agric. 18, 2242–2254.

ARTICLES FOR FACULTY MEMBERS

INVESTIGATING THE ROLE OF GIBBERELLIC ACID (GA) AND ABSCISIC ACID (ABA) CROSS-TALK IN ENHANCING TUBEROUS ROOT DEVELOPMENT IN SWEET POTATOES

Transcriptomic analysis of tuberous root in two sweet potato varieties reveals the important genes and regulatory pathways in tuberous root development. BMC / Cai, Z., Cai, Z., Huang, J., Wang, A., Ntambiyukuri, A., Chen, B., Zheng, G., Li, H., Huang, Y., Zhan, J., Xiao, D., & He, L.

BMC Genomics
Volume 23 (2022) 473 Pages 1-19
https://doi.org/10.1186/s12864-022-08670-x
(Database: Springer Nature)

BMC Genomics

RESEARCH

Open Access

Transcriptomic analysis of tuberous root in two sweet potato varieties reveals the important genes and regulatory pathways in tuberous root development

Zhaoqin Cai[1,2], Zhipeng Cai[1], Jingli Huang[1], Aiqin Wang[1,3], Aaron Ntambiyukuri[1], Bimei Chen[4], Ganghui Zheng[4], Huifeng Li[5], Yongmei Huang[5], Jie Zhan[1,3], Dong Xiao[1,3*] and Longfei He[1,3*]

Abstract

Background: Tuberous root formation and development is a complex process in sweet potato, which is regulated by multiple genes and environmental factors. However, the regulatory mechanism of tuberous root development is unclear.

Results: In this study, the transcriptome of fibrous roots (R0) and tuberous roots in three developmental stages (Rl, R2, R3) were analyzed in two sweet potato varieties, GJS-8 and XGH. A total of 22,914 and 24,446 differentially expressed genes (DEGs) were identified in GJS-8 and XGH respectively, 15,920 differential genes were shared by GJS-8 and XGH. KEGG pathway enrichment analysis showed that the DEGs shared by GJS-8 and XGH were mainly involved in "plant hormone signal transduction""starch and sucrose metabolism" and "MAPK signal transduction". Trihelix transcription factor (Tai6.25300) was found to be closely related to tuberous root enlargement by the comprehensive analysis of these DEGs and weighted gene co-expression network analysis (WGCNA).

Conclusion: A hypothetical model of genetic regulatory network for tuberous root development of sweet potato is proposed, which emphasizes that some specific signal transduction pathways like "plant hormone signal transduction""Ca^{2+}signal""MAPK signal transduction" and metabolic processes including "starch and sucrose metabolism" and "cell cycle and cell wall metabolism" are related to tuberous root development in sweet potato. These results provide new insights into the molecular mechanism of tuberous root development in sweet potato.

Keywords: Tuberous root, Transcriptomic analysis, Sweet potato, Development, Core genes

Introduction

Sweet potato (*Ipomoea batatas* L) is a dicotyledonous plant of the family Convolvulaceae, growing in tropical, subtropical, and temperate regions, it is the most important rhizome crop after potato and cassava, and one of the most important food crops in the world [1], with an annual global output of more than 100 million tons. China is the largest sweet potato producer in the world, accounting for 80–85% of the global output [1]. Sweet potato is nutritious and contains many ingredients for human health, which has the medicinal values such as anti-cancer, anti-diabetes and anti-inflammatory activity [2, 3], and has been selected as one of the test foods for long-term space travel [4]. The tuberous root of sweet

*Correspondence: xiaodong@gxu.edu.cn; lfhe@gxu.edu.cn

[1] National Demonstration Center for Experimental Plant Science Education, College of Agriculture, Guangxi University, Nanning 530004, People's Republic of China
Full list of author information is available at the end of the article

potato is rich in starch and soluble sugar, and its biomass is the highest in all crops. Sweet potato is listed as the key raw material for ethanol production because of its high starch content [5]. How to improve the yield and quality of sweet potato has become a top priority.

Endogenous hormones play an important role in the process of tuberous root expansion. Cytokinin (CTK) and abscisic acid (ABA) are involved in the formation of stored roots [6–11], t-zeatin is thought to play an important role in the induction of tuberous roots by activating the primary cambium. ABA regulates the thickening of tuberous roots by activating the cell division of meristem. The content of Auxin (IAA) increased gradually at the initial stage of root expansion in sweet potato tuberous root, and began to decrease after the beginning of secondary growth, while the content of ABA and cytokinin was steadily increased [12, 13]. In tuberous root, the content of jasmonic acid (JA) was very high, while the contents in burdock root and fibrous root were less [14].

The growth and expansion of tuberous root in sweet potato are genetically regulated. Previous studies have shown that MADS-box, KNOX genes were highly expressed and related to the expansion of tuberous root in sweet potato [15–17]. The overexpression of *SRD1* gene promoted the proliferation of cambium cells and xylem cells, and played a role in auxin-mediated initial root thickening [12]. SRF6 was the most abundantly expressed in tuberous root, and its mRNA was located around the primary cambium and meristem of the xylem, promoting the thickening of the tuberous root [18, 19]. Besides, an expansin coding gene *IbEXP1* was found to play an inhibitory role in the proliferation of cambium cells and xylem cells, which in turn inhibited the initial expansion of tuberous root in sweet potato [19]. The tuberous root development of sweet potato is regulated by multiple genes. However, few genes related to tuberous root development have been identified, and no specific genes regulating tuberous root development of sweet potato have been found, so more researches are needed to reveal the molecular mechanism of tuberous root development of sweet potato.

With the rapid development of sequencing and molecular technology, the study on the molecular mechanism of underlying tuberous root expansion in sweet potato has made great progress. However, the development of tuberous root in sweet potato is a complex biological process, and its mechanism is not clear. Sweet potato is a heterohexaploid plant (2n = 6x = 90) with a genome of 4.4 GB [20]. There are some studies on the development mechanism of sweet potato tuberous root at the transcriptional level. It was found that some specific genes and proteins associated with starch and phytohormone synthesis as well as various transcription factors are involved in storage root formation and development [17, 21–23], but there are many genes should be found at transcriptional level. In the meanwhile, previous studies were based on a single variety, however, there are great genetic differences among varieties. It is difficult to explain the general mechanism and variety specificity from transcriptomic analysis using a single variety. In this study, two main sweet potato cultivars with similar developmental processes but having great genetic differences and usually planted in Guangxi Zhuang Autonomous Region of PR China, Xiguahong (XGH, orange flesh sweet potato) and Guijingshu 8 (GJS-8, purple flesh sweet potato), were used as plant materials. RNA sequencing and weighted gene co-expression network analysis (WGCNA) were performed to identify the key candidate genes mediating tuberous root development.

Results

Identification of differentially expressed genes between fibrous root and tuberous root

To explore the molecular mechanism of the formation and development of tuberous roots of sweet potato, 8 cDNA libraries were generated from the fibrous roots(R0) and the tuberous roots at different development stages (R1, R2, R3) in GJS-8 and XGH. Based on Illumina sequencing, a total of 1,514,457,568 original readings were obtained. After removing the connectors, unknown bases and low-quality reads, 1,486,623,198 clean readings were obtained, with an error rate of less than 0.03, Q20 > 97%, Q30 > 93%, which met the quality requirements of database construction. These clean readings were compared to the sweet potato genome using HISAT2 platform, and each library compared the number of reads on the genome to more than 69%. The number of reads aligned to the unique location of the reference genome was more than 63%, and the number of reads aligned to multiple locations of the reference genome was about 3.2–3.8% (Table 1). The sample correlation heat map showed that the R2 value among three biological repetitive samples was greater than 0.8, and that of most of samples was greater than 0.9, indicating that this experiment was highly repeatable and the data were reliable (Fig. 1).

The expression levels of genes were measured and analyzed. Taking | log2 (FoldChange) | > 1 and padj < 0.05 as the standard, we identified 31,440 differentially expressed genes (DEGs) for the tuberous roots (R1, R2 and R3) vs. fibrous root in GJS-8 and XGH, of which 22,914 were in GJS-8, and 24,446 DEGs in XGH. GJS-8 and XGH shared 15,920 DEGs, of which 5133 DEGs in R1 stage, 5948 in R2 stage, and 11,607 in R3 stage (Fig. 2A). In addition, there were 2705 common genes involved in the whole

Table 1 Quality statistics of original sequencing data and alignment analysis of filtered data with reference genome sequence

Sample	Raw_reads	Clean_reads	Clean_bases	Q20	Q30	Total_map	Unique_map	Multi_map
RGJ8_0_1	54,855,784	53,608,048	8.04G	97.83	93.58	35,656,422(66.51%)	33,895,916(63.23%)	1,760,506(3.28%)
RGJ8_0_2	50,754,086	49,391,586	7.41G	98.02	93.98	33,894,841(68.62%)	32,215,839(65.23%)	1,679,002(3.4%)
RGJ8_0_3	60,342,940	58,716,810	8.81G	97.92	93.76	41,968,662(71.48%)	39,919,527(67.99%)	2,049,135(3.49%)
RGJ8_1_1	55,763,332	54,758,234	8.21G	97.84	93.58	41,532,205(75.85%)	39,473,934(72.09%)	2,058,271(3.76%)
RGJ8_1_2	54,963,332	53,697,528	8.05G	97.98	93.92	40,923,281(76.21%)	39,087,326(72.79%)	1,835,955(3.42%)
RGJ8_1_3	53,018,150	52,143,466	7.82G	98.06	94.11	38,338,903(73.53%)	36,568,391(70.13%)	1,770,512(3.4%)
RGJ8_2_1	62,021,164	60,915,180	9.14G	97.74	93.36	47,688,641(78.29%)	45,463,907(74.63%)	2,224,734(3.65%)
RGJ8_2_2	65,214,940	64,099,854	9.61G	98.07	94.11	47,955,582(74.81%)	45,694,127(71.29%)	2,261,455(3.53%)
RGJ8_2_3	63,298,644	62,034,718	9.31G	97.9	93.72	47,573,504(76.69%)	45,225,371(72.9%)	2,348,133(3.79%)
RGJ8_3_1	69,201,124	67,485,452	10.12G	97.84	93.58	50,006,430(74.1%)	47,384,881(70.21%)	2,621,549(3.88%)
RGJ8_3_2	77,918,304	76,533,928	11.48G	97.96	93.82	57,958,641(75.73%)	54,988,545(71.85%)	2,970,096(3.88%)
RGJ8_3_3	68,399,538	67,593,522	10.14G	97.91	93.77	51,855,415(76.72%)	49,265,248(72.88%)	2,590,167(3.83%)
RXGH_0_1	60,470,236	59,395,634	8.91G	97.77	93.47	42,773,878(72.02%)	40,808,492(68.71%)	1,965,386(3.31%)
RXGH_0_2	64,126,042	63,252,848	9.49G	98.08	94.18	46,675,900(73.79%)	44,499,900(70.35%)	2,176,000(3.44%)
RXGH_0_3	58,523,750	57,486,536	8.62G	97.82	93.59	42,259,753(73.51%)	40,308,434(70.12%)	1,951,319(3.39%)
RXGH_1_1	59,230,394	58,084,228	8.71G	97.92	93.82	41,855,180(72.06%)	40,072,574(68.99%)	1,782,606(3.07%)
RXGH_1_2	62,660,420	61,717,000	9.26G	97.79	93.49	45,089,703(73.06%)	43,198,530(69.99%)	1,891,173(3.06%)
RXGH_1_3	62,732,322	61,817,364	9.27G	97.78	93.45	46,399,696(75.06%)	44,450,491(71.91%)	1,949,205(3.15%)
RXGH_2_1	74,887,522	73,620,460	11.04G	97.74	93.36	56,299,859(76.47%)	53,684,052(72.92%)	2,615,807(3.55%)
RXGH_2_2	86,367,676	84,896,874	12.73G	97.66	93.14	66,256,302(78.04%)	63,046,641(74.26%)	3,209,661(3.78%)
RXGH_2_3	68,133,460	67,070,154	10.06G	98.34	94.79	51,470,162(76.74%)	49,089,797(73.19%)	2,380,365(3.55%)
RXGH_3_1	59,273,332	58,226,124	8.73G	97.77	93.46	45,695,896(78.48%)	43,444,717(74.61%)	2,251,179(3.87%)
RXGH_3_2	58,250,960	57,096,602	8.56G	97.81	93.5	44,842,303(78.54%)	42,632,664(74.67%)	2,209,639(3.87%)
RXGH_3_3	64,050,116	62,981,048	9.45G	97.91	93.77	49,630,747(78.8%)	47,242,197(75.01%)	2,388,550(3.79%)

tuberous root development process in GJS-8 and XGH (Fig. 2B).

GO and KEGG enrichment analysis of DEGs

To further determine the main biological functions of all DEGs shared by GJS-8 and XGH in the process of tuberous root development, functional annotation was performed by mapping all common DEGs to gene ontology (GO) terms in the GO database. GO enrichment analysis was implemented using a Bonferroni-corrected $p \leq 0.05$ as the threshold. Based on this criterion, 33 biological process terms, 3 cellular component terms and 36 molecular function terms were significantly enriched in R1 vs. R0 comparison. Among the DEGs between R1 vs. R0, the "cellular carbohydrate metabolic process" and "single-organism carbohydrate metabolic process" were the major terms of biological process, the "cell wall" and "external encapsulating structure" were the major terms of cellular component, and the "nucleic acid binding transcription factor activity" was the most represented molecular function term (Table S1). A total of 91 biological process terms, 7 cellular component terms and 49 molecular function terms were significantly enriched in R2 vs. R0 comparison. Among the DEGs between R2 vs. R0, the "response to stress" and "single-organism carbohydrate metabolic process" were the major terms of biological process, the "cell periphery", "cell wall" and "external encapsulating structure" were the major terms of cellular component, and the "nucleic acid binding transcription factor activity" was the most represented molecular function term (Table S2). Moreover, 75 biological process terms, 6 cellular component terms, and 39 molecular function terms were significantly enriched in R3 vs. R0 comparisons. Among the DEGs between R3 vs. R0, the "ion transport" and "cell communication" were the major terms of biological process, "cell periphery" "cell wall" and "external encapsulating structure" were major terms of cellular component, and "nucleic acid binding transcription factor activity" was the most represented molecular function term (Table S3).

To further determine the metabolic or signal transduction pathways that common DEGs may participate in tuberous root development, pathway enrichment analysis was performed by using KEGG database. A total of 5133 (R1 vs. R0), 5948 (R2 vs. R0), and 11,607 (R3 vs. R0) DEGs were respectively assigned to 101, 105, and 110 pathways by KEGG pathway enrichment

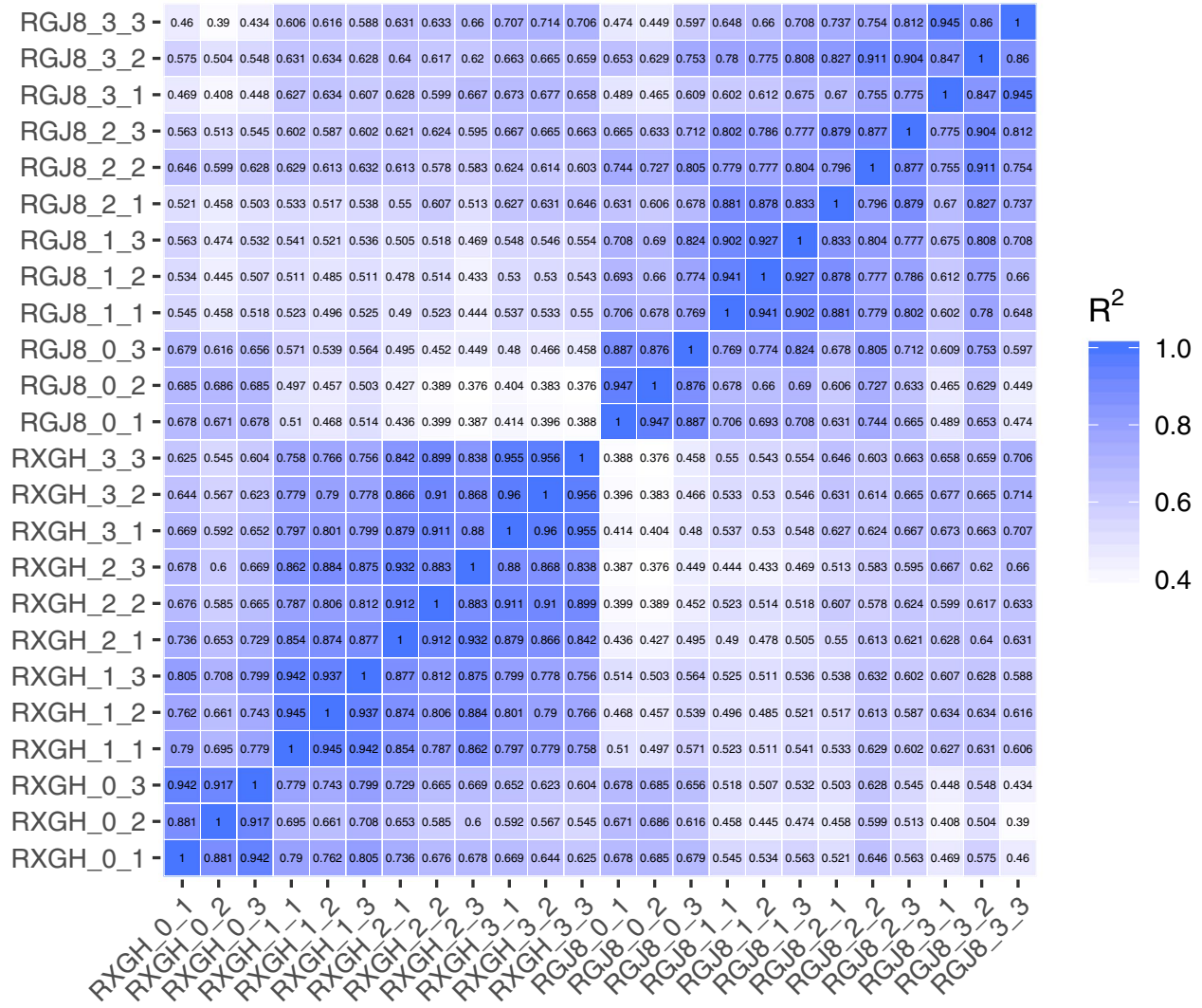

Fig. 1 Correlation analysis between sample replicates

analysis. Nine pathways were identified as significantly enriched pathways in R1 vs. R0 and R2 vs. R0, respectively, and 13 were identified as significantly enriched pathways in R3 vs. R0 ($Q \leq 0.05$) (Table 2; Fig. 3). The "Starch and sucrose metabolism (sot00500)" "MAPK signaling pathway - plant (sot04016)" "plant hormone signal transductiont (sot04075)" and "plant-pathogen interaction (sot04626)" were the major represented pathways among the DEGs of R1 vs. R0 and R2 vs. R0. Among the DEGs between R3 vs. R0, the "Starch and sucrose metabolism (sot00500)" "MAPK signaling pathway - plant (sot04016)" "Circadian rhythm - plant (sot04712)" and "Plant-pathogen interaction (sot04626)" were the major represented pathways. The results suggest that genes involved in regulation of plant hormone levels, metabolism and signal transduction played vital roles in tuberous root of sweet potato.

Comprehensive analysis of differential expression of signal transduction pathway genes

The KEGG enrichment analysis of the DEGs shared by GJS-8 and XGH during tuberous root expansion showed that they were significantly enriched in many signal transduction pathways. Furthermore, these DEGs were annotated using NR, GO, and KEGG annotations,

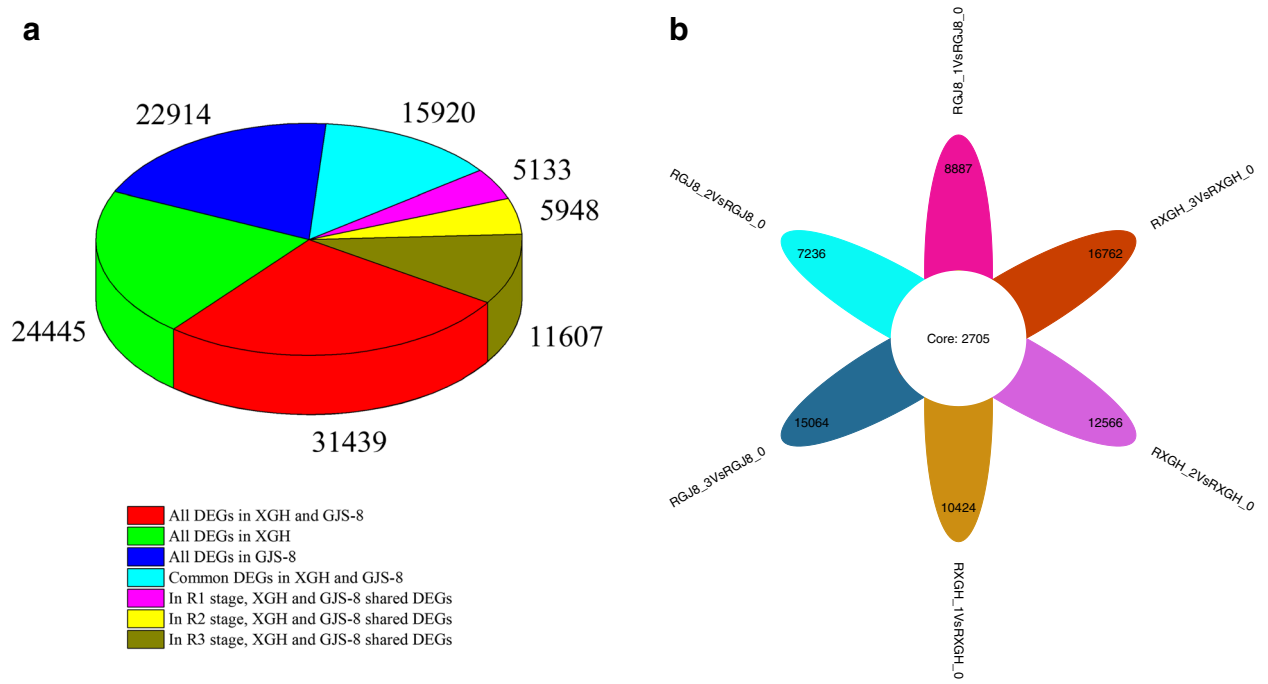

Fig. 2 The number of differentially expressed genes between tuberous root and fiber root at different stages of GJS-8 and XGH. **a** Statistics on the number of differential genes in different situations. **b** The number of differential genes between GJS-8 and XGH

and a large number of DEGs were involved in signal transduction, cell wall, cell division, starch and sucrose metabolism pathways, indicating that signal transduction pathways played an important role in the process of sweet potato tuberous root expansion. Therefore, we analyzed the related genes of these pathways.

Hormone signal

In this study, a total of 58 genes related to biosynthesis, metabolism and signal transduction of various hormones were identified (Table S4). The auxin signal transduction pathway was the most active, followed by ethylene signal transduction pathway. The genes related to hormone signal transduction in two varieties at the same developmental stage were further analyzed. In the auxin pathway, 3 AUX/IAA (Tai6.27980, Tai6.39648, and Tai6.22518) and 1 CH3(Tai6.36369) were significantly up-regulated in R1 phase; 1 AUX1(Tai6.1708), 1 SAUR (Tai6.14155), 1 AUX/IAA (Tai6.27980), and 2 ARF (Tai6.44587, Tai6.23113) were significantly up-regulated in R3 phase. In the ethylene pathway, 1 ERF (Tai6.17891) was significantly up-regulated in R1 phase, 1 ETR (Tai6.12247), 1 SIMKK (Tai6.10820) and 1 ERF (Tai6.10820) were significantly up-regulated in R2 phase, 5 ethylene-related genes (ETR: Tai6.12247, SIMKK: Tai6.10820, EIN2: Tai6.36354, EBF: Tai6.54900, and EIN3: Tai6.48960) were significantly up-regulated in R3 phase. In cytokinin signal transduction pathway, 1 AHP (Tai6.10485) was significantly enhanced during tuberous root development. In the abscisic acid pathway, 1 PYR/RYL (Tai6.18308) was significantly up-regulated in R1and R3 phase, 1 ABF (Tai6.48900) was significantly up-regulated in R2 phase. In the gibberellin pathway, 1 TF (Tai6.39357) was significantly up-regulated in R2, R2 and R3 phase. In the brassinolide pathway, 2 CYCD3(Tai6.43006, Tai6.37902) were significantly up-regulated in R2 phase. In the salicylic acid pathway, 2 NPR1(Tai6.32738, Tai6.52704) were significantly up-regulated in R1 phase,1 NPR1(Tai6.52704) was significantly up-regulated in R1 phase.

MAPK, calcium and phospholipid signaling

Among the DEGs shared by XGH and GJS-8, 1 mitogen-activated protein kinases (MAPK) gene (Tai6.51134) was up-regulated in whole expansion stage, 1 MAPK (Tai6.44720) was up-regulated in R1 and R2 stages, 1 MAPK (Tai6.10820) was up-regulated in R2 and R3 stages, 4 MAPK (Tai6.53239, Tai6.7760, Tai6.9123, and Tai6.4327) were up-regulated in R3 stage, 10 MAPK genes were down-regulated during whole expansion stage, 10 MAPK genes were down-regulated in R2 and R3 stages (Table S5).

A total of 147 calcium signal related to genes, including 36 calcium-dependent protein kinases (CDPKs), 40 calcium-binding proteins (CBPs), 45 calmodulin/

Table 2 KEGG enrichment analysis of common differential genes in different stages of GJS-8 and XGH

KEGGID	Term	p-value	Gene Number	
sot04016	MAPK signaling pathway - plant	1.40436E-05	23	R_1 Vs R_0
sot00500	Starch and sucrose metabolism	3.30079E-05	23	
sot04626	Plant-pathogen interaction	0.000156386	22	
sot00600	Sphingolipid metabolism	0.011080663	6	
sot00940	Phenylpropanoid biosynthesis	0.012234384	15	
sot00904	Diterpenoid biosynthesis	0.024164376	4	
sot04075	Plant hormone signal transduction	0.028135623	22	
sot00061	Fatty acid biosynthesis	0.038762762	7	
sot00592	alpha-Linolenic acid metabolism	0.038762762	7	
sot00500	Starch and sucrose metabolism	1.35885E-08	32	R_2 Vs R_0
sot04626	Plant-pathogen interaction	1.35835E-06	29	
sot04016	MAPK signaling pathway - plant	0.000622851	22	
sot00904	Diterpenoid biosynthesis	0.008765197	5	
sot00520	Amino sugar and nucleotide sugar metabolism	0.010132352	18	
sot04075	Plant hormone signal transduction	0.010903657	27	
sot00710	Carbon fixation in photosynthetic organisms	0.011375788	13	
sot00030	Pentose phosphate pathway	0.02528945	10	
sot00902	Monoterpenoid biosynthesis	0.032595474	4	
sot04626	Plant-pathogen interaction	1.658E-07	45	R_3 Vs R_0
sot04016	MAPK signaling pathway - plant	0.000129123	36	
sot00500	Starch and sucrose metabolism	0.000398031	36	
sot00561	Glycerolipid metabolism	0.007070632	22	
sot00904	Diterpenoid biosynthesis	0.007556666	7	
sot00940	Phenylpropanoid biosynthesis	0.008022448	28	
sot00564	Glycerophospholipid metabolism	0.015204748	23	
sot00520	Amino sugar and nucleotide sugar metabolism	0.017481772	28	
sot00073	Cutin, suberine and wax biosynthesis	0.019411125	7	
sot00600	Sphingolipid metabolism	0.021856661	9	
sot00710	Carbon fixation in photosynthetic organisms	0.029264501	19	
sot04712	Circadian rhythm - plant	0.0300729	12	
sot00230	Purine metabolism	0.032032208	25	

calmodulin-binding protein (CaM/CaM-binding), and 26 Calreticulin (CBL) were identified from the common DEGs of two varieties (Table S6). It is worth noting that most of genes were down-regulated in whole expansion stage.

A total of 22 phospholipid signal-related genes were identified from the common DEGs of two varieties (Table S7). Among them, 6 genes were significantly up-regulated in R1, R2 and R3 stages, 4 genes were significantly down-regulated in R1, R2 and R3 stages.

Light signal

Sixty-five photoperiod related genes were identified as DEGs shared by XGH and GJS-8 during tuberous root development (Table S8). These genes included 20 CONSTANS-likes (COL), 5 phototropins, 14 GATA transcription factors (GATA), 12 LOB domain-containing proteins (LOB), 6 COP-interactive proteins genes (COP) and 8 phytochromes. In R1 stage, 15 genes were significantly up-regulated, including 3 phototropins, 4 COLs, 1 LOB, 1 COP and 6 phytochromes. In R2 stage, 21 genes were significantly up-regulated, including 7 COLs, 1 phototropin, 1 GATA, 3 LOBs, 3 COPs and 6 phytochrome genes. In R3 stage, 24 genes, including 3 phototropins, 8 COLs, 1 GATA, 4 LOBs, 4 COPs and 6 phytochromes, were significantly up-regulated.

Cell wall and cell cycle

We identified 95 genes related to cell wall and cell cycle from the DEGs shared by GJS-8 and XGH (Table S9), including 29 xyloglucan endotransglucosylase/hydrolases (XTH), 22 expansins, 3 extensins, 8 cell division proteases (FtsZ), 6 cell division cycle 5-like proteins (CDC5), 9 cell division control proteins (CDC), 7 cyclin-dependent

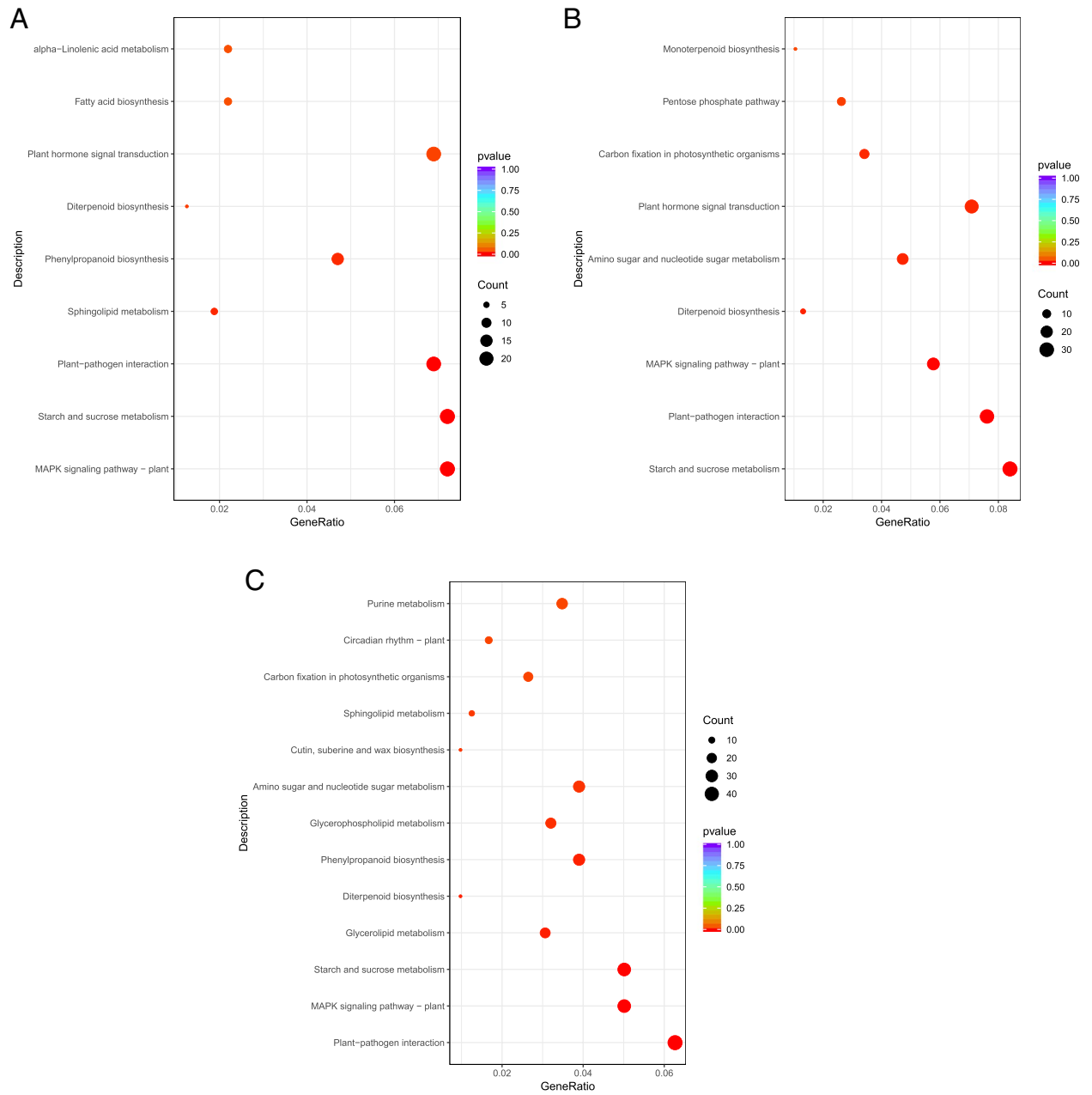

Fig. 3 KEGG enrichment analysis of DEGs shared by GJS-8 and XGH at R1, R2, R3 stages. **a** DEGs shared by GJS-8 and XGH at R1 stage; **b** DEGs shared by GJS-8 and XGH at R2 stage; **c** DEGs shared by GJS-8 and XGH at R3 stage

kinases (CDKs) and 11 cyclin-dependent kinase inhibitors (CDKIs). Among these genes, most of XTH and CDC genes were down-regulated, and most of the genes related to FtsZ, CDC5 and CDKIs were up-regulated.

Starch and sucrose metabolism

Seventy genes related to starch and sucrose metabolism were identified from the DEGs shared by GJS-8 and XGH (Table S10), including 13 sucrose synthases (SuSy), 2 sucrose phosphate synthases (SPS), 10 starch synthases (SS), 5 invertase genes (INV), 10 granule-bound starch synthases (GBSS), 4 soluble starch synthases (SSS), 11 starch branching enzymes (SBE), 5 Beta-amylases, 5 alpha-amylases, and 5 isoamylases. Most of the genes were significantly up-regulated during the root

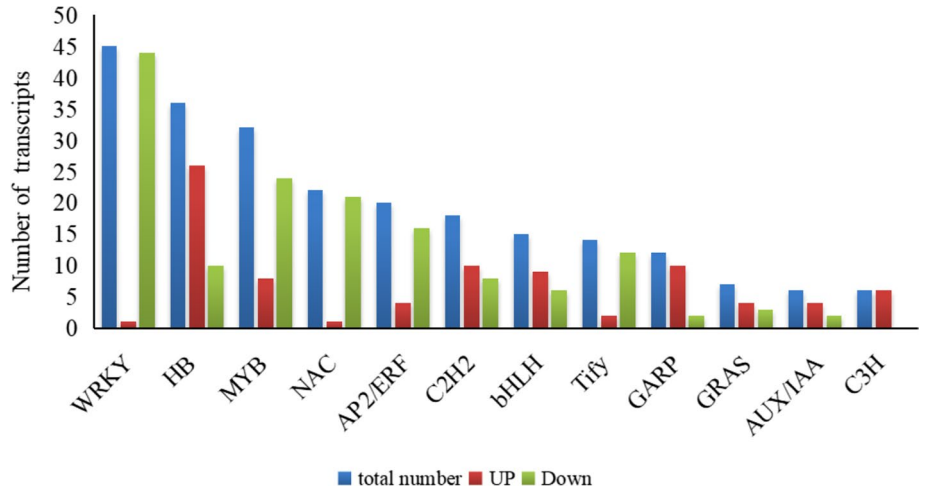

Fig. 4 The number of transcription factors expressed significantly differentially in the R1, R2 and R3 stages of tuberous root expansion in GJS-8 and XGH

expansion stage in sweet potato, and only a few genes were down-regulated.

Transcription factor

In this study, 296 TF genes were identified as DEGs shared by GJS-8 and XGH. Among them, 126 TFs were up-regulated, and 170 TFs were down-regulated during the tuberous root development (Table S11). WRKYs, HBs, MYBs were the major represented TF families (Fig. 4). Twenty-nine transcription factors in these families were significantly up-regulated, and their expression levels increased successively in the R1, R2 and R3 stages of tuberous root development in two cultivars, it mainly included the family of HB, C2H2, MYB transcription factors (Fig. 5).

Weighted gene co-expression network analysis

To further understand the relationship between gene expression and tuberous root development, the weighted gene co-expression network analysis (WGCNA) was performed. In this study, β (soft-power threshold) = 9 was set to guarantee high scale independence and low mean connectivity (near 0) (Fig. 6A). The dissimilarity of the modules was set as 0.75, and a total of 14 modules were generated (Fig. 6B). The module trait relationship was shown in Fig. 6C. Green modules are highly related to tuberous root development ($r > 0.80$, $p < 0.005$). GO enrichment analysis was further carried out on the genes of green module (Table S12). The result showed that the biological processes were the most enriched in this module related to energy metabolism and transport. In addition, it was also significantly enriched in mRNA processing, hormone response, endogenous stimulus response and stress response. KEGG enrichment analysis showed that the green module was significantly enriched in transcription factors, plant circadian rhythm (sot04712), MAPK plant signal pathway (sot04016), and plant hormone signal transduction (sot04075) (Table S13).

The gene connectivity in the modules represents the regulatory relationship between the gene and other genes. The higher the connectivity, the greater the regulatory role of the gene in the modules, the more likely it was a hub gene. The gene with the highest connectivity in the green module was selected as the core gene of the module. This gene encoded a trihelix transcription factor (Tai6.25300). The homology of this gene in Arabidopsis is AT1G13450.1 (trihelix transcription factor: GT-1). A total of 1272 genes interacted with trihelix, including genes related to light signaling, calcium signaling, and plant hormone signaling, implying the processes the genes involved were potentially co-regulated. The interaction network of core genes was visualized by Cytoscape software. Because there were many genes interacting with hub genes, only partial genes were shown here (Fig. 7).

Genes with significant differences in tuberous root development between two varieties

Taking | log2 (FoldChange) | > 1 and padj < 0.05 as the standard, we identified 18,028 differentially expressed genes (DEGs) for the GJS_8 vs. XGH (R1, R2 and R3), of which 12,792 were in R1 stage, 9979 in R2 stage and 8828 DEGs in R3. KEGG enrichment analysis showed that the up-regulated genes were significantly enriched to phenylpropanoid biosynthesis (sot00940), flavonoid

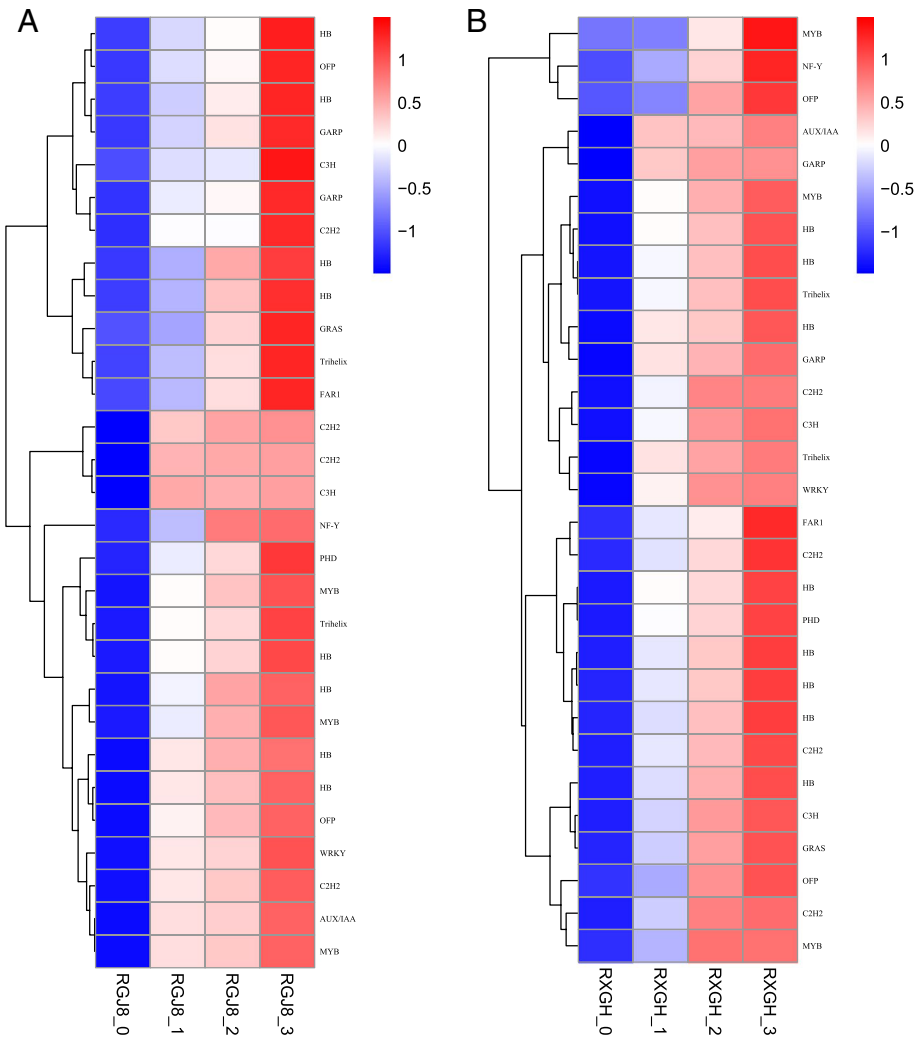

Fig. 5 Heat map of highly expressed transcription factors. Every row shows a different TF gene. Red, white, and blue indicate slow, middle and high levels of mRNA expression, respectively. (**a**) Expression of transcription factors in GJS-8; (**b**) Expression of transcription factors in XGH

biosynthesis (sot00941), starch and sucrose metabolism (sot00500) and pentose and glucuronate interconversions pathway (sot00040) in stage R1. In stage R2, the up-regulated genes were significantly enriched to the flavonoid biosynthesis pathway (sot00941). In R3 stage, the up-regulated genes were not significantly enriched to any pathway. In addition, 88 MYB, 86 bHLH, 3 WD40 transcription factors, and 30 anthocyanin biosynthesis related genes [6 trans-cinnamate 4-monooxygenases (C4H), 12 4-coumarate--CoA ligases (4CL), 8 chalcone synthases (CHS), 2 chalcone-flavanone isomerases (CHIL), 2 leucoanthocyanidin dioxygenases (LDOX/ANS)] were identified from these DEGs (Table S14). The difference of these anthocyanin related genes was the greatest in the R1 stage of the two varieties, and the difference was more than 10 times.

Verification of gene expression patterns by qRT-PCR

In order to verify the accuracy of RNA-Seq results, we randomly selected 6 genes (Tai6.25300, Tai6.22648, Tai6.3107, Tai6.42353, Tai6.46822, and Tai6.24971) for qRT-PCR analysis. The results showed that the expression pattern of these 6 differential genes was similar to that of RNA-Seq (Fig. 8). The results indicated that the RNA-Seq was reliable.

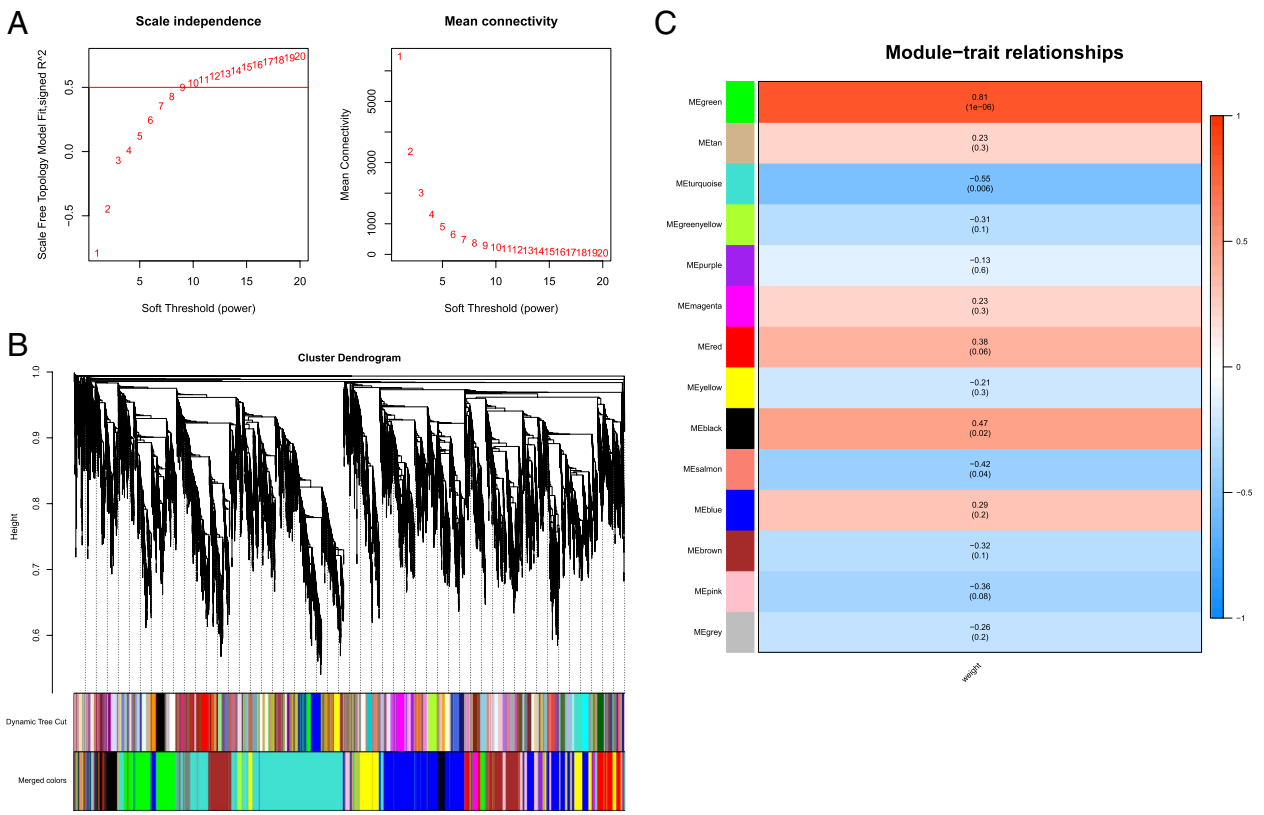

Fig. 6 Soft-thresholding values estimation and module identification. **a** Scale independence and mean connectivity of various soft-thresholding values (β). **b** Dendrogram of all filtered genes enriched according to a dissimilarity measure (1-TOM) and the cluster module colors. **c** Heatmap of the correlation between the root tuber expansion traits and MEs of bladder cancer. The darker the module color, the more significant their relationship

Discussion

The formation and development of the tuberous root of sweet potato is a complex process, which mainly involves the formation of vascular cambium and secondary cambium. After the formation of round vascular cambium, the tuberous root begins to thicken, then the cells continue to proliferate and expand to form a secondary cambium, which is accompanied by the continuous accumulation of starch and other substances, resulting in the continuous enlargement of the tuberous root.

Previous studies showed that the meristems are always active during tuberous root bulking, the transcriptome data obtained in this study reveal that the regulators of meristem development, such as LBD4 (LOB domain-containing protein 4, Tai6.18322, and Tai6.27010), WOX4 (WUSCHEL HOMEOBOX RELATED 14, Tai6.17770, and Tai6.44989) were significantly upregulated at tuberous root development, which is consistent with the results of previous studies [23]. Moreover, the genes are involved in cell division, including cell division protein FtsZ (FtsZ), cell division cycle 5 (CDC5), cell division control protein (CDC), and cyclin-dependent kinase (CDK), their expression levels were significantly enhanced in the tuberous root expansion stage (Table S9). The Genes involved in cell extension and expansion, including extension, XET, and expansin, also were significantly enhanced in the tuberous root expansion stage (Table S9). These results indicate that the formation and development of tuberous roots are inseparable from the active meristems and cell division.

A series of studies have shown that the initiation and induction of root/tuber is affected by the environment. For potatoes, photoperiod is essential for tuber formation [24]. Moreover, light is also important for the expansion of *Rehmannia glutinosa* tuberous root [25]. Photoperiod response protein, lateral organ boundaries protein (LOB), and GATA transcription factor are important members of photoperiod regulation. In this study, the expression of LOB (Tai6.27900) and GATA (Tai6.27468) were significantly enhanced during the tuberous root expansion stage. Furthermore, genes related to light signal transduction including phototropin, CONSTANS,

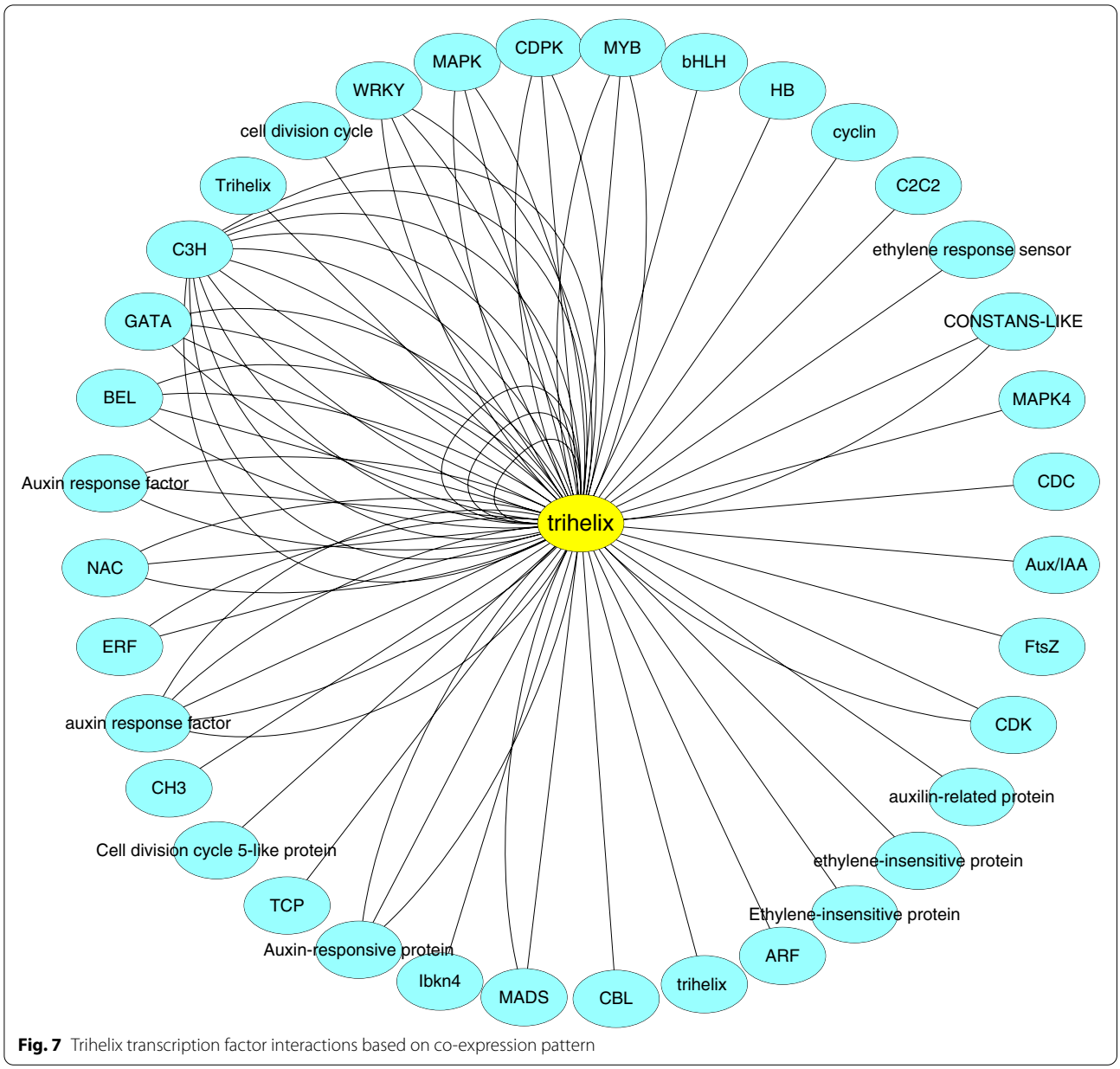

Fig. 7 Trihelix transcription factor interactions based on co-expression pattern

and COP-interactive proteins were also significantly enhanced during the tuberous root expansion stage (Table S8). However, their peaks and expression patterns were obviously different, suggesting that light regulation is very critical to tuberous root formation and continuous development.

Moreover, genes detected in the roots may also be transcribed in the leaves and then transported to the root. For example, after being transcribed in leaves, potato stBEL5 mRNA was transported through the phloem to the stolon tip for translation into protein, thereby promoting the formation of storage organs [26]. In this study, 14 BELs genes were consistently up-regulated during the tuberous root expansion stage (Table S8), which suggest that these genes may be functionally similar to the stBEL5. Although the storage organs of potato and sweet potato are different, they may have similar regulatory systems. Therefore, they may be involved in light signal-regulated tuberous root development via similar mechanisms.

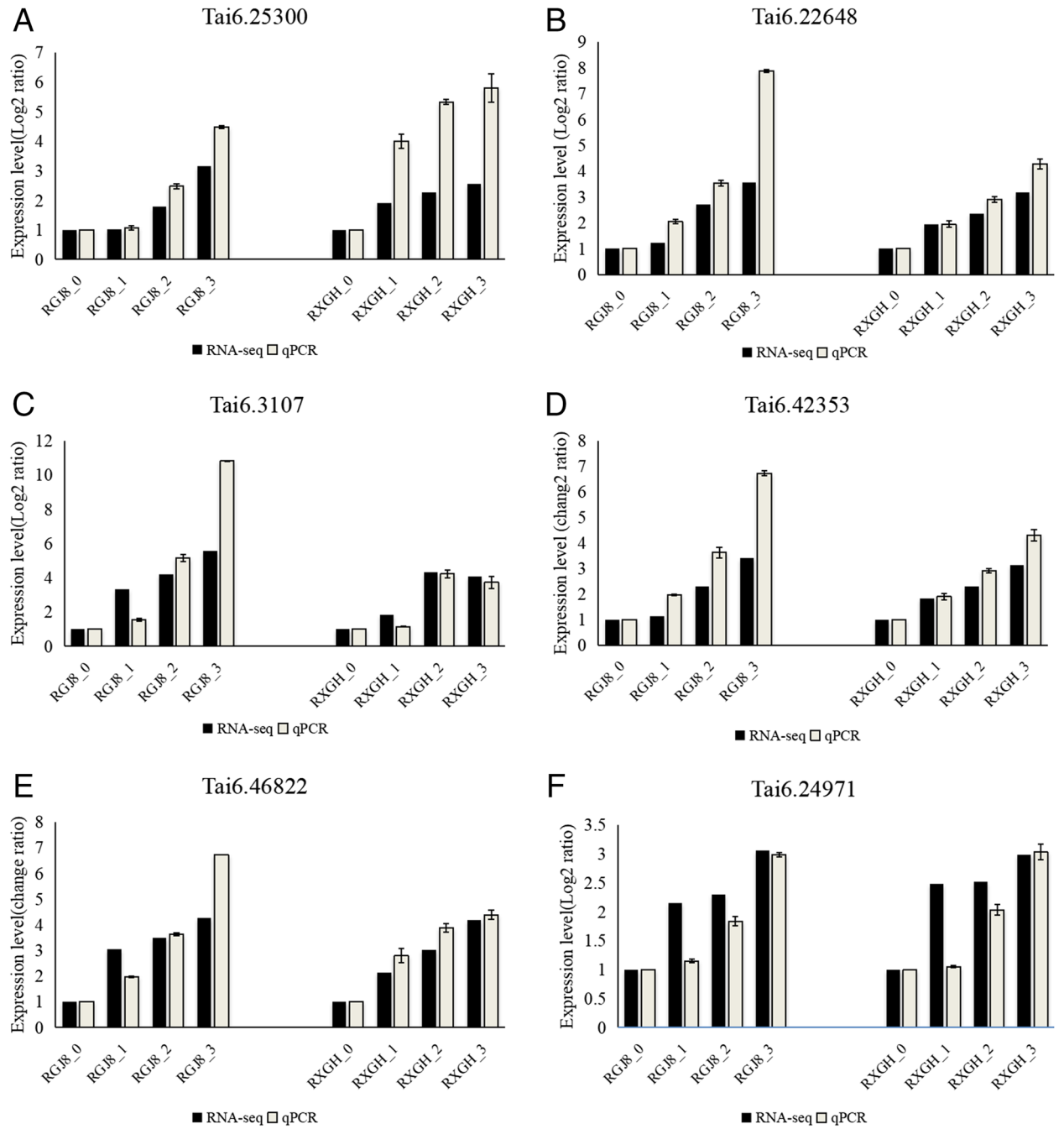

Fig. 8 qRT-PCR validation profiles of six randomly selected genes. The data was normalized by using UBI as an internal reference. The expression level of fibrous root(R0) in each cultivar was used as reference state, which was set to 1, and fold change values were shown here. (**a**) Trihelix transcription factor (Tai6.25300); (**b**) BEL (Tai6.22648); (**c**) CONSTANS-like (Tai6.3107); (**d**) BEL (Tai6.42353); (**e**) BEL (Tai6.46822); (**f**) auxin-responsive protein (Tai6.24971)

The relationship between hormones and tuberous root swelling

Hormones are important signals in plant root development [27, 28]. In this study, the plant hormone signal transduction pathway was one of the most enriched KEGG pathways in tuberous root expansion stage. Auxin plays an important role in cambium cell proliferation and cell expansion [12], also maintains the meristem state of cambium cells and increase the number of xylem elements [29]. In the studies of radish, *Rehmannia glutinosa*

and *Callerya speciosa*, the expressions of auxin-related genes were significantly up-regulated during tuberous root expansion stage [25, 30, 31]. In this study, 7 auxin-related genes (AUX / IAA, ARF, SAUR, and CH3) were up-regulated in tuberous root expansion stage, implying that they may relate to cell expansion in the secondary growth of cambium.

The results showed that cytokinin was involved in the proliferation and development of cambium cells, and the expression reached the highest level in the rapid growth stage of tuberous root, which was related to the development and formation of tuberous root / tuber [29, 32–34]. In this study, the expression of cytokinin related gene (Tai6.10485) was significantly up-regulated during tuberous root expansion, suggesting that cytokinin may promote root expansion by participating in the development of cambium.

Ethylene is a key regulator of rhizome induction and development [35], which promotes tuber formation by inhibiting GA biosynthesis [36]. Moreover, it has been shown that GA, auxin,and ethylene affect cell growth in the root by opposing the action of DELLA proteins. In this study, the expressions of ethylene-related genes were significantly up-regulated during tuberous root expansion (Table S4). Overall, these results suggest that these hormone signals related genes play vital roles during the tuberous root expansion stage.

Multiple signal pathways are activated to regulate tuberous root development

Cellular processes involved in a series of signaling pathways are usually triggered by specific stimuli and hormones. Phospholipid signal plays an important role in root growth, cell division, and hormone regulation [37, 38]. It was reported that the expression levels of phospholipid signal-related genes/proteins were increased in the early stage of tuberous root expansion in *Rehmannia glutinosa*. In addition, the phospholipid-calcium signal system regulated potato tuber formation [25, 39]. In this study, 6 phospholipid signal-related genes were up-regulated in the stage of tuberous root expansion in GJS-8 and XGH, and the expression profiles in two varieties were quite similar, indicating that phospholipid signal was involved in the initiation and of tuberous root expansion.

Calcium is one of the main nutrients and is involved in almost the whole process of plant growth, including the controls of cell division, differentiation, and stress response as the second messenger [40, 41]. Studies revealed that CDPK played a role in the signal pathway of root initiation in potato and cassava, and exogenous calcium levels could affect the quantity and weight of potato tuber [42–44]. In addition, Ca^{2+} concentration and calcium signal- related genes (CBP, CBL, CaM, and CDPK) were significantly up-regulated during tuberous root formation in *Rehmannia Glutinosa* [25]. In this study, there was an increase in the stage of tuberous root expansion in the expression level of calcium signaling-related genes, including 9 CDPKs, 8 CBLs, and 1 CaM (Table S6), which suggests that calcium signal is involved in the formation and expansion of tuberous root in sweet potato. In addition, some genes related to the MAPK signaling pathway were up-regulated during tuberous root expansion development (Table S5), suggesting that the MAPK signal participats in the initiation and expansion of tuberous root formation. It has been shown that the MAPK signal plays an important role in cell cycle regulation, hormone, and stress response [45].

Transcription factor regulation and weighted gene co-expression network analysis

Transcription factors play an important role in the regulation of plant growth and development and secondary metabolism. Many transcription factors have been identified to play key roles in organ development, including MADS, bHLH, MYB, NAC, GRAS et al. In this study, we identified 29 transcription factors that were significantly up-regulated during the tuberous root expansion stage in two varieties. Their expression levels increased successively (Fig. 5). Among these TFs, MYBs and HBs were the main transcription factors with large up-regulation multiples. One trihelix transcription factor gene (Tai6.25300) was identified as a tuberous root expansion-related gene through WGCNA analysis, its homologous gene in Arabidopsis was AT1G13450.1(Trihelix, GT-1), which was considered to be a molecular switch responded to light signals through Ca^{2+}-dependent phosphorylation/dephosphorylation [46]. The Trihelix factor is a plant-specific triple helix DNA binding transcription factor. Many studies have proved that the trihelix transcription factor was involved in plant light response [47, 48]. In this study, the expression of light signal related-genes was coordinated with Tai6.25300, and significantly up-regulated during tuberous root development. Moreover, qRT-PCR confirmed that the expression of Tai6.25300 was up-regulated and increased successively during tuberous root development in two varieties, suggesting that Tai6.23500 was closely related to tuberous root development. We infer that Tai6.25300 participates in tuberous root expansion by positively regulating light signal related genes.

MYBs were involved in cell cycle regulation, plant morphogenesis, cell wall synthesis, secondary metabolism, xylem/phloem differentiation, root radial pattern formation, and so on [49, 50]. Furthermore, previous studies have found that the transcriptional level of MYB

was significantly up-regulated during rhizome development [30, 51], and MYBs were highly expressed at the rapid thickening stages of *Callerya speciosa* [36]. In this study, 32 MYB transcription factors were significantly differentially expressed as tuberous root development, of which 8 were significantly up-regulated. Homeodomain (Homebox, HB) transcription factors are very important regulatory proteins in plants, which are mainly divided into 14 categories, including KNOX, BEL, and HD-ZIP, etc. Arabidopsis HB transcription factors were involved in cell division, differentiation, replication, growth, and regulation of the early development of vascular tissue [52, 53], In addition, the members of HB family were also involved in the regulation of cambium cell differentiation to phloem and lignin biosynthesis [54, 55]. RNA-Seq data revealed that 3 homeobox genes were notably upregulated during the formation and thickening of storage roots [22]. In this study, 36 HB transcription factors were significantly differentially expressed in tuberous root development, of which 26 were significantly up-regulated.

To sum up, these results suggest that transcription factors may drive root/stem growth through cell cycle regulation, cell division, and secondary wall strength. The TFs revealed in this study may be the important candidate genes for breeding sweet potato with high production in the future.

Starch and sucrose metabolism regulation

Sucrose and starch accumulation occurs during the bulking of storage roots, they are considered to be one of the most important carbohydrates, and play an important role in the formation of storage organs. Sucrose invertase and sucrose synthase were involved in the introduction and accumulation of sucrose in storage roots [56]. In addition, sucrose synthase was related to the tuber / tuberous root growth of potato and radish and was a key enzyme in the early development of radish storage root [57–60]. In this study, 5 SuSy genes were significantly up-regulated during tuberous root development in GJS-8 and XGH, while 2 INV genes were significantly down-regulated (Table S10), Invertase was active in fibrous roots of sweet potato but rapidly decreased to an undetectable level during storage root development [61]. Furthermore, Jackson showed that high content of sucrose was required as a necessary condition during the formation of storage organs [62]. In the present study, SPS (Tai6.24187), the major source of sucrose synthesis activity [63], was up-regulated during tuberous roots expansion. This result was consistent with previous studies in radish that found up-regulation of SPS playing a major role in the thickening stage of radish taproot [64].

The accumulation of starch occurs at the same time as the expansion of storage organs. It has shown that the expansions of potato and lotus root tubers were highly coordinated with the accumulation of starch [65, 66]. The expansion of cassava root was synchronized with the accumulation of starch [67], and granule-bound starch synthase (GBSS) has been shown to affect starch synthesis in storage organs [68]. In this study, 22 starch-related genes (6 GBSSs, 4 SSSs, 8 SBEs, and 4 isoamylases) were significantly up-regulated during root tuber expansion (Table S10), which was similar to previous studies. SBE, GBSS, and SS-related genes were significantly up-regulated during root expansion of *Panax notoginseng* [69]. These starch and sucrose metabolism genes play important roles in tuberous root expansion.

Genes with significant differences in tuberous root development between two varieties

GJS_8 and XGH are two varieties with different anthocyanin content. GJS_8 has higher anthocyanin content than XGH. Anthocyanins are water-soluble pigments and an important class of flavonoids. We found that there was a large number of genes with significant differences in tuberous root development between two varieties. KEGG enrichment analysis showed that the DEGs were significantly enriched to phenylpropanoid biosynthesis (sot00940), flavonoid biosynthesis (sot00941), and starch and sucrose metabolism pathway (sot00500). It was also found that phenylpropanoid biosynthesis and flavonoid biosynthesis was significantly enriched in the process of anthocyanin biosynthesis [70]. In addition, we identified a large number of MYB, bHLH, WD40 transcription factors, and anthocyanin biosynthesis genes from these differential genes, including 6 MYBs,17 bHLHs, 3 C4Hs, 5 4CLs,6 CHSs, 2CHILs, and 2 LDOX/ANSs, which were significantly differentially expressed between GJS_8 and XGH and also significant differentially expressed between tuberous root and fiber root, especially in GJS_8 tuberous root. A large number of studies have shown that MYB, bHLH, and WD40 transcription factors were the regulators of flavonoid biosynthesis, and the results also showed that *IbMYB1* controls the biosynthesis of anthocyanins in sweet potato [71]. It was found that 10 anthocyanin biosynthesis genes were significantly up-regulated during *Aronia melanocarpa* fruit development [72]. Hence, it shows that anthocyanin biosynthesis related-genes may be involved in the tuberous root development in sweet potato, and their regulatory mechanism should be studied in the next step.

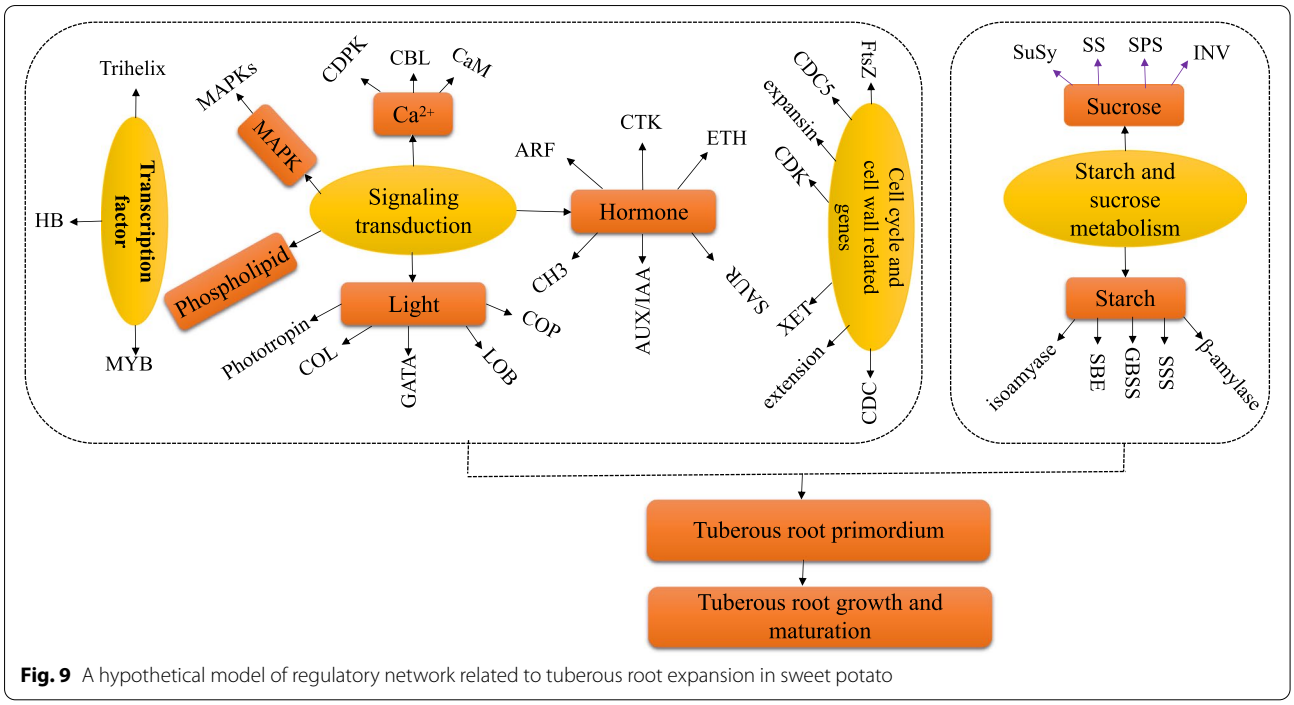

Fig. 9 A hypothetical model of regulatory network related to tuberous root expansion in sweet potato

Regulatory networks associated with tuberous root development

Tuberous root development is a complex regulatory process, which is affected by many factors. In this study, through transcriptome analysis, combined with previous research results, a hypothetical model of sweet potato tuberous root development regulatory network is proposed (Fig. 9). The cells in the vascular cambium divide and expand continuously to produce secondary xylem and secondary phloem, resulting in the expansion of tuberous root. Cell proliferation is regulated through several signal transduction pathways (light, Phospholipid, calcium, MAPK, hormone, and transcription signaling) and metabolism possesses (cell wall, sucrose, and starch metabolism). Several genes including photoperiod (LOB, GATA, Phototropin, COL, and COP), calcium signal (CDPK, CBL, and CaM), MAPK signal, auxin-related genes (Aux/IAA, CH3, ARF, and SAUR), HB transcription factors (BELL, KNOX, and HD-ZIP), are highly expressed to promote cell differentiation, division, expansion and sucrose and starch accumulation at the secondary structure. In addition, FtsZ, CDC, CDK, XTH, expansin, and extension, are involved in cell division extension and expansion. Finally, SuSy, SPS, SSS, GBSS, and SBE are involved in the hydrolysis of sucrose and the synthesis of starch. Further functional identification studies were needed to confirm the functions of these potential genes.

Conclusion

Integrated transcriptomic and WGCNA analyses were performed in the study, there were 15,920 differential genes shared by XGH and GJS-8. GO and KEGG pathway enrichment analysis revealed that these DEGs were mainly involved in plant hormone signal transduction, starch and sucrose metabolism, MAPK signal transduction, light signal, phospholipid signal, calcium signal, transcription factor, cell wall, and cell cycle. Furthermore, WGCNA and qRT-PCR analysis suggested that Tai6.25300 played an important role in tuberous root development in sweet potato. A hypothetical model of a genetic regulatory network associated with tuberous roots in sweet potato is put forward. The tuberous root development of sweet potato is mainly attributed to cell differentiation, division, and expansion, which are regulated and promoted by certain specific signal transduction pathways and metabolism processes. These findings can not only provide novel insights into the molecular regulation mechanism of tuberous root expansion, but also support theoretical basis for genetic improvement of sweet potato.

Materials and methods

Materials

Two sweet potato varieties, GJS-8 and XGH were used in this study. They were planted in the experimental farm of Hepu Institute of Agricultural Science in

Fig. 10 Anatomical diagram with sampling diagram. **a** GJS_8; **b** XGH

Beihai, Guangxi. At 90 days after planting, Sample collection refers to Ku et al's method [14], Fibrous roots (R0:RGJ8_0, RXGH_0; 1 mm diameter) and developing tuberous roots [(R1:RGJ8_1, RXGH_1; 1 cm diameter, less than 2 g), (R2:RGJ8_2, RXGH_2; 3 cm diameter, 5-10 g), (R3:RGJ8_3, RXGH_3; 5 cm diameter, approx 50 g)] were collected,respectively (Fig. 10). Three plants were selected randomly from every repetition each time. At least five roots were mixed as a biological biological repetition. For the big tuberous root samples, five fresh tuberous roots from a repetition were washed with distilled water, cut down into slices, and mixed as a biological repetition. Three biological replicates were performed. The samples were stored at − 80 °C for extracting total RNA.

RNA extraction, cDNA library construction, and RNA-Seq

A conventional trizol method was used to extract RNA from the samples. The concentration and purity of total RNA were determined by a NanoPhotometer® spectrophotometer (IMPLEN, CA, USA). RNA integrity was assessed using the RNA Nano 6000 Assay Kit of the Bioanalyzer 2100 system (AgilentTechnologies, CA, USA). Sequencing libraries were generated using NEBNext®UltraTM RNA Library Prep Kit for Illumina® (NEB, USA).

RNA sequencing and data analysis

3 μg total RNA from each sample was used as the input material, fragmentation was carried out using divalent cations under elevated temperature in NEBNext First Strand Synthesis Reaction Buffer (5X). First strand cDNA was synthesized using random hexamer primer and M-MuLV Reverse Transcriptase (RNase H-). Second strand cDNA synthesis was subsequently performed using DNA Polymerase I and RNase H. Remaining overhangs were converted into blunt ends via exonuclease/polymerase activities. After adenylation of 3′ ends of DNA fragments, NEBNext Adaptor with hairpin loop structure were ligated to prepare for hybridization. In order to select cDNA fragments of preferentially 250 ~ 300 bp in length, the library fragments were purified with AMPure XP system (Beckman Coulter, Beverly, USA). Then 3 μl USER Enzyme (NEB, USA) was used with size-selected, adaptor-ligated cDNA at 37 °C for 15 min followed by 5 min at 95 °C before PCR. Then PCR was performed with Phusion High -Fidelity DNA polymerase, Universal PCR primers and Index (X) Primer. At last, PCR products were purified (AMPure XP system) and library quality was assessed on the Agilent Bioanalyzer 2100 system. Clean reads were obtained by removing reads containing an adapter, reads containing ploy-N and low-quality reads from the raw data. The clean reads were then aligned with the sweet potato genome (http://public-genomes-ngs.molgen.mpg.de/cgi-bin/hgGateway?hgsid=9052&clade=plant&org=Ipomoea+batatas&db=ipoBat4) [23]. Feature Counts v1.5.0-p3 was used to count the read numbers mapped to each gene, and the FPKM of each gene was then calculated based on the length of the gene and the read count mapped to the gene [23]. Genes with an adjusted *P*-value < 0.05 and | log2 (FoldChange) | > 1 obtained by DESeq2 were considered DEGs.

Functional annotation

Gene Ontology (GO) enrichment analysis of the DEGs was implemented using the cluster Profiler R package, and the gene length bias was corrected during this process [73]. KOBAS software was used to test the statistical enrichment of the DEGs in Kyoto Encyclopedia of Genes and Genomes (KEGG) pathways [74]. To obtain more information about the DEGs, the DEGs were annotated using seven databases: NR (NCBI nonredundant protein), NT (NCBI Nucleotide Sequences), Gene Ontology (GO), KO (KO, KEGG Orthology), KOG (Eukaryotic Or Thologous Groups), Pfam (Protein Family Database) and Swiss-Prot (a manually annotated and reviewed protein sequence database). All the DEGs were subjected to hierarchical clustering analysis using the average linkage method [75].

Weighted gene co-expression network analysis

The DEGs detected with DESeq2 were combined and the TPM values for the 24 samples were determined. Each TPM value was increased by 0.01 and further transformed by a log10 calculation. The converted data were

analyzed with the R package WGCNA (version 1.66), with a power value of 9 [76, 77].

Validation of the DEGs data using qRT-PCR

Total RNAs were extracted from the tuberous samples (fibrous root, tuberous roots less than 2 g, tuberous roots 5-10 g, tuberous roots greater than 50 g) with Trizol® Reagent (Magen, China). and then reverse transcribed into cDNA with HiScript III SuperMix for qPCR(+gDNA wiper) (Vazyme, China). qRT-PCR was carried out using SYBR Premix Ex TaqII Kit (TaKaRa, Dalian, China) on a Bio-Rad iQ5 Real-time PCR System (Bio-Rad Laboratories, CA, USA), Ten μl reaction solution contained 5 μl SYBR Green I Master, 1 μl specific Primer, 1 μl cDNA samples, 3 μl RNase-Free H2O. One-third dilution of the cDNA sample was used, and the reaction conditions were: 30s at 95 °C followed by 40 cycles of 30s at 95 °C, and 30s at 60 °C. Each sample had three biological replicates with three technical replicates for each biological replicate. The relative expression level was calculated by the equation ratio $2^{-\Delta\Delta Ct}$. The primers of selected genes were designed using primer 5 software (Table S15), and UBI gene was used as the internal control.

Abbreviations

CTK: Cytokinin; ABA: Abscisic acid; IAA: Auxin; GA: Gibberellin; MAPK: Mitogen-activated protein kinases; CDPK: Calcium-dependent protein kinases; CBP: Calcium-binding proteins; CaM/CaM-Binding: Calmodulin/calmodulin-binding protein; CBL: Calreticulin; COL: CONSTANS-like; XTH: Xyloglucan endotransglucosylase/hydrolases; FtsZ: Cell division proteases; CDC5: Cell division cycle 5-like proteins; CDC: Cell division control proteins; CDK: Cyclin-dependent kinasess; CDKI: Cyclin-dependent kinase inhibitors; SuSy: Sucrose synthases; SPS: Sucrose phosphate synthases; INV: Invertase genes; GBSS: Granule-bound starch synthases; SSS: Soluble starch synthases; SBE: Starch branching enzymes; WGCNA: Co-expression network analysis.

Supplementary Information

The online version contains supplementary material available at https://doi.org/10.1186/s12864-022-08670-x.

Additional file 1.

Acknowledgements

We thank Miss Yunyi Zhou, Xia Li and Yuting Li for providing the experiment guidance.

Method declaration

All methods are implemented in accordance with relevant guidelines and regulations in this manuscript.

Authors' contributions

DX and LFH have designed experiments, and revised the manuscript. ZQC, ZPC, JLH, AQW,and Ntambiyukuri have analyzed the sequencing data for transcriptome assembly. BMC, GHZ, HFL, and YMH supported the materials. ZQC and JZ have developed qPCR experiments. ZQC have written the manuscript. The author(s) read and approved the final manuscript.

Funding

This work was supported by the National Natural Science Foundation of China (Grant No. 32060419, 32060469), the Guangxi Innovation Team Project of Tubers of Modern Agricultural Industrial Technology System of China (nycytxgxcxtd-11).

Availability of data and materials

The materials of this study were provided by the College of Agriculture at Hepu Institute of Agricultural Science. Correspondence and requests for materials should be addressed to Longfei He (lfhe@gxu.edu.cn). The raw sequencing data have submitted to the NCBI SRA database (PRJNA678375).

Declarations

Ethics approval and consent to participate

Not applicable.

Consent for publication

Not applicable.

Competing interests

The authors declare that they have no conflict of interest.

Author details

[1]National Demonstration Center for Experimental Plant Science Education, College of Agriculture, Guangxi University, Nanning 530004, People's Republic of China. [2]Guangxi South Subtropical Agricultural Science Research Institute, Chongzuo 532406, People's Republic of China. [3]Guangxi Colleges and Universities Key Laboratory of Crop Cultivation and Tillage, Nanning 530004, People's Republic of China. [4]Hepu Institute of Agricultural Sciences, Beihai 536101, People's Republic of China. [5]Maize Research Institute of Guangxi Academy of Agricultural Sciences, Nanning 530007, People's Republic of China.

Received: 20 January 2022 Accepted: 30 May 2022
Published online: 27 June 2022

References

1. Marques JM, da Silva TF, Vollu RE, Blank AF, Ding GC, Seldin L, et al. Plant age and genotype affect the bacterial community composition in the tuber rhizosphere of field-grown sweet potato plants. FEMS Microbiol Ecol. 2014;88(2):424–35.
2. Kang L, Ji CY, Kim SH, Ke Q, Park SC, Kim HS, et al. Suppression of the β-carotene hydroxylase gene increases β-carotene content and tolerance to abiotic stress in transgenic sweetpotato plants. Plant Physiol Biochem. 2017;117:24–33.
3. Wang S, Nie S, Zhu F. Chemical constituents and health effects of sweet potato. Food Res Int. 2016;89(Pt 1):90–116.
4. Wilson CD, Pace RD, Bromfield E, Jones G, Lu JY. Sweet potato in a vegetarian menu plan for NASA's advanced life support program. Life Support Biosph Sci. 1998;5(3):347–51.
5. Dai-Fu MA, Qiang L, Cao QH, Niu FX, Xie YP, Tang J. Development and prospect of sweetpotato industry and its technologies in China. Jiangsu Agric J. 2012;28(005):969–73.
6. Matsuo T, Yoneda T, Itoo S. Identification of free cytokinins and the changes in endogenous levels during tuber development of sweet potato (*Ipomoea batatas* lam.). Plant cell. Physiology. 1983;24(7):1305–1.
7. Matsuo T, Mitsuzono H, Okada R, Itoo S. Variations in the levels of major free cytokinins and free abscisic acid during tuber development of sweet potato. J Plant Growth Regul. 1988;7(4):249–58.
8. Suye S, Sugiyama T, Hashizume T. Mass spectrometric determination of Ribosyl trans-Zeatin from sweet potato tubers (*Ipomoea batatas* L. cv. Kohkei no. 14). Agric Biol Chem. 1983;47:1665–6.
9. Sugiyama T, Hashizume T. Cytokinins in developing tuberous roots of sweet potato (*Ipomoea batatas*). Agric Biol Chem. 1989;53:49–52.
10. Nakatani M, Komeichi M. Changes in the endogenous level of zeatin riboside, abscisic acid and indole acetic acid during formation and thickening of tuberous roots in sweet potato. Japan J Crop Sci. 2008;60(1):91–100.

11. Nakatani M, Komeichi M. Distribution of endogenous zeatin riboside and abscisic acid in tuberous roots of sweet potato. Japan J Crop Sci. 2008;60:322–3.
12. Noh SA, Lee HS, Huh EJ, Huh GH, Paek KH, Shin JS, et al. SRD1 is involved in the auxin-mediated initial thickening growth of storage root by enhancing proliferation of metaxylem and cambium cells in sweetpotato (*Ipomoea batatas*). J Exp Bot. 2010;61(5):1337–49.
13. Wang QM, Zhang LM, Guan YA, Wang ZL. Endogenous hormone concentration in developing tuberous roots of different sweet potato genotypes. Agric Sci China. 2006;5(012):919–27.
14. Ku AT, Huang YS, Wang YS, Ma D, Yeh KW. IbMADS1 (Ipomoea batatas MADS-box 1 gene) is involved in tuberous root initiation in sweet potato (*Ipomoea batatas*). Ann Bot. 2008;102(1):57–67.
15. Kim SH, Mizuno K, Fujimura T. Isolation of MADS-box genes from sweet potato (Ipomoea batatas (L.) lam.) expressed specifically in vegetative tissues. Plant cell. Physiology. 2002;43(3):314–22.
16. Tanaka M, Kato N, Nakayama H, Nakatani M, Takahata Y. Expression of class I knotted1-like homeobox genes in the storage roots of sweet potato (*Ipomoea batatas*). J Plant Physiol. 2008;165(16):1726–35.
17. Firon N, LaBonte D, Villordon A, Kfir Y, Solis J, Lapis E, et al. Transcriptional profiling of sweet potato (*Ipomoea batatas*) roots indicates down-regulation of lignin biosynthesis and up-regulation of starch biosynthesis at an early stage of storage root formation. BMC Genomics. 2013;14(1):460.
18. Tanaka M, Takahata Y, Nakatani M. Analysis of genes developmentally regulated during storage root formation of sweet potato. J Plant Physiol. 2005;162(1):91–102.
19. Noh SA, Lee HS, Kim YS, Paek KH, Shin JS, Bae JM. Down-regulation of the IbEXP1 gene enhanced storage root development in sweet potato. J Exp Bot. 2013;64(1):129–42.
20. Yang J, Moeinzadeh MH, Kuhl H, Helmuth J, Xiao P, Haas S, et al. Haplotype-resolved sweet potato genome traces back its hexaploidization history. Nature Plants. 2017;3(9):696–703.
21. Wang Z, Fang B, Chen J, Zhang X, Luo Z, Huang L, et al. De novo assembly and characterization of root transcriptome using Illumina paired-end sequencing and development of cSSR markers in sweet potato (*Ipomoea batatas*). BMC Genomics. 2010;11:726.
22. Wang Z, Fang B, Chen X, Liao M, Chen J, Zhang X, et al. Temporal patterns of gene expression associated with tuberous root formation and development in sweetpotato (*Ipomoea batatas*). BMC Plant Biol. 2015;15:180.
23. Dong T, Zhu M, Yu J, Han R, Tang C, Xu T, et al. RNA-Seq and iTRAQ reveal multiple pathways involved in storage root formation and development in sweet potato (*Ipomoea batatas* L.). BMC Plant Biol. 2019;19(1):136.
24. Kondhare KR, Malankar NN, Devani RS, Banerjee AK. Genome-wide transcriptome analysis reveals small RNA profiles involved in early stages of stolon-to-tuber transitions in potato under photoperiodic conditions. BMC Plant Biol. 2018;18(1):284.
25. Li M, Yang Y, Li X, Gu L, Wang F, Feng F, et al. Analysis of integrated multiple 'omics' datasets reveals the mechanisms of initiation and determination in the formation of tuberous roots in *Rehmannia glutinosa*. J Exp Bot. 2015;66(19):5837–51.
26. Chen H, Banerjee AK, Hannapel DJ. The tandem complex of BEL and KNOX partners is required for transcriptional repression of ga20ox1. Plant J. 2004;38(2):276–84.
27. Jung JK, McCouch S. Getting to the roots of it: genetic and hormonal control of root architecture. Front Plant Sci. 2013;4:186.
28. Ljung K. Auxin metabolism and homeostasis during plant development. Development. 2013;140(5):943–50.
29. Nieminen K, Immanen J, Laxell M, Kauppinen L, Tarkowski P, Dolezal K, et al. Cytokinin signaling regulates cambial development in poplar. Proc Natl Acad Sci U S A. 2008;105(50):20032–7.
30. Yu R, Wang J, Xu L, Wang Y, Wang R, Zhu X, et al. Transcriptome profiling of taproot reveals complex regulatory networks during taproot thickening in radish (*Raphanus sativus* L.). Front Plant Sci. 2016;7:1210.
31. Yao S, Lan Z, Huang R, Tan Y, Huang D, Gu J, et al. Hormonal and transcriptional analyses provides new insights into the molecular mechanisms underlying root thickening and isoflavonoid biosynthesis in *Callerya speciosa* (champ. Ex Benth.) Schot. Sci Rep. 2021;11(1):9.
32. Hejátko J, Ryu H, Kim GT, Dobesová R, Choi S, Choi SM, et al. The histidine kinases CYTOKININ-INDEPENDENT1 and ARABIDOPSIS HISTIDINE KINASE2 and 3 regulate vascular tissue development in Arabidopsis shoots. Plant Cell. 2009;21(7):2008–21.
33. Kumar D, Wareing PF. Factors controlling stolon development in the potato plant. New Phytol. 1972;71(4):639–48.
34. Yasunori K. Changes in levels of butanol- and water-soluble cytokinins during the life cycle of potato tubers. Plant Cell Physiol. 1982;23(5):843–9.
35. Rayirath UP, Lada RR, Caldwell CD, Asiedu SK, Sibley KJ. Role of ethylene and jasmonic acid on rhizome induction and growth in rhubarb (*Rheum rhabarbarum* L.). Plant Cell Tissue Organ Cult. 2011;105(2):253–63.
36. Mingo-Castel AM, Negm FB, Smith OE. Effect of carbon dioxide and ethylene on tuberization of isolated potato stolons cultured in vitro. Plant Physiol. 1974;53(6):798–801.
37. Lee Y, Bak G, Choi Y, Chuang W, Cho HT, Lee Y. Roles of phosphatidylinositol 3-kinase in root hair growth. Plant Physiol. 2008;147(2):624–35.
38. Xue HW, Chen X, Mei Y. Function and regulation of phospholipid signalling in plants. Biochem J. 2009;421(2):145–56.
39. Cenzano A, Cantoro R, Racagni G, De Los S-BC, Hernandez-Sotomayor T, Abdala G. Phospholipid and phospholipase changes by jasmonic acid during stolon to tuber transition of potato. Plant Growth Regul. 2008;56(3):307–16.
40. Dudits D, Abrahám E, Miskolczi P, Ayaydin F, Bilgin M, Horváth GV. Cell-cycle control as a target for calcium, hormonal and developmental signals: the role of phosphorylation in the retinoblastoma-centred pathway. Ann Bot. 2011;107(7):1193–202.
41. Chen T, Wu X, Chen Y, Li X, Huang M, Zheng M, et al. Combined proteomic and cytological analysis of Ca^{2+}-calmodulin regulation in Picea meyeri pollen tube growth. Plant Physiol. 2009;149(2):1111–26.
42. Gargantini PR, Giammaria V, Grandellis C, Feingold SE, Maldonado S, Ulloa RM. Genomic and functional characterization of StCDPK1. Plant Mol Biol. 2009;70(1–2):153–72.
43. Sojikul P, Kongsawadworakul P, Viboonjun U, Thaiprasit J, Intawong B, Narangajavana J, et al. AFLP-based transcript profiling for cassava genome-wide expression analysis in the onset of storage root formation. Physiol Plant. 2010;140(2):189–98.
44. Yao Y, Min Y, Geng MT, Wu XH, Hu XW, Fu SP, et al. The effects of calcium on the *in vitro* cassava storage root formation. Adv Mater Res. 2013;726-731:4529–33.
45. Hirt H. Connecting oxidative stress, auxin, and cell cycle regulation through a plant mitogen-activated protein kinase pathway. Proc Natl Acad Sci U S A. 2000;97(6):2405–7.
46. Nagata T, Niyada E, Fujimoto N, Nagasaki Y, Noto K, Miyanoiri Y, et al. Solution structures of the trihelix DNA-binding domains of the wild-type and a phosphomimetic mutant of Arabidopsis GT-1: mechanism for an increase in DNA-binding affinity through phosphorylation. Proteins. 2010;78(14):3033–47.
47. Nagano Y. Several features of the GT-factor trihelix domain resemble those of the Myb DNA-binding domain. Plant Physiol. 2000;124(2):491–4.
48. Kuhn RM, Caspar T, Dehesh K, Quail PH. DNA binding factor GT-2 from Arabidopsis. Plant Mol Biol. 1993;23(2):337–48.
49. Zhao C, Craig JC, Petzold HE, Dickerman AW, Beers EP. The xylem and phloem transcriptomes from secondary tissues of the Arabidopsis root-hypocotyl. Plant Physiol. 2005;138(2):803–18.
50. Zhong R, Lee C, McCarthy RL, Reeves CK, Jones EG, Ye ZH. Transcriptional activation of secondary wall biosynthesis by rice and maize NAC and MYB transcription factors. Plant Cell Physiol. 2011;52(10):1856–71.
51. Xie Y, Xu L, Wang Y, Fan L, Chen Y, Tang M, et al. Comparative proteomic analysis provides insight into a complex regulatory network of taproot formation in radish (*Raphanus sativus* L.). horticulture. Research. 2018;5:51.
52. Chan RL, Gago GM, Palena CM, Gonzalez DH. Homeoboxes in plant development. Biochimica et Biophysica Acta (BBA). 1998;1442(1):1–19.
53. Hur YS, Um JH, Kim S, Kim K, Park HJ, Lim JS, et al. *Arabidopsis thaliana* homeobox 12 (ATHB12), a homeodomain-leucine zipper protein, regulates leaf growth by promoting cell expansion and endoreduplication. New Phytol. 2015;205(1):316–28.
54. Tornero P, Conejero V, Vera P. Phloem-specific expression of a plant homeobox gene during secondary phases of vascular development. Plant J. 1996;9(5):639–48.
55. Xu XR, Gao ZM, Lou YF, Yang KB, Shan XM, Zhu CL. Identification of homeobox genes associated with lignification and their expression patterns in bamboo shoots. Biomolecules. 2019;9:862.
56. Ruan YL. Sucrose metabolism: gateway to diverse carbon use and sugar signaling. Annu Rev Plant Biol. 2014;65:33–67.

57. Zrenner R, Salanoubat M, Willmitzer L, Sonnewald U. Evidence of the crucial role of sucrose synthase for sink strength using transgenic potato plants (*Solanum tuberosum* L.). Plant J. 1995;7(1):97–107.
58. Rouhier H, Usuda H. Spatial and temporal distribution of sucrose synthase in the radish hypocotyl in relation to thickening growth. Plant Cell Physiol. 2001;42(6):583–93.
59. Hideaki U, Taku D, Kousuke S, Hiroo F. Development of sink capacity of the "storage root" in a radish cultivar with a high ratio of "storage root" to shoot. Plant Cell Physiol. 1999;4:4.
60. Mitsui Y, Shimomura M, Komatsu K, Namiki N, Shibata-Hatta M, Imai M, et al. The radish genome and comprehensive gene expression profile of tuberous root formation and development. Sci Rep. 2015;5:10835.
61. Li XQ, Zhang D. Gene expression activity and pathway selection for sucrose metabolism in developing storage root of sweet potato. Plant Cell Physiol. 2003;44(6):630–6.
62. Jackson SD. Multiple signaling pathways control tuber induction in potato. Plant Physiol. 1999;119(1):1–8.
63. Ren X, Zhang J. Research progresses on the key enzymes involved in sucrose metabolism in maize. Carbohydr Res. 2013;368:29–34.
64. Yu R, Xu L, Zhang W, Wang Y, Luo X, Wang R, et al. De novo taproot transcriptome sequencing and analysis of major genes involved in sucrose metabolism in radish (*Raphanus sativus* L.). Front Plant Sci. 2016;7:585.
65. Abelenda JA, Navarro C, Prat S. From the model to the crop: genes controlling tuber formation in potato. Curr Opin Biotechnol. 2011;22(2):287–92.
66. Yang M, Zhu L, Pan C, Xu L, Liu Y, Ke W, et al. Transcriptomic analysis of the regulation of rhizome formation in temperate and tropical Lotus (*Nelumbo nucifera*). Sci Rep. 2015;5:13059.
67. Wang X, Chang L, Tong Z, Wang D, Yin Q, Wang D, et al. Proteomics profiling reveals carbohydrate metabolic enzymes and 14-3-3 proteins play important roles for starch accumulation during cassava root Tuberization. Sci Rep. 2016;6:19643.
68. Kuipers A, Jacobsen E, Visser R. Formation and deposition of amylose in the potato tuber starch granule are affected by the reduction of granule-bound starch synthase gene expression. Plant Cell. 1994;6(1):43–52.
69. Li XJ, Yang JL, Hao B, Lu YC, Qian ZL, Li Y, et al. Comparative transcriptome and metabolome analyses provide new insights into the molecular mechanisms underlying taproot thickening in *Panax notoginseng*. BMC Plant Biol. 2019;19(1):451.
70. Qin Z, Hou F, Li A, Dong S, Huang C, Wang Q, et al. Comparative analysis of full-length transcriptomes based on hybrid population reveals regulatory mechanisms of anthocyanin biosynthesis in sweet potato (*Ipomoea batatas* (L.) lam). BMC Plant Biol. 2020;20(1):299.
71. Mano H, Ogasawara F, Sato K, Higo H, Minobe Y. Isolation of a regulatory gene of anthocyanin biosynthesis in tuberous roots of purple-fleshed sweet potato. Plant Physiol. 2007;143(3):1252–68.
72. Mahoney JD, Wang S, Iorio LA, Wegrzyn JL, Dorris M, Martin D, et al. De novo assembly of a fruit transcriptome set identifies AmMYB10 as a key regulator of anthocyanin biosynthesis in Aronia melanocarpa. BMC Plant Biol. 2022;22(1):143.
73. Young MD, Wakefield MJ, Smyth GK, Oshlack A. Gene ontology analysis for RNA-seq: accounting for selection bias. Genome Biol. 2010;11(2):R14.
74. Mao X, Tao C, Olyarchuk JG, Wei L. Automated genome annotation and pathway identification using the KEGG Orthology (KO) as a controlled vocabulary. Bioinformatics. 2005;21(19):3787.
75. Eisen MB, Spellman PT, Brown PO, Botstein D. Cluster analysis and display of genome-wide expression patterns. Proc Natl Acad Sci U S A. 1998;95(25):14863–8.
76. Langfelder P, Horvath S. WGCNA: an R package for weighted correlation network analysis. BMC Bioinformatics. 2008;9:559.
77. Zhang B, Horvath S. A general framework for weighted gene co-expression network analysis. Stat Appl Genet Mol Biol. 2005;4:Article17.

Publisher's Note

ABOUT UMT FACULTY

SDI

Selective Dissemination of Information (SDI) service is a current-awareness service offered by the PSNZ for UMT Faculty Members. The contents selection criteria include current publications (last 5 years), highly cited and most viewed/downloaded documents. The contents with pdf full text from subscribed databases are organized and compiled according to a monthly theme which is determined based on the topics of specified interest.

For more information or further assistance, kindly contact us at 09-6684185/4298 or email to psnz@umt.edu.my/sh_akmal@umt.edu.my

Thank you.

Perpustakaan Sultanah Nur Zahirah
Universiti Malaysia Terengganu
21030 Kuala Nerus, Terengganu.

Tel. : 09-6684185 (Main Counter)
Fax : 09-6684179
Email : psnz@umt.edu.my